UNIVERSITY OF HULL

Investigation of the effects of anticoagulants on tissue factor mediated cellular processes

being a thesis submitted in fulfilment of the requirements for the degree of Doctor of Biomedical Science in the University of Hull by Sophie Featherby (BSc, MSc)

May 2021

To my family,

Thank you.

Acknowledgements

I would like to sincerely thank Dr. Camille Ettelaie for giving me the confidence to undertake this PhD. Her time, supervision, guidance, patience and continuous support over the last four years has been invaluable. Also, I would like to thank Prof. Anthony Maraveyas for his guidance, support and knowledge. I also thank Dr Xiao Yu Pei for her time and expertise in teaching me the CAM techniques required for this work.

I acknowledge the support of Bristol Myers Squibb for funding this work as well as providing pure apixaban. I also thank LeoPharma and Castle Hill Hospital Cancer Trust Fund for additional funding contributions and Bayer of providing pure rivaroxaban for this project.

A huge thank you to my parents for their unending support and encouragement. I also thank my sister, Katie and my friends for listening through both the highs and the lows. I would also like to thank the members of the PGR writing group for their inspiration and encouragement during the writing up process. I am deeply grateful to my colleagues from over the years Xiao Yu Pei, Ali Ethaeb, Naima Benelhaj, Yahya Madkhali, Mohammad Mohammad and Farzana Haque for their friendship and advice, and generally making the lab a pleasant place to be, even when experiments weren't going to plan. Additionally, thank you to Dr. Leonid Nikitenko and the members of his laboratory for sharing their knowledge and experiences.

Publications and Conferences

Papers

Ettelaie, C., Collier, M. E. W., Featherby, S., Greenman, J. & Maraveyas, A. (2018) Peptidyl-prolyl isomerase 1 (Pin1) preserves the phosphorylation state of tissue factor and prolongs its release within microvesicles. *Biochim Biophys Acta Mol Cell Res*, 1865(1), 12-24.

Featherby, S., Madkhali, Y., Maraveyas, A. & Ettelaie, C. (2019) Apixaban suppresses the release of TF-positive microvesicles and restrains cancer cell proliferation through directly inhibiting TF-fVIIa activity. *Thromb Haemost*, 119(9), 1419-1432.

Featherby, S., Xiao, Y. P., Ettelaie, C., Nikitenko, L. L., Greenman, J. & Maraveyas, A. (2019) Low molecular weight heparin and direct oral anticoagulants influence tumour formation, growth, invasion and vascularisation by separate mechanisms. *Sci Rep*, 9(1), 6272.

Madkhali, Y., Featherby, S., Collier, M. E., Maraveyas, A., Greenman, J. & Ettelaie, C. (2019) The ratio of factor VIIa:Tissue factor content within microvesicles determines the differential influence on endothelial cells. *TH Open*, 3(2), e132-e145.

Ethaeb, A. M., Mohammad, M. A., Madkhali, Y., Featherby, S., Maraveyas, A., Greenman, J. & Ettelaie, C. (2020) Accumulation of tissue factor in endothelial cells promotes cellular apoptosis through over-activation of Src1 and involves beta1-integrin signalling. *Apoptosis*, 25(1-2), 29-41.

Madkhali, Y., Rondon, A. M. R., Featherby, S., Maraveyas, A., Greenman, J. & Ettelaie, C. (2021) Factor VIIa regulates the level of cell-surface tissue factor through separate but cooperative mechanisms. *Cancers*, 13(15), 3718.

Ettelaie, C., Featherby, S., Rondon, A. M. R., Greenman, J., Versteeg, H. H. & Maraveyas, A. (2021) De-palmitoylation of tissue factor regulates its activity, phosphorylation and cellular functions. *Cancers*, *13*(15), 3837.

Presentations

Featherby, S., Xiao, Y. P., Maraveyas, A. & Ettelaie, C. (2017) Tinzaparin reduces angiogenesis and vasculogenesis in a chorio-allantoic membrane model. Presented at the 14th international medical postgraduate conference. Prague, Czech Republic.

Featherby, S., Maraveyas, A. & Ettelaie, C. (2018) Apixaban and rivaroxaban reduce the release of TF-bearing microvesicles from fXa activated cancer cell line. Presented in BSHT Annual Scientific Meeting. University of Warwick, UK.

Featherby, S., Maraveyas, A. & Ettelaie, C. (2018) Dissimilar effects of direct oral anticoagulants on the release of TF-positive microvesicles and cancer cell proliferation. Presented at the 9th international conference on thrombosis & hemostasis issues in cancer. Bergamo, Italy.

Featherby, S., Ettelaie, C. & Maraveyas, A. (2019) Low molecular weight heparin reduces tumour formation, invasion and vascularisation. Presented at congress of the international society on thrombosis and haemostasis. Melbourne, Australia.

Featherby, S., Mohammad, M. A., Madkhali, Y., Collier, M. E., Maraveyas, A. & Ettelaie, C. (2019) Identification of the interacting domains between the extracellular domains of tissue factor and β1-intergin and their influence on cell proliferation. Presented at congress of the international society on thrombosis and haemostasis. Melbourne, Australia.

Posters

Featherby, S., Ettelaie, C. & Maraveyas, A. (2017) Factor Xa inhibitors apixaban and rivaroxaban suppress the release of TF-bearing microvesicles from cancer cell lines. Presented at congress of the international society on thrombosis and haemostasis. Berlin, Germany.

Featherby, S., Maraveyas, A. & Ettelaie, C. (2017) Apixaban and rivaroxaban reduce the release of TF-bearing microvesicles from fXa activated cancer cell line. Presented at annual conference of extracellular vesicles. Cambridge, UK.

Featherby, S., Xiao, Y. P., Maraveyas, A. & Ettelaie, C. (2017) Tinzaparin reduces angiogenesis and vasculogenesis in a Chorio-allantoic membrane model. Presented in BSHT Annual Scientific Meeting. University of Warwick, UK.

Featherby, S., Xiao, Y. P., Maraveyas, A. & Ettelaie, C. (2018) Low molecular weight heparin reduces tumour formation, invasion and vascularisation. Presented in BSHT Annual Scientific Meeting. University of Warwick, UK.

Featherby, S., Madkhali, Y., Maraveyas, A. & Ettelaie, C. (2019) Apixaban suppresses the release of TF-positive microvesicles and restrains cancer cell proliferation through directly inhibiting TF-fVIIa

activity. Presented at congress of the international society on thrombosis and haemostasis. Melbourne, Australia.

Featherby, S., Mohammad, M. A., Madkhali, Y., Collier, M. E., Maraveyas, A. & Ettelaie, C. (2019) Examination of the interacting domains between the extracellular domains of tissue factor and β1-intergin and their influence on cell proliferation. Presented at European Congress on Thrombosis and Haemostasis. Glasgow, UK.

Featherby, S. & Ettelaie, C. (2021) Elucidation of the signalling properties of the two fibronectin-like domains of tissue factor. Presented at BSHT Virtual Scientific Meeting.

Abstract

Thrombotic complications are common in cancer patients and are amongst the leading causes of morbidity and mortality. Recently, it was reported that treatment of cancer patients with the low molecular weight heparin (LMWH) family of anticoagulants can result in a significant reduction in mortality compared with those receiving other conventional anticoagulants. Therefore, the mechanisms by which different anticoagulants interact with cancer cells were investigated. First, the influence of two preparations of LMWH (tinzaparin and dalteparin) and two direct fXa inhibitors (apixaban and rivaroxaban) on cancer invasion, angiogenesis and tumour growth was explored. Tinzaparin and to a lesser extent dalteparin, were shown to inhibit cancer cell invasion and angiogenesis, using matrix invasion and chorioallantoic membrane (CAM) assays, respectively. In addition, apixaban, but not rivaroxaban inhibited the growth of CAM-implanted xenografts which indicated a mechanism independent of the anti-fXa property of apixaban. The anti-tumour property of apixaban was further explored by comparing the influence of apixaban and rivaroxaban on cancer cell proliferation and microvesicle (MV) release. Apixaban was shown to inhibit the release of MV in response to exogenous fXa and fVIIa, as well as endogenous fVIIa expressed by the cancer cells. In contrast rivaroxaban was effective in suppressing MV release in response to fXa only. The mechanism of inhibition of endogenous fVIIa by apixaban was also shown to include the suppression of complex formation with TF and therefore, preventing the activation of protease activated receptor (PAR) 2 by the TF/fVIIa complex.

In addition to signalling through PAR2, the interaction of tissue factor (TF) with β1 integrin is known to be required for induction of cell proliferation and contact-independent survival of cancer cells. Therefore, in the next section of the study an attempt was made to identify the function of the potential interacting domains between TF and β1 integrin. The cDNA corresponding to the upper or lower fibronectin-like domains, and also that encoding the complete extracellular domain of TF were separately cloned into an expression plasmid. These were expressed in human dermal blood endothelial cells (HDBEC) and MDA-MB-231 cell line and the ability of the resulting peptides to bind to β1 integrin was assessed *in situ*, using the proximity ligation assay (PLA) and also, by co-immunoprecipitation. The upper fibronectin-like domain (UED) was shown to bind to the EGF4 domain of β1 integrin and the lower fibronectin-like domain (LED) with the βTD domain. To examine the proliferative properties of these peptides, the expression of cyclin D1 and ERK1/2 phosphorylation were measured and changes in cell numbers determined. The interaction of either the UED or the LED peptide with β1 integrin in HDBEC, which do not express endogenous TF, was shown to induce ERK1/2 phosphorylation. However, displacement of endogenous TF by the UED peptide in MDA-MB-231 cells resulted in a reduction in ERK1/2 phosphorylation, cyclin D1

expression and cell numbers. In contrast, expression of LED peptide in MDA-MB-231 cells did not influence these parameters for proliferative signalling, indicating that the TF-signalling was maintained by the LED peptide. Collectively, these findings suggested that although both the upper and lower extracellular domains of TF can induce cell signalling, the lower domain may be essential for the promotion of proliferation.

The last section of the study was based on previous work showing that prevention of the phosphorylation of TF can block the release of the protein in MV, resulting in a build-up of TF within cells. This study explored the role of TF depalmitoylation which is also known to precede and be essential for TF phosphorylation. It was hypothesised that such alterations may regulate the translocation of TF to lipid rafts and its release within MV. Mutant forms of TF with substitutions to prevent, or to mimic palmitoylation at cysteine 245, or with altered lengths of the transmembrane domain were prepared and expressed in cells. The influence of these proteins on cell proliferation and apoptosis were then examined. Expression of mutant forms of TF which could not be palmitoylated or containing a longer transmembrane domain resulted in decreased levels of apoptosis. However, neither the mutant mimicking palmitoylation, or containing a shortened transmembrane domain were not released within MV and resulted in increased cell apoptosis.

In conclusion, this study has demonstrated the anti-cancer properties and some of the mechanisms involved, in a set of anticoagulants. In particular, apixaban was shown to suppress cancer cell growth by preventing the activation of PAR2 by the TF/fVIIa complex. In addition, this study has elucidated the role of the various extracellular and intracellular domains within TF, in promoting the signals that regulate cell proliferation and apoptosis.

Contents

List of Figures

List of Tables

List of symbols and abbreviations

%	Percentage
°C	Degree celsius
2D	2-dimensional
3D	3-dimensional
Å	Angstrom
Ab	Antibody
ADP	Adenosine diphosphate
ANOVA	Analysis of variance
AP	Alkaline phosphatase
Apix	Apixaban
ARF6	ADP-ribosylation factor 6
asTF	Alternative spliced TF
ATIII	Antithrombin III
bFGF	Basic fibroblast growth factor
bp	Base pair
BSA	Bovine serum albumin
Ca^{+2}	Calcium ion
CAM	Chorioallantoic membrane
cAMP	Cyclic adenosine monophosphate
cDNA	Complementary deoxyribonucleic acid
CO_2	Carbon dioxide
co-IP	Co-immunoprecipitation
Ct	Cycle Threshold
Da	Dalton
DAPI	4',6-diamidino-2-phenylindole
DCTA	Trans-1,2-Diaminocyclohexane-*N,N,N',N'*-tetraacetic acid monohydrate
DMEM	Dulbeco's modified essential medium
DMSO	Dimethyl sulphoxide
DNA	Deoxyribonucleic acid
dNTP	Deoxyribose nucleoside triphosphate
DOAC	Direct oral anticoagulant
DTT	Dithiothreitol
E. coli	Escherichia coli
EC50	Half maximal effective concentration
ECM	Extracellular matrix
EDD	Embryo development day
EDTA	Ethylenediaminetetraacetic acid
EGF	Epidermal growth factor
EGFR	Epidermal growth factor receptor
ELISA	Enzyme-linked immunosorbent assay
EpCAM	Epithelial cell adhesion molecule
ERK	Extracellular signal-regulated kinase
Ex/Em	Excitation/Emission
f	Factor
FAK	Focal adhesion kinase
FCS	Foetal calf serum

FITC	Fluorescein isothiocyanate
FSC	Forward scatter
g	Gram
g	Gravity
GAPDH	Glyceraldehyde-3-phosphate dehydrogenase
GDP	Guanosine diphosphate
GLA	Vitamin K-dependent carboxylation/gamma-carboxyglutamic
GPCR	G-protein-coupled receptor
GTP	Guanosine triphosphate
h	Hour
H_2SO_4	Sulfuric acid
HA	Human influenza hemagglutinin
HCAEC	Human coronary artery endothelial cells
HCl	Hydrochloric acid
HDBEC	Human dermal blood endothelial cells
HEPES	4-(2-hydroxyethyl)-1-piperazineethanesulfonic acid
HGF	Hepatocyte growth factor
HRP	Horseradish peroxidase
HSPG	Heparan sulphate proteoglycan
HUVEC	Human umbilical vein endothelial cells
Ig	Immunoglobulin
IL	Interleukin
IU	International units
k	Kilo
KLD	Kinase-Ligase-DpnI
l	Litre
LB	Lysogeny broth
LED	Lower extracellular domain
LMWH	Low molecular weight heparin
m	Milli
M	Molarity
MAPK	Mitogen-activated protein kinase
min	Minute
MLC2	Myosin light chain 2
MLCK	Myosin light chain kinase
MLCP	Myosin light chain phosphatase
M-MLV	Moloney murine leukemia virus reverse transcriptase
MMP	Matrix metalloproteinase
$MnCl_2$	Manganese Chloride
mol	Mole
mRNA	Messager RNA
MV	Microvesicles
MW	Molecular weight
n	Nano
NaCl	Sodium Chloride
NaOH	Sodium Hydroxide
NCBI	National Center for Biotechnology Information
NFκB	Nuclear factor-κB

p	Pico
PAR	Protease activated receptor
PAR2-AP	Protease activated receptor 2-activating peptide
PBS	Phosphate buffered saline
PBST	PBS containing Tween-20
PC	Phosphatidylcholine
PCR	Polymerase chain reaction
PDGF	Platelet-derived growth factor
PE	Phosphatidylethanolamine
PECAM-1	Platelet endothelial cell adhesion molecule-1
PF4	Platelet factor-4
PI3K	Phosphoinositide 3-kinase
PLA	Proximity ligation assay
PS	Phosphatidylserine
PTEN	Phosphatase and tensin homolog
RCSB	Research Collaboratory for Structural Bioinformatics
RhoA	Ras homolog family member A
Riv	Rivaroxaban
RNA	Ribonucleic acid
rNAP	Recombinant nematode anticoagulant protein
RNase	Ribonuclease
ROCK	Rho associated coiled-coil containing protein kinase
rpm	Revolutions per minute
RT-PCR	Real-time PCR
s	Second
SDS	Sodium dodecyl sulphate
SDS-PAGE	Sodium dodecyl sulphate - polyacrylamide gel electrophoresis
SFM	Serum free media
siRNA	Short interfering RNA
SOC	Super optimal broth with catabolite repression
SSC	Side scatter
TBE	Tris Borate EDTA
TBS	Tris-HCl buffered saline
TBST	TBS containing Tween-20
TdT	Terminal deoxynucleotidyl transferase
TED	Total extracellular domain
TEMED	N,N,N’,N’-tetramethylethylenediamine
TF	Tissue factor
TFPI	Tissue factor pathway inhibitor
$TF^{\Delta CT}$	Cytoplasmic domain deleted tissue factor
tGFP	Turbo green fluorescent protein
Tinz	Tinzaparin
TNF-α	Tumour necrosis factor-α
Tris	Tris(hydroxymethyl)aminomethane
U	Unit
U	Arbitrary unit
UED	Upper extracellular domain
v/v	Volume to volume

VE-cadherin	Vascular endothelial cadherin
VEGF	Vascular endothelial growth factor
VEGFR	Vascular endothelial growth factor receptor
VTE	Venous thromboembolism
vWF	von Willebrand factor
w/v	Weight to volume
α	Alpha
β	Beta
βTD	β-tail domain
µ	Micro

Chapter 1

Introduction

1.1 General Introduction

The bidirectional association between coagulation and cancer has been reported since the 1800s and the ability of tumours to promote a hypercoagulable state in cancer patients has been established (Trousseau, 1867). The clinical manifestation of this hypercoagulable state includes the increased prevalence of thrombotic events in cancer patients including deep-vein thrombosis (DVT) and pulmonary embolism (PE) (Ay et al., 2017; Walker et al., 2013). In addition, the activation of the coagulation system in cancer patients appears to contribute to tumour growth and angiogenesis (Rickles et al., 2001; Shoji et al., 1998), as well as the dissemination of the tumour through metastasis (Rickles et al., 1988). Consequently, it has been proposed that treatment of cancer patients with anticoagulants may be effective at reducing tumour development and angiogenesis. More recently, it has been reported that treatment of cancer patients with the LMWH family of anticoagulants resulted in a reduction in patient mortality, compared with those receiving other types of anticoagulants (Akl et al., 2007; Lazo-Langner et al., 2007). Furthermore, the development of a new class of anticoagulants, known as direct oral anticoagulants (DOAC) has given impetus to the research for the understanding of the mechanisms of the association between coagulation and cancer. This study aimed to examine the effectiveness of a limited set of anticoagulants, and to elucidate the underlying mechanisms by which these may influence cancer cells.

A main initiator of the coagulation mechanism is the protein tissue factor (TF) which has been shown to be closely associated with cancer and angiogenesis (Belting et al., 2004; Cirillo et al., 2004). The signals arising from TF are reported to be mediated by the activation of protease-activated receptors (PAR) (Camerer et al., 2000a; Camerer et al., 2000b) and also through interaction with the cell adhesion molecule β1 integrin (Collier & Ettelaie, 2010; Rothmeier et al., 2018; Versteeg et al., 2008b). However, many of the mechanisms involved in these signalling pathways and their regulators are currently unclear. By examining the TF-mediated cellular signalling, this study aimed to examine the effectiveness of a limited set of anticoagulants, and to elucidate the underlying mechanisms by which these may influence cancer cells.

1.2 Blood haemostasis and the coagulation pathways

Haemostasis is the process by which bleeding is arrested following damage to a blood vessel, to prevent excessive blood loss (Hatton, 2013). The four components of the haemostatic system are the coagulation system, together with the fibrinolytic system, platelets and the vasculature, which together maintain blood fluidity and regulate clot formation (Hatton, 2013; Palta et al., 2014). The coagulation system consists of a series of proteases known as coagulation factors, the majority of which circulate in the blood stream in inactive, precursor forms known as zymogens (summarised in

Table 1.1)(Davie & Ratnoff, 1964; Macfarlane, 1964). Following vascular injury these proteases, together with their cofactors, sequentially activate each other in what is known as the coagulation cascade. The initial sections of the coagulation cascade are divided into the extrinsic pathway and the intrinsic pathway (Figure 1.1)(Palta et al., 2014; Triplett, 2000). The extrinsic pathway is activated following damage to the vascular tissue which results in the exposure of the protein tissue factor (TF) to the bloodstream. The exposure of TF results in the binding of circulating factor (f)VII to the extracellular domain of TF and promotes the conversion of fVII to the active form of the protein, fVIIa. The TF/fVIIa complex proteolytically cleaves fIX and fX, generating the active enzymes, fIXa and fXa (Komiyama et al., 1990). The generation of fXa is a point of convergence between the intrinsic and extrinsic pathways as well as the initiation point of the common pathway. FXa activates prothrombin to produce thrombin which in turn converts fibrinogen to fibrin monomers which go on to aggregate to produce a clot. Furthermore, thrombin activates fXIII, a transglutaminase that covalently cross-links the fibrin chains further stabilising the clot (Hatton, 2013). Thrombin also feeds back and activates fV and fVIII producing fVa and fVIIIa. FVa forms a complex with fXa on the surface of cells or platelets and acts as a co-factor for the conversion of prothrombin to thrombin at an accelerated rate, compared to fXa alone (Morrissey et al., 2010; Palta et al., 2014). Thrombin also acts as an agonist which promotes the activation of platelets. Additionally, platelets can be activated following the binding of glycoprotein adhesion molecules on the platelets to ligands including collagen, fibrinogen and von Willebrand factor (vWF) within exposed subendothelial layers. The activation of platelets induces a morphological change which results in an increase in the surface area of the platelet and the exposure of negatively charged phospholipids on the platelet surface. The activated platelets aggregate together with the fibrin clot to form a haemostatic plug. This haemostatic plug prevents further loss of blood and preserves vascular integrity (Mackman, 2004). The intrinsic pathway is initiated through the activation of fXII following contact between the blood and sub-endothelial collagen or the plasma membrane of activated platelets (Grover & Mackman, 2018). FXIIa catalyses the activation of fXI to fXIa which in turn activates fIX to fIXa. FIXa forms a complex with the co-factor fVIIIa, which itself is activated by the feedback of thrombin. The fIXa/fVIIIa complex activates fXa, which feeds into the common pathway.

Coagulation proteases including prothrombin, fVII, fIX, and fX contain a series of negatively charged γ-carboxyglutamate residues located at the c-terminus, called a GLA-domain (Suttie, 1980). These residues bind to a Ca^{2+} ion, which in turn interacts with exposed negatively charged phospholipids, particularly phosphatidylserine (PS). High concentrations of PS are exposed on the surface membrane of activated platelets and damaged cells, at the site of vessel injury (Morrissey et al., 2010; Paborsky et al., 1991). The binding of coagulation factors, together with their respective

Table 1.1: Coagulation factors

Clotting factor number	Clotting factor name	Function	Plasma half-life (h)	Plasma concentration (mg/L)
I	Fibrinogen	Clot formation	90	3000
II	Prothrombin	Activation of I, V, VII, VIII, XI, XIII, protein C, platelets	65	100
III	TF	Co factor of VIIa	-	-
IV	Calcium	Facilitates coagulation factor binding to phospholipids	-	-
V	Proacclerin, labile factor	Co-factor of X-prothrombinase complex	15	10
VI	Unassigned			
VII	Stable factor, proconvertin	Activates factors IX, X	5	0.5
VIII	Antihaemophilic factor A	Co-factor of IX-tenase complex	10	0.1
IX	Antihaemophilic factor B or Christmas factor	Activates X: Forms tenase complex with factor VIII	25	5
X	Stuart-Prower factor	Prothrombinase complex with factor V: Activates factor II	40	10
XI	Plasma thromboplastin antecedent	Activates factor IX	45	5
XII	Hageman factor	Activates factor XI, VII and prekallikrein		-
XIII	Fibrin-stabilising factor	Crosslinks fibrin	200	30
XIV	Prekallikerin (F Fletcher)	Serine protease zymogen	35	
XV	HMWK- (F Fitzgerald)	Co factor	150	
XVI	vWf	Binds to VIII, mediates platelet adhesion	12	10 µg/mL
XVII	Antithrombin III	Inhibits IIa, Xa, and other proteases	72	0.15-0.2 mg/mL
XVIII	Heparin cofactor II	Inhibits IIa	60	-
XIX	Protein C	Inactivates Va and VIIIa	0.4	-
XX	Protein S	Cofactor for activated protein C		-

HMWK – High molecular weight kininogen; vWf – Von Willebrand factor; TF – Tissue factor

Name, function and plasma concentration of the coagulation proteases/clotting factors which make up the blood clotting pathways. Proteases highlighted by red boxes are of particular interest for the current study (Originally published in Palta et al. (2014)).

Figure 1.1: Blood clotting pathways

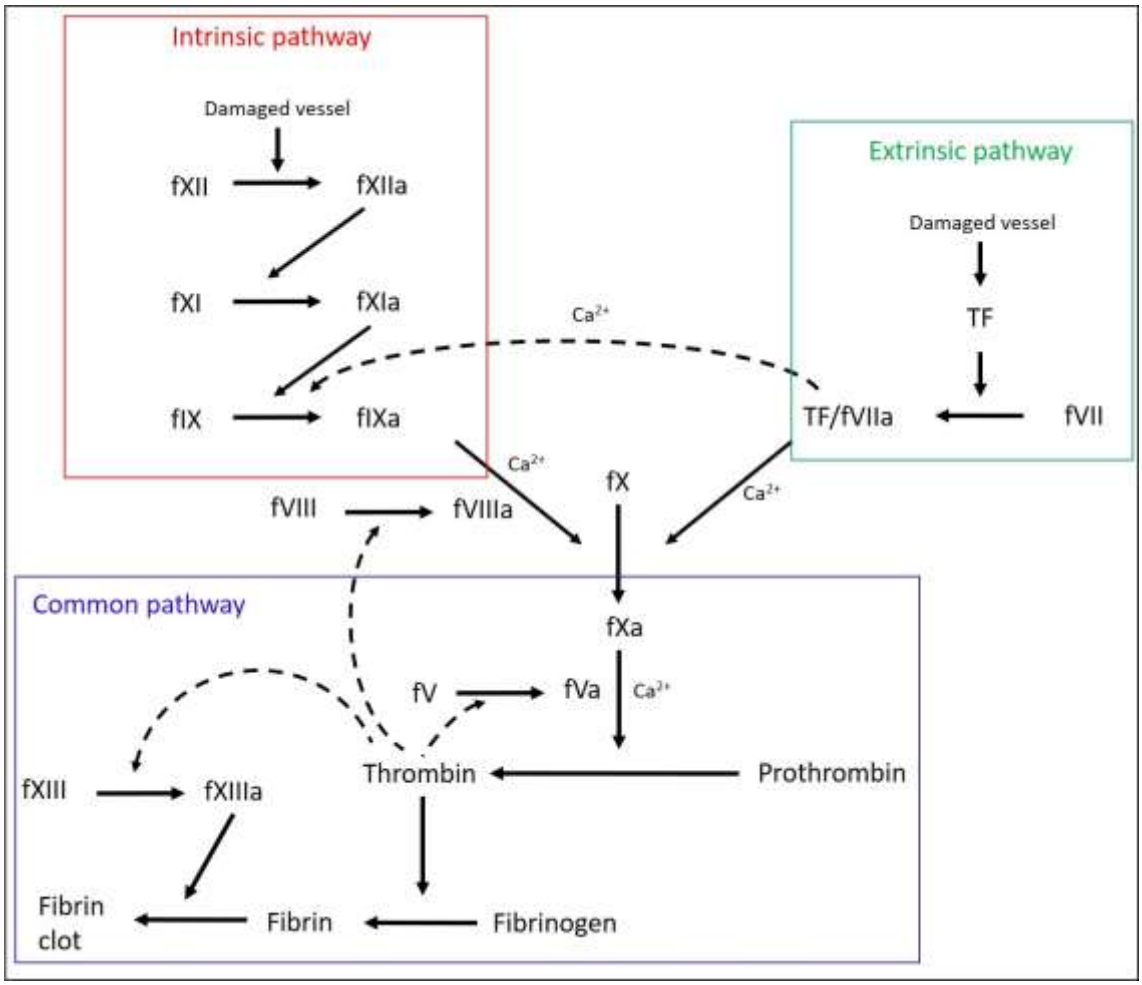

The blood clotting pathways can be divided into the extrinsic, intrinsic and common pathways. The extrinsic pathway is triggered upon injury to the blood vessel which exposes TF on the surface of injured tissue. The intrinsic pathway is initiated by the activation of factor XII on exposure of negatively charged molecules, including adenosine diphosphate (ADP) and collagen. The intrinsic and extrinsic pathways converge to initiate the common pathway.

substrates and cofactors, on these membranes increases the rate of contact between the molecules and accelerates the rate of activity of the enzymes. Therefore, the fIXa/fVIIIa complex and the fVa/fXa complex rapidly generate a large quantity of fXa and thrombin, respectably.

The coagulation system is stringently regulated by anticoagulant proteins and the fibrinolytic system. These systems limit the size of a forming clot and localise it to the site of injury. In addition, the anticoagulant and fibrinolytic systems prevent aberrant clotting, and also contribute to the initiation of wound healing and subsequent removal of the clot (Hatton, 2013). The key inhibitor of the extrinsic coagulation pathway is an anticoagulant protein called tissue factor pathway inhibitor (TFPI) (Broze, 1995). TFPI functions by initially binding to and inhibiting fXa. The TFPI/fXa complex then binds to TF/fVIIa on the surface of cells, resulting in the formation of a fully inhibited quaternary complex. The formation of this complex prevents further initiation of the blood coagulation cascade by TF (Broze, 1995).

Finally, in addition to the containment of bleeding, the activation of the coagulation system has also been shown to be a precursor for subsequent biological processes involved in wound healing, including angiogenesis. However, dysregulation of these processes is known to have substantial influences on the development of various chronic diseases, including cancer and cardiovascular disease, and is discussed later in this chapter.

1.3 Tissue factor (TF)

TF also known as coagulation factor III, thromboplastin or CD142, is a 47 kDa transmembrane glycoprotein (Butenas, 2012). TF is a type I integral membrane protein that consists of an extracellular domain (residues 1-219), a transmembrane domain (residues 220-242) and a cytoplasmic domain (residues 243-263) (Morrissey et al., 1987; Spicer et al., 1987). The extracellular domain of TF is composed of two fibronectin type III domains, joined at an angle of 125 degrees (Harlos et al., 1994) regardless of whether the protein is in the free state, or bound to fVIIa (Teplyakov et al., 2017). As stated in section 1.2, TF is the principal initiator of the coagulation cascade and is crucial for haemostasis. TF functions as a receptor and co-factor for coagulation factor fVII(a), promoting fVIIa cleavage of fX and fXI. The amino acid residues responsible for the interaction with fVII(a) are located mainly in the upper fibronectin-like domain (residues 1-107) whereas the residues responsible for interacting with fX or fXI are located in the lower fibronectin-like domain (residues 108-219) (Figure 1.2A) (Krudysz-Amblo et al., 2011). Each of the fibronectin type III domains contains a disulphide bridge located at Cys49-Cys57 and Cys186-Cys209 (Butenas et al., 2012). Alterations in the reduction status of the Cys186-Cys209 disulphide bonds have been reported to reduce the binding affinity for fVIIa and also to completely prevent the interaction of TF

Figure 1.2: The structure of TF extracellular domain and asTF

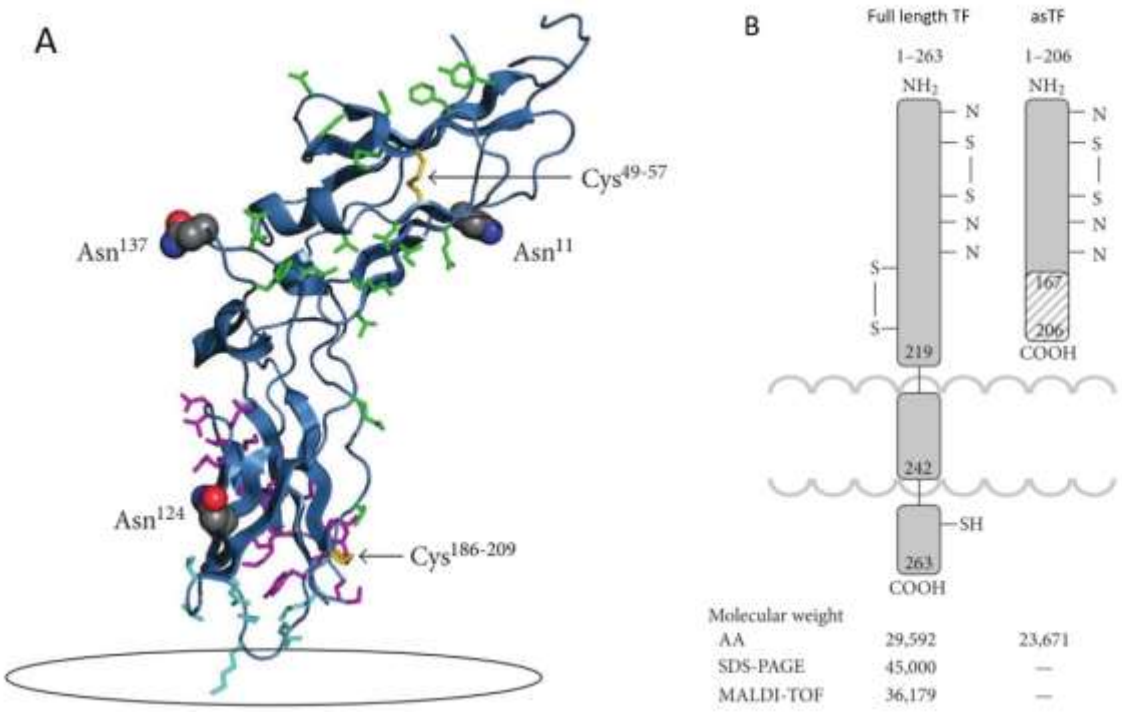

A) TF extracellular domain contains residues which are responsible for complexing with both fVII(a) (green) and fX or fXI (magenta). In addition, residues at the C-terminal end of TF extracellular domain form interactions with the cell membrane (aqua). TF also contains three potential glycosylation sites (red) and two disulphide bridges (yellow) (Originally published in Krudysz-Amblo et al. (2011)). B) Comparison of the domain structures of TF and asTF. The asTF protein lacks the transmembrane or cytoplasmic domains and instead possesses a unique C-terminus (Adapted from Butenas (2012)).

with fX or fXI (Ahamed et al., 2006). TF has also been shown to be glycosylated and the extracellular domain contains 3 glycosylation sites at Asp11, Asp124 and Asp137 (Butenas et al., 2012; Paborsky & Harris, 1990). However, it has been reported that the glycosylation of TF is not essential for its function (Aberg & Siegbahn, 2013).

Many cell types including fibroblasts, epidermal keratinocytes and astrocytes constitutively express TF (Drake et al., 1989). In addition, TF is located in vascular smooth muscle cells, pericytes and fibroblasts within the blood vessel walls. However, although TF is expressed in monocytes, the protein is absent from all other circulating blood cells and vascular endothelial cells that are in contact with the bloodstream (Osterud, 2010). Therefore, in order for coagulation to be initiated the integrity of the endothelial layer must be disrupted to expose the underlying TF (Drake et al., 1989; Mackman, 2009). However, endothelial cells have been shown to express TF in response to stimulation with inflammatory cytokines, growth factors or lipopolysaccharides (Mackman et al., 1993). Consequently, during diseases such as cardiovascular disease, chronic inflammation and diabetes, TF has been shown to be expressed on the surface of endothelial cells. These disease states can also lead to TF circulating within the blood stream, located on blood cells, platelets and small phospholipid vesicles called microvesicles. However, it has been reported that a large proportion of cell surface TF, such as that on monocytes, is in an encrypted form which has very little procoagulant activity (Rao et al., 2012). This form of TF can be converted to the procoagulantly active form (decrypted) following activation of the cell expressing the protein (Bach, 2006; Chen & Hogg, 2013). The cellular mechanisms responsible for the encryption and decryption of TF are poorly defined. Suggested mechanisms include exposure of negatively charged phospholipids on the cell membrane in proximity to the TF (Chen & Hogg, 2013; Paborsky et al., 1991) or the sequestering of TF within lipid rafts (Bach, 2006). Similarly, reduction of the Cys186-Cys209 disulphide bond and TF dimerization have been proposed as possible mechanisms for TF encryption (Ahamed et al., 2006).

In addition to its role in coagulation, TF also functions as a signalling receptor and is capable of controlling cellular functions. For example, cleavage of protease-activated receptors (PAR) by TF/fVIIa has been shown to influence cell proliferation, migration and apoptosis (see sections 1.7.2 and 1.8.2) (Schaffner & Ruf, 2008). Additionally, the interaction of TF with integrin adhesion molecules has been shown to induce cell migration and promote angiogenesis (see sections 5.1.2) (Kocaturk & Versteeg, 2013). In addition, the signals arising from TF have been suggested to be initiated and/or regulated by the cytoplasmic domain of the protein (Ruf & Mueller, 1999; Zioncheck et al., 1992). Although the domain does not possess enzymatic activity (Dorfleutner & Ruf, 2003; Zioncheck et al., 1992), it does contain a palmitoylation site (Cys245), two phosphorylation sites

(Ser253 and Ser258) and a ubiquitination site (Lys255) (see section 1.11). Modifications to these sites have been shown to influence TF signalling (see section 1.11.2).

In addition to the full-length TF, a splice variant of TF pre-mRNA, which excludes exon 5, has been shown to lead to translation of a 26 kDa isoform of TF termed alternatively-spliced TF (asTF) (Figure 1.2B). This isoform lacks the usual transmembrane and cytoplasmic domains but instead contains a unique c-terminus (van den Berg et al., 2009) that is poorly homologous to any other known protein sequence (Kocaturk et al., 2013). The unique c-terminus contains a cluster of five positively charged residues that allow asTF to interact with cell membranes, despite lacking a transmembrane domain (Unruh & Horbinski, 2020). The asTF protein retains the ability to bind fVII(a) but lacks large portions of the fX and fXI binding site and therefore has no procoagulant activity. However, despite the lack of procoagulant activity, asTF has been reported to be capable of inducing cellular signalling (see sections 5.1.2) (Kocaturk et al., 2015; Kocaturk et al., 2013; Unruh et al., 2014; van den Berg et al., 2009).

1.4 Protease-activated receptors (PAR)

In addition to the cessation of bleeding, the coagulation system is also capable of influencing other biological processes by activating a family of receptors called PAR. There are currently 4 known proteins within the family named PAR1-4, which are each activated by a range of different proteases (Table 1.2) (Wojtukiewicz et al., 2015). PAR are a sub-class of the G-protein-coupled receptor (GPCR) superfamily and therefore, like all GPCR, consist of an extracellular N-terminal domain, a transmembrane domain consisting of seven helices connected by three extracellular and three intracellular loops and ending in an intracellular C-terminus (Adams et al., 2011; Dery et al., 1998). However, the mechanism of activation of PAR is unique among GPCR. PAR are activated following the proteolytic cleavage of the extracellular N-terminal domain, resulting in the exposure of a sequence of residues that acts as a tethered ligand (Dery et al., 1998; Heuberger & Schuepbach, 2019). This tethered ligand can then fold over and interacts with specific regions within the extracellular and transmembrane domains of the receptor (Figure 1.3). The engagement of these domains results in the induction of conformational changes in the PAR, which are transduced to G proteins bound to the intracellular portion of the protein. These G proteins are a group of heterotrimeric proteins consisting of an α-subunit (Gα) and a βγ-dimer (Gβγ). Activation of the receptor induces GDP to be exchanged for GTP within Gα and disassociation from the G proteins from the PAR. PAR are known to couple to heterogeneous populations of Gα subunits and therefore can induce an array of downstream signalling events (McCoy et al., 2010). The physiological outcomes of activation of any particular PAR depend on the cell type it is expressed in and the

Table 1.2: The list of known proteases that activate PAR

	PAR1	PAR2	PAR3	PAR4
Proteases	Thrombin fXa TF/fVIIa/fXa aPC Plasmin Granzyme A, B, K Gingipains-R Trypsin MMP-1, -2, -3, -8, -9, -12 & -13 Cathepsin G, Kallikrein-1, -4, -5, -6 & -14 Calpain-1 Neutrophil elastase	Trypsin Tryptase fVIIa fXa TF/fVIIa/fXa TF/fVIIa Plasmin Matriptase/MT-SP1 Testisin Gingipains-R Cathepsin G, S Kallikrein -4, -5, -6 & -14 Proteinases-3 Calpain-2 Neutrophil elastase	Thrombin aPC Trypsin fXa	Thrombin Plasmin Cathepsin G Trypsin fXa Gingipains-R Kallikrein -1 & -14 MASP-1

List of proteases which have been reported to cleave the PAR1-4 proteins. Proteases which are members of the coagulation system are denoted in blue (Compiled from Adams et al. (2011); Heuberger & Schuepbach (2019); Wojtukiewicz et al. (2015)).

Figure 1.3: The mechanism of activation of PAR

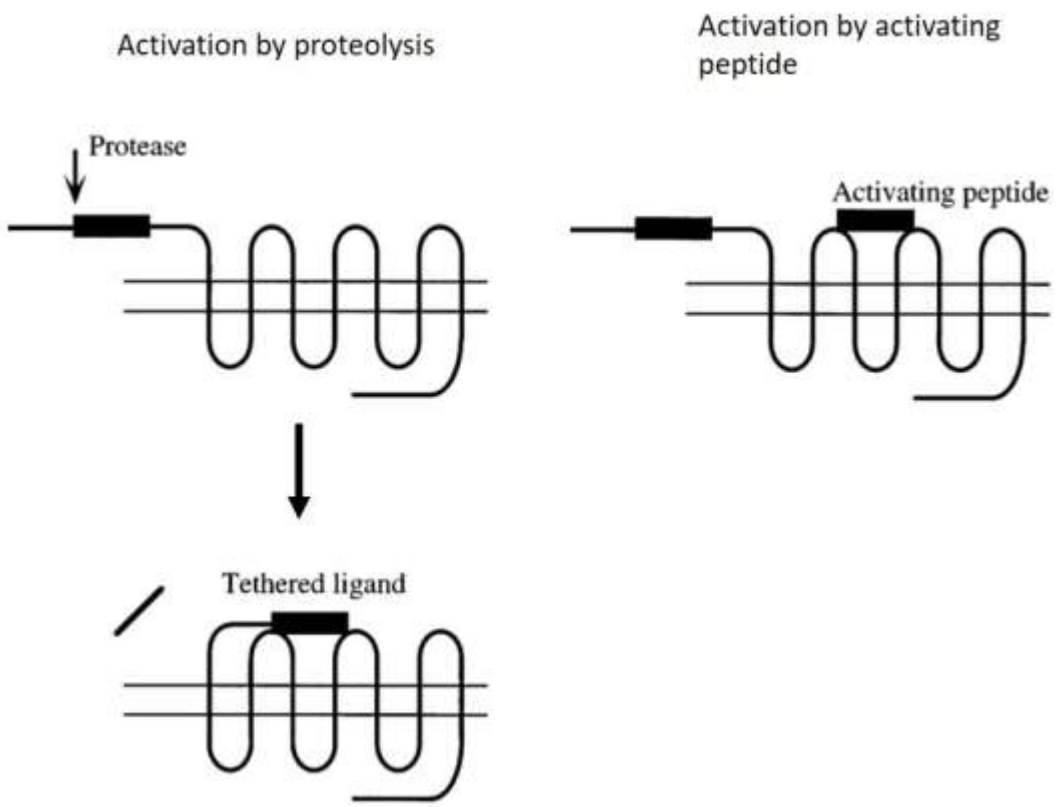

PAR are activated by cleavage of the extracellular domain of the receptor by a protease which results in the exposure of a tethered ligand. Alternatively, an activating peptide with the same amino acid sequence as the tethered ligand can activate the receptor in the absence of proteolysis (Adapted from Dery et al. (1998)).

protease/agonist responsible for activating the receptor. In addition, heterodimerization with other members of the PAR family and interaction of the PAR with co-receptors such as TF or the endothelial cell protein C receptor have been shown to influence the physiological outcomes of activation (Majewski et al., 2020).

1.4.1 PAR2

The member of the PAR family which is of interest to this study is PAR2 since it can be activated by the TF/fVIIa complex. Human PAR2 consists of 397 amino acids and has a molecular weight of 44 kDa (Nystedt et al., 1994). In addition to the TF/fVIIa complex, PAR2 is also activated by a range of proteases, including trypsin, fXa and matrix metalloproteinases (MMP). The enzymes activate PAR2 by cleaving the Arg34-Ser35 bond within the N-terminus of the receptor (Camerer et al., 2000b) producing a tethered ligand with the sequence SLIGKV (Maryanoff et al., 2001; Nystedt et al., 1995) which interacts with regions in the 2nd extracellular loop and 7th transmembrane domain of the protein (Lerner et al., 1996; Yau et al., 2013). The activation of PAR2 can result in a range of cellular responses that vary depending on cell type as well as on the nature of the activating stimulus. For example, activation of PAR2 with a synthetic activating peptide that mimics the tethered ligand (termed PAR2-activating peptide (PAR2-AP)) results in a different pattern of gene expression compared to activation of the PAR by trypsin (Suen et al., 2010). The PAR2 gene is widely expressed in the human body, with especially high levels in epithelial cells (lung, gastrointestinal tract), endothelial cells, smooth muscle cells, fibroblasts, nerves, immune and inflammatory cells (Nystedt et al., 1994; Nystedt et al., 1995). PAR2 signalling pathways are involved in circulatory, cardiovascular, central nervous, gastrointestinal, metabolic and respiratory systems (Table 1.3). However, like TF, PAR2 expression is influenced by environmental stimuli and can be increased in injured tissues or after stimulation by inflammatory mediators. Consequently, the expression and activation of PAR2 is associated with the pathogenesis of a number of diseases as well as normal physiological processes. PAR2 is particularly associated with inflammatory outcomes associated with respiratory, gastrointestinal, cardiovascular and neurological diseases (Yau et al., 2013). In addition, PAR2 has been shown to be upregulated in certain malignancies including colon, lung pancreatic, prostate and stomach adenocarcinoma as well as, acute myeloid leukemia (Arakaki et al., 2018).

1.4.2 PAR2 is activated by fXa and TF/fVIIa

PAR2 is activated by a number of proteases including fXa and the TF/fVIIa complex, as detailed in section 1.4.1. It should be noted that fXa is known to activate PAR1 and PAR2, whereas the TF/fVIIa complex has only been shown to activate PAR2 (Wojtukiewicz et al., 2015). FXa and fVIIa are

Table 1.3: Localization of human PAR

	PAR1	PAR2	PAR3	PAR4
Tissue	Brain Lung Heart Stomach Colon Kidney Testis	Small intestine Colon Pancreas Kidney Liver Airway Prostate Ovary Eye Trachea	Bone marrow Heart Kidney Brain Placenta Liver Pancreas Thymus Small intestine Stomach Lymph nodes Trachea	Liver Small intestine Colon Pancreas Megakaryocytes Lung Placenta Thyroid Prostate Placenta Uterus Testis Adrenal gland Skeletal muscle
Cell type	Platelets Endothelial cells Fibroblasts GI tract epithelial cells Neurons Brain glial cells Vascular smooth muscle cells Mast cells Astrocytes Immune cells (monocytes, T cells, neutrophils, lymphocytes, macrophages) Cancer cells	Neurons Endothelial cells Fibroblasts GI tract and lung epithelial cells Airway and vascular smooth muscle cells Mast cells Keratinocytes, Immune cells (T cells, lymphocytes, neutrophils) Cancer cells	Airway smooth muscle cells Platelets Cancer cells	Platelets Neurons Endothelial cells Immune cells Cancer cells

List of the tissues and cell types which have been reported to express PAR1-4 proteins (Compiled from Dery et al. (1998); O'Brien et al. (2001); (Hollenberg & Compton, 2002)).

coagulation factors with trypsin-like serine protease activity. The active site of both proteins contains the catalytic triad Asp102-His57-Ser195 (chymotrypsin numbering system) (Hedstrom, 2002) which is capable of cleaving and activating PAR2. These blood coagulation factors are produced as precursors in the liver and then secreted into the bloodstream. In physiological conditions it is not known if TF/fVIIa and fXa act alone to activate PAR2 or in the tertiary TF/fVIIa/fXa complex. In *in-vitro* experiments low concentrations of fVIIa (8 pM) have been observed to induce PAR2 signalling by converting fX to fXa, which goes on to cleave PAR2 (Camerer et al., 2000b). However individually, the EC50 values for PAR2 activation by fVIIa and fXa have been determined to be 3.5-7 nM and 7-70 nM, respectively and vary depending on the cell type tested (Camerer et al., 2000b; Camerer et al., 2002; Morris et al., 2006). The activation of PAR2 by low concentrations of fXa (<2.5 nM) is dependent on the presence of fVIIa (Camerer et al., 2000b; Riewald & Ruf, 2001). Therefore, the interaction of the different proteases with PAR2 appears to be concentration dependant. However, since the blood circulation is a dynamic and heterogeneous system it is extremely difficult to determine the concentration of a particular coagulation factor at any specific location. Furthermore, fXa and fVIIa may be released into the tumour microenvironment enabling activation of PAR2 on the cancer cells which is independent of the circulatory system.

1.5 Cell-derived microvesicles (MV)

Cell-derived MV are a type of extracellular vesicle released from the surface of cells (Figure 1.4A) (Thery et al., 2018). MV are spherical phospholipid bilayers which can contain a range of cargo including mRNA, microRNA, DNA including genomic and mitochondrial DNA, proteins, lipids and carbohydrates (Figure 1.4B). There are also other types of extracellular vesicles which are also lipid bilayer spheres, including exosomes and apoptotic bodies, and differ from MV in size, cargo and mechanism of formation (Borges et al., 2013; Raposo & Stoorvogel, 2013). The size of MV were classically estimated to range between 100 and 1000 nm in diameter (Borges et al., 2013) however more recently, more stringent criteria used to differentiate between extracellular vesicles, organelles and cell debris estimate the maximum diameter of MV to be closer to 200 nm (Cocucci et al., 2009). MV are formed by budding directly from the cell surface membrane (see section 1.5.1) and therefore include a complement of cell-surface proteins which are similar to that of the plasma membrane of the cell of origin. Therefore, MV originating from different cells can be molecularly different from each other (Cocucci et al., 2009). However, MV do not simply contain a random set of cellular components but, rather, the cargo is selectively incorporated into the MV during the formation of the vesicles. For example, the quantity of TF on the surface of MV derived from THP-1 cells is greater than that found on the surface of the cell plasma membrane (Del Conde et al., 2005).

Figure 1.4: The structure and content of MV

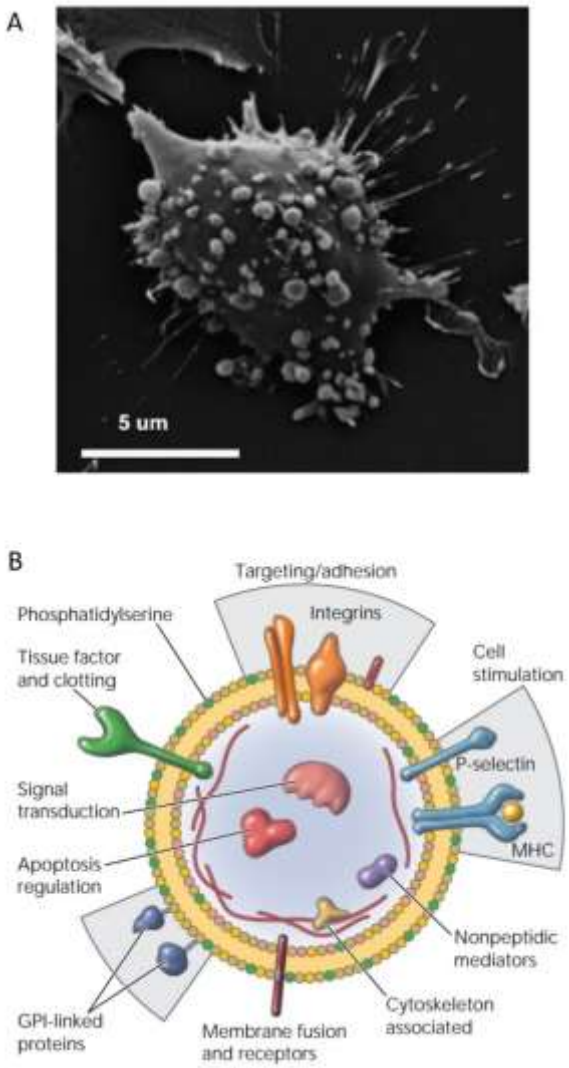

A) A scanning electron microscopy image of MV being shed from the surface of an MDA-MB-231 cell (Originally published in Li et al. (2012)). B) MV are composed of a lipid bilayer which contains cytoplasmic and transmembrane proteins derived from their original donor cell (Originally published in Hugel et al. (2005)).

Consequently, the content of the MV may also be variable and dependent on the type of inducing stimuli.

The involvement of MV in the regulation of blood coagulation has been well documented (Del Conde et al., 2005; Fox et al., 1991). The procoagulant properties of MV arise from the high proportion of PS on the outer membrane which provide a suitable phospholipid surface for the assembly of coagulation factor complexes (Davizon et al., 2010). In addition, MV derived from a number of sources and particularly those derived from monocyte/macrophages and cancer cells can express TF and fVIIa (Biro et al., 2003; Yokota et al., 2009). TF-bearing MV are produced as part of normal physiological processes, however, elevated levels may be detectable during diseases such as cancer, cardiovascular disease, neurodegenerative diseases and diabetes (Tricarico et al., 2017).

In addition to participating in coagulation, MV have recently been shown to be mediators of cell-cell communication (Al-Nedawi et al., 2008). MV-mediated communication occurs by transporting the cargo within MV over both short and long distances to recipient cells throughout the body. This communication is an active process and MV shed from particular cell types are targeted to and interact with specific recipient cells (Losche et al., 2004). On interaction with the recipient cells, MV may induce signals by interacting with cell surface receptors. Alternatively, MV may be taken up by the recipient cell either through endocytosis, or by fusion with the cell membrane (Del Conde et al., 2005). Subsequently, the MV-associated material is either delivered to the cell cytoplasm (Skog et al., 2008) or incorporated into the cell membrane (Al-Nedawi et al., 2009a). An important example of protein transfer by MV is the transfer of TF from monocytes/macrophages and cancer cells onto platelets (Del Conde et al., 2005; Rauch et al., 2000). Platelets are not capable of synthesising the TF protein (Bouchard et al., 2012; Osterud & Olsen, 2013) therefore, the transfer of TF to platelets by MV plays a critical role in coagulation. In addition to contributing to coagulation, a number of other signalling pathways have been reported to be induced following the activation of cellular receptors and/or the delivery of MV-associated material. These signals participate in a range of physiological and disease-related processes (Buzas et al., 2014; Tricarico et al., 2017). For example, the influence of MV-mediated cell-cell communication on cancer development is described further in section 1.7.3.

1.5.1 The formation and release of MV

The process of MV release includes two concurrent and interrelated steps which involve the redistribution of lipids on the plasma membrane, and the reorganisation of the sub-membrane cytoskeleton. MV production can be triggered by a variety of biological processes, including by cellular differentiation events, shear stress on the cell, cell senescence and apoptotic breakdown of the membrane (Al-Nedawi et al., 2009b; Ayers et al., 2015). In addition, stimulation of cells with

cytokines, growth factors, coagulation proteases or adenosine triphosphate (ATP) can induce the release of MV (Al-Nedawi et al., 2009b; Ayers et al., 2015).

In unstimulated/resting cells, the distribution of cell membrane lipids is maintained by three proteins called aminophospholipid translocase, scramblase and floppase (Hugel et al., 2005). Aminophospholipid translocase is highly specific for the transport of aminophospholipids (PS and phosphatidylethanolamine (PE)) from the outside layer of the cell membrane to the inside. Floppase is a non-specific transporter of lipids from inside the cell to the outside and is thought to work in conjunction with aminophospholipid translocase. Scramblase transports all phospholipid types across the cell membrane, in both directions (Piccin et al., 2007). The initial signalling event that leads to MV release is an increase in cytosolic Ca^{2+} ions (Hankins et al., 2015). The increase of Ca^{2+} ions results in the inhibition of aminophospholipid translocase as well as an increase in the activity of scramblase (Piccin et al., 2007). As a result of changes in the activity of these enzymes, the phospholipid asymmetry is disrupted and PS is expressed on the outer leaflet of the membrane. This loss of asymmetry allows the physical curvature of the membrane which favours the formation of MV (van Niel et al., 2018). Furthermore, activation of acid sphingomyelinase converts the membrane phospholipids sphingomyelin, to ceramide (Bianco et al., 2009; Menck et al., 2017; Wang et al., 2017). The production of the cone-shaped lipid ceramides further accentuates the membrane curvature which facilitates MV formation. Concurrent with the lipid redistribution, some molecules are transported to the site of MV release whilst others are excluded, resulting in selective enrichment of cargo molecules within the MV (Clancy et al., 2015). The small GTPases, ADP-ribosylation factor 6 (ARF6) and RAB22A have been identified as regulators of selective loading of cargo proteins (D'Souza-Schorey & Chavrier, 2006; Muralidharan-Chari et al., 2009a; Wang et al., 2014). However, the mechanisms by which nucleic acid cargo are loaded into the MV is not well understood (van Niel et al., 2018).

The second process involved in the release of MV is the rearrangement of the peripheral cytoskeleton. This entails the reorganisation of actin filaments and stimulation of acto-myosin contraction. It is hypothesised that the reorganisation of actin filaments may aid membrane curvature during MV formation by pushing up against the membrane (Figure 1.5B) (Holliday et al., 2019). The polymerization of actin filaments is accelerated during early stages of MV formation, while the latter phases are associated with actin depolymerization (Das et al., 2018b). The regulatory signals which control this sequence of events have not been fully deduced, although a few key steps have been identified (Figure 1.5A). For instance, activation of the AKT and p38 MAP kinase signalling cascades which results in an increase in actin polymerization have been shown to promote MV release (Das et al., 2018a; Das et al., 2018b). In addition, activation of Rho-associated protein kinase

Figure 1.5: Signalling pathways of cytoskeletal rearrangement during MV formation

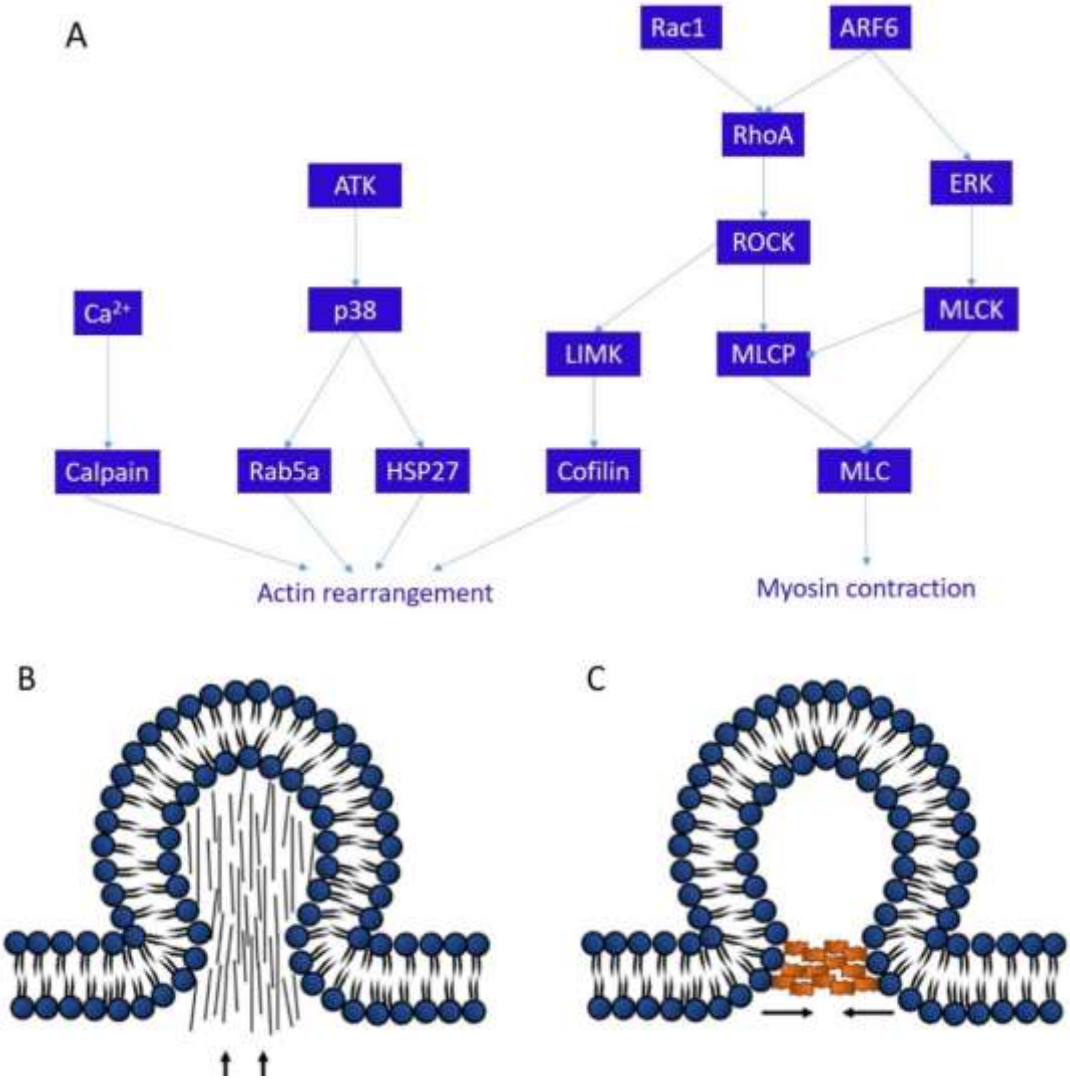

A) Schematic of the signalling pathways associated with the rearrangement of the cell cytoskeleton during MV formation (Compiled from Das et al. (2018a); Das et al. (2018b); Li et al. (2012); Sedgwick et al. (2015)). Proposed mechanisms by which B) actin filaments promote membrane curvature during MV formation and C) myosin contraction facilitates the 'pinching off' of MV from the cell surface membrane (Originally published in Holliday et al. (2019)).

(ROCK) regulates MV release by promoting the phosphorylation of cofilin. Phosphorylated cofilin has a reduced ability to breakdown actin filaments and therefore, prolongs the extension of actin fibres (Li et al., 2012). Finally, increases in cytoplasmic Ca^{2+} ions activate calpain resulting in the cleavage of long actin filaments (Piccin et al., 2007). The signals which initiate acto-myosin contraction during MV formation occur concurrently with those which regulate actin reorganisation. Acto-myosin contraction is initiated by the small GTPases ARF6 and Rac1 (Sedgwick et al., 2015). The GTPases activate the Ras homolog family member A (RhoA) and extracellular signal-regulated kinase (ERK) signalling cascades which lead to the concurrent activation of myosin light chain kinase (MLCK) and deactivation of myosin light chain phosphatase (MLCP) (Das et al., 2018b; Sedgwick et al., 2015)(Figure 1.5A). The activation of MLCK and deactivation of MLCP results in the accumulation of phosphorylated myosin light chain. The presence of phosphorylated myosin light chain leads to increases in the myosin contraction and has been suggested to be involved in the 'pinching off' and release of MV (Figure 1.5C) (Holliday et al., 2019).

1.6 The prevalence and causes of thrombotic complications in cancer patients

The association between cancer and excessive blood coagulation was first identified in the 1800s when Jean-Baptiste Bouillaud and subsequently Armand Trousseau described the relationship (Trousseau, 1867). Thrombotic complications are common in cancer patients and are amongst the leading causes of morbidity and mortality (Ay et al., 2017; Khorana et al., 2007b). The prevalence of thrombotic events has been measured to be ~15% across all cancer types, with rates as high as 50% in palliative care inpatients (Johnson et al., 1999). The severity of the thrombotic events ranges from venous thromboembolism (VTE), including deep vein thrombosis and pulmonary embolism, to more disseminated abnormalities in the clotting system that may not manifest clinical indications (Khorana et al., 2007a; Varki, 2007).

The pathogenesis of cancer-associated thrombosis is complex and includes direct factors such as the release of procoagulant factors from tumours into the blood stream (Ay et al., 2017; Timp et al., 2013) and indirect factors such as vascular injury caused by chemotherapy or surgery (Ay & Unal, 2016). The procoagulant factors which can be released by tumours include haemostatic proteins (TF, fVIIa) (Callander et al., 1992; Koizume et al., 2006), inflammatory cytokines (tumour necrosis factor (TNF)-α, interleukin (IL)-1β) and proangiogenic factors (VEFG, basic fibroblast growth factor (bFGF)) (Falanga et al., 2015; Khalil et al., 2015). The expression and release of TF and/or fVIIa by cancer cells is thought to be the main promoter of cancer associated thrombosis since these proteins are responsible for the initiation of coagulation (Mousa et al., 2006). The induction of TF expression in the cancer cells is mediated through various pathways including oncogenic mutations, epithelial-

mesenchymal transition, tumour hypoxia, inflammatory cytokines and alterations in tumour cell metabolism (Hisada & Mackman, 2019). The oncogenic mutations which have been shown to influence TF expression include the dysregulation of p53, K-ras and PTEN (Rao et al., 2011; Rong et al., 2009; Rong et al., 2006; Yu et al., 2005). Furthermore, the expression of fVIIa in cancer cells was first reported in hypoxic areas of tumours although, more recently, has also been demonstrated under normoxic conditions (Koizume et al., 2012; Yokota et al., 2009). The procoagulant activity of cancer-derived TF and fVIIa can be further exacerbated by packaging of the proteins into MV and release into the blood circulation (Gong et al., 2015; Yokota et al., 2009). MV that present TF and/or fVIIa are able to systemically activate the coagulation system (Ender et al., 2020; Rousseau et al., 2017). In addition to initiating coagulation through TF, cancer cells can also directly alter the haemostatic balance of the blood by activating platelets. The expression of adhesion molecules and receptors, such as the glycoprotein Ib-IX-V complex, αvβ3 integrin and P-selectin, on the surface of cancer cells promotes the binding and activation of platelets (Graf & Ruf, 2018; Jurasz et al., 2004). In addition, cancer cells have been shown to secrete platelet-activating molecules, such as ADP and thromboxane A2 (Schlesinger, 2018).

In addition to directly altering haemostatic mechanisms, cancer cells can increase coagulability through the release of growth factors, cytokines and proangiogenic factors that influence the properties of vascular endothelial cells (Falanga et al., 2017; Khalil et al., 2015; Liu & Mueller, 2006). For example, the expression of IL-6 and TNF-α by cancer cells can stimulate the expression of adhesion molecules, such as P- and E-selectin, on the surface of endothelial cells and the release of vWF into the blood stream (Ay et al., 2017; Graf & Ruf, 2018). The expression of these adhesion molecules facilitates the binding and activation of platelets (Graf & Ruf, 2018; Mousa & Petersen, 2009). Another protein expressed by cancer cells that influences the properties of vascular endothelial cells is heparanase (Masola et al., 2020; Tang et al., 2002). Heparanase is an endoglycosidase which influences vascular endothelial cells by cleaving the anticoagulant heparan sulphate proteoglycan (HSPG) molecules that coat the luminal side of the cells (Vlodavsky et al., 2007). In addition, heparanase has been shown to stimulate the up-regulation of TF expression in cancer and endothelial cells (Nadir et al., 2006).

Finally, the presence of a tumour can also indirectly alter blood coagulability. For example, the restriction of blood vessels or vascular injury caused by invading tumours can result in the activation of the coagulation system. These risk factors are further exacerbated by cancer treatments such as chemotherapies and surgeries, and contribute to the risk of thrombosis in cancer patients (Ay & Unal, 2016).

1.7 The role of the coagulation system in cancer development and progression

In addition to tumours causing a hypercoagulable state in patients, the patient's activated coagulation system can feedback to alter the behaviour of the tumour cells (Hjortoe et al., 2004; Langer & Bokemeyer, 2012; Morris et al., 2006). The components of the haemostatic system have been shown to facilitate cancer growth, invasion and metastasis (Figure 1.6). Significant to the current study, the expression of TF in cancer cells has been demonstrated to enhance proliferation, invasion and migration through mechanisms which are both dependent and independent of its role in coagulation (see sections 1.7.1) (Hempel et al., 2016; Unruh & Horbinski, 2020). Additionally, the activation of coagulation on the surface of metastasising cancer cells results in the deposition of fibrin and adhesion of platelets which encapsulate the cells (Bobek & Kovarik, 2004). This encapsulation can protect the cells from recognition by the immune system (Nieswandt et al., 1999) as well as facilitating the embedding of cells into metastatic sites (Bereczky et al., 2005; Jones et al., 1971; Mueller et al., 1992).

1.7.1 The role of TF in cancer development and progression

The expression of high levels of TF within a tumour is associated with poor prognosis (Kakkar et al., 1995; Seto et al., 2000). This association with poor prognosis partly arises due to the contribution of TF to the development of cancer associated thrombosis. However, the expression of TF in cancer cells is also capable of initiating signals which promote cell proliferation, migration and invasion (Kakkar et al., 1995; Shigemori et al., 1998; Ueno et al., 2000). For example, treatment of human umbilical vein endothelial cells (HUVEC) or H9c2 cells with TF resulted in an increase in the rate of cell proliferation (Alkistis Frentzou et al., 2010; Pradier & Ettelaie, 2008). Additionally, cells transfected to express TF produce larger xenograft tumours than wild type cells whereas, xenograft tumours devoid of TF are smaller in size (Zhang et al., 1994). Furthermore, the rate of growth of xenografts was reduced following the inhibition of the activity of the TF/fVIIa or TF/fVIIa/fXa complexes using a variety of inhibitors (Carneiro-Lobo et al., 2009; de Oliveira et al., 2012; Hembrough et al., 2003; Zhao et al., 2009). In addition to enhancing cancer cell proliferation, TF also appears to increase the rate of cancer cell invasion. In support of this, TF expression levels positively correlate with invasiveness in multiple cancer cell types (Poon et al., 2003; Vrana et al., 1996). Additionally, TF is prominently located at the leading edge of migrating tumour cells (Muller et al., 1999) and TF has also been shown to participate in cell migration (Dorfleutner et al., 2004; Ott et al., 1998; Sato et al., 1996). Finally, the expression of TF by cancer cells also influences the surrounding tumour microenvironment (Han et al., 2014) by altering the rate of angiogenesis (see section 1.8.1) and modulating the immune system (Han et al., 2014). Given these numerous roles of TF in cancer

Figure 1.6: The influence of the coagulation system on cancer and angiogenesis

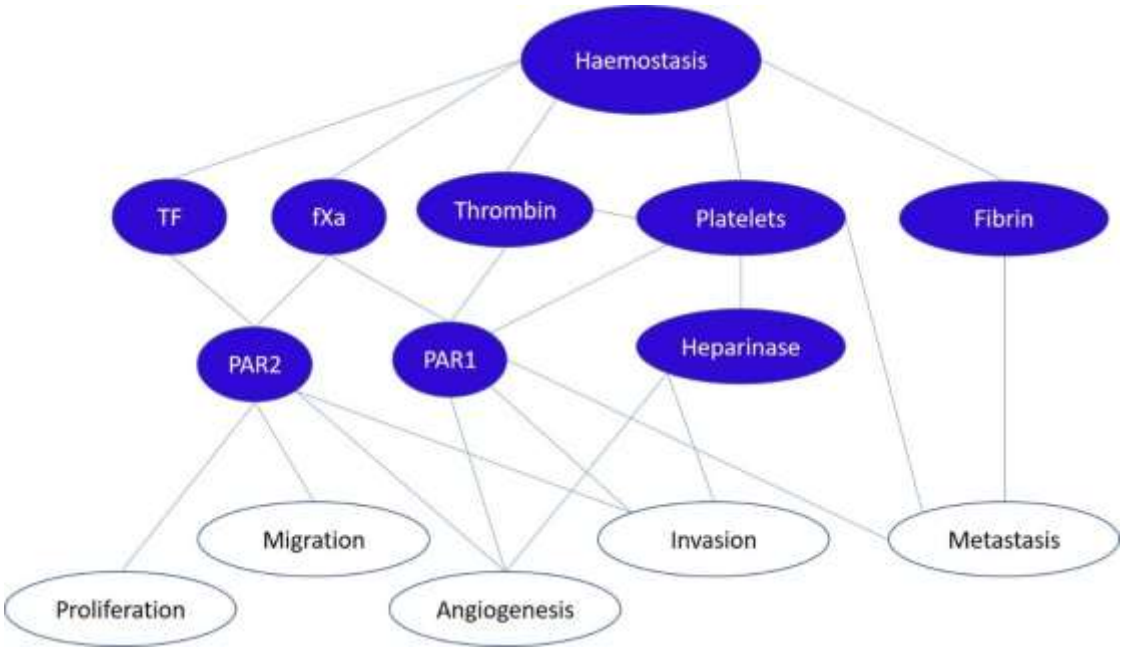

Diagram of which components of the haemostatic system contribute to the various aspects of cancer development and progression.

growth and progression, the protein is a promising target for cancer therapies. Recent stage II clinical trials of an antibody conjugated drug which targets TF called Tisotumab vedotin have shown encouraging antitumour outcomes in patients with a range of cancer types (de Bono et al., 2019; Hong et al., 2020).

TF participates in cancer development using mechanisms which can be both dependent and independent of fVII(a). The mechanisms that are independent of fVII(a) are primarily attributed to direct signalling initiated through TF cytoplasmic domain (see section 1.11.2) (Belting et al., 2005; Unruh & Horbinski, 2020). In addition to the direct TF signalling, fVII(a)-dependant mechanisms involve the activation of PAR by the TF/fVIIa complex or downstream proteases of the coagulation cascade (see section 1.7.2) (Hempel et al., 2016).

1.7.2 The role of PAR signalling in cancer development and progression

As stated above, one of the mechanisms by which the coagulation system supports tumour growth and progression is through the activation of PAR on the surface of cancer cells. PAR are commonly overexpressed in cancer cells (Arakaki et al., 2018; Pawar et al., 2019). In addition, the expression level of PAR2 has been shown to correlate with the TNM stage and size of tumours, as well as with patient overall and disease-free survival (Sun et al., 2018a). PAR on cancer cells can be activated by proteases, including TF/fVIIa, expressed by the cancer cells or other cells in the tumour microenvironment as well as, by circulating coagulation factors, including fXa and thrombin. PAR1 primarily influences cancer cell invasion, whereas PAR2 has a more diverse role and has been reported to promote cancer cell proliferation, invasion, migration and metastasis (Albrektsen et al., 2007; Fan et al., 2005; Hjortoe et al., 2004; Morris et al., 2006; Versteeg et al., 2008a). Activation of PAR1 by thrombin in breast cancer cells has been shown to stimulate invasion (Booden et al., 2004). Conversely, suppression of the activation of PAR1 using the thrombin inhibitor dabigatran resulted in a reduction in cancer cell invasion (Defeo et al., 2010). The activation of PAR2 has also been demonstrated to increase the rate of invasion of cancer cells (Lin et al., 2014; Morris et al., 2006). The increase in invasiveness was shown to be mediated through the up-regulation of the expression of MMP-9 (Lin et al., 2014). Conversely, prevention of the activation of PAR2 using TFPI-2 reduced cancer cell invasion (Rao et al., 2001). The involvement of PAR2 in cancer cell growth has also been demonstrated. For example, activation of PAR2 using a variety of methods has been shown to increase cancer cell proliferation (Carvalho et al., 2018; Hu et al., 2013; Shimamoto et al., 2004; Xie et al., 2012). Conversely, genetic deletion of PAR2 in PyMT cells resulted in a reduction in the rate of growth of tumour xenografts (Schaffner et al., 2010). Similarly, treatment of xenograft tumours with an inhibitory anti-PAR2 antibody attenuated tumour growth and spontaneous metastasis (Versteeg

et al., 2008b). PAR2 has also been shown to participate in the migration of multiple cancer cell types (Ge et al., 2003; Guo et al., 2011; Wu et al., 2013). For example, shRNA-mediated silencing of the expression of PAR2 in breast cancer cells reduced cell migration induced by fXa (Morris et al., 2006). Similarly, treatment of colon or breast cancer cells with a PAR2 antagonist was shown to inhibit cell migration in these cells (Jiang et al., 2018). Finally, genetic deletion of PAR2 in MMTV-PyMT mice used as a model of spontaneous breast cancer development resulted in delays in the development of advanced adenocarcinoma tumours in the animals (Versteeg et al., 2008a). Collectively, these data indicate that PAR2 signalling can initiate multiple processes involved during the progress of cancer.

1.7.3 The role of MV in cancer development and progression

Cells from the majority of cancer types have been shown to release elevated levels of MV compared to their non-malignant counterparts (Martins et al., 2013). These MV can contain TF, fVIIa and PS, and therefore may contribute to the development of cancer associated thrombosis (Falanga, 2005; Yokota et al., 2009). However, while elevated levels of MV are associated with the hypercoagulable state (Campello et al., 2011; Geddings & Mackman, 2013; Thaler et al., 2014) there is no direct correlation between the concentration of circulating MV and incidence of thromboembolism (Hernandez et al., 2013; Thaler et al., 2012; Thaler et al., 2014). Such discrepancies may arise as a result of the cells releasing bursts of MV following activation, temporarily resulting in high levels of MV within the blood stream (Al-Nedawi et al., 2009b; Ayers et al., 2015). However, clearance of MV from the blood stream occurs within a timeframe ranging from 10 minutes to a few hours (Collier et al., 2013; Kawamoto et al., 2012; Rand et al., 2006) and consequently, the levels of MV may have subsided by the time of sampling.

In addition to contributing to the development of the hypercoagulable state in cancer patients, MV can influence cancer progression by transporting oncogenic and proangiogenic cargo between cells (Martins et al., 2013). For example, MV have been reported to transport TF from cancer cells expressing high levels of the protein to those expressing lower levels. The transposed TF may then be taken up and expressed on the surface of the recipient cell (Lima et al., 2013). Alternatively, TF on the surface of MV may be capable of initiating cellular signalling through activating PAR2 on the recipient cell (Ender et al., 2020). Additionally, the exchange of TF between cancer and endothelial cells has been reported to enhance angiogenesis within the tumour microenvironment (Yu et al., 2008). Cancer-derived MV additionally influence angiogenesis by transporting proangiogenic cargo including vascular endothelial growth factor (VEGF) (Feng et al., 2017; Munster et al., 2014), IL-6 and miRNA1246 (Muralidharan-Chari et al., 2010). In support of this exchange, experiments using

epidermoid carcinoma xenografts have shown that the development of capillaries within tumours may be reduced following treatment with the PS blocker, Diannexin. The PS blocker was shown to reduce the rate of angiogenesis and tumour growth specifically through disrupting the binding of cancer-derived MV to endothelial cells (Al-Nedawi et al., 2009a). Another mechanism by which cancer-derived MV can influence cancer progression is by transporting oncogenic factors such as growth factor receptors (EGFRvIII) (Al-Nedawi et al., 2008), drug resistance proteins (P-glycoprotein and multidrug resistance-associated protein 1) (Rackov et al., 2018) and immune system regulating proteins (programmed death-ligand 1 (PD-L1), TNF-related apoptosis-inducing ligand (TRAIL)) (Muralidharan-Chari et al., 2010; Tricarico et al., 2017). Finally, in addition to participating in cell-cell communications, cancer-derived MV may also influence developing tumours by carrying MMP, such as MMP-14 (Clancy et al., 2015; Muralidharan-Chari et al., 2009a). MMP are known to participate in the degradation and remodelling of the extracellular matrix (ECM) which further aids cancer invasion, metastasis and angiogenesis (Nawaz et al., 2018; Rackov et al., 2018).

1.8 The association between coagulation and angiogenesis

Angiogenesis is the process by which new blood vessels form from pre-existing vascular networks. Angiogenesis takes place in several stages (Table 1.4); the first of which is the activation of endothelial cells. Following this activation, regions within the ECM are degraded by MMP. The activated endothelial cells can then begin to proliferate and migrate to fill the cleared space. Finally, the endothelial cells are rearranged to form into new capillaries (Carmeliet & Jain, 2000; Lodish, 2008). Angiogenesis occurs at an accelerated rate during embryo development however, is mostly arrested in healthy adults and only occurs during the female reproductive cycle and during wound healing (Carmeliet, 2005). However, aberrant activation of endothelial cells by stimuli including inflammatory cytokines, hypoxia, hypoglycaemia or genetic mutation can promote angiogenesis (Carmeliet & Jain, 2000). Initiation of angiogenesis under these conditions has been detected in a number of pathological conditions including atherosclerosis and cancer (Richard et al., 2001).

Following injury to the vasculature, the activation of haemostatic processes can induce angiogenesis as part of the wound healing process in order to restore the circulation (Browder et al., 2000; Carmeliet, 2005). Both the cellular and protein components of the haemostatic system can contribute to angiogenesis (Figure 1.6). For example, the deposition of fibrin during coagulation promotes angiogenesis by facilitating endothelial cell adhesion and migration (Dvorak et al., 1995). In addition, fibrin networks provide a surface for the binding of proangiogenic factors, such as VEGF and platelet factor-4 (PF4) (Hadjipanayi et al., 2015). Furthermore, the activation and degranulation of platelets during haemostasis, results in the release of multiple angiogenic factors, including VEGF,

Table 1.4: Stages of angiogenesis

Stages	Description
1	Endothelial cell activation
2	Controlled proteolytic degradation of the extracellular matrix
3	Proliferation endothelial cells
4	Migration of newly synthesised endothelial cells
5	Formation of capillary vessel lumina

HGF, bFGF and PF4 (Wojtukiewicz et al., 2017). The released platelet granules also contain heparanase (Cui et al., 2016) which has been reported to enhance angiogenesis (Edovitsky et al., 2004; Ilan et al., 2006) by cleaving HSPG and releasing HSPG-bound proangiogenic growth factors (Ilan et al., 2006; Sato et al., 2004). In support of this, transgenic mice overexpressing heparanase were found to exhibit increased vascularisation with abnormal over-branching of vessels (Zcharia et al., 2004). Heparanase activity has also been shown to up-regulate the expression of TF and VEGF in endothelial cells (Nadir et al., 2006; Zetser et al., 2006). In addition to the mechanisms mentioned above, members of the coagulation cascade can initiate angiogenesis through protease-dependent and independent mechanisms. These mechanisms include the activation of PAR1 and PAR2 (see section 1.8.2) and the direct signalling arising from the interaction of TF with cell surface proteins (see section 1.8.1). These mechanisms are referred to later in this chapter.

1.8.1 The role of TF in angiogenesis

The involvement of TF in angiogenesis was first demonstrated by deletion of the murine TF gene which resulted in embryonic lethality by around day 10.5 *post coitum,* due to failure in the formation of vasculature in the yolk sac (Carmeliet et al., 1996; Toomey et al., 1996). In addition, endothelial tube formation was promoted following supplementation of HUVEC with exogenous TF and fVIIa (Mousa & Mohamed, 2004b). Conversely, downregulation of TF in endothelial cells and vascular smooth muscle cells reduced the formation of tubules in matrigel (Arderiu et al., 2012). Furthermore, inhibition of the activity of the TF/fVIIa complex using recombinant nematode anticoagulant protein (rNAP) c2 reduced the density of the vessels within colorectal xenograft tumours (Hembrough et al., 2003; Zhao et al., 2009).

One of the mechanisms by which TF influences angiogenesis is by regulating the expression of the proangiogenic growth factor VEGF. Indicative of this, suppression of TF expression in Meth-A sarcoma cells resulted in a decrease in the expression of VEGF, whereas artificial enhancement of the expression of TF resulted in increased VEGF expression (Zhang et al., 1994). In addition, immunohistochemical staining of cancer biopsies indicated a strong positive correlation between TF and VEGF expression (Shoji et al., 1998). TF can regulate VEGF expression by either activating PAR2 (see section 1.8.2) or independently of PAR2, through signalling that is mediated by TF cytoplasmic domain (Abe et al., 1999; Belting et al., 2004).

In addition, TF is capable of influencing angiogenesis through mechanisms that are independent of VEGF expression. In support of this, the promotion of tube formation following the treatment of HUVEC with endogenous TF was not influenced by the presence of an inhibitory anti-VEGF antibody (Pradier & Ettelaie, 2008). In this instance, TF was thought to be regulating angiogenesis by directly

initiating cell signals which enhanced the rate of endothelial cell proliferation (Collier & Ettelaie, 2010; Pradier & Ettelaie, 2008). This influence on proliferation was independent of fVIIa and PAR2, but required the interaction between TF and β1 integrin (Collier & Ettelaie, 2010). Another mechanism by which TF influences angiogenesis is by aiding the recruitment of smooth muscle cells to developing vessels. This was demonstrated by the lack of a smooth muscle cell layer surrounding the blood vessels in embryonic $TF^{-/-}$ mice (Carmeliet et al., 1997). This may be as consequence of the suppression of vascular smooth muscle cell chemoattractant, C-C motif chemokine 2 which was shown to be reduced in endothelial cells, following the knockdown of TF expression (Arderiu et al., 2011).

In addition to full length TF, the splice isoform asTF has also been shown to promote angiogenesis. In support of the role of asTF in angiogenesis, overexpression of the protein in pancreatic cancer cells increased the growth of xenograft tumours as well as the extent of the xenograft vascularisation (Hobbs et al., 2007). Furthermore, supplementation of cultured aortic rings with asTF resulted in an increased sprouting of capillaries (van den Berg et al., 2009). AsTF regulates angiogenesis through interacting with integrins and the association between asTF and αvβ3 integrin was reported to enhanced endothelial cell migration. In addition, promotion of endothelial cell tubule formation by asTF was blocked following treatment with inhibitory anti-α6 and β1 integrin antibodies (van den Berg et al., 2009).

1.8.2 The role of PAR in angiogenesis

As stated above, coagulation proteases can induce angiogenesis through activation of either PAR1 or PAR2. Previous studies showed that around half of $PAR1^{-/-}$ mice and around 10% of $PAR2^{-/-}$ mice died during gestation due to deficiencies in vessel formation (Damiano et al., 1999; Griffin et al., 2001; Saffarzadeh et al., 2020). The involvement of PAR2 in angiogenesis was previously demonstrated by injection of murine skeletal muscles with PAR2-AP which resulted in increased capillary density (Milia et al., 2002). In addition, treatment of primary endothelial cells with PAR2-AP resulted in an increased rate of cell proliferation (Mirza et al., 1996). Conversely, a reduction in the level of vascularisation was observed in xenograft tumours grown in $PAR2^{-/-}$ mice, compared with wild-type animals (Schaffner et al., 2010; Versteeg et al., 2008a). Similarly, inhibition of PAR2 with a blocking anti-PAR2 antibody reduced the density of vessels in xenograft tumours (Versteeg et al., 2008b). The mechanisms by which the activation of PAR2 results in increases in angiogenesis include the up-regulation and release of proangiogenic factors, including VEGF, C-X-C motif ligand 1 and IL-8 (Albrektsen et al., 2007; Liu & Mueller, 2006). Interestingly, within the tumour microenvironment, the TF/fVIIa complex and not fXa has been reported to be responsible for PAR2 mediated regulation

of angiogenesis (Hembrough et al., 2003). In addition, angiogenesis was accelerated in transgenic mice expressing TF in which the cytoplasmic domain was deleted ($TF^{\Delta CT}$) (Belting et al., 2004). However, the enhanced angiogenesis was abolished in animals which were also deficient in PAR2 (Uusitalo-Jarvinen et al., 2007). This indicated that the cytoplasmic domain of TF negatively regulates PAR2-mediated angiogenesis.

In addition to the effects of TF/fVIIa on PAR2, downstream coagulation proteases are also known to be capable of influencing angiogenesis through the activation of PAR1. For example, thrombin activity can induce tubule formation by activating PAR1, in endothelial cells cultured in matrigel (Haralabopoulos et al., 1997). In addition, treatment of primary endothelial cells with either PAR1-AP or thrombin resulted in increases in the rate of cell proliferation (Mirza et al., 1996). Additionally, thrombin activity has been shown to enhance angiogenesis in chick chorioallantoic membrane (CAM) by activating PAR1 (Caunt et al., 2003). Conversely, inhibition of PAR1 using the PAR1-antagonist SCH79797 was shown to reduce the rate of angiogenic-dependent wound healing (Ma et al., 2005). The activation of PAR1 is known to promote angiogenesis by up-regulating a range of proteins including growth factors (VEGF, Angiopoietin-2), growth factor receptors (VEGFR-2) and metalloproteinases (MMP-1 and MMP-2) (Caunt et al., 2006; Caunt et al., 2003; Ollivier et al., 2000; Tsopanoglou & Maragoudakis, 1999).

1.9 The use of anticoagulants in the treatment of cancer patients

As discussed in section 1.6, the association between cancer and coagulation often manifests as venous thrombosis in cancer patients. Additionally, cancer patients who develop thrombosis often exhibit poorer prognoses than those without. Currently, the family of anticoagulants most commonly prescribed to cancer patients with thrombosis include the various preparations of low molecular weight heparin (LMWH) (Ay et al., 2017; Lyman et al., 2007; Mandala et al., 2006). However, the use of anticoagulants in cancer patients, particularly those with complex multi-organ disease, significantly increases the risk for bleeding (Levine et al., 2012). Furthermore, the use of LMWH for extended periods can lead to thrombocytopenia and osteopenia (Krishnamurthy & Freedman, 2005). Therefore, the use of a new class of anticoagulant, known as direct oral anticoagulants (DOAC), may have advantages over LMWH. An obvious advantage of DOAC is that they can be administered orally and have a faster onset of action. Additionally, DOAC do not require laboratory monitoring and cause fewer side effects than LMWH (Ay et al., 2017). In recent years, a number of trials have examined the safety and efficacy of DOAC for the treatment of VTE in cancer patients. The results of these studies have been varied, with some reporting superior reduction in VTE and less bleeding complications following the use of DOAC compared to LMWH (McBane et al.,

2020; Wygant et al., 2019) whereas others indicated that although DOAC were superior to LMWH in the prevention of VTE, their use was associated with higher rates of bleeding (Raskob et al., 2018; Young et al., 2018). Finally, a separate study reported no differences in incidences of both VTE and bleeding complications in patients treated with either agent type (Wysokinski et al., 2019).

1.9.1 Heparin and low molecular weight heparin (LWMH)

Heparin molecules are naturally occurring polymers of glucosamine and iduronic/galacturonic acid disaccharide repeats (Casu, 1985). The polysaccharide chains are heterogeneous in length, varying between 5-40 kDa (mean MW ~13 kDa) (Linhardt & Gunay, 1999). Heparin is located within the granules of mast cells and platelets and pharmaceutical heparin is derived from bovine and porcine mucosal tissues which are rich in mast cells (Linhardt, 2003). The anticoagulant activity of heparins arises from the ability of these molecules to simultaneously bind antithrombin III (ATIII) and either fXa or thrombin. Once bound, heparin accelerates a reaction that covalently links ATIII to the active site of the fXa or thrombin enzyme (Olson et al., 1992) and therefore prevents the enzyme from participating in the coagulation cascade.

Heparin can be chemically fractionated to generate smaller chains known as low molecular weight heparins (LWMH). LMWH are capable of facilitating fXa/ATIII complex formation but are less efficient in binding thrombin and hence supporting thrombin/ATIII complex formation. The administration of LMWH has a number of advantages over unfractionated heparin including greater bioavailability and longer half-life within the blood stream (Norrby, 2006). Most LMWH are depolymerised using chemical methods such as benzylation followed by alkaline hydrolysis or nitrous acid digestion (Table 1.5). Uniquely, tinzaparin is produced by enzymatic digestion with heparinase (Norrby, 2006). The different depolymerisation methods result in LMWH preparations with different average chain-lengths (Dogan et al., 2011; Norrby, 2006). In addition, the termini of the chains differs depending on the method of depolymerisation used (Fareed et al., 1996). As a result of these structural differences, LMWH preparations have dissimilar chemical and pharmaceutical properties including different affinities for fXa, thrombin and ATIII (Fareed et al., 1996; Norrby, 2006). Therefore, regulatory agencies, such as the U.S. Food and Drug Administration and European Medicines Agency regard different LMWH as distinct pharmacological agents that may not be regarded as interchangeable (Norrby, 2006).

In addition to the fXa/ATIII and thrombin/ATIII complexes, both LMWH and unfractionated heparin are capable of interacting with multiple other proteins and biological molecules within the blood stream. Consequently, LMWH preparations have been shown to possess biological activities which are independent of their anticoagulant function, including influencing cancer growth and

Table 1.5: Depolymerisation methods of different LMWH preparations

LMWH	Preparation	Mean MW
Tinzaparin	Heparanase digestion	6.5 kDa
Daltaparin	Nitrous acid digestion	6.0 kDa
Certoparin	Isoamyl nitrate digestion	5.4 kDa
Enoxaparin	Benzylation followed by alkaline depolymerisation	4.5 kDa
Parnaparin	Peroxide cleavage	4.5 kDa
Nadroparin	Nitrous acid digestion	4.3 kDa
Reviparin	Nitrous acid digestion	3.9 kDa
Bemiparin	Benzylation followed by alkaline depolymerisation	3.6 kDa

List of different LMWH preparations with the methods of fractionation and mean MW of the produced fragments (Compiled from Dogan et al. (2011); Norrby (2006)).

development (see section 3.1.1) (Mousa & Petersen, 2009). Indicative of this, treatment of cancer patients with LMWH has been reported to reduce patient mortality (Kakkar et al., 2004; Klerk et al., 2005). Moreover, meta-analyses studies indicate a significant reduction in mortality in cancer patients receiving LMWH versus those receiving unfractionated heparin or warfarin (Lazo-Langner et al., 2007). The LMWH preparations were shown to be particularly effective at reducing mortality in patients with less aggressive cancers. However, it should be noted that a different set of studies reported that the usage of LMWH treatment did not confer any improvement in patient mortality (Conti et al., 2003; Sideras et al., 2006).

1.9.2 Direct oral anticoagulants (DOAC)

DOAC also known as novel oral anticoagulants or non-vitamin k oral anticoagulants (NOAC), are small-molecular inhibitors which directly inhibit specific coagulation proteases. Apixaban and rivaroxaban are two common examples of DOAC that inhibit fXa and were developed by Bristol-Meyer-Squibb and Bayer, respectively (Pinto et al., 2007; Roehrig et al., 2005). Despite the dissimilar structures of these compounds, both function by binding within the active site of fXa (Figure 1.7). The binding of these inhibitors prevents the approximation of the substrates cleaved by fXa to the catalytic amino acids within the active site of the enzyme.

1.10 The signalling of TF in conjunction with β1 integrin

1.10.1 Integrins

Integrins are a family of transmembrane glycoproteins which are receptors for ECM proteins and immunoglobulin (Ig) superfamily molecules. This allows these receptors to act as adhesion molecules and participate in cell-ECM and cell-cell interactions. Integrin complexes are formed from non-covalently associated heterodimers of alpha (α) and beta (β) subunits. In vertebrates there are 18 distinct α and 8 different β subunits (Campbell & Humphries, 2011). These α and β subunits combine into 24 different heterodimers which bind to overlapping but distinct sets of ECM proteins (Humphries et al., 2006). The current study will be focusing mainly on β1 integrin which is the predominantly expressed β subunit in both normal and cancerous cells (Sun et al., 2018b). The β integrin proteins are composed of a large extracellular domain, a single transmembrane domain and a small intercellular cytoplasmic tail (Campbell & Humphries, 2011). The extracellular domain is divided into a 'head' group and a 'leg' group. The 'leg' group consists of 4 cysteine-rich epidermal growth factor (EGF) repeats and a beta tail domain (βTD)(Hynes, 2002). The 'head' group consists of 3 globular domains, the β-inserted (I) domain, the hybrid

Figure 1.7. X-ray crystal structures and chemical structures of apixaban and rivaroxaban

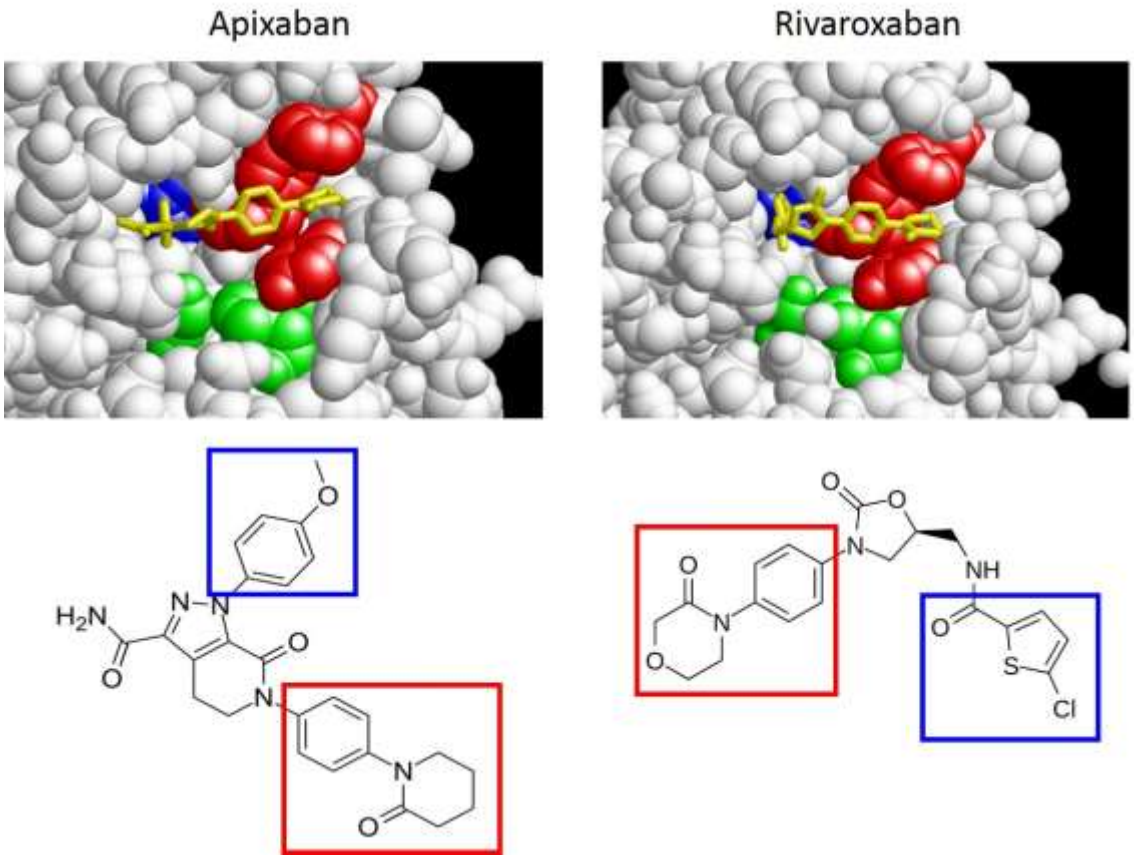

X-ray crystal structures of fXa with either apixaban or rivaroxaban (yellow) bound within the active site. The catalytic triad of fXa (His236-Asp282-Ser379 (Venkateswarlu et al., 2002)) is highlighted in green. Both apixaban and rivaroxaban bind within the S1 (blue) and S4 (red) pockets of the active site of fXa (Pinto et al., 2007; Roehrig et al., 2005). The functional groups within the chemical structures of apixaban and rivaroxaban which interact with these respective pockets are indicated by red and blue boxes.

domain and the plexin-semaphorin-integrin (PSI) domain (Luo et al., 2007) (Figure 1.8A). The 'head' group of the β integrin subunit forms a complex with a 'head' group of an α integrin to construct the ligand binding region. The binding of divalent cations at sites within or near to this ligand binding region regulates the affinity of the receptor for ligands (Humphries, 1996; Valdramidou et al., 2008). More specifically, the binding of Mn^{2+} and Mg^{2+} ions promotes ligand binding whereas, Ca^{2+} ions have an inhibitory effect (Humphries, 1996; Zhang & Chen, 2012). The crystal structures of β2 integrin (4NEH)(Xie et al., 2010) and β3 integrin (4G1E)(Xiong et al., 2001) have been resolved and previously published, however to date no crystal structure of the complete β1 integrin protein is currently available. Integrins are normally expressed on the cell surface with the complex in a folded/closed configuration (Figure 1.8C). In response to either internal or external stimuli, the proteins can rapidly switch to a fully extended, open conformation (Zhu et al., 2008) (Figure 1.8C). The folded/closed configuration and the extended/open configuration are generally considered to reflect the inactive and active states of the receptor, respectively. However, electron microscopy studies indicate that integrin dimers are flexible and capable of adopting a variety of conformations (Su et al., 2016; Zhu et al., 2008). Integrins have both structural and signalling functions within cells (Alberts, 2015; Desgrosellier & Cheresh, 2010). Whilst the extracellular domain of the integrins binds to ECM proteins, the cytoplasmic domain interacts with actin filaments within the cell. Therefore, the receptors form structural connections between the cytoskeleton and the matrix (Brakebusch & Fassler, 2003). Additionally, the binding of integrins to the ECM activates the receptor and induces a conformational change in the proteins from the closed to the open configuration (Luo et al., 2007). The conformational change in the integrins is also transmitted to the intracellular domain of the receptor (Harburger & Calderwood, 2009). Signalling molecules are associated with the intracellular domain of integrins and consequently, the conformational change can initiate signalling cascades within the cell. These signalling cascades regulate responses to damage to the ECM which allow repair and remodelling of the affected area (Campbell & Humphries, 2011; Desgrosellier & Cheresh, 2010).

1.10.2 The role of integrin signalling in cellular proliferation

Integrin signalling has been demonstrated to be essential for cell adhesion, survival, proliferation, differentiation, migration and apoptosis in most cell types (Campbell & Humphries, 2011; Cooper & Giancotti, 2019; Desgrosellier & Cheresh, 2010). The current study aims to focus on the role of β1 integrin in the regulation of cellular proliferation. Integrin signalling regulates progression through the cell cycle and detachment of normal cells from the ECM prevents progression through the G1 phase (Jeanes et al., 2012; Stoker et al., 1968). Additionally, the dysregulation of the control of cell

Figure 1.8: Representation of the structure of an αβ integrin complex

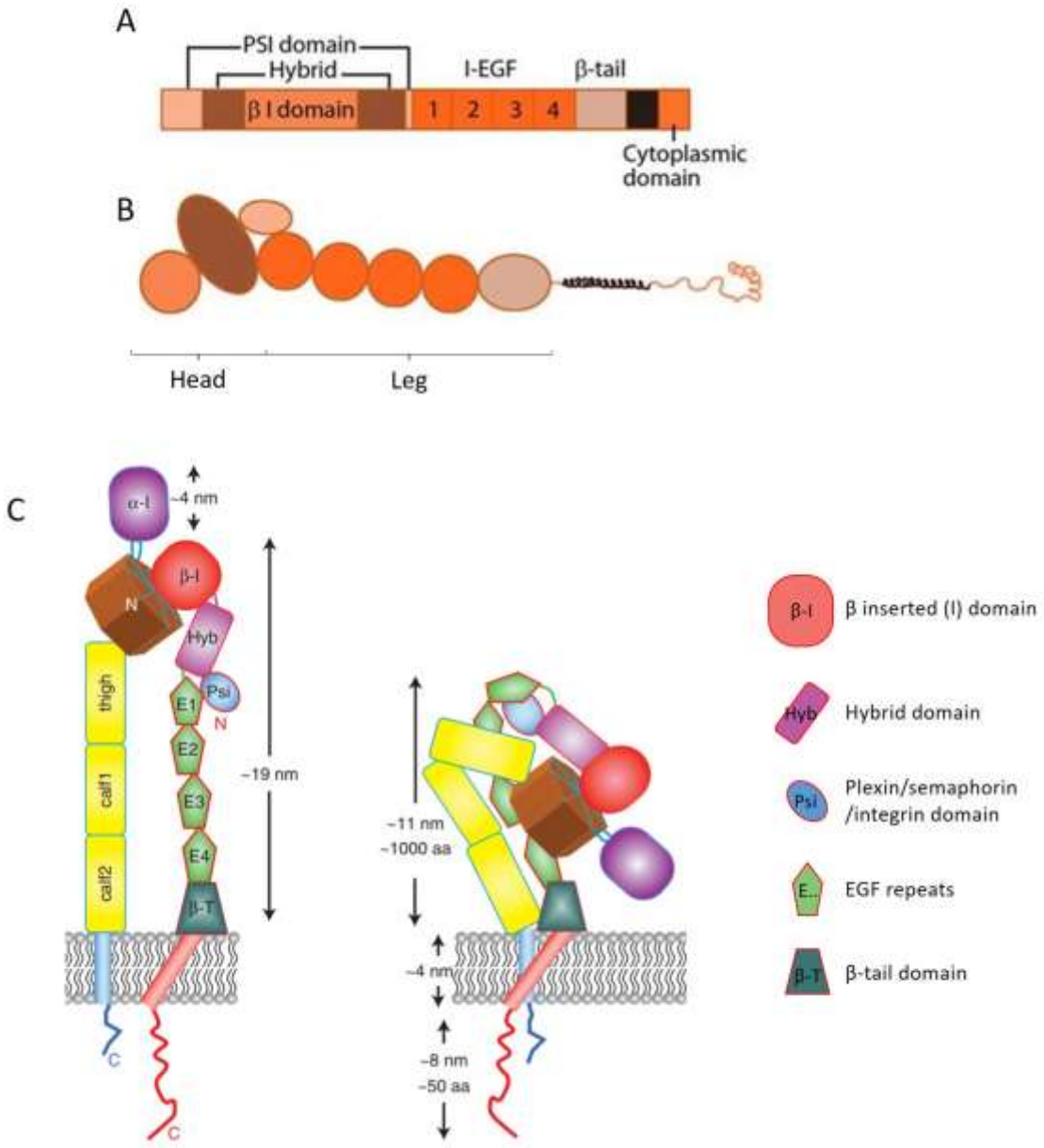

Schematic of the domain structure of β integrins showing A) the linear arrangement of the domains within the primary protein sequence and B) a representation of the tertiary protein structure. C) Schematic of an αβ integrin complex in the open/active or closed/inactive conformations (Adapted from Campbell & Humphries (2011); MBinfo (2018)).

survival and proliferation is known to be a key stage in the development of cancer. One of the mechanisms by which dysregulation of cell proliferation occurs is through changes in integrin expression and signalling which in turn results in increased cell proliferation (Blandin et al., 2015; Desgrosellier & Cheresh, 2010). Consequently, up-regulation of the expression of specific integrins in human cancer has been associated with poor prognosis. For example, the expression of high levels of β1 integrin is associated with reduced overall survival in lung and breast cancer patients (Sun et al., 2018b). In addition, treatment of breast cancer xenografts with an inhibitory anti-β1 integrin antibody (AIIB2) resulted in a reduction in the growth of the xenografts (Park et al., 2006). Furthermore, knockdown of β1 integrin expression in cells significantly reduced the weight and volume of xenograft tumours compared to xenografts formed of wild-type cells (Hou et al., 2016). In addition, the disruption of integrin signalling can have different outcomes depending on the surrounding environment of cells. For example, antibody mediated blockage of β1 integrin reduced the rate of proliferation in cells cultured in laminin-rich ECM (Park et al., 2006). However, the same antibody had no inhibitory influence on the proliferation of cells when grown in reconstituted basal membrane (Howlett et al., 1995). To further complicate the outcome, the cell cycle is concurrently regulated by both soluble growth factors and cell adhesion via integrins in most cell types (see section 5.1.1) (Assoian & Schwartz, 2001).

As mentioned earlier, the interaction of TF with integrins has been shown to influence cellular signalling (Kocaturk & Versteeg, 2013). It has therefore been suggested that TF may act as a physiological regulatory factor for integrin signalling and may be capable of inducing cell proliferation through this mechanism.

1.11 Posttranslational modification of the cytoplasmic domain of TF

In addition to its role in coagulation, TF has been shown to function as a cell signalling receptor (Ruf & Mueller, 1999; Zioncheck et al., 1992). Furthermore, the signals initiated by TF can be regulated by posttranslational modification of the cytoplasmic domain of the TF protein. This domain contains two phosphorylation sites at residues Ser253 and Ser258, which are phosphorylated by protein kinase C (Wu et al., 2013; Zioncheck et al., 1992) and proline-directed kinase p38α MAP kinase (Dorfleutner & Ruf, 2003; Ettelaie et al., 2013b), respectively. The phosphorylation of TF is induced following the activation of PAR2 (Ahamed & Ruf, 2004). The phosphorylation of Ser253 triggers signalling that results in the subsequent phosphorylation of Ser258. Likewise, phosphorylation of Ser258 accelerates or induces the dephosphorylation of Ser253, by potentially either enhancing the activity of phosphatases 1/2A or through structural alterations within the cytoplasmic domain of TF (Collier & Ettelaie, 2011). The cytoplasmic tail of TF also contains a single S-palmitoylation site

located close to the inner membrane surface at Cys245 (Bach et al., 1988). The palmitic acid chains which are added to the site have affinity for specific fatty acids (including sphingolipids and cholesterol) and therefore may targets TF to specific subdomains of the cell membrane which are enriched in those fatty acids (Edidin, 2003; Levental et al., 2010). Palmitoylation of the Cys245 residue also negatively regulates phosphorylation of TF cytoplasmic domain. This regulation was demonstrated by the observation that the level of phosphorylation of TF, following activation of protein kinase C in cells, was higher in a Cys245Ser TF mutant, which could not be palmitoylated, than in wild-type TF (Dorfleutner & Ruf, 2003).

1.11.1 The role of the cytoplasmic domain of TF in the incorporation of TF into MV

The release of TF-bearing MV can be triggered by the activation of PAR2 (Collier & Ettelaie, 2011; Fox et al., 1991). The first stage in the incorporation of TF into MV following the activation of PAR2 is the phosphorylation of TF at Ser253 (Ahamed & Ruf, 2004; Collier & Ettelaie, 2011). Phosphorylation of Ser253 promotes the interaction between TF and the cytoskeletal protein filamin-A, which results in the packaging of TF into MV and subsequent release from the cell (Collier et al., 2014; Ott et al., 1998). Additionally, phosphorylation of Ser253 induces the phosphorylation of TF at Ser258 (Dorfleutner & Ruf, 2003; Ettelaie et al., 2013b). TF which is phosphorylated at Ser258 binds less efficiently to filamin-A and therefore, the incorporation of TF into MV is reduced. It has been proposed that sequential phosphorylation of TF permits rapid bursts of release of TF-bearing MV. However, the termination of the incorporation of TF into MV does not alter the ability of cells to release MV (Collier & Ettelaie, 2011; Collier et al., 2014), indicating that the incorporation of TF into MV occurs via different mechanisms to that of the formation of the MV themselves.

1.11.2 The role of the cytoplasmic domain of TF in the regulation of cell signalling

As previously described in sections 1.7.1 and 1.8.1, the cytoplasmic domain of TF has been implicated in signalling which enhances cancer development and angiogenesis. In support of this, deletion of the cytoplasmic tail of TF in transgenic $TF^{\Delta CT}$ mice was shown to lead to accelerated angiogenesis (Belting et al., 2004). The mechanism by which the cytoplasmic domain of TF influences angiogenesis appears to be mediated through regulating the signals initiated by the activation of PAR2. Support for this hypothesis is provided by the lack of accelerated angiogenesis in $TF^{\Delta CT}$ mice with concurrent deletion of PAR2 (Belting et al., 2004). Therefore, the cytoplasmic domain of TF appears to negatively regulate signalling arising from PAR2 activation. Furthermore, the negative regulatory function of the cytoplasmic domain appears to be switched off following the phosphorylation of this domain (Figure 1.9). Further support for this observation includes studies

Figure 1.9: The influence of the cytoplasmic domain of TF on PAR2 signalling

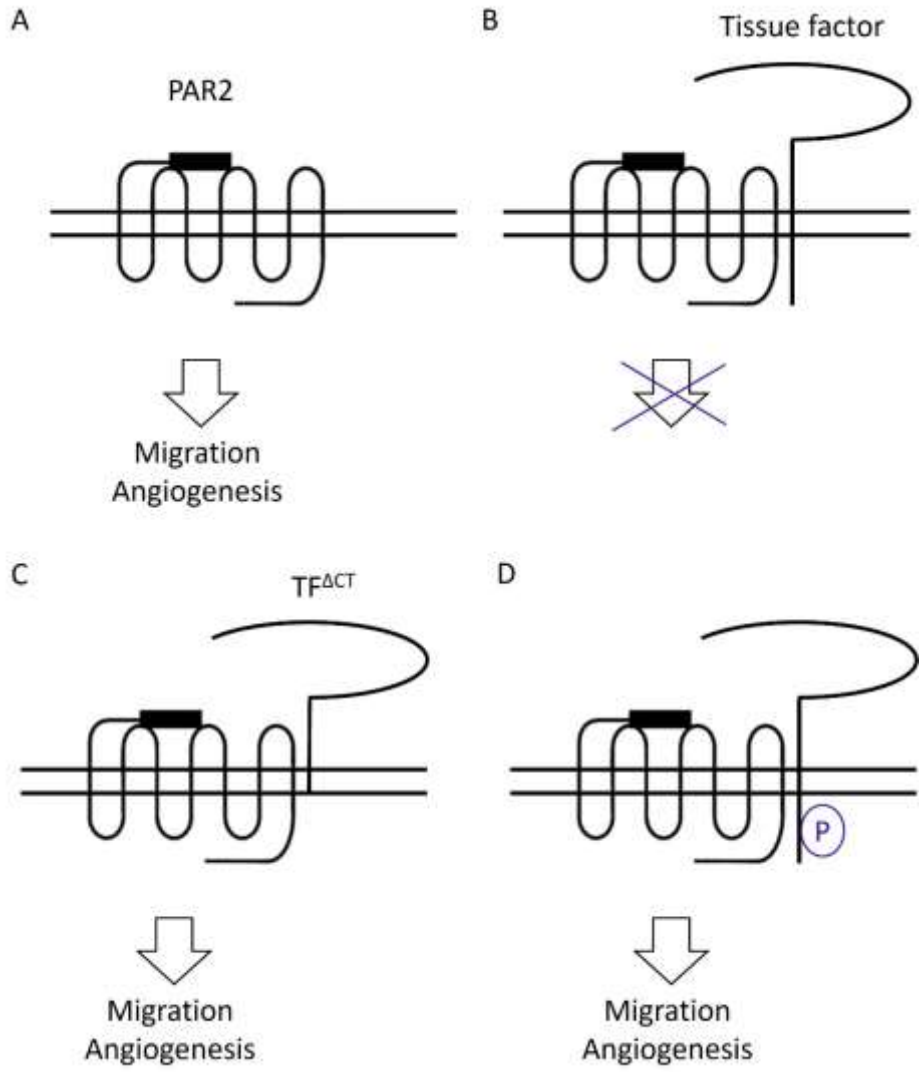

A) Activation of PAR2 results in increased cell migration and the induction of angiogenesis. B) The presence of non-phosphorylated TF negatively regulates the induction of angiogenesis and migration by PAR2. This negative regulation can be eliminated by either C) the deletion of the cytoplasmic tail oof TF or D) phosphorylation of the cytoplasmic tail at Ser253 or Ser258.

using TF mutants with substitutions in the two phosphorylation sites. The expression of phosphorylation-disabled mutants of TF, through Lys255Ala, Pro259Ala and Ser258Ala substitutions, resulted in a reduction in cell migration in A7 melanoma cells (Dorfleutner et al., 2004). Conversely, either expression of Ser253Asp and Ser258Asp substituted TF to mimic phosphorylation or induction of TF phosphorylation through activation of PAR2, resulted in increased cell migration (Dorfleutner et al., 2004). Further i*n vivo* evidence for the role of TF phosphorylation comes from biopsies of invasive breast cancer tissue which exhibit significantly more TF phosphorylation than the non-invasive tumours (Ryden et al., 2010). However, the cytoplasmic domain of TF does not influence all signals which arise from the activation of PAR2. For example, TF-dependent up-regulation of early growth response protein 1 mRNA in response to fVIIa was not influenced by the presence/absence of the TF cytoplasmic domain (Camerer et al., 1999). Similarly, deletion of the cytoplasmic domain of TF did not influence the ability of TF/fVIIa to induce ERK signalling following the activation of PAR2 (Sorensen et al., 1999).

In addition to influencing PAR2-mediated signalling, the cytoplasmic domain of TF is capable of initiating signals independently. For example, treatment of cells transfected to express full-length TF, with either active fVIIa or an active-site-inhibited fVIIa resulted in the activation of p38. However, this signal was absent on expression of $TF^{\Delta CT}$ (Ott et al., 2005). These observations suggest that the induction of p38 activation was independent of proteolytic cleavage of PAR2 (Ott et al., 2005). In other studies, deletion of the cytoplasmic domain of TF in transgenic mice delayed the development of spontaneous breast cancer tumours. Additionally, the delay in the development of the tumours was not further influenced by simultaneous deletion of PAR2 in the mice (Schaffner et al., 2010). This further supports the role of the cytoplasmic domain of TF in influencing spontaneous tumour development independently of PAR2.

1.12 Aims

There is a bidirectional association between coagulation and cancer and the ability of tumours to promote thrombosis has been established. Therefore, thrombotic complications are common in cancer patients and are amongst the leading causes of morbidity and mortality. Recently, it was reported that treatment of cancer patients with anticoagulants can result in a significant reduction in mortality that extends beyond the prevention of thrombosis. Therefore, it is hypothesised that anticoagulants may inference bidirectional association between coagulation and cancer. Consequently, this study aimed to investigate the mechanisms by which different anticoagulants interact with cancer cells.

Furthermore, TF is one of the key interlinking factors between coagulation and cancer. TF has been reported to promote cell proliferation by activating PAR2 and through interacting with β1 integrin. Therefore, this study aimed to examine TF-mediated cellular signalling to elucidate the underlying mechanisms by which these may influence cancer cells.

The main objectives of this study are:

- To examine the influence of the LMWH tinzaparin and dalteparin on cancer invasion, angiogenesis and the growth of cancer cell xenografts.
    - Additionally, to compare the outcomes to those of the fXa inhibitors, apixaban and rivaroxaban.
- To determine if apixaban and rivaroxaban were capable of reducing cancer cell proliferation as well as MV release.
    - To elucidate the mechanism by which the inhibition of PAR2 activation by apixaban and rivaroxaban was accomplished.
- To determine domains within TF and β1 integrin which were responsible for the interaction of the proteins.
    - To examine the influence of the individual domains on the proliferative signals resulting from the interaction of TF and β1 integrin.
    - To determine if the presence of fVIIa is a pre-requisite for the interaction of TF and β1 integrin.
- To investigate the influence of phosphorylation and palmitoylation of the cytoplasmic domain of TF on the regulation of cell proliferation and apoptosis.

Chapter 2

Materials and methods

2.1 Materials

Company	Material
Abcam, Cambridge, UK	CytoPainter Phalloidin-iFluor 488 Reagent, Rabbit anti-TF polyclonal antibody, AP-conjugated Mouse anti-rabbit IgG2b-light chain (lambda) antibody, AP-conjugated Rabbit anti-mouse IgG-light chain (kappa) antibody
Addgene, LGC Standards Teddington, UK	FLAG-HA pcDNA3.1 plasmid
Ambion – supplied by ThermoFisher, Paisley, UK	Cells-2-cDNA™ II Kit, Silencer® Select Pre-designed siRNA (fVII), Silencer® Select Negative Control #1 siRNA
Applied Biosystems - supplied by ThermoFisher, Paisley, UK	SYBR™ Select Master Mix
American Type Cell Collection, Manassas, Virginia, USA	MDA-MB-231 breast cancer cell line, MCF-7 breast cancer cell line, AsPC-1 pancreatic cancer cell line, WM-266-4 melanoma cell line
Bayer, Leverkusen, Germany	Rivaroxaban (Xarelto)
BD BioSciences, Wokingham, Berkshire, UK	BD Matrigel™ basement membrane matrix, Rat anti-β1 integrin antibody (9EG7), 10-well chamber slides, Mouse anti-VE-cadherin antibody
BioLegand UK Ltd, London, UK	Mouse anti-αv integrin antibody (NKI-M9)
Bristol-Myers Squibb, New York, USA	Apixaban (Eliquis)
Cell signalling - supplied by New England Biolabs, Hitchin, UK	HRP-conjugated Goat anti-rabbit IgG antibody, HRP-conjugated Rabbit anti-mouse IgG antibody, Rabbit anti-phosphorylated ERK1/2 antibody, Rabbit anti-ERK1/2 antibody, Rabbit anti-HA-tag antibody
Dade Behring, Deerfield, Illinois, USA	Recombinant relipidated human TF (Innovin®)
Diagnostica Stago UK Ltd, Theale, UK	FluCa reagent kit, Thrombin calibrator, PPP-reagent
eBiosciences - supplied by ThermoFisher, Paisley, UK	Mouse anti-TF antibody (HTF-1), Mouse anti-FLAG-tag antibody, Mouse anti-PECAM-1 antibody, Mouse anti-EpCAM antibody, Rabbit anti-vWF antibody

Eurofins, Wolverhampton, UK	PCR & mutagenic primers
Fisher Scientific, Loughborough, UK	FCS, Butanol, Methanol, Tris base, Glycine, SDS, LB broth powder, Mr Frosty Freezing container, Isopropanol
GE Healthcare illustra - supplied by Fisher Scientific, Loughborough, UK	PuReTaq Ready-To-Go™ PCR beads, Nitrocellulose membrane
Henry Stewart & Co. Eggs, Norfolk, UK	Live fertilised white leghorn chicken eggs
GeneTex - supplied by Insight Biotechnology Ltd, Wembley, UK	Rabbit anti-β1 integrin polyclonal antibody
Gibco - supplied by ThermoFisher, Paisley, UK	Opti-MEM I reduced serum medium, Cell dissociation buffer, TrypLE Select enzyme (10x), HEPES
Invitrogen - supplied by ThermoFisher, Paisley, UK	Platinum™ Taq DNA Polymerase, SYBR™ Green I nucleic acid gel stain, T4 DNA ligase
Hyphen BioMed/Quadratech Diagnostics Ltd, Epsom, UK	Zymuphen MP-activity kit, BIOPHEN Normal control plasma, BIOPHEN Factor VII deficient plasma, fXa chromogenic substrate CS-11(32), thrombin chromogenic substrate CS-01(38)
Leo Pharma, Ballerup, Denmark	Tinzaparin (Innohep)
Lipocalyx - supplied by Cambridge bioscience, Cambridge, UK	Viromer® RED transfection reagent
Merck Millipore, Watford Hertfordshire, UK	Rat anti-β1 integrin antibody (AIIB2)
Mirus Bio - supplied by Cambridge bioscience, Cambridge, UK	TransIT-2020 transfection reagent
New England Biolabs, Hitchin, UK	Q5® Site-Directed Mutagenesis Kit, Instant Sticky-end Ligase Master Mix, Monarch Plasmid Mini-prep kit, Monrach PCR & DNA cleanup kit, Quick-Load® Purple 1Kb DNA ladder, Quick-Load® Purple 100 bp DNA ladder, Protein A magnetic beads

NovusBio - supplied by R&D Systems, Abingdon, UK	Rabbit anti-fVII(a) polyclonal antibody
Origene - supplied by Cambridge bioscience, Cambridge, UK	pCMV6-XL5 vector containing ITGB1 gene, pCMV6-AC-GFP vector containing F3 gene plasmids
Pfizer, Tadworth, UK	Gelfoam® gelatin sponge, Dalteparin (Fragmin)
Promega, Southampton, UK	TMB-one solution substrate for HRP, TMB stabilised substrate for HRP, Western blue stabilized substrate for AP, *XbaI* restriction enzyme, *NotI* restriction enzyme, *BamHI* restriction enzyme, *BsrGI* restriction enzyme, Wizard Midi-prep DNA purification kit
PromoCell, Heidelberg, Germany	HDBEC, HCAEC, Endothelial cell growth medium (MV), Endothelial cell growth supplement pack, Serum free freezing media
Qiagen, Manchester, UK	β-Actin primers for RT-PCR
R&D systems, Abingdon, UK	Human Tissue Factor Quantikine ELISA, Northen-light493-conjugated Donkey anti-mouse IgG antibody, Northen-light493-conjugated Donkey anti-rabbit IgG antibody, Northen-light637-conjugated Donkey anti-rabbit IgG antibody, HRP-conjugated Goat anti-rat IgG antibody, Mouse anti-fX(a) antibody, Mouse anti-fVII(a) antibody
Roche, Welwyn Garden City, UK	Bevacizumab (Avastin)
Santa Cruz Biotechnology-supplied by Insight Biotechnology, Wembley, Middlesex, UK	Mouse anti-PAR2 antibody (SAM11), Mouse IgG Isotype control, Rabbit IgG Isotype control, AP-conjugated Mouse anti-rabbit IgG antibody, AP-conjugated Mouse anti-goat IgG antibody, AP-conjugated Goat anti-mouse IgG antibody, Goat anti-GAPDH antibody, Mouse anti-PAR1 antibody (ATAP2)
Sigma-Aldrich, Gillingham Dorset, UK	Crystal violet powder, Glutaraldehyde, Formaldehyde (37%), PAR2-AP, DMSO, Sulfuric acid, Hydrochloric acid, LB agar powder, Tween-20, Triton-X100, RNAse-free ethanol, BSA, Hydrogen peroxide, Duolink® In Situ Detection Reagents Red, In Situ PLA® Probe Anti-Mouse PLUS, In Situ PLA® Probe Anti-Rabbit MINUS, Purified fXa, Purified fVIIa, Ammonium persulfate, Laemmli buffer

	(2x), Carbenicillin, Bradford reagent, Sodium acetate, Sodium azide, TEMED, DAPI, Glycerol
Scientific Laboratory Supplies Limited, Wilford, Nottingham, UK	DMEM media, RPMI-1640 media, PBS buffer (10x), Trypsin/EDTA solution (10x), Penicillin-streptomycin, TBE buffer (5x)
Reckitt Benckiser, Hull, UK	Dettol disinfectant
ThermoFisher, Paisley, UK	Rabbit anti-β1 integrin polyclonal antibody (PA1-37318), Spectra™ Multicolor Broad Range Protein Ladder, Nunclon Sphera 96-well plate
Trevigen - supplied by Bio Techne Ltd, Abingdon, UK	Cultrex® 3D Spheroid Cell Invasion Assay
VWR International Ltd, Lutterworth, UK	Absolute ethanol

2.2 Equipment

Equipment Name	Manufacturer	Model
3UV transilluminator	UVP	LMS-26E
Flow cytometer	Becton Dickinson	FACSCalibur
Fluorescent Microscope	Carl Zeiss Microscopy	AXIO Vert.A1
Light Microscope	Nikon	TMS
pH meter	Seven compact	pH/ion S220
Plate reader	BMG labtech	PolarStar Optima
RT-PCR machine	BIORAD	iCycler Real-Time
Refrigerated microfuge	Sigma	1 - 14 K
Stereomicroscope	Leica/GT Vision	
Thermal cycler	Teche	FTGENE2D
Vacuum pump	KNF Neuberger UK	D-79112 Freiburg
Ultracentrifuge	Beckman	TL-100
Ultracentrifuge rotor	Beckman	TLA-100.2

2.3 Methods

2.3.1 Preparation of reagents

The fXa inhibitors, apixaban and rivaroxaban, were provided in a powdered pure compound form from Bristol-Myers Squibb and Bayer, respectively. The fXa inhibitors were dissolved in dimethyl sulphoxide (DMSO) to 4 mg/ml stock solutions. These were then diluted in sterile phosphate buffered saline (PBS) to concentrations of 200 μg/ml for used in experimental procedures. The experimental concentrations of apixaban were 0.1 and 1 μg/ml and for rivaroxaban were 0.06 and 0.6 μg/ml. These are equivalent to 2.18 μM and 0.22 μM for apixaban and 1.38 μM and 0.14 μM for rivaroxaban. These concentrations were determined beforehand using an fXa activity assay as part of this work and are in line with the pharmacokinetic studies carried out in phase III testing of the drugs (Frost et al., 2013; Mueck et al., 2014). The mean blood concentration of apixaban has been reported to be between 0.05-0.72 μg/ml and between 0.10-0.46 μg/ml for rivaroxaban depending on the treatment intervals and concentrations. The final concentration of the vehicle DMSO in experiments was 0.05% (v/v) or lower which was not toxic to the cells and in line with other experiments using pure compound apixaban and rivaroxaban (Ellinghaus et al., 2016). The LMWH tinzaparin was provided by LeoPharma and bevacizumab was purchased from Roche. Tinzaparin and bevacizumab were diluted to required concentrations for experimental procedures with sterile PBS. The concentrations of Tinzaparin utilised (0.063-5 IU/ml) were designed to extend either side of the average concentrations of LMWH detectable in patients' blood (0.73-1.04 IU/ml) following treatment with LMWH (Deitcher et al., 2006; Katagiri et al., 1999).

2.3.2 Cellular methods

2.3.2.1 Cell culture

All procedures were carried out in a sterile environment in a class II biological safety laminar flow cabinet. Diluted Dettol and industrial methylated spirit (70% v/v) were used for cleaning all surfaces before commencing any work. Only sterile plasticware and pipette tips were used. All cells were incubated in a humidified environment at 37°C, in a 5% CO_2 atmosphere. All media were prewarmed by placing in a 37°C water bath for 15 min before use. The culture media were replaced every 2-3 days to ensure the presence of sufficient nutrients and to prevent the build-up of waste products.

2.3.2.2 Maintenance and subculture of cancer cell lines

Cell lines were cultured in the appropriate medium according to the instruction of the supplier's (outlined in Table 2.1). The media were supplemented with foetal calf serum (FCS; 10% v/v). Cancer cells were propagated as monolayers until approximately 90% confluent. To subculture the cells, the

Table 2.1: Cancer cell line culturing conditions

Cell name	Origin cancer type	Media	Supplements	Subcultivation ratio
MDA-MB-231	Breast cancer	DMEM	2mM Glutamine + 10% FCS	1:2 - 1:4
AsPC-1	Pancreatic cancer	RPMI-1640	2mM Glutamine + 1mM Sodium Pyruvate + 10% FCS	1:3 - 1:8
WM-266-4	Melanoma	RPMI-1640	2mM Glutamine + 1% Non Essential Amino Acids + 1% Sodium Pyruvate + 10% FCS	1:3 - 1:6
MCF-7	Breast cancer	EMEM	2mM Glutamine + 1% Non Essential Amino Acids + 10% FCS	1:3 - 1:6
SK-OV-3	Ovarian cancer	McCoy's 5a	2mM Glutamine + 10% FCS	1:2 - 1:3
LoVo	Colo-rectal cancer	F-12K	2mM Glutamine + 10% FCS	1:3 - 1:10
BxPC-3	Pancreatic cancer	RPMI-1640	2mM Glutamine + 10% FCS	1:3 - 1:6

Media and supplements used in culture of cancer cell lines used for experimental procedures.

medium was removed from the flask and the cells were washed with 5 ml of sterile PBS (pH 7.2) to remove any traces of serum. To detach the cells from the flask 2-3 ml of Trypsin-EDTA solution (0.25% w/v Trypsin, 0.02% w/v EDTA) was pipetted into the flask and incubated at 37°C for 3-4 min. The flasks were tapped to detach the cells from the surface and complete medium was then added (2-3 ml) to neutralise the trypsin. The cells were counted and used in experiments or were subcultured at ratios outlined in Table 2.1.

2.3.2.3 Maintenance and subculture of primary cells

Human dermal blood endothelial cells (HDBEC) and human coronary artery endothelial cells (HCAEC) were obtained from PromoCell. The cells were cultured in endothelial cell growth medium (MV) containing FCS (5% v/v), endothelial cell growth supplement (4 µl/ml), epidermal growth factor (10 ng/ml), heparin (90 µg/ml) and hydrocortisone (0.2 µg/ml). The cells were propagated as monolayers until approximately 80% confluent. To subculture the cells, the medium was removed from the flask and the cells were washed with 5 ml of sterile PBS (pH 7.2). To detach the cells from the flask 2-3 ml of TrypLE was pipetted into the flask and incubated at 37°C for 3-4 min. TrypLE contains a highly specific recombinant cell-dissociation enzyme instead of trypsin, and therefore is not detrimental to sensitive cells such as primary endothelial cells. The flasks were tapped to detach the cells from the surface and complete medium was added (2-3 ml) to neutralise the cell-dissociation enzymes. The cells were either counted and used in experiments or were subcultured at ratios of between 1:2 - 1:4. All primary cells used for experiments were used at passage 5 or lower.

2.3.2.4 Determination of cell numbers using a haemocytometer

To determine the number of cells, the cell suspension (20 µl) was loaded into a haemocytometer and the number of cells in 1 mm² area counted. The number of cells was then calculated as:

$$\text{Total number of cells in flask} = \text{number of cells counted per mm}^2 \times \text{volume cell suspension} \times 10{,}000$$

2.3.2.5 Cryopreservation of cells

The harvested cells were centrifuged at 400 *g* for 5 min and the supernatant was discarded. The cells were resuspended in serum free freezing media (containing 10% v/v DMSO and methylcellulose) at a concentration of 10^6 cells/ml and 500 µl aliquots were added to cryovials labelled with the cell type, cell numbers, passage number and the date of freezing. The vials were then transferred to a freezing chamber (Mr Frosty) that contained 100% isopropanol and placed into a -70°C freezer overnight. The

chamber ensures the cells were cooled at a rate of -1°C/min to maintain the cell viability throughout cryopreservation and recovery. After a minimum 24 h, the cryovials were transferred to liquid nitrogen container for long-term storage. To start a new culture from frozen cells, cryovials containing the cells were thawed in a 37°C water bath for 1-2 min. The cells were immediately transferred to flasks that contained prewarmed complete medium.

2.3.2.6 Transfection of plasmid DNA using the Trans-IT 2020 reagent

Cells were seeded at varying densities and in varying dish sizes depending on cell type and experiment length (specified in each chapter). The cells were incubated at 37°C overnight to allow cells to adhere. The medium was then removed from each well and replaced with fresh medium. To transfect the cell lines a transfection mixture was prepared to contain the Trans-IT 2020 reagent, plasmid DNA and Opti-MEM I reduced serum media at a ratio of 3 µl : 1 µg : 100 µl. To transfect primary cells a transfection mixture was prepared to contain Trans-IT 2020 reagent, plasmid DNA and Opti-MEM I reduced serum media at a ratio of 1.5 µl : 1 µg : 100 µl. The transfection mixture was incubated at room temperature for 15 min before adding to the cells at a ratio of 100 µl : 1 ml of cell culture media. The transfection mixture was added dropwise to different areas of the wells and the plates were gently shaken. The cells were then incubated at 37°C for 2 days to permit the expression of the proteins, prior to experiments.

2.3.2.7 Transfection of plasmid DNA using the Viromer® RED reagent

Cells were seeded at varying densities and in varying dish sizes depending on cell type and experiment length (specified in each chapter). The cells were incubated at 37°C overnight to allow cells to adhere. The medium was then removed from each well and replaced with fresh medium. The plasmid DNA was diluted (11 ng/ml) in the provided buffer (45 µl). A droplet containing 0.2 µl of Viromer reagent per reaction was placed on the wall of a microfuge tube, followed by 4.8 µl of the provided buffer and the mixture was vortexed for 3-5 s. The plasmid DNA solution was added to the tube containing the Viromer reagent, mixed and incubated for 15 min at room temperature. 50 µl of the transfection complex was added dropwise to different areas of the wells and the plates were gently shaken. The cells were incubated at 37°C for up to 2 days to permit the expression of the proteins, prior to experiments.

2.3.2.8 Transfection of short interfering RNA (siRNA) using the Trans-IT 2020 reagent

In order to reduce the expression of the fVII protein, cells were transfected with synthetic siRNA specific to mRNA of the F7 gene, that is translated into the fVII protein. SiRNA is made of double

stranded RNA that hybridises with the complementary mRNA, targeting it for degradation and so inducing gene silencing. Cells were seeded at varying densities and in varying dish sizes depending on cell type and experiment length (specified in each chapter). The cells were incubated at 37°C overnight to allow cells to adhere. The medium was then removed from each well and replaced with fresh medium. A transfection mixture was prepared by adding Trans-IT 2020 reagent (3 µl) and Silencer® Select fVIIa siRNA (300 pmol) to Opti-MEM I reduced serum media (100 µl) and was mixed by pipetting. The transfection mixture was incubated at room temperature for 15 min and then added to the cells dropwise to different areas of the wells and the plates were gently shaken. The cells were then incubated at 37°C for up to 2 days. The expression levels of the target protein were assessed using the western blot assay (sections 2.3.4.4 and 2.3.4.5).

2.3.2.9 Transfection of siRNA using the Viromer RED reagent

Cells were plated out and incubated at 37°C overnight to allow adherence. The medium was then removed from each well and replaced with fresh medium. The Silencer® Select fVIIa siRNA was diluted (6.6 pmol/µl) in the provided buffer (45 µl). A droplet containing 0.2 µl of Viromer reagent per reaction was placed on the wall of a microfuge tube, followed by 4.8 µl of the provided buffer and the mixture was vortexed for 3-5 s. The siRNA solution was added to the tube containing the Viromer reagent, mixed and incubated for 15 min at room temperature. The final amount of siRNA in each well was 300 pmol. 50 µl of the transfection complex was added dropwise to different areas of the wells, the plates were gently shaken and incubated at 37°C for up to 2 days. The expression levels of the target protein were assessed as above.

2.3.2.10 Determination of cell numbers using the crystal violet assay

Crystal violet solution was obtained at 0.2% (w/v) in ethanol. Working stocks were prepared by diluting in PBS (0.02% w/v crystal violet in the final solution) (Bonnekoh et al., 1989). All cells to be counted were fixed with 3% (v/v) glutaraldehyde for 30 min and washed three times with PBS. Crystal violet solution was added to each well and the plate was incubated at room temperature for 30 min with shaking. The crystal violet solution was then removed from the wells and the plate washed three times with PBS. Care was taken not to dislodge the cells from the wells during washing. 1% (w/v) sodium dodecyl sulphate (SDS) solution was added to each well. Reverse pipetting was used to ensure a consistent volume of the detergent was added to each well. The plates were incubated at room temperature for 10 min with shaking after which, aliquots from each well (100 µl) were transferred to a 96-well plate and the absorption measured at 584 nm using a plate reader. A standard curve of the average absorption at 584 nm for a given number of cells was generated for

each cell line separately. In order to generated standard curves, samples of the cells of interest (specified in each chapter) were counted and plated at a range of concentrations of 5-200 x 10^5 cells/well in 12-well plates. The cells were incubated for 5 h to allow the cell to adhere to the plates. Primary cells were incubated overnight. The media was removed and the cells were washed twice with PBS. The cells were then fixed with 3% (v/v) glutaraldehyde (300 µl) for 30 min before counting using crystal violet, as described above.

2.3.3 Microvesicle methods

2.3.3.1 Isolation of MV by ultracentrifugation

It has been confirmed that FCS contains large amounts of bovine MV (Thery et al., 2006; Thery et al., 2018). Therefore, to obtain cell-derived MV free of contamination, the cells were adapted to serum free media (SFM). Cells were cultured in plates or flasks as described in section 2.3.2.2. The cell culture media was removed, the cells were washed with PBS and the media was replaced with an appropriate amount of SFM. The cells were incubated for 1 h, and the SFM was exchanged for fresh SFM containing the test reagents (specified in chapter). The cells were incubated with the reagents for 30 min at 37°C which was optimised previously, for maximum MV release following PAR2 activation (Ettelaie et al., 2015). The media containing the released MV were collected and centrifuged at 4,800 *g* to remove cell debris. The media were then transferred to clean ultracentrifuge tubes and centrifuged using a TLA 100.2 rotor at 100,000 *g* for 1 h to isolate the MV. The speed and duration of the ultracentrifugation for the collection of MV was also previously optimised (Che et al., 2017; Ettelaie et al., 2014; Schecter et al., 2000). The MV pellet was washed once with PBS (1 ml) before a second centrifugation at 100,000 *g* for 1 h. The MV pellet was then resuspended in 20 mM Tris-HCl pH 7.4 (150 µl) and either used in the stated experiments or stored at -20°C for later use. Small vesicles have been shown to be relatively insensitive to freeze/thaw cycles (Szatanek et al., 2015; Witwer et al., 2013). Therefore, a single freeze-thaw cycle does not alter the properties of the isolated MV. The cell plates/flasks were retained and the number of cells were determined using crystal violet assay as described in 2.3.2.10.

2.3.3.2 Methods for quantification of MV

A number of methods exist which are used to quantify and characterise MV (Hartjes et al., 2019). These are broadly split into physical and functional analysis. The most popular physical analysis approaches in recent literature are transmission electron microscopy to confirm MV structure and nanoparticle tracking analysis (NTA) to quantify the number and size distribution of MV. Flow cytometry is used to identify proteins expressed on the MV and also detect the size distribution of

the particles, however most conventional flow cytometers are only able to detect single MV above ~300 nm in size. More recent improvements have enabled detection and quantification of MV as small as 100 nm (van der Pol et al., 2014). There are also a range of biological/functional assays for MV. These assays included western blot assay of specific proteins to confirm the MV origin and assays which measure either the thrombin or fXa generating potential of either the PS alone or in combination with other procoagulant proteins expressed on the MV (Enjeti et al., 2016). In this study the functional Zymuphen assay (detailed below) was selected for the quantification of MV since the MV procoagulant properties was of paramount interest to this study. Furthermore, the Zymuphen assay results have previously been demonstrated to correlate to, and are comparable to MV quantitation by NTA and high performance flow cytometry (Ayers et al., 2014; Burger et al., 2017).

2.3.3.3 Quantification of MV using the Zymuphen MP-activity kit

2.3.3.3.1 Principles of the Zymuphen MP-activity assay

The density of MV in the isolated samples was detected using Zymuphen MP-activity kit. The assay is carried out by adding a mixture of bovine fXa/fVa, purified human prothrombin and Ca^{2+} ions to the isolated MV. The fXa and fVa bind to the negatively charged PS expressed on the surface of the MV via the Ca^{2+} ions and form a prothrombinase complex (Figure 2.1). This complex activates the prothrombin, producing thrombin. The amount of thrombin generated is then measured by adding a thrombin specific chromogenic substrate.

2.3.3.3.2 Protocol of the Zymuphen MP-activity assay

The Zymuphen kit was removed from 4°C storage and reagent required for the reaction were aliquoted out and warmed to 37°C for 15 min before the experiment was performed. A control MV solution was provided with the kit which contained 2.6 nM MV. A standard curve with serial dilutions ranging 0.2-1.6 nM was generated and added to the 96-well plate alongside the MV samples. The isolated MV (10 µl) were added to a flat-bottom 96-well plate along with the fXa/fVa mixture (40 µl, R1 reagent) and prothrombin (20 µl, R2 reagent). The plate was incubated at 37°C for 10 min and the thrombin substrate (50 µl, R3 reagent) was added and the plate was incubated for a further 10 min at 37°C. The reaction was terminated with 3% (v/v) citric acid (50 µl) and the absorptions measured at 410 nm using a plate reader. The generated standard curve was used to calculate the density of MV in each sample in nM. The reading was normalised to the number of cells present in the well or flask from which the MV were collected as determined by crystal violet assay (section 2.3.2.10). Therefore, the quantities of the isolated MV were recorded as nM/million cells.

Figure 2.1: Diagram representing the Zymuphen MP-activity kit assay

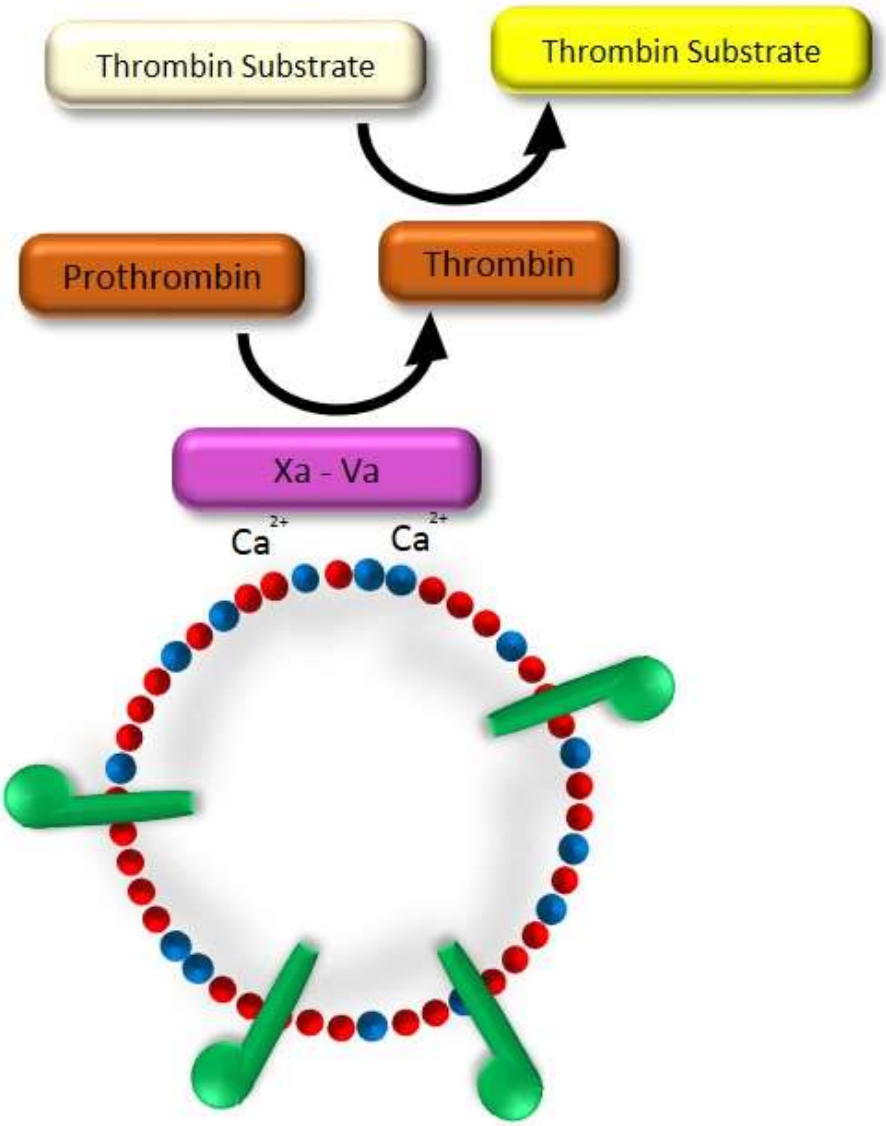

FXa and fVa bind to PS (blue dots) exposed on the MV surface via Ca^{2+} ions to form the prothrombinase complex. The complex activates prothrombin to produce thrombin which digests a synthetic chromogenic thrombin substrate.

2.3.4 Proteomic methods

2.3.4.1 Estimation of protein concentration using the Bradford assay

Bradford assay was used to measure the protein concentration of samples to be used for western blot experiments. A standard curve was generated by preparing a bovine serum albumin (BSA) stock solution (10 mg/ml) which was then diluted to a range of concentrations (5-200 µg/ml). Samples and standards (20 µl) were added to a 96-well plate with 200 µl of Bradford reagent diluted in distilled water (60% v/v). The plate was incubated for 15 min in the dark at room temperature and the absorption measured at 584 nm using a plate reader.

2.3.4.2 Quantification of TF antigen using Quantikine enzyme-linked immunosorbent assay (ELISA) kit

TF antigen was measured using the Quantikine Human TF ELISA kit according to the manufacturer's instructions. The MV samples (150 µl) were diluted with the Calibrator Diluent (150 µl). Recombinant TF provided with the kit was diluted to concentrations of 3.9-500 pg/ml in the calibration diluent and tested alongside the samples to generate a standard curve. MV samples and standards (50 µl) were added to the ELISA plate in triplicate together with the assay diluent (50 µl) and the plate sealed with an adhesive film and incubated for 2 h at room temperature. The wells were washed four times with wash buffer (300 µl) and the provided horseradish peroxidase (HRP)-conjugated anti-TF antibody solution (200 µl) was added to each well. The plate was resealed and incubated for a further 2 h at room temperature. The substrate solution was prepared by mixing equal volumes of the provided substrate solutions A and B. The mixed solution was protected from light at all times. The wells were washed four times with wash buffer and the substrate solution (200 µl) was added to each well. The plate was incubated at room temperature in the dark for 30 min and the reaction was stopped with the provided stop solution (50 µl). The absorption of the samples was measured at 450 nm using a plate reader. The generated standard curve was used to calculate the concentration of TF in each MV sample in pg/ml. The values were then normalised to the number of cells, as determined by crystal violet assay (section 2.3.2.10), in the well or flask from which the MV were collected. The quantities of TF associated with the isolated MV were expressed in pg/ml/million cells.

2.3.4.3 Flow cytometric methods

2.3.4.3.1 Principles of flow cytometry

Flow cytometry is performed by passing individual cells through a 488 nm laser beam. This results in the scattering of the beam which is detected and measured. The amount of scattered light, deflected by the surface of the cell is called forward scatter (FSC) and is proportional to the size of

the cell. The amount of light scattered at 90° to the axis of the laser beam is called side scatter (SSC) and reflects the granularity of the cell. Furthermore, cell surface and cytosolic antigens can be quantified by tagging or labelling with a fluorophore. The laser beam excites the fluorophores to a higher energy state, which results in emission of light at a different wavelength. Different wavelengths of light are selected for using filters and the intensity quantified by different detectors. The FL1 channel detects light at 530 nm, while the FL2 channel measures at 585 nm and the FL3 channel at 670 nm (Biosciences, 2007). During the flow cytometry experiments samples of 10,000 cells are analysed by the flow cytometer. Untreated control cells are examined alongside every experimental sample to determine the amount of background fluorescence (auto-fluorescence) produced by the cells alone. The intensity of the FSC and SSC of each cell is recorded for all samples. The FL detector used depends on the fluorophore present in the experiment (outlined below). A gate is then set to contain approximately 3% of the control cells as measured by the fluorescence intensity at the FL detectors. The percentage of the treated cells that emit within the gate is then calculated.

2.3.4.3.2 Analysis of transfection efficiency using flow cytometry

In order to examine the efficiency of different transfection reagents, cells were transfected as described in sections 2.3.2.6 or 2.3.2.7 with the pCMV-XL5-tGFP mammalian expression vector. This plasmid encodes for the turbo green fluorescent protein (tGFP) (max emission 509 nm). The cells were incubated for 2 days to allow the expression of the protein. The cells were then detached using cell dissociation buffer to prevent loss of cell surface antigens by trypsin cleavage. The cells were centrifuged at 4,800 *g* for 5 min and washed twice with PBS (500 µl). Finally, the cells were resuspended in 500 µl of flow cytometry buffer (PBS, 10% v/v FCS, 1% w/v sodium azide) transferred to polypropylene FACS tubes and analysed by flow cytometry as described above. The intensity at the FL1 detector was measured to determine the expression of tGFP.

2.3.4.4 Separation of protein using sodium dodecyl sulphate-polyacrylamide gel electrophoresis (SDS-PAGE)

Samples were prepared for SDS-PAGE by lysing cells in Laemmli buffer (2% w/v SDS, 10% v/v glycerol, 5% v/v 2-mercaptoethanol, 0.002% w/v bromphenol blue and 62.5 mM Tris-HCl, pH 6.8). The samples were transferred to microfuge tubes and heated for 5 min at 95°C to denature the proteins. A 12% (w/v) separating gel was prepared by mixing 4 ml acrylamide solution (30% w/v acrylamide, 0.8% w/v bisaacrylamide), 2.6 ml resolving buffer (1.5 M Tris-HCl pH 8.8, 0.4% w/v SDS), 3.3 ml de-ionised water and 100 µl ammonium persulphate (10% w/v). The solution was then gently mixed and

5 µl of N,N,N',N'-tetramethylethylenediamine (TEMED) added to initiate polymerisation. The solution was then poured in between the glass electrophoresis plates in a gel caster and covered with a layer of butanol (100%) and allowed to polymerise for 1 h at room temperature. Once the gel was set, the butanol was removed and a 4% (w/v) stacking gel was prepared by mixing 0.65 ml of the acrylamide solution, 1.3 ml stacking buffer (0.5 M Tris-HCl pH 6.8, 0.4% w/v SDS), 3 ml de-ionised water and 100 µl ammonium persulphate (10% w/v). The solution was gently mixed and 5 µl of TEMED was added. The solution was poured on top of the separating gel, a comb was inserted and the gel allowed to polymerise for about 1 h at room temperature. The comb was removed and the gel was transferred to an electrophoresis tank. Samples were loaded into the wells in volumes that contained 20 µg of protein lysate/well as determined used the Bradford assay (section 2.3.4.1). Pre-stained protein molecular weight markers (10 - 260 kDa) were loaded into an adjacent well. The gel was covered with electrophoresis buffer (25 mM Tris-HCl pH 8.3, 192 mM glycine, 0.1% w/v SDS) and electrophoresis carried out at 100 V for between 90 - 120 min.

2.3.4.5 Analysis of separated proteins using western blot assay

Following electrophoresis, the separated proteins were transferred onto a nitrocellulose membrane. The gel was removed from the glass plates and sandwiched between nitrocellulose membrane and blotting paper and placed in a holder. The holder was transferred to a transfer tank containing transfer buffer (10 mM Tris-HCl pH 8.3, 20 mM glycine, 20% v/v methanol). The proteins were transferred at 70 V for 1 h. Non-specific binding was blocked by incubating the membrane in Tris-HCl buffered saline (TBS) (10 mM Tris-HCl pH 8, 150 mM NaCl) containing 0.05% (v/v) Tween-20 (TBST) for a minimum of 1 h at room temperature. The membrane was transferred to TBST solution containing antibody against the protein of interest (specified in each chapters) and incubated overnight at 4°C. One membrane in every experiment was incubated with antibody against the house keeping gene glyceraldehyde-3-phosphate dehydrogenase (GAPDH). This was to ensure equal protein loading in each lane and to confirm the successful transfer of the proteins from the gel to the membrane. On the next day, the membranes were washed three times with TBST and incubated with alkaline phosphatase (AP)-conjugated antibodies against mouse, rabbit or goat (specified in each chapters) diluted in TBST. During western blot analysis of co-immunoprecipitation (co-IP) experiments (section 2.3.4.9) the membranes were incubated with AP-conjugated antibodies against rabbit IgG2b-light chain (lambda) or mouse IgG-light chain (kappa) diluted 1:3000 (v/v) in TBST. The membranes were incubated with the antibodies at room temperature for 1 h. The membranes were washed three times with TBST and once with distilled water and the protein bands were visualised using Western Blue stabilised substrate for alkaline phosphatase. Images of the membranes were

recorded using a digital camera and the bands analysed using ImageJ v1.48 software.

2.3.4.6 Assessment of cell surface expression of specific proteins using the antibody binding assay

To assess the cell surface expression of various proteins, cells (10^4) were plated in 96-well plates and allowed to adhere overnight. The media were removed, the cells were washed once with PBS and fixed with 4% (v/v) formaldehyde for 20 min at room temperature. The cells were washed three times with PBST (PBS containing 0.1% v/v Tween-20). Endogenous peroxidases within the cells were quenched by the addition of 100 µl of quenching buffer (0.1% w/v sodium azide, 1% v/v hydrogen peroxide diluted in PBST) and incubated for 10 min at room temperature. The wells were then washed three times with PBST. To prepare the antibody solutions, antibodies against the proteins of interest (stated in each chapter) were diluted in PBST. The solutions were added to the wells and incubated for 90 min at room temperature. The wells were then washed three times with PBST. HPR-conjugated antibodies against rabbit or rat IgG (specified in each chapter) was diluted 1:100 (v/v) in PBST. The cells were incubated with the antibody (100 µl) for 1 h at room temperature. The cells were washed three more times with PBST. The TMB-one solution HRP substrate (100 µl) was added to each well and incubated for 10 min at room temperature, in the dark. The reactions were stopped with 2 M sulphuric acid (50 µl) and the absorption was measured at 450 nm using a plate reader (Figure 2.2). The values were then normalised to the number of cells in each well, as determined by crystal violet assay (section 2.3.2.10). The amount of bound antibody was semi-quantitatively expressed as the amount of antigen/million cells.

2.3.4.7 Immunofluorescence microscopy

Immunofluorescence microscopy was used to visualise antigens on both cell and tissue sample prepared as specified in each chapter. The samples were fixed for 20 min with 4% (v/v) formaldehyde at room temperature and washed three times with PBST (100 µl) for 1 min. The samples were then blocked with the provided blocking buffer (100 µl) for 1 h at room temperature. Solutions were prepared containing antibodies against the protein of interest (specified in each chapter) diluted in the provided antibody diluent. The samples were incubated with the antibody (100 µl) at 4°C overnight. The samples were washed three times with PBST (100 µl) each for 1 min. Solutions were prepared containing fluorophore-conjugated antibodies against rabbit or mouse IgG (specified in each chapter) diluted in the provided antibody diluent. The diluted fluorophore-conjugated antibodies (100 µl) were added to the samples. Additional control samples were incubated with fluorophore-conjugated antibodies against rabbit or mouse IgG (100 µl) individually alongside. The samples were incubated in the antibody for 1 h at room temperature and then

Figure 2.2: Diagram representing the antibody binding assay

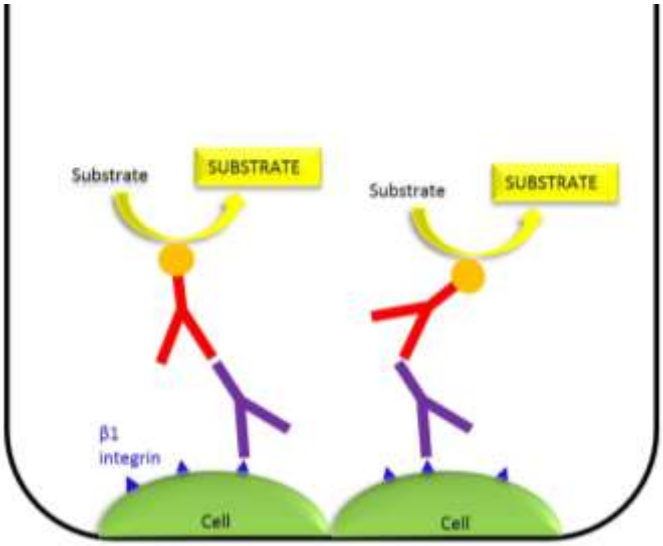

Cell surface antigens are probe with antibodies (purple). These antibodies are then bound by HRP-conjugated antibody (red) against the IgG of the species the first antibody was raised in. A HRP substrate in then added.

washed three times with PBST (100 µl) each for 1 min. The nuclei were stained with 4',6-diamidino-
washed three times with PBST (100 µl) each for 1 min. The nuclei were stained with 4',6-diamidino-
2-phenylindole (DAPI; 0.4 µg/ml diluted in PBS) for 20 min at room temperature. The samples were then washed twice in PBS and visualised using a florescence microscope.

2.3.4.8 Examination of protein proximity using the Proximity ligation assay (PLA)

2.3.4.8.1 Principles of the PLA

The PLA is used to study the proximity of two proteins of interest and is carried out using the Duolink™ PLA kit (Figure 2.3). The principles of the assay are that each of the potentially interacting proteins are labelled with a specific antibody raised in different species (mouse or rabbit). Oligonucleotide-conjugated antibodies, termed 'plus and minus PLA probes' are then added. In this study the antibody conjugated to the plus probes recognised mouse IgG and the antibody conjugated to the minus probes recognised rabbit IgG. If the proteins of interest are within 40 nm of each other the oligonucleotide sequences on the probes hybridise. A ligase enzyme is added which ligates the hybridised oligonucleotides resulting in a closed circular loop of DNA. A polymerase enzyme is then able to amplify the circular DNA template. Finally, fluorophore-conjugated detection oligonucleotides hybridise to a repeating sequence within the amplified DNA product. The signal can then be visualised using fluorescence microscopy as discrete dots at the sites of the protein interactions.

2.3.4.8.2 Protocol of the PLA

Cells were plated out into 29 mm culture dish with a 10 mm glass bottomed micro-well. The cells were incubated at 37°C overnight to allow cells to adhere to the plates and then treated as described in the experiments (specified in each chapter The cells were fixed with 4% (v/v) formaldehyde for 20 min at room temperature, washed three times with PBS each for 1 min and then incubated with the provided blocking buffer for 1 h at 37°C. The two antibodies against each of the potentially interacting proteins were diluted together 1:50 (v/v) in the provided antibody diluent. The dishes were incubated with the antibodies (50 µl) at 4°C overnight. On the next day, the dishes were washed twice with Wash Buffer A (10 mM Tris-HCl pH 7.4, 150 mM NaCl, 0.05% v/v Tween-20) for 5 min. The Plus and Minus PLA probes were diluted together (1:50 v/v each) in the provided antibody diluent. The mixture was added to the dishes and incubated at 37°C for 1 h. The dishes were washed twice with Wash Buffer A, each for 5 min. To prepare the ligase solution, the ligase enzyme was diluted 1:40 (v/v) in the provided Ligase Buffer and added to the dishes and incubated at 37°C for 30 min. The dishes were then washed twice with Wash Buffer A for 2 min. From this point

Figure 2.3: Diagram representing the PLA procedure

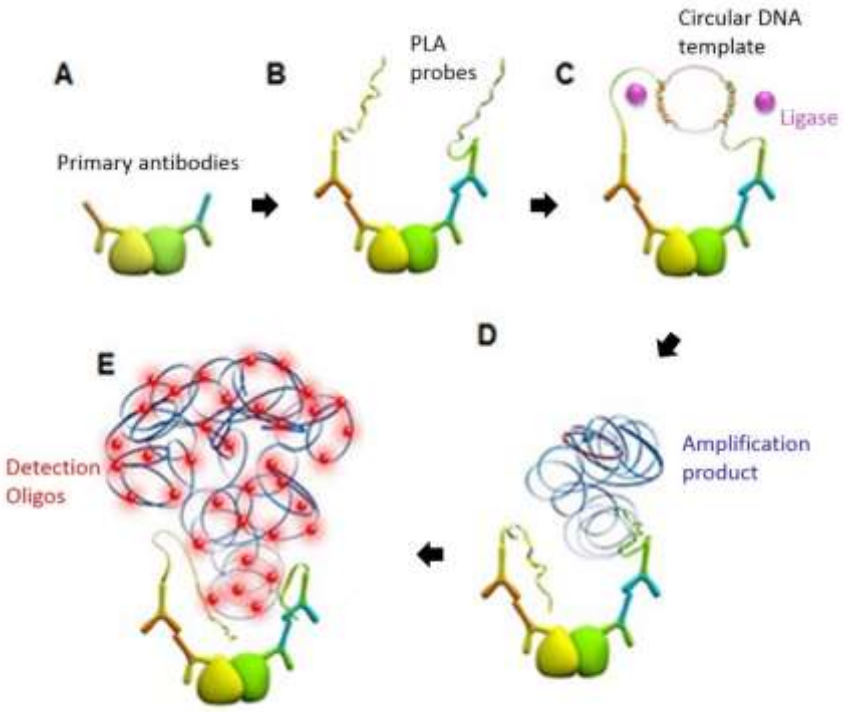

A) Potentially interacting proteins are labelled with specific antibodies raised in different species (e.g orange antibody = mouse and blue antibody = rabbit). B) Oligonucleotide-conjugated antibodies are then added. C) If the potentially interacting proteins are within 40 nm of each other the oligonucleotide sequences will hybridise. Next a ligase enzyme ligates the oligonucleotides resulting in a closed circular loop of DNA. D) A polymerase enzyme amplifies the circular DNA template. E) Finally, fluorophore-conjugated detection oligonucleotides hybridise to a repeating sequence within the amplified DNA product. (Adapted from MERCK (2019)).

onward all samples were kept in the dark during incubation periods. To prepare the polymerase solution, the polymerase enzyme was diluted 1:80 (v/v) in the provided polymerase buffer. The solution was added to the dishes and incubated at 37°C for 100 min. The dishes were washed twice with Buffer B (200 mM Tris-HCl pH 7.5, 100 mM NaCl) for 10 min and once in Buffer B (diluted 1:100 v/v in distilled water) for 1 min. A staining solution was prepared by diluting DAPI (0.4 µg/ml) and Phalloidin-iFluor 488 Reagent (diluted 1:1000 v/v) in Buffer B (diluted 1:100 v/v). The staining solution was added to the dishes and incubated for 10 min at room temperature. The dishes were washed twice with Buffer B (diluted 1:100 v/v) for 2 min and visualised using a florescence microscope. All images were captured with a 40× objective and ten images were acquired for each sample. A 'Particle Analysis' macro used with ImageJ v1.48 software was used to quantify the number of cells (blue incidences) and the number of protein interactions (red incidences) in each field of view. From these data, the number of incidences/cell were calculated.

2.3.4.9 Examination of protein interactions using co-immunoprecipitation (co-IP)

To confirm the interaction of selected proteins, one of the target proteins was immunoprecipitated using a specific antibody and the presence of co-immunoprecipitated proteins were examined by western blot analysis (Figure 2.4). Cells were lysed in phospho-safe buffer (25 mM Tris-phosphate pH 7.8, 2 mM DTT, 2 mM DCTA, 10% w/v glycerol, 1% v/v Triton X-100) for 10 min on ice. The samples were collected into microfuge tubes and centrifuged at 4,800 *g* for 5 min at 4°C to remove any insoluble material. The supernatant was diluted in ice cold PBS and divided between microfuge tubes. An antibody (20 µg/ml) against one of the interacting proteins of interest (specified in each chapter) was added to each sample. The samples were incubated at 4°C overnight on a rotary shaker at 4 rpm. On the next day, recombinant Protein A conjugated magnetic beads were diluted 1:10 (v/v) in PBST and added to each sample (100 µl). The samples were incubated for 3 h at 4°C on a rotary shaker at 10 rpm to allow the Protein A to bind the antibody. The tubes were then placed in a magnetic stand to retain the magnetic beads within the tube and the supernatant was removed. Samples of the supernatant from each sample were retained for later analysis. The magnetic beads were washed three times with PBST with vortexing during each washing step. The beads were collected using the magnetic stand and the proteins dissolved in Laemmli buffer (50 µl). The samples were then heated at 95°C for 10 min to denature all proteins present, releasing the antibodies and any captured proteins from the magnetic beads. The magnetic beads were retained on the magnetic stand and the samples were removed to clean microfuge tubes for analysis by western blot assay (sections 2.3.4.4 and 2.3.4.5). An aliquot of the retained supernatant was mixed 1:1 (v/v) with 2x Laemmli buffer and heated at 95°C for 10 min and examined alongside.

Figure 2.4: Diagram representing the co-IP procedure

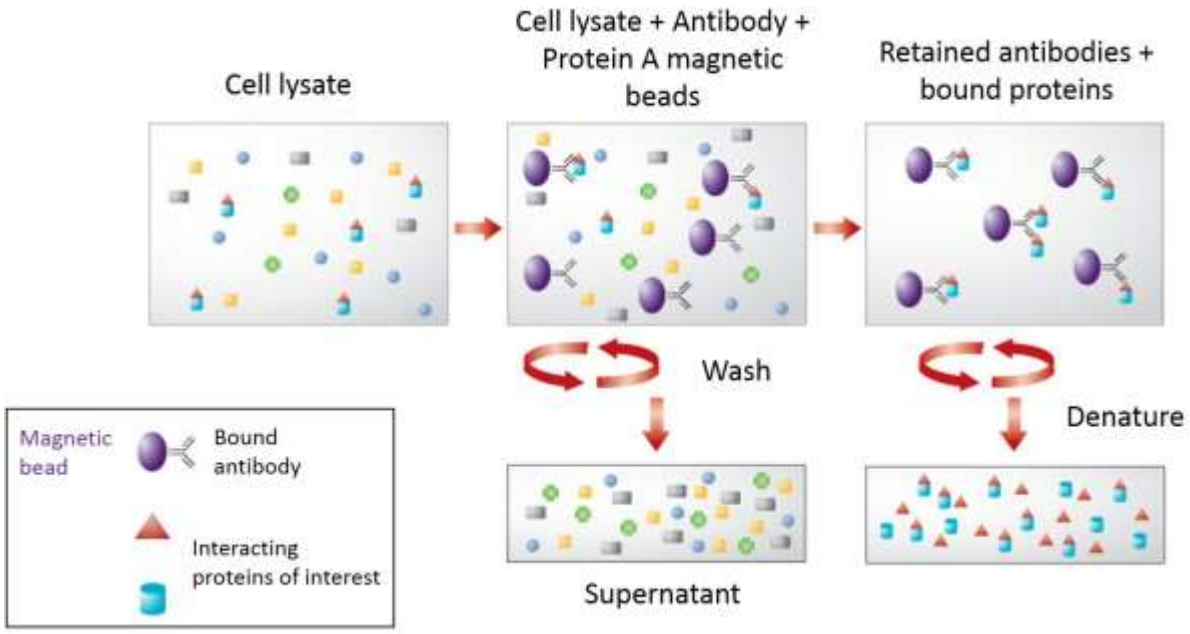

First, proteins of interest (red triangles) within cell lysate are bound by a specific antibody. Next, the bound antibodies are captured using antibody-binding proteins (such as Protein A or G) which are immobilised onto a magnetic beads. The magnetic beads are then retained using a magnet whilst the sample is washed. The primary proteins of interest (red triangles) as well as any other macromolecules that are bound to those proteins (blue squares) are retained along with the beads, whilst all other proteins are washed away. Finally, the retained proteins are denatured and eluted from the magnetic beads. The eluted samples are analysed by SDS-PAGE followed by western blot to verify the identity of the collected proteins (Adapted from ThermoFisherScientific (2020)).

2.3.5 Microbiology methods

2.3.5.1 Bacterial cell culture

LB media was prepared by dissolving LB broth powder (10 g) in 400 ml of distilled water and autoclaving it at 121°C, 15 pounds/square inch for 1 h. In order to expand cultures of 5-alpha competent *Escherichia coli* (*E. coli)* transformed with specified plasmids (specified in each chapter), the bacteria were incubated in 100 ml of LB media at 37°C, overnight.

2.3.5.2 Cryopreservation of bacterial cells

Bacterial freezing media was prepared by adding glycerol (20% w/v) to LB media. The freezing solution was mixed by vortexing and was sterilised by filtration through a 0.22-µm filter. In order to prepare stock of *E. coli* for storage*,* bacterial cultures were pelleted by centrifugation 15 min at 2500 *g.* The cells were resuspended in of freezing medium (1-2 ml), divided into 500 µl aliquots and transferred to 1.5 ml microfuge tubes. The samples were stored at -20°C for short term storage (1-2 months) or -80°C for long term storage.

2.3.5.3 Preparation of LB media plates

To prepare plates of agar media containing carbenicillin antibiotic, the LB agar powder (3.5 g) was dissolved in distilled water (100 ml) and autoclaved at 121°C, 15 psi for 1 h. The agar media was cooled to 50°C and the carbenicillin solution (100 µg/ml) was added and mixed. Aliquots of the LB agar (20 ml) were poured into 75 mm Petri dishes and allowed to solidify at room temperature in a sterile environment. The dishes were sealed and stored at 4°C until required.

2.3.5.4 Transformation of plasmid DNA into bacterial cells

In order to transform bacteria with plasmid DNA, competent 5-alpha *E. coli* cells were thawed on ice. Plasmid DNA (20-50 ng) was pipetted into the cells and incubated on ice for 30 min. The cells were then heat shocked at 42°C for 30 s in a thermal cycler and returned to ice for 5 min. SOC medium (150 µl) was added to each sample and incubated at 37°C for 1 h, to allow the expression of the antibiotic resistance gene by the transformed bacteria. An aliquot of each sample (20-50 µl) was spread over the selection plates containing carbenicillin (100 µg/ml) and incubated at 37°C, overnight. Single colonies were pick from the plates using a sterile pipette tip, placed in LB media (10 ml) and incubated at 37°C with shaking (130 rpm) overnight.

2.3.5.5 Isolation of plasmid DNA from bacterial cultures using the Midi-prep kit

Plasmid DNA was isolated from 100-150 ml cultures of bacteria using Wizard plus Midi-prep DNA Purification kit. The overnight bacterial culture was cooled to 4°C and centrifuged for 15 min at 2500 *g* to pellet the bacteria. The pellet was resuspended in the provided resuspension buffer (3 ml) and transferred to a 20 ml tube. The cells were then lysed by adding the provided lysis buffer (3 ml) and the tube was gently inverted to mix the solution without damaging any genomic DNA. The solution was the neutralised by adding the provided neutralisation buffer (4 ml) simultaneously precipitating the genomic DNA. The sample was centrifuged at 3000 *g* for 15 min to pellet the genomic DNA. The supernatant was transferred to a 15 ml tube and centrifuged again at 3000 *g* for 15 min to remove any remaining trace of cell debris or genomic DNA. The supernatant was transferred to a Midi-prep column along with provided purification resin (10 ml) to capture the plasmid DNA. The mixture was cleared through the column under vacuum. The column was washed with wash buffer (15 ml) and cleared through the column under vacuum. The neck of the Midi-prep column was removed and the filter section (containing the resin) was transferred to a 1.5 ml microfuge tube. The tube was centrifuged at 12,000 *g* for 3 min to clear residual wash buffer from the resin. The resin was transferred to a clean 1.5 ml tube and 300 µl of pre-warmed (50°C) DNase-free water was added to the column neck and incubated for 1 min at room temperature. The tube was then centrifuged for 2 min at 12,000 *g* to elute the plasmid DNA.

2.3.5.6 Isolation of plasmid DNA from bacterial cultures using the Mini-Prep kit

Plasmid DNA was isolated from small volume (4-10 ml) bacterial cultures using the Monarch Plasmid Mini-prep Kit. The overnight bacterial culture was centrifuged at 12,000 *g* for 1 min to pellet the bacteria. The pellet was resuspended in Resuspension Buffer (200 µl) and the bacteria lysed by adding Lysis Buffer (200 µl). The solution was then neutralised by adding the provided Neutralisation Buffer (400 µl) which also precipitated the genomic DNA. The sample was centrifuged at 12,000 *g* for 3 min to pellet the genomic DNA and the supernatant was transferred to a provided spin column. The column was centrifuged at 12,000 *g* for 1 min and the flow-through discarded. The column was washed with Plasmid Wash Buffer 1 (200 µl) and then with Plasmid Wash Buffer 2 (400 µl) and centrifuged each time at 12,000 *g* for 1 min. The column was transferred to a clean 1.5 ml microfuge tube and the DNA eluted using the provided DNA Elution Buffer (30 µl, 50°C) and incubated for 1 min. The column was centrifuged for 1 min to elute the plasmid DNA.

2.3.5.7 Purification of DNA using ethanol precipitation

In order to remove any traces of salts and endotoxins from the isolated plasmid DNA, the plasmid DNA was precipitated with ethanol. Sodium acetate (5 M; pH 5.2) (150 µl) and absolute ethanol (600 µl) were mixed with the DNA solution (150 µl) and the sample was incubated at -20°C for 30 min. The sample was then centrifuged at 16,600 *g* for 20 min at 2°C to pellet the precipitated DNA. The pellet was washed with 300 µl of ice-cold ethanol solution (75% v/v) and the sample centrifuged at 16,600 *g* for a further 10 min at 2°C. The supernatant was removed and the pellet was dried in a sterile environment for 10 min to remove any remaining ethanol. Finally, the pellet was resuspended in DNAse-free water (150 µl) and the concentration of the plasmid DNA was determined using a spectrometer (section 2.3.5.8). The DNA was either used in the stated experiments or stored at -20°C for later use.

2.3.5.8 Quantification of the concentration and purity of isolated DNA

To determine the concentration of the eluted plasmid DNA, the absorption of a 1:10 dilution (v/v) of the DNA sample was measured at 260 nm using a spectrometer.

The DNA concentration (µg/ml) was calculated as:

DNA concentration (µg/ml) = Absorption (260 nm) x 50 x 10 (dilution factor)

The 260:280 ratio was also calculated to determine the purity of the DNA. A DNA sample with a ratio of above 1.7 was deemed to have sufficient purity for transfection into mammalian cells.

2.3.5.9 Examination of DNA using agarose gel electrophoresis

After various procedures (polymerase chain reaction (PCR), plasmid preparation and ligation) DNA product were examined using agarose gel electrophoresis. The agarose gel was prepared by adding 0.25 g of agarose to 50 ml of Tris-Borate-EDTA (TBE) buffer (89 mM Tris-borate pH 8.3, 2 mM EDTA). The mixture was heated in a microwave oven to dissolve the agarose. The mixture was allowed to cool for around 5 min and then poured into a pre-sealed gel tray, a comb was placed in the gel and it was allowed to solidify for a minimum of 1 h at room temperature. DNA samples were prepared by adding 1 µl SYBR™ Green I nucleic acid gel stain (diluted 1:100 in distilled water) and 5 µl Loading buffer (glycerol (30% v/v) bromophenol blue (0.25% w/v)) to a 5 µl sample of each DNA. In addition, the DNA Ladder (10 µl) was mixed with 1 µl of SYBR Green I. The Quick-Load® Purple 100 bp DNA Ladder was used alongside any PCR products and the Quick-Load® Purple 1 kb DNA Ladder was used together with plasmid DNA samples. The samples and markers were loaded into the wells and

electrophoresis was carried out at 100 V for approximately 1 h. The bands were examined using an ultraviolet transilluminator and images captured using a digital camera.

2.3.5.10 Polymerase chain reaction (PCR) amplification of DNA using platinum *Taq* polymerase

DNA inserts used for ligation into expression vectors were generated using platinum *Taq* polymerase to ensure maximal accuracy of the sequences. The PCR reactions were prepared to contain 1x reaction buffer, $MgCl_2$ (1.5 mM), dNTP (0.2 mM each), primers (0.2 mM of forward and reverse), template DNA (100 ng/reaction) and platinum *Taq* DNA polymerase (2 U). In order to test for the presence of contamination or foreign DNA, negative control reactions devoid of either the template DNA or the primers were also prepared. The PCR tubes were transferred to a thermal cycler and amplification carried out according to the protocol outlined in Table 2.2. The annealing temperature of the primers was determined using the online tool Tm Calculator from Life Technologies (specified in each chapter). A sample of PCR product (5 µl) was examined by agarose gel electrophoresis (section 2.3.5.9). The remaining product was either used in the stated experiments or stored at -20°C for later use.

2.3.5.11 PCR amplification of DNA using illustra PuReTaq Ready-To-Go PCR Beads

Confirmation of successful ligation of inserts into the expression vectors was performed using illustra PuReTaq Ready-To-Go PCR Beads. Reactions were prepared to contain 2.5 µl template DNA (10 ng/µl), 1 µl primers (10 µM of both forward and reverse) and 21.5 µl RNAse-free water added to a PCR tube containing a PuReTaq Bead. Each bead contained BSA, mixed dNTP, ~2.5 U of PuReTaq DNA polymerase and the reaction buffer. Following reconstitution to a 25 µl final volume, the concentration of each dNTP is 200 µM in 10 mM Tris-HCl pH 9.0, 50 mM KCl, and 1.5 mM $MgCl_2$. In order to test for the presence of contamination or foreign DNA, negative control reactions devoid of either the template DNA or the primers were also prepared. The PCR tubes were placed in a thermal cycler and amplification performed according to the protocol outlined in Table 2.3. The annealing temperature of primers was calculated using the online tool Tm Calculator from Life Technologies (specified in each chapter). A sample of the PCR product (5 µl) was examined by agarose gel electrophoresis (section 2.3.5.9).

2.3.5.12 Digestion of DNA using restriction enzymes

In order to clone the amplified DNA inserts into the expression vectors both the plasmid vector and the insert sequences were digested with the same two restriction enzymes. Digestion with two enzymes was performed to ensure the directional insertion of the PCR was reproduced into the

Table 2.2: PCR cycle protocol using the platinum *Taq* polymerase

STEP	TEMP	TIME
Initial Denaturation	94°C	10 min
35 Cycles - Denaturation	94°C	30 s
- Annealing	50–72°C*	30 s
- Extension	72°C	1 min
Final Extension	72°C	10 min
Hold	4°C	

* The annealing temperature used varied depending on the primer set.

Table 2.3: PCR cycle protocol using the Ready-To-Go PCR Beads

STEP	TEMP	TIME
Initial Denaturation	94°C	2 min
35 Cycles - Denaturation	94°C	30 s
- Annealing	50–72°C*	30 s
- Extension	72°C	30 s
Final Extension	72°C	5 min
Hold	4°C	

* The annealing temperature used varied depending on the primer set.

expression vector. The plasmid and the amplified DNA insert were digested with the two enzymes separately, with a DNA clean-up procedure (section 2.3.5.13) in between, since the two enzymes required different buffers for effective digestion. Restriction digest reactions were assembled using the indicated volumes in Table 2.4 and contained BSA (1 mg/ml), restriction enzyme buffer, DNA (either plasmid or insert), restriction enzyme (10 U/ml) and were made up to the total volumes stated with RNAse-free water. Prior to the second restriction digest, the amount of DNA recovered after the clean-up was determined using a spectrometer (section 2.3.5.8) and the proceeding reaction setup was adjusted according to Table 2.4. All reactions were carried out at 37°C for 1 h in a thermal cycler. Samples of products (5 µl) were analysed by agarose gel electrophoresis (section 2.3.5.9) to confirm successful digestion.

2.3.5.13 Purification of DNA using DNA clean-up kit

In order to remove traces of reaction buffer and enzymes between restriction enzyme reactions the Monarch® PCR & DNA Cleanup Kit was used. Following each digestion, the samples were mixed with the DNA Cleanup Binding Buffer in a ratio of 2:1 (v/v). The samples were pipetted into a provided column and centrifuged at 12,000 *g* for 1 min. The flow-through was discarded and the columns were washed twice with 200 µl DNA Wash Buffer and centrifuged at 12,000 *g* for 1 min each time. The columns were centrifuged at 12,000 *g* for a further 5 min to ensure the removal of all traces of wash buffer. The columns were transferred to a clean 1.5 ml microfuge tube and 6 µl of DNA Elution Buffer, preheated to 50°C, was added to each column. The columns were incubated for 1 min and centrifuged at 12,000 *g* for 2 min to elute the DNA. The concentrations of the eluted DNA samples were measured using a spectrometer (section 2.3.5.8) and used in further procedures or stored at -20°C.

2.3.5.14 Ligation methods

2.3.5.14.1 Ligation of DNA using T4 DNA ligase

To optimise the ligation reaction, the ability of the T4 DNA ligase to recyclise linearised plasmid DNA was assessed. The reaction was prepared to contain the digested plasmid (30 ng), T4 ligase (0.2 µl; 5 U/µL), reaction buffer (2 µl) and the reaction was made-up to a final volume of 20 µl using RNAse-free water. A negative control reaction devoid of the ligase enzyme was also prepared. The tubes were incubated for 15 min at 22°C in a thermal cycler and a sample of each reaction (5 µl) was analysed by agarose gel electrophoresis (section 2.3.5.9).

Table 2.4: Components of the restriction digestion reaction adjusted for the amount of DNA

DNA (µg)	10x BSA (µl)	10x Buffer (µl)	Restriction Enzyme (µl)	Total reaction volume (µl)
0.1	0.3	0.3	0.1	3
0.5	1.5	1.5	0.5	15
1	3	3	1	30
2	6	6	2	60
3	9	9	3	90

2.3.5.14.2 Ligation of DNA using NEB instant sticky ends ligase master mix

To optimise the ligation reaction, the ability of New England Biolabs (NEB) instant sticky ends ligase master mix to recyclise linearised plasmid DNA was assessed. The reaction was prepared by mixing the digested plasmid (30 ng) and sticky-end master mix (5 µl) and the reaction was made-up to a final volume of 10 µl using RNAse-free water. A negative control reaction devoid of the master mix was also prepared. The tubes were incubated for 15 min at 22°C in a thermal cycler and a sample of each reaction (5 µl) was analysed by agarose gel electrophoresis (section 2.3.5.9).

2.3.5.15 Site-Directed mutagenesis of the DNA using the Q5 mutagenesis Kit

Substitution and deletion mutagenesis of DNA sequences were performed using Q5® Site-Directed Mutagenesis Kit. Primers were designed to include the desired mutation (specified in section 5.2.3) using the NEBaseChanger website program (Figure 2.5). Mutagenic PCR reactions were assembled to contain 12.5 µl of Q5 Hot Start High-Fidelity 2X Master Mix (containing polymerase buffer, dNTPs, 2 mM Mg^{2+} and Q5 Hot Start High-Fidelity DNA Polymerase), 1 µl of template plasmid DNA (1 ng/µl), 2.5 µl of primers (10 µM of forward and reverse) and 9 µl of RNAse-free water. The tubes were transferred to a thermal cycler the PCR performed using the protocol shown in Table 2.5. The annealing temperatures used (specified in each chapter) were calculated by the NEBaseChanger website for each specific set of primers. The PCR products (5 µl) were examined by agarose gel electrophoresis as described in section 2.3.5.9. Samples of the PCR products (1 µl) were then incubated with 1 µl of 10x Kinase-Ligase-DpnI (KLD) enzyme mix, 3 µl of 2x KLD reaction buffer and 3 µl of RNAse-free water and incubated for 5 min at room temperature. The DpnI domain within the KLD enzyme digests any methylated DNA and so removes the original template DNA leaving only the newly synthesised unmethylated PCR product. The kinase domain of the KLD enzyme phosphorylates the 5' end of the PCR product and the ligase domain joins the two ends together resulting in a circular mutant plasmid (Figure 2.5). After incubation with the KLD enzyme, the reaction mixtures were transformed into high-efficiency NEB 5-alpha Competent *E. coli* cells using the procedure described in section 2.3.5.4.

2.3.5.16 One-step preparation of complementary DNA (cDNA) from cells using cell-2-cDNA kit

In order to generate cDNA from cellular mRNA for use in real-time (RT)-PCR analysis, a direct one-step procedure was employed using the cells-to-cDNA™ II Kit according to manufacturer's instructions. Cells (10^5) were transferred to PCR tubes, centrifuged at 4,800 *g* for 5 min at 4°C and resuspended in 100 µl in ice-cold Cell Lysis II Buffer (provided in cell-2-cDNA kit). The tubes were transferred to a thermal cycler and incubated for 10 min at 75°C. 2 µl of DNase I (2 U/µL) was added

Figure 2.5: Diagram representing the Site-Directed Mutagenesis procedure

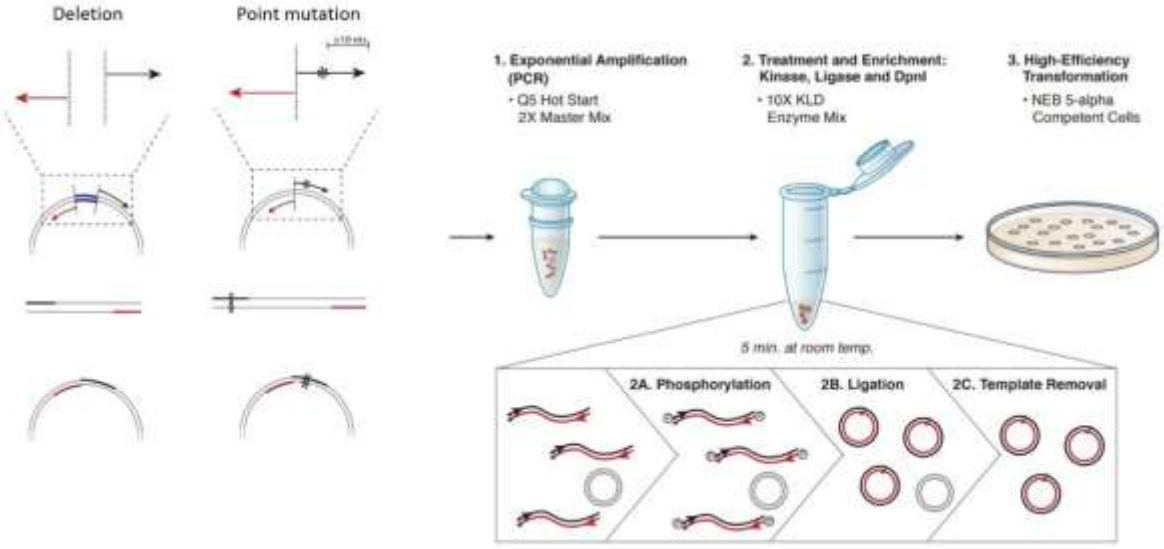

For deletion mutagenesis, primers are designed which bind to sequences directly adjacent to the sequence that requires deletion. For point mutations, a forward mutagenic primer containing the desired substituted base(s) is designed which produces a mismatch to the plasmid template (indicated by the *). These primers are used to amplify the template DNA in mutagenic PCR reactions. The products of the mutagenic PCR reactions are treated with Kinase-Ligase-DpnI (KLD) enzyme mix. 2A) The kinase domain of the KLD enzyme phosphorylates the 5' end of the PCR product and 2B) the ligase domain joins the two ends together resulting in a circular mutant plasmid. 2C) The DpnI domain within the KLD enzyme digests any methylated DNA and so removes the original template DNA leaving only the newly synthesised unmethylated PCR product. The KLD treated product is then transformed into high-efficiency NEB 5-alpha Competent *E. coli* cell (Diagram adapted from NEBiolabs (2020)).

Table 2.5: PCR cycle protocol used for Site-Directed Mutagenesis

STEP	TEMP	TIME
Initial Denaturation	98°C	30 s
25 Cycles - Denaturation	98°C	10 s
- Annealing	50–72°C*	30 s
- Extension	72°C	3 min
Final Extension	72°C	2 min
Hold	4°C	

* The annealing temperature used varied depending on the primer set.

to each tube and the tubes returned to the thermal cycler and incubated for a further 15 min at 37°C to degrade the genomic DNA. The samples were then heated at 75°C for 5 min to inactivate the DNase I. A mixture containing dNTP Mix (2.5 mM each dNTP), random decamers (50 µM) and RNAse-free water was prepared and divided into the tubes. A sample of each cell lysate (5 µl) was added to the tubes and heated for 3 min at 70°C to denature any secondary structures present in the mRNA, and then placed on ice. A mixture containing Reverse Transcriptase Buffer (provided by the kit), M-MLV Reverse Transcriptase enzyme and RNase Inhibitor (10 U/µL) was added to each tube. A negative control reaction devoid of the Reverse Transcriptase enzyme was also prepared. The tubes were incubated at 42°C for 60 min to synthesis the cDNA and then the enzyme was inactivated by heating to 95°C for 10 min. The resulting cDNA samples were either used for RT-PCR or stored at -20°C.

2.3.5.17 Quantification of cDNA using semi-quantitative real-time (RT)-PCR

The amounts of the prepared cDNA, corresponding to the expression of mRNA in the cells, were measured using iCycler Real-Time PCR machine (BioRad), and the SYBR™ Select Master Mix according to manufacturer's protocols. RT-PCR reactions were prepared to contain SYBR Select Master Mix (30 µl), specific primer (specified in each chapter) (3 µl; 0.4 µM final conc), cDNA samples (15 µl; 7.5-10 ng/µl final conc) and RNAse-free water (12 µl). In order to test for the presence of contamination or foreign DNA a reaction was performed omitting the reverse transcription steps, also reactions devoid of either the template DNA or the primers were prepared. Each reaction was divided between 3 wells in a 96-well PCR plate and placed in the iCycler Real-Time PCR machine. Amplification was performed using the protocol shown in Table 2.6. The cycle threshold (Ct) for each sample was calculated automatically by iCycler iQ v3.1 software and the relative gene expression levels were calculated using the following equation (Livak & Schmittgen, 2001):

$$2^{-((Ct(TE)-Ct(HE)) - (Ct(TC)-Ct(HC)))}$$

TE = Test gene experimental sample, HE = Housekeeping gene experimental sample, TC = Test gene control sample, HE = Housekeeping gene control sample.

β-actin was used as the housekeeping gene in these experiments since the gene expression level has been reported to remain constant in the cell lines used in this study (Ettelaie et al., 2016). In order to ensure specific binding of the primers, a melt curve was performed using the protocol shown in step 6 in Table 2.6. This was performed to ensure the presence of a single amplicon was produced for

Table 2.6: Thermocycling conditions for RT-PCR

			Temp	Time
Cycle 1:	(1X)	Step 1:	50.0 °C	02:00
Cycle 2:	(1X)	Step 1:	95.0 °C	02:00
Cycle 3:	(40X)	Step 1:	95.0 °C	00:15
		Step 2:	60.0 °C	00:30
			Data collection.	
Cycle 4:	(1X)	Step 1:	95.0 °C	01:00
Cycle 5:	(1X)	Step 1:	50.0 °C	01:00
Cycle 6:	(44X)	Step 1:	70.0 °C	00:05
		Increase set point temperature after cycle 2 by 0.5 °C		
			Melt curve data collection.	
Cycle 7:	(1X)	Step 1:	4.0 °C	HOLD

each primer set. For experiments performed using designed primers with known sequences a predicted melt curve peak temperature was calculated using the µMelt online tool (v2.0.2). If the melt curve peak temperature for a well was more than 0.5°C either side of the predicted melt curve peak value, then the Ct value from the well would not be used, as an incorrect sequence had been amplified.

2.3.6 Statistical analysis

The data represented in all graphical figures are the mean value of the number of experiments ± the standard error of mean (SEM) or standard deviation (SD), as stated in the legends. Statistical analysis of data was carried out using the Statistical Package for the Social Sciences (SPSS) program v25 (IBM). To test for normal distribution the Kolmogorov Smirnov test was used. A reading of $p > 0.05$ indicated the data was normally distributed. To test if the variances of two groups were equal the Levene's Test of Equality of Variance was used. A reading of $p > 0.05$ indicated the group variances could be treated as equal. Comparison between two normally distributed groups with equal variables was performed using the independent sample t-test and a p-value of <0.05 was considered significant. For experiments with multiple variables, one-way ANOVA test were used and a p-value of < 0.05 was considered significant.

Chapter 3

The influence of LMWH and direct fXa inhibitors on tumour properties

3.1 Introduction

Thrombotic complications are among the leading causes of morbidity and mortality in cancer patents (section 1.6). Therefore, cancer patients frequently receive anticoagulant drugs alongside chemotherapy (Khorana et al., 2018). Two pharmaceutical LMWH agents, dalteparin and tinzaparin are currently the anticoagulants recommended for prophylaxis against VTE in cancer patients (Horton, 2005). Interestingly, studies of cancer patients receiving LMWH reported favourable biological outcomes that extended beyond the prevention and/or treatment of thrombosis (Akl et al., 2007). However, the mechanisms that give rise to these favourable biological outcomes are not fully understood. Furthermore, it is not known if other classes of anticoagulants, such as DOAC, possess similar properties. However, the use of LMWH for extended periods comes with the risk of bleeding, thrombocytopenia and osteopenia (Krishnamurthy & Freedman, 2005). Therefore, if DOAC do possess anticancer activities, these agents may have advantages over the traditional prophylactic treatments. Therefore, a study of the anticancer actions of different anticoagulants and their mechanisms may provide alternative therapies for the treatment of cancer patients.

3.1.1 Recorded anticancer properties of anticoagulants

As stated above, favourable biological effects extending beyond the treatment of thrombosis have been reported in cancer patients receiving LMWH (Akl et al., 2007). Furthermore, administration of LMWH in experimental animal models, has been shown to reduce the growth of xenograft tumours (Lee et al., 2009; Takahashi et al., 2005). However, it is not clear if these properties of LMWH arise directly from suppressing the rate of cancer cell proliferation, or alternatively, through reduction of angiogenesis (Bertolesi et al., 1994; Carmazzi et al., 2012; Halper & Carter, 1989). Treatment of A549 lung cancer cells with the LMWH nadroparin, reduced cancer cell proliferation by arresting the cells at the G_2/M phase of the cell-cycle (Carmazzi et al., 2012). In contrast, a number of other *in vitro* studies did not detect any anti-proliferative properties against cancer cells, associated with LMWH treatment (Bereczky et al., 2005; Lee et al., 2009; Takahashi et al., 2005). Therefore, alternative mechanisms for the anticancer properties of LMWH may include the inhibition of angiogenesis. Previously, a range of LMWH preparations were shown to inhibit endothelial capillary tube formation *in vitro* (Khorana et al., 2003; Marchetti et al., 2008; Mousa & Mohamed, 2004b). In addition, tinzaparin has been shown to inhibit angiogenesis *in vivo*, using a rat mesentery assay (Norrby, 2000). However, it must be noted that these antiangiogenic outcomes were specific to the LMWH preparations stated in each study and therefore, variations in the activities of the preparations is expected.

The mechanism by which LMWH preparations influence angiogenesis may itself be either dependent or independent of the anticoagulant properties of these compounds. For example, LMWH disrupt the binding of proangiogenic growth factors and cytokines including bFGF, VEGF and TNFα (Khorana et al., 2003; Marchetti et al., 2008; Mousa & Mohamed, 2004b). Another mechanism by which LMWH may influence cancer cells and angiogenesis is through the disruption of cell-cell and cell-ECM interactions (Beauvais & Rapraeger, 2004; Jung et al., 2016; Luo et al., 2008). Cell-cell and cell-ECM interactions transmit signals into the cell which encourage proliferation, migration and invasion in both cancer cells and endothelial cells (Baker & Chen, 2012; Smyrek et al., 2019). Therefore, disruption of these interactions by LMWH is likely to reduce cancer progression through enhanced angiogenesis. In addition, LMWH may also influence angiogenesis by coagulation-dependent mechanisms mediated through PAR. Activated coagulation proteases, including fXa, cleave PAR which is present on a number of cells including cancer cells and the associated endothelial cells. The activation of PAR has been reported to promote cancer cell proliferation, migration and invasion (section 1.7.2) (Hempel et al., 2016) whereas PAR activation on endothelial cells induces angiogenesis (section 1.8.2) (Kawaguchi et al., 2020). Therefore, any reduction in the activation of PAR, through inhibition of coagulation fXa activity, may suppress tumour growth. In addition to LMWH, apixaban and rivaroxaban are therapeutically used oral anticoagulants which also inhibit fXa. While LMWH acts as a co-factor for the approximation of ATIII and fXa (Olson et al., 1992), apixaban and rivaroxaban inhibit fXa directly by binding at the catalytic site of the protease (Pinto et al., 2007; Roehrig et al., 2005). Therefore, it may be hypothesised that these DOAC also possess some similar anticancer properties to LMWH. Furthermore, DOAC may even have advantages over LMWH as they can be administrated orally and possess a faster onset of action. Additionally, DOAC do not require laboratory monitoring and although they can cause bleeding complications (Ay et al., 2017), they do not induces the addition side effects, thrombocytopenia and osteopenia, associated with LMWH (Krishnamurthy & Freedman, 2005).

3.1.2 Use of 3D spheroid cultures to study the anticancer properties of anticoagulants

While previous studies have indicated that LMWH are capable of reducing the growth of xenograft tumours, these agents did not influence cancer cell proliferation *in vitro* (Bereczky et al., 2005; Lee et al., 2009; Takahashi et al., 2005). The reasons for the discrepancies between the various observations are currently unclear. Therefore in this study, it is proposed that 3D cultures of cancer cells may be used as an intermediary between 2D *in vitro* and *in vivo* studies and may aid the understanding of the anticancer properties of LMWH. 3D cultures of cells form into spheroids comprising of a layered structure with a necrotic core, surrounded by a layer of quiescent cells and

an outer layer of proliferating cells (Figure 3.1). This occurs due to the limited diffusion of molecules including oxygen, nutrients and growth factors, into and out of the spheroid and mimics *in vivo* tumour morphology (Lin & Chang, 2008). In addition, cells grown in 3D cultures form cell-cell and cell-ECM interactions, rather than cell-plastic interactions which are observed in cells grown in 2D cultures (Baker & Chen, 2012). Due to these properties, 3D culture assays may be used to assess the influence of LMWH on cell-cell and cell-ECM interactions as well as growth factor binding and examine the outcomes for spheroid formation and cell invasion.

3.1.3 Use of chorioallantoic membrane (CAM) for the study of angiogenesis and tumour vascularisation

The CAM is the membrane which allows exchange of gases to and from a developing chick embryo (Cimpean et al., 2008; Deryugina & Quigley, 2008; Dohle et al., 2009). The CAM is first formed around days 3-4 of chick embryo development (embryo development day (EDD) 3-4) (Figure 3.2A) (Cimpean et al., 2008; Deryugina & Quigley, 2008) and is initially vascularised by undifferentiated capillaries (Mangieri et al., 2008). These vessels develop between EDD4 to EDD12, subsequently recruiting mesenchymal cells to surround the endothelium, gaining a basal lamina and differentiating into distinct arterioles and venules (Figure 3.2B & Figure 3.2C) (Mangieri et al., 2008). The expression VEGF and bFGF has been previously demonstrated to be responsible for the initiation and progression of vessel development (Mangieri et al., 2008). The development of the vasculature within the CAM makes this membrane a suitable model for studying the molecular mechanisms involved in angiogenesis (Jakob et al., 1978). Consequentially, CAM has also been used to test the effectiveness of potential antiangiogenic agents, including both unfractionated heparin and LMWH (Dogan et al., 2011; Katrancioglu et al., 2012; Mousa, 2013; Mousa & Mohamed, 2004a). However, caution is essential in interpreting the data from such studies since the concentrations of LMWH used in these studies often far exceeded those used as therapeutic doses (Dogan et al., 2011; Katrancioglu et al., 2012). In contrast, any influence of direct fXa inhibitors such as apixaban and rivaroxaban, on CAM vessel angiogenesis have not been explored to date. Another advantage of the CAM model is that the developing chick embryo remains immunodeficient during the majority if its development. This permits the transplantation of cells and tissues from various organisms and species onto the CAM without the risk of triggering an immune response. Vascularisation of these implanted cells and tissues occurs by growth of host vessels into the cell mass, attracted by the angiogenic factors released from the xenograft (Ribatti, 2014). The CAM model has previously been used to examine the influence of LMWH on the growth of xenografts made from colon carcinoma,

Figure 3.1: Structure of spheroids formed in 3D cell culture

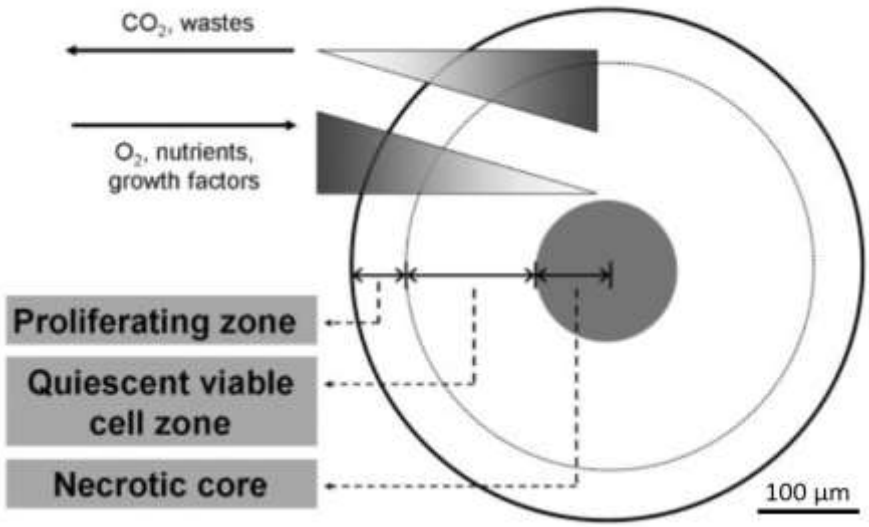

Cells grown in 3D cultures form into spheroids with a layered structure of necrotic, quiescent and proliferating cells. The layered structure develops because the diffusion of molecules, including oxygen, carbon dioxide, nutrients and growth factors, through cell boundaries is limited to about 150-200 µm (Lin & Chang, 2008). Therefore, in spheroids greater than 500 µm in diameter the concentration of oxygen, nutrients and growth factors is reduced in the centre of spheroids and metabolic waste accumulates.

Figure 3.2: The development and structure of chick embryo CAM

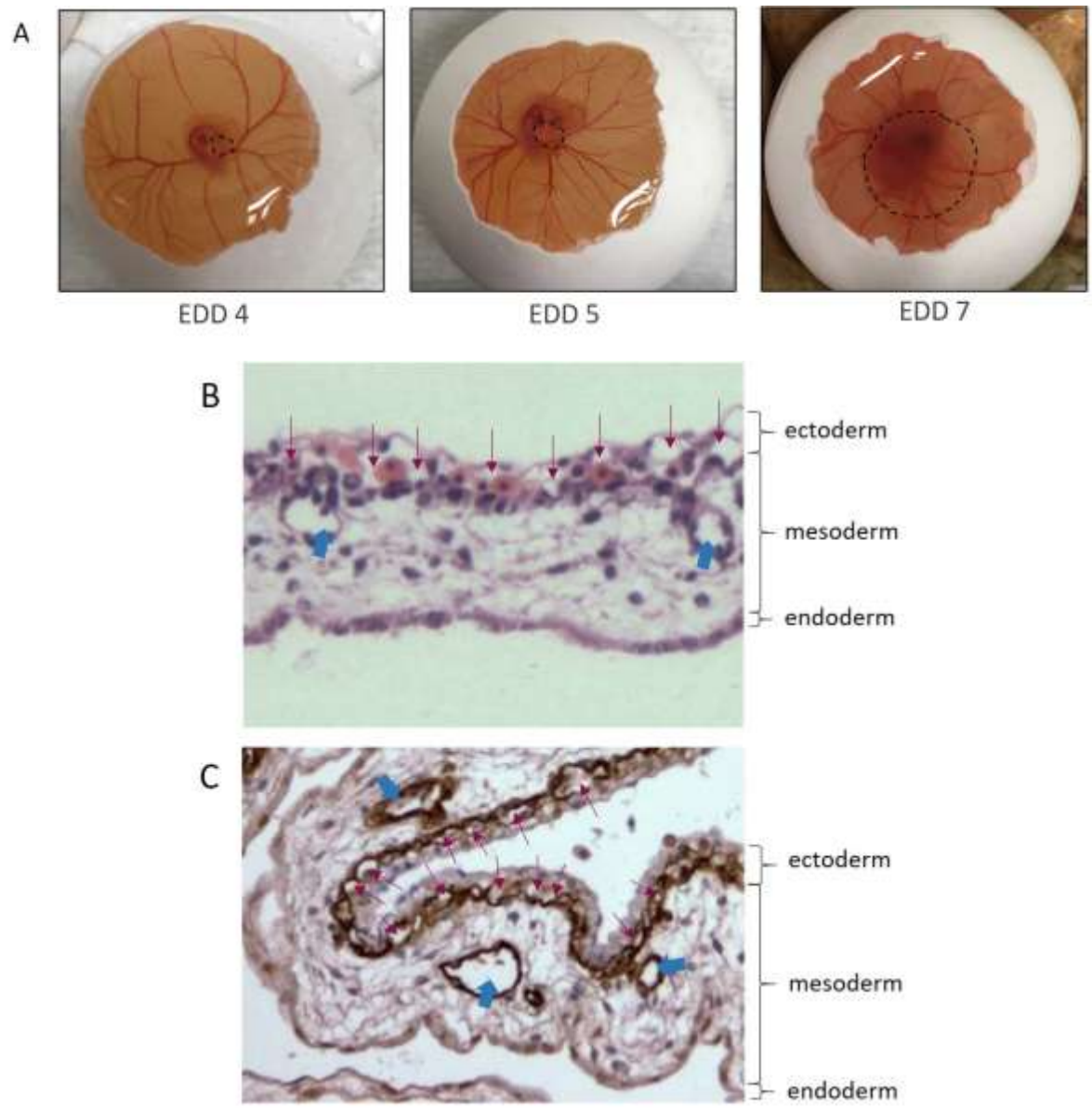

A) Representative images of CAM taken at EDD 4-7. Sections of CAM collected on EDD 12 and stained with either B) Hematoxylin and eosin staining or C) immunohistochemical staining with endothelium-specific lectin *sambucus nigra* agglutinin. In image B, the vessels are visible as dark brown structures. Histologically, the CAM contains three major layers; the ectoderm, mesoderm and endoderm (Deryugina & Quigley, 2008). In both images, smaller vessels (thin red arrows) are present directly below the ectoderm layer, while the larger vessels (thick blue arrows) are distributed throughout the mesoderm. Images are shown at x100 magnification (Originally published in Deryugina & Quigley (2008) with no scale bars included).

fibrosarcoma, lung carcinoma and pancreatic cancer cells (Mousa & Mohamed, 2004a; Sudha et al., 2014).

The activation of the coagulation system in cancer patients appears to contribute to tumour growth and angiogenesis (Rickles et al., 2001; Shoji et al., 1998), as well as the dissemination of the tumour through metastasis (Rickles et al., 1988). Consequently, it was hypothesised that treatment of cancer with anticoagulants may be effective at reducing tumour development and angiogenesis. Furthermore, it has been reported that treatment of cancer patients with the LMWH family of anticoagulants resulted in a reduction in patient mortality (Akl et al., 2007; Lazo-Langner et al., 2007). However, the mechanisms of action of the LMWH remain under investigation. A new class of anticoagulants, called DOAC, inhibit fXa by a dissimilar mechanism to LMWH. Therefore, if the anti-cancer properties of LMWH arise from their ability to inhibit fXa then it is hypothesised that the DOAC with also impact cancer development and angiogenesis.

3.1.4 Aims

In this study, the anticancer properties of the LMWH, tinzaparin and dalteparin and the fXa inhibitors, apixaban and rivaroxaban were examined and compared. The influence of the anticoagulants on cancer cell invasion was assessed using spheroid growth and invasion assays in which both the size of the spheroid and the invasiveness of the cells into a matrix were recorded. In addition, the influence of the anticoagulants on angiogenesis was examined by measuring the density and diameter of treated blood vessels, using the CAM model. Finally, the rate of tumour growth was explored by implanting cell masses onto the CAM model and monitoring the overall size of the xenograft tumours following treatment with the anticoagulants.

3.2 Methods

3.2.1 Optimisation of the formation of cancer cell spheroids

Prior to studies, five cell lines including A375, WM-266-4 and SK-MEL-2 melanoma cells, AsPC-1 pancreatic cancer cells and MDA-MB-231 breast cancer cells were assessed to see if they were capable of forming spheroids when grown in 3D cultures. To achieve this, the cells (2 x 10^3) were cultured in Nunclon Sphera non-adherent 96-well plates and incubated at 37°C for up to 4 days. Spheroid formation was monitored by white-light microscopy and images were capture daily. In additional experiments, the number of cells required for consistent spheroid formation was determined. A375, WM-266-4 and SK-MEL-2 cells were plated at a range of densities (0.5-2.5 x 10^3) in the non-adherent 96-well plates. The cells were incubated at 37°C for up to 4 days and spheroid formation was monitored by white-light microscopy.

3.2.2 Assessment of the influence of LMWH on spheroid formation

The potential of anticoagulants to interfere with the formation of cancer cell spheroids was assessed next. For these experiments, WM-266-4 or AsPC-1 cells (2 x 10^3) were suspended in media (100 µl) containing tinzaparin (0.2 & 2 IU/ml) or dalteparin (0.2 & 2 IU/ml) in non-adherent 96-well plates. In other experiments, WM-266-4 cells (2 x 10^3) were suspended in media (100 µl) containing an inhibitory anti-β1 integrin antibody (10 µg/ml) in non-adherent plates. The cells were maintained at 37°C for up to 3 days to permit the formation of the spheroids (Figure 3.3A), monitored by white-light microscopy, and images were obtained daily. The numbers of spheroids formed following the 3-day incubation were counted and the diameters of the spheroids were measured using ImageJ.

3.2.3 Assessment of the influence of anticoagulant agents on cell invasion

The spheroid invasion assay aims to mimic *in vivo* invasion of cancerous cells through the stroma leading to metastasis. To achieve this, spheroids were encased within a matrix (Figure 3.3B) consisting of a mixture of basement membrane extract and collagen I (Trevigen, 2016). Prior to the experiments, the abilities of different cell lines to invade through this matrix were assessed. Five candidate cell lines; A375, WM-266-4, SK-MEL-2, AsPC-1 and MDA-MB-231 cells (2 x 10^3) were cultured in the non-adherent 96-well plates and incubated at 37°C for 4 days to permit spheroid formation, as above. The spheroids were then embedded into invasion matrix by dropwise adding 20 µl of Cultrex spheroid invasion matrix to each well. The plate was incubated for 1 h at 37°C to allow the matrix to solidify. The spheroids were then examined daily by white-light microscopy, for up to 4 days.

Figure 3.3: Schematic protocol of spheroid formation and spheroid invasion assays

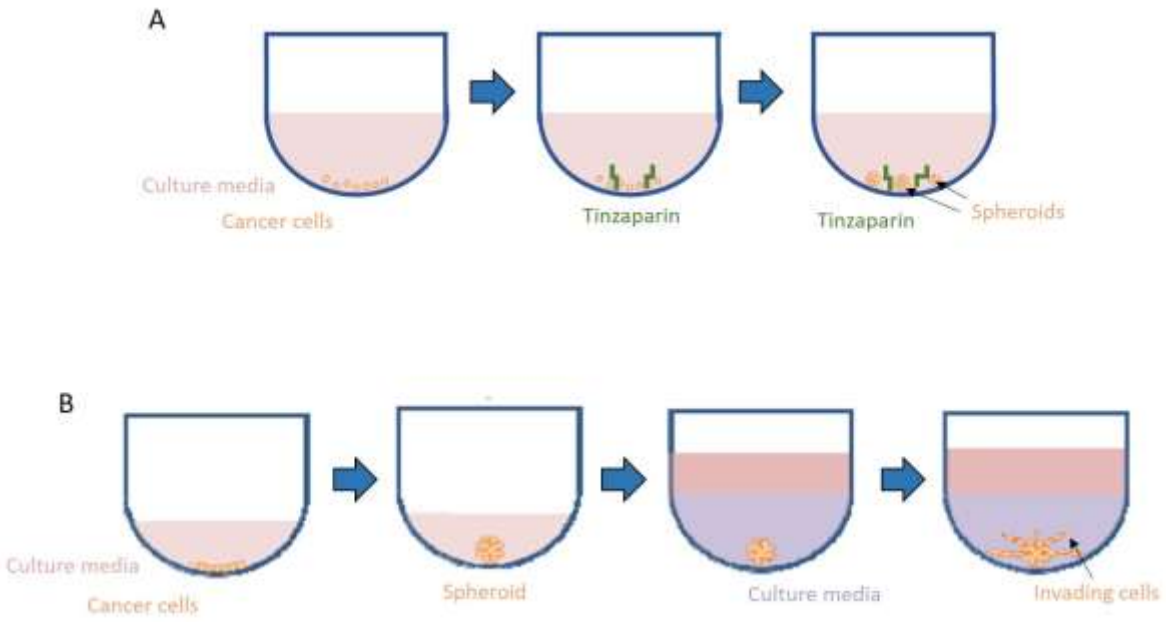

A) The influence of anticoagulants on the formation of spheroids was assessed by suspending cells in media containing the test reagents (e.g tinzaparin) in non-adherent plates and incubating for 3 days at 37°C. B) To assess the invasive properties of cells, spheroids were embedded in Culture invasion matrix. The spheroids were then incubated for up to a further 5 days at 37°C to allow cell invasion into the matrix. The influence of anticoagulants on cell invasion was assessed by supplementing the culture media with the test reagents during these 5 days of incubation.

To assess the influence of anticoagulant agents on cell invasion, WM-266-4 and AsPC-1 cell spheroids were prepared and embedded into invasion matrices as above. Selected wells were then supplemented with media (100 µl) containing tinzaparin (0.2 & 2 IU/ml), dalteparin (0.2 & 2 IU/ml), apixaban (0.1 & 1 µg/ml) or rivaroxaban (0.06 & 0.6 µg/ml). The spheroids were examined by white-light microscopy and images were captured daily for up to 5 days. The extent of the invasion of cells out from the spheroids was assessed using ImageJ. In addition, an invasion ratio was calculated as the ratio of the area of spread cells following the final day of treatment (Figure 3.4B) to that of the initial area of the spheroid measured on the day of embedding (Figure 3.4A).

3.2.4 Assessment of the influence of anticoagulant agents on angiogenesis using the CAM assay

The study was carried out under the UK home office animal licence 40/3564. Live fertilized white leghorn chicken (Gallus gallus domesticus) eggs were stored at 12-18°C for up to 2 days before use. Embryo development was stimulated by placing the eggs in an incubator at 37°C and 70% relative humidity, on the day designated as embryo development day (EDD) 0. On EDD 4, an opening of approximately 30 mm diameter was cut into the shell above the air sack of the egg. The shell membrane was then removed from the exposed area under the opening. The opening was covered with a plastic cap and the eggs returned to the incubator. On EDD 11, sections of sterile gelatin sponge (8 mm^3) were soaked in solution of tinzaparin (0.063-5 IU/ml), apixaban (0.1 & 1 µg/ml), rivaroxaban (0.06 & 0.6 µg/ml) or bevacizumab (0.5-12.5 µg/ml) for 2 min. In addition, sections of sponge were also soaked in the respective vehicle controls, PBS or DMSO (0.05% v/v). Two sponges were placed on each exposed CAM (Figure 3.5A), one containing a test reagent and the other the respective vehicle control solution. These treatments were repeated daily for 3 days (until EDD 14) (Figure 3.6). The extent of vascularisation within the CAM directly adjacent to the sponges was monitored over the 3 days using a Leica stereomicroscope and real-time images were captured. The chick embryos were then sacrificed by incubating the eggs at 4°C for 2 h. In order to assess the influence of the anticoagulants on the CAM vessels, the sets of images captured on day 0 of treatment (EDD 11) and following 3 days of treatment (EDD 14) were grouped together and electronically randomised. All the images were then compared against a reference image of CAM vessels which had not been touched by the gelatin sponge (Figure 3.5B). The images were awarded a vessel density score of 0 if there was more than a 50% reduction in vessels compared with the reference image, or 1 if there was less than 50% reduction. The random numbers were “decrypted” and an average vessel density score calculated for each treatment area. Eggs in which any images taken on EDD 11 were scored 0 were deemed to have not developed properly and were therefore

Figure 3.4: Analysis of the invasiveness of the cells from the spheroid using ImageJ

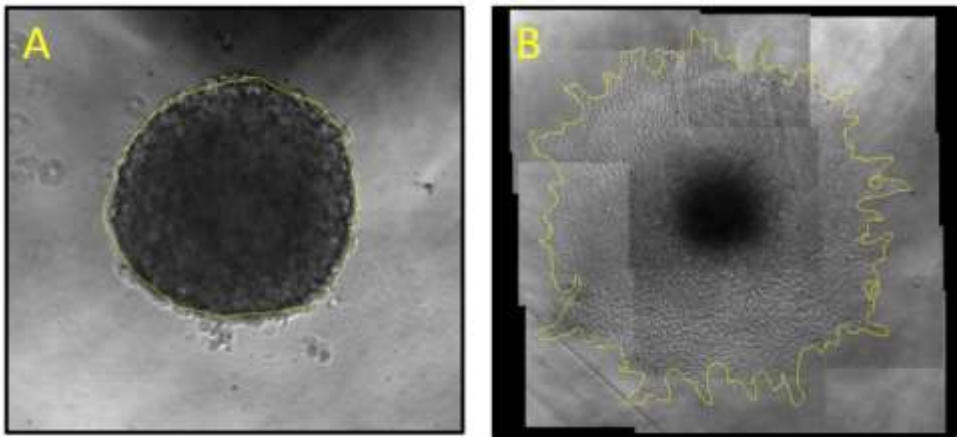

In order to quantify the extent of the invasion of cells out from the spheroids A) the area of the spheroid on the day of embedding and B) the total area of invaded cells on the final day of treatment was measured using ImageJ. To achieve this, the boundaries of either the spheroids or the invading cells were defined manually (shown by the yellow line), and the respective areas were calculated by ImageJ. The invasion ratio was calculated as the ratio of the area of spread cells following the final day to the initial area of the spheroid measured on the day of embedding.

Figure 3.5: CAM angiogenesis assay set up

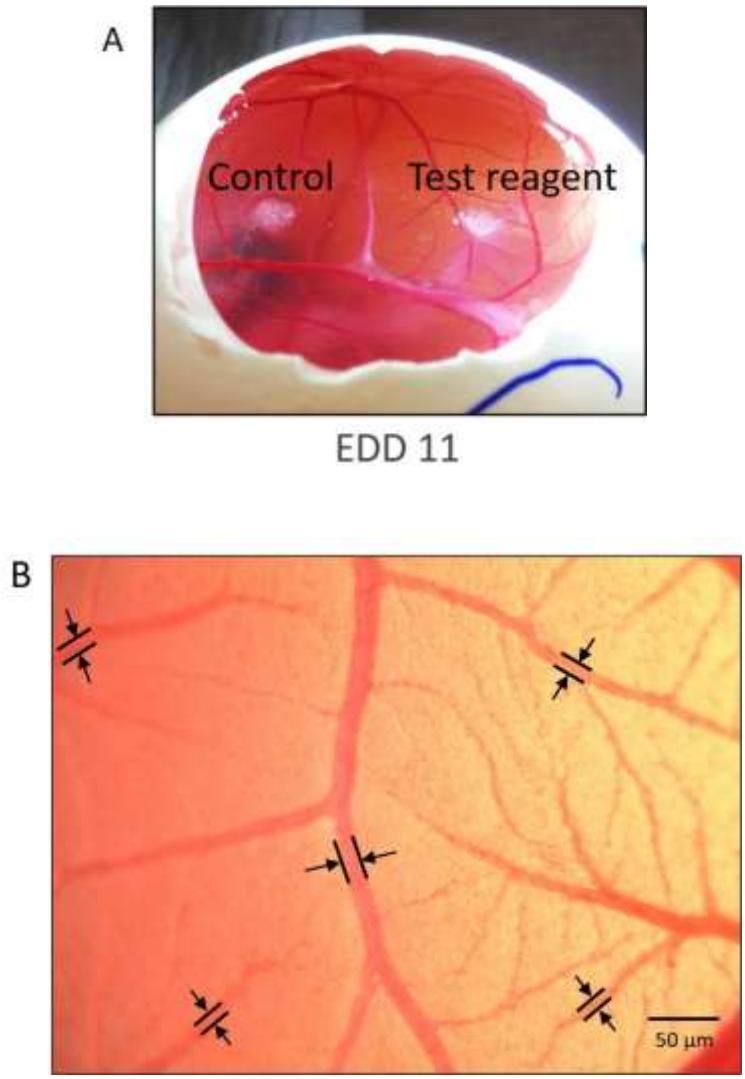

A) The CAM angiogenesis assay is started on EDD 11 by placing two sterile gelatin sponges containing an antiangiogenic reagent and the respective vehicle control onto an area of exposed CAM. B) The reference image of CAM vessels which had not been touched by gelatin sponge against which images of vessels treated with the antiangiogenic agents were compared during the assessment of vessel density. Arrows indicate randomly selected vessels (one from each quarter of the image) of which the diameters were measured.

Figure 3.6: Timelines for the CAM angiogenesis assay and establishment and treatment of cellular tumour xenografts

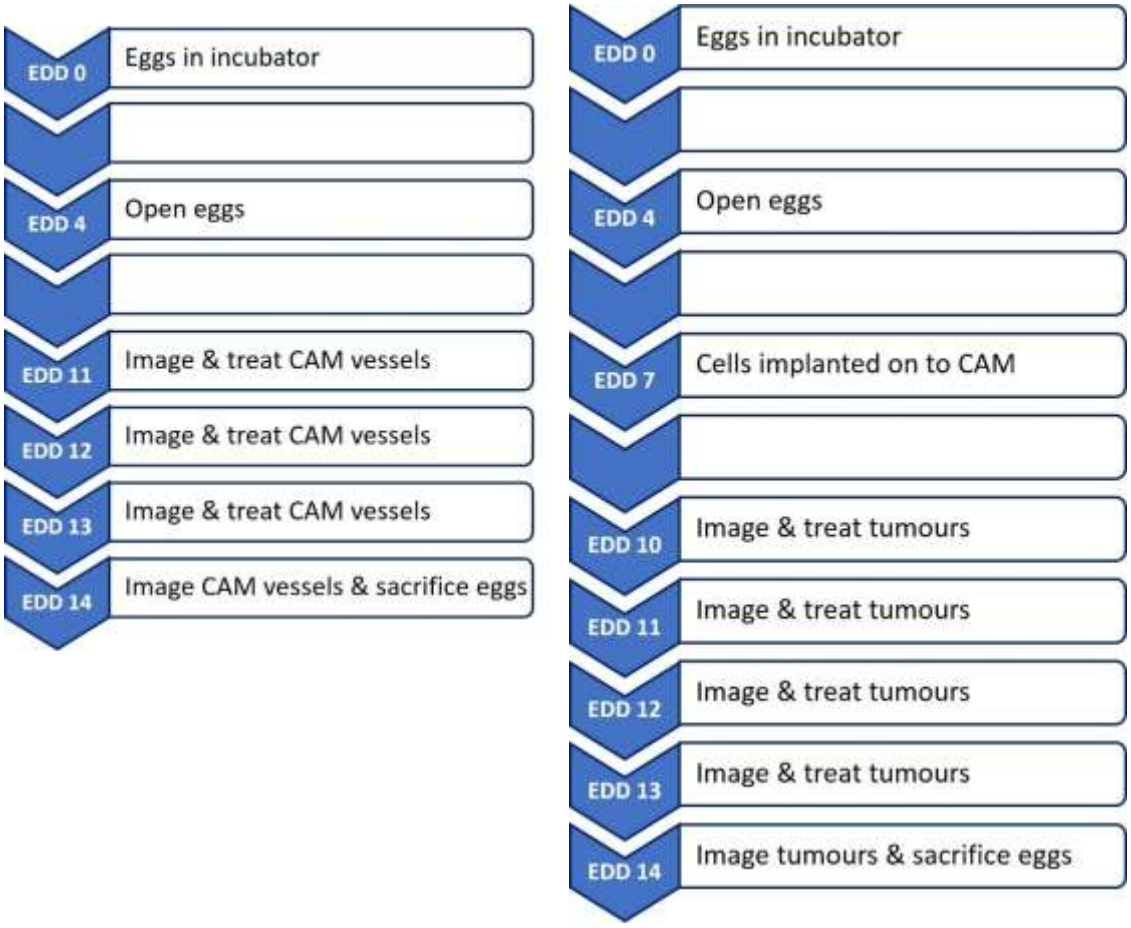

Timeline of which day each of the stages of the CAM model experiments were carried out.

discounted. Any eggs in which the area treated with the vehicle control scored 0 were deemed to have been irritated by the addition of the sterile gelatin sponge and all images from that egg (control and test areas) were discounted. In addition to vessel density, the diameters of 4 randomly selected vessels (one from each quarter of the image) within each image were measured using ImageJ (Figure 3.5B). The measurements were "decrypted" after the experiments and an average vessel diameter was calculated for each treatment area.

3.2.5 Optimisation of the establishment of cellular tumour xenografts implanted onto CAM

Prior to studies, the abilities of cancer cell lines to establish cellular tumour xenografts implanted onto CAM was assessed. Live fertilized chicken eggs were incubated at 37°C and 70% relative humidity to induce embryo development. On EDD 4, the eggs were opened as described above. On EDD 7, cell suspensions were prepared by resuspending WM-266-4 cells in ice cold matrigel at a range of concentrations (1-4 x 10^5 cells/µl) and were kept on ice. In addition, AsPC-1, MDA-MB-231 and MCF-7 cells were resuspended in ice cold matrigel (4 x 10^5 cells/µl) and kept on ice. Blood vessels on the surface of the CAM were disrupted by dabbing with a sterile cotton swab and 5 µl of cell suspension was added to the disrupted area. The eggs were then incubated at 37°C which promoted the solidification of the matrigel into a gel (Hughes et al., 2010), restricting the cells to a small area on the surface of the CAM. The eggs were incubated for 3 days (until EDD 10) to allow the cells to consolidate into tumours and the rates of tumour formation and embryo survival was reported.

3.2.6 Assessment of the influence of anticoagulant agents on the growth of cellular tumour xenografts

Embryo development was induced in live fertilized chicken eggs which were then opened, as described above, on EDD 4. AsPC-1 and WM-266-4 cells (4 x 10^5 cells/µl) were resuspended in ice cold matrigel (5 µl) and implanted onto CAM as described above. The eggs were returned to the incubator at 37°C for 3 days to allow the tumour xenografts to consolidate. To assess the influence of anticoagulants on the growth of the xenografts, they were treated with tinzaparin (1.25-5 IU/ml), apixaban (0.1 & 1 µg/ml) or rivaroxaban (0.6 µg/ml) daily, for up to 4 days (EDD 13) (Figure 3.6). The xenografts were imaged daily using a Leica stereomicroscope and the areas were analysed using ImageJ. The chick embryos were then sacrificed by incubating the eggs at 4°C for 2 h and the sections of CAM containing the tumour xenografts were dissected. The sections were washed once in PBS and then incubated in paraformaldehyde (4% v/v) for 20 min at room temperature. The

sections were either examined immediately or washed twice in 70% (v/v) ethanol and stored in 100% ethanol at 4°C for later assessment.

3.2.7 Visualisation of the blood vessels within CAM sections using white-light microscopy

In order to optimise the visualisation of CAM blood vessels, the expression of a range of endothelial cell markers by the CAM vessels was assessed. Sections of CAM were then excised from the eggs at EDD 13 and cut into 25 mm^2 segments. These were placed into 10-well chamber slides and fixed with 4% (v/v) paraformaldehyde (100 µl) for 20 min at room temperature. The sections were then washed three times with PBST (200 µl) and labelled with antibodies against platelet endothelial cell adhesion molecule-1 (PECAM-1), vascular endothelial (VE)-cadherin or epithelial cell adhesion molecule (EpCAM) (diluted 1:700 v/v in PBST; Table 3.1) at 4°C, overnight. Additional sections were incubated with mouse IgG isotype control antibody (diluted 1:700 v/v in PBST). All the sections were then washed three times with PBST (200 µl) and incubated with HRP-conjugated anti-mouse antibody (diluted 1:2000 v/v in PBST) for 2 h, at room temperature. The samples were developed with HRP-substrate (TMB stabilised substrate for HRP) for 30 min at room temperature and images of the section were captured by white-light microscopy.

3.2.8 Verification of the lack of endothelial cell antigens in AsPC-1 and WM-266-4 cancer cell lines

In order to highlight the infiltration of CAM vessels into tumours, AsPC-1 and WM-266-4 xenografts were implanted onto CAM. However, to ensure that these cell lines did not express any of the endothelial cell surface antigens, first the absence of these antigens on the cells was confirmed. AsPC-1 and WM-266-4 cells (5×10^4) were seeded in a 96-well plate and allowed to adhere overnight. Any cell surface expression of endothelial cell markers PECAM-1, VE-cadherin and vWF on the cell lines was examined by antibody binding assay (section 2.3.4.6) using the appropriate antibodies at dilutions stated in Table 3.1. The expression of the cancer cell marker EpCAM was also assessed alongside as a positive control.

3.2.9 Analysis of the influence of tinzaparin on the vessels associated with CAM-implanted tumours

To assess the vascularisation of the tumour xenografts implanted onto CAM which were dissected in section 3.2.6, the CAM sections were removed from ethanol and the xenografts carefully separated from the CAM using a scalpel. The sections were added to 10-well chamber slides and washed three times with PBST (200 µl). The sections were then incubated overnight with anti-PECAM-1 antibody

Table 3.1: Antibodies used for immunostaining for microscopy and antibody binding assay

Probing antibody				**Detection antibody**			
Antigen	Clone	Host species	Dilution	Antigen		Host species	Dilution
PECAM-1		Mouse	1:700	**Mouse IgG**	HRP	Rabbit	1:2000
EpCAM	1B7	Mouse	1:700	**Mouse IgG**	HRP	Rabbit	1:2000
VE-cadherin	55-7H1	Mouse	1:700	**Mouse IgG**	HRP	Rabbit	1:2000
vWF		Rabbit	1:700	**Rabbit IgG**	HRP	Goat	1:2000

(diluted 1:700 v/v in PBST) at 4°C. Selected sections were then washed three times in PBST, incubated with HRP-conjugated anti-mouse IgG antibody and assessed according to the protocol described in section 3.2.7. Images of the sections were captured by light microscopy and electronically randomised. The diameters of 4 randomly selected vessels (one from each quarter of the image) for each field of view were measured using ImageJ. The measurements were "decrypted" after the experiments and an average vessel diameter was calculated.

Alternatively, to precisely highlight the blood vessel densities, lengths and diameters, other CAM sections which had been incubated with the anti-PECAM-1 antibody, where developed with the fluorochrome NL493-conjugated anti-mouse IgG antibody (diluted 1:200 v/v in PBST). The sections were incubated for 2 h at room temperature and were then washed three times in PBST. Images were captured using a fluorescence microscope controlled by the Zen 2012 SP1 v8.1 software (Carl Zeiss Microscopy). The amount of fluorescence of the captured fields of view was assess using ImageJ as a measure of the density of vessels present.

3.3 Results

3.3.1 Assessment of the influence of LMWH on spheroid formation

Prior to experiments, studies were carried out to establish the cell lines which were capable of forming compact spheroids when cultured in non-adherent Nunclon Sphera 96-well plates. WM-266-4, AsPC-1 and MDA-MB-231 cells were shown to aggregate into spheroids following 4 days of incubation, whereas A375 and SK-MEL-2 cells did not aggregate (Figure 3.7). In addition, the optimal number of cells required for the formation of consistent spheroids was determined to be 2 x 10^3 cells when using either WM-266-4, AsPC-1 or MDA-MB-231 cells.

The influence of anticoagulants on spheroid formation was assessed, next. Supplementation of the AsPC-1 cells with 2 IU/ml of dalteparin resulted in reductions in spheroid diameter to an average of 1.7 mm compared to the untreated samples which averaged 2.5 mm (Figure 3.8). In addition, supplementation of WM-266-4 cells with either tinzaparin or dalteparin (2 IU/ml) resulted in the formation of multiple spheroids with an average diameter of between 0.9-1.2 mm (Figure 3.9) compared to untreated WM-266-4 cells which formed single spheroids, with average diameters of 2.0 mm. This indicated that the LMWH were impacting spheroid formation and preventing the cells from aggregating into a single spheroid. In order to investigate if the disruption in spheroid formation was due to LMWH influencing integrin mediated cell aggregation, WM-266-4 cell suspensions were treated with an inhibitory anti-β1 integrin antibody (AIIB2). Supplementation of the cells with this inhibitory antibody resulted in an increase in the average diameter of the spheroids formed to 3.4 mm, compared to untreated control cells (2 mm diameter) (Figure 3.10).

3.3.2 Assessment of the influence of LMWH and fXa inhibitors on cell invasion

Prior to the experiments, the ability of WM-266-4, MDA-MB-231 and AsPC-1 cells to invade into Cultrex spheroid invasion matrix was assessed. WM-266-4 and AsPC-1 cells were shown to invade into the matrix (Figure 3.11) with dissimilar rates, with WM-266-4 cells invading at a faster rate. Consequently, the matrix-invasion experiments were carried out for 3 days with WM-266-4 cells but for 5 days when using AsPC-1 cells. However, spheroids formed using MDA-MB-231 cells did not invade into the matrix within the period of the experiment and were not used further.

The influence of anticoagulants on cell invasion was assessed, next. Treatment of WM-266-4 cells with 2 IU/ml of tinzaparin or dalteparin resulted in reductions in invasion ratios to 0.15 ± 0.02 and 0.17 ± 0.01, respectively, compared to that of the untreated cells (0.22 ± 0.05) (Figure 3.12). Treatment of AsPC-1 cells produced a similar but smaller reduction in invasion ratio to 0.08 ± 0.02 and 0.09 ± 0.02 respectively, compared to untreated cells (0.10 ± 0.01) (Figure 3.13). Incubation of the spheroids

Figure 3.7: Optimisation of the number of cells required for spheroid formation

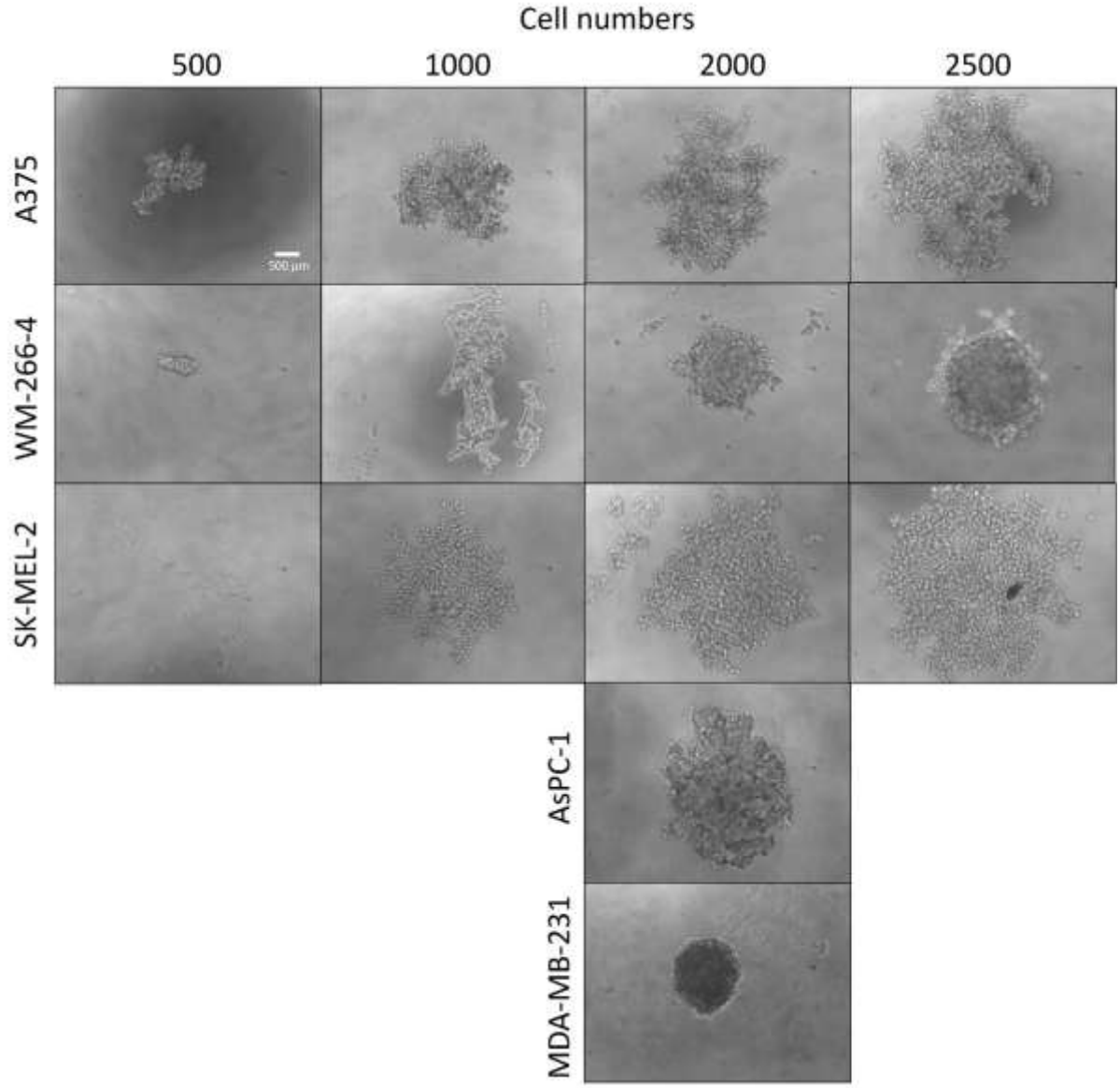

A range of numbers (0.5-2.5 x 10^3) of A375, WM-266-4, SK-MEL-2, AsPC-1 and MDA-MB-231 cancer cell lines were seeded in non-adherent 96-well plates. The cells were incubated for 4 days and monitored by bright field microscopy at x10 magnification (Images are representative of an experiment carried out in triplicate).

Figure 3.8: Assessment of the influence of tinzaparin and dalteparin on AsPC-1 cell spheroid formation

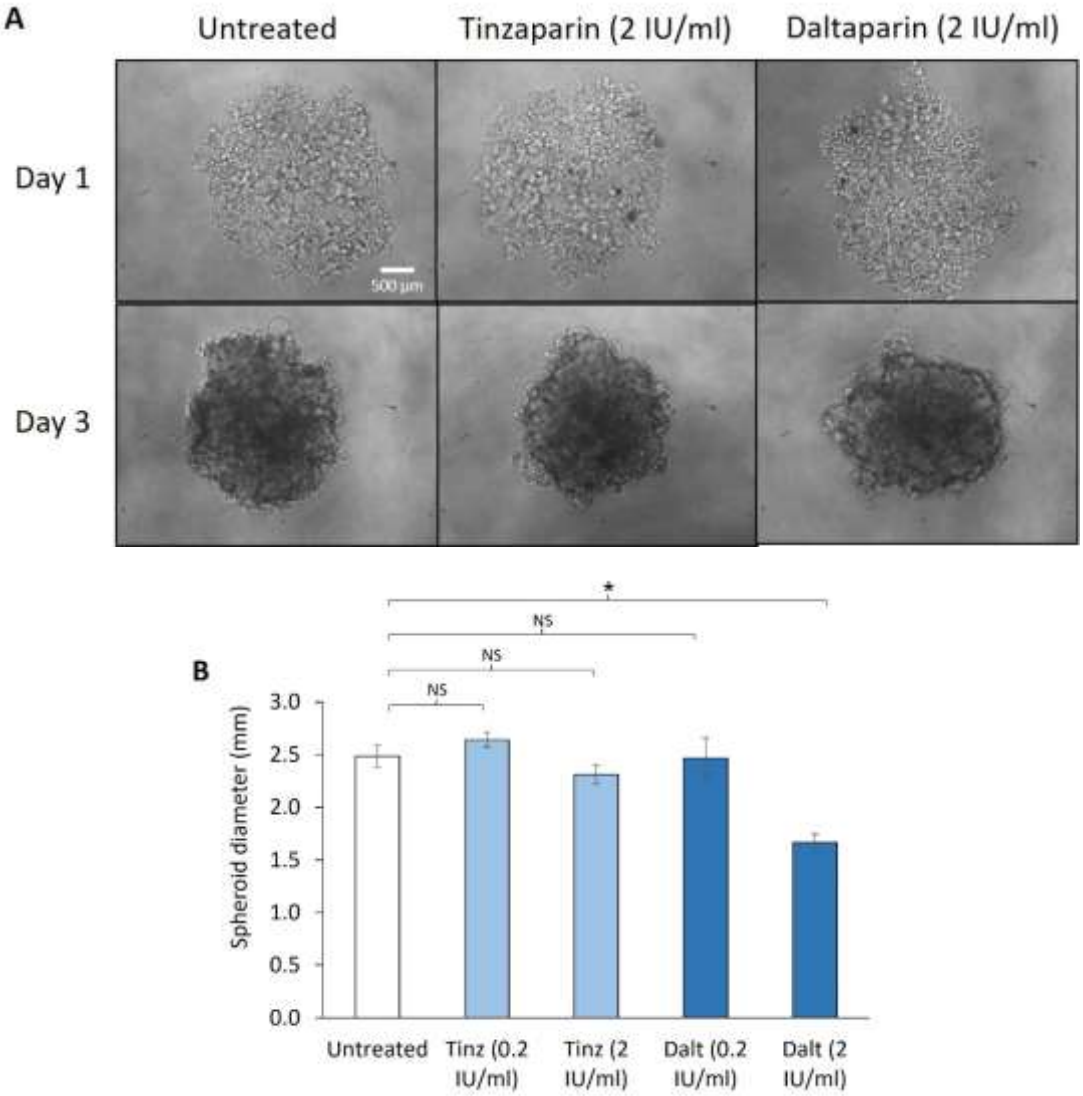

AsPC-1 cells (2×10^3) were seeded in non-adherent 96-well plates and supplemented with tinzaparin (0.2 & 2 IU/ml) or dalteparin (0.2 & 2 IU/ml). The plates were incubated at 37°C for 3 days and A) the spheroids were monitored by bright field microscopy at x10 magnification. B) The diameter of the spheroids formed were measured using ImageJ (n=6, two independent experiments carried out in triplicate; data = mean values ± SEM; independent t-test, NS = not significant * = $p < 0.05$).

Figure 3.9: Assessment of the influence of tinzaparin and dalteparin on WM-266-4 cell spheroid formation

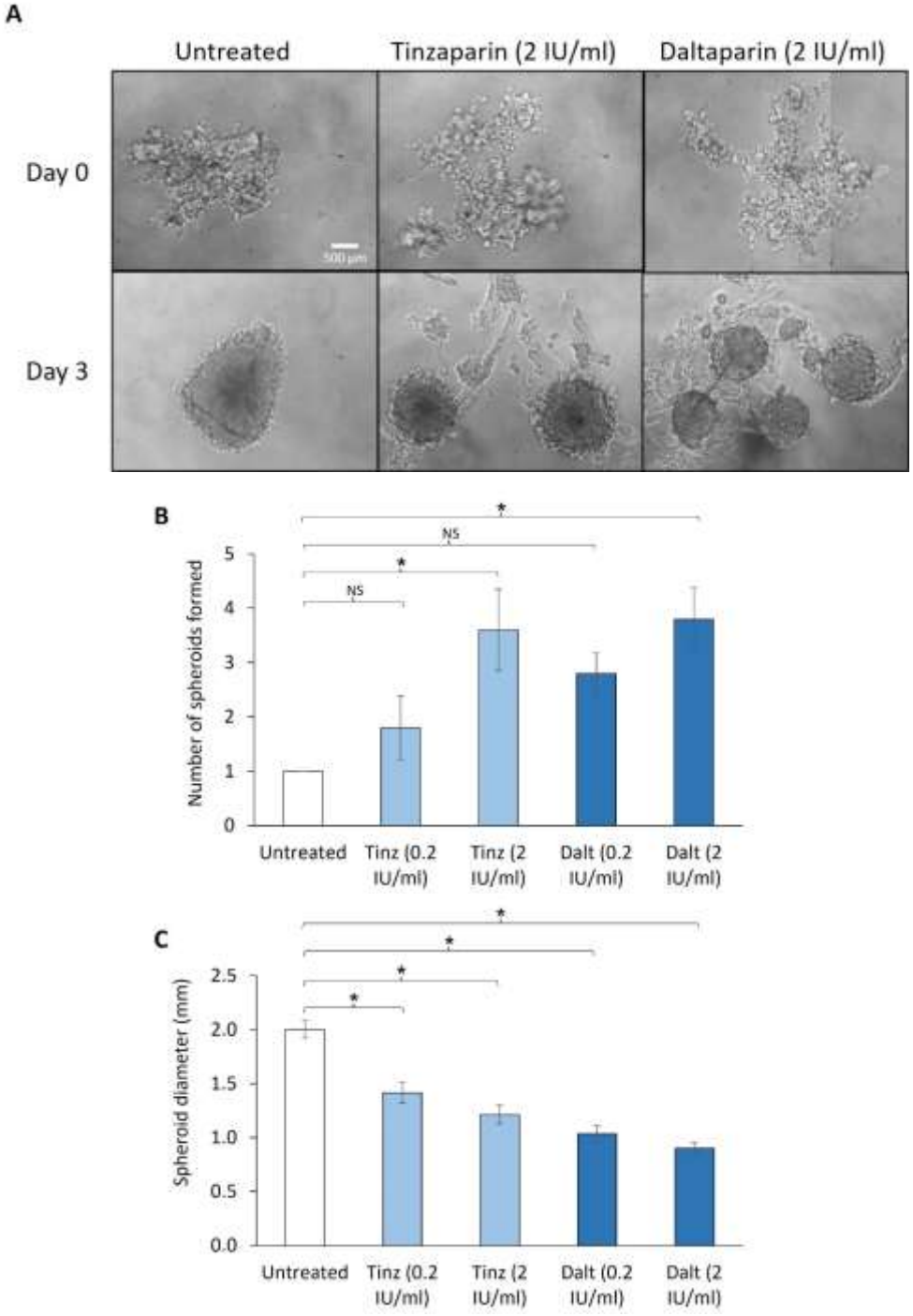

WM-266-4 cells (2×10^3) were seeded in non-adherent 96-well plates and supplemented with tinzaparin (0.2 & 2 IU/ml) or dalteparin (0.2 & 2 IU/ml). The plates were incubated at 37°C for 3 days and A) the spheroids were monitored by bright field microscopy at x10 magnification. B) The numbers of spheroids formed were recorded and C) the diameter of the spheroids formed were measured using ImageJ (n=6, two independent experiments carried out in triplicate; data = mean values ± SEM; independent t-test, NS = not significant * = $p < 0.05$)

Figure 3.10: Assessment of the influence of anti-β1 integrin antibody on WM-266-4 cell spheroid formation

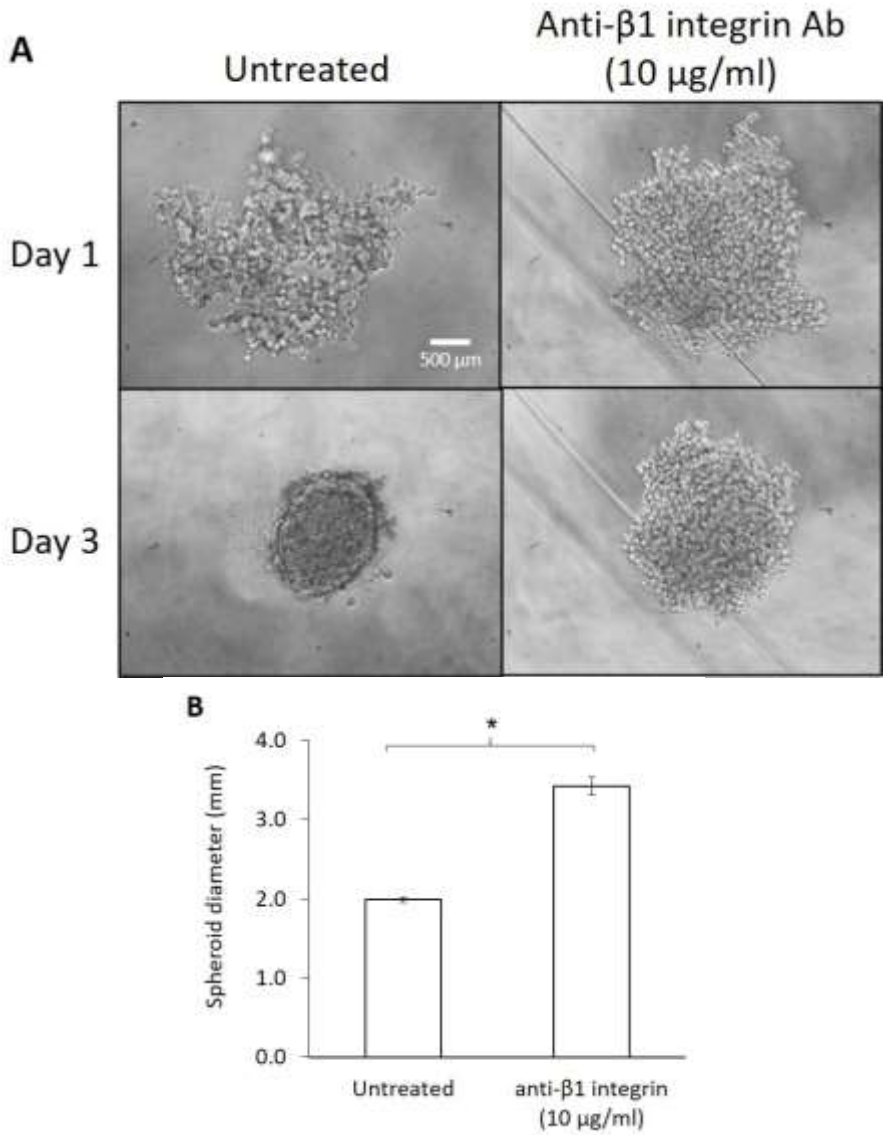

WM-266-4 cells (2×10^3) were seeded in non-adherent 96-well plates and supplemented with an inhibitory anti-β1 integrin antibody (AIIB2; 10 µg/ml). The plates were incubated at 37°C for 3 days and A) the spheroids were monitored by bright field microscopy at x10 magnification. B) The diameters of the formed spheroids were measured using ImageJ (n=6, two independent experiments carried out in triplicate; data = mean values ± SEM; independent t-test * = $p < 0.05$).

Figure 3.11: Assessment of the ability of cancer cells to invade into invasion matrix

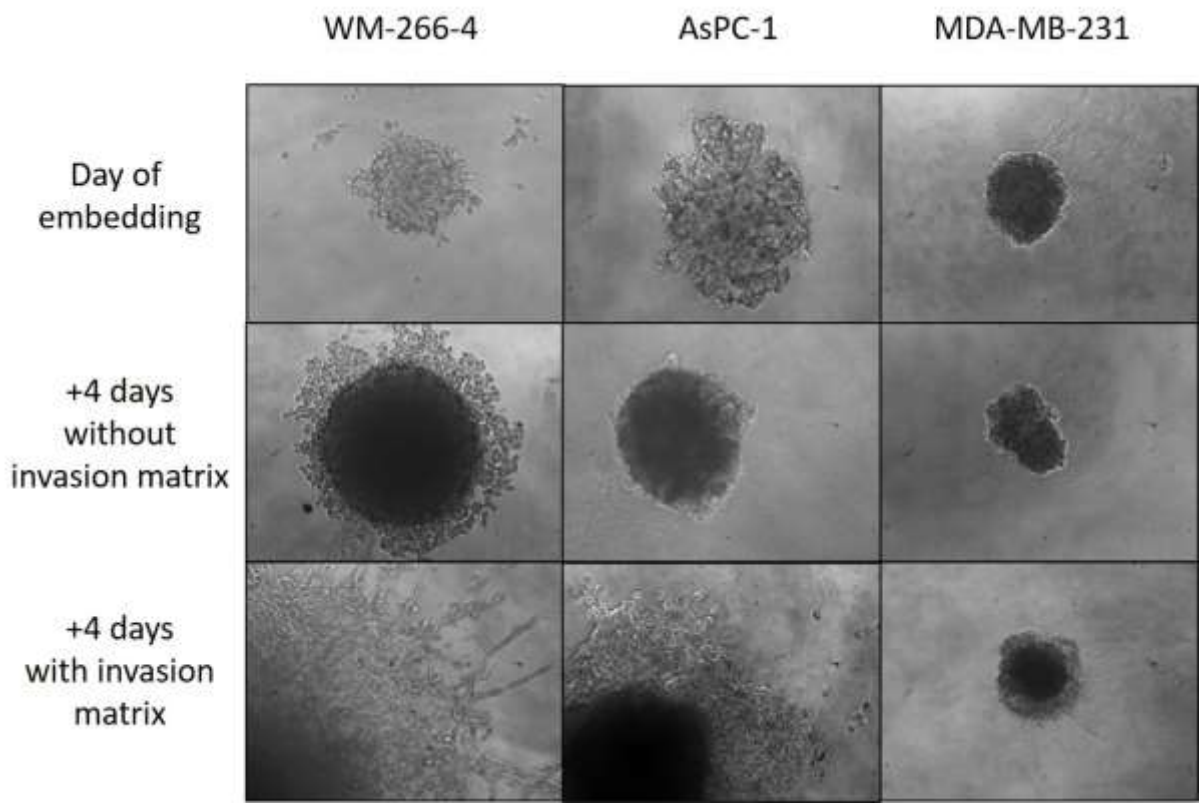

WM-266-4, AsPC-1 and MDA-MB-231 cells (2 x 10^3) were plated in non-adherent plates and allowed to form into spheroids for 4 days. The spheroids were then either embedded into invasion matrix or left in culture medium and incubated for an additional 4 days and the spheroids were monitored by bright field microscopy at x10 magnification (Images are representative of an experiment carried out in triplicate).

Figure 3.12: Assessment of the influence of tinzaparin and dalteparin on WM-266-4 cell spheroid invasion

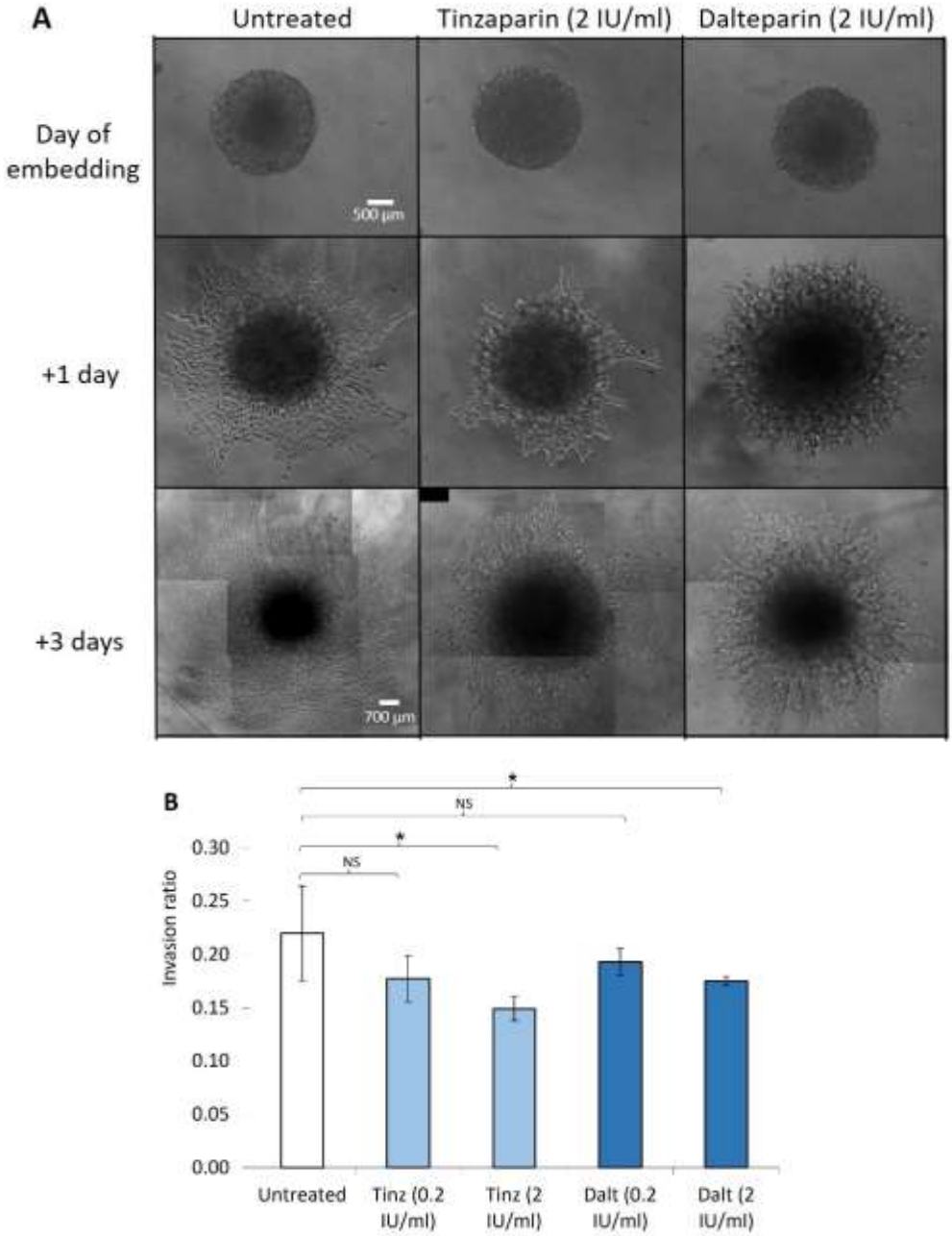

WM-266-4 cells (2×10^3) were seeded in non-adherent 96-well plates and incubated for 4 days to allow spheroids to form. The spheroids were embedded in invasion matrix and treated with tinzaparin (0.2 & 2 IU/ml) or dalteparin (0.2 & 2 IU/ml) for an additional 3 days. A) The spheroids were monitored by bright field microscopy at x10 magnification. B) The degree of invasion was assessed using ImageJ and the invasion ratios were calculated as the total area of invaded cells on the final day of treatment divided by the area of the spheroid on the day of embedding. Scale bar = 500 µm unless otherwise stated (n=6, 2 independent experiments carried out in triplicate; data = mean values ± SEM; independent t-test, NS = not significant * = $p < 0.05$).

Figure 3.13: Assessment of the influence of tinzaparin and dalteparin on AsPC-1 cell spheroid invasion

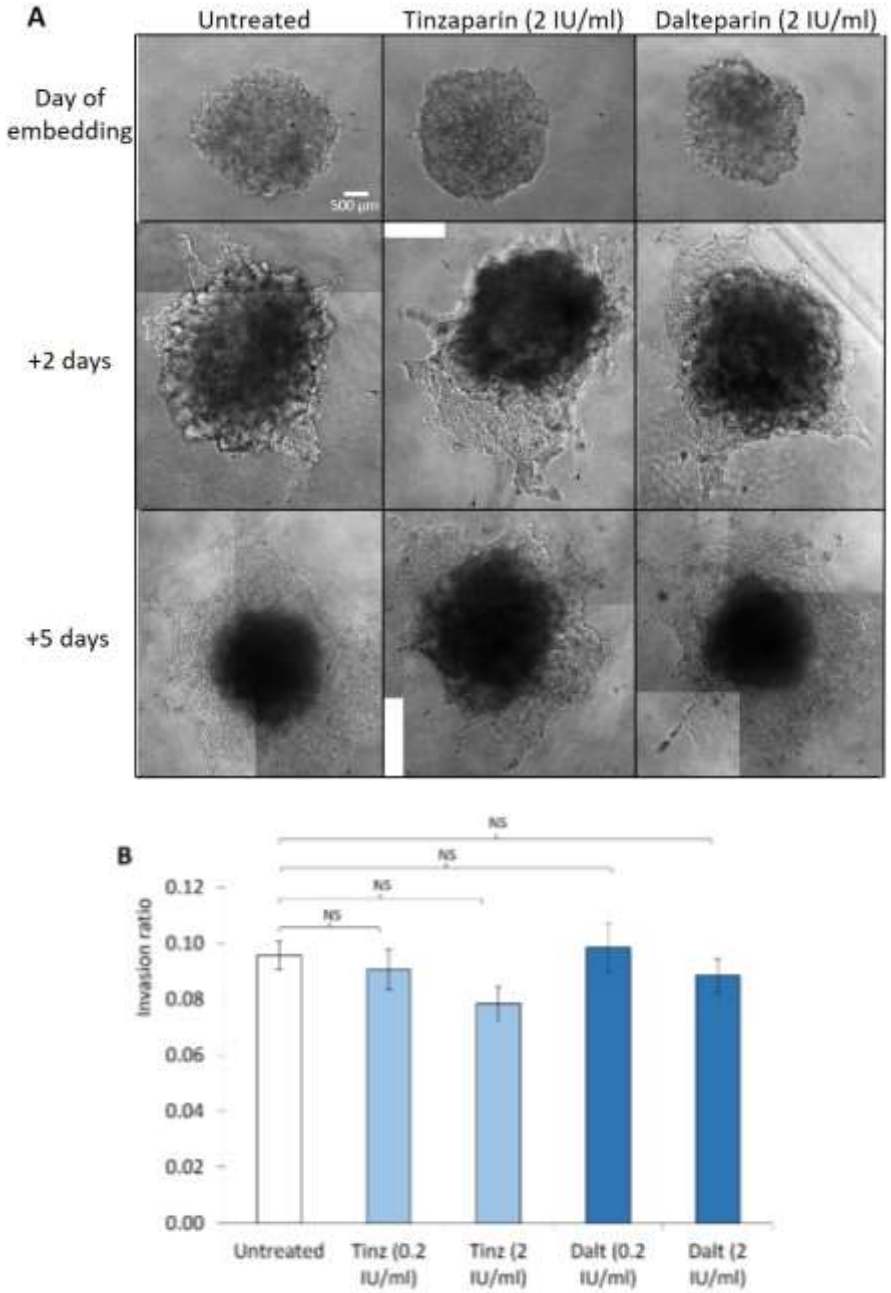

AsPC-1 cells (2×10^3) were seeded in non-adherent 96-well plates and incubated for 4 days to allow spheroids to form. The spheroids were embedded in invasion matrix and treated with tinzaparin (0.2 & 2 IU/ml) or dalteparin (0.2 & 2 IU/ml) for an additional 5 days. A) The spheroids were monitored by bright field microscopy at x10 magnification. B) The degree of invasion was assessed using ImageJ and the invasion ratios were calculated as the total area of invaded cells on the final day of treatment divided by the area of the spheroid on the day of embedding (n=6, 2 independent experiments carried out in triplicate; data = mean values ± SEM; independent t-test NS = not significant).

formed from either cell lines with apixaban or with rivaroxaban did not have any detectable influence on tumour invasiveness (Figure 3.14 & Figure 3.15).

3.3.3 Assessment of the influence of anticoagulants on CAM vessel angiogenesis

Supplementation of CAM with 5 IU/ml of tinzaparin resulted in reductions in vessel density score to 0.44 ± 0.1, compared to that of CAM treated with PBS (0.75 ± 0.06) (Figure 3.16B). Additionally, treatment with tinzaparin (5 IU/ml) reduced the average diameter of CAM vessels to 24 µm ± 4.1 compared to those observed with PBS (44 µm ± 3.7) (Figure 3.16C). As a comparison, the influence of tinzaparin on CAM vessels was compared to that of the established antiangiogenic agent, bevacizumab. Treatment of CAM with bevacizumab (12.5 µg/ml) resulted in reductions in vessel density score to 0.56 ± 0.13 compared to that of CAM treated with PBS (0.75 ± 0.06) (Figure 3.17B). Furthermore, treatment with bevacizumab marginally reduced the average diameter of CAM vessels from 44 µm ± 3.7 in CAM treated with PBS, to 38 µm ± 3.8 (Figure 3.17C).

In order to determine if the reductions in vessel density and diameter following tinzaparin treatment, arose from the anti-fXa activity of this anticoagulant, CAM were also treated with the direct fXa inhibitors, apixaban and rivaroxaban. However, treatment of CAM with these inhibitors did not alter either the density or the diameter of the CAM vessels (Figure 3.18).

3.3.4 Assessment of the influence of anticoagulants on the growth of cancer cell xenografts implanted into CAM

Prior to experiments, the number of cells required to establish cellular tumour xenografts on CAM was determined. Studies using a range of cell numbers indicated that inoculation of CAM with 2 x 10^6 WM-266-4 cells resulted in tumour formation on 80% of the samples (Table 3.2A). In contrast, inoculation of CAM with 5 x 10^5 and 10^6 cells resulted in the establishment of tumours on 20% and 60% of CAM, respectively. Similarly, 63% of CAM inoculated with AsPC-1 cells (2 x 10^6) developed tumours (Table 3.2B) but the rate of successful xenografts was lower with MDA-MB-231 (43%) and MCF-7 cells (13%). Therefore, only AsPC-1 and WM-266-4 cell lines were used in further experiments.

Any independent ability of anticoagulants to influence the growth of CAM-implanted tumour xenografts was assessed, next. Treatment of implanted AsPC-1 tumours with apixaban (1 µg/ml) resulted in a reduction in the average tumour area from 3.85 mm^2 ± 2.03 on the first day of treatment to 2.58 mm^2 ± 1.10 following 4 days of treatment. In contrast, tumours treated with the DMSO control remained unchanged (Day 0 = 4.52 mm^2 ± 1.18, Day 4 = 4.27 mm^2 ± 0.88) (Figure 3.19). Similarly, treatment of WM-266-4 tumours with apixaban (1 µg/ml) reduced the area of the tumour xenografts from 10.52 mm^2 ± 1.46 on day 0 to 7.17 mm^2 ± 1.67 on day 4, whereas those treated with

Figure 3.14: Assessment of the influence of apixaban and rivaroxaban on WM-266-4 cell spheroid invasion

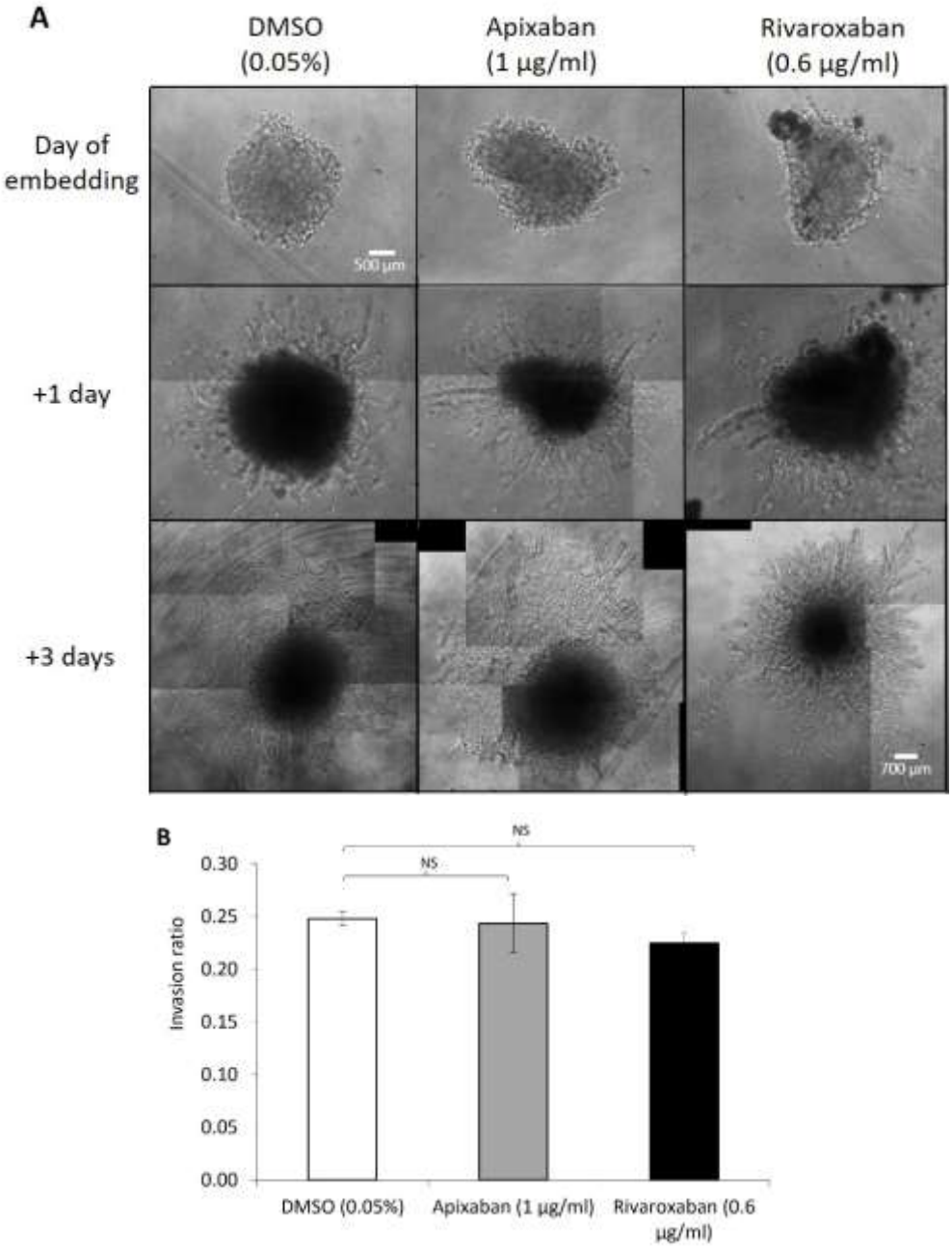

WM-266-4 cells (2×10^3) were seeded in non-adherent 96-well plates and incubated for 4 days to allow spheroids to form. The spheroids were embedded in invasion matrix and treated with apixaban (1 µg/ml) or rivaroxaban (0.6 µg/ml) for an additional 3 days. A) The spheroids were monitored by bright field microscopy at x10 magnification. B) The degree of invasion was assessed using ImageJ and the invasion ratio was calculated as the total area of invaded cells on the final day of treatment divided by the area of the spheroid on the day of embedding. Scale bar = 500 µm unless otherwise stated (n=6, 2 independent experiments carried out in triplicate; data = mean values ± SEM; independent t-test NS = not significant).

Figure 3.15: Assessment of the influence of apixaban and rivaroxaban on AsPC-1 cell spheroid invasion

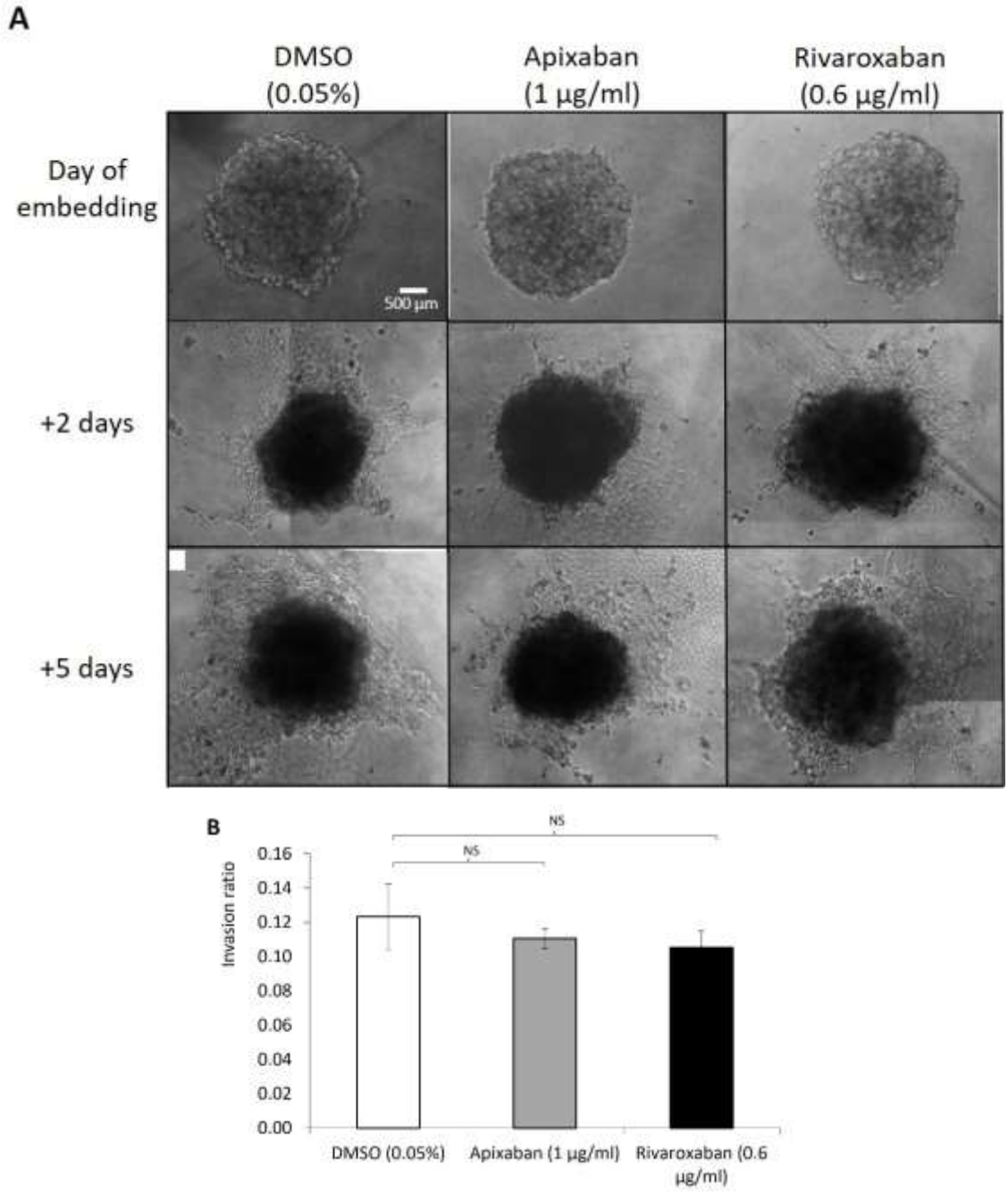

AsPC-1 cells (2 x 10^3) were seeded in non-adherent 96-well plates and incubated for 4 days to allow spheroids to form. The spheroids were embedded in invasion matrix and treated with apixaban (1 µg/ml) or rivaroxaban (0.6 µg/ml) for an additional 5 days. A) The spheroids were monitored by bright field microscopy at x10 magnification. B) The degree of invasion was assessed using ImageJ and the invasion ratio was calculated as the total area of invaded cells on the final day of treatment divided by the area of the spheroid on the day of embedding (n=6, 2 independent experiments carried out in triplicate; data = mean values ± SEM; independent t-test NS = not significant).

Figure 3.16: Assessment of the influence of tinzaparin on CAM vessel formation

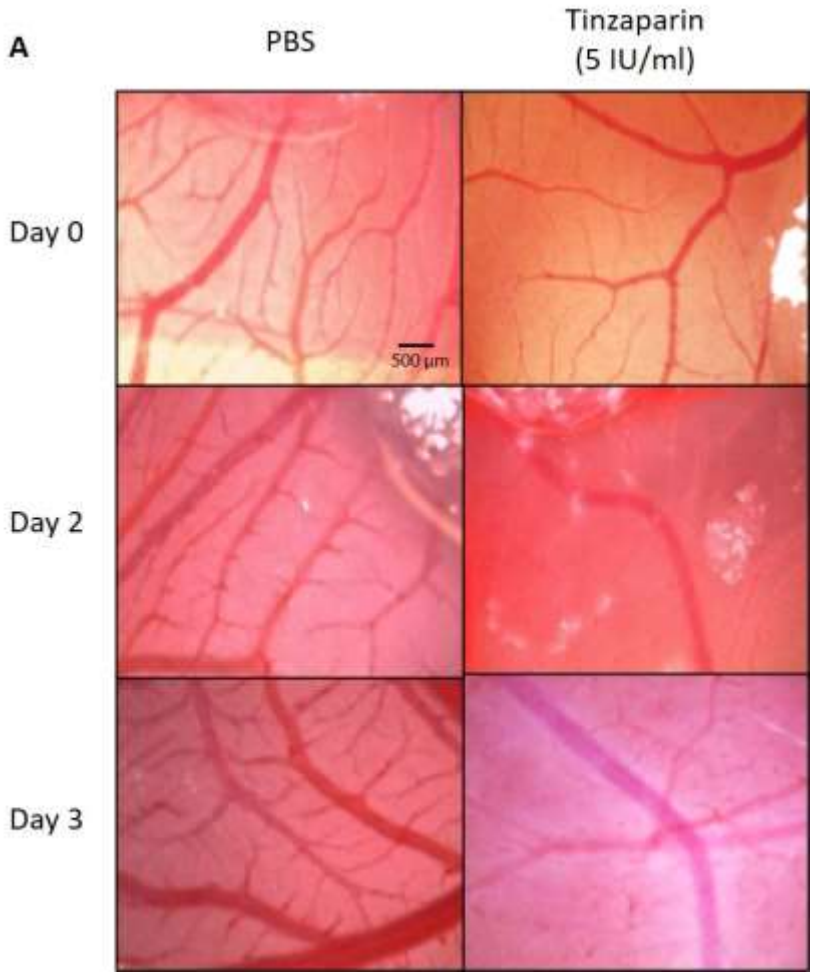

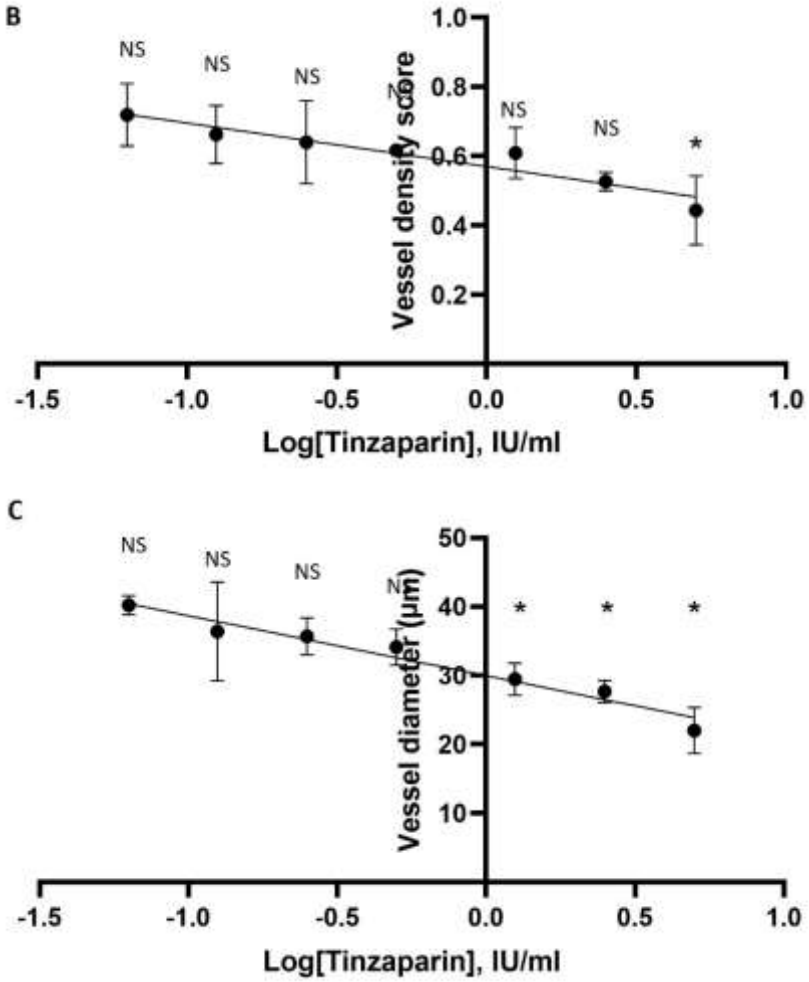

CAM was treated with sterile gelatin sponge containing tinzaparin (0.063-5 IU/ml) or PBS control for 3 days. A) The CAM were monitored daily and real time images of the CAM vessels were captured using a stereomicroscope at x10 magnification. B) The vessel density of each field of view was scored and C) the vessel diameters were measured using ImageJ (n = 7; 4 fields of view from 7 independent experiments; data = mean values ± SEM; independent t-test vs PBS, * = $p < 0.05$, NS = not significant).

Figure 3.17: Assessment of the influence of bevacizumab on CAM vessel formation

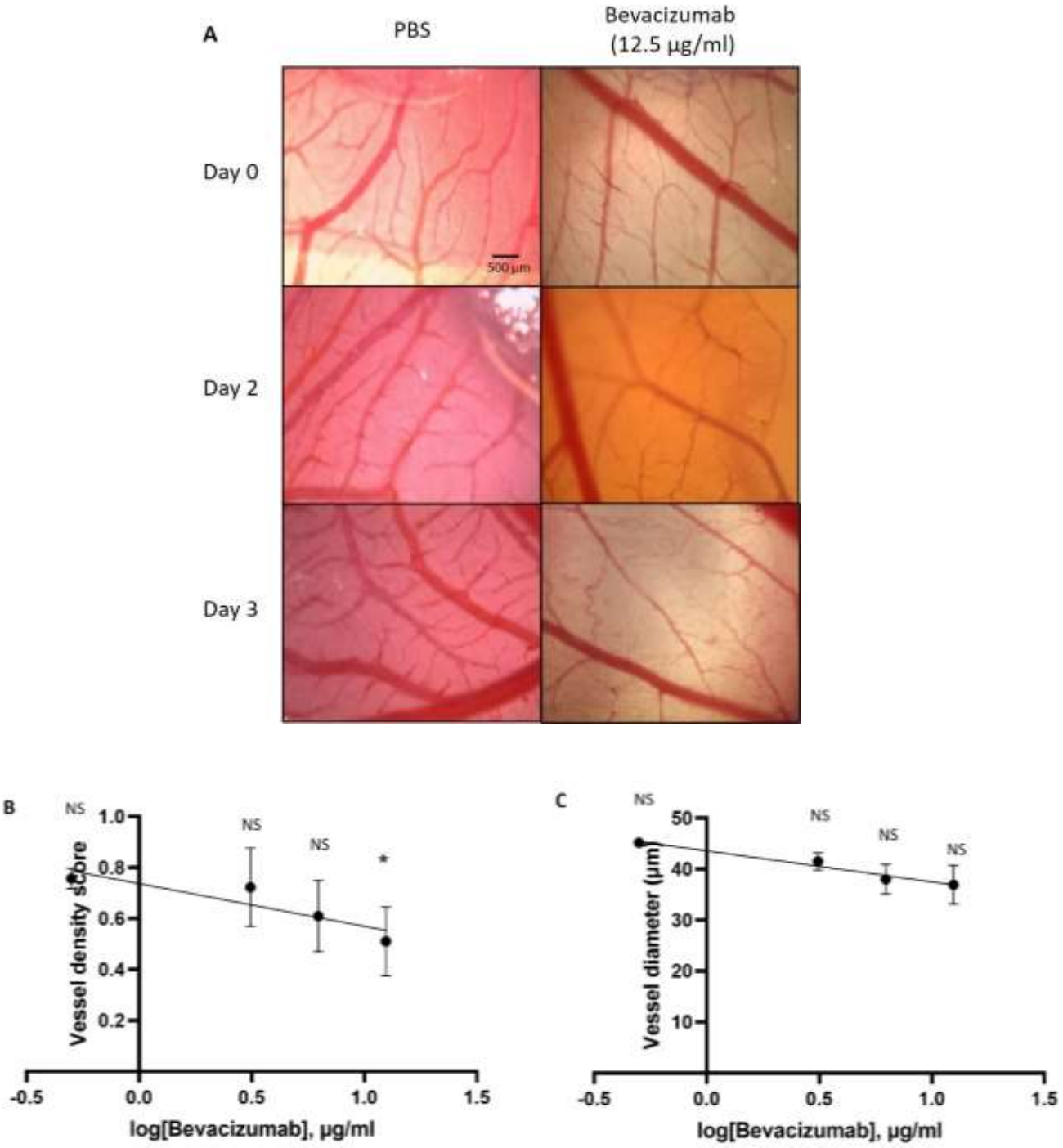

CAM was treated with sterile gelatin sponge containing bevacizumab (0.5-12.5 µg/ml) or PBS control for 3 days. A) The CAM were monitored daily and real time images of the CAM vessels were captured using a stereomicroscope at x10 magnification. B) The vessel density of each field of view was scored and C) the vessel diameters were measured using ImageJ (n = 7; 4 fields of view from 7 independent experiments; data = mean values ± SEM; independent t-test vs PBS, NS = not significant * = $p < 0.05$).

Figure 3.18: Assessment of the influence of rivaroxaban and apixaban on CAM vessel formation

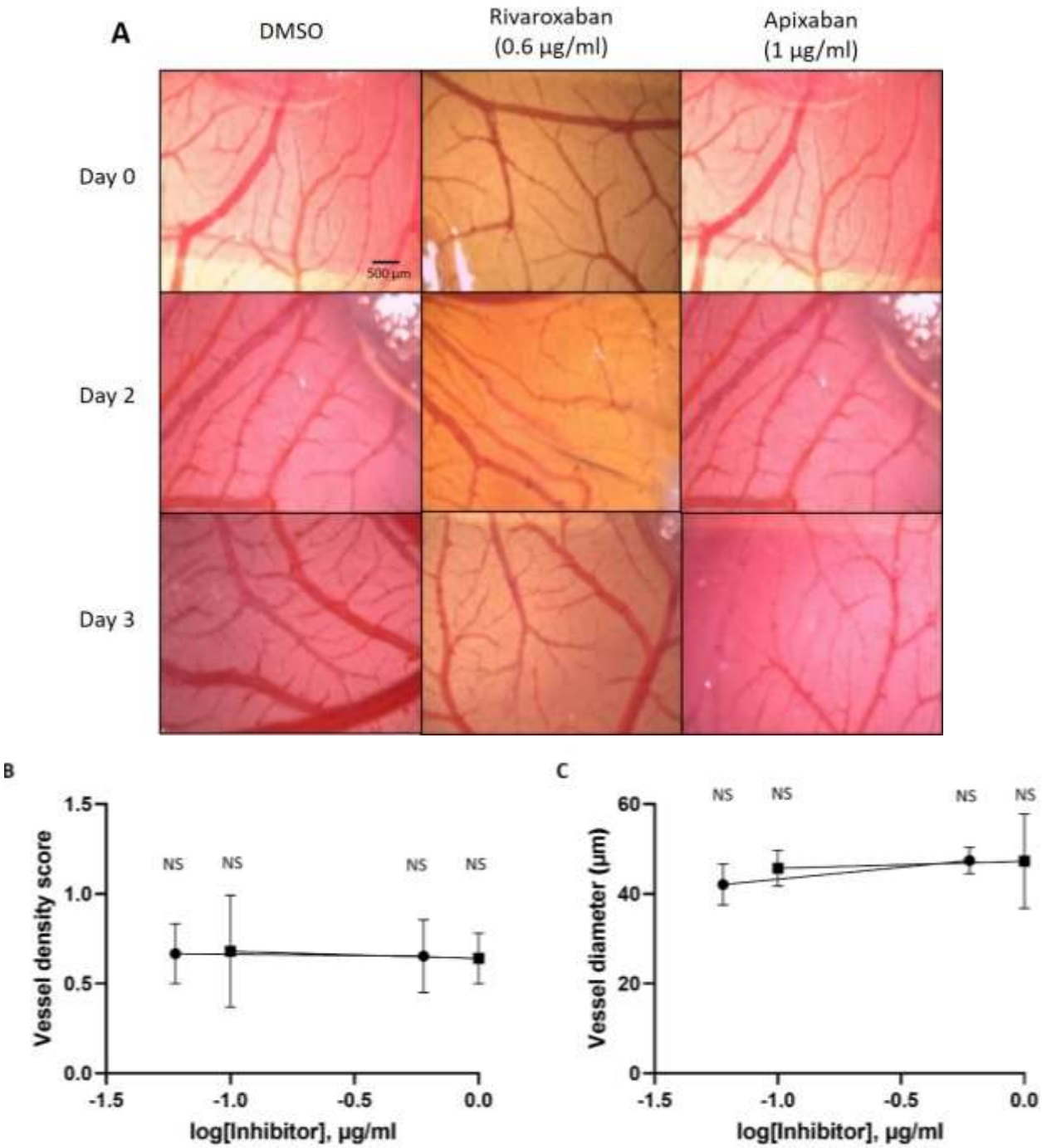

CAM was treated with sterile gelatin sponge containing apixaban (-■-, 0.1 & 1 µg/ml), rivaroxaban (-●-, 0.06 & 0.6 µg/ml) or DMSO control for 3 days. A) The CAM were monitored daily and real time images of the CAM vessels were captured using a stereomicroscope at x10 magnification. B) The vessel density of each field of view was scored and C) the vessel diameters were measured using ImageJ (n = 7; 4 fields of view from 7 independent experiments; data = mean values ± SEM; independent t-test vs PBS, NS = not significant).

Table 3.2: Optimisation of implantation of cancer cell lines onto CAM

A

Cell concentration (cells/µl)	Tumour development rate
1 x 10^5	20%
2 x 10^5	60%
4 x 10^5	80%

B

Cancer cell line	Tumour development rate
AsPC-1	63%
MDA-MB-231	43%
MCF-7	13%

A) WM-266-4 cells were resuspended in ice cold matrigel at a range of concentrations of 1-4 x 10^5 cells/µl. B) AsPC-1, MDA-MB-231 and MCF-7 cells (4 x 10^5 cells/µl) were resuspended in ice cold matrigel. Vessels within exposed CAM were disrupted by dabbing with a sterile cotton swab and 5 µl of the cell suspensions were added to the areas. The eggs were incubator at 37°C for 3 days to allow tumour to consolidate and the rate of tumour formation was recorded.

Figure 3.19: Assessment of the influence of apixaban on the growth of CAM-implanted tumours

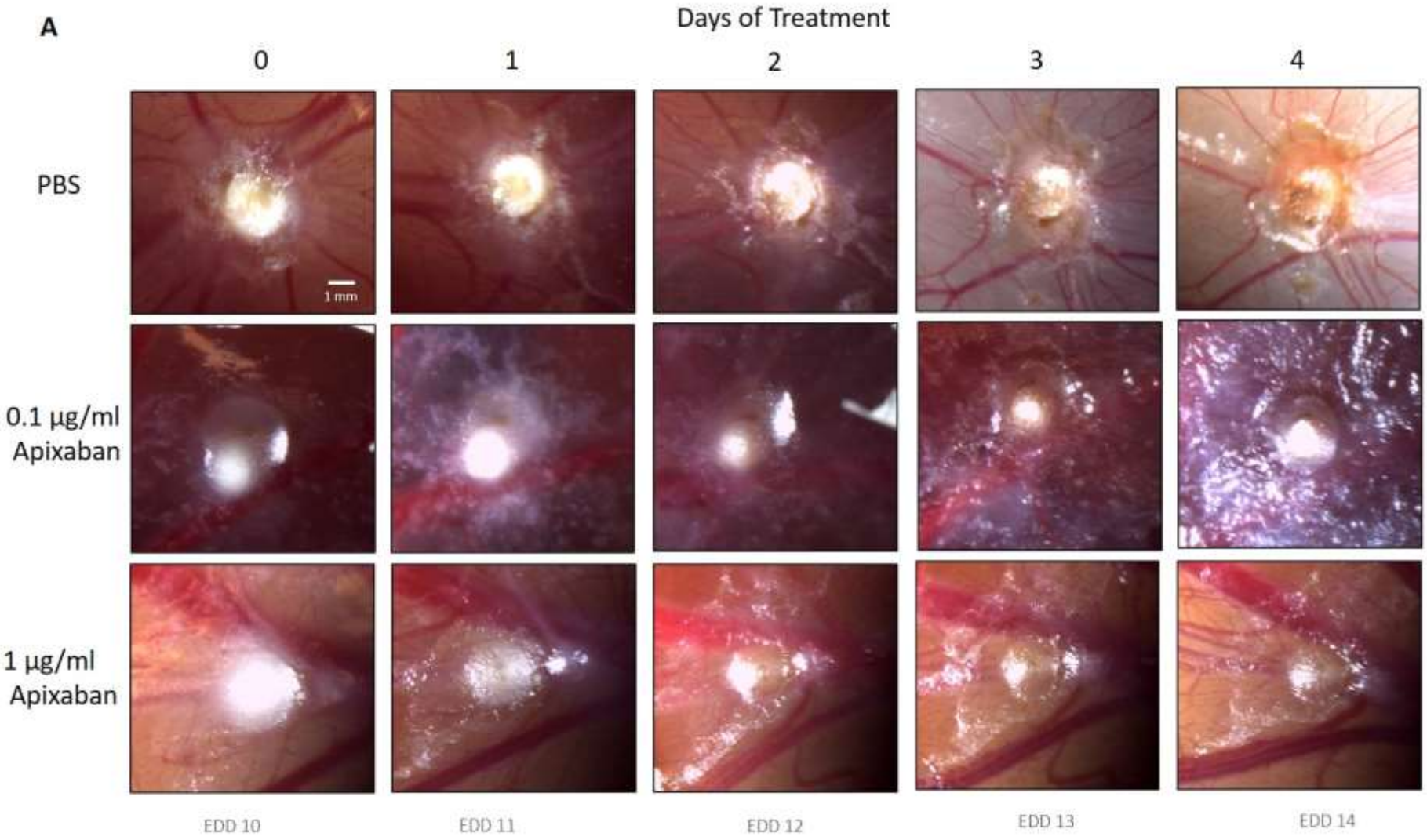

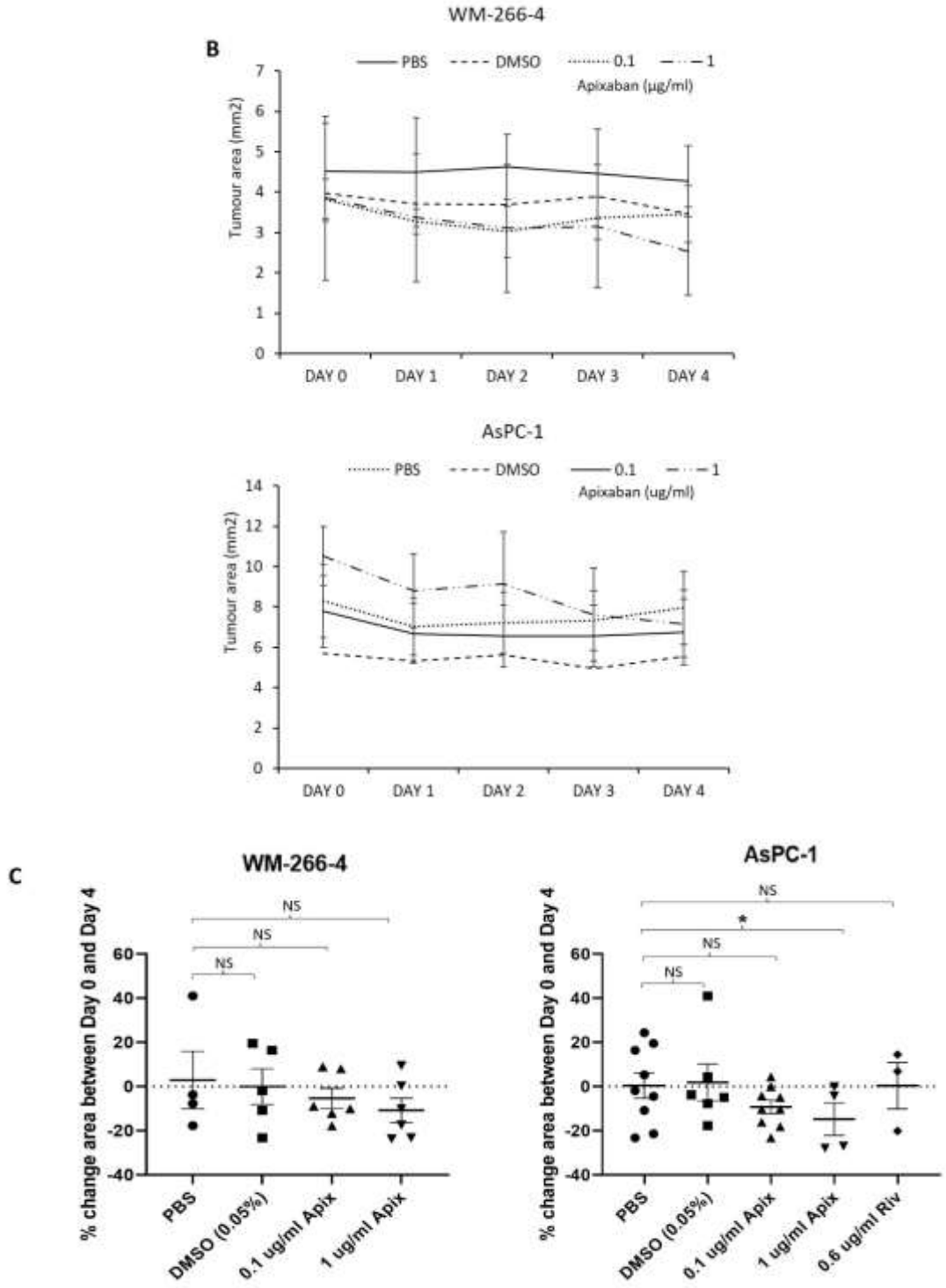

WM-266-4 and AsPC-1 cells (2 x 10^6) were implanted onto CAM and allowed to form into tumours for 3 days. Tumours were treated with apixaban (0.1 & 1 µg/ml), rivaroxaban (0.6 µg/ml) and DMSO vehicle control daily, for up to 4 days. The tumours were monitored daily and real time images were captured using a stereomicroscope at x5 magnification. A) Representative images of AsPC-1 cell xenografts. B) The tumour areas were measured using ImageJ and C) the percentage change values were calculated as 100 x (area on day 4 – area on day 1) / area on day 1 (n = 4, Images represent 4 experiments; data = mean values ± SEM; independent t-test, NS = not significant * = $p < 0.05$).

DMSO vehicle control remained unchanged (Day 0 = 8.29 mm^2 ± 1.82, Day 4 = 7.95 mm^2 ± 1.80) (Figure 3.19). In contrast, treatment of WM-266-4 tumour xenografts with rivaroxaban (0.6 µg/ml) did not influence the overall tumour areas, over the course of the experiments (Figure 3.19). Finally, treatment of either AsPC-1 or WM-266-4 tumour xenografts with tinzaparin also did not influence the area of the tumour xenografts over the course of the experiments (Figure 3.20).

3.3.5 Optimisation of the visualisation of infiltrating CAM vessels into implanted tumour xenografts

Prior to the examination of the vascularisation of the implanted CAM tumours, the visualisation of CAM blood vessels using immunomicroscopy was optimised. Vessels were visible in CAM sections probed with antibodies against VE-cadherin, PECAM-1 and EpCAM (Figure 3.21). In contrast, vessels were absent in the control CAM sections probed with mouse IgG isotype antibody.

In addition, any aberrant expression of endothelial cell antigens in cancer cells was discounted. To achieve this, AsPC-1 and WM-266-4 cells were probed with anti-VE-cadherin, PECAM-1 and vWF antibodies. Examination of either of these cell lines using the appropriate antibodies confirmed the absence of VE-cadherin and PECAM-1 (Figure 3.22A & Figure 3.22B). However, examination of AsPC-1 cells showed the presence of vWF on the surface of these cells indicated by an increase in absorption to 1.19 ± 0.16 compared to control cells (0.08 ± 0.08) (Figure 3.22A). Similarly, WM-2664 cells were shown to express cell surface vWF, indicated by an increase in absorption to 0.94 ± 0.07 compared to control cells (0.02 ± 0.01) (Figure 3.22B). Consequently, vWF was not used to examine the vascularisation of the implanted CAM tumours. Finally as a positive control, the expression of the cancer cell marker EpCAM on the cell surface was assessed alongside. Examination of AsPC-1 cells showed the presence of EpCAM on the cell surface as indicated by an increase in absorption to 0.71 ± 0.04 compared to control cells (0.07 ± 0.06) (Figure 3.22A). In contrast, examination of WM-2664 cells indicated an absence of cell surface EpCAM (Figure 3.22B). These observations are consistent with previous studies demonstrating the presence of EpCAM on the surface of AsPC-1 cells (Bao et al., 2011; Kim et al., 2012) but not WM-266-4 cells (Jung et al., 2014).

3.3.6 Examination of the influence of LMWH on the vascularisation of implanted CAM tumours

The influence of LMWH on the vascularisation of CAM-implanted tumour xenografts was assessed next. AsPC-1 and WM-266-4 cell xenografts were treated with tinzaparin for 4 days and then excised from the egg and separated from the CAM. The extent of vascularisation of the CAM beneath the

Figure 3.20: Assessment of the influence of tinzaparin on CAM-implanted tumour growth

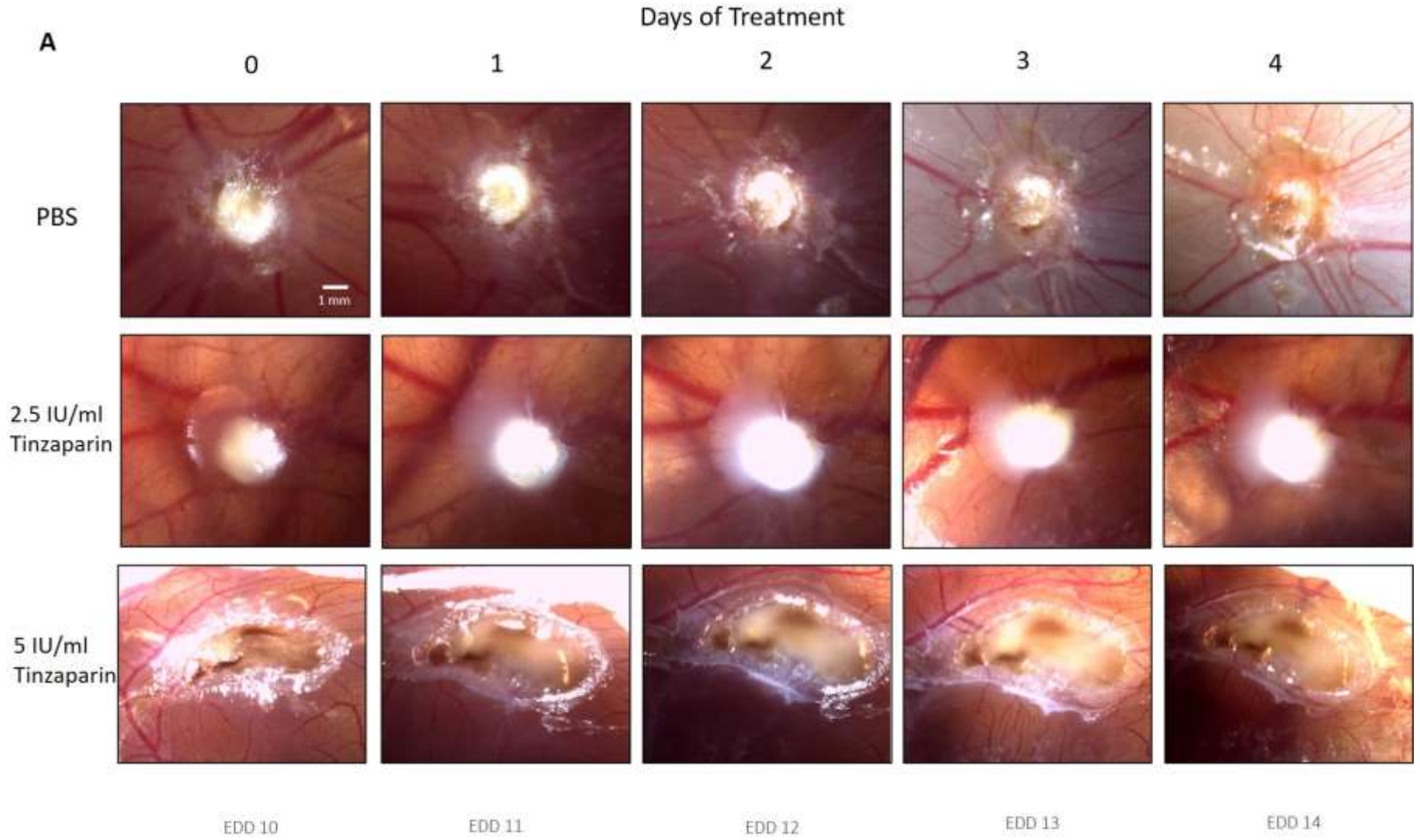

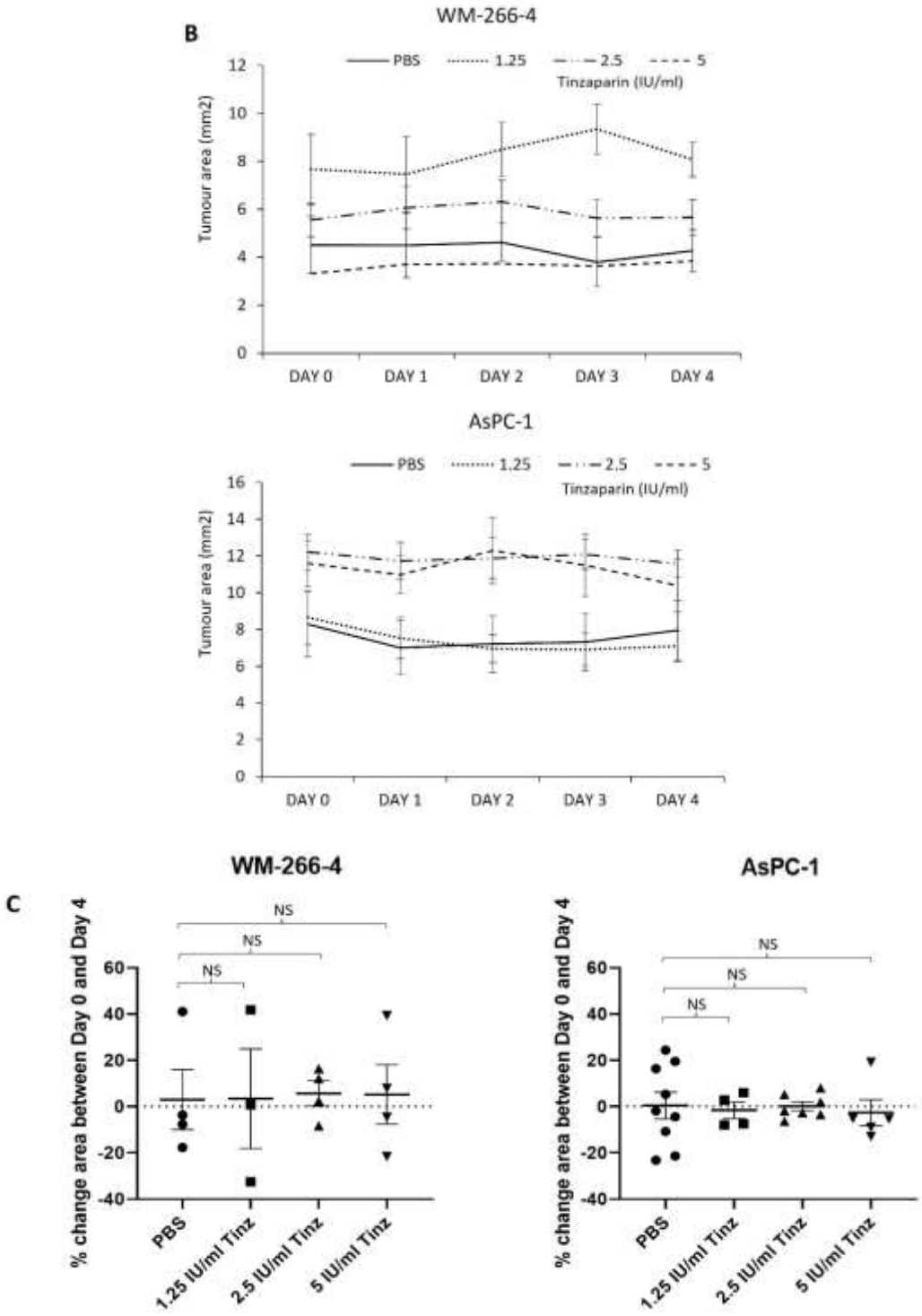

WM-266-4 and AsPC-1 cells (2 x 10^6) were implanted onto CAM and allowed to form into tumours for 3 days. Tumours were treated with tinzaparin (1.25-5 IU/ml) or PBS control daily, for up to 4 days. The tumours were monitored daily and real time images were captured using a stereomicroscope at x5 magnification. A) Representative images of AsPC-1 cell xenografts. B) The tumour areas were measured using ImageJ and C) the percentage change values were calculated as 100 x (area on day 4 – area on day 1) / area on day 1 (n = 4, Images represent 4 experiments; data = mean values ± SEM; independent t-test, * = $p < 0.05$ NS = not significant).

Figure 3.21: Assessment of the expression of endothelial cell markers by CAM tissue

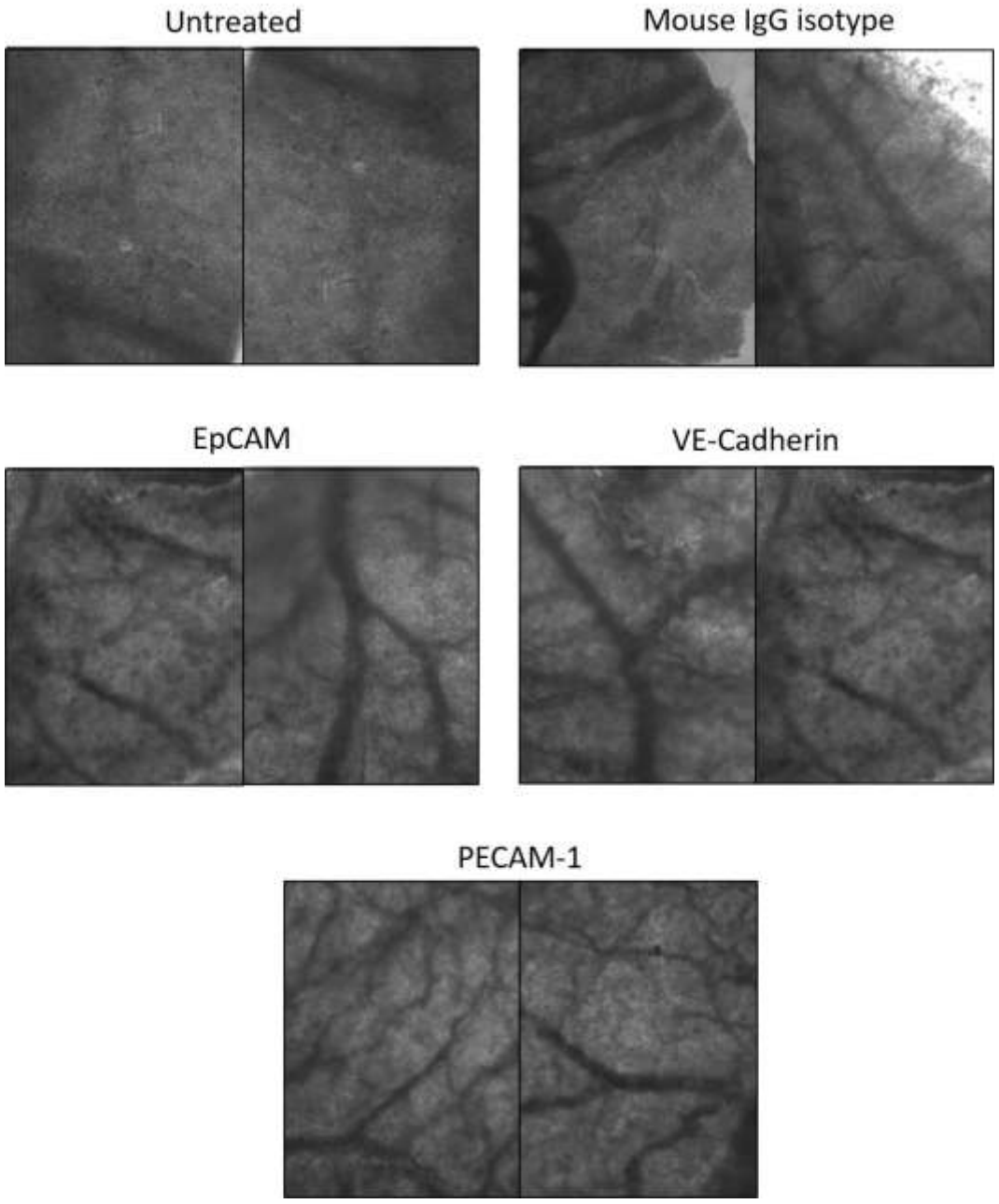

Sections of CAM excised from eggs at EDD 13 were cut into 25 mm^2 sections and fixed in 4% (v/v) paraformaldehyde. The sections were probed with anti-EpCAM, VE-cadherin and PECAM-1 antibodies as well as mouse IgG isotype antibody (diluted 1:700 v/v in PBST). The sections were then probed with an HRP-conjugated anti-mouse antibody (diluted 1:2000 v/v in PBST) and developed using TMB stabilised substrate for HRP. The samples were imaged by white-light microscopy at x10 magnification (Images represent four fields of view from two independent experiments).

Figure 3.22: Assessment of the expression of endothelial cell markers by cancer cell lines

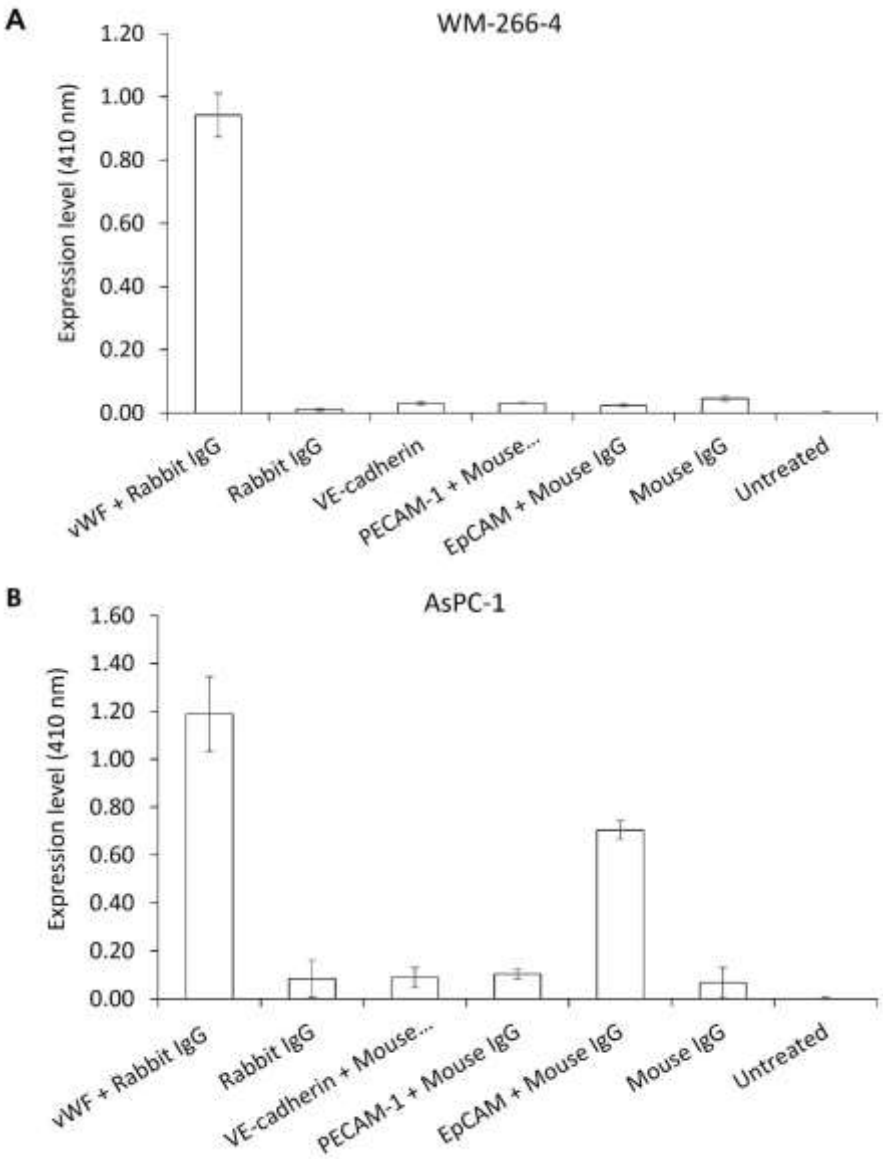

WM-266-4 and AsPC-1 cells (5 x 10^4) were plated in 96-well plates. The cells were probed with antibodies against vWF, VE-cadherin, PECAM-1, and EpCAM (diluted 1:700 v/v in PBST). The cells were probed with HRP-conjugated anti-rabbit IgG or anti-mouse IgG antibody as appropriate (diluted 1:2000 v/v in PBST) and developed using TMB-one solution HRP substrate. The amount of bound antibody was quantified by measuring the absorptions at 450 nm using a plate reader (n=4 two experiments carried out in duplicate; data = mean values ± SEM).

tumour masses was analysed. The implantation of the tumour xenografts resulted in an increase in CAM vascularisation as indicated by increases in average vessel diameter beneath the xenografts (AsPC-1 = 45.5 µm ± 2.9, WM-266-4 = 42.9 µm ± 7.1, no tumour = 37.5 µm ± 3.28). Treatment of the AsPC-1 cell xenografts with tinzaparin (5 IU/ml) for 4 days resulted in a reduction in vessel diameter to 35.3 µm ± 3.0 (Figure 3.23B). Similarly, treatment of the WM-266-4 cell xenografts with tinzaparin (5 IU/ml) resulted in a reduction in vessel diameter to 30.9 µm ± 4.9 (Figure 3.23B). These observations were further confirmed using fluorescence microscopy to highlight the vascular tissue. In addition, the amount of fluorescence of the captured fields of view was assessed as a measure of the density of vessels present. The treatments with tinzaparin (5 IU/ml) resulted in a decrease in vessel density beneath the xenografts as indicated by a decrease in fluorescence compared with control CAM sections treated with PBS (Figure 3.24).

Figure 3.23: Examination of the influence of tinzaparin on the diameter of CAM vessels supporting the implanted tumours

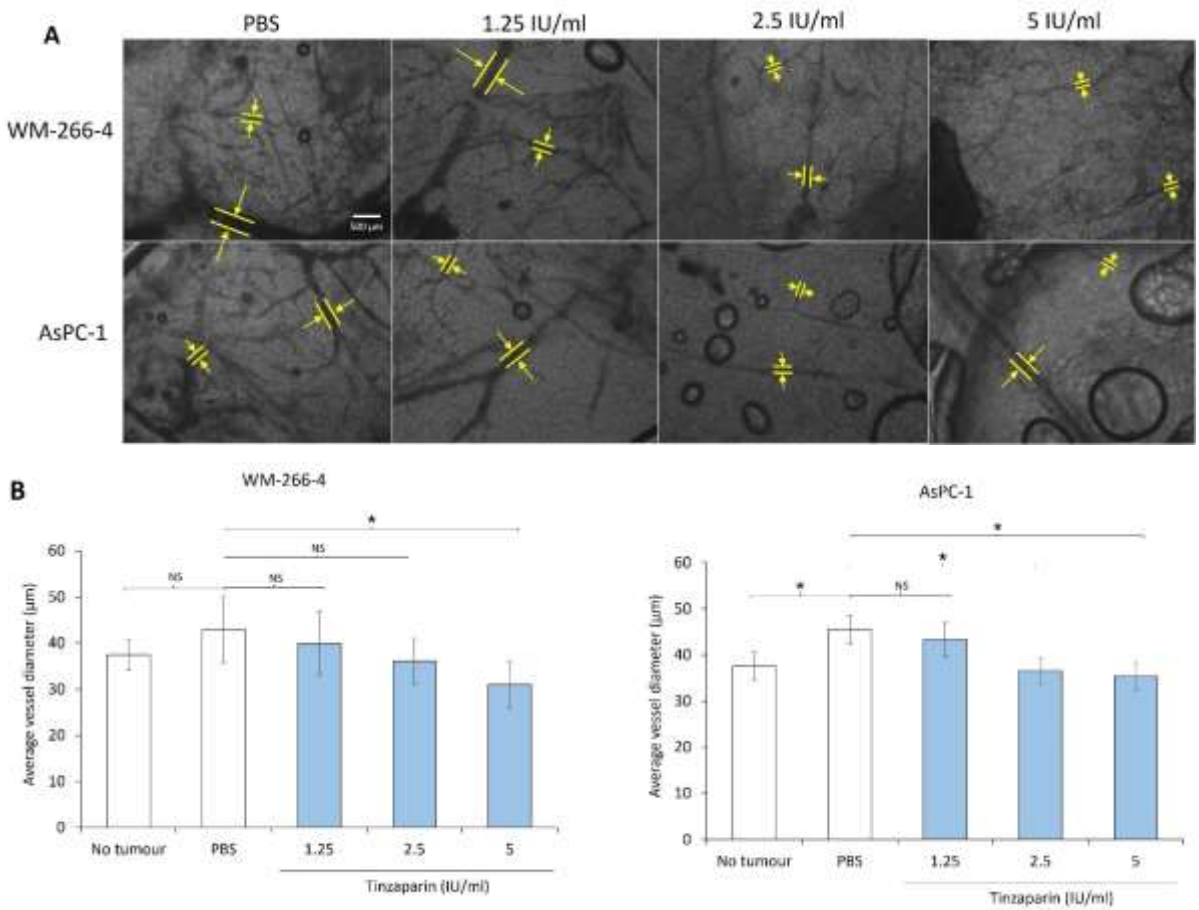

CAM-implanted WM-266-4 and AsPC-1 cell tumours were treated with tinzaparin (1.25-5 IU/ml) or PBS control for 4 days. The tumours and surrounding CAM tissue were excised and fixed in 4% (v/v) paraformaldehyde. The tumours were then separated from the underlying CAM and the CAM sections were probed with anti-PECAM-1 antibody (diluted 1:700 v/v in PBST). The sections were then probed with an HRP-conjugated anti-mouse antibody (diluted 1:2000 v/v in PBST) and developed using TMB stabilised substrate for HRP. A) The samples were imaged by white-light microscopy at x10 magnification. B) The average diameters of the CAM vessels were measured using ImageJ (n = 12, 4 fields of view from 3 independent samples; data = mean values ± SEM; independent t-test, * = $p < 0.05$ NS = not significant).

Figure 3.24 Examination of the influence of tinzaparin on the vessel density of CAM supporting the implanted tumours

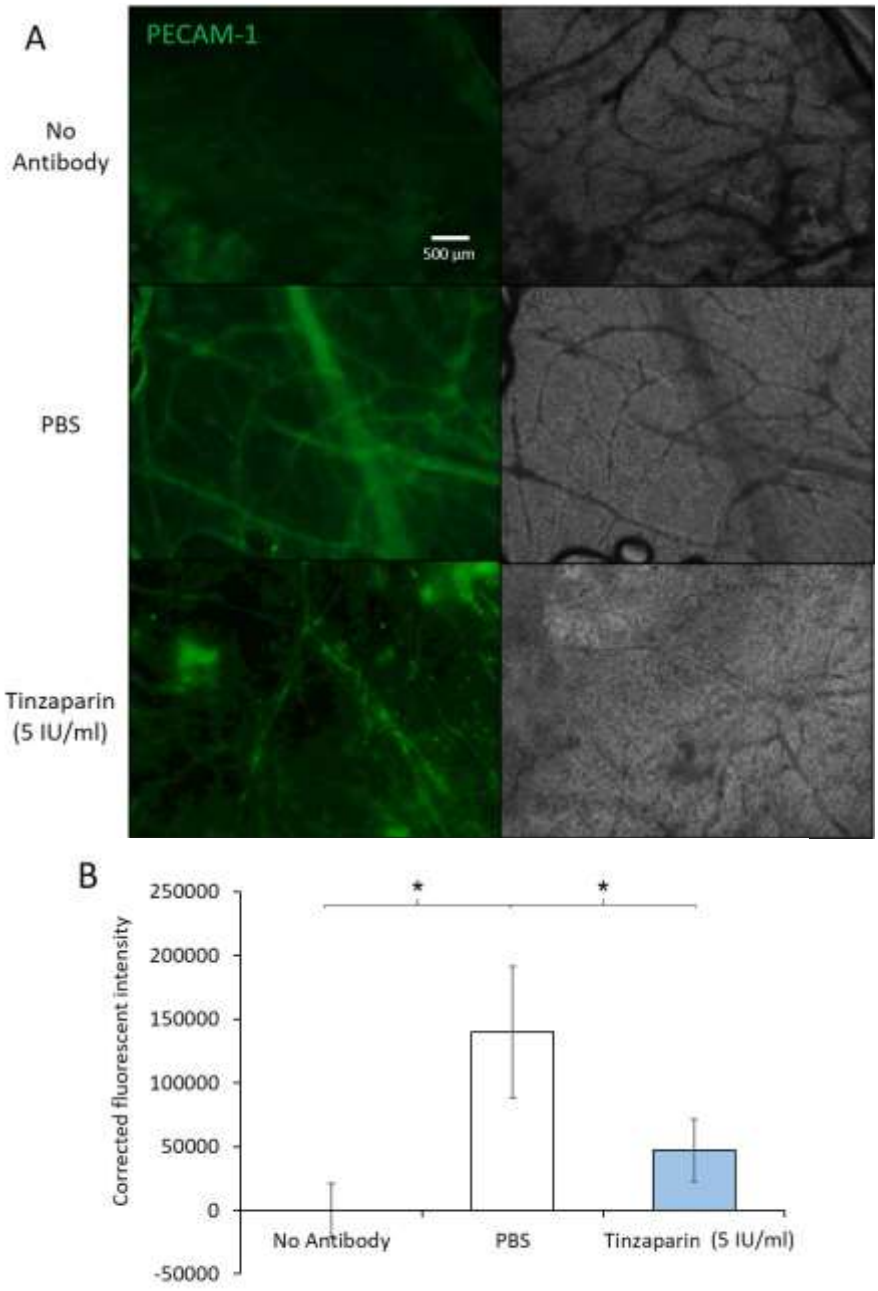

CAM-implanted AsPC-1 cell tumours were treated with tinzaparin (5 IU/ml) or PBS control for 4 days. The tumours and surrounding CAM tissue were excised and fixed in 4% (v/v) paraformaldehyde. The tumours were removed from the underlying membrane and the membrane was probed with anti-PECAM-1 antibody (diluted 1:700 v/v in PBST) and developed with NL493-conjugated anti-mouse IgG antibody (diluted 1:200 v/v in PBST). A) The sections were imaged by fluorescence microscopy at x10 magnification. B) The fluorescence intensities of the images were quantified using ImageJ (n = 12, 4 fields of view from 3 independent samples; data = mean values ± SEM; independent t-test * = $p < 0.05$).

3.4 Discussion

Studies of cancer patients receiving LMWH have previously reported favourable biological outcomes that extended beyond the prevention and/or treatment of thrombosis (Akl et al., 2007; Maraveyas et al., 2012). These favourable biological outcomes appear to arise due to LMWH interfering with mechanisms including tumour formation, invasion (Ettelaie et al., 2011a; Maraveyas et al., 2010) and angiogenesis (Dogan et al., 2011; Katrancioglu et al., 2012; Mousa, 2013; Mousa & Mohamed, 2004a). Furthermore, it appears that the LMWH may function by mechanisms besides the inhibition of fXa. Therefore, this study examined the direct effects of tinzaparin and dalteparin on tumour formation, invasion and angiogenesis, and compared the outcomes to those of direct fXa inhibitors, apixaban and rivaroxaban.

The examination of spheroid formation indicates that LMWH are capable of interfering with the processes involved in the adhesion of cells to form the tumour masses. This was evident by the formation of multiple small spheroids in the presence of both tinzaparin and dalteparin instead of single larger spheroids (Figure 3.8 & Figure 3.9). Heparins have previously been shown to influence cell-cell adhesion by inhibiting the function of selectins, (Bereczky et al., 2005; Stevenson et al., 2005; Stevenson et al., 2007) as well as reducing cancer cell adhesion to endothelial cell layers by blocking the engagement of intercellular adhesion molecules (Lever et al., 2000; Manduteanu et al., 2002). In addition to cell-cell adhesion, the binding of integrins to secreted ECM fibres is essential and in fact, the first step in spheroid formation (Figure 3.25) (Lin et al., 2006; Smyrek et al., 2019; Tzanakakis et al., 2001). It has also been proposed that LMWH can disrupt the binding of integrins to ECM proteins including fibronectin, vitronectin and laminin (Smorenburg & Van Noorden, 2001). Consequently, it was proposed that LMWH may interfere with the initiation of spheroid formation by inhibiting integrin binding. However, cells grown in 3D cultures in the presence of an inhibitory anti-β1 integrin antibody (AIIB2) failed to aggregate and remained as individual cells (Figure 3.10). Therefore, since cells cultured in the presence of LMWH aggregated into multiple small spheroids, LMWH does not appear to inhibit integrin binding.

In addition to influencing spheroid formation, tinzaparin and dalteparin were also shown to reduce the rate of cancer cell invasion into the supporting matrix (Figure 3.12 & Figure 3.13). It is known that the activation of PAR can lead to increased rate of invasion by cancer cells (Booden et al., 2004; Henrikson et al., 1999). Among the coagulation proteases, fXa is known to be capable of activating both PAR1 and PAR2 (Jiang et al., 2004; Wojtukiewicz et al., 2015; Xue et al., 2011). However, the supplementation of cells with apixaban and rivaroxaban did not alter the rate of cell invasion (Figure

Figure 3.25: The steps of spheroid formation in 3D cell culture

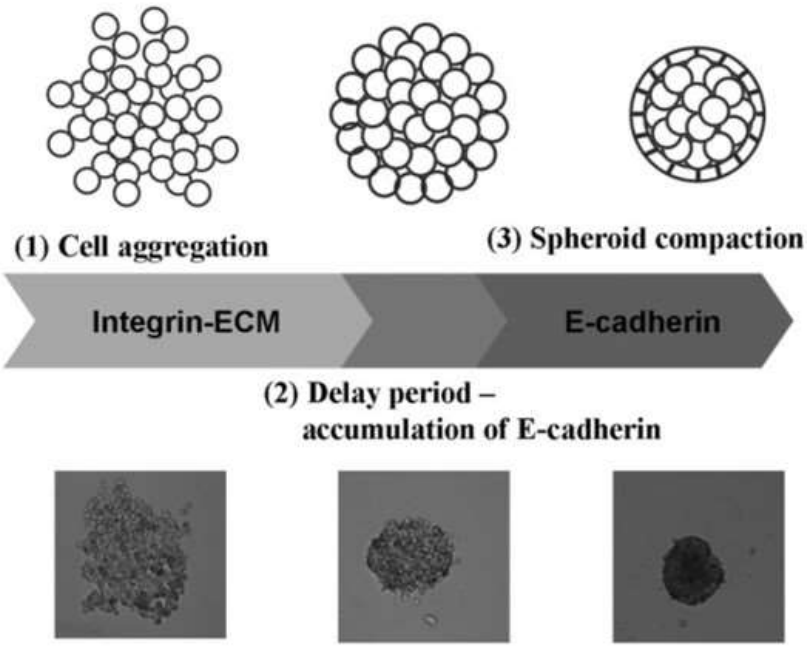

Spheroid formation takes place through three steps. First, the binding of integrins to secreted ECM fibres results in aggregation of suspended cells. The engagement of the integrins then results in the up-regulation of E-cadherin. Finally, the formation of E-cadherin junctions results in the cell aggregates transforming to form compact spheroids (Lin et al., 2006).

3.14 & Figure 3.15). FXa is not commonly expressed by cancer cells (Graf et al., 2019; Sierko et al., 2012) which explains the ineffectiveness of the anticoagulant in the current *in vitro* studies. However interestingly, the presence of fXa within the tumour microenvironment has been demonstrated *in vivo* and may arise from infiltration of the tumour stroma by cells such as macrophages (Graf et al., 2019; Graf, 2018). Therefore, it is possible that fXa inhibitors may influence cancer cell invasion *in vivo*.

Moreover, LMWH have been demonstrated to influence the rate of cell invasion through mechanisms other than by inhibiting fXa. For example, LMWH have been shown to alter the expression of TF in cell lines which consequently reduces the rate of cell invasion (Ettelaie et al., 2011a). Furthermore, LMWH have also been reported to interfere with the engagement of cell-surface receptors by a number of growth factors including VEGF (Ettelaie et al., 2011b; Soker et al., 1994) and bFGF (Ettelaie et al., 2011a; Jayson & Gallagher, 1997), and chemokines including CXCL12 (Harvey et al., 2007). These growth factors and chemokines are known to stimulate cancer cell invasion (Khajah et al., 2012; Shen et al., 2013; Wells, 2000). Finally, LMWH preparations are also potent inhibitors of the endoglycosidase heparanase (Bar-Ner et al., 1987; Hostettler et al., 2007). Heparanase degrades the heparan sulphate components of the ECM which results in the weakening of the matrix structure (Vlodavsky et al., 2007). Since this degradation is a prerequisite for tumour invasion (Tryggvason et al., 1987), LMWH may reduce the rate of cancer cell invasion by inhibiting heparanase.

Treatment of CAM with tinzaparin also inhibited vessel formation, as evident by the reduction in the density and diameter of the vessels within the CAM (Figure 3.16). Moreover, tinzaparin was effective in significantly reducing vessel diameter at 2.5 IU/ml, which is comparable to the concentrations of LMWH detectable in patients' blood (0.73-1.04 IU/ml) following treatment with LMWH (Deitcher et al., 2006; Katagiri et al., 1999). Since the activation of PAR2 has been shown to promote angiogenesis (Chang et al., 2013; Milia et al., 2002), it was proposed that LMWH may influence angiogenesis by inhibiting the activation of PAR2 by fXa. However, neither apixaban (1 µg/ml) nor rivaroxaban (0.6 µg/ml) were capable of influencing the formation of CAM vessels (Figure 3.18). Therefore, the antiangiogenic activities of LMWH appear to be independent of the anticoagulant properties of these molecules. This is in agreement with reports which demonstrate that non-anticoagulant heparin derivatives are capable of inhibiting CAM angiogenesis (Casu et al., 2002; Pisano et al., 2005). However, it is contradictory to the observations by a different study which reported that rivaroxaban (0.4 ng/ml) has the ability to inhibit CAM angiogenesis (Yavuz et al., 2014).

An alternative mechanism by which LMWH may inhibit vessel formation is through interfering with the binding of growth factors to their respective receptors. Therefore, the antiangiogenic influence of tinzaparin was compared to that of the VEGF blocker, bevacizumab. Bevacizumab (12.5 μg/ml) reduced vessel density to a similar degree as tinzaparin (2.5 IU/ml) (Figure 3.16B & Figure 3.17B). However, bevacizumab did not alter the average vessel diameter whereas treatment with tinzaparin resulted in the reduction in vessel dimeter (Figure 3.16C & Figure 3.17C). The differences in vessel diameter were indicative of the fact that tinzaparin inhibited the formation of larger arterioles and venules, in addition to capillaries. In contrast, bevacizumab only inhibited the formation of capillaries and smaller CAM vessels. These observations suggest that tinzaparin and bevacizumab may disrupt the binding of different sets of growth factors to their receptors and therefore, have dissimilar influences on the formation of different types of blood vessels. Bevacizumab is known to impede the formation of capillaries through blocking the engagement of VEGFR (Leung et al., 1989). In contrast, LMWH are capable of inhibiting the function of multiple growth factors, including VEFG (Soker et al., 1994), bFGF (Ettelaie et al., 2011a; Jayson & Gallagher, 1997), EGF (Ettelaie et al., 2011b), hepatocyte growth factor (HGF) and platelet-derived growth factor (PDGF) (Norrby, 2006). These growth factors participate in the different stages of tumour angiogenesis (Lugano et al., 2020). For example, PDGF stimulates the recruitment of pericytes to blood vessel endothelium (Franco et al., 2011; Lindblom et al., 2003). Consequently, tinzaparin is capable of influencing both the endothelial cells and the surrounding pericytes which may influence the maturation of existing capillaries into larger vessels.

Moreover, LMWH have been reported to influence angiogenesis through mechanisms other than by inhibiting growth factor binding. For example, LMWH is capable of displacing TFPI from HSPG, on the surface of endothelial cells (Mousa et al., 2000). The released TFPI, in turn, is able to inhibit the TF/fVIIa complex and suppress TF-induced tumour angiogenesis (Mousa & Mohamed, 2004b). Finally, as mentioned above, LMWH inhibit the endoglycosidase heparanase (Bar-Ner et al., 1987; Hostettler et al., 2007). The degradation of the ECM by heparanase is an important step during angiogenesis (section 1.8) (Masola et al., 2020). In addition, degradation of the ECM also aids angiogenesis by releasing proangiogenic growth factors, such as bFGF and VEGF, which are bound within the matrix (Vlodavsky et al., 2007). Therefore, LMWH may suppress angiogenesis by inhibiting the degradation of the ECM by heparanase.

The examination of the growth of CAM-implanted xenografts indicated that tinzaparin did not directly influence the rate of tumour growth (Figure 3.20). This is in contrast to previous studies showing that treatment of CAM-implanted xenografts with either tinzaparin (0.128 mg/egg) or

sulphated non-anticoagulant heparin (1 μg/egg) resulted in the reduction in xenograft growth (Mousa & Mohamed, 2004a; Sudha et al., 2014). However, the differences between these observations may arise from the variations in the length of exposure of the xenografts to the LMWH as well as the LMWH concentrations utilised (Mousa & Petersen, 2009). In the current study, although no reduction in xenograft growth was detectable, there was a statistically significant reduction in vessel density of the CAM supporting the xenograft tumours (Figure 3.23 & Figure 3.24). Therefore, it is likely that this reduction in vessel density may eventually lead to a reduction in the rate of growth of the xenografts in extended experiments.

In contrast to the observations using LMWH, treatment of the CAM-implanted xenografts with apixaban resulted in a significant reduction in the xenograft growth (Figure 3.19). This is in agreement with previous reports that apixaban reduced the rate of proliferation in a range of cancer cell types (Guasti et al., 2017). The ability of PAR2 signalling to stimulate cell proliferation has previously been established (Hu et al., 2013; Nishibori et al., 2005; Sun et al., 2018a). Therefore, apixaban may influence the growth of the xenografts by inhibiting the activation of PAR2 by fXa. However, since neither rivaroxaban nor tinzaparin influenced the growth of the CAM-implanted tumours, inhibition of fXa activity does not appear to be the mechanism by which apixaban reduces CAM xenograft growth. Therefore, the possibility of mechanisms other than anti-fXa inhibition were considered next.

In conclusion, this study has highlighted the dissimilar outcomes of treating cancer cells with therapeutic concentrations of the anticoagulants tinzaparin, dalteparin, apixaban and rivaroxaban. The LMWH tinzaparin and dalteparin inhibited spheroid formation and cell invasion by mechanisms which were independent of their anticoagulant activities. Tinzaparin was also capable of inhibiting CAM angiogenesis, but not the growth of CAM-implanted xenografts. Conversely, apixaban did not influence angiogenesis but was shown to inhibit the growth of CAM-implanted xenografts. The finding that apixaban, but not rivaroxaban or tinzaparin, suppressed xenograft growth suggest that apixaban has additional properties aside from the inhibition of fXa, which require further investigation.

Chapter 4

The effect of apixaban on cancer cell growth and the release of procoagulant MV

4.1 Introduction

In the previous chapter it was shown that the treatment of CAM embedded xenograft tumours with the anticoagulant apixaban, but not rivaroxaban or tinzaparin, resulted in a reduction in xenograft growth. Since all these anticoagulants function through the inhibition of fXa, the dissimilar anti-cancer activities of the drugs may be due to these agents influencing biological processes beyond that of the blood coagulation system. It is known that there is a bidirectional association between coagulation and cancer (Varki, 2007) which leads to enhanced tumour progression (Falanga et al., 2013). One of the key mediators in this interaction is the receptor PAR2 which is activated by coagulation proteases, included fXa (Camerer et al., 1999; Schaffner & Ruf, 2009). Activation of PAR2 results in increased cancer cell proliferation, invasion and angiogenesis, as well as the release of MV (Schaffner & Ruf, 2009). Therefore, the reduction in the growth of the CAM embedded tumours may arise from the inhibition of coagulation protease-activation of PAR2. Furthermore, due to the dissimilar activities of these anticoagulants, the mechanism by which these agents influence PAR2 activation in cancer cells needs further study, in order to explore any potential beneficial influences on cancer patients.

4.1.1 PAR2 signalling in cancer cells

PAR2 is a GPCR that is activated by a number of extracellular serine proteases (section 1.4.1). Activation of PAR2 in cancer cells leads to a range of different cellular responses, including increased cell proliferation, migration and invasion, as well as promotion of proangiogenic signalling (Schaffner & Ruf, 2009; Yau et al., 2013). The diversity of these responses stems from the mechanism by which PAR2 induces signalling within cells. Following activation, PAR2 releases G-proteins bound to the intracellular side of the receptor. PAR2 can be coupled with a number of different Gα subunit types, including $G\alpha_i$, $G\alpha_{12/13}$ and $G\alpha_q$ (Ayoub & Pin, 2013; McCoy et al., 2010; Sriwai et al., 2013). Depending on which Gα subunit is coupled to PAR2 a number of different responses can be triggered. Activation of PAR2 bound to $G\alpha_i$ results in reduced cyclic AMP (cAMP) formation, $G\alpha_{12/13}$ increases Rho-Kinase activity (Scott et al., 2003) and $G\alpha_q$ mediates Ca^{2+} mobilization from the endoplasmic reticulum (Bohm et al., 1996). All three of these responses give rise to further downstream signals, which include mitogen-activated protein kinase (MAPK) cascades and the nuclear factor-κB pathway (DeFea et al., 2000; Stalheim et al., 2005). The Gα subunit that is coupled to PAR2 and consequently the downstream signalling varies in different cell types. For example, activation of PAR2 in endometriotic stromal cells results in activation of three MAPK cascades (Hirota et al., 2005), whereas activation in cardiomyocytes only causes p38 MAPK and ERK1/2 signalling (Sabri et al., 2000). In addition, PAR2 signalling differs depending on the nature of the PAR2 activating enzyme.

For example, activation of cells by either PAR2-AP, TF/fVIIa or fXa has been shown to result in dissimilar durations and magnitudes of ERK1/2 phosphorylation (Camerer et al., 2002; Guo et al., 2011; Rothmeier et al., 2018). Finally, PAR2 is also known to signal through β-arrestin-1 and -2. β-arrestins usually play a role in receptor internalization and control the magnitude and duration of GPCR signalling (van Gastel et al., 2018). However, β-arrestins recruited to PAR2 appear to act as scaffold proteins and target activated ERK1/2 to specific areas of the cell (Ruf et al., 2010).

4.1.1.1 The role of PAR2 in the induction of cell proliferation

Multiple studies have demonstrated that activation of PAR2 with various agonists results in increased cellular proliferation (Darmoul et al., 2004; Hu et al., 2013; Jiang et al., 2017; Shanshan et al., 2019). The role of PAR2 in proliferation is further indicated by the finding that knockdown or overexpression of PAR2 in cells results in decreased or increased proliferation rates, respectively (Sun et al., 2018a). This is mediated through PAR2 signalling resulting in activation of MAPK cascades, including p38 MAPK, ERK1/2 (Poulsen et al., 1998) and SAPK/JNK (Camerer et al., 2000a; Hirota et al., 2005). These cascades are downstream signalling pathways of $G\alpha_q$ mediated Ca^{2+} mobilization (Bohm et al., 1996), $G\alpha_i$ inhibition of cAMP formation, as well as, β-arrestin signalling. The MAPK signalling cascades ultimately influence proliferation by altering the expression and/or activation of the proteins that control cell cycle checkpoint progression (Mebratu & Tesfaigzi, 2009; Zhang & Liu, 2002). These are mediated through the action of transcription regulators, including proliferating cell nuclear antigen and activator protein-1 (Hirota et al., 2005; Hu et al., 2013; Xie et al., 2012). For example, PAR2 influences cell cycle progression in HEK293 kidney cells, through regulating the expression of p53 and members of the cyclin and cyclin-dependent kinases families (Parisis et al., 2013; Suen et al., 2010). Furthermore, treatment of HepG2 cells with PAR2-AP results in an increase in the percentage of cells in the S and G_2/M phases of the cell cycle and a reduction in the G_0/G_1 phase (Xie et al., 2012). Collectively, these studies demonstrate that PAR2 influences cell cycle progression resulting in changes in cellular proliferation.

4.1.1.2 The role of PAR2 in the release of MV

In addition to influencing proliferation, the activation of PAR2 has been shown to induce MV release from both normal and cancerous cells (Collier & Ettelaie, 2011; Das et al., 2018a; Das et al., 2018b; Ettelaie et al., 2016; Koizume et al., 2016). Activation of PAR2 gives rise to both the cytoskeleton reorganisation and changes in membrane composition required for MV formation and release (see section 1.5.1). Three signalling pathways were found to contribute to PAR2 induced cytoskeleton reorganisation that resulted in MV release in MDA-MB-231 cells (Figure 4.1) (Das et al., 2018b). Two

Figure 4.1: Proposed signalling pathways for MV generation following PAR2 activation in MDA-MB-231 cells

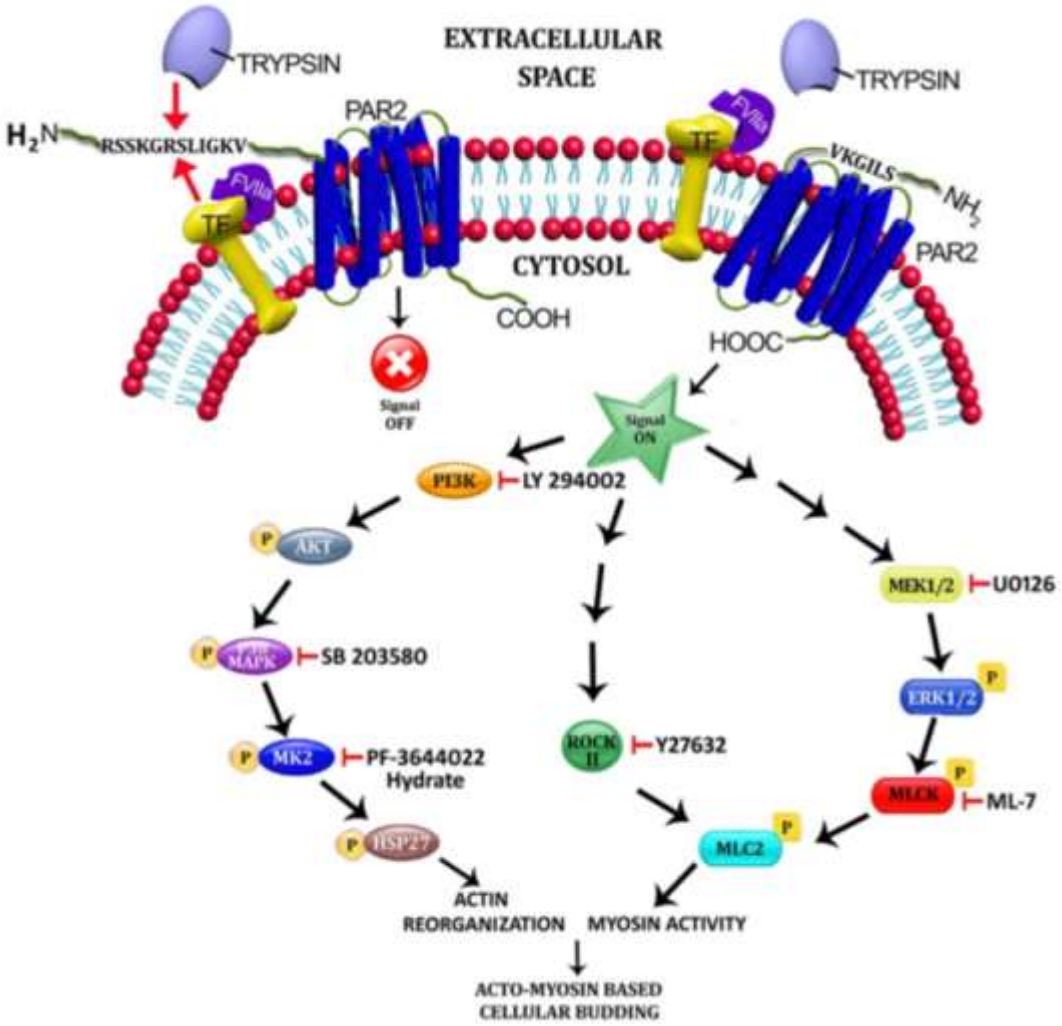

Activation of PAR2 by trypsin or the TF/fVIIa complex results in signalling through the p38 and ERK MAPK cascades as well as, the RhoA-ROCK-II pathway, that leads to MV release (Originally published in Das et al. (2018b)).

of these pathways involved the same MAPK cascades, p38 MAPK (Curtis et al., 2009) and ERK1/2 (Muralidharan-Chari et al., 2009a), which are involved in PAR2-induced increases in proliferation. In the case of MV release, the activation of these cascades results in changes in regulation of actin dynamics and phosphorylation of myosin light chain 2 (MLC2), which results in myosin reorganization. The third pathway consists of RhoA dependent ROCK-II activation which also leads to myosin reorganization (Das et al., 2018b; Li et al., 2012). In addition, PAR2 activation induces recruitment of β-arrestins to the receptor and triggers cytoskeleton reorganization through the cofilin pathway (Ruf et al., 2010). These changes to the cytoskeleton are required to allow vesicle budding and the subsequent pinching off from the plasma membrane upon MV release. Finally, changes to the lipid composition of the plasma membrane are also required for MV formation. These changes are regulated by a number of aminophospholipid translocases (Hugel et al., 2005; Stachowiak et al., 2012). These translocases are selectively activated or deactivated by an increase of cytosolic Ca^{2+} (Hankins et al., 2015). The mobilization of Ca^{2+} from the endoplasmic reticulum is triggered by PAR2 activation and is mediated through the interaction with $G\alpha_q$.

4.1.2 Factor VII

Factor VII (fVII) consists of an N-terminal GLA-domain, two EGF-like domains, and a C-terminal serine protease domain (Figure 4.2). The inactive precursor form of fVII is a single polypeptide chain, approximately 50 kDa in size (Broze & Majerus, 1980) which is converted into the active form of the enzyme (fVIIa) comprising of a light chain (~20 kDa) and a heavy chain (~30 kDa) linked by a disulphide bond (Eigenbrot, 2002; Pike et al., 1999). In the absence of TF, fVIIa exhibits very low proteolytic activity towards its substrates fX and fIX. However, following complex formation with TF, a conformational change in fVIIa stabilizes the active site and increases catalytic activity of the enzyme (Gale & Gordon, 2001). In healthy individuals fVII circulates in the blood at a concentration of 0.25-0.5 µg/ml (5-10 nM) (Hillyer, 2009; Wildgoose et al., 1992). Approximately 1-3% (0.1-0.3 nM) of the circulating fVII is in the active form (Mann, 1999; Morrissey et al., 1993) and this active fVIIa has a half-life of between 3-6 hours within the circulation (Sevenet et al., 2017).

4.1.3 Factor X

Factor X (fX) is an approximately 72 kDa protein which consists of two polypeptide chains (~55 and ~19 kDa) in the inactive precursor form (Mertens & Bertina, 1980). The light chain contains the GLA-domain and two EGF-like domains. The heavy chain contains the catalytic serine protease domain (Figure 4.2). The activated form of fX (fXa) is generated by the cleavage of a 52 amino acid 'activation peptide' from the heavy chain by either the TF/fVIIa or fIX/fVIII complexes. The cleavage produces a

Figure 4.2: The structure of fXa and fVIIa enzymes

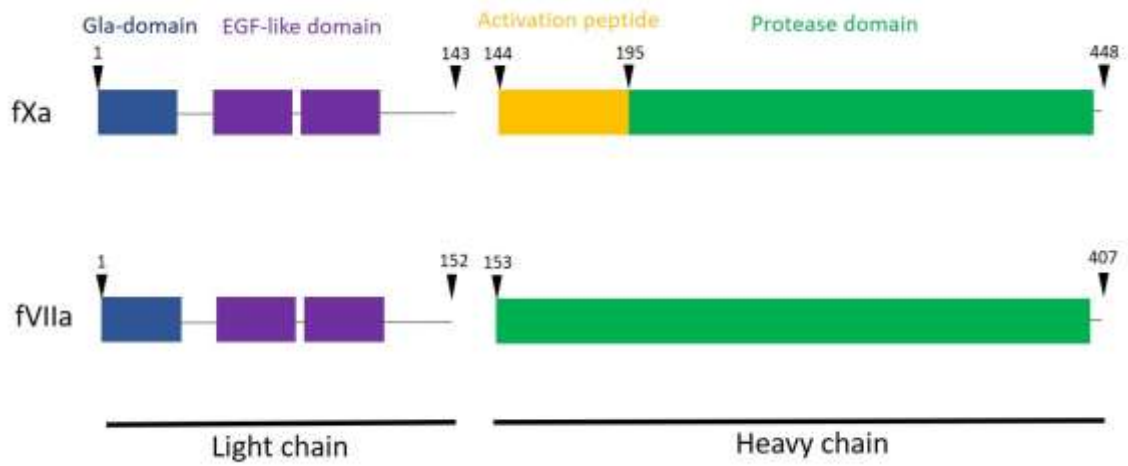

FXa and fVIIa share a similar, trypsin-like serine protease domain structure. The proteins contain the GLA-domain (blue), two EGF-like domains (purple) and a serine protease-domain (green). FX contains an additional activation peptide domain (yellow) which is removed upon activation of the protein to fXa.

modified heavy chain with a molecular weight of approximately 49 kDa. The concentration of fX circulating in the blood is around 174 nM (Hillyer, 2009). However, the amount of active fXa is more difficult to measure than that for fVIIa. This is due to the short half-life of fXa in the blood and the rapid inhibition by circulating inhibitors, including TFPI and ATIII (Mann, 1999). The rapid inhibition is essential to prevent the excessive generation of thrombin within the circulation. However, it has been estimated that within specialised areas of the blood stream, such as within a platelet plug, the majority of the fXa could remain uninhibited in the active form (Kempton et al., 2005).

4.1.4 Sources of fXa and fVIIa within the tumour microenvironment

Activation of PAR2 on the surface of cancer cells, by fXa or TF/fVIIa, requires the cells to be in direct contact with the enzymes. Such conditions may arise on the exposure of the cancer cells to the circulatory system or the release of fXa or TF/fVIIa into the tumour microenvironment. Both of these events may arise as a consequence of increased vascular permeability surrounding and within the tumour allowing coagulation factors to access the tumour, as well as for cancer cells to enter the blood stream (Liu et al., 2011). Additionally, cancer cells are capable of expressing coagulation factors. It has been established that many cancer types are capable of endogenously expressing TF (Hisada & Mackman, 2019). More recently, a number of studies have reported the expression of fVII(a) by cells obtained from patient biopsies and also in cultured cancer cell lines (Koizume et al., 2012; Koizume et al., 2006; Koizume et al., 2009; Madkhali et al., 2019; Magnus et al., 2010; Yokota et al., 2009). Furthermore, the endogenous fVII expression appears to be up-regulated by the hypoxic conditions often encountered in the tumour microenvironment (Koizume et al., 2006; Yokota et al., 2009). The expression of fX by cancer cells appears to be less prevalent and studies have reported both the absence (Guasti et al., 2017; Koizume et al., 2006) and the presence (Sierko et al., 2012; Zhang et al., 2018) of fX in various cancer cell types. In addition to cancer cells, the surrounding cells within the tumour microenvironment may also be induced to express coagulation factors. For example, the expression of TF is increased in tumour associated fibroblasts (Shaker et al., 2020) and endothelial cells (Contrino et al., 1996; Drake et al., 1989) when compared to normal tissues. Furthermore, the expression of fVIIa and fXa has been documented in tumour-associated macrophages (Graf et al., 2019; Graf, 2018). Therefore, the regulation of the activity of fVIIa and fXa by anticoagulants may be beneficial in suppressing the progression of disease in cancer patients.

The beneficial effects of treating cancer patients with anticoagulants to prevent thrombotic events are well established (Di Nisio et al., 2016; Khorana et al., 2018). However, it has become evident that such treatments may also impact aspects of tumour development which are influenced by the direct association between cancer and coagulation. One crucial mediator of this association entails the activation of PAR on the surface of cancer cells by coagulation proteases. In particular, PAR2 is activated by both TF/fVIIa and fXa, which are known to be present within the tumour microenvironment. Activation of PAR2 gives rise to a number of responses in cancer cells, including increased cell proliferation and MV release, which further participate in tumour development. Therefore, it was hypothesised that inhibition of coagulation proteases with direct fXa inhibitors, apixaban and rivaroxaban, may lead to a reduction in cancer progression.

4.1.5 Aims

The primary aim of this study was to determine if apixaban and rivaroxaban were capable of reducing the release of MV from cancer cells. The influence of apixaban and rivaroxaban on the release of TF bearing MV in response to activation of PAR2 by exogenous fXa, exogenous fVIIa as well as fVIIa endogenously expressed by cancer cells was examined. The release of MV was measured using the Zymuphen assay, and the levels of MV-associated TF antigen and activity were assessed using the TF-ELISA and CAT assays, respectively. Furthermore, the influence of apixaban and rivaroxaban on the enhancement of cell proliferation and up-regulation of IL-8 caused by activation of PAR2 was also assessed. Finally, the study aimed to elucidate the mechanism by which apixaban inhibited activation of PAR2 using PLA and *in silico* modelling of ligand binding.

4.2 Methods

4.2.1 Reagent preparation

Apixaban and rivaroxaban were prepared as described in section 2.3.1. The experimental concentrations of apixaban were 0.1 and 1 µg/ml and for rivaroxaban were 0.06 and 0.6 µg/ml. These are equivalent to 2.18 µM and 0.22 µM for apixaban and 1.38 µM and 0.14 µM for rivaroxaban. These concentrations were determined beforehand using an fXa activity assay as part of this work and are in line with the pharmacokinetic studies carried out in phase III testing of the drugs. The mean blood concentration of apixaban has been reported to be between 0.05-0.72 µg/ml and between 0.10-0.46 µg/ml for rivaroxaban depending on the treatment intervals and concentrations (Frost et al., 2013; Mueck et al., 2014).

4.2.2 Induction of MV release by activation of PAR2 with fXa and PAR2-AP

AsPC-1 and MDA-MB-231 cells were plated in T25 flasks (10^6) or 6-well plates (2 x 10^5) in complete medium and allowed to adhere overnight. The media was removed, the cells were washed with PBS and adapted to SFM (2 ml in T25 flask, 1 ml in 6-well-plate) for 1 h. The media was removed and replaced with fresh SFM containing either PAR2-agonist peptide (PAR2-AP) (SLIGKV-NH; 20 µM) or fXa (10 nM). The concentration of PAR2-AP was previously optimised and was equal to that used in previous published studies (Collier & Ettelaie, 2011; Hirota et al., 2005). The concentration of fXa used was based on the experimental amounts determined to be capable of activating PAR2 (Camerer et al., 2000b). Cells were incubated with these activating reagents for 30 min at 37°C to induce MV release (Ettelaie et al., 2016). The conditioned media was then collected and the MV isolated as described in section 2.3.3.1. The MV density was determined by Zymuphen assay (section 2.3.3.3), the MV-associated TF antigen by ELSIA (section 2.3.4.2) and the MV-associated procoagulant activity by CAT assay (section 4.2.6.4). The cell plates/flasks were retained in order to determine the number of cells present using the crystal violet assay as described in section 2.3.2.10.

To confirm the role of PAR2 activation in fXa-mediated MV release from cells AsPC-1 and MDA-MB-231 cells were plated out as described above. The cells were pre-incubated for 1 h in SFM containing either a verified inhibitory anti-PAR2 antibody, (SAM11; 20 µg/ml), a mouse IgG isotype antibody (20 µg/ml) or left untreated. The media was then exchanged for SFM containing the antibodies as above in combination with either fXa (10 nM) or PAR2-AP (20 µM). The cells were incubated for 30 min at 37°C and the conditioned media was then collected and the MV isolated and assessed as before. The culture plates were retained and the number of cells determined using the crystal violet assay.

4.2.3 Examination of the induction of MV release by fVIIa

In order to assess if fVIIa was capable of inducing MV release, AsPC-1 and MDA-MB-231 cells (2 x 10^5) were plated out and adapted to SFM as described above. As with fXa, the concentration of fVIIa used was based on the experimental amounts determined to be capable of activating PAR2 (Albrektsen et al., 2007; Morris et al., 2006). Samples of purified fVIIa (5 nM) enzyme were pre-incubated for 5 min with either an inhibitory polyclonal anti-fVII(a) antibody (20 μg/ml) or a rabbit IgG isotype antibody (20 μg/ml) diluted in SFM. The pre-incubated enzymes were added to the cells and incubated for 30 min at 37°C. MV were then isolated from the conditioned media and quantified as before. In a separate experiment to explore the role of endogenously expressed fVIIa in MV release, a set of cells were pre-incubated for 1 h with the two antibodies as above. The cells were supplemented with either purified fXa (10 nM) or fVIIa (5 nM) and incubated for 30 min at 37°C. The conditioned media was then collected and the MV were isolated and assessed as before. The culture plates were retained and the number of cells determined using the crystal violet assay.

4.2.4 Examination of the inhibition of MV release in response to fXa and fVIIa, by apixaban or rivaroxaban

AsPC-1 and MDA-MB-231 cells were plated out and adapted to SFM as described above. The SFM was removed and replaced with fresh SFM containing either purified fXa (10 nM) or fVIIa (5 nM), in the presence or absence of either apixaban (0.1 & 1 μg/ml), rivaroxaban (0.06 & 0.6 μg/ml) or DMSO (0.05% v/v) vehicle control. The cells were incubated for 30 min at 37°C and the conditioned media was collected and the MV isolated and assessed as before. The culture plates were retained and the number of cells determined using the crystal violet assay.

4.2.5 Examination of the inhibition of MV release in resting cells

To examine the inhibition of MV release in resting cells, by apixaban and rivaroxaban, AsPC-1 and MDA-MB-231 cells were plated out and adapted to SFM as described above. The SFM was removed from the cells and replaced with fresh SFM containing either apixaban (1 μg/ml), rivaroxaban (0.6 μg/ml) or DMSO (0.05% v/v) vehicle control. The cells were incubated for 30 min at 37°C and the conditioned media was collected and the MV isolated and assessed as before. In addition, experiments were preformed to examine the role of PAR2 in MV release from resting cells. MDA-MB-231 cells were plated out and adapted to SFM in the presence of either blocking antibodies to PAR2 (SAM11; 20 μg/ml), PAR1 (ATAP2; 20 μg/ml), a combination of both antibodies or a mouse IgG isotype antibody (20 μg/ml) for 1 h. The media was exchanged from fresh media containing the above antibodies either alone or in combination with apixaban (1 μg/ml) and incubated for 1 h at

37°C. The conditioned media was collected and the MV isolated and assessed as before. The culture plates were retained and the number of cells determined using the crystal violet assay.

4.2.6 Quantification of the TF activity associated with isolated MV using the Calibrated Automated Thrombogram (CAT) asaay

4.2.6.1 Prinicipals of the CAT assay

The CAT assay is based on the release of a fluorogenic product from a synthetic thrombin substrate which is added to plasma samples and then activated using a coagulation inducer. The generated thrombin in the plasma digests the substrate and releases the fluorophore which is measured. A thrombin calibrator with a defined thrombin activity is added to a parallel plasma sample. The measured thrombin activity of these samples is compared to the thrombin activity of the calibrator allowing for the differences in plasma colour and opacity to be accounted for. The relative thrombin concentration is then calculated in the parallel test. The fluorescence signal is continuously measured by a fluorometer called a Thrombinoscope which monitors the change in thrombin generated over time and Thrombinoscope analysis software (version 5.0.0.742) converts this to a thrombin generation curve. The software also calculates a number of parameters from each curve; namely the Lag time, endogenous thrombin potential (ETP), Cmax and Tmax (Figure 4.3). Lag time is the time in min for thrombin levels to reach 10 nM as clot formation occurs when approximately 10 nM thrombin is generated and coincides with the onset of the major burst of thrombin generation (Brummel-Ziedins et al., 2005). The ETP is the total amount of thrombin that a sample is able to generate as measured by the area under the thrombin generation curve. The Cmax is the maximum amount of thrombin generated over the course of the reaction as indicated by the peak height of the graph and Tmax is the time taken to reach this peak. The CAT assay can measure the influence of both the procoagulant PS and expressed procoagulant proteins present on MV, on thrombin generation.

4.2.6.2 Preparation of the standards for use with CAT assay

In order to assess the suitability of the CAT assay for measuring the TF activity associated with isolated MV, thrombin generation was tested in plasma samples supplemented with either recombinant relipidated human TF or MV devoid of TF. The influence of the two procoagulant components of cancer cell-derived MV, TF protein and procoagulant phospholipids, on CAT measured thrombin generation was then examined. The recombinant relipidated human TF (Innovin®) was diluted according to manufacturer's instructions. Since the concentration of TF within the reagent was not revealed by the manufacturer, the relative activity of the TF was calculated in

Figure 4.3: Thrombin generation curve

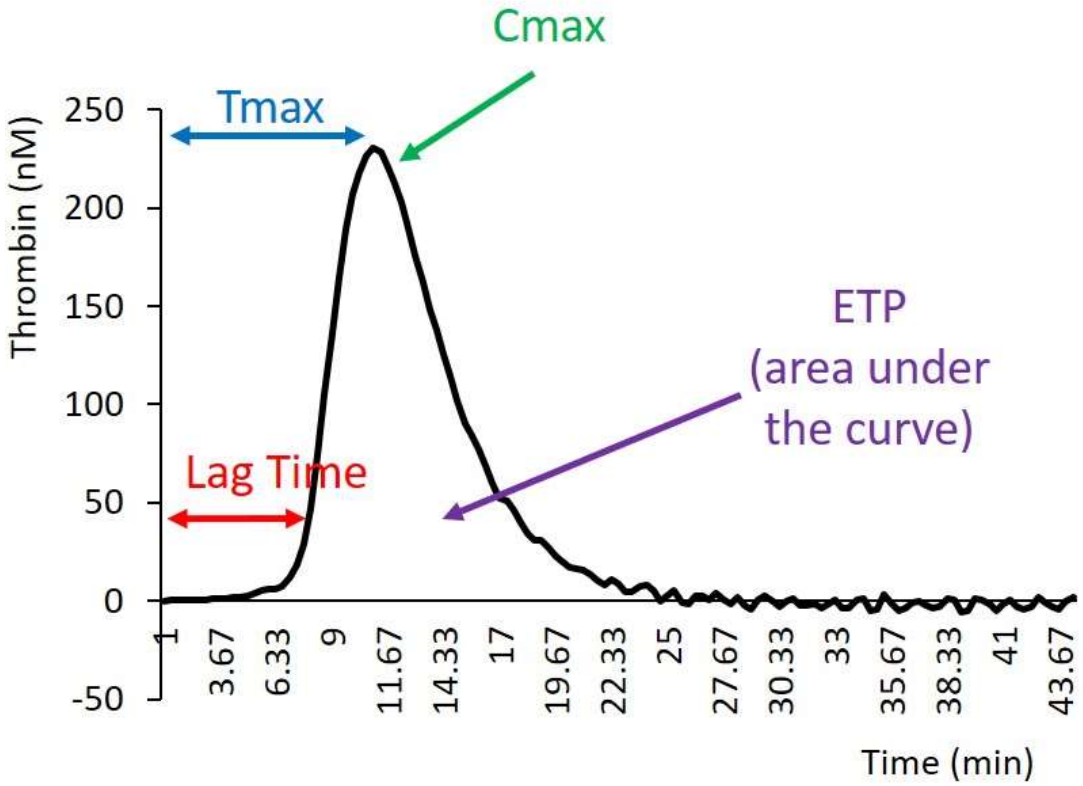

Diagram of a thrombin generation curve with the parameters assessed by the Thrombinoscope analysis software depicted. The parameters measured are the Lag time of thrombin generation, the time to reach the maximum concentration of thrombin (Tmax), the maximum concentration of thrombin (Cmax) and the total amount of thrombin activity assessed as the area under the curve (i.e. the endogenous thrombin potential – ETP).

arbitrary units of activity/ml (U/ml) with the starting solution being assumed to contain 1000 U/ml. The 1000 U/ml stock solution was diluted to between 0.01-10 U/ml prior to use. A control MV reagent, provided with the Zymuphen MP-activity kit was used as a source of procoagulant MV. The reagent contained 2.6 nM of MV and was diluted to between 0.005-0.5 nM MV were used. The MV were confirmed to be devoid of TF using the TF-ELISA kit.

4.2.6.3 Assessment of the suitability of the regular CAT assay for the analysis of the procoagulant activity of MV

As the regular CAT assay was not designed to measured isolated MV it was necessary to assess if it was capable of detecting the procoagulant activity of TF bearing MV at the concentrations yielded following the ultracentrifugation of conditioned media. Normal plasma (480 µl) was supplemented with a range of concentrations of either recombinant relipidated TF (0.01-10 U/ml) or Zymuphen MV (0.005-0.5 nM)(120 µl) and aliquots the mixtures (80 µl) were added to 6 wells in a round-bottom 96-well plate. An activator solution (20 µl; 5 pM of TF and 4 µM of procoagulant phospholipids (PS, PC, PE)) was added to 3 of the wells containing the treated plasma to initiate thrombin generation. The thrombin calibrator (20 µl) was added to the other 3 wells. The plate was incubated for 10 min at 37°C and 20 µl of FluCa reagent (HEPES (pH 7.35), $CaCl_2$ and a fluorogenic thrombin substrate (Z-Gly-Gly-Arg-AMC)) was automatically dispensed into each well by the Thrombinoscope instrument. The added Ca^{2+} ions initiate thrombin generation in the citrated plasma. The fluorescence signal of the wells was measured at 390/460 nm (Ex/Em) by the Thrombinoscope every 30 s for 60 min. The thrombin generation curves of the samples supplemented with the different controls were compared to highlight the influence of the added TF or MV on thrombin generation.

4.2.6.4 Analysis of the procoagulant activity of isolated MV samples using a modified CAT assay

In the modified CAT assay the provided activator reagent was omitted from the assay. In order to assess the suitability of a modified CAT assay for the study of isolated MV, normal plasma (480 µl) was supplemented a range of concentrations of recombinant TF or Zymuphen MV (120 µl) as above. 100 µl of the supplement plasma samples were added to 3 wells in a round-bottom 96-well plate and 80 µl was added to another 3 wells along with the provided thrombin calibrator (20 µl). The plate was incubated for 10 min at 37°C and assay carried out as described above. Once the suitability of the assay was confirmed, the assay was also carried out with the MV isolated from the cancer cell lines (Sections 4.2.2- 4.2.5) (120 µl). Of the different parameters measured by the CAT assay (Lag time, ETP, Cmax and Tmax) the Lag time was shown to correlate most closely with the concentration of recombinant TF utilised to initiate thrombin generation (Table 4.2**Error! Reference source not**

found.). Therefore, Lag time The Lag time values of the plasma supplemented with the isolated MV were compared to a standard curve (Figure 4.4) of Lag time values of plasma treated with recombinant TF (0.01-10 U/ml) to calculate the TF activity of the isolated MV samples. In addition, to assess the influence of any fVIIa present on the isolated MV, the above experiments were performed using fVII-deficient plasma instead of the normal complete plasma and assessed as above.

Finally, in order to confirm the procoagulant activity associated with the isolated MV arose from TF activity, samples of isolated MDA-MB-231 cell-derived MV (0.5 nM) were pre-incubated with an inhibitory anti-TF antibody (HTF-1; 20 µg/ml), a mouse IgG isotype antibody (20 µg/ml) or the buffer (20 mM Tris-HCl pH 7.4) for 15 min. The pre-incubated MV samples (120 µl) were added to normal plasma (480 µl) and analysed by CAT as above.

4.2.7 Optimisation of the measurement of MV-associated TF antigen using the Quantikine TF-ELISA

During an ELISA, the TF proteins are sandwiched between the capture antibodies and the detection antibodies. However, as MV are generally spherical, the MV surface may make the captured antigen inaccessible to the detection antibodies. Consequently, only a fraction of the antigen molecules would be detected. To examine this possibility, MV (150 µl) were diluted in the provided Calibrator Diluent (150 µl) in the presence or absence of additional Triton-X (0.5% v/v) and incubated for 5 min at room temperature. The TF antigen concentration was then determined using the Quantikine TF-ELISA as detailed in section 2.3.4.2.

4.2.8 FXa activity assay

4.2.8.1 Assessment of the inflence of apixaban and rivaroxaban on fXa activity

To establish the concentration of apixaban and rivaroxaban required to completely inhibit fXa activity, a range of concentrations of the inhibitors (0.001-2 µg/ml) were added to a mixture of fXa enzyme (10 nM) and a fXa substrate (Suc-Ile-Glu(γPip)-Gly-Arg-pNa, HCl; 0.5 mg/ml) in 20 mM Tris-HCl pH 7.4 buffer, in a flat bottom 96-well plate. The plate was incubated for 15 min at 37°C and the absorption of the samples was measured at 410 nm using a plate reader. In addition, to assess if MV generated in the presence of apixaban or rivaroxaban were capable of inhibiting fXa, MDA-MB-231 cells were activated with PAR2-AP (20 µM), in the presence or absence of either apixaban (1 µg/ml), rivaroxaban (0.6 µg/ml) or DMSO (0.05% v/v) vehicle control, as described in section 4.2.4. The released MV were collected by ultracentrifugation, washed with PBS (1 ml) and collected again by ultracentrifugation, as described in section 2.3.3.1. Samples of the MV (40 µl) were collected prior to and after the PBS wash and incubated with fXa (10 nM) together with the fXa-chromogenic substrate

Figure 4.4: A standard curve for determining TF activity using the CAT assay

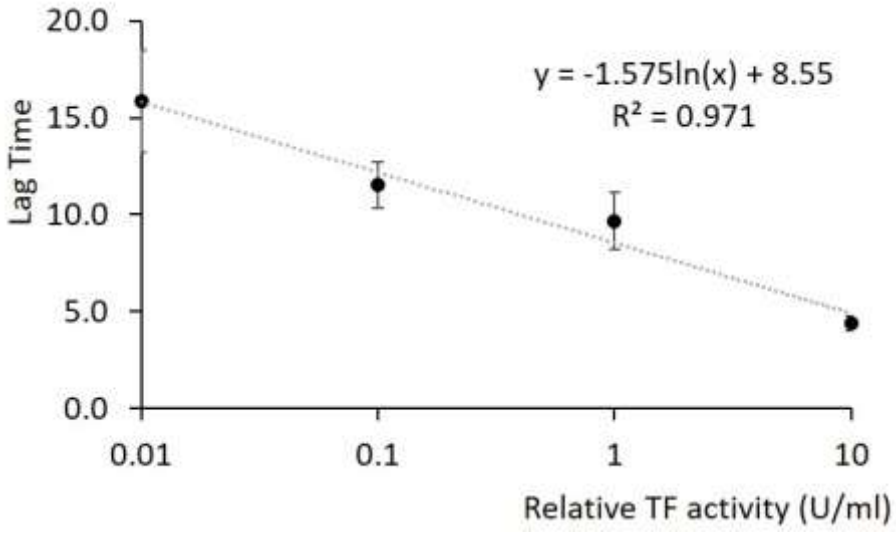

The standard curve was constructed by supplementing normal plasma with different concentrations of recombinant TF (0-10 U/ml). Thrombin generation in the samples were assess using the CAT assay. The Lag time values of the samples were used to generate a standard curve of TF activity (n=4).

(0.5 mg/ml in 20 mM Tris-HCl pH 7.4 buffer) in a flat bottom 96-well plate. The plate was incubated for 20 min at 37°C and the absorption of the samples was measured at 410 nm using a plate reader.

4.2.8.2 Determining if MDA-MB-231 cells express fXa on the cell surface using the fXa activity assay

To assess cell surface fXa activity on the surface of the MDA-MB-231 cell line, the cells (2 x 10^4) were plated in a 96-well plate and allowed to adhere overnight. The culture media was removed, and the wells were washed once with PBS (200 µl). The fXa substrate (0.5 mg/ml) was diluted in buffer (20 mM HEPES pH 7.4) and added to each well (50 µl) and the plate was incubated for 1 h at 37°C. The absorption of the samples was measured at 410 nm using a plate reader. To calculate the fXa values, a standard curve was constructed using purified fXa (0-0.3 nM) which was incubated with the fXa substrate (0.5 mg/ml) in buffer (20 mM HEPES pH 7.4) for 1 h at 37°C and the absorption were measured at 410 nm (Figure 4.5A).

4.2.8.3 Assessment of the release of fXa from MDA-MB-231 cells into cell conditioned media

To assess the fXa activity released from MDA-MB-231 cells into the culture media, cells (10^6) were plated in a T25 flask and incubated for 24 h. The media was collected and added (100 µl) to a 96-well plate. The fXa substrate (0.5 mg/ml) was diluted in buffer (20 mM HEPES pH 7.4), added to the plate (50 µl) and incubated for 1 h at 37°C. The absorption of the samples was measured at 410 nm using a plate reader. To generate a standard curve, purified fXa (0-0.3 nM) was diluted in fresh media and placed (100 µl) in a 96-well plate. The fXa substrate was added as above and incubated for 1 h at 37°C. The absorption values were measured at 410 nm using a plate reader and fXa activities in the conditioned cell culture media samples were determined (Figure 4.5B).

4.2.9 Assessment of alteration in cell surface TF following MV release

The packaging of TF and subsequent release within MV may lead to a reduction in the amount of TF remaining on the cell surface. Therefore, preventing the constitutive release of MV from MDA-MB-231 cells may result in increases in the amount of TF on the cell surface. In order to assess how the release of MV following the activation of cells influences cell surface TF, the release of MV from cells was inhibited using apixaban or encouraged by incubation with PAR2-AP and the cell surface TF was then quantified using the TF-ELISA kit. MD-MB-231 cells (5 x 10^4) were plated in a 96-well plate, allowed to adhere and were then treated with PAR2-AP (20 µM), apixaban (1 µg/ml) or the respective vehicle controls and incubated for 1 h at 37°C. The media were removed, the cells were washed once with PBS and fixed with 4% (v/v) formaldehyde and then washed three times in the

Figure 4.5: Standard curves for determining fXa activity

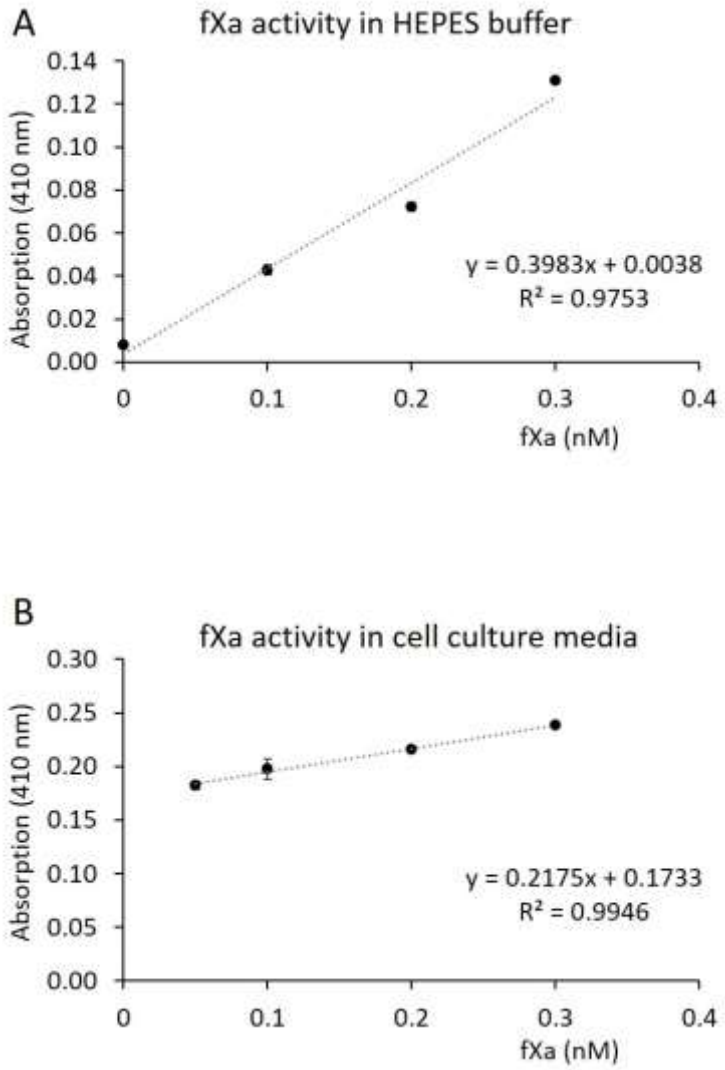

A) Purified fXa (0-0.3 nM) and fXa substrate (0.5 mg/ml) were incubated for 1 h at 37°C. The absorption at 410 nm was measured and a standard curve generated (n=4). B) Purified fXa (0-0.3 nM) and fXa substrate (0.5 mg/ml) diluted in DMEM media (100 µl) were incubated for 1 h at 37°C. The absorption at 410 nm was measured and a standard curve generated (n=4).

provided wash buffer. The cell-associated peroxidase activity in the samples was quenched as described in section 2.3.4.6 and the wells were washed twice with the wash buffer (300 µl) for 5 min. The provided HRP-conjugated anti-TF antibody (50 µl) was added to each well and incubated for 2 h at room temperature and the wells then were washed twice with the wash buffer (300 µl) for 5 min. The provided HRP-substrate solution was prepared as described in section 2.3.4.2 and was added to the wells (100 µl). The plate was incubated at room temperature in the dark for 30 min and the reaction was stopped with stop solution (50 µl). The absorption of the samples was measured at 450 nm using a microplate reader. The values were determined from the standard curve (Figure 4.6) and the amount of surface TF in pg/ml was calculated. The plates were retained in order to determine the number of cells using the crystal violet assay as described in section 2.3.2.10.

4.2.10 Examination of the influence of PAR2 activation on interleukin (IL)-8 expression using semi-quantitive RT-PCR

MDA-MB-231 cells (2 x 10^5) were plated in 6-well plates and allowed to adhere overnight. The media was removed and fresh media containing the inhibitory anti-PAR2 antibody (SAM11; 10 µg/ml), PAR2-AP (20 µM), apixaban (1 µg/ml) or DMSO (0.05% v/v) was added. The cells were incubated for 16 h to permit the expression of IL-8 mRNA (Wang et al., 2006). The cells were lysed, the mRNA extracted and converted to cDNA using the cell-2-cDNA kit (section 2.3.5.16). The relative quantity of IL-8 mRNA was quantified by RT-PCR as described in section 2.3.5.17. A previously confirmed set of primers for IL-8 (Jia et al., 2016) were used with the sequences 5'- ATG ACT TCC AAG CTG GCC GTG GCT-3' (forward) and 5'-TCT CAG CCC TCT TCA AAA ACT TCT-3' (reverse). The data were normalised against the housekeeping gene β-Actin which was quantified using a confirmed commercial primer set, obtained from Qiagen (sequence not disclosed). The change in IL-8 mRNA expression in cells following treatment with the SAM11 antibody, or with the PAR2-AP was calculated using the $2^{-\Delta\Delta Ct}$ method and expressed relative to the untreated cells. The change in IL-8 mRNA expression in the apixaban treated cells was calculated using the $2^{-\Delta\Delta Ct}$ method relative to the DMSO vehicle treated cells.

4.2.11 Crystal violet assay

4.2.11.1 Assessment of cell numbers using the crystal violet assay

The cell culture plates and flasks used to produce the MV in sections 4.2.2 - 4.2.5 were retained. The cells were fixed with 3% (v/v) glutaraldehyde for 30 min at room temperature. The number of cells in each well or flask were then determined using the crystal violet assay (section 2.3.2.10) and used to normalise the amounts of MV, TF antigen and TF activity.

Figure 4.6: Standard curve for determining TF antigen concentrations using TF-ELISA

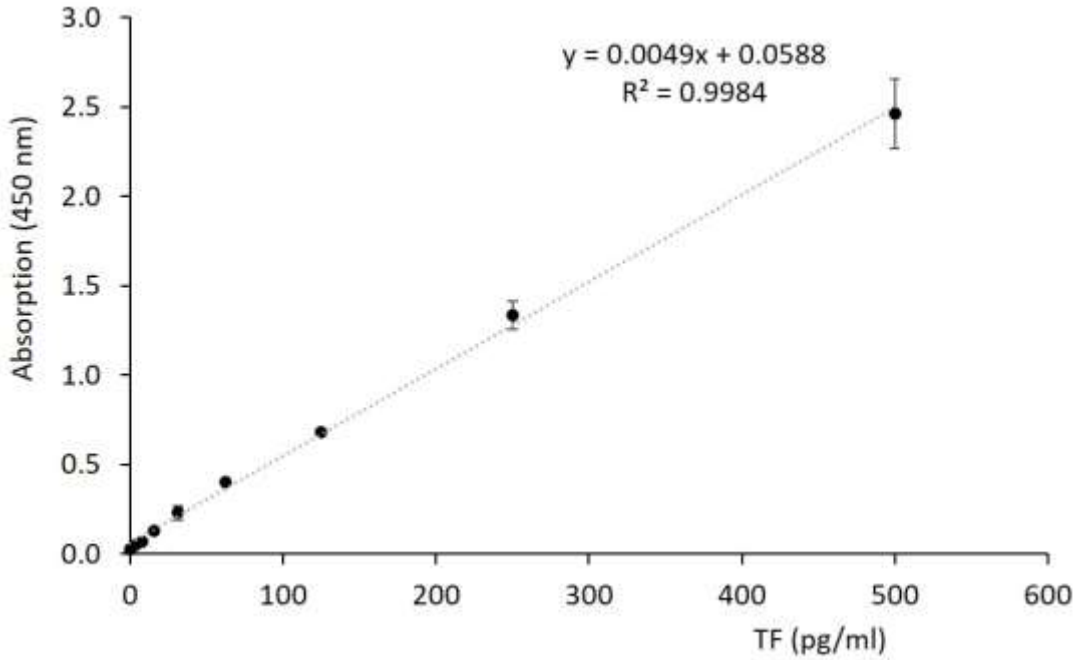

The standard curve was constructed using a serial dilution (0-500 pg/ml) of recombinant TF provided with the kit. The standards (150 µl) were placed in 96-well plates and assessed by ELISA. The absorption of the samples was then measured at 450 nm using a plate reader (n=6).

4.2.11.2 Assessment of the inflence of apixaban and rivaroxaban on cell growth using crystal violet assay

MDA-MB-231 cells, AsPC-1 cells and HDBEC (2×10^4) were plated out in three sets of 12-well plates and allowed to adhere overnight. On the next day, one set of plates were fixed with 3% (v/v) glutaraldehyde and stored at -20°C for future assessment. In all other sets of plates, the media was removed and replaced with fresh media containing apixaban (0.1-5 µg/ml), rivaroxaban (0.06-3 µg/ml) or DMSO (0.05% v/v) and the plates incubated at 37°C. The treatment was repeated every 2 days for up to 4 days and one set of plates was collected and fixed every 2 days, and stored as above. Once all the plates were collected the number of cells in each well were determined using the crystal violet assay (section 2.3.2.10). As cancer cell lines contain aberrant DNA content and chromosomal ploidy, individual standard curves were generated for each cell type. In order to produce a standard curve, sets of MDA-MB-231 cells, AsPC-1 cells and HDBEC (0.005-0.15 million cells) were plated in 12-well plates. The cancer cell lines were incubated for 5 h and the primary cells were incubated overnight to allow the cells to adhere. The cells were fixed and the crystal violet assay performed as above. The absorption values were determined at 584 nm using a plate reader and standard curves constructed (Figure 4.7).

4.2.12 Analysis of the expression of fXa and fVIIa in cancer cell lines using the western blot assay

MDA-MB-231 and AsPC-1 cells were cultured in T25 flasks as described in section 2.3.2.2 until 80% confluent. The cells were then lysed in Laemmli buffer (1 ml) and heated at 95°C for 5 min. The protein concentration was determined using the Bradford assay (section 2.3.4.1) and equal quantities (20 µg/well) were separated by SDS-PAGE (section 2.3.4.4). The expression of fXa and fVIIa were assessed using the western blot assay (section 2.3.4.5) using the antibodies and dilutions shown in Table 4.1. Semi-quantitative analysis of the western blot membranes was carried out using ImageJ.

4.2.13 Examination of the influence of apixaban on the interaction between fVIIa with PAR2 and fVIIa with TF using the PLA

To examine the influence of apixaban on the interaction between fVIIa with either PAR2 or TF, MDA-MB-231 cells (10^4) were plated out into 29 mm culture dishes with a 10 mm glass bottomed micro-well. The cells were incubated at 37°C overnight to allow cells to adhere. The media was removed and replaced with fresh media containing either apixaban (1 µg/ml) or DMSO (0.05% v/v) vehicle control and incubated for 1 h at 37°C. The media was removed and the plates were fixed. The

Figure 4.7: Standard curves for determining cell numbers using the crystal violet assay

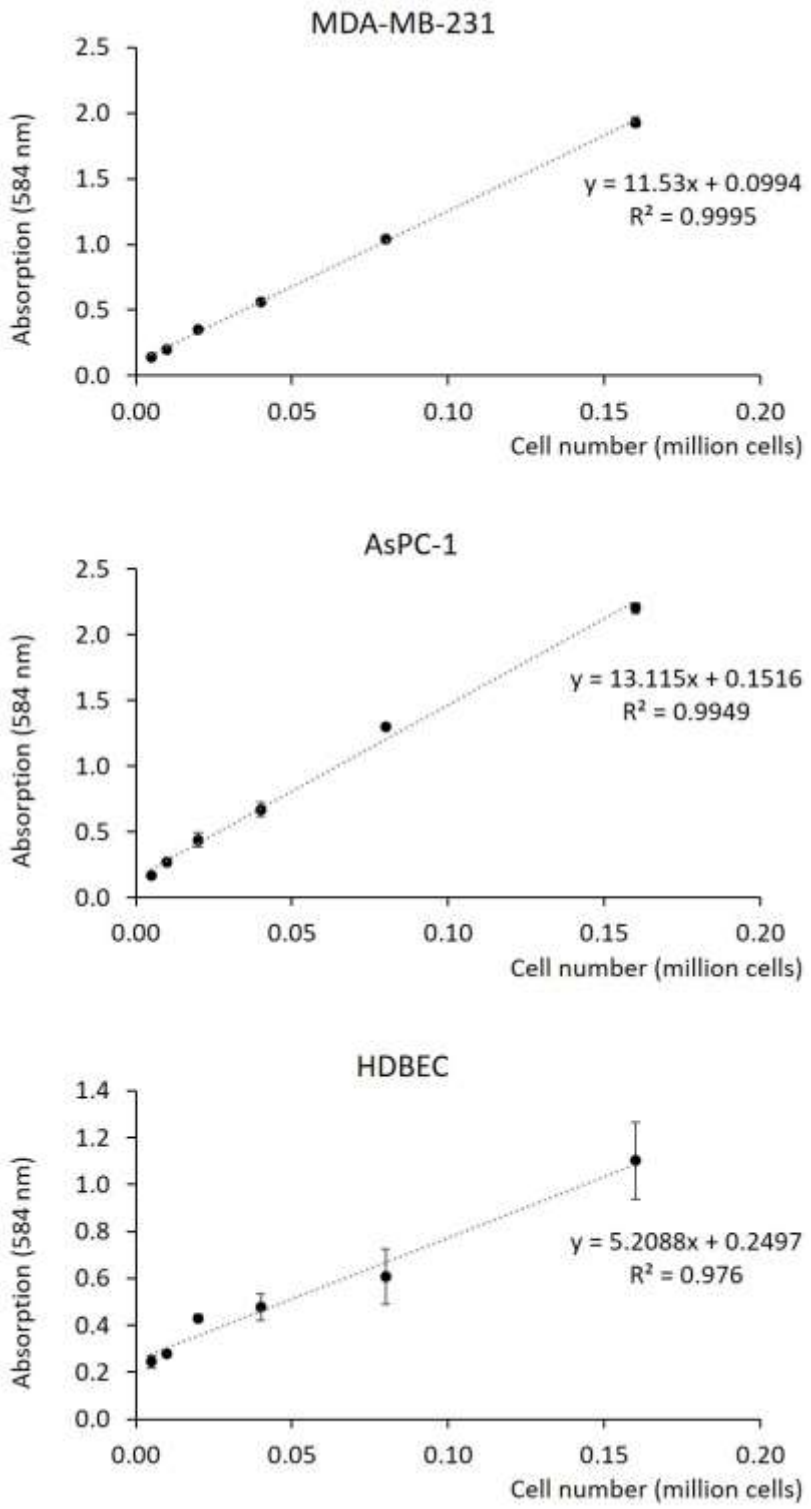

MDA-MB-231 cells, AsPC-1 cells and HDBEC (0.005-0.15 million cells) were plated in 12-well plates and allowed to adhere overnight. The number of cells were determined using the crystal violet assay and the absorption measured at 584 nm using a plate reader. The values were used to create a standard curve for each cell line (n=4).

Table 4.1: Antibodies used for western blot assays

Probing antibody				**Detection antibody**		
Antigen	Clone	Host species	Dilution	Antigen	Host species	Dilution
GAPDH	v-18	Goat	1:5000	**Goat IgG**	Mouse	1:3000
fVII	polyclonal	Rabbit	1:3000	**Rabbit IgG**	Mouse	1:3000
fX	156106	Mouse	1:3000 or 1:6000	**Mouse IgG**	Goat	1:3000

proximity and possible interaction of fVIIa with either PAR2 or TF, on the surface of the cells was then examined using PLA (section 2.3.4.8.2). To detect the interactions between fVIIa and PAR2, a rabbit anti-fVII(a) antibody was used in conjunction with a mouse anti-PAR2 antibody (SAM11). To detect the interactions between fVIIa and TF, the rabbit anti-fVII antibody was used in conjunction with a mouse anti-TF antibody (HTF-1). The results were visualised using a florescence microscope and the number of incidences of interaction and the number of cells in each field of view was quantify using ImageJ. The number of incidences/cell were compared between the apixaban and vehicle control treated samples.

4.2.14 *In silico* modelling of the binding of apixaban and rivaroxaban to fXa and fVIIa using the Autodock program

The binding energies for apixaban and rivaroxaban with fXa and fVIIa were predicted using the Autodock 4v2.6 program. FXa (2P16) and fVIIa (4ylq) crystal structures, as well as apixaban (GG2) and rivaroxaban (RIV) ligands were acquired from the Protein Data Bank. The fXa and fVIIa crystal structures were imported into the Autodock 4v2.6 program running the AutoDockTools 1.5.6 graphical interface (Seeliger & de Groot, 2010). The polar hydrogens and partial charges were added to the proteins and the Gasteiger charges calculated. For modelling of the ligand binding sites a 20 × 20 × 20 Å box was centred around the –OH group of Ser195 in fXa and Ser344 in fVIIa, located in the active sites of the enzymes. For each pairing of enzyme and ligand, 25 predicted binding conformations were obtained. The estimated binding energy, ligand efficiency and inhibition constant were calculated for the most likely configuration for each of the enzyme-ligand pairings.

4.3 Results

4.3.1 Optimisation of experimental procedures

4.3.1.1 Optimisation of the CAT assay to detect procoagulant activity of isolated MV

In order to assess if the CAT assay was capable of detecting the procoagulant activity of TF-bearing MV at the concentrations yielded by the ultracentrifugation of conditioned media, first the limit of the sensitivity of the assay to low concentrations of TF and phospholipids was examined. The assay was carried out using two experimental protocols; a regular protocol where the provided activator reagent was included and a modified protocol without the additional activator. In experiments performed using the modified protocol, the Lag time to initiation of thrombin generation decreased in a TF concentration-dependant manner (Figure 4.8A & Figure 4.8C). However, in experiments performed using the regular protocol there was little change in Lag time values following the supplementation with the recombinant TF (Figure 4.8B & Figure 4.8C). This may be due to the high concentration of TF (5 pM) present in the provided activator reagent which superseded any activity of the recombinant TF. Finally, statistical assessment of the Lag time, ETP, Cmax and Tmax (Figure 4.3) of the thrombin generation curves produced by the different concentrations of recombinant TF indicated that the Lag time of the curves most closely correlated with TF concentration (Table 4.2). Therefore, in all further experiments the Lag times of plasma treated with the isolated MV samples were compared to a standard curve of those of plasma treated with recombinant TF to determine the relative TF activity within the isolated MV. The authenticity of TF activity on isolated MV was determined using an inhibitory antibody and is described later in section 4.3.1.5. Supplementation of plasma with control MV, which lacked TF (Figure 4.9), did not alter the rate of thrombin generation in normal plasma as tested with either protocol (Figure 4.10).

4.3.1.2 Selection of suitable cell lines for the analysis of MV release following PAR2 activation

This study required cancer cell lines in which treatment with PAR2 activators resulted in an increase in the amount of MV released. Activation of MDA-MB-231 cells with PAR2-AP resulted in an increase in MV-associated procoagulant activity from 1.44 U/ml ± 0.53 to 5.03 U/ml ± 1.10 (Figure 4.11A). Similarly, activation of AsPC-1 cells resulted in an increase in MV-associated procoagulant activity from 1.11 U/ml ± 0.37 to 3.33 U/ml ± 0.90 (Figure 4.11A). The MV derived from BxPC-3 cells, SK-OV-3 and LoVo cells did not produce a significant increase in procoagulant activity following PAR2 activation. This may arise from the differences in PAR2 expression levels on the surface of these cell lines (Ettelaie et al., 2016). Next, to determine the optimal concentration of fXa capable of inducing maximal MV release, MDA-MB-231 and AsPC-1 cells were incubated for 30 min with a range of concentrations of fXa (0-10 nM). Incubation of the MDA-MB-231 cells with all tested concentrations

Figure 4.8: Assessment of the influence of low concentrations of TF on thrombin generation measured using the CAT assay

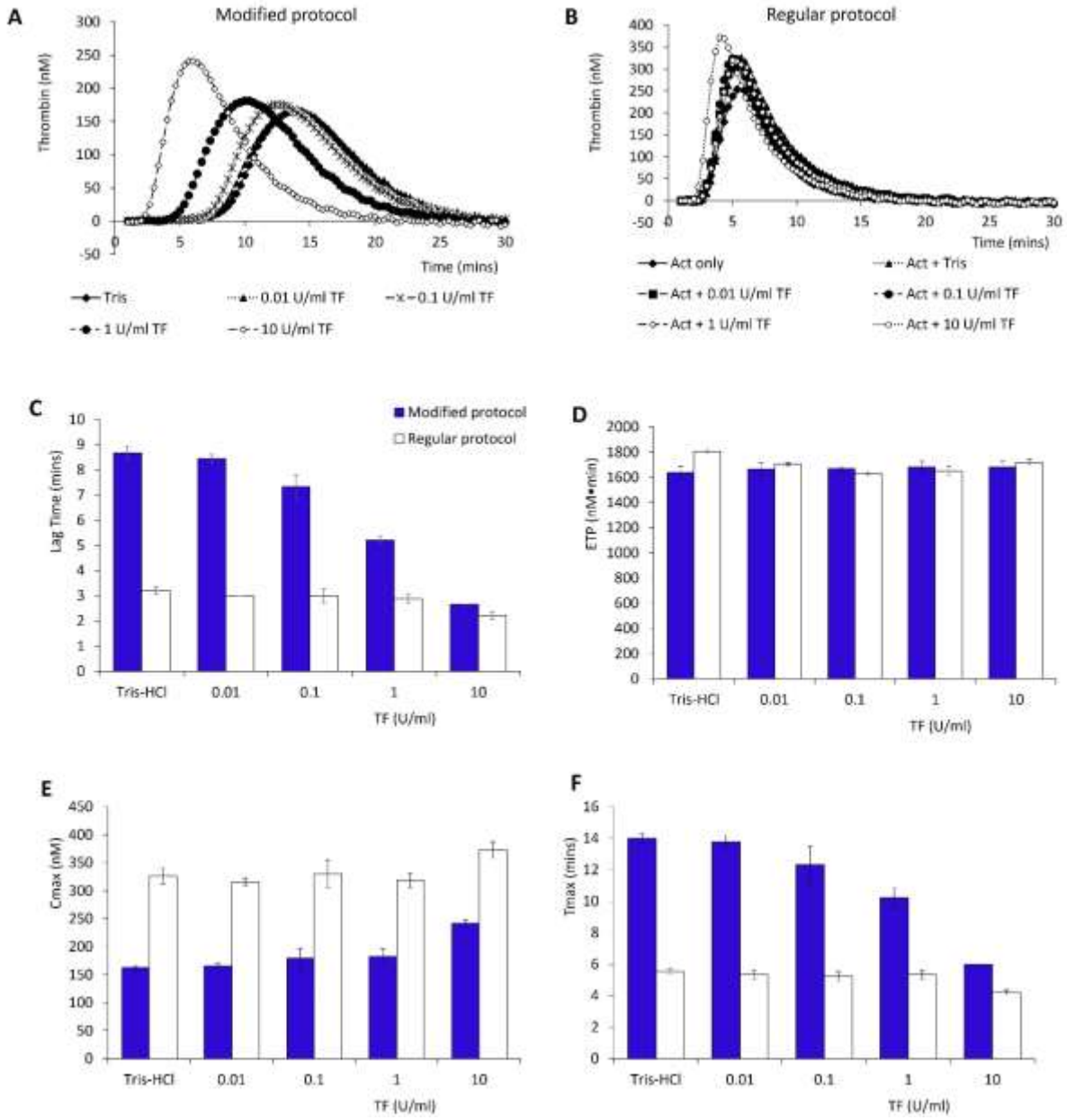

Normal plasma was supplemented with recombinant TF (0.01-10 U/ml) and thrombin generation measured using either the A) modified or B) regular CAT assay. The C) Lag time, D) ETP, E) Cmax and F) Tmax values for each sample in the modified (Blue) and regular (White) assay were then calculated using the onboard analysis software (n=3, one experiment carried out in triplicate; data = mean values ± SD).

Figure 4.9: Assessment of the presence of TF in samples of control phospholipid MV

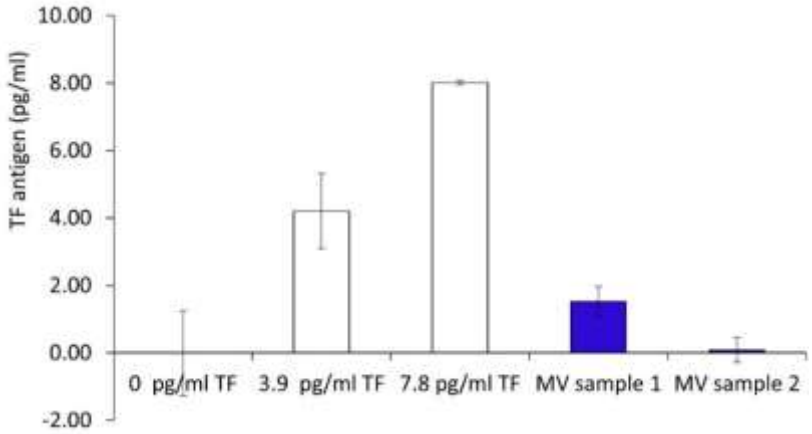

The TF content of the control phospholipid MV (1.3 nM) provide with the Zymuphen assay kit was quantified using TF-ELSIA (n=3; data = mean values ± SEM).

Figure 4.10: Assessment of the influence of phospholipid MV, devoid of TF, on thrombin generation measured using the CAT assay

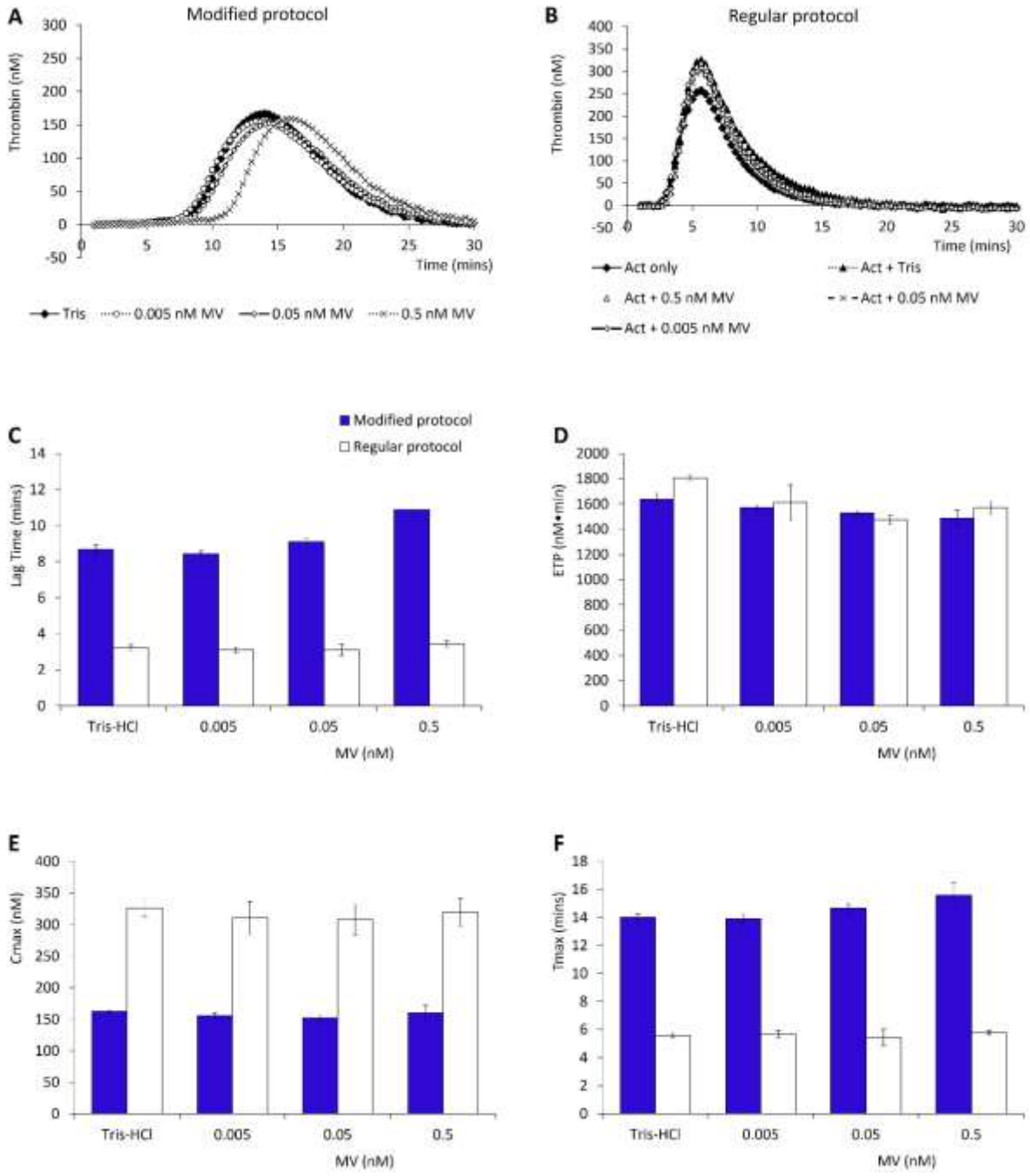

Normal plasma was supplemented with control MV (0.005-0.5 nM) and thrombin generation measured using either the A) modified or B) regular CAT assay. The C) Lag time, D) ETP, E) Cmax and F) Tmax values for each sample in the modified (Blue) and regular (White) assay were then calculated using the onboard analysis software (n=3, one experiment carried out in triplicate; data = mean values ± SD).

Table 4.2: Correlations between TF concentration and measured CAT assay parameters

Correlations

		TF concentration
Lag Time	Pearson Correlation	-.649**
	Sig. (2-tailed)	.005
ETP	Pearson Correlation	-.023
	Sig. (2-tailed)	.931
Cmax	Pearson Correlation	.459
	Sig. (2-tailed)	.064
Tmax	Pearson Correlation	-.634**
	Sig. (2-tailed)	.006
** Correlation is significant at the 0.01 level (2-tailed).		

Normal plasma was supplemented with recombinant TF (0.01-10 U/ml) and thrombin generation measured using the modified CAT assay. The Lag time, ETP, Cmax and Tmax values were calculated using the onboard analysis software. The Pearson correlation coefficient between the concentration of recombinant TF and the resultant Lag time, ETP, Cmax and Tmax was calculated using the SPSS program.

Figure 4.11: Analysis of the release of MV from cancer cells lines following activation with PAR2-AP and fXa

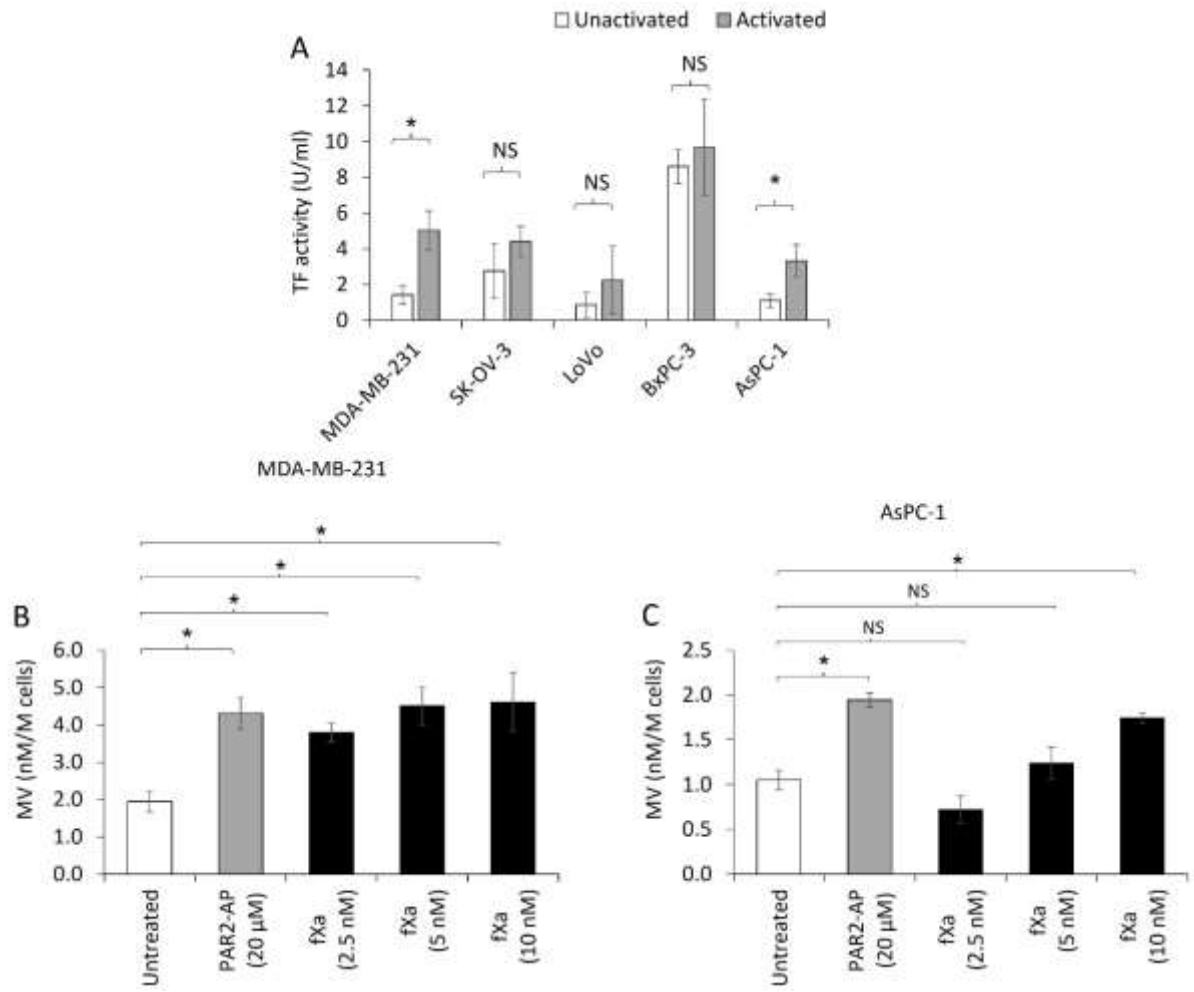

A) MDA-MB-231, SK-OV-3, LoVo, BxPC-3 and AsPC-1 cells were used untreated or were activated with PAR2-AP (20 µM) for 30 min. The released MV were collected by ultracentrifugation and the procoagulant activity of the isolated MV were measured by CAT (n=6, two independent experiments carried out in triplicate; data = mean values ± SEM; independent t-test * = $p < 0.05$). B) MDA-MB-231 cells or C) AsPC-1 cells were used untreated or were activated with either PAR2-AP (20 µM) or fXa (2.5-10 nM) for 30 min. The released MV were collected by ultracentrifugation and quantified using the Zymuphen assay (n=3, one experiment carried out in triplicate; data = mean values ± SEM; one-way ANOVA, * = $p < 0.05$, NS = not significant).

of fXa resulted in increases in MV release (2.5 nM = 3.80 nM/M cells ± 0.26, 5 nM = 4.51 nM/M cells ± 0.50, 10 nM = 4.61 nM/M cells ± 0.80) (Figure 4.11B). Additionally, incubation with 10 nM of fXa resulted in maximal MV release in the AsPC-1 cells of 1.74 nM/M cells ± 0.11 (Figure 4.11C). Activation of the MDA-MB-231 and AsPC-1 cell lines with PAR2-AP (20 µM) resulted in MV release of 4.30 nM/M cells ± 0.42 and 1.95 nM/M cells ± 0.16 respectively, which were comparable to that observed with 10 µM of fXa.

4.3.1.3 Inhibition of PAR2 reduces the release of MV from fXa-activated cells

Next it was verified that the induction of MV release by fXa was mediated through PAR2 (Figure 4.12). Pre-incubation of MDA-MB-231 cells with the inhibitory anti-PAR2 antibody reduced the release of MV following fXa treatment from 3.55 nM/M cells ± 0.05 to 2.48 nM/M cells ± 0.16 (Figure 4.13A). Similarly, pre-incubation of AsPC-1 cells with the inhibitory anti-PAR2 antibody resulted in a reduction in MV release to 1.10 nM/M cells ± 0.27 following fXa activation compared to cells treated with control IgG (1.67 nM/M cells ± 0.14) (Figure 4.13B). In contrast, the inhibitory anti-PAR2 antibody had no influence on MV release from cells activated with PAR2-AP (Figure 4.13A and Figure 4.13B). The inhibitory SAM11 antibody is known to bind to the epitope of residues 37-50 of PAR2 (Santa Cruz Biotechnology, 2020) and therefore prevents cleavage by fXa between residues Arg36/Ser37 (Nystedt et al., 1995). In contrast, PAR2-AP binds the second extracellular loop and seventh transmembrane domain of PAR2 (Adams et al., 2011; Al-Ani et al., 1999; Yau et al., 2013) and therefore is not influenced by inhibitory antibody binding.

4.3.1.4 The release of MV from cells by fXa is not dependant on the presence of fVIIa

To examine if fVIIa was essential for the induction of MV release by fXa, MDA-MB-231 and AsPC-1 cells (3×10^4) were pre-incubated with an inhibitory anti-fVII(a) antibody (20 µg/ml) and then activated with fXa (10 nM) (Figure 4.12). The pre-incubation of the cells with inhibitory anti-fVII(a) antibody had no significant effect on the release of MV from fXa-activated cells, indicating that activation of PAR2 by fXa was independent of the presence of fVIIa (Figure 4.14).

4.3.1.5 Analysis of the procoagulant activity of released MV

Firstly, a set of experiments was preformed to determine the concentration of an inhibitory anti-TF antibody (HTF-1) capable of preventing thrombin generation initiated by cancer cell-derived MV. Pre-incubation of the isolated MV (0.5 nM) with HTF-1 reduced thrombin generation in a concentration-dependant manner, with 20 µg/ml producing maximal inhibition (to 18% of untreated plasma) (Figure 4.15). Next, to assess the procoagulant potential of isolated MV, normal plasma

Figure 4.12: Experimental procedure for the assessment of the influence of PAR2 or fVIIa on the release of MV from fXa treated cells

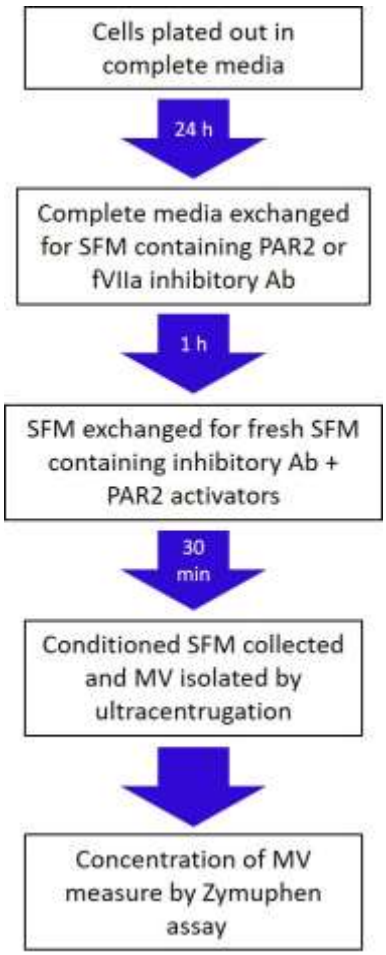

Figure 4.13: Assessment of the influence of PAR2 on the release of MV from fXa treated cells

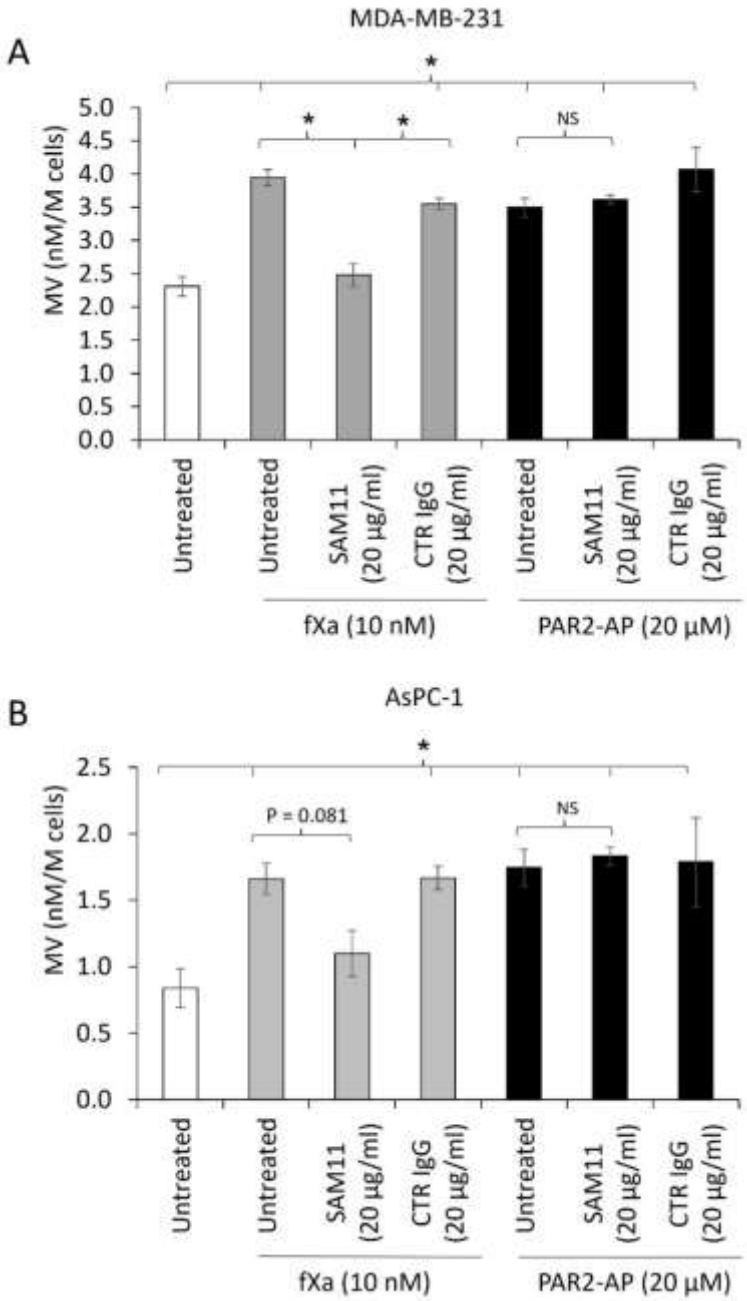

A) MDA-MB-231 cells and B) AsPC-1 cells (2 x 10^5) were adapted to SFM supplemented with either an inhibitory anti-PAR2 antibody (SAM11; 20 µg/ml) or the equivalent isotype control antibody (CTR IgG; 20 µg/ml) for 1 h. The cells were then activated with either fXa (10 nM) or PAR2-AP (20 µM) in combination with the above antibodies for 30 min. The released MV were collected by ultracentrifugation and quantified using the Zymuphen assay (n=4, two independent experiments carried out in duplicate; data = mean values ± SEM; one-way ANOVA, * = $p < 0.05$, NS = not significant).

Figure 4.14: Assessment of the influence of fVIIa on the release of MV from fXa treated cells

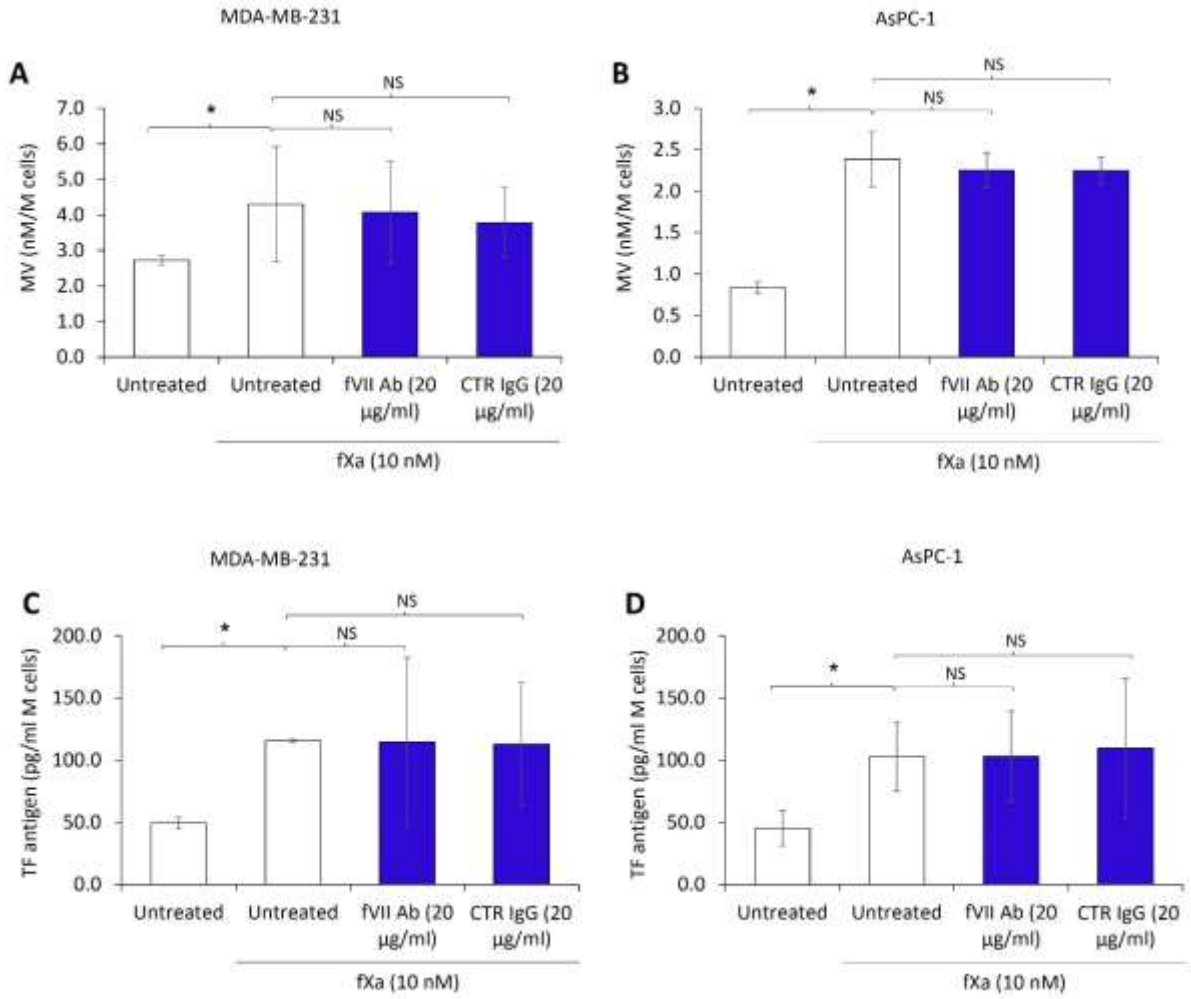

A) & C) MDA-MB-231 and B) & D) AsPC-1 cells (2 x 10^5) were adapted to SFM containing an inhibitory anti-fVII(a) antibody (fVII Ab; 20 µg/ml) or the equivalent isotype control antibody (CTR IgG; 20 µg/ml) for 1 h. The cells were then activated with fXa (10 nM) in combination with the above antibodies for 30 min. The released MV were collected by ultracentrifugation and A) & B) the density of the released MV was determined using the Zymuphen assay and C) & D) the MV-associated TF antigen was determined using TF-ELISA. (n=6, two independent experiments carried out in triplicate; data = mean values ± SEM; independent t-test, * = $p < 0.05$, NS = not significant).

Figure 4.15: Optimisation of the concentration of HTF-1 antibody required to inhibit MV-induced thrombin generation

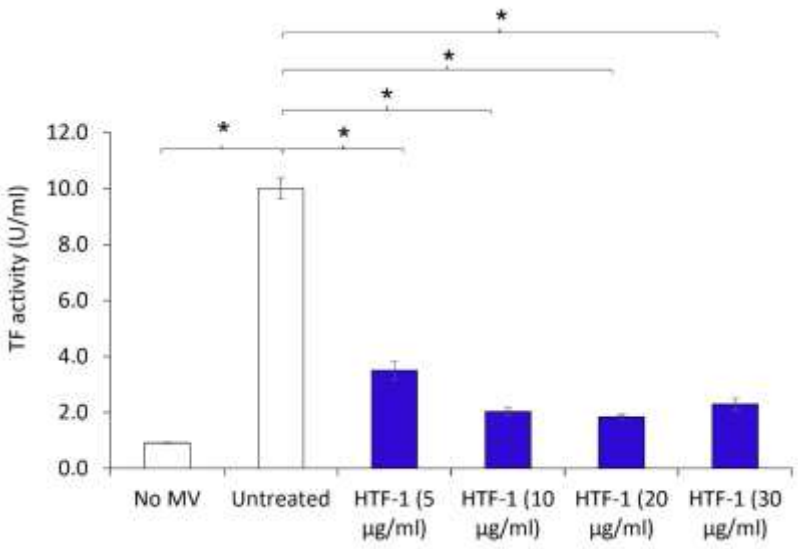

MDA-MB-231 cell-derived MV (0.5 nM) were pre-incubated with an inhibitory anti-TF antibody (HTF-1; 0-20 µg/ml) for 15 min. Normal plasma was supplemented with the pre-incubated MV and thrombin generation was assessed using the CAT. The Lag time values of each plasma sample were recorded and MV-associated TF activity calculated (n=6, two independent experiments carried out in triplicate; data = mean values ± SEM; independent t-test * = $p < 0.05$).

samples were supplemented with MV (0.5 nM) derived from MDA-MB-231 or AsPC-1 cells. Supplementation of normal plasma with the cell-derived MV resulted in an accelerated rate of thrombin generation to 9.65 U/ml ± 0.22 with MB-MB-231 cell-derived MV (Figure 4.16A) and 4.55 U/ml ± 0.53 with AsPC-1 cell-derived MV (Figure 4.16B). Furthermore, pre-incubation of the MV with the HTF-1 antibody reduced the rate of thrombin generation to 2.97 U/ml ± 0.42 with MB-MB-231 cell-derived MV (Figure 4.16C) and 2.06 U/ml ± 0.18 with AsPC-1 cell-derived MV (Figure 4.16D). These data suggest that the procoagulant activity of the MV is derived from the TF present on the surface of the MV. However, the initiation of coagulation was not completely inhibited by pre-incubation of the MV with the HTF-1 antibody.

Finally, to examine if the released MV contained any fVIIa activity on the surface, fVII-deficient plasma was supplemented with cancer cell-derived MV and thrombin generation was monitored using the CAT. The MV from both cell lines were capable of promoting thrombin generation in fVII-deficient plasma, with those derived from AsPC-1 cells exhibiting higher activity of 4.25 U/ml ± 0.19 compared to those from MDA-MB-231 cells (3.06 U/ml ± 0.30) (Figure 4.17). Therefore, these data suggest the presence of active fVIIa on MV from these cell lines.

4.3.1.6 Optimisation of the measurement of MV-associated TF antigen with the TF-ELISA

Prior to the study, it was necessary to assess whether lysis of the isolated MV would result in a more accurate measurement of the TF antigen associated with the MV. MV samples were dispersed in Triton-X (0.5% v/v) for 5 min at room temperature prior to quantification by ELISA. Comparison of the lysed and intact MV showed no difference in the measured amounts of the released TF antigen (Figure 4.18).

4.3.1.7 Optimisation of the concentrations of apixaban and rivaroxaban for the inhibition of fXa activity

To determine the concentrations of apixaban and rivaroxaban capable of inhibiting fXa, samples of fXa (10 nM) were pre-incubated with apixaban or rivaroxaban (0.001-2 µg/ml) and the fXa activity measured by addition of a fXa-chromogenic substrate. Both apixaban and rivaroxaban inhibited fXa activity in a dose-dependent manner. Complete inhibition of the fXa activity was achieved with 1 µg/ml of apixaban or 0.6 µg/ml of rivaroxaban (Figure 4.19).

Next, the risk of any carry-over of the fXa inhibitors onto later experiments was assessed and eliminated. Samples of the MV were collected prior to and after the PBS wash during the isolation procedure. Incubation of fXa with MV, generated in the presence of apixaban or rivaroxaban and collected prior to the PBS wash, resulted in a 99% or 73% reduction in the fXa activity, respectively.

Figure 4.16: Assessment of the influence of TF on MV-associated procoagulant activity

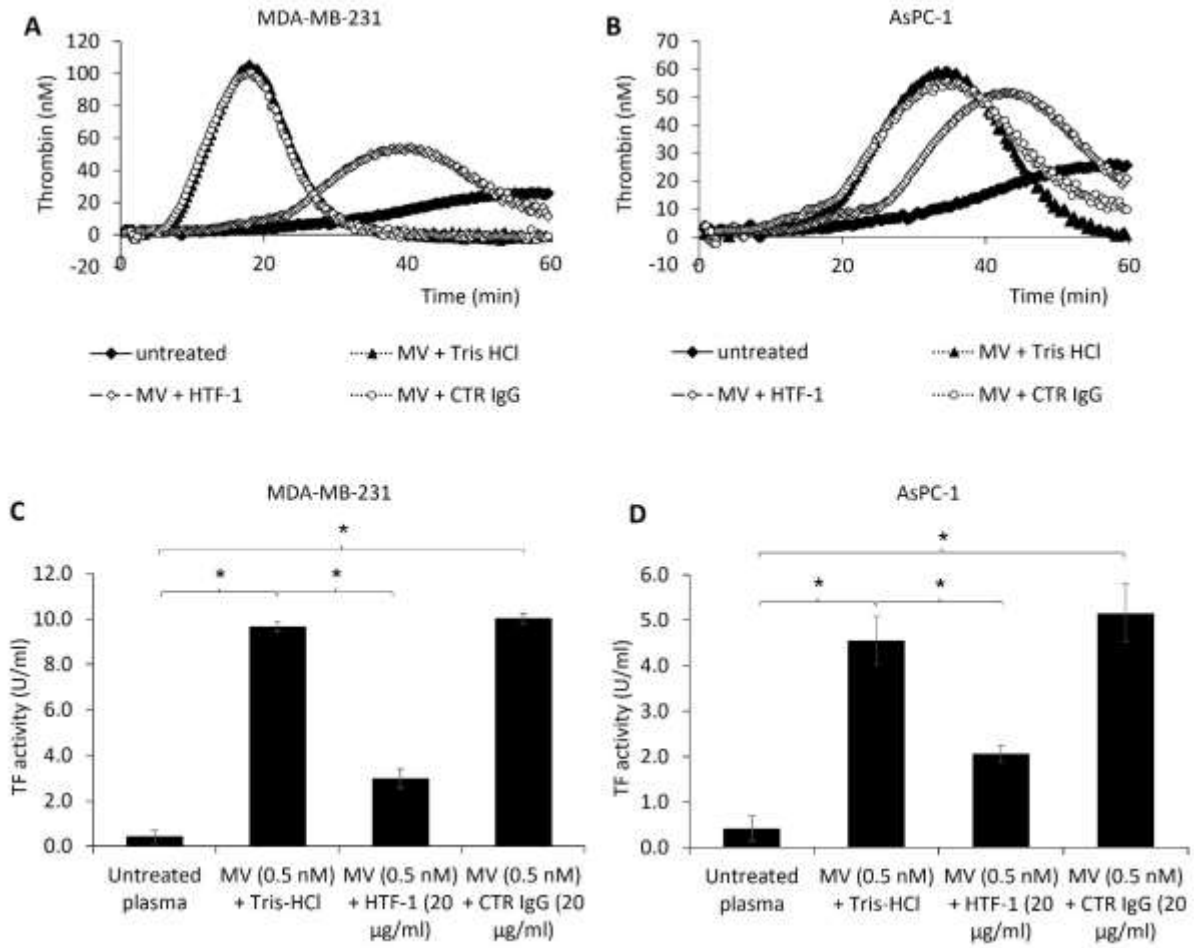

MV (0.5 nM) derived from A) & C) MDA-MB-231 cells or B) & D) AsPC-1 cells were pre-incubated with either an inhibitory anti-TF antibody (HTF-1; 20 µg/ml), the equivalent isotype control antibody (CTR IgG; 20 µg/ml) or the vehicle buffer (Tris-HCl, pH 7.4) for 15 min. Normal plasma was supplemented with the pre-incubated MV and thrombin generation in the samples was monitored by CAT. C) & D) Lag time values of each plasma sample were recorded and the TF activity calculated (n=3, one experiment carried out in triplicate; data = mean values ± SEM; independent t-test * = $p < 0.05$).

Figure 4.17: Assessment of the capability of cancer cell-derived MV to promote thrombin generation in fVII-deficient plasma

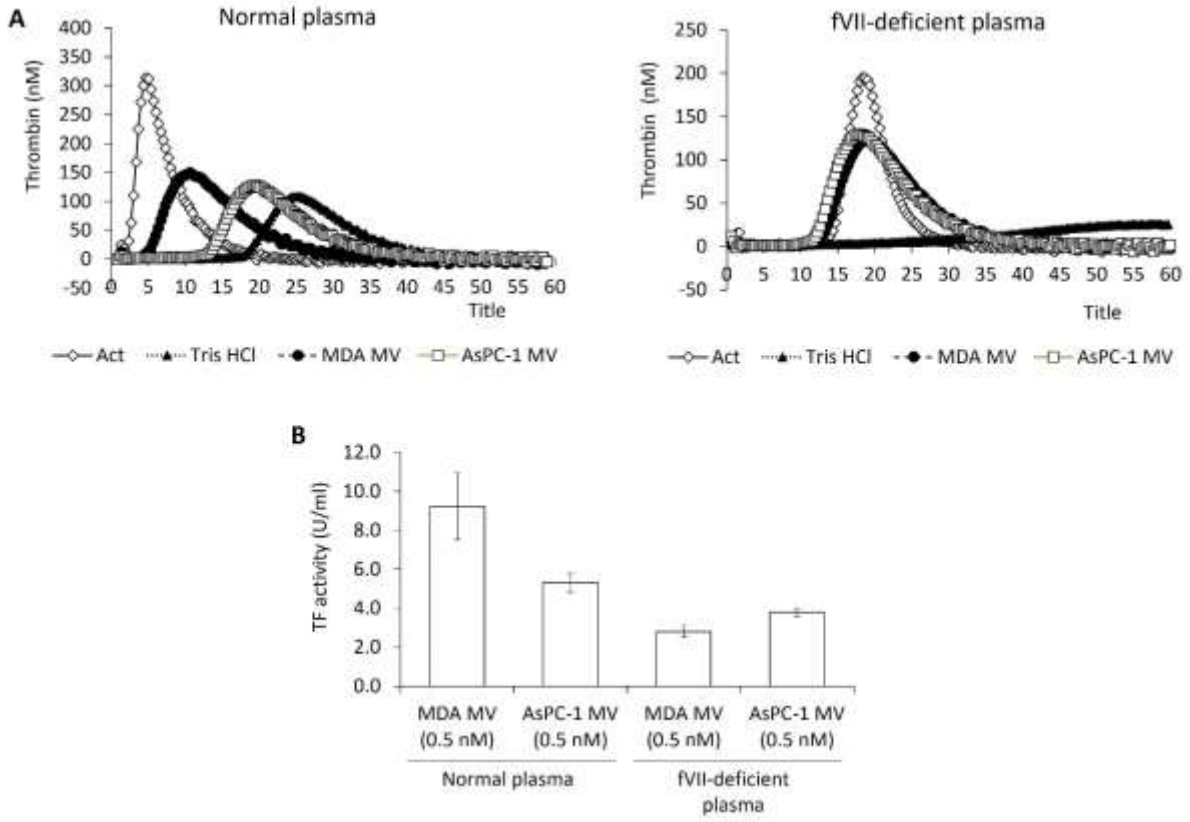

FVII-deficient plasma or normal plasma was supplemented with MV (0.5 nM) derived from MDA-MB-231 cells or AsPC-1 cells and A) thrombin generation in the samples was monitored by CAT. B) Lag time values of each sample were recorded and TF activity calculated (n=3, one experiment carried out in triplicate; data = mean values ± SEM).

Figure 4.18: Assessment of the influence of the lysis of MV on the detection of MV-associated TF antigen

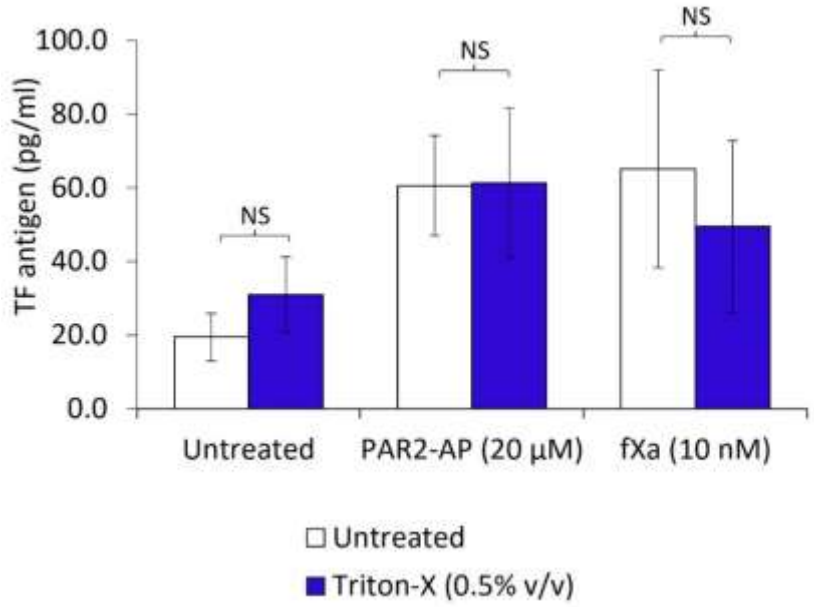

MDA-MB-231 cells (2×10^5) were adapted to SFM for 1 h before being activated with PAR2-AP (20 µM) or fXa (10 nM) for 30 min. The MV were collected by ultracentrifugation. Samples of isolated MV were incubated with Triton-X (0.5% v/v) for 5 min prior to quantification of MV-associated TF antigen using by ELISA (n=3, the data represent one experiment carried out in triplicate; data = mean values ± SEM; independent t-test, NS = not significant).

Figure 4.19: Analysis of the effective concentrations of apixaban and rivaroxaban on fXa

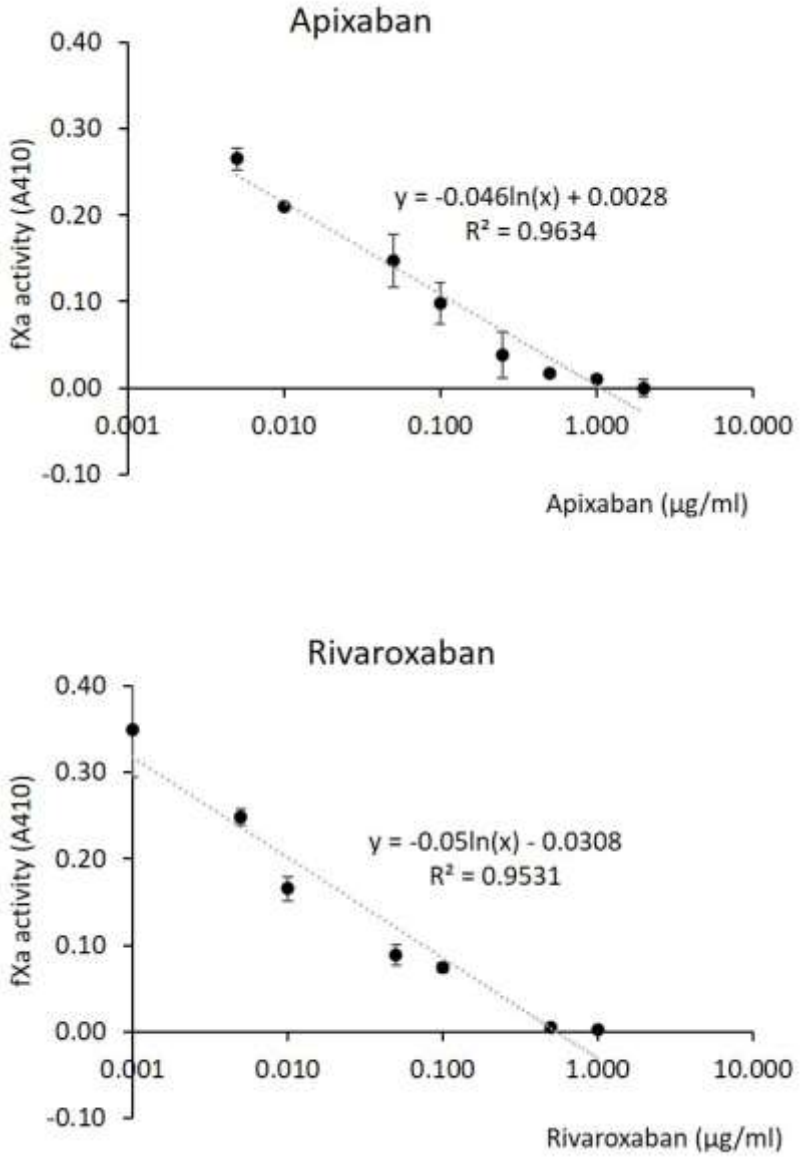

Samples of fXa (10 nM) were pre-incubated with a range of concentrations of apixaban or rivaroxaban (0.001-2 µg/ml) and then incubated with a fXa substrate (0.5 mg/ml) at 37°C for 20 min. The absorption of the samples was measured at 410 nm using a plate reader. Logarithmic regression lines and R^2 values were calculated in Microsoft Excel (n=6, two independent experiments carried out in triplicate; data = mean values ± SEM).

However, MV collected following the single PBS wash did not alter fXa activity as measured with the chromogenic substrate (Figure 4.20). Consequently, it was determined that a single wash of the MV with PBS was sufficient to eliminate the presence of any residual apixaban/rivaroxaban.

4.3.2 Examination of the influence of apixaban and rivaroxaban on the release of MV from cell lines

MDA-MB-231 and AsPC-1 cells were incubated with fXa (10 nM) which had been pre-incubated with either apixaban (0.1 & 1 μg/ml) or rivaroxaban (0.06 & 0.6 μg/ml) (Figure 4.21). Incubation of MDA-MB-231 and AsPC-1 cells with fXa (10 nM) resulted in an increased release of MV (Figure 4.22). This was concurrent with an increase in MV-associated TF antigen (Figure 4.23) and MV associated procoagulant activity (Figure 4.24). Inclusion of apixaban (1 μg/ml) or rivaroxaban (0.6 μg/ml) reduced the release of MV and the MV-associated TF antigen and procoagulant activity (Figure 4.22-Figure 4.24) to levels comparable to that of resting/non-activated cells (results have been summarised in Table 4.3). Incubation of the cells with the DMSO vehicle had no detectable effect on the release of MV from either cell line (Figure 4.25).

In addition, the capability of apixaban or rivaroxaban to influence the release of MV beyond that mediated through fXa inhibition was assessed. Incubation of cells with either apixaban or rivaroxaban did not result in a significant change in the release of MV following PAR2 activation with PAR2-AP (Figure 4.26). Interestingly, apixaban did reduced the release of MV from resting MDA-MB-231 cells as well as the MV-associated TF antigen levels (Figure 4.27). In contrast, rivaroxaban had no significant effect on the MV release from resting cells (results have been summarised in Table 4.4).

A further set of experiments was carried out to determine if the reduction in release of MV from resting MDA-MB-231 cells observed with apixaban treatment was mediated through PAR2 and/or PAR1 (Figure 4.28). Pre-incubation of cells with the inhibitory anti-PAR2 antibody resulted in a reduction in MV release from 2.39 nM/M cell ± 0.28 in cells treated with control IgG antibody to 1.41 nM/M cell ± 0.25 in cells treated with SAM11 antibody (Figure 4.29A). In contrast, pre-incubation of cells with the inhibitory anti-PAR1 antibody did not influence MV release (2.21 nM/M cell ± 0.14). The combined treatment of cells with both apixaban and the inhibitory anti-PAR2 antibody (1.31 nM/M cell ± 0.11) did not reduce MV release below that of the treatment with apixaban alone (1.15 nM/M cell ± 0.31) (Figure 4.29B). Therefore, these data suggest that the inhibition of MV release by apixaban in resting cells is mediated through PAR2.

4.3.3 Examination of the alterations in cell surface TF expression following MV release

To examine the possibility that the release of MV may regulate the amount of cell surface TF, the release of MV was inhibited using apixaban (1 μg/ml) or alternatively, encouraged by incubation of

Figure 4.20: Analysis of the inhibition of fXa activity by apixaban and rivaroxaban present in isolated MV

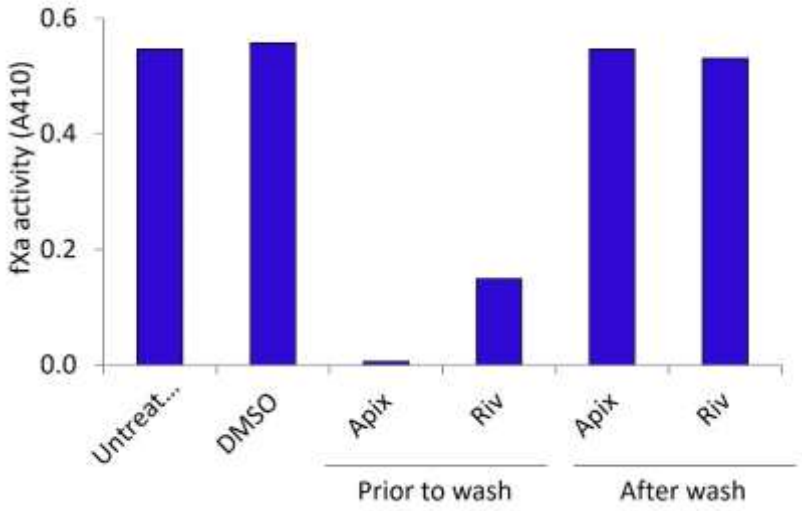

MDA-MB-231 cells (2×10^5) were adapted to SFM for 1 h before being activated with PAR2-AP (20 µM) in the presence or absence of either apixaban (1 µg/ml), rivaroxaban (0.6 µg/ml) or DMSO (0.05% v/v) for 30 min. Samples of MV were collected by ultracentrifugation either prior to or after the PBS wash. The MV samples (40 µl) were incubated with purified fXa (10 nM) and fXa substrate (0.5 mg/ml) for 20 min at 37°C. The fXa activity was determined by measuring absorption at 410 nm (n=2; data = mean values).

Figure 4.21: Experimental procedure for examining the inhibition of MV release from fXa- or fVIIa-activated cells by apixaban and rivaroxaban

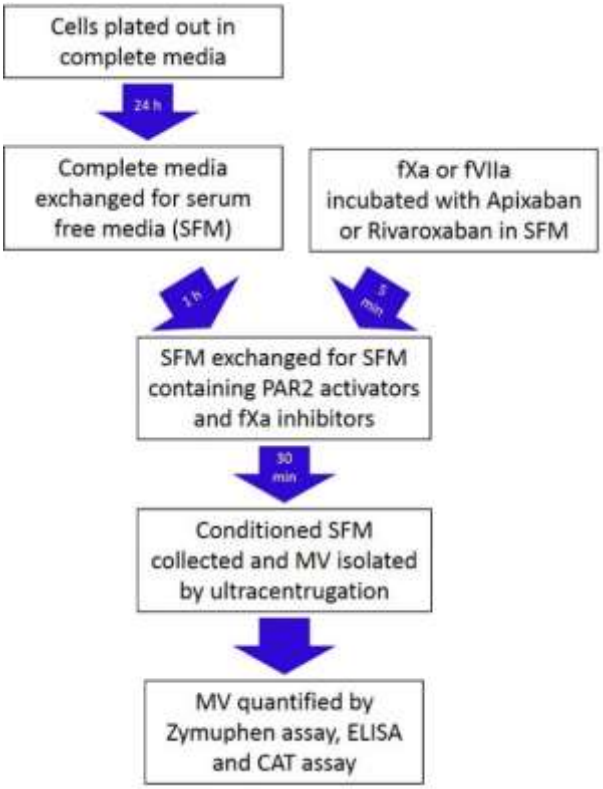

Figure 4.22: Assessment of the influence of apixaban and rivaroxaban on MV release from fXa-activated cells

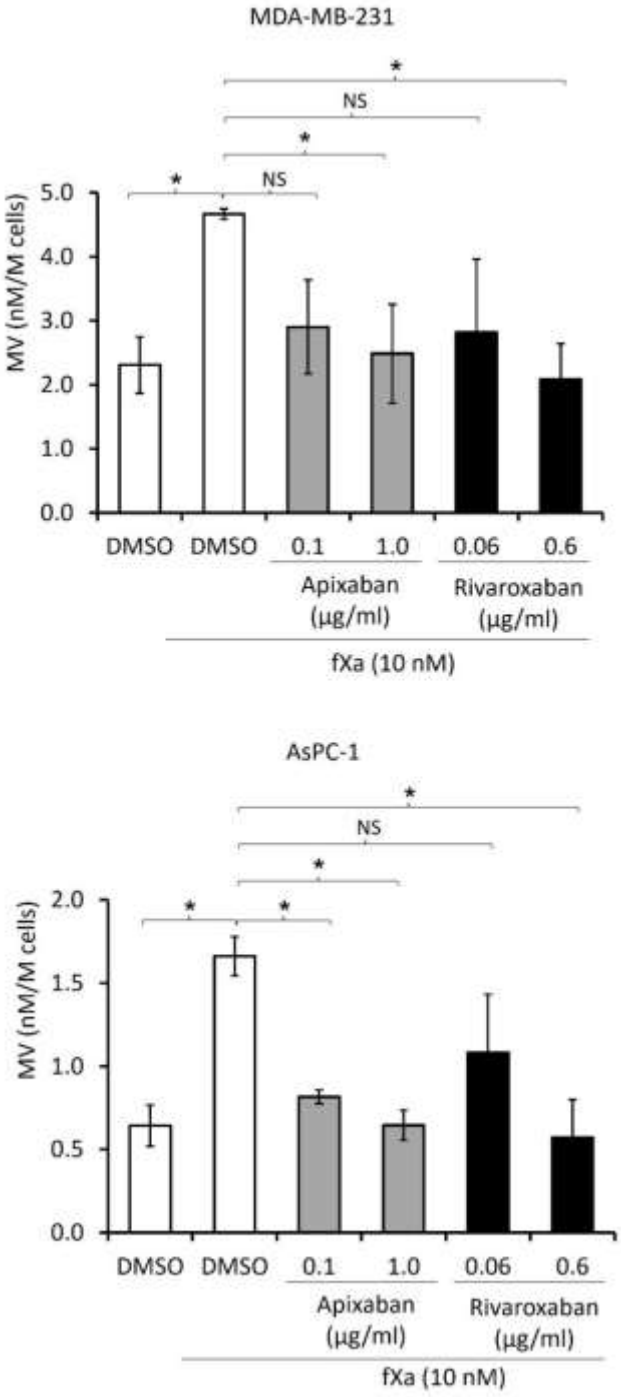

MDA-MB-231 and AsPC-1 cells (10^6) were adapted to SFM for 1 h. Purified fXa (10 nM) was pre-incubated in either apixaban (0.1 & 1 µg/ml), rivaroxaban (0.06 & 0.6 µg/ml) or DMSO (0.05% v/v) vehicle control in SFM for 5 min. The pre-incubated enzyme was added to the cells and incubated for 30 min at 37°C. MV were collected and quantified using Zymuphen assay (n=6, two independent experiments carried out in triplicate; data = mean values ± SEM; independent t-test, * = $p < 0.05$, NS = not significant).

Figure 4.23: Assessment of the influence of apixaban and rivaroxaban on MV-associated TF antigen release from fXa-activated cells

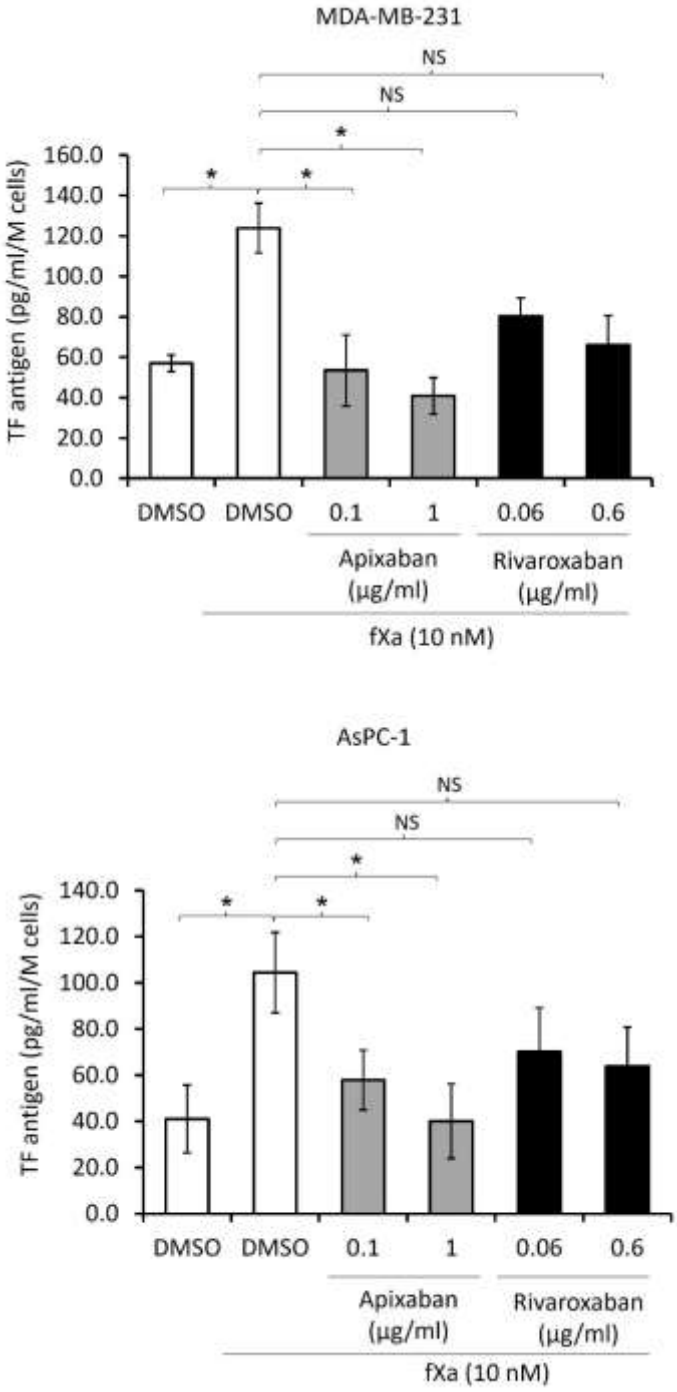

MDA-MB-231 and AsPC-1 cells (10^6) were adapted to SFM for 1 h. Purified fXa (10 nM) was pre-incubated in either apixaban (0.1 & 1 µg/ml), rivaroxaban (0.06 & 0.6 µg/ml) or DMSO (0.05% v/v) vehicle control in SFM for 5 min. The pre-incubated enzyme was added to the cells and incubated for 30 min at 37°C. MV were collected by ultracentrifugation and the MV-associated TF antigen was quantified using ELISA (n=6, two independent experiments carried out in triplicate; data = mean values ± SEM; independent t-test, * = $p < 0.05$, NS = not significant).

Figure 4.24: Assessment of the influence of apixaban and rivaroxaban on the procoagulant activity associated with MV released from fXa-activated cells

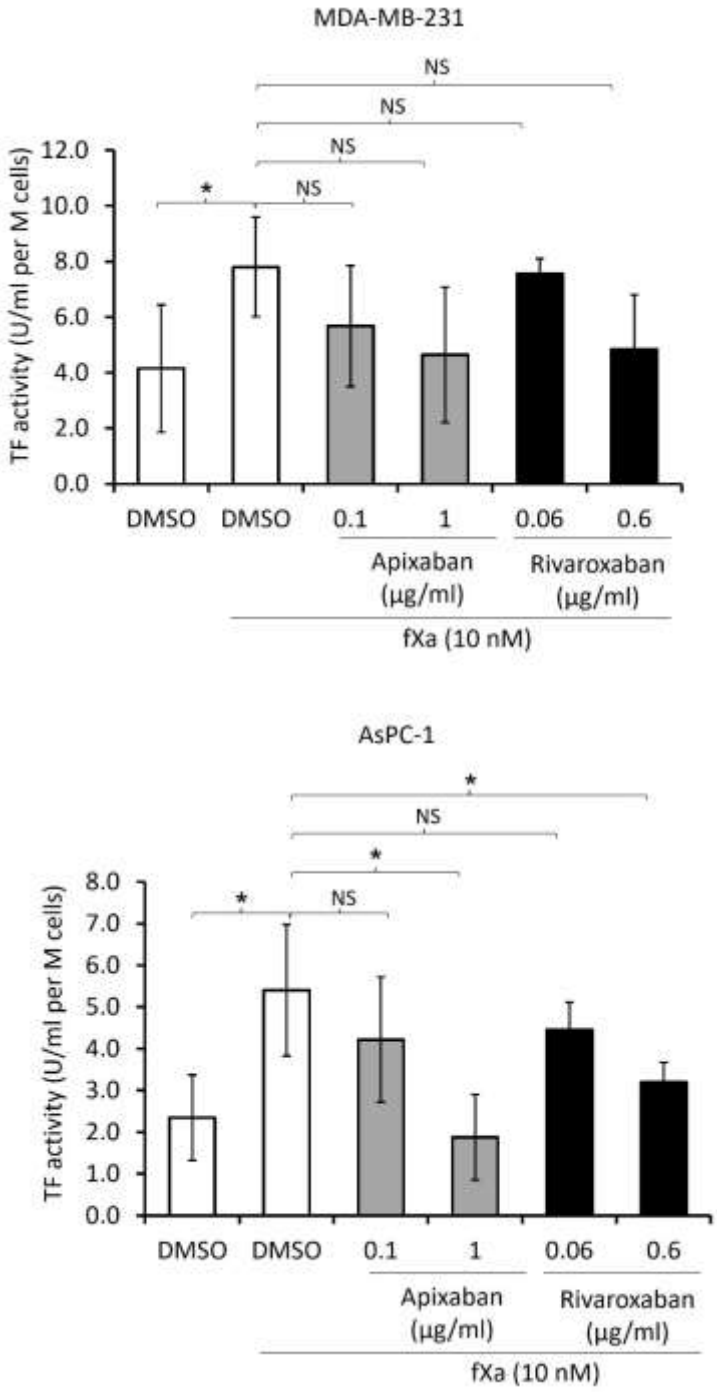

MDA-MB-231 and AsPC-1 cells (10^6) were adapted to SFM for 1 h. Purified fXa (10 nM) was pre-incubated in either apixaban (0.1 & 1 µg/ml), rivaroxaban (0.06 & 0.6 µg/ml) or DMSO (0.05% v/v) vehicle control in SFM for 5 min. The pre-incubated enzyme was added to the cells and incubated for 30 min at 37°C. MV were collected by ultracentrifugation and the MV-associated procoagulant activity was quantified by CAT (n=6, two independent experiments carried out in triplicate; data = mean values ± SEM; independent t-test, * = $p < 0.05$, NS = not significant).

Table 4.3: The reduction in MV and TF release from fXa-activated cells following treatment with apixaban and rivaroxaban

MDA-MB-231	1 µg/ml Apixaban	0.6 µg/ml Rivaroxaban
MV concentration	29% * +/- 22	41% * +/- 16
MV associated TF antigen	36% * +/- 16	19% +/- 18
MV associated pro-coagulant activity	41% +/- 31	38% +/- 25

AsPC-1	1 µg/ml Apixaban	0.6 µg/ml Rivaroxaban
MV concentration	31% * +/- 10	43% * +/- 17
MV associated TF antigen	33% * +/- 20	21% +/- 21
MV associated pro-coagulant activity	39% * +/- 30	34% * +/- 10

MDA-MB-231 and AsPC-1 cells were activated with fXa (10 nM) pre-incubated with of either apixaban (1 µg/ml), rivaroxaban (0.6 µg/ml) or DMSO (0.05% v/v) vehicle control. MV were collected and quantified using the Zymuphen assay, the MV-associated TF antigen measured by ELISA and the MV-associated-procoagulant activity measured by CAT. Percentage inhibition was calculated as 100 x (control - treated) / control (Data = mean values ± SEM; independent t-test * = $p < 0.05$ vs DMSO control).

Figure 4.25: Assessment of the influence of DMSO on MV released

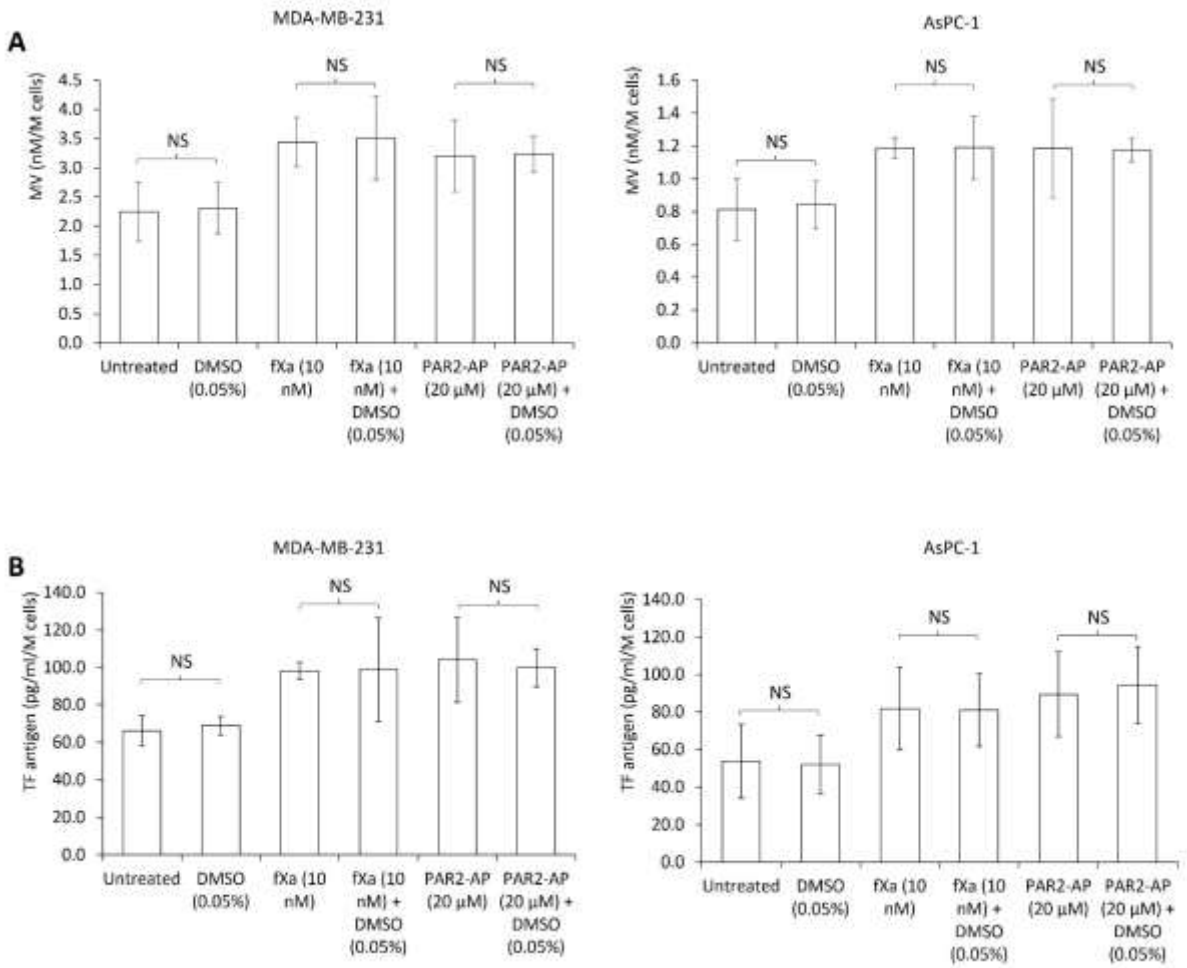

MDA-MB-231 and AsPC-1 cells (2×10^5) were adapted to SFM for 1 h. Purified fXa (10 nM) or PAR2-AP (20 µM) were pre-incubated in the presence or absence of DMSO (0.05% v/v), in SFM for 5 min. The pre-incubated fXa and PAR2-AP was then added to the cells and incubated for 30 min at 37°C. MV were collected, A) quantified using the Zymuphen assay and B) the MV-associated TF antigen was measured by ELISA (n=6, two independent experiments carried out in triplicate; data = mean values ± SEM; independent t-test, NS = not significant).

Figure 4.26: Assessment of the influence of apixaban and rivaroxaban on MV released from PAR2-AP-activated cells

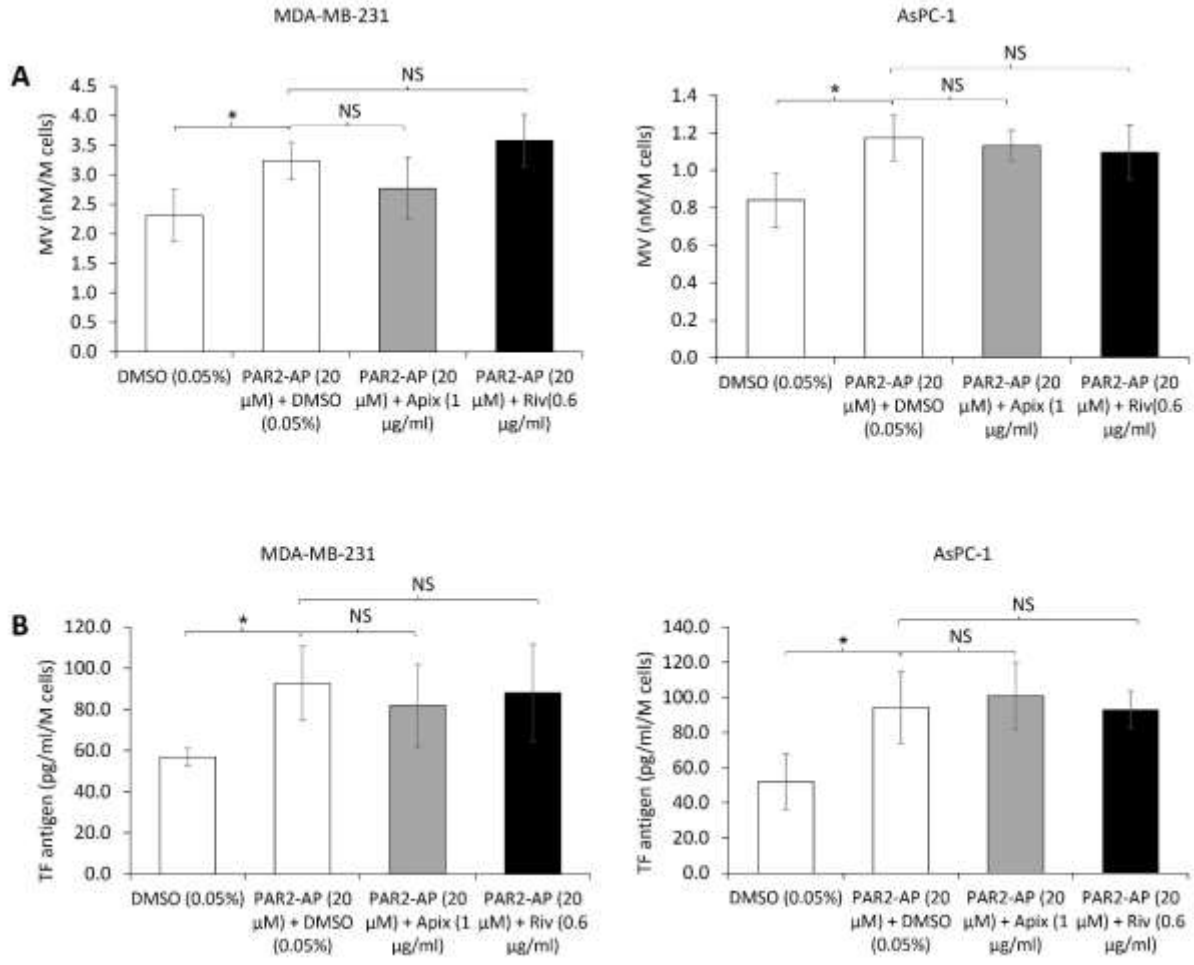

MDA-MB-231 and AsPC-1 cells (2×10^5) were adapted to SFM for 1 h. PAR2-AP (20 µM) was pre-incubated in the presence or absence of either apixaban (1 µg/ml), rivaroxaban (0.6 µg/ml) or DMSO (0.05% v/v) vehicle control, in SFM for 5 min. The pre-incubated PAR2-AP was then added to the cells and incubated for 30 min at 37°C. MV were collected, A) quantified using the Zymuphen assay and B) the MV-associated TF antigen was measured by ELISA (n=6, two independent experiments carried out in triplicate; data = mean values ± SEM; independent t-test, * = $p < 0.05$, NS = not significant).

Figure 4.27: Assessment of the influence of apixaban and rivaroxaban on MV released from resting cells

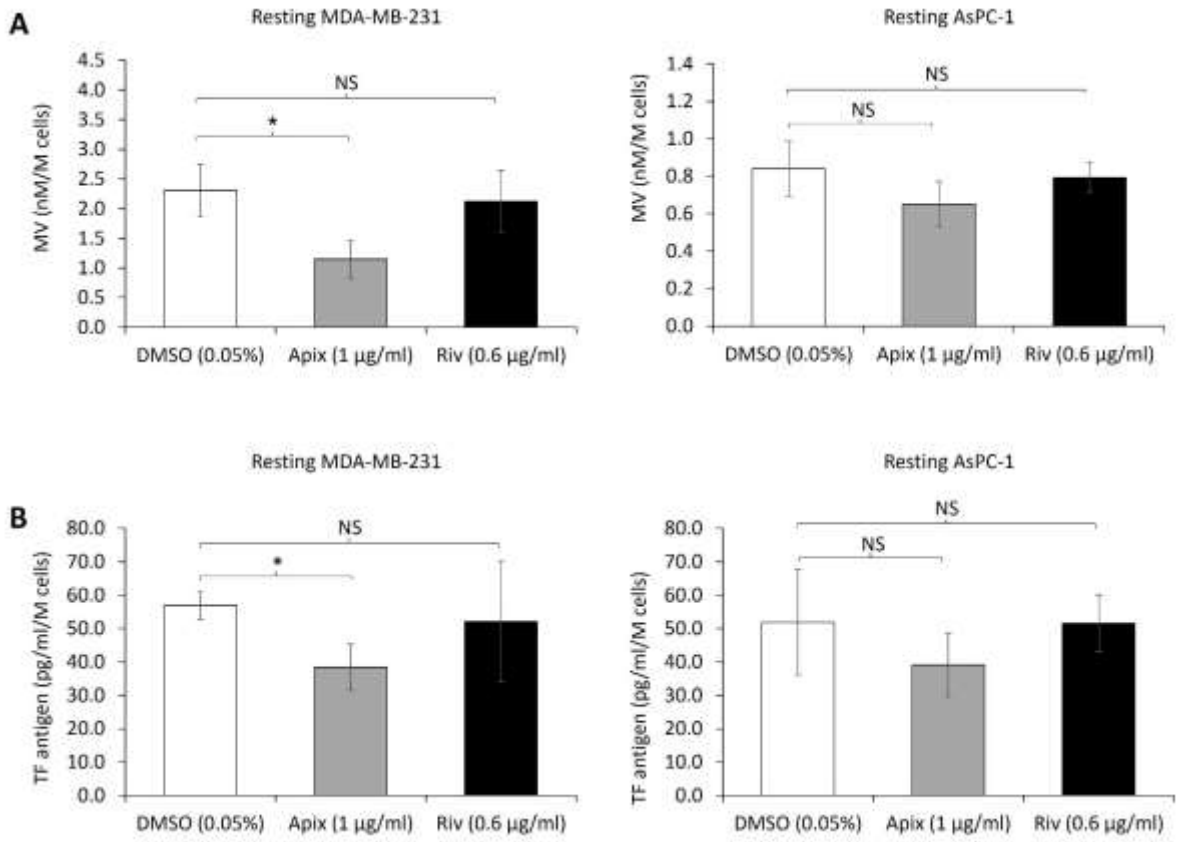

MDA-MB-231 and AsPC-1 cells (2×10^5) were adapted to SFM for 1 h. The cells were then incubated with either apixaban (1 µg/ml), rivaroxaban (0.6 µg/ml) or DMSO (0.05% v/v) vehicle control for 30 min at 37°C. The released MV were collected, A) quantified using the Zymuphen assay and B) the MV-associated TF antigen was measured by ELISA (n=6, two independent experiments carried out in triplicate; data = mean values ± SEM; independent t-test * = $p < 0.05$).

Table 4.4: The reduction in MV and TF release from resting cells following treatment with apixaban and rivaroxaban

MDA-MB-231	1 µg/ml Apixaban	0.6 µg/ml Rivaroxaban
MV concentration	50% * +/- 14	8% +/- 23
MV assosiated TF antigen	32% * +/- 12	9% +/- 32

AsPC-1	1 µg/ml Apixaban	0.6 µg/ml Rivaroxaban
MV concentration	23% +/- 14	5% +/- 9
MV associated TF antigen	25% +/- 18	1% +/- 16

MDA-MB-231 and AsPC-1 cells were incubated with either apixaban (1 µg/ml), rivaroxaban (0.6 µg/ml) or DMSO (0.05% v/v) vehicle control for 30 min. MV were collected, quantified by Zymuphen assay and the MV-associated TF antigen was measured by ELISA. Percentage inhibition was calculated as 100 x (control - treated) / control. (Data = mean values ± SEM; independent t-test * = $p < 0.05$ vs DMSO control).

Figure 4.28: Experimental procedure for examining the role of PAR1 and PAR2 in the inhibition of MV release in resting cells by apixaban

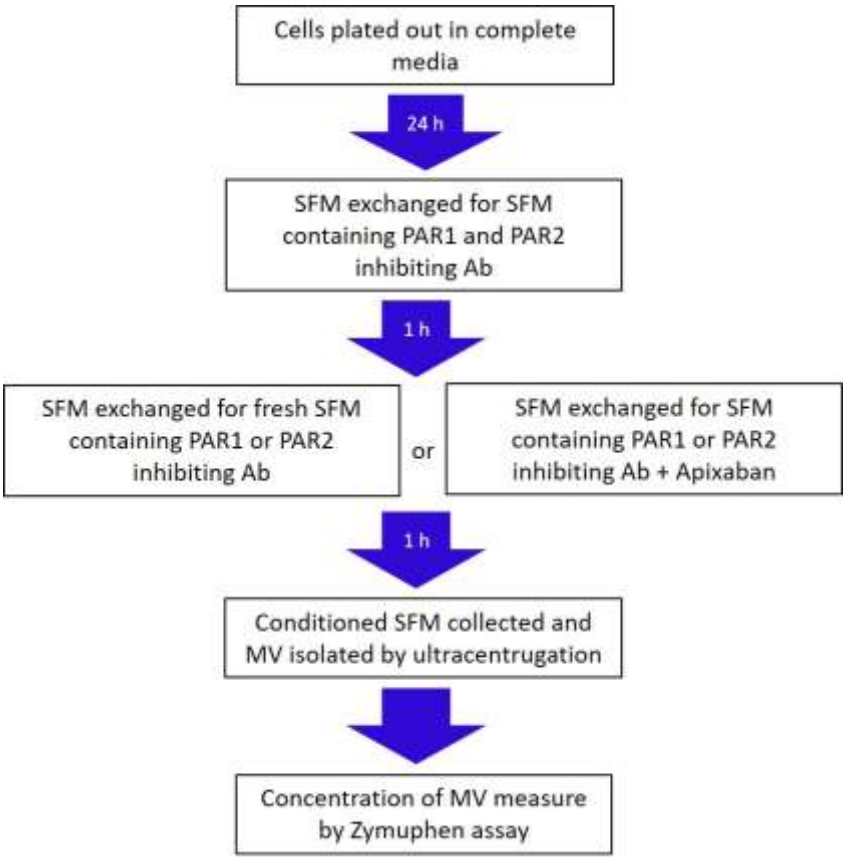

Figure 4.29: Examination of the role of PAR1 and PAR2 in the inhibition of MV release in resting cells by apixaban

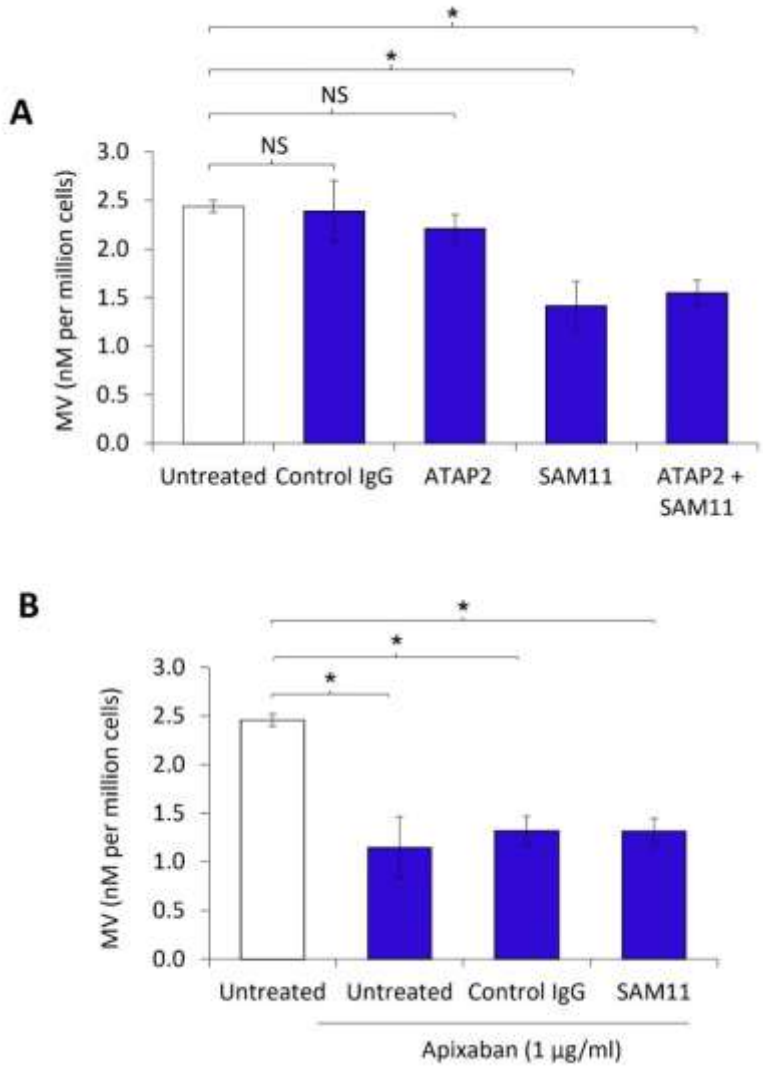

MDA-MB-231 cells (2×10^5) were adapted to SFM in the presence of either blocking antibodies to PAR2 (SAM11; 20 µg/ml), PAR1 (ATAP2; 20 µg/ml), a combination of the two antibodies or the equivalent isotype control antibody (Control IgG; 20 µg/ml) for 1 h. The media was exchanged for fresh media containing the above antibodies either A) alone or B) in combination with apixaban (1 µg/ml) and the cells were incubated for 30 min. MV were collected and quantified using the Zymuphen assay (n=4, two independent experiments carried out in duplicate; data = mean values ± SEM; independent t-test, * = $p < 0.05$, NS = not significant).

cells with PAR2-AP (20 μM) and the cell surface TF was then quantified using the TF-ELISA. Although inclusion of apixaban (1 μg/ml) resulted in an increase in the amount of cell surface TF antigen from 0.61 pg/ml/M cells ± 0.05 in cells treated with DMSO to 0.68 pg/ml/M cells ± 0.05, due to the large variation in the data these differences were not statistically significant (Figure 4.30). In addition, treatment of cells with PAR2-AP (20 μM) resulted in a minor reduction in the cell surface TF to 0.55 pg/ml/M cells ± 0.02 (Figure 4.30). Again, due to large variation in the data these differences were not statistically significant. However, together, these data indicate that TF may be lost from the surface of the cell when released in MV and that apixaban may diminish this loss.

4.3.4 Examination of the influence of apixaban on IL-8 expression

Activation of PAR2 has been reported to induce IL-8 expression (Hirota et al., 2005; Jiang et al., 2017) therefore, the use of IL-8 expression as an indicator of PAR2 activation in cells was confirmed. The activation of MDA-MB-231 cells with PAR2-AP (20 μM) resulted in the up-regulation of IL-8 expression to 4.5 ± 1.48 compared to the untreated cells. Conversely, blocking of PAR2 with the SAM11 antibody resulted in the downregulation of IL-8 expression to 0.40 ± 0.03 (Figure 4.31). These data agree with previous studies showing IL-8 levels in MDA-MB-231 cells can be regulated through PAR2 activation (Hjortoe et al., 2004). As a control, to ensure the absence of any contaminating DNA, the reverse transcription process preceding the PCR amplification was omitted. The omission prevented amplicon production confirming the absence of contaminating genomic DNA. A melt curve was also constructed which produced a single peak for each of the amplicons tested confirming the specificity of the primers used (Figure 4.31B).

The influence of apixaban on IL-8 expression in resting cells was investigated next. Treatment of resting MDA-MB-231 cells with apixaban resulted in a downregulation in IL-8 expression to 0.6 ± 0.10 compared to cells treated with the DMSO vehicle (1.0 ± 0.12) (Figure 4.32). This reduction in IL-8 expression was comparable in magnitude to that observed following the treatment of cells with an inhibitory anti-PAR2 antibody (0.4 ± 0.14).

4.3.5 Examination of the influence of apixaban and rivaroxaban on cell growth

PAR2 activation has previously been reported to increase cell proliferation (Hu et al., 2013; Nishibori et al., 2005; Sun et al., 2018a). Therefore, the influence of apixaban and rivaroxaban on the growth of MDA-MB-231 cells, AsPC-1 cells and HDBEC was examined next (Figure 4.33). Incubation of MDA-MB-231 cells with apixaban (1 μg/ml) resulted in a reduction in cell numbers to 122,000 cells ± 10,000 compared with DMSO treated control cells (170,000 cells ± 5,000). Similarly, incubation of AsPC-1 cells with apixaban resulted in a reduction in cell numbers to 186,000 cells ± 3,000 compared

Figure 4.30: Examination of the alterations in cell surface TF expression following MV release

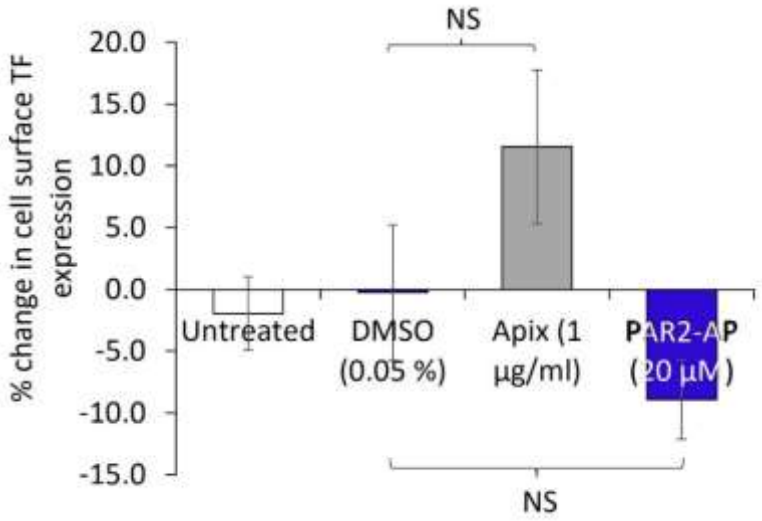

MDA-MB-231 cells (5 x 10^4) were treated with apixaban (1 µg/ml), PAR2-AP (20 µM) or the respective vehicle controls and incubated for 1 h. The surface TF antigen expression of the cells was measured by ELISA (n=8, two independent experiments carried out in quadruplicate; data = mean values ± SEM; independent t-test, NS = not significant).

Figure 4.31: Examination of IL-8 expression as an indicator of PAR2 activation

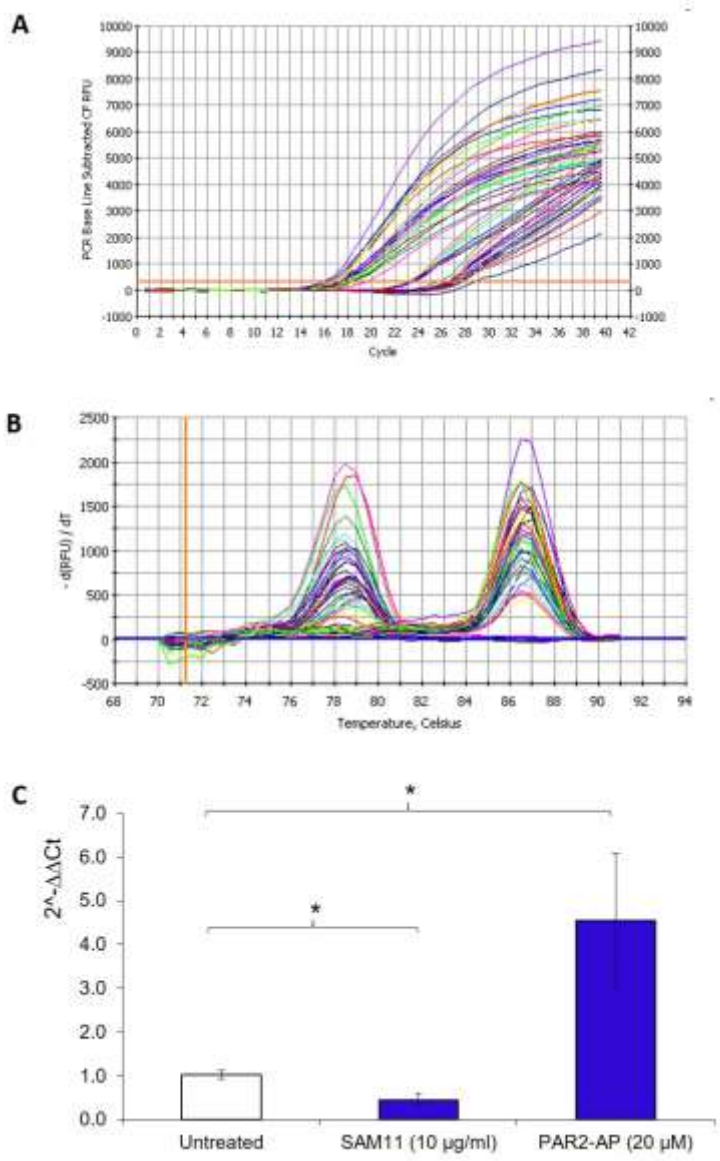

MDA-MB-231 cells (2 x 10^5) were incubated with PAR2-AP (20 µM) or an inhibitory anti-PAR2 antibody (SAM11; 10 µg/ml) for 16 h. The cells were then lysed, mRNA extracted and converted to cDNA using cell-2-cDNA kit. The expression of IL-8 and β-actin mRNA were measured using RT-PCR. A) RT-PCR traces and B) melt curves were generated by the onboard analysis software and C) the relative IL-8 expression levels calculated using the $2^{-\Delta\Delta Ct}$ method (n=6, two independent experiments carried out in triplicate; data = mean values ± SEM; independent t-test * = $p < 0.05$).

Figure 4.32: Assessment of the influence of apixaban on IL-8 expression in resting cells

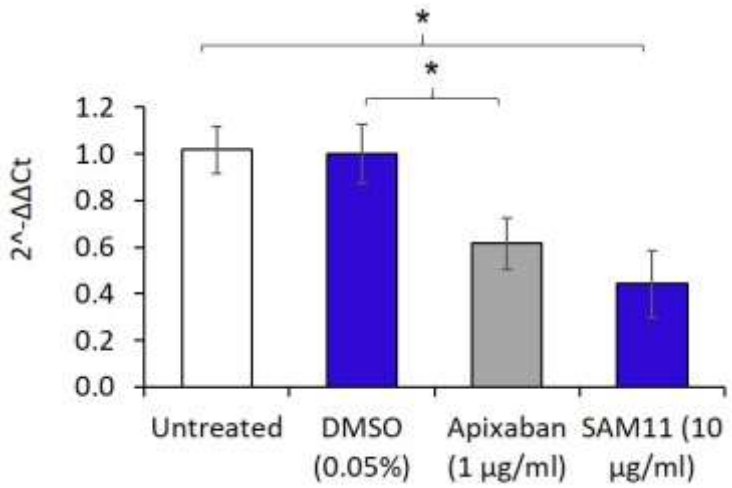

MDA-MB-231 cells (2 x 10^5) were incubated with either an inhibitory anti-PAR2 antibody (SAM11; 20 µg/ml), apixaban (1 µg/ml) or DMSO (0.05% v/v) vehicle control, for 16 h. The cells were lysed, the mRNA was extracted and then converted to cDNA using cell-2-cDNA kit. The expression of IL-8 and β-actin mRNA were measured using RT-PCR and the relative IL-8 expression levels calculated (n=6, two independent experiments carried out in triplicate; data = mean values ± SEM; independent t-test * = $p < 0.05$).

Figure 4.33: Examination of the influence of apixaban and rivaroxaban on cell growth curves

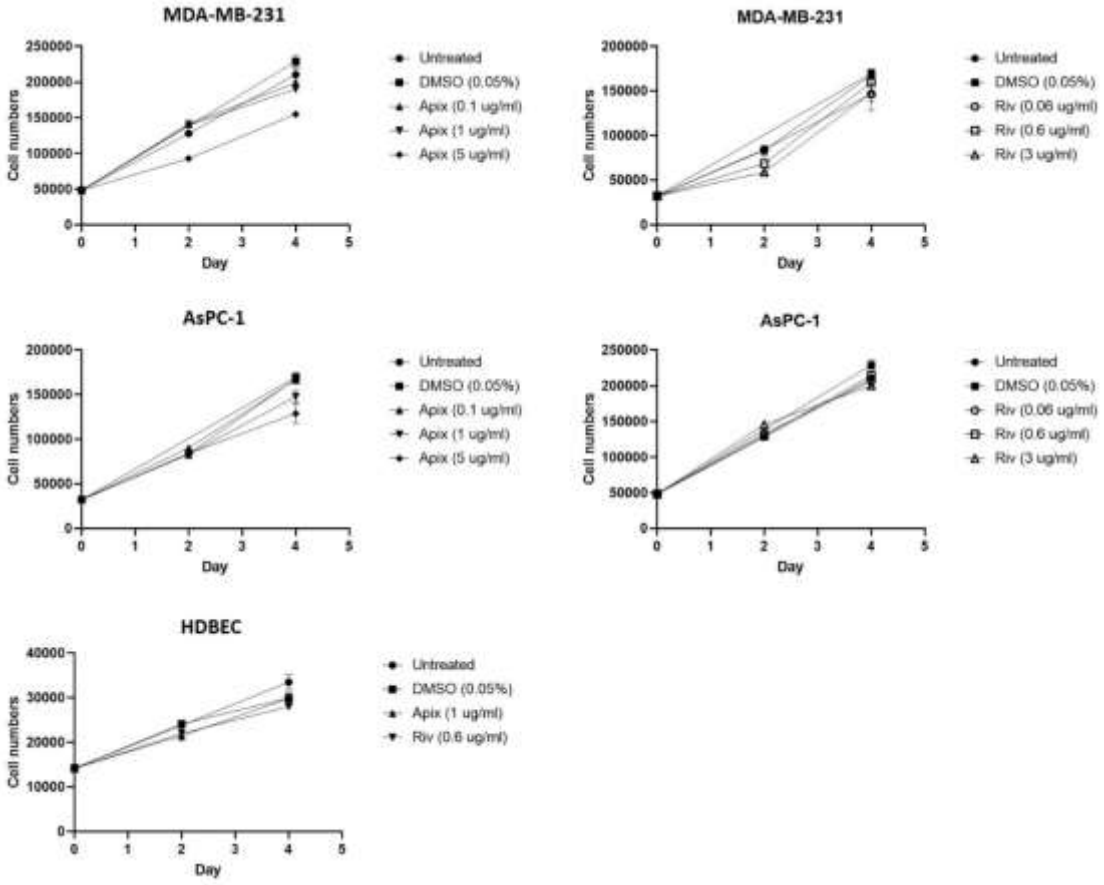

MDA-MB-231 cells, AsPC-1 cells and HDBEC (2×10^4) were plated in 12-well plates and treated with apixaban (0.1-5 µg/ml), rivaroxaban (0.06-3 µg/ml) or DMSO (0.05% v/v) vehicle control for up to 4 days. Plates were collected on day 0, day 2 and day 4 and the cell numbers were determined using the crystal violet assay (n=6; two experiments carried out in triplicate; data = mean values ± SEM).

with DMSO treated control cells (229,000 cells ± 8,000) (Figure 4.34). However, incubation with apixaban did not appear to have any detectable influence on cell growth in HDBEC (apixaban = 29,800 cells ± 1,400, DMSO = 30,000 cells ± 800) (Figure 4.34). Finally, incubation of all cell types with rivaroxaban had no observable influence on cell numbers at any of the concentrations tested.

4.3.6 Examination of the ability of apixaban to inhibit fVIIa activity

Prior to experiments the capability of fVIIa to promoting MV release from MDA-MB-231 and AsPC-1 cells was assessed. Activation of the cells with fVIIa resulted in an increase in MV release from 2.72 nM/M cells ± 0.14 to 4.31 nM/M cells ± 0.62 in MDA-MB-231 cells and from 0.83 nM/M cells ± 0.19 to 2.0 nM/M cells ± 0.32 in AsPC-1 cells (Figure 4.35A). These increases were comparable to that observed following activation with fXa (Figure 4.14). In addition, activation of the cells with fVIIa resulted in an increase in MV-associated TF antigen from 49 pg/ml/M cells ± 13 to 462 pg/ml/M cells ± 53 in MDA-MB-231 cells and from 45 pg/ml/M cells ± 21 to 506 pg/ml/M cells ± 59 in AsPC-1 cells (Figure 4.35A). This indicated that activation with fVIIa may result in increased loading of TF into the MV since the amount of TF associated with the MV isolated from fVIIa-activated cells was much higher than MV isolated from fXa-activated cells (Figure 4.14). This data is contrary to a previous study which reported that MV derived from fVIIa-activated MDA-MB-231 cells did not contain any TF antigen (Das et al., 2018b). Moreover, pre-incubation of the fVIIa enzyme with the inhibitory anti-fVII(a) antibody reduced the release of MV from the cells to 3.15 nM/M cells ± 0.23 in MDA-MB-231 cells and to 1.30 nM/M cells ± 0.06 in AsPC-1 cells (Figure 4.35B). In addition, pre-incubation with the inhibitory anti-fVII(a) antibody also reduced MV-associated TF antigen to 213 pg/ml/M cells ± 24 in MDA-MB-231 cells and to 289 pg/ml/M cells ± 26 in AsPC-1 cells (Figure 4.35B).

In order to test if apixaban was capable of inhibiting fVIIa mediated PAR2 activation, the influence of apixaban on fVIIa induced MV release was assessed in comparison to rivaroxaban, which has been shown not to inhibit fVIIa (Madkhali, 2020). Pre-incubation of the fVIIa with apixaban (1 μg/ml) reduced MV release to levels comparable to that observed from resting MDA-MB-231 and AsPC-1 cells (Figure 4.36A). Furthermore, apixaban reduced the release of MV-associated TF antigen following fVIIa activation. However, this remained at a higher concentration than the levels observed in the resting cells. This data supported the hypothesis that activation of cells with fVIIa may increase the amount of TF antigen associated with each MV. Finally, pre-incubation of fVIIa with rivaroxaban (0.6 μg/ml) did not influence MV release or MV-associated TF antigen levels (Figure 4.36B). The results have been summarised in Table 4.5.

Figure 4.34: Examination of the influence of apixaban and rivaroxaban on cell numbers

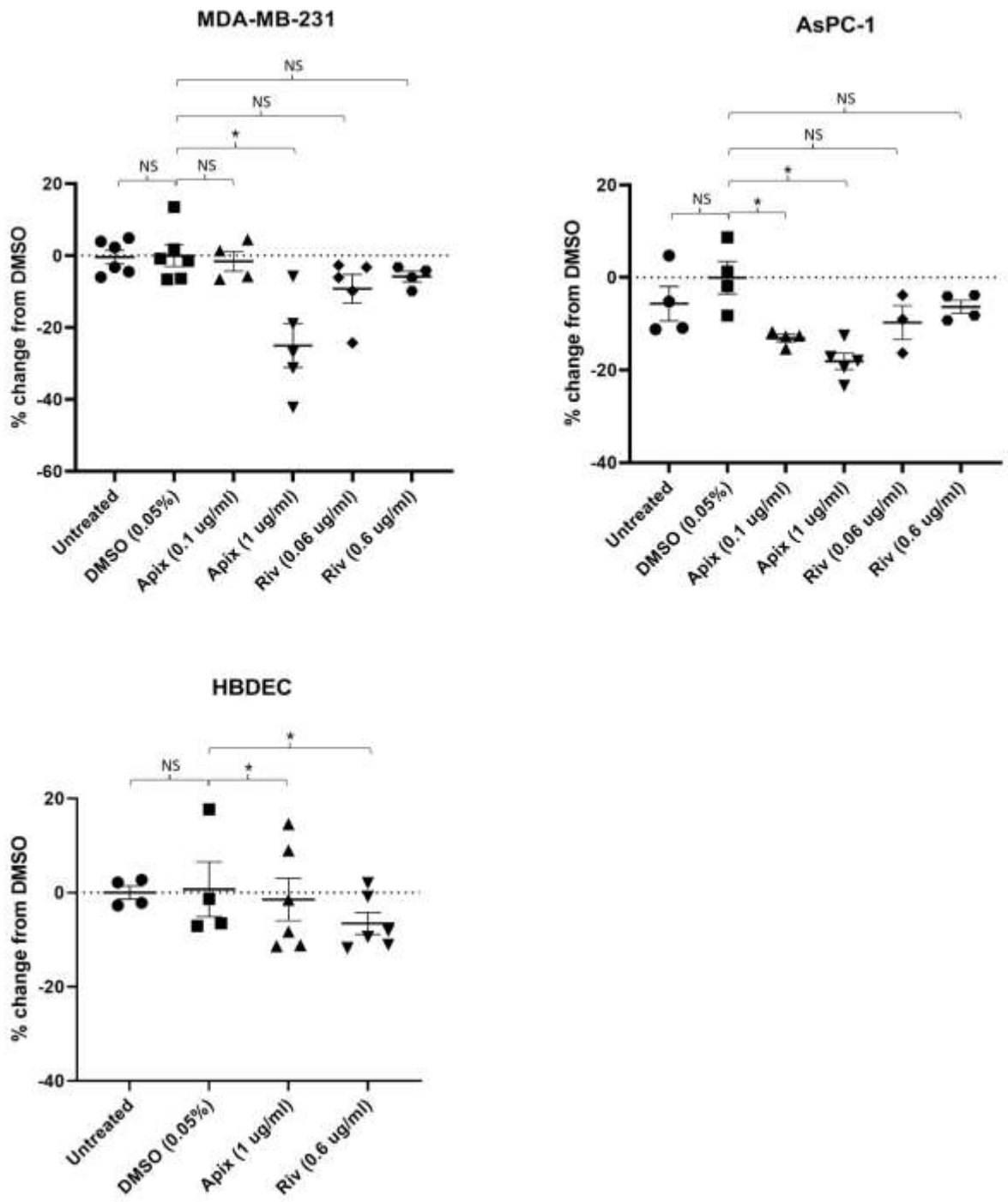

MDA-MB-231 cells, AsPC-1 cells and HDBEC (2×10^4) were plated in 12-well plates and treated with apixaban (0.1 & 1 µg/ml), rivaroxaban (0.06 & 0.6 µg/ml) or DMSO (0.05% v/v) vehicle control for 4 days. The cell numbers were determined using the crystal violet assay. Percentage change was calculated as 100 x (treated - control) / control (n=6; two experiments carried out in triplicate; data = mean values ± SEM; independent t-test, * = $p < 0.05$, NS = not significant).

Figure 4.35: Assessment of the influence of an inhibitory anti-fVIIa antibody on the release of MV from fVIIa-activated cells

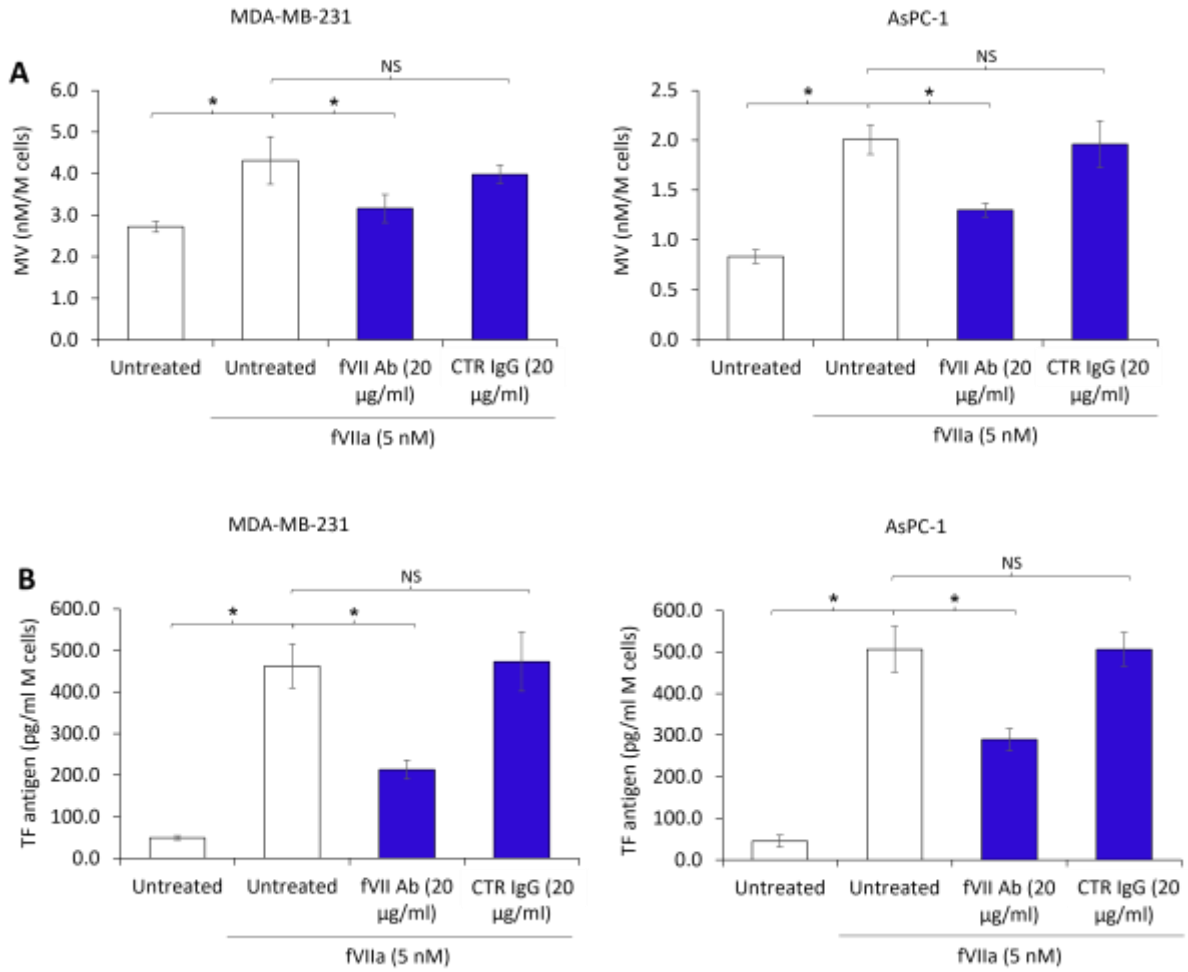

MDA-MB-231 and AsPC-1 cells (2 x 10^5) were adapted to SFM for 1 h. Purified fVIIa (5 nM) was incubated with an inhibitory anti-fVIIa polyclonal antibody (fVII Ab; 20 µg/ml) or an equivalent isotype control antibody (CTR IgG; 20 µg/ml) for 5 min. The pre-incubated fVIIa was then added to the cells and incubated for 30 min at 37°C. MV were collected, A) quantified using the Zymuphen assay and B) the MV-associated TF antigen was measured by ELISA (n=6; two experiments carried out in triplicate; data = mean values ± SEM; independent t-test, * = $p < 0.05$, NS = not significant).

Figure 4.36: Assessment of the influence of apixaban on the release of MV from fVIIa-activated cells

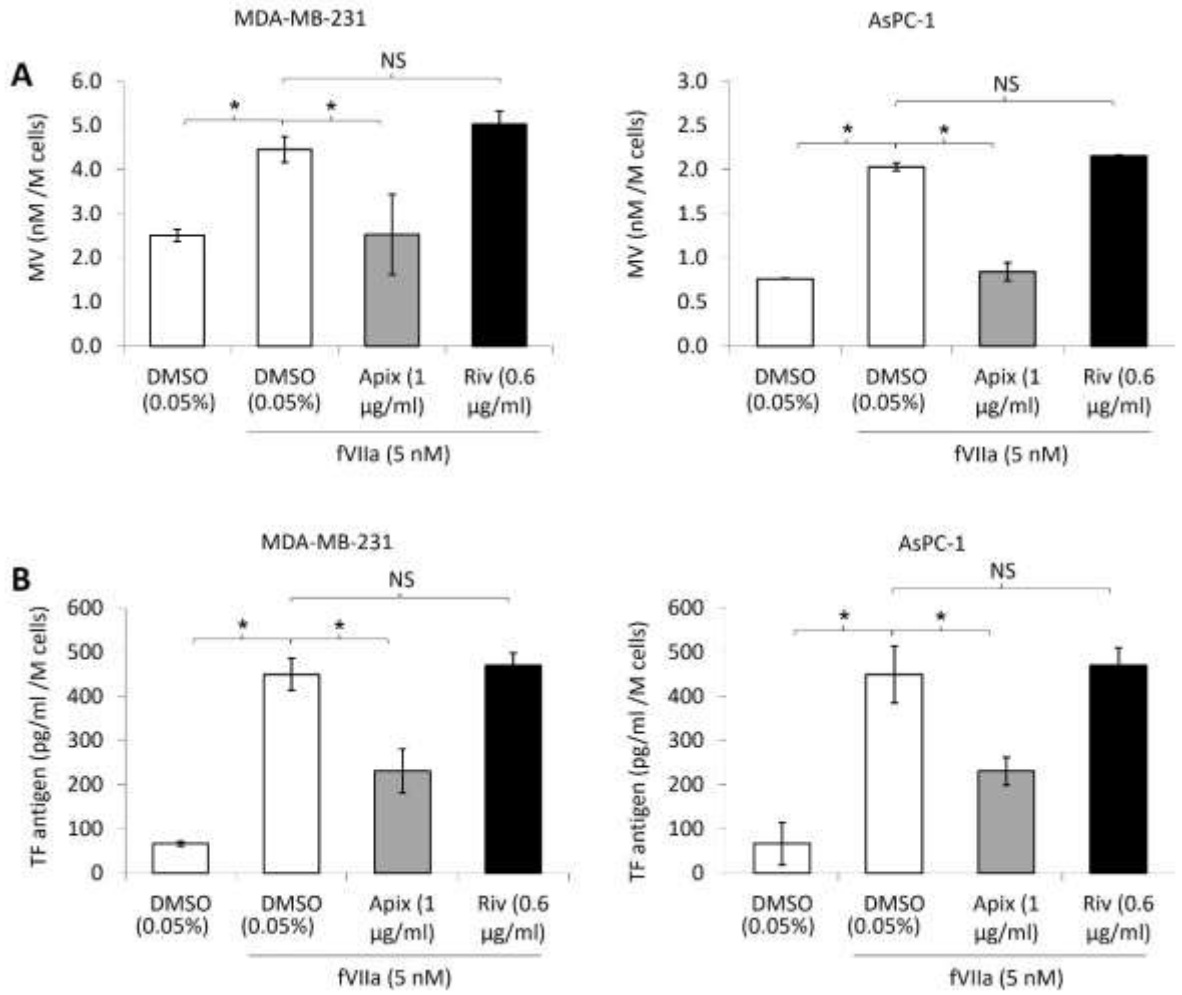

MDA-MB-231 and AsPC-1 cells (2×10^5) were adapted to SFM for 1 h. Samples of fVIIa (5 nM) were pre-incubated in the presence or absence of either apixaban (1 µg/ml), rivaroxaban (0.6 µg/ml) or DMSO (0.05% v/v) vehicle control, in SFM for 5 min. The pre-incubated fVIIa was then added to the cells and incubated for 30 min at 37°C. MV were collected, A) quantified using the Zymuphen assay and B) the MV-associated TF antigen was measured by ELISA (n=6, two independent experiments carried out in triplicate; data = mean values ± SEM; independent t-test, * = $p < 0.05$, NS = not significant).

Table 4.5: The reduction in MV and TF release from fVIIa-activated cells following treatment with apixaban and rivaroxaban

MDA-MB-231	1 µg/ml Apixaban	0.6 µg/ml Rivaroxaban
MV concentration	43% * +/- 7	6% increase +/- 20
MV associated TF antigen	49% * +/- 8	5% increase +/- 11

AsPC-1	1 µg/ml Apixaban	0.6 µg/ml Rivaroxaban
MV concentration	59% * +/- 2	6% increase +/- 5
MV associated TF antigen	56% * +/- 12	1% increase +/- 6

MDA-MB-231 and AsPC-1 cells were activated with fVIIa (5 nM) pre-incubated with either apixaban (1 µg/ml), rivaroxaban (0.6 µg/ml) or DMSO (0.05% v/v) vehicle control, for 30 min. MV were collected, quantified using Zymuphen assay and the MV-associated TF antigen measured by ELISA. Percentage inhibition was calculated as 100 x (control - treated) / control (Data = mean values ± SEM; independent t-test * = $p < 0.05$ vs DMSO control).

4.3.7 Examination of the expression of fVII and fX by cancer cell lines and primary endothelial cells

In order to determine if MDA-MB-231 cells, AsPC-1 cells and HDBEC expressed fVII and/or fX, samples were analysed using SDS-PAGE and western blot. In addition, the liver cancer cell line, HepG2, was used as a positive control as these cells are known to express the coagulation proteins (Fair & Bahnak, 1984; Koizume et al., 2006). The inactive form of fVII was expressed in all the above cell lines, as indicated by the band at ~70 kDa; the AsPC-1 cells exhibited the highest expression levels and the HDBEC the lowest. In addition, the active form, fVIIa, was detectable in the MDA-MB-231, AsPC-1 and HepG2 cell lines. The fVIIa could be identified by the presence of a major band at ~30 kDa corresponding to the light chain of the fVIIa protein and less prominent multiple bands at 35-37 kDa corresponding to the heavy chain (Figure 4.37). Due to extensive and differential glycosylation of the protein, the molecular weights observed for all forms of the protein were greater than would be estimated from the amino acid sequence of fVII. This may also explain the multiple bands observed for the heavy chain of fVIIa, since the patterns of glycosylation are known to vary (Bohm et al., 2015; Kaufman, 1998).

The western blot membrane was also probed with the anti-fX antibody but did not produce any clear data due to non-specific binding of the antibody (Figure 4.38). In an attempt to detect the expression of fXa in the cell lines, fXa was measured using a chromogenic substrate, on the surface of the cells and also in the culture media. Incubation of MDA-MB-231 cells with the fXa chromogenic substrate indicated the presence of 0.07 nM +/- 0.03 of fXa activity (Figure 4.39A). To examine the ability of the cells to release the fXa, conditioned media was incubated with the fXa substrate. The fXa activity of the media was determined to be 0.018 nM +/- 0.04 which was not significantly different to that measured in the fresh non-conditioned media (Figure 4.39B), indicating the MDA-MB-231 cells did not secrete a detectable amount of fXa into the media.

4.3.8 Investigation of the mechanism of fVII inhibition by apixaban

4.3.8.1 Examination of the influence of apixaban on interaction between fVIIa, TF and PAR2

FVIIa must form a complex with TF in order to be capable to activate PAR2 (Camerer et al., 2000b). Furthermore, the TF/fVIIa complex closely associates with the N-terminal domain of PAR2 in order to cleave and activate the receptor (Nystedt et al., 1995). Therefore, a possible mechanism by which apixaban may inhibit the activation of PAR2 is by interfering with the interaction of fVIIa with either TF or PAR2. PLA analysis indicated that incubation of the cells with apixaban did not influence the number of interactions between fVIIa and PAR2 on the cell surface (apixaban = 8.6 ± 0.9 incidences/cell, DMSO = 9.4 ± 1.4 incidences/cell) (Figure 4.40). This suggests that apixaban does not interfere with the approximation and possible association of fVIIa with PAR2. Moreover, treatment

Figure 4.37: Examination of the expression of fVII(a) in cells by western blot

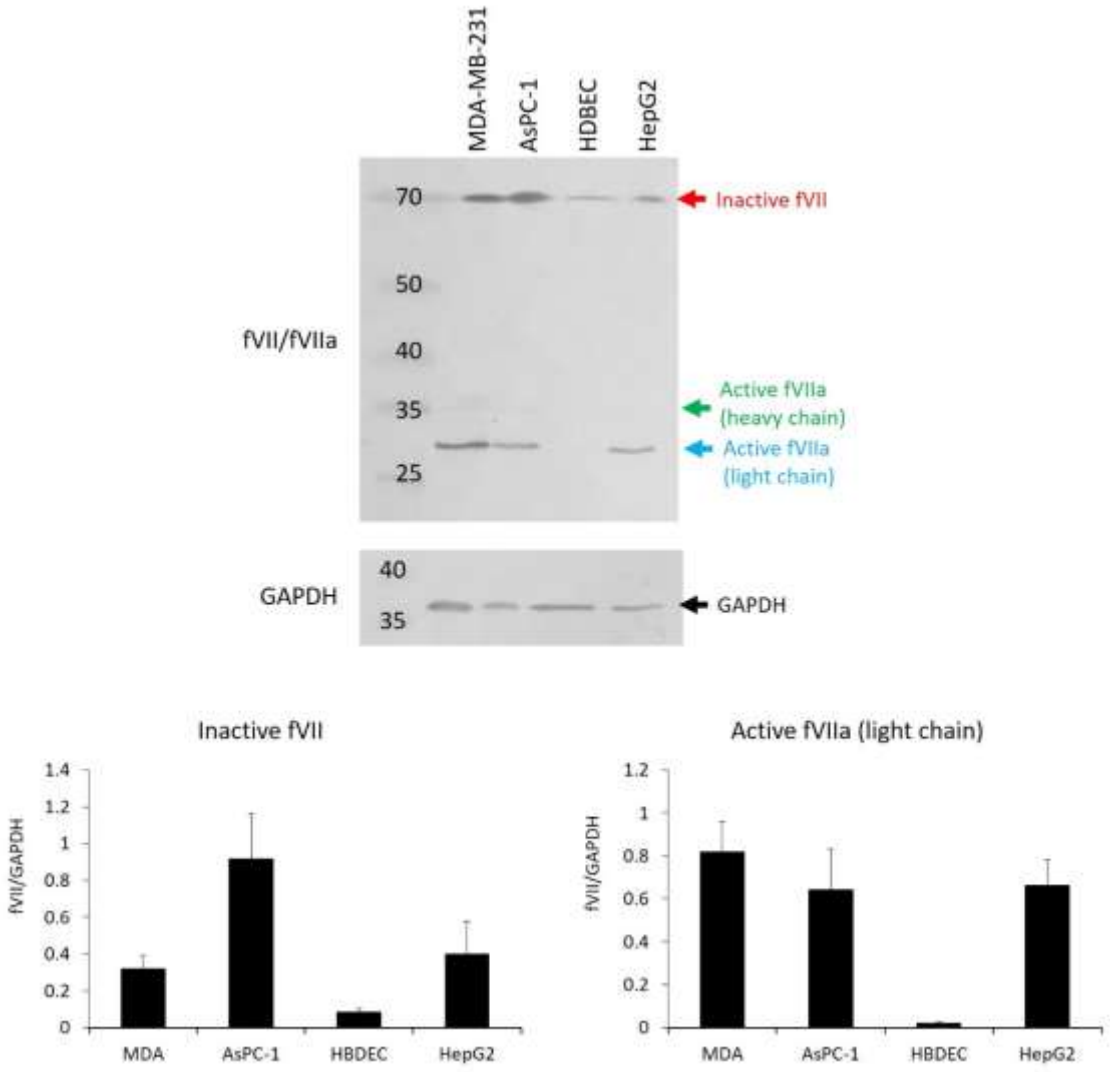

MDA-MB-231 cells, AsPC-1 cells, HDBEC and HepG2 cells were lysed in Laemmli buffer and heated at 95°C for 5 min. The proteins were separated by SDS-PAGE and then probed using the western blot assay with anti-fVII antibody (diluted 1:3000 v/v in TBST) and anti-GAPDH antibody (diluted 1:5000 v/v in TBST). The membranes were then incubated with AP-conjugated anti-rabbit IgG and AP-conjugated anti-goat IgG antibodies (diluted 1:3000 v/v in TBST), respectively. The membranes were developed using Western Blue stabilised substrate for AP and the intensities of the bands were quantified using ImageJ (n=3; data = mean values ± SEM).

Figure 4.38: Examination of the expression of fX(a) in cells by western blot

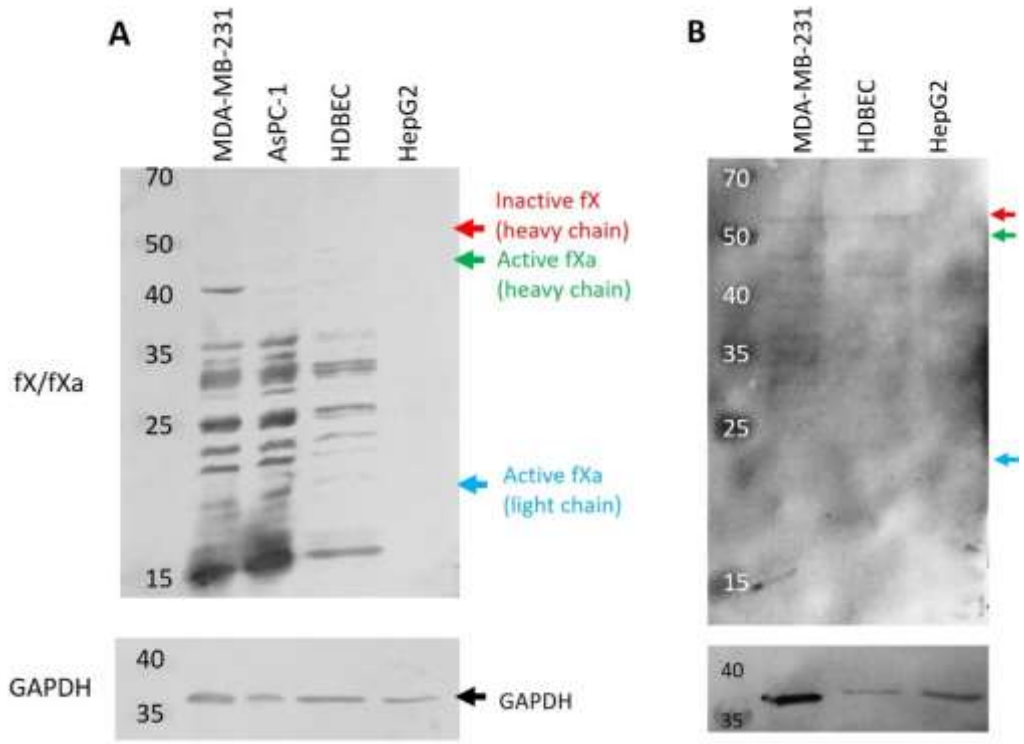

MDA-MB-231 cells, AsPC-1 cells, HDBEC and HEPG2 cells were lysed in Laemmli buffer and heated at 95°C for 5 min. The proteins were separated by SDS-PAGE and then probed by western blot with an anti-fX antibody diluted A) 1:6000 (v/v) B) 1:3000 (v/v) in TBST or an anti-GAPDH antibody diluted 1:5000 (v/v) in TBST. The membranes were incubated with AP-conjugated anti-rabbit IgG or AP-conjugated anti-goat IgG antibodies (diluted 1:3000 v/v in TBST), respectively. The membranes were then developed using Western Blue stabilised substrate for AP (Images are representative of 2 experiments carried out in in duplicate).

Figure 4.39: Assessment of the expression of fX(a) in MDA-MB-231 cells by fXa activity assay

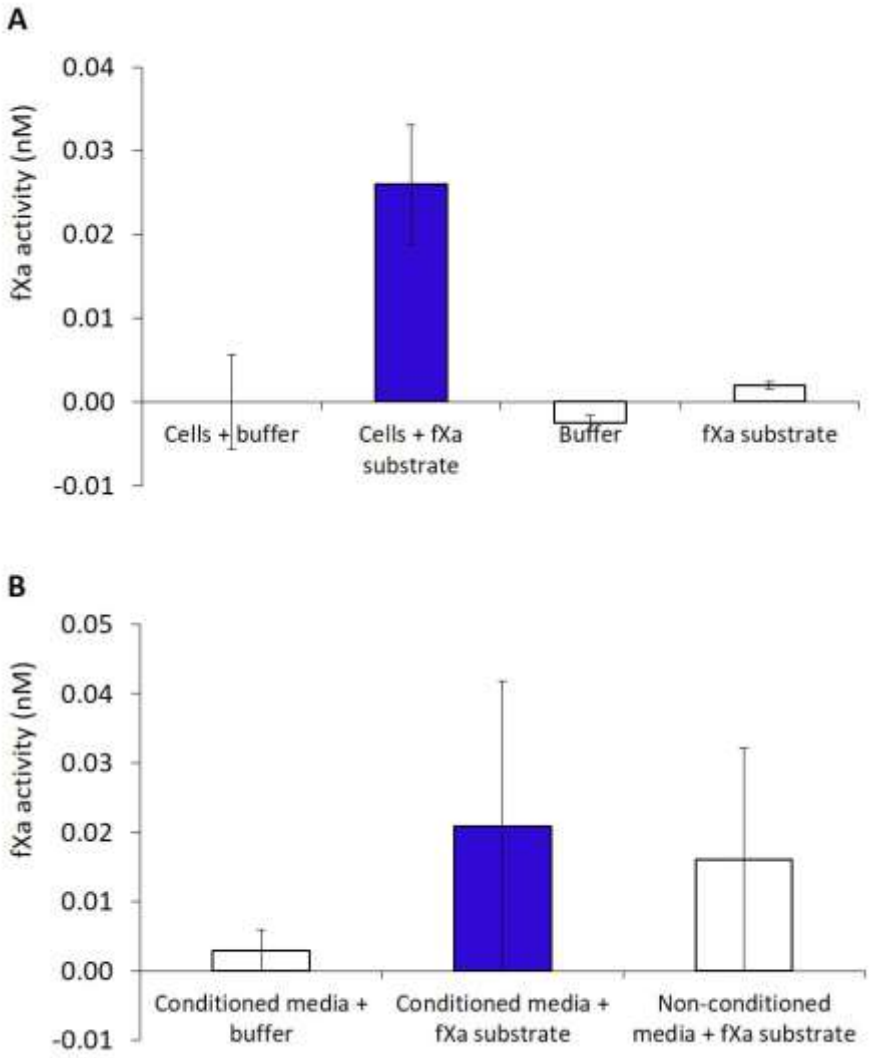

A) MDA-MB-231 cells (2 x 10^4) were incubated in the presence or absence of the fXa substrate (0.5 mg/ml) for 1 h at 37°C. The fXa activity was determined by measuring the absorption at 410 nm (n=4, one experiment carried out in quadruplicate). B) Conditioned or non-conditioned media (100 µl) was incubated in the presence or absence of the fXa substrate (0.5 mg/ml) for 1 h at 37°C. The fXa activity was determined by measuring the absorption at 410 nm (n=4, one experiment carried out in quadruplicate; data = mean values ± SEM).

Figure 4.40: Assessment of the influence of apixaban on the interaction between fVIIa and PAR2

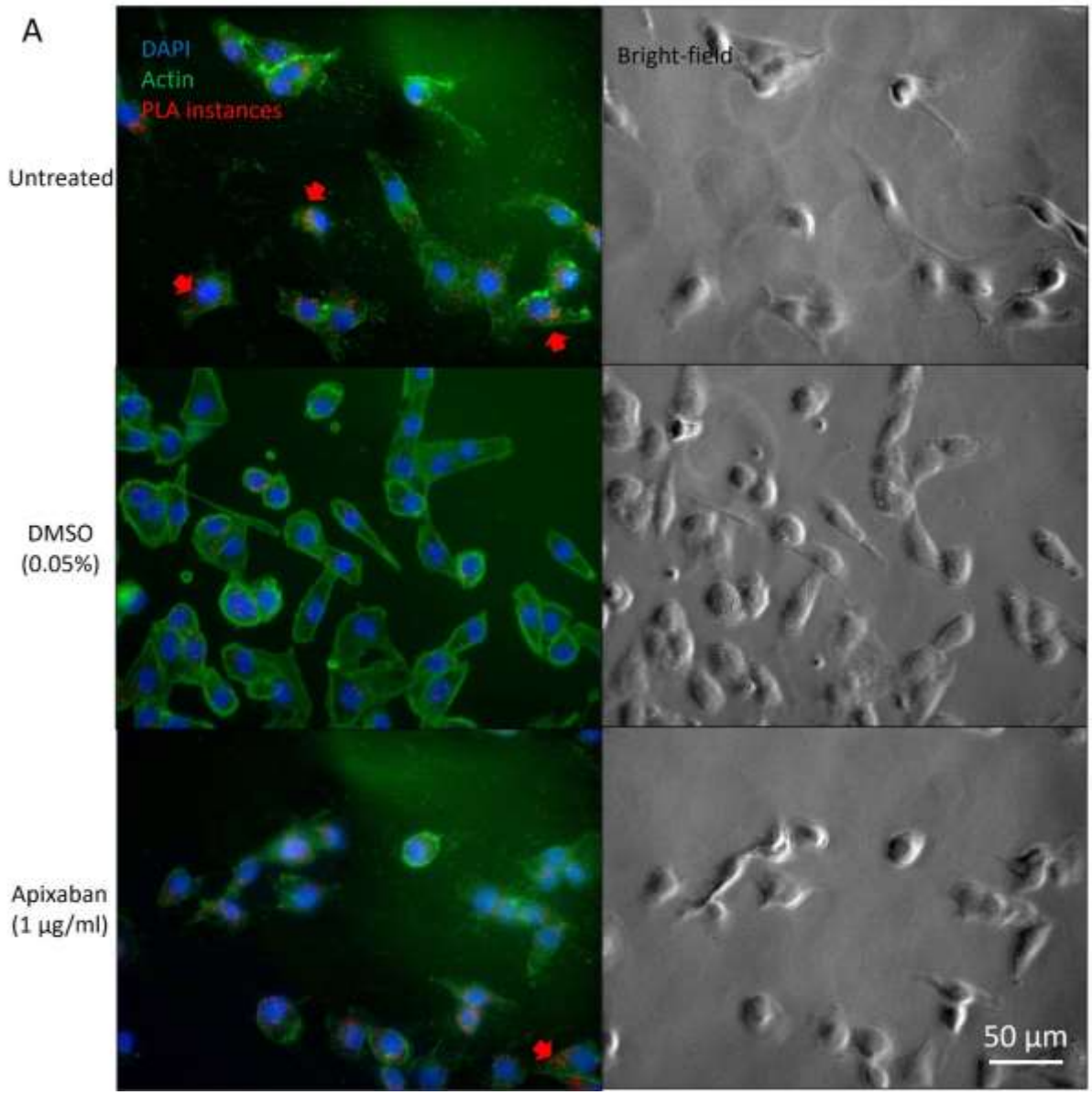

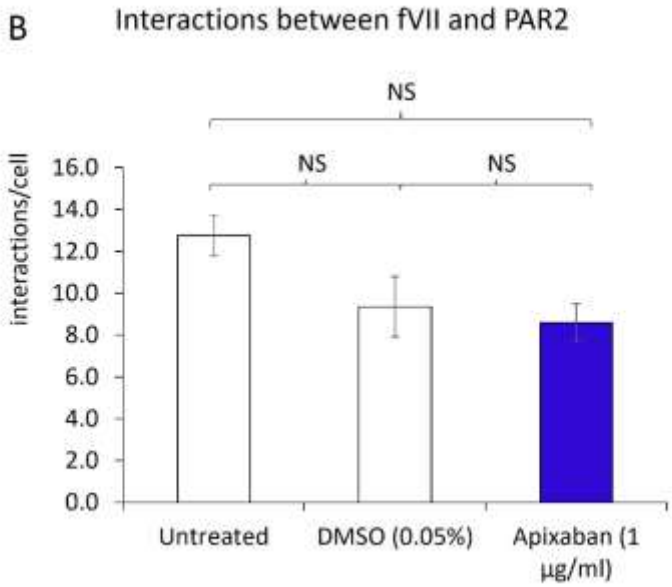

MDA-MB-231 cells (10^4) were seeded into glass bottomed cell culture plates. The cells were incubated with apixaban (1 µg/ml) or DMSO (0.05% v/v) vehicle control and incubated for 1 h at 37°C. The interactions between fVIIa and PAR2 were assessed by PLA using rabbit anti-fVII and mouse anti-PAR2 (SAM11) antibodies (diluted 1:50 v/v in antibody diluent). A) Results were visualised by fluorescence microscopy at x40 magnification. Areas with high densities of interactions are indicated with red arrows. B) The number of interactions in each field of view was quantified using ImageJ (Images represent 10 fields of view from 2 independent experiments; data = mean values ± SEM; independent t-test, NS = not significant).

of cells with apixaban increased the number of interactions between TF and fVII from 1.9 ± 0.3 incidences/cell in cells treated with DMSO control to 4.0 ± 0.6 incidences/cell (Figure 4.41). However, it was demonstrated in section 4.3.3 that treatment of cells with apixaban increased the amount of TF on the cell surface by preventing the loss of the protein when packaged and released in MV (Figure 4.30). Therefore, the increase in the number of associations observed may be due to the increase in available TF.

4.3.8.2 Computer docking simulation of fXa inhibitors into fXa and fVIIa proteins

Another mechanism by which apixaban may inhibit fVIIa activation of PAR2 is by binding within the active site of the enzyme. To explore this, the possible interactions of apixaban or rivaroxaban with fVIIa and fXa were modelled using the computer docking simulator Autodock (Figure 4.42A & Figure 4.42B). The simulation indicated that apixaban was capable of binding to fVIIa and fXa with similar binding energies of -9.78 and -11.66 kcal/mol, respectively (Figure 4.42C). The modelled rivaroxaban also bound to fVIIa and fXa with similar binding energies of -9.98 and -11.01 kcal/mol, respectively. Furthermore, the estimated inhibition constant for rivaroxaban against fVIIa was 48 μM, which was marginally lower than estimated for apixaban inhibition of fVIIa (67.5 μM) (Figure 4.42D). In addition, both these values were an order of magnitude higher than the estimated constants for the inhibitors against fXa, of 2.84 μM with apixaban and 8.56 μM with rivaroxaban. These data indicated that apixaban and rivaroxaban are predicted to be less effective at inhibiting fVIIa than fXa. Furthermore, apixaban and rivaroxaban were predicted to have similar potential to inhibit fVIIa. These findings are contrary to the experimental data where only apixaban was capable of inhibiting fVIIa and with a similar potency to that observed with fXa (Madkhali, 2020).

Figure 4.41: Assessment of the influence of apixaban on the interaction between TF and fVIIa

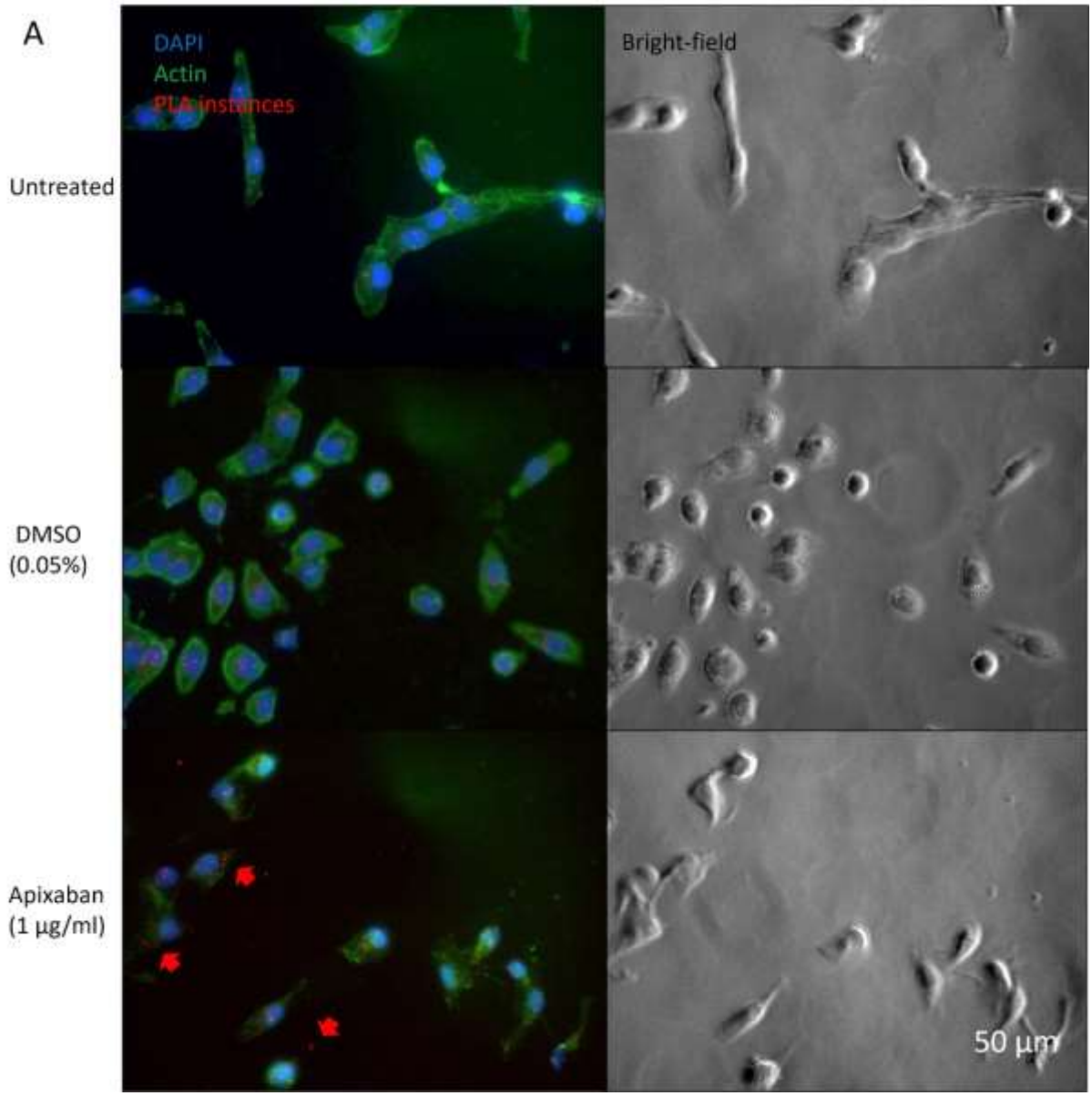

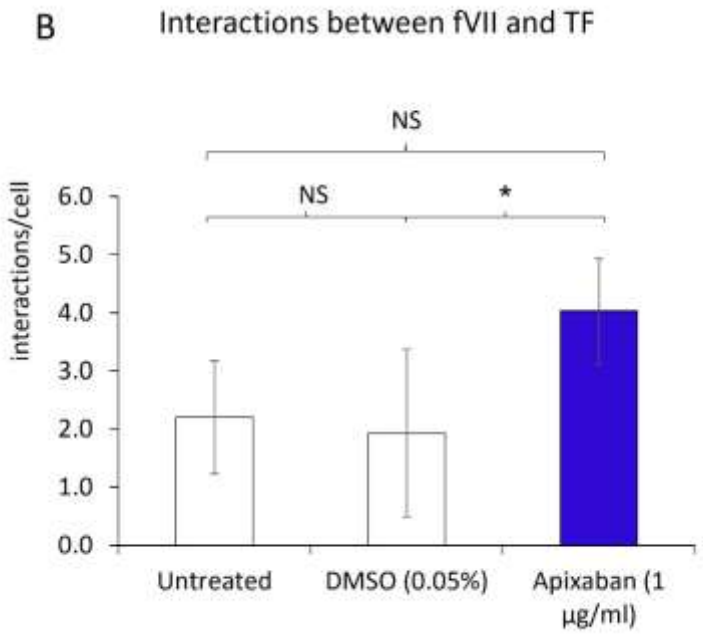

MDA-MB-231 cells (10^4) were seeded into glass bottomed cell culture plates. The cells were incubated with apixaban (1 µg/ml) or DMSO (0.05% v/v) vehicle control and incubated for 1 h at 37°C. The interactions between fVIIa and TF were assessed by PLA using rabbit anti-fVII(a) and mouse anti-TF (HTF-1) antibodies (diluted 1:50 v/v in antibody diluent). A) The results were visualised by fluorescence microscopy at x40 magnification. Areas with high density of interactions are indicated with red arrows. B) The number of interactions in each field of view was quantified using ImageJ (Images represent 10 fields of view from 2 independent experiments; data = mean values ± SEM; independent t-test, * = $p < 0.05$, NS = not significant).

Figure 4.42: Computerised docking of apixaban and rivaroxaban into fXa and fVIIa

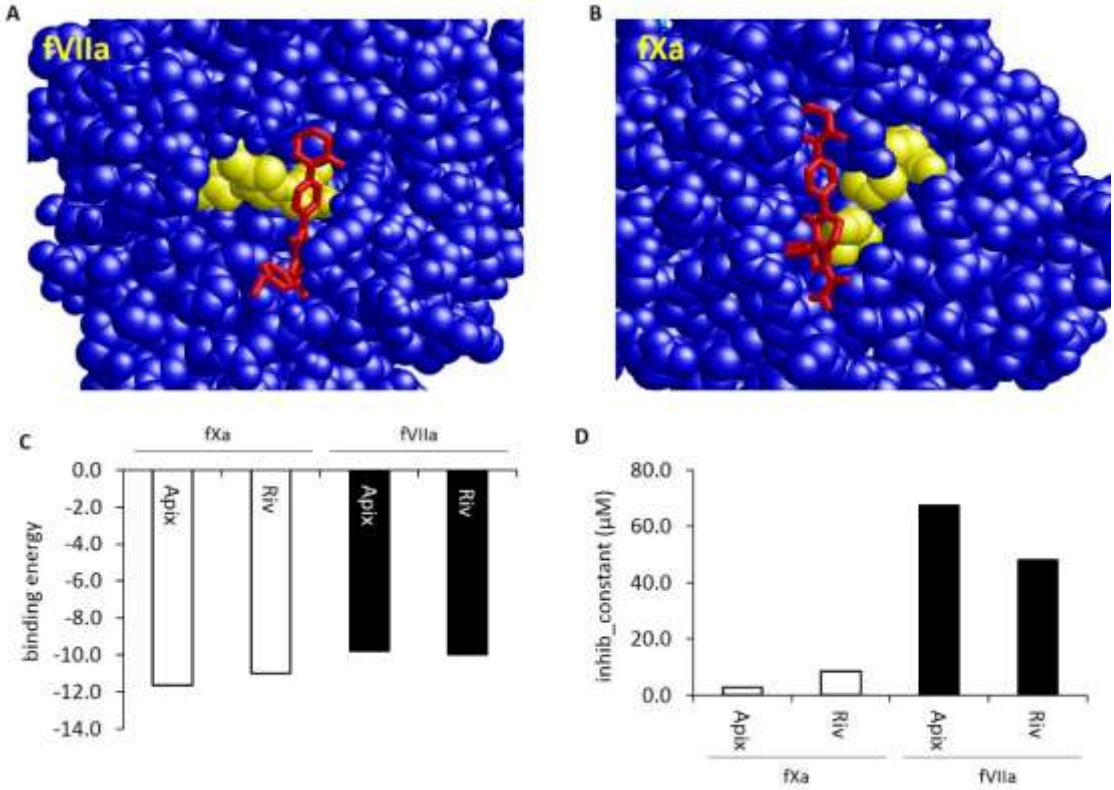

Crystal structures of apixaban (red) bound with A) fXa and B) fVIIa in the most energy efficient binding conformation as calculated by the Autodock program. The catalytic triad of the enzymes (Asp102-His57-Ser195) are indicated in yellow. Estimated C) binding energies and D) inhibition constants for apixaban and rivaroxaban with fXa and fVIIa were calculated by the Autodock program.

4.4 Discussion

PAR2 is often overexpressed in cancer cells and a number of studies have linked the activation of PAR2 with the accelerated progression of cancer (Schaffner & Ruf, 2009; Yau et al., 2013). Therefore, the inhibition of the proteases responsible for the activation of PAR2 may provide a means of attenuating the downstream signalling and functional consequences in cancer cells. The direct fXa inhibitor apixaban has previously been reported to reduce the rate of proliferation in cancer cells (Guasti et al., 2017). Furthermore, in the previous chapter it was shown that the treatment of CAM-embedded tumours with apixaban resulted in a reduction in tumour growth (Figure 3.19). Therefore, in this study the ability of two direct fXa inhibitor compounds to influence the activation of PAR2 in cancer cell lines were explored further.

The fXa inhibitors apixaban and rivaroxaban reduced the release of MV from MDA-MB-231 and AsPC-1 cells, in response to fXa (Figure 4.22). Moreover, the amount of the incorporated TF antigen within the released MV and consequently the associated procoagulant activity were also reduced following treatment with these anticoagulants (Figure 4.23 & Figure 4.24). Interestingly, apixaban, but not rivaroxaban, also reduced the release of MV from unstimulated cells in the absence of exogenous PAR2 activators (Figure 4.27). Moreover, the magnitude of this reduction in MV release in unstimulated cells was comparable to that achievable by incubating the cells with an inhibitory anti-PAR2 antibody (Figure 4.29A). Treatment of the cells with a combination of apixaban, together with the inhibitory anti-PAR2 antibody did not reduce MV release below that of the treatment with apixaban alone (Figure 4.29B). This suggests that apixaban acts to reduce MV release, in a PAR2-dependant manner and not through an alternative mechanism. This observation was further reflected in reductions in the expression of IL-8 in cells incubated with apixaban (Figure 4.32). The up-regulation in the expression of IL-8 has been used in a number of studies as a measure of PAR2 activation (Carneiro-Lobo et al., 2012; Hirota et al., 2005; Jiang et al., 2017). In this study, the induction of IL-8 expression was attributed and hence used as indicative of active PAR2 signalling (Figure 4.31). PAR2 activation has also been associated with accelerated cell proliferation (Jiang et al., 2017; Nishibori et al., 2005; Shimamoto et al., 2004; Sun et al., 2018a; Xie et al., 2015). The treatment of MDA-MB-231 and AsPC-1 cells with apixaban also attenuated the rate of proliferation in these cells (Figure 4.34). However, it must be noted that the crystal violet assay used in this study determines cell numbers at the time of measurement and is not a direct measure of the metabolic activity of cells. The activation of PAR2 has also been associated with resistance to cellular apoptosis (Guo et al., 2011; Luo et al., 2014; Shanshan et al., 2019). Therefore, it was envisaged that the prevention of PAR2 activation using apixaban may contribute to increased rate of cell apoptosis

under experimental conditions. Consequently, the reduction in the number of cells observed following treatment with apixaban may be attributed to the combined effects of inhibiting proliferation, as well as the increased rate of cellular apoptosis.

Since apixaban blocked the activation of PAR2 in cells in the absence of exogenous fXa, the mechanism underlying the effect of apixaban was investigated next. First, the involvement of any cellular fXa was discounted since the amount of fXa activity detected on the surface of MDA-MB-231 cells (0.07 nM) (Figure 4.39A) was measured to be substantially lower than that required in order to be capable of activating PAR2 (Camerer et al., 2000b; Camerer et al., 2002; Morris et al., 2006). Moreover, since all cells were adapted to SFM prior to experiments, the possibility of the fXa being introduced in the cell culture media could be ruled out. Therefore collectively, these data indicated that apixaban may be capable of inhibiting both fXa-dependant and -independent activation of PAR2. This is in agreement with previous reports that apixaban was capable of reducing the rate of proliferation in cancer cells in which the expression of fX(a) mRNA or protein was shown to be absent (Guasti et al., 2017). Furthermore, these data suggested that an alternative protease that is endogenously expressed and present on the surface of the cancer cells, may be responsible for the PAR2 activation. Cancer cells can express a number of membrane-associated serine proteases, including matriptase, testisin, trypsinogen, KLK14 and the TF/fVIIa complex. All these serine proteases have been reported to be capable of activating PAR2 on the host cell previously (Ma et al., 2013; Pawar et al., 2019). For example, expression of trypsinogen and KLK14 by colorectal carcinomas cells has been shown to result in acceleration of the rate of cell proliferation (Ma et al., 2013; Miyata et al., 1998). SiRNA mediated suppression of the expression of either PAR2 or fVIIa in MDA-MB-231 cells has also been shown to reduce cell proliferation (Featherby et al., 2019). In addition, the endogenous expression of TF and fVIIa has been observed to induce the release of MV (Koizume et al., 2016), promote the growth of xenograft tumours (Hembrough et al., 2003) and promote tumour invasion and metastasis (Tang et al., 2010). Finally, in xenograft tumour studies, a specific fXa inhibitor, rNAP5, only had a small influence on tumour growth whereas a TF/fVIIa-specific inhibitor, rNAPc2, was shown to have a larger effect (Hembrough et al., 2003). Collectively, these studies indicate that fVIIa may be capable of initiating PAR2-mediated MV release and inducing cell proliferation following complex formation with cell-surface TF (Featherby et al., 2019; Koizume et al., 2016). A number of cancer cell types, including MDA-MB-231 cells, have previously been reported to express fVII(a) (Das et al., 2018b; Koizume et al., 2012; Koizume et al., 2006; Koizume et al., 2009; Madkhali et al., 2019; Magnus et al., 2010; Yokota et al., 2009). In agreement with these studies, both MDA-MB-231 and AsPC-1 cells were shown to express fVII, a significant

proportion of which was in the activated fVIIa form (Figure 4.37). Therefore, fVIIa was presumed to be a likely candidate for the alternative protease, responsible for the activation of PAR2 which may also be inhibited by apixaban. In this study it was shown that apixaban was capable of directly reducing the release of MV from MDA-MB-231 and AsPC-1 cells in response to exogenous fVIIa (Figure 4.36). Moreover, the magnitude of this inhibition was comparable to that attainable following the incubation of the fVIIa enzyme with an inhibitory anti-fVII(a) antibody prior to addition to the cells (Figure 4.35). Therefore, these data for the first time demonstrate a function of apixaban in reducing the release of MV and suppressing cell proliferation through a mechanism that involves the inhibition of the activation of PAR2 by endogenously expressed TF/fVIIa (Figure 4.43). In addition, as a part of a larger study, apixaban was also demonstrated to possess direct inhibitory potential towards the proteolytic activity of fVIIa (Madkhali, 2020). Finally, since a number of fXa-blocking DOAC exist which include edoxaban, darexaban, otamixaban, betrixaban, letaxaban and eribaxaban, the examination of the potential of these compounds in inhibiting fVIIa activity would be an interesting future study.

To further examine and confirm the mechanism by which apixaban suppresses cell proliferation, it was hypothesised that cells which lack either fVIIa or TF would not respond to treatment by the inhibitor. Therefore, the influence of apixaban on the growth of primary endothelial cells, that lack TF (Contrino et al., 1996; Drake et al., 1989), was studied. Although these cells are known to express PAR2 and fVII (Figure 4.37), the lack of TF under normal conditions, precludes the activation of PAR2 under physiological conditions. In agreement with the above hypothesis, treatment of primary endothelial cells with apixaban did not influence the rate of growth in the cells (Figure 4.34). Similarly, previous studies have shown that, treatment of primary fibroblasts which lack fVII expression with apixaban also does not alter the rate of proliferation (Guasti et al., 2017). This indicates that the ability of apixaban to inhibit cell proliferation is dependent on the presence of TF, fVIIa and PAR2 on the cell surface. The specificity of apixaban in suppressing proliferation in cancer cells may prove to be a useful therapeutic agent for suppressing cancer growth in patients, without the undesirable detrimental effects on healthy cells.

In addition to reducing the rate of cell proliferation, apixaban also reduced the release of MV from cancer cells, which are associated with tumour invasiveness and increased proangiogenic signalling, as well as the promotion of the hypercoagulable state in cancer patients (Bian et al., 2019; Gong et al., 2015). Again, to date few investigations have examined the influence of apixaban on cancer progression *in vivo*. One such clinical study compared the effects of apixaban to placebo and determined the drug to be safe for use in cancer patients. However, the short duration of treatment

Figure 4.43: Schematic diagram showing the mechanism of activation of PAR2 by endogenously expressed fVIIa

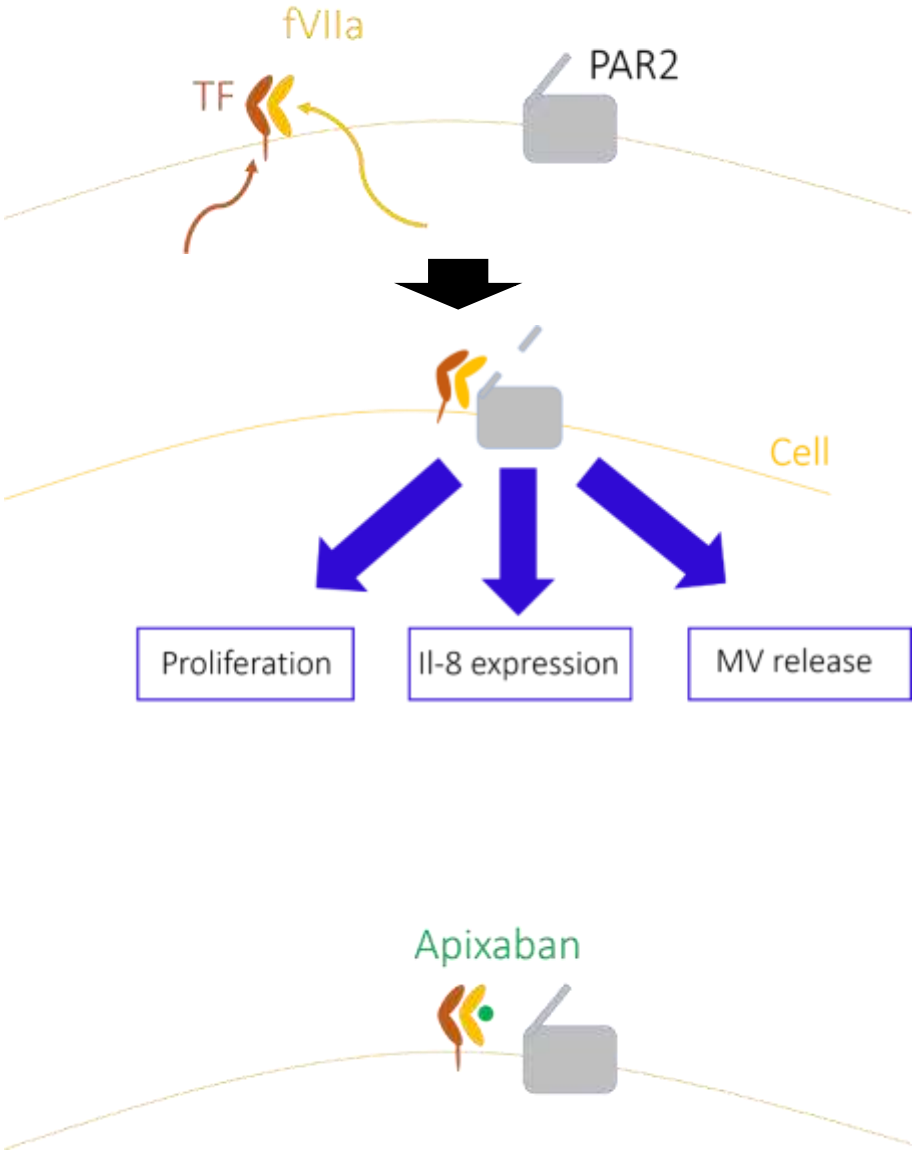

Endogenously expressed fVIIa and TF on the surface of cancer cells interact to form the TF/fVIIa complex. This complex associates with PAR2 resulting in the activation of the latter protein. Signalling arising from PAR2 activation promotes cell proliferation, up-regulates the expression of IL-8 and induces the release of MV. Inhibition of fVIIa by apixaban prevents PAR2 and suppresses the cellular outcomes.

and the small number of recruited patients prevented the generation of conclusive data regarding any influence of apixaban on patient survival (Levine et al., 2012). In contrast, rivaroxaban has recently been shown to be ineffective at reducing the growth of xenograft tumours (Buijs et al., 2019; Maqsood et al., 2019). This also agrees with the data obtained in this study since rivaroxaban only reduced MV release from fXa activated cell lines and was ineffective in either preventing MV release from resting cells, or reducing the rate of cancer cell proliferation. The data presented in this study suggest that the activation of PAR2 by TF/fVIIa and not by fXa may be responsible for the aggressive behaviour in cancer cells. Interestingly, it was previously demonstrated that a small molecule fVIIa inhibitor (PCI-27483) was also capable of inhibiting the growth of tumour xenografts (Loury et al., 2007; Prescott, 2008). This may indicate that apixaban might have similar beneficial properties *in vivo,* by suppressing cancer cell proliferation through inhibiting fVIIa, rather than fXa. However in clinical trials, treatment of advanced pancreatic cancer patients with PCI-27483 in combination with the chemotherapy agent Gemcitabine did not improve overall survival when compared to the Gemcitabine alone (Ramanathan et al., 2019). Therefore, future paired studies are essential to establish the anti-cancer properties of apixaban observed in the current *in vitro* study, and to translate these observations into therapeutic usage of apixaban for the control of cancer progression *in vivo*.

In the last section of the study, the mechanism by which apixaban inhibits PAR2 activation by fVIIa of was investigated. However, data obtained from docking simulations indicated that apixaban and rivaroxaban would have similar potential to bind to the active site of fVIIa and inhibit the enzyme (Figure 4.42). These findings are contrary to the experimental data where only apixaban was shown to be capable of inhibiting fVIIa (Figure 4.36) (Madkhali, 2020). Although computer molecular docking simulations are constantly improving such programs have a number of limitations. These limitations arise from the insufficient modelling of ligand induced alterations in the protein structure, as well as exclusion of solvent molecules from docking simulations (Prieto-Martínez FD, 2018). It is not known if apixaban inhibits fVIIa cleavage of all potential substrates or specifically the cleavage of PAR2. A concurrent study carried out in this laboratory showed that apixaban inhibited the ability of fVIIa to digest a specific fVIIa chromogenic substrate (Madkhali, 2020) indicating apixaban was capable of specifically blocking the enzymatic activity of fVIIa in a competitive manner. However, *in vivo* studies where excessive anticoagulation by apixaban could be counteracted by administration of recombinant fVIIa (Escolar et al., 2013). This suggests that fVIIa is still capable of cleaving coagulation proteases in the presence of apixaban. It has been suggested that TF within the TF/fVIIa complex may be present on the surface of cells in different conformations which preferably

participate in either coagulation or cell signalling via PAR2 (Ahamed et al., 2006). In this mechanism, the interaction with integrins has been shown to direct the TF/fVIIa complex away from coagulation and towards PAR2 activation by positioning the complex in a favourable conformation to cleave the receptor (Versteeg et al., 2008b). It is therefore possible that apixaban may interact more efficiently with fVIIa when in complex with TF that is in the conformation which is responsible for PAR2 cleavage. However, contradictory evidence showed that the inhibition of the proteolytic activity of fVIIa by apixaban, as measured using the chromogenic substrate remains unaffected by the presence of TF (Madkhali, 2020). Another explanation for the variation in the capacity of apixaban to inhibit fVIIa cleavage of different substrates is that apixaban may be capable of interfering with the association of the fVIIa and PAR2 proteins. The association between fVIIa and PAR2 on the surface of MDA-MB-231 cells was not influenced by the presence of apixaban (Figure 4.40). In contrast, experiments performed concurrently in our laboratory indicated that apixaban was capable of disrupting the association between TF and PAR2 (Madkhali et al, unpublished data). Therefore, further studies are required in order to elucidate the mechanism by which apixaban prevents PAR2 activation by fVIIa.

In conclusion, this study has shown that MDA-MB-231 and AsPC-1 cells express TF, fVIIa and PAR2 endogenously. These cell lines were shown to release high levels of MV which was positively regulated through the activation of PAR2 by TF/fVIIa. The activation of PAR2 in turn, leads to signalling mechanisms which enhance the rate of cell proliferation in these cells. In addition, this study has produced data to demonstrate the potential of apixaban to inhibit fVIIa activity. The evidence presented indicated that apixaban may selectively inhibit fVIIa which, in complex with TF, induces cellular signalling through activating PAR2 whilst having less influence on the procoagulant activity of fVIIa. Taken together, these findings provide evidence that apixaban may prove to be a useful agent in controlling cancer cell proliferation as well as reducing the risk of thrombosis through the inhibition of fXa.

Chapter 5

Identification of the interacting domains between TF and β1 integrin, and the resultant signalling properties

5.1 Introduction

In the previous chapters it was shown that coagulation mechanisms are capable of enhancing the rate of cell proliferation in cancer cells. This mechanism was shown to arise through the engagement of TF and fVIIa, and was also shown to involve the activation of PAR2. However, TF is also known to modulate cellular signalling through other mechanisms apart from the activation of PAR2 (Aberg & Siegbahn, 2013; Ruf et al., 2011). One such mechanism is mediated through the interaction of TF with the cell adhesion protein, β1 integrin (Collier et al., 2008; Versteeg et al., 2008b). The interaction of TF and β1 integrin has been reported to influence cell migration and proliferation, as well as promoting angiogenesis (Kocaturk & Versteeg, 2013). Although the consequences of the interaction between TF and β1 integrin on these cellular functions have been observed, it is not known if signalling arises from direct interaction of these proteins, and if there are any specific requirements for complex formation. Therefore, in this section of the study an attempt was made to identify the domains within TF and β1 integrin which are responsible for the interaction between the two proteins, on the surface of the cell. Furthermore, the outcome of these interactions on the regulation of cell proliferation signals was investigated.

5.1.1 Mechanisms of regulation of cell proliferation by integrins

Integrins are cell-surface glycoprotein receptors that interact with ECM proteins and therefore act as sensors of the environment surrounding the cell (section 1.10.1). Integrin signalling influences a range of cellular behaviors including changes to the rate of cell proliferation, migration, differentiation, survival and apoptosis (Campbell & Humphries, 2011; Cooper & Giancotti, 2019; Desgrosellier & Cheresh, 2010). The mechanisms by which integrins regulate cell signalling are initiated by a conformational switch from a folded/inactive form of the receptor to a fully extended/active conformation. The conformational changes are transmitted to the cytoplasmic tail of the integrin subunits and results in the recruitment of adaptor proteins including talin, vinculin, paxillin, and kindlin (Wolfenson et al., 2013). Engagement of these adaptor proteins brings the integrins together into multiple receptor clusters known as focal adhesions. The clustering enables the recruitment and activation of secondary signalling proteins, including focal adhesion kinase (FAK), integrin-linked kinase, Src and small GTPases (Rac, Rho and Cdc42) (Mitra & Schlaepfer, 2006; Olson et al., 1995; Wolfenson et al., 2013). As a result of the activation of these secondary signals, downstream pathways are induced, including the JNK/c-Jun, ERK-MAPK and PI3K-AKT cascades (Aoudjit & Vuori, 2001; Khwaja et al., 1997; Short et al., 1998; Zhao et al., 1998) (Figure 5.1). These signalling cascades are responsible for the induction of the expression of cyclin D1, as well as

Figure 5.1: Integrin mediated cell signalling

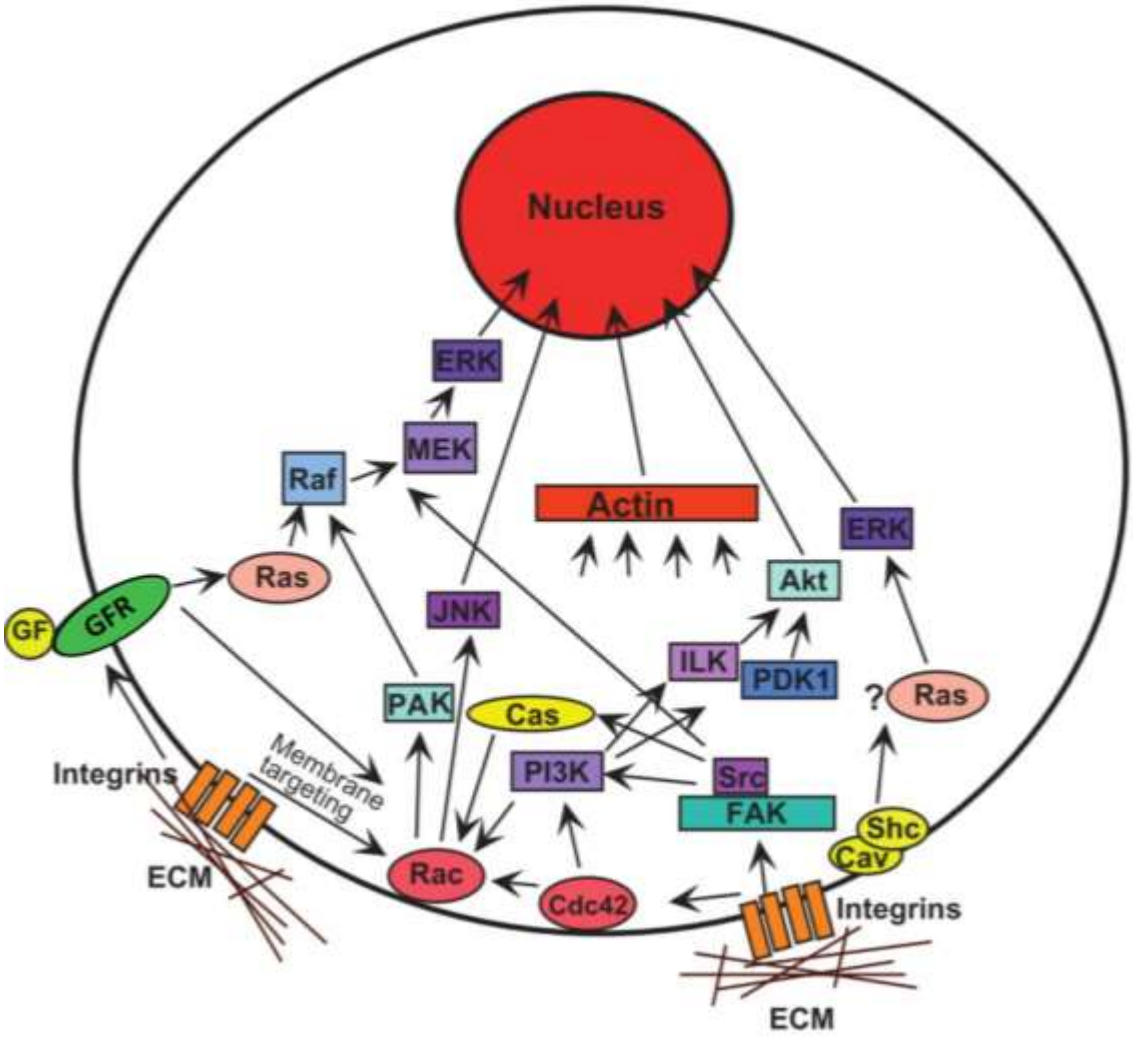

The interaction of integrins with ECM proteins results in the activation of secondary signalling proteins, including FAK, Src and small GTPase (Rac and Cdc42). Activation of these second messanger proteins results in the induction of downstream signalling cascades, including the ERK-MAPK, JNK and PI3K-AKT pathways. These signalling cascades terminate in the cell nucleus where they influence the proteins that regulate the progression of the cell cycle. (Originally published in Schwartz & Assoian (2001)).

the downregulation of the cyclin-dependent kinase inhibitors, p21 and p27 (Zhao et al., 1998; Zhu et al., 1996). In addition, following integrin adhesion FAK has been shown to translocate to the nucleus. Within the nucleus, FAK stabilises a p53-Mdm2 complex resulting in the ubiquitination and subsequent degradation of p53 (Lim et al., 2008). Collectively, the changes in the levels and activities of these proteins allows a cell to progress through the G_1 checkpoint of the cell cycle (Harris & Levine, 2005; Vermeulen et al., 2003).

In most cells, cell cycle regulation is orchestrated through signals resulting from the adhesion of integrins, together with those initiated through the engagement of growth factor receptors (Moreno-Layseca & Streuli, 2014). In fact, it has been proposed that 'integrin and growth factor receptor signalling pathways are interwoven to such an extent that it is difficult to consider their effects on cell proliferation separately' (Assoian & Schwartz, 2001). The cross-talk between integrin and growth factor receptors signalling is evident by the sensitivity of multiple growth factor pathways to cell adhesion. For example, the induction of the Rac pathway following growth factor stimulation is dependent on the recruitment of both Rac and its downstream effector proteins to the focal adhesions (del Pozo et al., 2000). In addition, activation of PI3K and AKT in response to EGF is reduced in suspended cells compared with adherent cells (Khwaja et al., 1997). This was shown to be as the result of phosphorylation of EGFR which takes place following integrin binding to extracellular components (Moro et al., 2002). Consequently, the outcome of integrin-initiated signals may vary in different cells, depending on the cohort of growth factor receptors expressed by the cells. Due to these differences, it is essential that the influences of integrin signalling are examined in different cells and with respect to any additional influences exerted by each cell type. Finally, TF has been shown to influence integrin signalling with outcomes that affect cell migration, proliferation and angiogenesis (Collier et al., 2008; Versteeg et al., 2008b). These changes to typical integrin signalling exerted following ligation of TF, have been shown to contribute to a number of disease processes including cancer progression and endothelial cell dysfunction (Cooper & Giancotti, 2019).

5.1.2 An overview of the interaction of TF and β1 integrin and the outcomes on the cellular signals

The co-localisation between TF and β1 integrin was first observed in the lamellipodia and filopodia at the leading edge of migrating cancer cells (Dorfleutner et al., 2004; Muller et al., 1999). Direct binding of TF and β1 integrin was demonstrated more recently, by co-IP experiments (Collier et al., 2008; Versteeg et al., 2008b). As mentioned above, the interaction between TF and β1 integrin has been shown to influence signalling pathways normally induced by integrin adhesion. For example, treatment of primary human coronary artery or umbilical vein endothelial cells with recombinant TF

resulted in increases in ERK1/2 phosphorylation as well as the rate of cell proliferation. Furthermore, pre-incubation of the recombinant TF with a peptide corresponding to a membrane proximal region of β1 integrin prevented these increases in proliferation (Collier & Ettelaie, 2010; Pradier & Ettelaie, 2008). The influence of the interaction between TF and β1 integrin on proliferation has also been demonstrated in cell lines. The overexpression of both full-length TF and the splice isoform asTF in MCF-7 breast cancer cells resulted in increases in the rate of cell proliferation that were reduced following the knockdown of β1 integrin expression (Kocaturk et al., 2013). Additionally, treatment of immortalised human endothelial cells with asTF resulted in activation of FAK, together with increased ERK1/2 and AKT phosphorylation. However, the rate of cell proliferation in the immortalised endothelial cells was not significantly altered (van den Berg et al., 2009). Rather, these signals resulted in increased angiogenesis, as measured by capillary formation in a matrigel matrix (van den Berg et al., 2009). Furthermore, this increased rate of angiogenesis following treatment with asTF was shown to be dependent on the presence of α6β1 integrin and was inhibited by antibodies against either of the integrin subunits. Collectively these data indicate that in line with other integrin signalling, the signals arising from the interaction of TF and β1 integrin lead to variable outcomes and are cell type-dependant. Finally, the interaction between TF and β1 integrin influences additional cellular processes along with cell proliferation and angiogenesis. For example, TF has been shown to modify the ability of integrins to influence cell migration in HUVEC and A7 melanoma cells (Dorfleutner et al., 2004; Ott et al., 2005) as well as influencing the expression of estrogen receptor α in MCF-7 and T47D breast cancer cells (Collier et al., 2008).

5.1.3 Current evidence for the direct interaction between β1 integrin and TF

Although the interaction between TF and β1 integrin has been reported to result in a number of different cellular outcomes, the mechanisms by which these proteins interact with each other and influence cellular signalling has not been determined. The evidence for direct complex formation between TF and β1 integrin has mainly been obtained from co-IP experiments (Collier et al., 2008; Versteeg et al., 2008b). Furthermore, purified TF extracellular domain acts as an adhesive ligand for several integrin heterodimers expressed by chinese hamster ovary cells (Dorfleutner et al., 2004). Additional evidence that the 4th EGF repeat (EGF4) and βTD domains within β1 integrin are crucial for complex formation with TF were obtained from functional studies. These studies indicated that although treatment of HCAEC with recombinant TF increased the rate of proliferation, this could be interrupted by the inclusion of a competitor-peptide corresponding to the EGF4-βTD domains of β1 integrin (Collier & Ettelaie, 2010). Similarly, the overexpression of asTF in MCF-7 cells resulted in increased rates of cell proliferation but was abolished on inclusion of an antibody

targeting the EGF4-βTD domains (Kocaturk et al., 2013). Additionally, studies on the influence of asTF on cell proliferation have produced clues to the regions within TF which are involved in complex formation with β1 integrin (Kocaturk et al., 2013). The absence of the transmembrane and cytoplasmic domains in asTF, together with the lack of any detectable procoagulant activity suggests that the interacting domains responsible for influencing β1 integrin signalling are located within the extracellular domain of TF. For example, overexpression of asTF in MCF-7 cells resulted in the up-regulation of genes responsible for the progression through the cell cycle (Kocaturk et al., 2013). In addition, overexpression of asTF in Mia-Paca-2 cells resulted in the formation of larger, more vascularised xenograft tumours (Hobbs et al., 2007). Finally, the association of asTF with α6β1 enhanced the activation of FAK and increased ERK1/2 and AKT phosphorylation in immortalised endothelial cells (van den Berg et al., 2009).

In addition to the likelihood of a direct interaction between TF and β1 integrin, it is possible that other proteins, which may act as adaptors, may be required to facilitate the complex formation. In fact, incubation of cells with exogenous fVIIa has been shown to facilitate the association of TF and β1 integrin in some, but not all cell types (Rothmeier et al., 2018; Rothmeier et al., 2019; Versteeg et al., 2008b). Conversely, the binding of TF and β1 integrin does not appear to be dependent on exogenous fVIIa in MDA-MB-231mfp cells (Versteeg et al., 2008b). Furthermore, the presence of an inhibitory anti-fVIIa antibody did not influence the increase in the rate of cell proliferation observed in HUVEC following treatment of with TF, but was blocked by an inhibitory-β1 integrin peptide (Pradier & Ettelaie, 2008).

The interaction of TF and β1 integrin has been shown to promote cellular migration and proliferation, as well as angiogenic signalling in both normal and cancerous cells. Moreover, the ability of asTF, which lacks the transmembrane and cytoplasmic domains, to bind to β1 integrin and influence cellular proliferation (Kocaturk et al., 2013; van den Berg et al., 2009) leads to the hypothesis that the interaction between TF and β1 integrin occurs through the extracellular domains of these proteins. Furthermore, since a peptide corresponding to the EGF4 and βTD domains of β1 integrin can disrupt the proliferative abilities of full-length TF (Collier & Ettelaie, 2010) and asTF (Kocaturk et al., 2013), it was hypothesised that the binding site between TF and β1 integrin was located within the EGF4 and/or βTD domains of the latter protein. Finally, identification of additional proteins which may be pre-requisites for the interaction of TF and β1 integrin would further elucidate the mechanisms by which cells respond to external circumstances. Signalling

arising from the interaction between TF and β1 integrin has been shown to be enhanced by the addition of fVIIa. Therefore, it was hypothesised that fVIIa may be an essential co-factor for TF-β1 integrin binding.

5.1.4 Aims

This section of the study aimed to determine if the extracellular domain of TF and the EGF4 and βTD domains of β1 integrin are involved in the interaction of these two proteins. The cDNA corresponding to the complete extracellular domain of TF as well as the first or second fibronectin-like domains were separately cloned into an expression plasmid in tandem with a HA-FLAG tag sequence. The constructs were then expressed in cell lines and primary cells, and the ability of the resulting peptides to bind to β1 integrin was assessed. Similarly, the cDNA corresponding to the EGF4 and βTD domains of β1 integrin as well as the combined EGF4-βTD domains were cloned into the expression plasmid and the binding of the resulting peptides to TF was studied.

In further studies, proliferative signals resulting from the interaction of TF and β1 integrin with each of the expressed peptides were assessed by measuring the expression of cyclin D1, ERK1/2 phosphorylation and cell numbers, in both cell lines and primary cells.

Finally, to determine if the presence of fVIIa is a pre-requisite for the interaction of TF and β1 integrin, the interactions of the proteins were assessed in the presence and absence of fVIIa.

5.2 Methods

5.2.1 *In Silico* analysis of the protein structures of integrins and TF

5.2.1.1 Identification of the boundaries of the EGF4 and βTD domains of β1 integrin

The exact boundaries of the EGF4 and βTD domains of β1 integrin have not been defined. In addition, the crystal structure for the entirety of β1 integrin has not yet been resolved. Therefore, the boundaries of the EGF4 and βTD domains were first identified within the crystal structures of β2 integrin (4NEH) and β3 integrin (4G1E), which were obtained from the Research Collaboratory for Structural Bioinformatics (RCSB) protein databank, using the RasWin program. The respective amino acid residues were then identified within the amino acid sequences of β2 integrin (NG_007270.2) and β3 integrin (P05106.2) which were obtained from the National Center for Biotechnology Information (NCBI). These sequences were aligned with the sequence of β1 integrin (P05556.2) using the Clustal Omega online alignment tool (EMBL-EBI). By homology comparison of the amino acid sequences, the locations of EGF4 and βTD domains were then estimated within β1 integrin. Finally, the cDNA sequence for human β1 integrin (AK291697.1) was obtained from the NCBI and the nucleotide sequences coding for the amino acid sequences encompassing the EGF4 and βTD domains were determined.

5.2.1.2 Identification of the boundaries of the upper and lower extracellular domains of TF

The crystal structure of the extracellular domain of TF (1TFH) was obtained from the RCSB protein databank. The boundary between the two fibronectin-like domains within the crystal structure was identified using the RasWin program. The 'linking region' between these two domains was also identified. The cDNA sequence of human TF (NM_001993.4) was obtained from the NCBI and the DNA sequences corresponding to the identified amino acid sequences were determined. The whole of the extracellular domain of TF containing both fibronectin-like domains and hereafter referred to as the "total extracellular domain" (TED), the first fibronectin-like domain including the linking region, referred to as the "upper extracellular domain" (UED), and the second fibronectin-like domain including the linking region referred to as the "lower extracellular domain" (LED) were identified for the purpose of amplification and cloning as described below.

5.2.2 PCR based cloning

5.2.2.1 Generation of insert sequences using PCR with platinum *Taq* polymerase

To facilitate the cloning of the identified DNA sequences into the FLAG-HA-pcDNA3.1 plasmid (FLAG-HA plasmid), primers were designed to contain restriction sites (Figure 5.2) which were also uniquely

Figure 5.2: Strategy for the design of the PCR primers for the cloning procedures

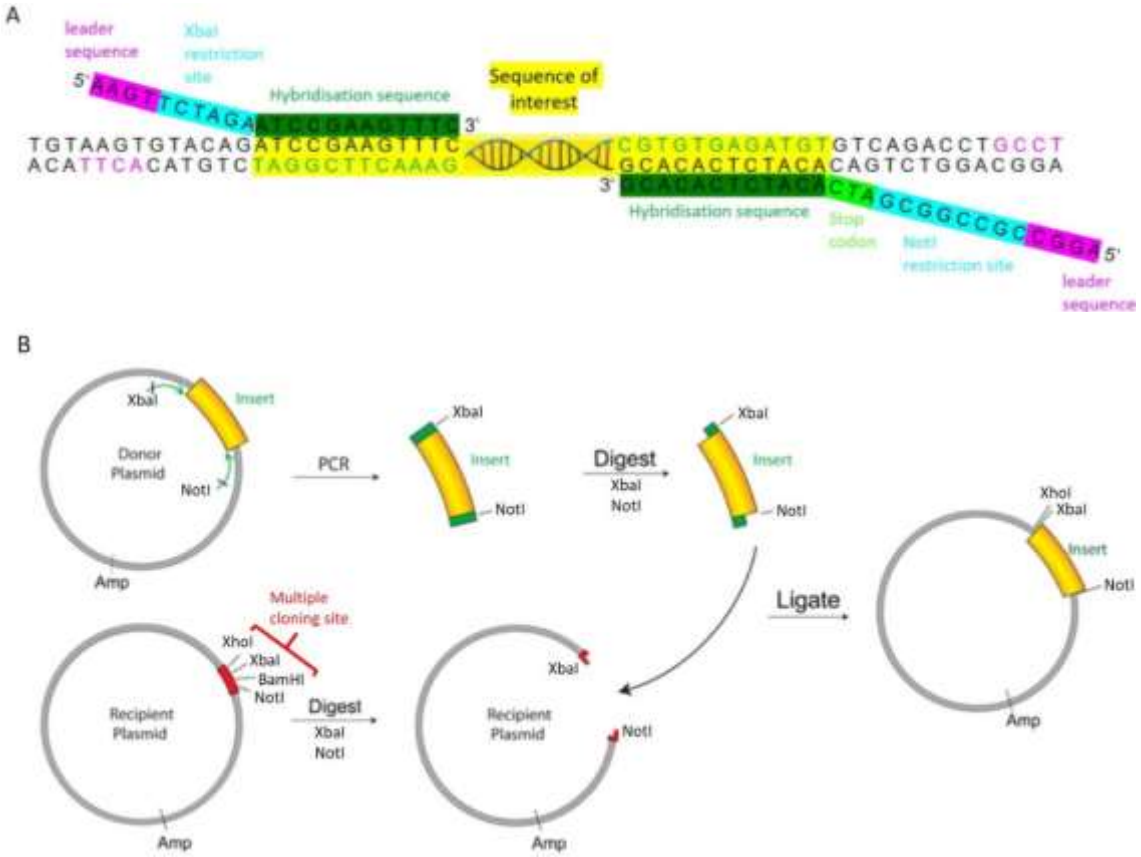

A) Primers were designed to include a leader sequence (purple), a restriction site (blue) and a complementary/hybridisation sequence (green). The primers were designed to amplify a sequence of interest (yellow) whilst simultaneously incorporating restriction sites into the ends of the amplicon. B) Amplification of the desired DNA sequence using these PCR primers permits the unidirectional cloning of the amplified DNA. The restriction sites within the insert and in the multiple cloning site of the recipient plasmid are unique and may be digested with the same two enzymes. The insert is then ligated into the recipient plasmid. (Diagram adapted from Addgene (2020)).

present in the multiple cloning site of the plasmid (Figure 5.3). The forward primers were designed to include an *XbaI* restriction site and the reverse primers to include either a *NotI* or a *BamHI* restriction site (Table 5.1). The use of different restriction sites on the forward and reverse primers ensured the unidirectional insertion of the DNA into the plasmid. The designed primers were synthesised and used to generate DNA inserts by PCR using high fidelity platinum *Taq* polymerase to ensure accuracy (section 2.3.5.10). The pCMV6-AC turbo-GFP tagged plasmid containing human TF cDNA (F3 gene NM_001993) was used as the template DNA for the generation of the UED, LED and TED sequences. The pCMV6-XL5 plasmid containing human β1 integrin cDNA (ITGB1 gene NM_002211) was used for the generation of the EGF4-βTD sequence. The PCR products were analysed by agarose gel electrophoresis (section 2.3.5.9), the sizes of the amplicons were determined and compare to the calculated values shown in Table 5.2.

5.2.2.2 Restriction digestion of the insert and plasmid DNA

Prior to ligation, the insert and plasmid DNA were digested with the same two restriction enzymes (section 2.3.5.12). Cloning of the UED, LED and TED DNA was carried out by digesting the insert and the plasmid DNA with the *XbaI* and *NotI* enzymes. When sub-cloning the β1 integrin fragment, the EGF4-βTD DNA and the plasmid DNA were digested with the *XbaI* and *BamHI* enzymes. The DNA were digested with each enzyme sequentially with a DNA clean-up carried out in between the digestion steps to remove unwanted proteins and salts as detailed in section 2.3.5.12.

5.2.2.3 Cloning the insert sequences into the FLAG-HA plasmid

Prior to the ligation of the insert DNA into the plasmid, the ligation reagents and conditions were optimised. Ligation of linearised plasmid (30 ng) was carried out using T4 DNA ligase (sections 2.3.5.14.1) or NEB instant sticky-end master mix (sections 2.3.5.14.2). The degree of recyclisation of the ligated products (5 µl) were then examined by agarose gel electrophoresis.

For ligation of the insert DNA into the plasmid, ligation mixes were assembled to contain the digested FLAG-HA plasmid (30 ng) and the digested insert DNA at molar ratios of 1:5, 1:15 and 1:30 (plasmid:insert). The mixtures were then ligated using NEB instant sticky-end master mix (section 2.3.5.14.2). After the incubation, samples of the ligation mixtures (5 µl) were examined by agarose gel electrophoresis. In addition, NEB 5-alpha competent *E. coli* (20 µl) were transformed with the ligation mixtures (1 µl) as described in section 2.3.5.4. A negative control, containing the competent *E. coli* without any DNA was included alongside. The cells (10 µl) were plated out on LB agar plates containing carbenicillin (100 µg/ml) and incubated at 37°C overnight. Single colonies were picked from the plates using a sterile pipette tip, transferred to LB media (10 ml) and incubated at 37°C with

Figure 5.3: FLAG-HA-pcDNA3.1 plasmid expression vector map

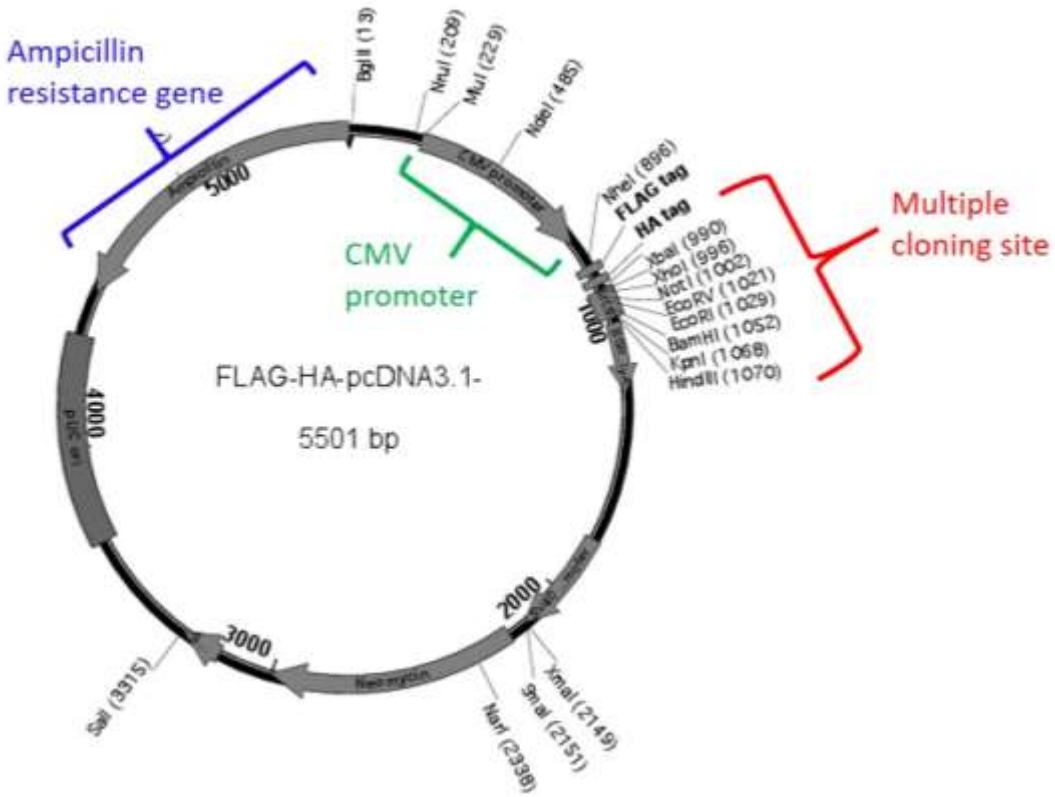

The FLAG-HA-pcDNA3.1 plasmid expression vector contains a sequence that encodes of FLAG-5xGly-HA-5xGly which directly precedes a multiple cloning site. This allows for the production of peptides which include both a FLAG- and HA-tag at the N-terminal. The plasmid also contains a pUC origin facilitates replication of the vector in bacterial culture and an ampicillin resistance gene which permits selection of transformed bacteria. The CMV promoter allowing mammalian expression.

Table 5.1: PCR primer set used for the preparation of insert sequences

	Primers			
	Forward	Reverse	Anneal Temp	Product size
UED	tcgcctctagagccggatcctcaggcact	ctctggcggccgcCTAtggctgtccgaggtttgt	62 °C	368 bp
LED	acctgtctagaaacctcggacagccaaca	atgtagcggccgcCTAttctctgaattccccttt	54 °C	366 bp
TED	tcgcctctagagccggatcctcaggcact	atgtagcggccgcCTAttctctgaattccccttt	54 °C	693 bp
EGF-4-βTD	ggatctagaggtgtttgcaagtgtcgt	acaatggatccTTAgtctggaccagtgggac	52 °C	494 bp

Sequences of the primers used for the amplification step of PCR based cloning. Restriction sites for *XbaI* (Green), *NotI* (red) and *BamHI* (blue) enzymes are highlighted. The stop codon sequences are denoted in capital letters.

Table 5.2: Length of cDNA sequences encoding for peptides and the expected molecular weight of peptides

	Insert DNA	**Fusion protein**	
	bp	aa	kDa
TED	669	252	28.04
UED	345	144	15.91
LED	342	143	15.69
EGF4-βTD	564	208	22.76
EGF4	210	69	7.09
Tags only	186	61	6.48

shaking (130 rpm) overnight. The plasmid DNA was isolated from the cultures using the mini-prep kit (section 2.3.5.6).

5.2.2.4 Examination and confirmation of sub-cloning of the inserts into the plasmid

The successful sub-cloning of the DNA inserts into the FLAG-HA plasmid was confirmed by at least two analysis procedures, as follows. Initially, the presence of each DNA insert was assessed by attempting to amplify the insert using the plasmids recovered in section 5.2.2.3 as template for PCR reactions. The PCR reactions were carried out using the respective primers as indicated in Table 5.1 and the reactions were performed using PuReTaq Ready-To-Go PCR Beads (section 2.3.5.11). Negative control reactions devoid of template DNA were included to ensure reaction fidelity. The PCR products were examined by agarose gel electrophoresis. Successful ligations were identified by the presence of the amplified DNA at the correct length for each insert.

The successful sub-cloning of the EGF4-βTD DNA into the plasmid was further confirmed by restriction enzyme digestion. A unique *BsrGI* restriction site was identified within the EGF4-βTD DNA but otherwise absent from the FLAG-HA plasmid. Samples (1 µg) of the construct plasmids isolated from the colonies in section 5.2.2.3 were digested with the *BsrGI* enzyme using the procedure detailed in section 2.3.5.12. Samples of the digested product (5 µl) were then examined by agarose gel electrophoresis. Successful sub-clones were identified by the presence of a linear DNA product which migrated as a single band on the agarose gel, as opposed to the multiple banding observed by the undigested plasmid.

Finally, positive samples from either of the previous two analysis procedures were examined externally by DNA sequencing, performed by Eurofins MWG. Sequencing reactions contained 50 ng/µl of plasmid DNA and 10 µM of T7 sequencing primer prepared in RNAse-free water (total volume 17 µl). The sequence of the T7 primer used for the sequencing reactions was 5'-TAA TAC GAC TCA CTA TAG GG-3'.

5.2.3 Preparation of EGF4 and βTD domain constructs using site directed mutagenesis

Plasmid constructs containing the individual EGF4 and βTD domains were prepared from the plasmid containing the sub-cloned EGF4-βTD DNA by site directed mutagenesis. The mutagenesis procedure involves 3 stages. Firstly, mutagenic PCR is performed using primers designed to include the desired mutation(s). The EGF4 domain was prepared by point mutation which introduced a stop codon (TAG) directly following the EGF4 domain (Gly611→Stop) (Figure 5.4). In order to achieve this, back-to-back mutagenic primers were designed and the desired substituted bases (coloured red in Table 5.3) were incorporated into the forward primer. To express the βTD domain alone, the sequence

Figure 5.4: Diagram representing the design of primers for site-directed mutagenesis

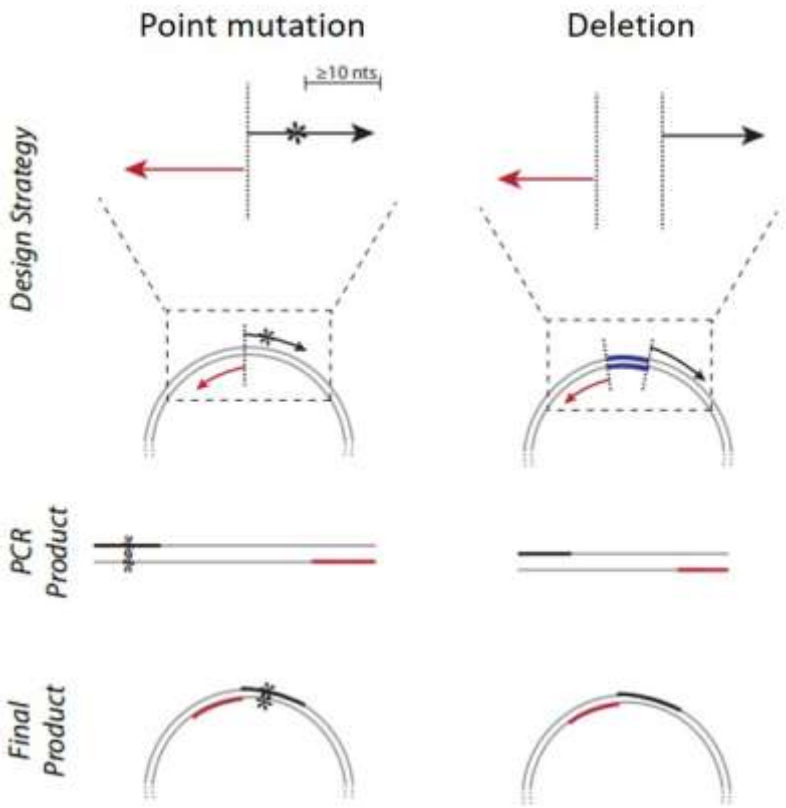

Point mutations can be generated using a forward mutagenic primer containing the desired substituted base(s) which produced a mismatch to the plasmid template (indicated by the *). On amplification, the mismatched mutant DNA accumulates rapidly as the major DNA present. Deletion mutagenesis is performed using primers that bind to sequences directly adjacent to the sequence that required deletion. These are then used to amplify the remained of the DNA and exclude the region to be deleted. (Diagram adapted from NEBiolabs (2020)).

Table 5.3: PCR primer used for site directed mutagenesis

Reaction	Mutation	Forward	Reverse	Annealing Temp
Add STOP	Point mutation	CAATGGCCGGTAGATCTGCGAGTG	CAGATCTGTCCGTTGCTG	62 °C
Del EGF-4	Deletion	GGCATCTGCGAGTGTGGT	TCTAGAACCTCCACCTCCAC	67 °C

encoding the EGF4 domain was deleted from the sub-cloned plasmid. To achieve this, mutagenic primers were used which hybridised to sequences directly adjacent to the EGF4 domain sequence that required deletion (Figure 5.4). The mutagenic PCR reactions were preformed using the Q5 site directed mutagenesis kit (section 2.3.5.15). The annealing temperature for each set of primers was determined using the NEBaseChanger online program and are specified in Table 5.3. To improve the efficacy of the deletion mutagenesis reaction, experiments were prepared containing either additional DMSO (3% v/v) or Mg^{2+} ions (1 mM magnesium chloride) (NEBiolabs). During the second stage of the mutagenesis procedure the PCR product was incubated with the provided KLD enzyme. Finally, the resultant products were transformed into NEB 5-alpha competent *E. coli* cells (section 2.3.5.4). The cells (10 µl) were plated out on LB agar plates containing carbenicillin (100 µg/ml) and incubated overnight at 37°C. Single colonies were picked from the plates using a sterile pipette tip, transferred to LB media (10 ml) and incubated at 37°C with shaking (130 rpm) overnight. The plasmid DNA were then isolated from the cultures using the mini-prep kit (section 2.3.5.6). The presence of the desired mutations within the isolated plasmid DNA was verified by sequencing performed by Eurofins MWG.

5.2.4 Optimisation of the transfection of cells with plasmid DNA

Prior to experiments, the transfection efficiency of two transfection reagents was assessed in MDA-MB-231 cells. Cells (2 x 10^5) were plated in 6-well plates and allowed to adhere overnight. The cells were transfected with the pCMV-XL5-tGFP mammalian expression plasmid using either Trans-IT 2020 transfection reagent (sections 2.3.2.6) or Viromer RED reagent (sections 2.3.2.7) and incubated for 2 days to allow the expression of the tGFP. The cells were harvested and the proportion of cells expressing tGFP was assessed by flow cytometry (section 2.3.4.3.2).

In addition, the amount of Trans-IT 2020 transfection reagent required for optimal transfection of the cells was determined. MDA-MB-231 cells (1.5 x 10^5) were plated in 12-well plates and allowed to adhere overnight. A range of volumes (2-4 µl) of Trans-IT 2020 were mixed with the FLAG-HA plasmid DNA (1 µg) in Opti-MEM I (100 µl) and incubated at room temperature for 15 min. The transfection mixture was then added dropwise to different areas of the wells and the cells were incubated at 37°C for 2 days. The cells were lysed in Laemmli buffer (200 µl) and heated at 95°C for 5 min. The samples (4.5 µl) were dotted onto separate areas of a nitrocellulose membrane and allowed to air dry at room temperature for 5 min. The membrane was blocked with TBST and processed using the same procedure as used for the western blot assay (section 2.3.4.5) using an anti-HA-tag antibody (C29F4). Finally, MDA-MB-231 cells (1.5 x 10^5) were plated in 12-well plates and transfected with the FLAG-HA plasmid either containing TED, LED, UED or EGF4-βTD DNA, or the

empty plasmid using Trans-IT 2020 transfection reagent (sections 2.3.2.6). The concentrations of denatured samples were determined using the Bradford assay (section 2.3.4.1) and equal quantities of the samples were separated by SDS-PAGE (section 2.3.4.4). To test the efficiency of gene silencing, the samples were examined by western blot (section 2.3.4.5) using anti-HA-tag and anti-GAPDH antibodies (Table 5.4). The sizes of the visualised bands were compared to the calculated values shown in Table 5.2.

5.2.5 Optimisation of the knockdown of fVII expression using small interfering RNA (siRNA)

Small interfering RNA (siRNA) are synthetically produced, small, double-stranded RNA molecules (consisting of 21-25 nucleotides) which can interfere with the translation of mRNA coding for specific proteins by enhancing the degradation. A set of pre-designed siRNA (Ambion® silencer select®), which specifically target three separate regions of the fVII mRNA, was used to suppress the expression of the fVII protein in MDA-MB-231 cells. In order to optimize the suppression of the fVII protein, a range of siRNA quantities (30-300 pmol) as well as a range of transfection reagents from various manufacturers were assessed. MDA-MB-231 cells (1.5×10^5) were plated in 12-well plates and allowed to adhere overnight. The cells were transfected with either the fVII siRNA or silencer select negative control #1 siRNA (300 pmol) using either TransIT 2020 (section 2.3.2.8) or Viromer RED (section 2.3.2.9) transfection reagents. The cells were incubated for 2 days at 37°C and were then lysed in Laemmli buffer (200 µl). The concentrations of protein in the samples were determined using the Bradford assay (section 2.3.4.1) and equal quantities of the samples were separated by SDS-PAGE (section 2.3.4.4). To test the efficiency of gene silencing, the samples were examined by western blot (section 2.3.4.5) using anti-fVII and anti-GAPDH antibodies (Table 5.4). The membranes were analysed using ImageJ to determine the level of expression of the fVII protein. The expression levels were normalised against that of GAPDH in the respective sample.

5.2.6 Optimisation of the detection of cell-surface antigens using immunofluorescence microscopy

MDA-MB-231 cells (5×10^4) were plated in glass 10-well chamber slides and allowed to adhere overnight. The presence of TF and β1 integrin on the surface of the cells was assessed by immunofluorescence microscopy (section 2.3.4.7) using a mouse anti-TF antibody (HTF-1) and a rabbit polyclonal anti-β1 integrin antibody. The cells were probed with NL493-conjugated anti-mouse IgG and NL637-conjugated anti-rabbit IgG antibodies, respectively. Images were captured using a fluorescence microscope controlled by the Zen 2012 SP1v8.1 software (Carl Zeiss Microscopy). The amount of fluorescence in each sample was quantified using the ImageJ program.

Table 5.4: Antibodies used for western blot experiments

Probing antibody				Detection antibody		
Antigen	Clone	Host species	Dilution	Antigen	Host species	Dilution
GAPDH	v-18	Goat	1:5000	**Goat IgG**	Mouse	1:3000
HA tag	C29F4	Rabbit	1:3000	**Rabbit IgG**	Mouse	1:3000
p-ERK1/2	D13.14.4E	Rabbit	1:2000	**Rabbit IgG**	Mouse	1:3000
ERK1/2	137F5	Rabbit	1:2000	**Rabbit IgG**	Mouse	1:3000
fVII	polyclonal	Rabbit	1:3000	**Rabbit IgG**	Mouse	1:3000

In a separate set of experiments, the expression of the cloned FLAG-HA-tagged TED peptide and subsequent presentation of the peptide on the cell surface was confirmed. MDA-MB-231 cells (5 x 10^4) were plated as above. The cells were transfected with the FLAG-HA plasmid containing TED DNA using TransIT 2020 (section 2.3.2.6) and incubated for 2 days at 37°C. The presence of the FLAG-HA-tagged TED peptide on the surface of intact cells was detected by immunofluorescence microscopy (section 2.3.4.7) using either an anti-FLAG-tag antibody (FG4R) or an anti-HA-tag antibody (C29F4). The cells were then probed with NL493-conjugated anti-rabbit IgG antibody. Images were captured using the fluorescence microscope and assessed using the ImageJ program as above.

5.2.7 PLA

5.2.7.1 Detecting the interaction between TF and β1 integrin using PLA

Prior to experiments, the suitability of the PLA procedure for examining the interaction of TF and β1 integrin on the surface of cells was assessed. MDA-MB-231 cells (10^4) or HDBEC (5 x 10^4) were plated in 29 mm culture dishes with a 10 mm glass bottomed micro-well and allowed to adhere overnight. One set of HDBEC were transfected with the pCMV6-AC-F3-tGFP plasmid using TransIT 2020 (section 2.3.2.6) and incubated for 2 days at 37°C prior to the PLA. The proximity of TF and β1 integrin was then examined as described in section 2.3.4.8.2, using a rabbit anti-β1 integrin antibody paired with a mouse anti-TF antibody (HTF-1). As a positive control, the association of αv integrin and β1 integrin was also examined using the rabbit anti-β1 integrin antibody paired with a mouse anti-αv integrin antibody. Negative control experiments were performed using the anti-β1 integrin antibody alone or paired with a mouse IgG isotype.

Additional sets of experiments were carried out to determine the potential role of fVIIa in the interaction of TF and β1 integrin. MDA-MB-231 cells (10^4) were plated as above and transfected with either a fVII siRNA (300 pmol), or the silencer® select negative control #1 siRNA (300 pmol). The transfections were performed using Viromer RED transfection reagent (section 2.3.2.9) and the cells were incubated for 2 days at 37°C. An additional set of cells, transfected with the fVII siRNA, was included as above, but the cells were pre-incubated with purified fVIIa (10 nM) for 1 h prior to the PLA. The proximity of TF and β1 integrin was then examined by PLA using a rabbit anti-β1 integrin antibody paired with a mouse anti-TF antibody (HTF-1).

5.2.7.2 Analysis of the interaction of TF extracellular domain peptides with β1 integrin using PLA

Non-specific interactions between the cloned peptides and cell-surface proteins may prevent the accurate assessment of the interaction between the peptides and the cellular TF or β1 integrin. Prior to the experiments, the likelihood of non-specific interaction between the expressed peptides and

cell-surface proteins was examined and precluded. MDA-MB-231 cells (10^4) were plated in 29 mm culture dishes with a 10 mm glass bottomed micro-well and allowed to adhere overnight. Sets of cells were transfected with the FLAG-HA plasmid either containing TED DNA or the empty plasmid using TransIT 2020 (section 2.3.2.6). The cells were incubated for 2 days at 37°C. In order to eliminate peptide which non-specifically associated with the cell membrane, the cells were washed three times with PBST. Samples of cells were collected prior to and after the washing. The interactions of the HA-tagged TED peptide with β1 integrin were assessed by PLA using an anti-HA-tag antibody (C29F4) paired with a rabbit polyclonal anti-β1 integrin antibody. Images were captured using the fluorescence microscope and assessed using the ImageJ program.

In further experiments, MDA-MB-231 cells (10^4) or HDBEC (5×10^4) were plated and transfected with the FLAG-HA plasmid either containing TED, LED or UED DNA, or the empty plasmid as above. The cells were washed with PBST and the interaction of the peptides with β1 integrin was assessed by PLA. To examine the interactions an anti-HA-tag antibody (C29F4) was used in conjunction with a rabbit polyclonal anti-β1 integrin antibody. Images were captured using the fluorescence microscope and assessed using the ImageJ program (section 2.3.4.8.2). The number of interactions observed in the cells expressing the peptide construct were quantified and compared to those of the cells expressing the empty plasmid. In addition, experiments were performed in which the capability of β1 integrin to enter the active conformation was blocked prior to the analysis of the interaction with the TF peptides. HDBEC (5×10^4) were plated and transfected as above. Sets of cells were incubated with an inhibitory anti-β1 integrin antibody (AIIB2; 10 μg/ml) which only recognises the closed/inactive conformation of this proteins and prevents its activation (Park et al., 2006; Spiess et al., 2018). The cells were incubated with the antibody for 1 h prior to the PLA experiment. The interactions between the expressed peptides and β1 integrin was then assessed as above using the anti-HA-tag antibody (C29F4) paired with a rabbit polyclonal anti-β1 integrin antibody. Images were captured using the fluorescence microscope and assessed using the ImageJ program (section 2.3.4.8.2).

5.2.7.3 Analysis of the interaction of the β1 integrin EGF4 and βTD domain peptides of with TF using PLA

MDA-MB-231 cells (10^4) were plated and transfected with the FLAG-HA plasmid either containing EGF4-βTD or EGF4 DNA, or the empty plasmid as above. The cells were washed with PBST and then the interaction of the peptides with TF was assessed by PLA using a rabbit anti-HA-tag antibody (C29F4) in conjunction with a mouse anti-TF (HTF-1) antibody. Images were captured using the fluorescence microscope and assessed using the ImageJ program (section 2.3.4.8.2). The number of

interactions observed in the cells expressing the peptide constructs were quantified and compared to those of the cells expressing the empty plasmid.

5.2.8 Examination of the interaction of the expressed peptides with target proteins using co-IP

MDA-MB-231 cells (1.5 x 10^5) were plated in 12-well plates and allowed to adhere overnight. The cells were transfected with the FLAG-HA plasmid containing the EGF4-βTD, EGF4, TED, LED or UED DNA, or the empty plasmid as described above. The cells were harvested and the expressed FLAG-HA-tagged peptides were immunoprecipitated using an anti-HA-tag antibody (section 2.3.4.9). The isolated proteins were then separated by SDS-PAGE (section 2.3.4.4) and the presence of either TF or β1 integrin was assessed by western blot assay (section 2.3.4.5) using anti-TF or anti-β1 integrin antibodies, respectively (Table 5.5). Conversely, cellular TF or β1 integrin were immunoprecipitated using anti-TF or anti-β1 integrin antibodies. The isolated proteins were separated by SDS-PAGE and the presence of the expressed FLAG-HA-tagged peptides was assessed using the anti-HA-tag or anti-FLAG-tag antibodies (Table 5.5).

5.2.9 Examination of the influence of the TF and β1 integrin peptides on ERK1/2 phosphorylation

In order to investigate any potential alterations to cellular signalling arising from the interaction of TF and β1 integrin, the influence of the expression of the TF extracellular domain peptides on ERK1/2 phosphorylation was measured. MDA-MB-231 cells (1.5 x 10^5) and HDBEC (5 x 10^5) were plated in 12-well plates and allowed to adhere overnight. The cells were transfected with FLAG-HA plasmid containing the EGF4-βTD, TED, LED or UED DNA, or the empty plasmid as described above. Another set of cells were transfected with the UED expression plasmid or empty plasmid and were then incubated with an inhibitory anti-β1 integrin antibody (AIIB2; 10 µg/ml) for 16 h prior to harvesting. The cells were lysed in Laemmli buffer (200 µl) and heated at 95°C for 5 min. The concentrations of protein in the samples were determined using the Bradford assay (section 2.3.4.1) and equal quantities (20 µg/well) were separated by SDS-PAGE (section 2.3.4.4). Western blot analysis (section 2.3.4.5) was performed using an anti-ERK1/2 antibody together with an anti-phosphorylated ERK1/2 antibody, which recognises T202/185 phosphorylation of ERK1/2 both in the presence or absence of phosphorylated Y204/187 (Table 5.4). The membranes were analysed using ImageJ and the expression level of phosphorylated ERK1/2 were normalised against that of total ERK1/2 in each sample.

Table 5.5: Antibody combinations used for co-IP and subsequent western blot analysis

Peptides expressed	Precipitate target	Antibody Species		Western blot target	Antibody Species
EGF4-βTD	**HA**	Rabbit	→	**TF**	Mouse
TED, LED, UED	**HA**	Mouse	→	**β1 integrin**	Rabbit
EGF4-βTD	**TF**	Mouse	→	**HA**	Rabbit
TED, LED, UED	**β1 integrin**	Rabbit	→	**HA**	Mouse

Properties of the antibodies used for co-IP, including the host species of the antibodies targeting each target. In addition, the antibodies used to probe for the co-immunoprecipitated antigens are indicated alongside each line.

5.2.10 Examination of the influence of the TF and β1 integrin peptides on cyclin D1 expression using semi-quantitative RT-PCR

To further investigate any influence of the TF extracellular domain peptides on cellular signalling, the outcome on cyclin D1 expression was assessed next. MDA-MB-231 cells (1.5 x 10^5) and HDBEC (5 x 10^5) were plated in 12-well plates and allowed to adhere. The cells were transfected with the FLAG-HA plasmid containing the EGF4-βTD, TED, LED or UED DNA, or the empty plasmid as described above. Another set of cells were transfected with the UED expression plasmid or empty plasmid and were then incubated with an inhibitory anti-β1 integrin antibody (AIIB2; 10 μg/ml) for 16 h prior to harvesting. The cells were then lysed, and the mRNA was extracted and converted to cDNA using the cell-2-cDNA kit (section 2.3.5.16). The relative quantity of cyclin D1 mRNA present in the cell lysate was quantified uses RT-PCR (section 2.3.5.17). A previously confirmed set of primers for cyclin D1 (Bijwaard et al., 2001) with the sequences 5'-CCG TCC ATG CGG AAG ATC-3' (forward) and 5'-ATG GCC AGC GGG AAG AC-3' (reverse) were used. The data were normalised against the housekeeping gene β-Actin which was quantified using a confirmed commercial primer set, obtained from Qiagen (sequence not disclosed). The change in cyclin D1 mRNA expression in the cells expressing the TF or β1 integrin peptides was calculated in relation to that in cells expressing the empty plasmid, using the $2^{-\Delta\Delta Ct}$ method (Livak & Schmittgen, 2001).

5.2.11 Examination of the influence of the TF and β1 integrin peptides on cell numbers using the crystal violet assay

To examine the influence of the TF extracellular domain peptides on cell proliferation, the influence of the expression of the peptides on cell numbers was assessed. MDA-MB-231 cells and HDBEC (5 x 10^4) were plated in 12-well plates and allowed to adhere. The cells were transfected with the FLAG-HA plasmid containing EGF4-βTD, TED, LED or UED DNA, or the empty plasmid as described above. The cells were then incubated for 3 days at 37°C. The cells were then fixed with 3% (v/v) glutaraldehyde and assessed by crystal violet assay (section 2.3.2.10). The resulting absorption values were converted to cell numbers using previously generated standard curves for MDA-MB-231 cells and HDBEC (Figure 4.7).

5.2.12 Monoclonal antibody assay

5.2.12.1 Assessment of the binding of TF extracellular domain peptides to the EGF4-βTD domain of β1 integrin

In order to assess if TF associated with the EGF4-βTD domains within β1 integrin, the ability of the TF extracellular domain peptides to compete with the binding of an antibody specific to the EGF4-βTD

region was evaluated. MDA-MB-231 cells (10^4) and HDBEC (5 x 10^4) were plated in 96-well plates and allowed to adhere. The cells were transfected with the FLAG-HA plasmid expressing TED, LED or UED DNA, or the empty plasmid as described above. The cells were then fixed with 4% formaldehyde and the cells were probed with an antibody specific for the EGF4-βTD domain (residues 579-799) and detected using a previously described antibody binding assay (section 2.3.4.6).

5.2.12.2 Examination of the influence of the TF peptides on the conformation of β1 integrin

The ability of the TF extracellular domain peptides to induce a conformational change in β1 integrin was assessed using monoclonal antibodies specific for the open and closed conformations of the latter protein. The use of monoclonal antibodies to study changes in the conformation of β1 integrin is well established (Takada & Puzon, 1993). The monoclonal antibody 9EG7 recognises an epitope of β1 integrin that only becomes exposed when the protein is in the active/open conformation (Bazzoni et al., 1995). The monoclonal antibody AIIB2 recognises an epitope that is only available when the protein is in the inactive/closed conformation (Park et al., 2006; Spiess et al., 2018). Prior to the experiments, the specificity of the 9EG7 and AIIB2 antibodies to distinguish between the two different conformations of β1 integrin was confirmed. Incubation of cells with Mn^{2+} ions is known to induce switching to the active/open conformation in cell-surface integrins, even in the absence of ligand binding (Kim et al., 2004; Luo et al., 2007). Sets of MDA-MB-231 cells (5 x 10^4) were incubated in HEPES buffer (20 mM HEPES, pH 7.4) containing 1 mM Mn^{2+} ions ($MnCl_2$) at 37°C for 30 min. The cells were then fixed with 4% formaldehyde and assessed by antibody binding assay (section 2.3.4.6) using the 9EG7 and AIIB2 antibodies.

In order to assess if the binding of the TF extracellular domain peptides to β1 integrin was capable of inducing, or preventing a change in the protein conformation, MDA-MB-231 cells (10^4) and HDBEC (5 x 10^4) were plated in 96-well plates and allowed to adhere. The cells were transfected with the FLAG-HA plasmid expressing TED, LED or UED, along with a separate set transfected with the empty plasmid as described above. The cells were then fixed with 4% formaldehyde and assessed using the above procedure utilising the 9EG7 and AIIB2 antibodies.

5.3 Results

5.3.1 Examination of the molecular structure of integrins and TF using Raswin

5.3.1.1 Identification of the boundaries of the EGF4 and βTD domains of β1 integrin

The putative TF binding domain within β1 integrin has previously been suggested to lie within the EGF4 and βTD domains in the membrane-proximal region of the latter protein (Collier & Ettelaie, 2010). To examine this hypothesis, the cDNA corresponding to the EGF4 and βTD domains were cloned into an expression vector and the binding of the resulting peptides to TF examined. However, the exact boundaries of the EGF4 and βTD domains within β1 integrin cDNA have not previously been defined. Therefore, in order to determine the boundaries of the EGF4 and βTD domains, the domains were first identified within the crystal structures of β2 and β3 integrin using the RasWin program (Figure 5.5). In β2 integrin, the EGF4 was identified to span residues 556-594 and the βTD was localised to residues 595-676. Similarly, in β3 integrin, the EGF4 was identified to span residues 563-603 and the βTD was localised to residues 604-695. The amino acid sequences of β1, β2 and β3 integrin were then aligned and the boundaries of EGF4 and βTD domains within β1 integrin were then estimated by homologous comparison (Figure 5.6). The EGF4 domain in β1 integrin was estimated to span residues 572-610 and βTD was localised to residues 611-728.

5.3.1.2 Identification of the boundaries of the upper and lower extracellular (fibronectin-like) domains of TF

The boundary between the upper and lower fibronectin-like domains was identified within the crystal structure of the extracellular domain of TF using the RasWin program (Figure 5.7). The upper and lower domains were identified as residues 1-105 and 111-219, respectively. A linking region between the two domains consisting of 5 amino acids was also identified. In this study the region including the whole of the extracellular domain of TF is referred to as the “total extracellular domain” (TED), and the upper and lower fibronectin-like domains including the linking region are referred to as the “upper extracellular domain” (UED) and the “lower extracellular domain” (LED), respectively.

5.3.2 Generation of the insert DNA by PCR

In order to sub-clone the DNA sequences identified above into the FLAG-HA plasmid, DNA inserts were generated by PCR. The PCR products were assessed by agarose gel electrophoresis and the sizes of the amplicons were determined and compare to the calculated values shown in Table 5.2. A band corresponding to the EGF4-βTD insert DNA was observed at ~500 base pairs (bp), which corresponded to the expected size for this insert (Figure 5.8A). In separate amplifications, bands corresponding to the TED, UED and LED insert DNA were detected at approximately 750, 350 and

Figure 5.5: The EGF4 and βTD domains in β2 and β3 integrin

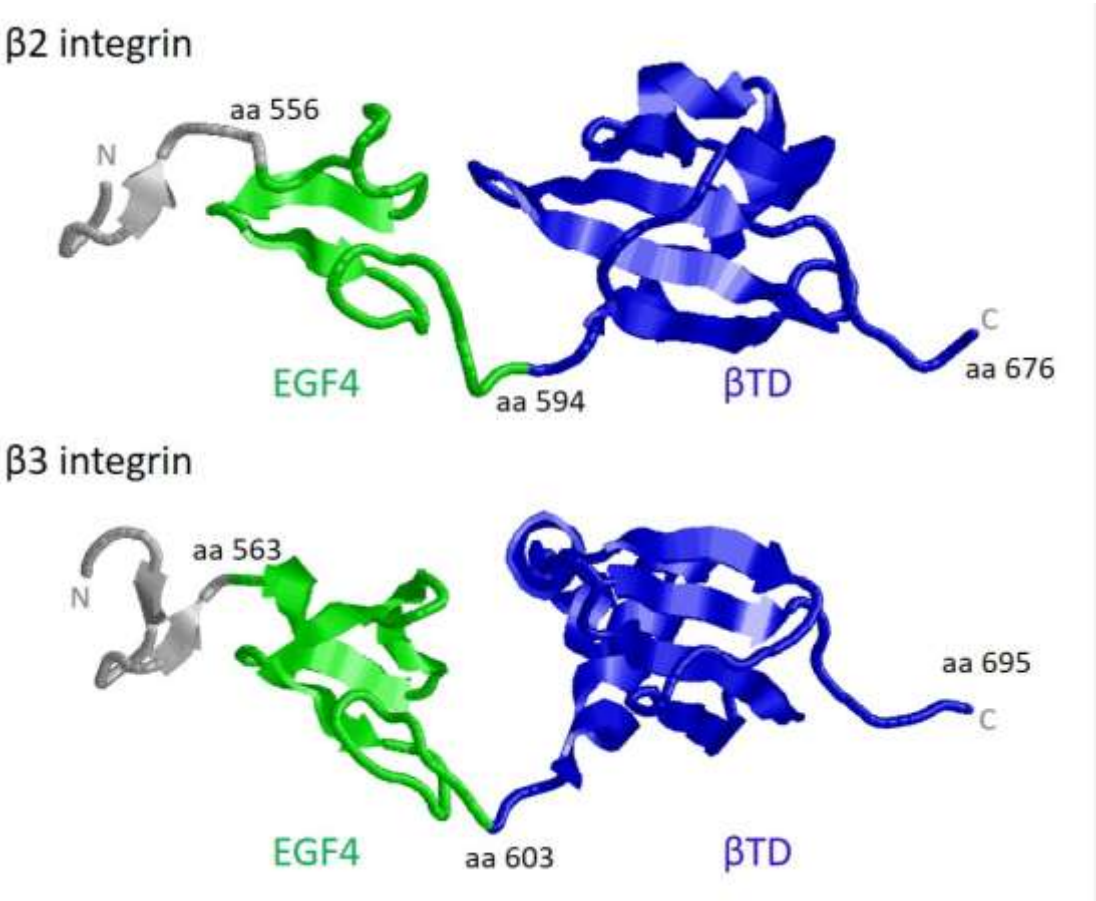

The structures of β2 integrin and β3 integrin were visualised using the RasWin program and the files were edited to limit the structures to the amino acids corresponding the EGF4 and βTD domains.

Figure 5.6: Alignment of the amino acid sequences of β1, β2 and β3 integrin

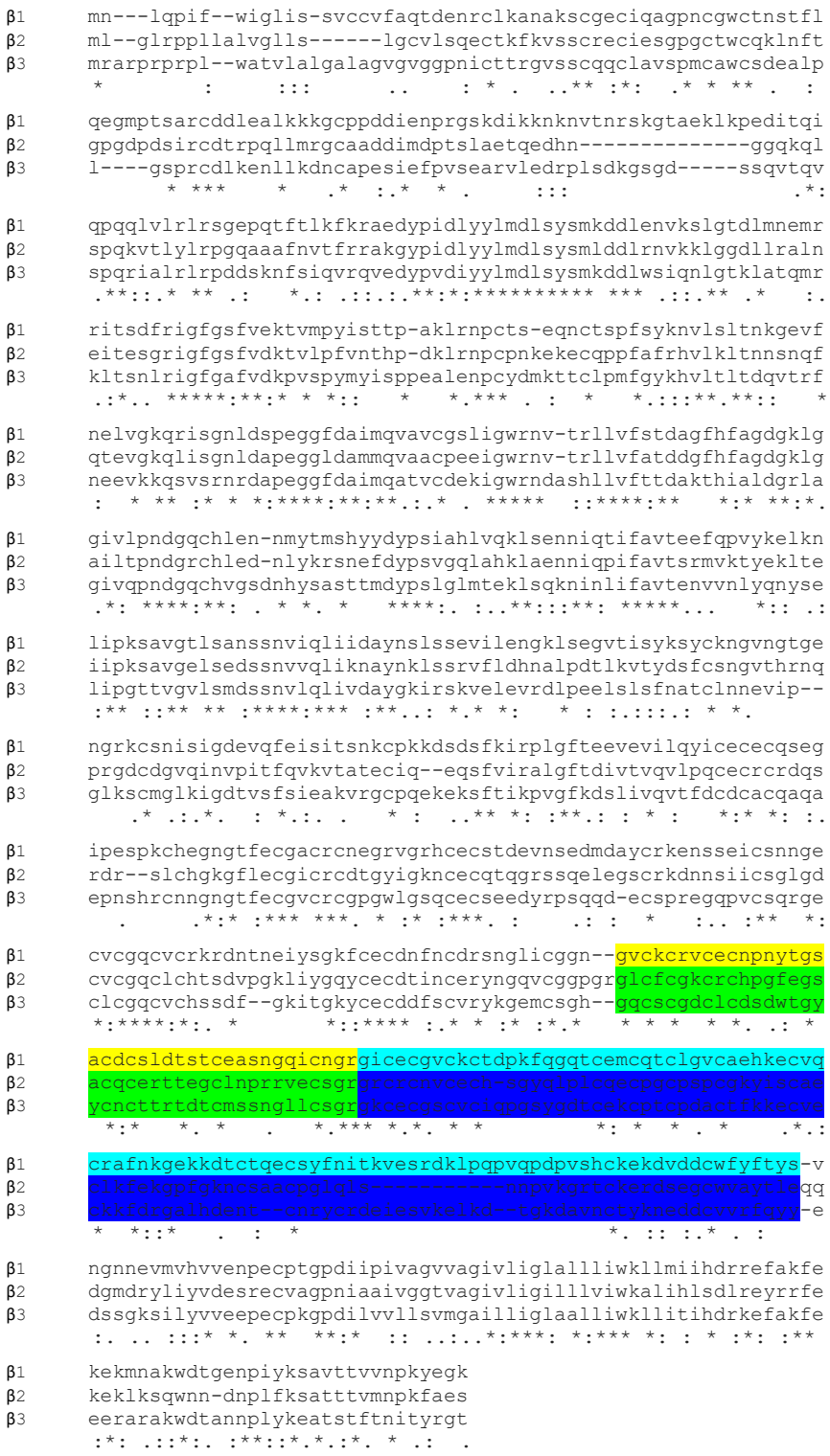

Alignment of the amino acid sequence of β1 integrin with that of β2 and β3 integrin using the Clustal Omega program (EMBL-EBI). Using homology comparisons, the EGF4 (yellow) and βTD (cyan) domains were estimated within β1 integrin.

Figure 5.7: Crystal structure and amino-acid sequence of the extracellular domain of TF

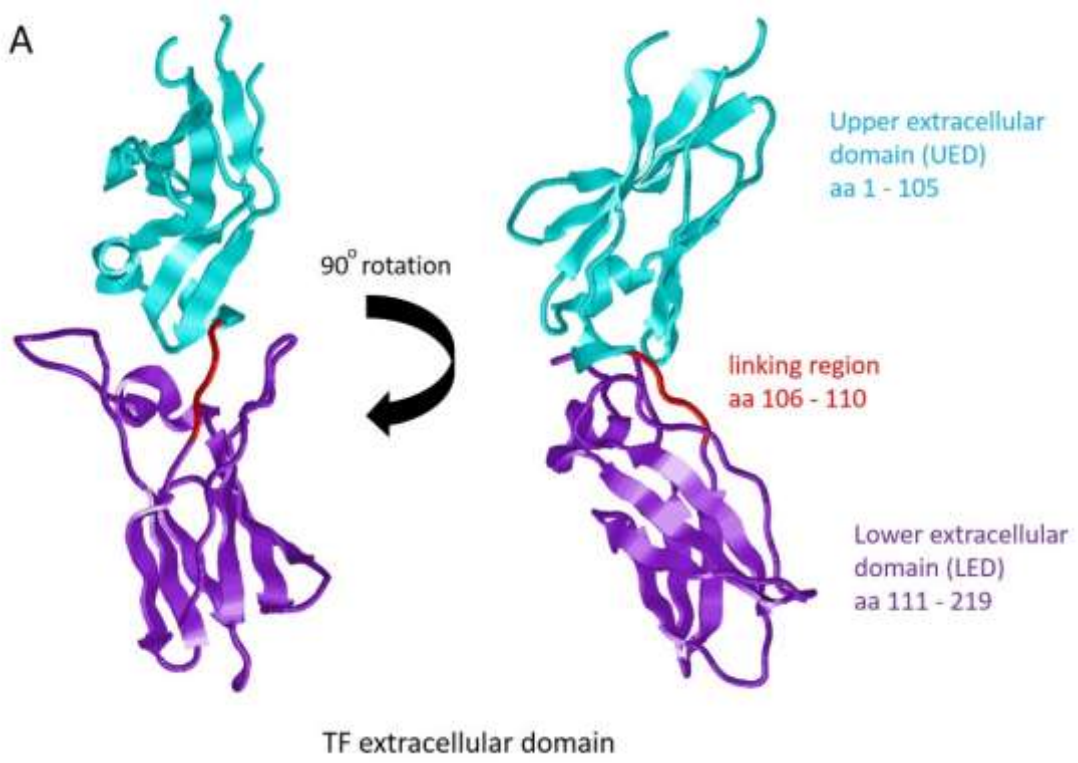

B

S G T T N T V A A Y N L T W K S T N F K T I L E W E P K P V N Q V Y T V
Q I S T K S G D W K S K C F Y T T D T E C D L T D E I V K D V K Q T Y L
A R V F S Y P A G N V E S T G S A G E P L Y E N S P E F T P Y L E T N L
G Q P T I Q S F E Q V G T K V N V T V E D E R T L V R R N N T F L S L R
D V F G K D L I Y T L Y Y W K S S S S G K K T A K T N T N E F L I D V D
K G E N Y C F S V Q A V I P S R T V N R K S T D S P V E C M G Q E K G E
F R E *I F Y I I G A V V F V V I I L V I I L A I S L* h k c r k a g v g q s w
k e n s p l n v s

The boundary between the UED (cyan) and LED (purple) was identified within the crystal structure of TF using the RasWin program. A 'linking region' (red) between these two domains was also identified.

Figure 5.8: Generation of insert DNA by PCR

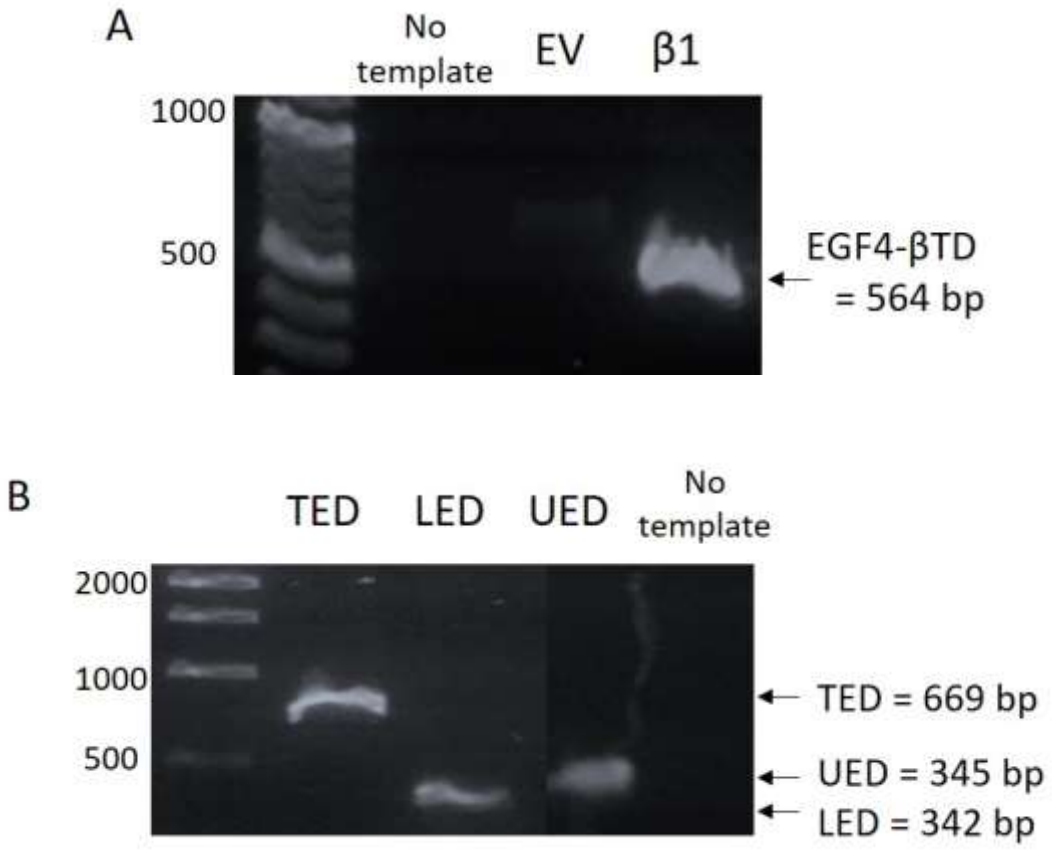

A) The EGF4-βTD of β1 integrin was amplified by PCR using the pCMV6-XL5-ITGB1 plasmid as template. B) The TED, LED and UED of TF were amplified by PCR using the pCMV6-AC-F3-tGFP plasmid as template. The amplified PCR products were confirmed by agarose gel electrophoresis. EV = empty pCMV6-XL5 vector.

300 bp, respectively (Figure 5.8B). Control experiments performed devoid of the template DNA, did not produce an amplicon and confirmed the absence of contaminating DNA in the PCR reagents. In addition, no amplicon was produced in control experiments performed using the empty pCMV6-XL5 plasmid as template DNA. This indicated that the primers used for the generation of the EGF4-βTD insert DNA were specific to the desired sequences.

5.3.3 Optimisation of digestion and ligation procedures

In order to ligate the insert DNA into the FLAG-HA plasmid it was first necessary to digest both DNA strands with two restriction enzymes. To confirm that the XbaI and NotI restriction enzymes were capable of efficient digestion of the FLAG-HA plasmid, samples of the plasmid were incubated with each of the enzymes. Digestion of the plasmid with either the XbaI or NotI enzyme produced a single band at ~4000 bp which corresponded to the linearised plasmid. In contrast, the undigested plasmid was observed as multiple bands between 3500-10000 bp which corresponded to the circular plasmid in supercoiled and relaxed conformations (Figure 5.9). Therefore, both enzymes were deemed suitable for digestion of the circular FLAG-HA plasmid.

Next, the conditions used for the ligation of DNA were optimised using samples of FLAG-HA plasmid which had been previously linearised using the XbaI enzyme. Successful ligations were identified by measuring the ratio of linear plasmid (visible at ~4000 bp) to the relaxed circular plasmid (visible at ~10000 bp). Incubation of the linearised plasmid with the NEB sticky end master mix resulted in a ratio of circular:linear DNA of 1.3, which was higher than that of the T4 ligase (0.2 circular:linear ratio) (Figure 5.10). Therefore, the NEB sticky end master mix was used in all further ligation procedures. Additionally, by ligating the digested TED DNA and the digested plasmid DNA together, at molar ratios of 1:5, 1:15 and 1:30 (plasmid:insert), the optimal molar ratio of plasmid:insert was explored. Initial examination of the ligated products by electrophoresis did not reveal any differences in the ratios of circular:linear plasmid between these samples (Figure 5.11A). Therefore, to further examine the efficiency of ligation, samples were transformed into competent *E. coli* and grown overnight on carbenicillin selection plates. Three individual colonies were selected from each plate and the plasmids were extracted. The presence of the inserted TED DNA within the extracted plasmids was examined by PCR. Analysis of the extracted plasmids from the set of colonies containing DNA ligated at the molar ratio of 1:30 produced a band at ~750 bp (Figure 5.11B). This indicated that the TED DNA was present in this set of plasmids and confirmed the success of the ligation. In contrast, only one out of three plasmids extracted from the set of colonies containing DNA ligated at the molar ratios of 1:5 or 1:15 produced a band at ~750 bp following PCR. Therefore, in all further ligation procedures, insert DNA and plasmid DNA were mixed at a molar ratio of 1:30.

Figure 5.9: Restriction digest of the FLAG-HA plasmid

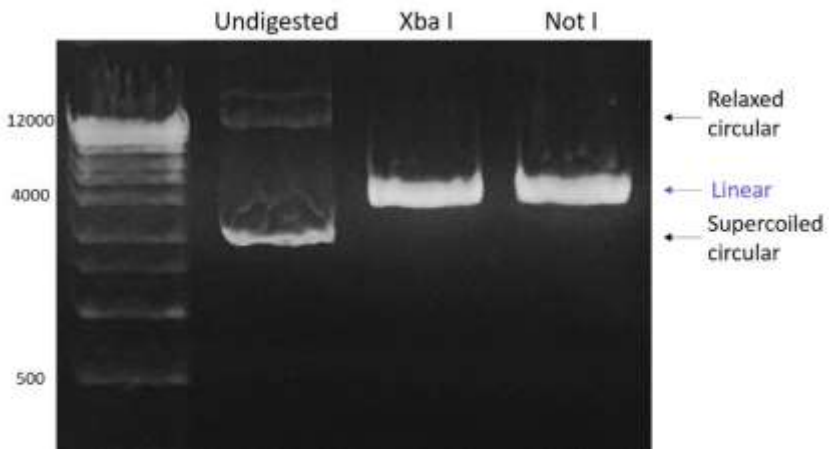

FLAG-HA-pcDNA plasmid DNA (1 µg) was incubated with *XbaI* or *NotI* restriction enzymes (10 U) for 1 h at 37°C. The reaction products was assessed by agarose gel electrophoresis for the presence of linearised DNA.

Figure 5.10: Recircularisation of linear plasmid using different ligation reagents

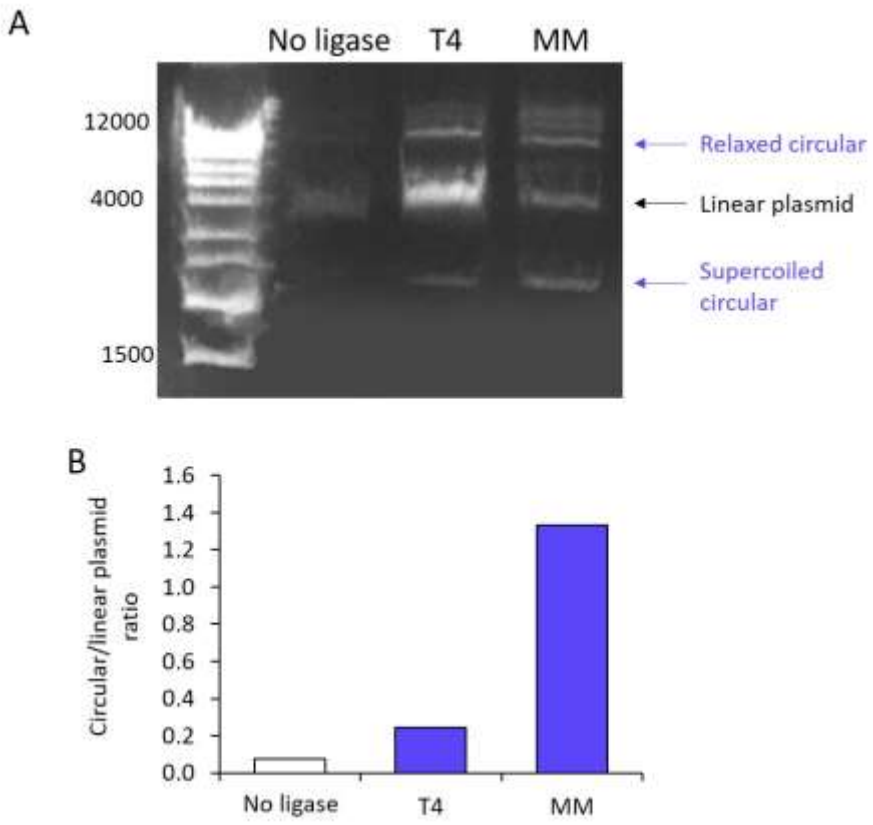

Linearised plasmid DNA (30 ng) was incubated with either T4 ligase (T4), NEB sticky end master mix (MM) or in the absence of ligase, at 22°C for 15 min. The ligation products was A) assessed by agarose gel electrophoresis and B) the intensities of the bands were quantified using ImageJ and the ratio of circularised/linear plasmid was calculated (n=1).

Figure 5.11: Optimisation of the ligation of insert DNA into the FLAG-HA plasmid

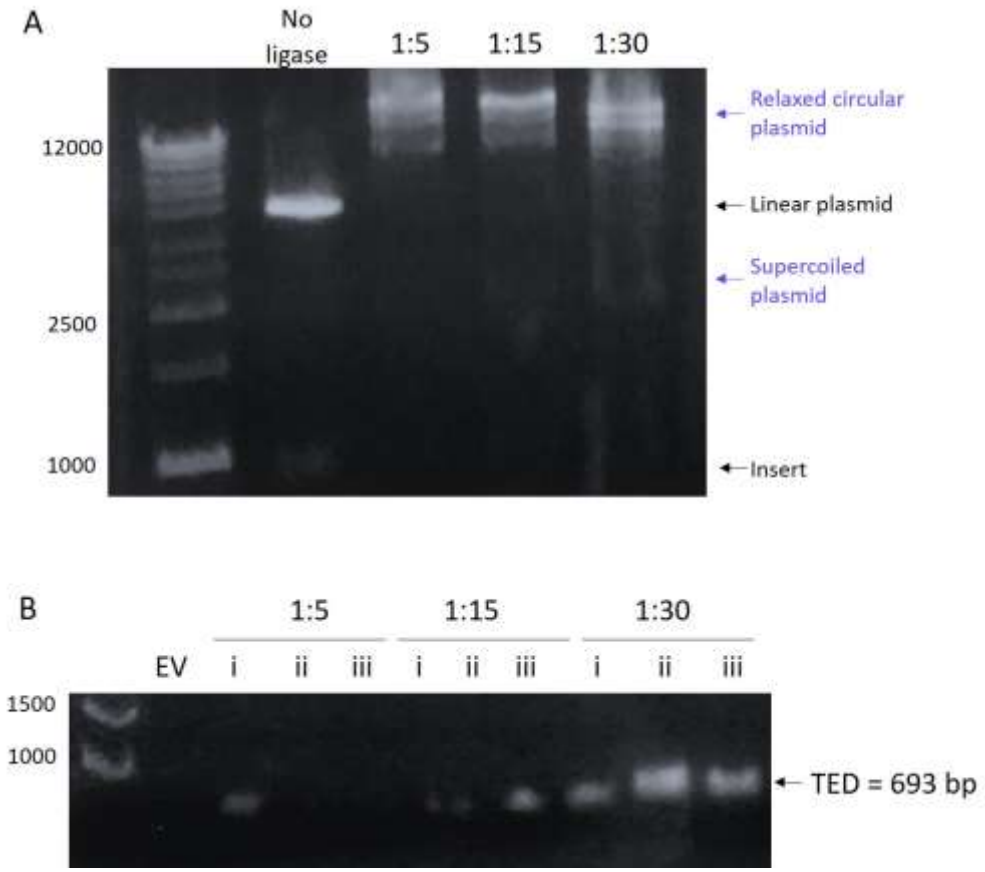

TED DNA (1 µg) and FLAG-HA plasmid (1 µg) were separately digested with *XbaI* and *NotI* restriction enzymes (10U). The FLAG-HA plasmid (30 ng) and TED DNA were then ligated at range of molar ratios of 1:5, 1:15 and 1:30 (plasmid:insert) using NEB sticky end master mix. A) Ligation products were examined by agarose gel electrophoresis. B) *E. coli* were then transformed with the ligated DNA constructs and grown of selection plates. Three individual colonies (i, ii and iii) were selected from each plate, expanded overnight and the plasmid DNA isolated. The presence of the inserted TED DNA within the isolated plasmids was assessed by PCR. EV = empty FLAG-HA-pcDNA3.1 vector.

5.3.4 Validation of the sub-cloning of insert DNA into the plasmid

The amplified DNA coding for LED, UED and EGF4-βTD were individually ligated into the FLAG-HA plasmid using the NEB sticky end master mix. To confirm the successful insertion of the DNA, PCR reactions were performed as described above. Electrophoresis analysis of the samples showed bands that corresponded to the LED (~300 bp), UED (~400 bp) and EGF4-βTD (~500 bp) DNA in each of the positive samples (Figure 5.12 & Figure 5.13A). To ensure the absence of contaminating DNA and to confirm the specificity of the primers used, a reaction was also performed using the empty FLAG-HA plasmid. Amplification of the empty FLAG-HA plasmid using either LED or EGF4-βTD primer sets did not produce an amplicon (Figure 5.12 & Figure 5.13A). In contrast, a nonspecific amplicon was observed following amplification of the empty FLAG-HA plasmid using the UED primer set (Figure 5.12). However, the molecular weight of this nonspecific amplicon was ~500 bp, rather than the expected ~400 bp, indicating the product arose from off-target binding by this primer set.

Successful sub-cloning of the EGF4-βTD DNA was further confirmed by restriction digestion of the ligated plasmid construct with *BsrGI* enzyme. This was possible since the EGF4-βTD DNA contains a single *BsrGI* restriction site that is otherwise absent from the FLAG-HA plasmid. Digestion of plasmid isolated from one of the four colonies (ii) produced a single band at ~4000 bp (Figure 5.13B). This band corresponded to the linearised plasmid and indicated the presence of the EGF4-βTD DNA within the construct. Additionally, digestion of the plasmids from two other colonies (iii and iv) resulted in multiple bands at approximately 500, 1000, 2000 and 4000 bp. Since the EGF4-βTD DNA was 500 bp in length, this indicated the presence of multiple tandem copies of the EGF4-βTD DNA inserted into these plasmids. In contrast, digestion of the negative sample did not result in the linearisation or release of any DNA fragments which was indicated by the presence of multiple bands between 3500-10000 bp corresponding to the supercoiled and relaxed conformations of the circular plasmid.

Finally, to confirm the correct orientation of the DNA within the plasmid, the positive samples were examined by DNA sequencing. The sequencing results were aligned against the published DNA sequences for the respective insert DNA contained within the FLAG-HA plasmid. Sequence-analysis of the samples confirmed the correct orientation of the insert DNA.

5.3.5 Preparation of plasmid DNA for the expression of EGF4 and βTD domains using site directed mutagenesis

Plasmid constructs containing the individual EGF4 and βTD domains were prepared from the plasmid containing the sub-cloned EGF4-βTD DNA using site directed mutagenesis. Successful amplification using primers designed to insert a stop codon after the EGF4 resulted in an amplicon at ~4000 bp

Figure 5.12: Verification of the success of the insertion of TF extracellular domain DNA into the FLAG-HA plasmid using PCR

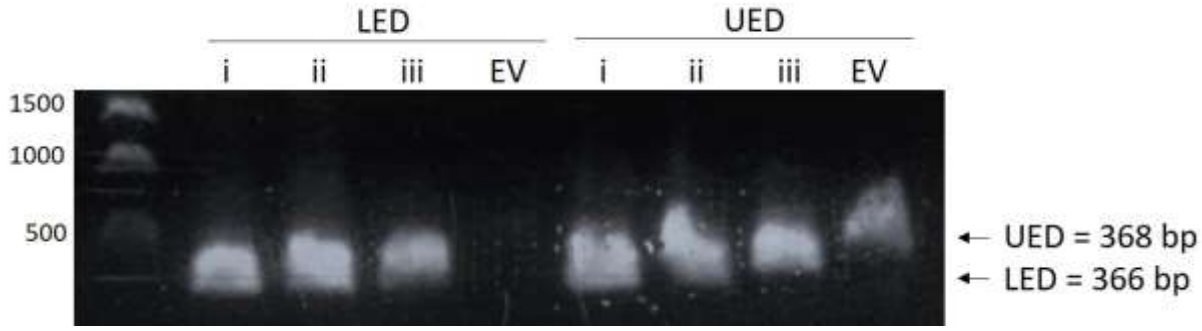

LED and UED DNA (1 µg) and FLAG-HA plasmid (1 µg) were digested with the *XbaI* and *NotI* restriction enzymes (10U). The FLAG-HA plasmid (30 ng) and LED and UED DNA were then mixed at a molar ratio of 1:30 (plasmid:insert) and ligated using NEB sticky end master mix. *E. coli* were transformed with ligated DNA and grown of selection plates. Three individual colonies (i, ii and iii) were selected, expanded overnight and the plasmid DNA isolated. The presence of the inserted LED and UED DNA within the isolated plasmids was assessed by PCR. EV = empty FLAG-HA-pcDNA3.1 vector.

Figure 5.13: Products of PCR and restriction enzyme digestion reactions used to verify the insertion of EGF4-βTD DNA into the FLAG-HA plasmid

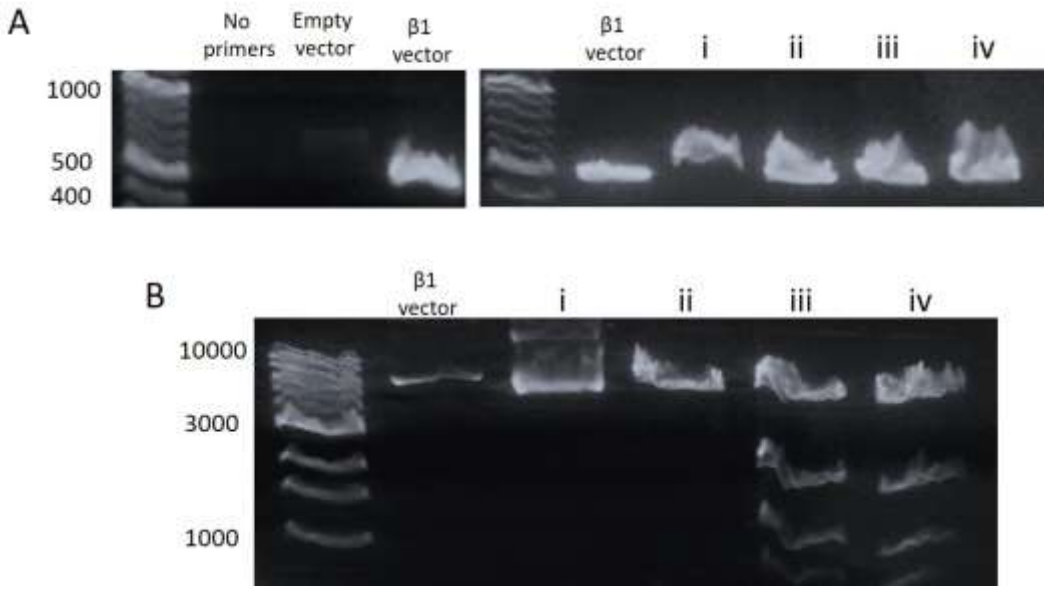

EGF4-βTD DNA (1 µg) and FLAG-HA plasmid (1 µg) were digested with the *XbaI* and *BamHI* restriction enzymes (10U). The FLAG-HA plasmid (30 ng) and EGF4-βTD DNA were then mixed at a molar ratio of 1:30 (plasmid:insert) and ligated using NEB sticky end master mix. *E. coli* were transformed with ligated DNA and grown of selection plates. Four individual colonies (i, ii, iii and iv) were selected, expanded overnight and the plasmid DNA isolated. The presence of the inserted EGF4-βTD DNA within the isolated plasmids was assessed by A) PCR and B) restriction enzyme digest using the *BsrGI* enzyme. Empty Vector = empty FLAG-HA-pcDNA3.1 vector, β1 vector = pCMV6-ITGB1-XL5 vector.

(Figure 5.14) which was then used for the remainder of the mutagenesis procedure. The successful mutants were then identified by DNA sequencing and shown to contain a point mutation that converted the Gly611 residue of β1 integrin (GGC) into a stop codon (TAG). Therefore, this mutation terminates the transcription of the plasmid after the expression of EGF4 domain only, in tandem to the FLAG- and HA-tags.

In another mutagenesis reaction, amplification using PCR primers designed to delete the EGF4 sequence leaving the βTD sequence did not produce any detectable products (Figure 5.15A). In an attempt to improve the efficacy of this reaction, experiments were prepared containing either additional DMSO (3% v/v) or Mg^{2+} ions (1 mM) (NEBiolabs) and carried out at a range of annealing temperatures. However, no PCR products were produced using any of the alterations in reaction conditions (Figure 5.15B).

5.3.6 Optimisation of transfection of plasmid DNA into mammalian cells

In order to maximise the expression of the plasmid constructs, preliminary studies were carried out to determine the transfection efficiency of TransIT 2020 and Viromer RED transfection reagents. MDA-MB-231 cells were transfected with a plasmid encoding tGFP using the two transfection reagents and the expression of tGFP was examined by flow cytometry. A gate (M1) was drawn to include the 3% of control cells with the highest fluorescence. The transfection efficiency of the tested reagents was determined by the proportion of the resulting transfected cells which were within this gate (Figure 5.16A). Transfection of cells using TransIT 2020 resulted in an increase the number of fluorescent cells within the gated region (32%) together with an increase in the mean fluorescence (19.6 ± 1.2). Transfection of cells using Viromer RED also resulted in an increase in the number of cells within the gate (23%) together with an increase in the mean fluorescence (13.8 ± 1.1) (Figure 5.16B). This indicated that both reagents were capable of transfecting the plasmid with similar efficiencies. However, the fluorescent signal of all transfected cells was deemed to be more homogeneous when performed using the TransIT 2020 reagent (Figure 5.16C). This indicates that the TransIT 2020 reagent was capable of transfecting a similar copy number of the plasmid into each cell. In contrast, transfection of cells using Viromer RED resulted in diverse fluorescent signals ranging from those remaining unchanged from the control cells to those emitting fluorescence at levels 3-4 orders of magnitude higher than the controls (Figure 5.16C). This variation in fluorescence was deemed to have arisen from the transfection of a disproportionate number of plasmid copies into cells. Therefore, the TransIT 2020 reagent was used to transfect cells in all further experiments.

Next, the concentration of TransIT 2020 transfection reagent required for the transfection of the FLAG-HA plasmid in MDA-MB-231 cells was optimised. Sets of cells were transfected using a range of

Figure 5.14: Analysis of the PCR product from the substitution mutagenesis reaction

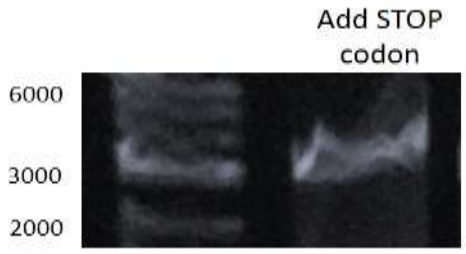

The FLAG-HA plasmid containing the EGF4-βTD DNA was amplified by PCR using primers designed to introduce a stop codon (TAG) following the EGF4 domain (Gly611→Stop). Reactions were assessed for the presence of amplified DNA by agarose gel electrophoresis.

Figure 5.15: Analysis of the PCR product of the deletion mutagenesis reaction

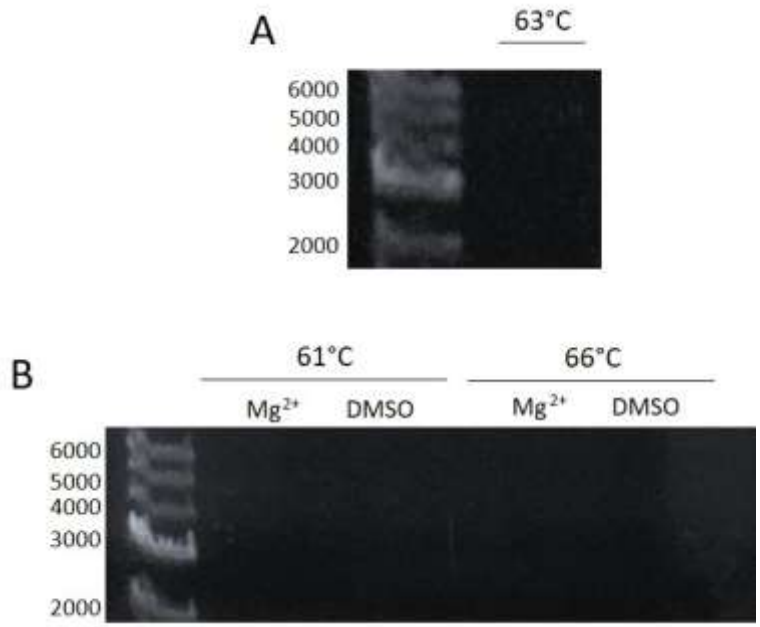

The FLAG-HA plasmid containing the EGF4-βTD DNA was amplified by PCR using primers designed to hybridised to sequences directly adjacent to the EGF4 domain sequence that required deletion. PCR reactions were performed at a range of annealing temperatures (61-66°C) as well as in the presence of additional DMSO (3% v/v) or Mg^{2+} ions (1 mM magnesium chloride) as indicated. Reactions were assessed for the presence of amplified DNA by agarose gel electrophoresis.

Figure 5.16: Assessment of transfection efficiency using flow cytometry

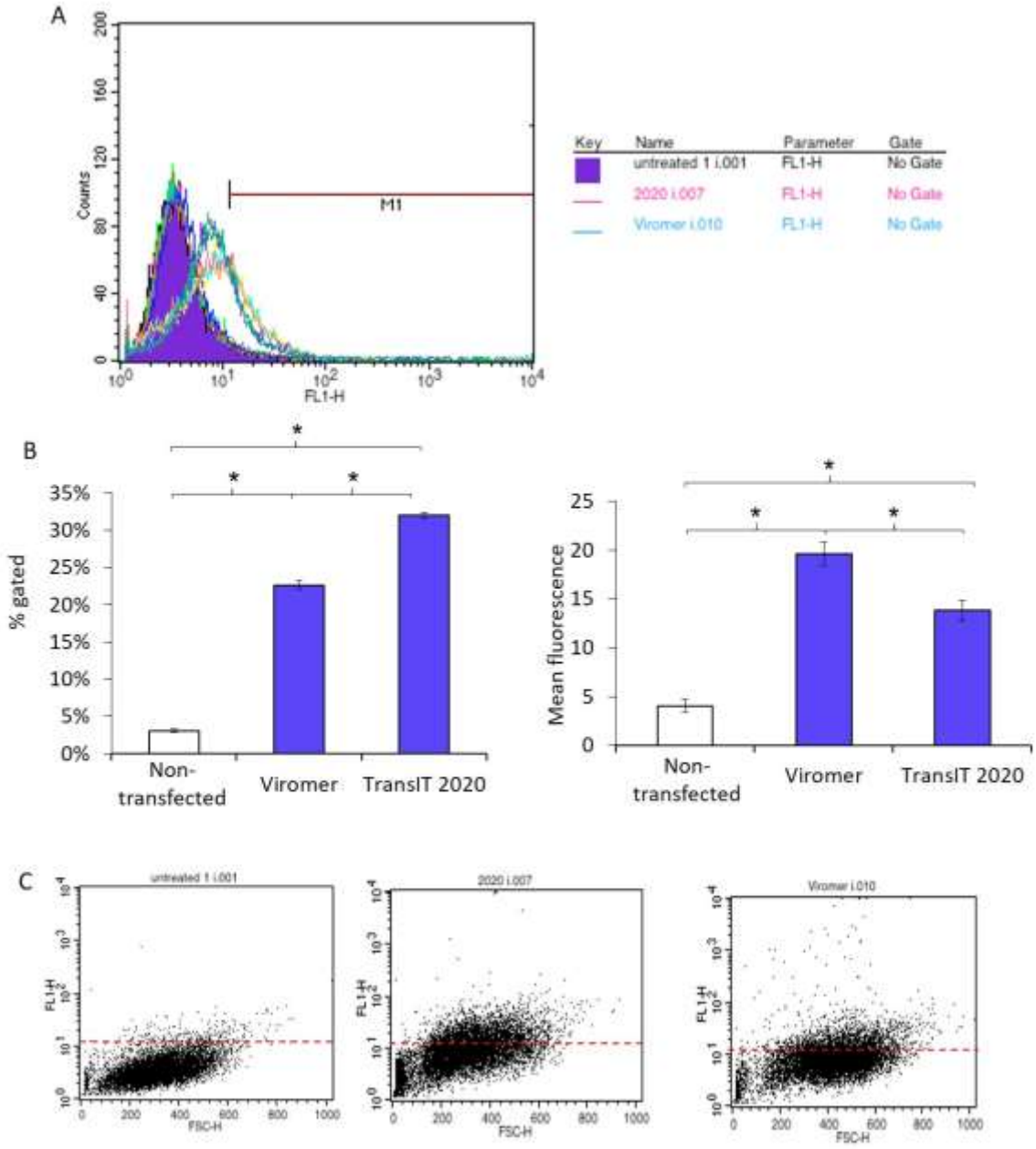

MDA-MB-231 cells (2 x 10^5) were transfected with pCMV-XL5-tGFP plasmid using either TransIT 2020 or Viromer RED transfection reagents and incubated for 2 days. The expression levels of tGFP were then determined by flow cytometry and fluorescence intensities measured with the FL1 detector. A gate was set containing approximately 3% (M1) of the non-transfected control cells (purple) and used to compare the fluorescence of the transfected cells (n=6, plots represent two experiments carried out in triplicate; data = mean values ± SEM; independent t-test * = $p < 0.05$).

quantities (2-4 µl) of TransIT 2020. The expression of the FLAG-HA-tagged peptides were measured by dot blot using an anti-HA antibody. Transfection of MDA-MB-231 cells (1.5 x 10^5) using either 3 µl or 4 µl of the reagent resulted in an increase in the expression FLAG-HA-tagged protein after 2 days in both instances (Figure 5.17A). Subsequently, in all further experiments, MDA-MB-231 cells were transfected using 3 µl of TransIT 2020 to express the TED, LED, UED or EGF4-βTD peptides. The expression of the peptides was also examined by western blot and bands corresponding to the TED (~36 kDa), UED (~20 kDa), LED (~18 kDa) and EGF4-βTD (~26 kDa) peptides were observed (Figure 5.17B). The observed molecular weights of the TF extracellular domain peptides were 3-8 kDa higher than the expected size for the TED (28 kDa), UED (16 kDa) and LED (15 kDa) peptides (Table 5.2). This is likely to have been due to the glycosylation of these peptides, since TF is known to have 3 glycosylation sites at Asp11, Asp124 and Asp137 (Butenas et al., 2012). The molecular weight of the band corresponding to the EGF4-βTD peptide construct matched the expected size for this peptide.

5.3.7 Confirmation of the suitability of the PLA for the analysis of the interaction between TF and β1 integrin

Prior to the experiments, the expression of β1 integrin and TF on the cell surface of MDA-MB-231 cells was confirmed. To detect the expression of TF, the cells were incubated with a range of dilutions of an anti-TF antibody (HTF-1) or a mouse IgG isotype antibody and were then probed with NL493-conjugated anti-mouse IgG antibody. The stained cells were examined by fluorescence microscopy. An increase in fluorescence was detected on the cells that were probed with the anti-TF antibody compared to the IgG isotype control. The use of intact cells, without any permeabilization agent, indicated that the TF was present on the cell surface. The highest signal was detected on cells incubated with a 1:50 (v/v) dilution of the antibody (Figure 5.18) and this dilution was used in all further immunofluorescence and PLA procedures. To detect the expression of β1 integrin, cells were incubated with a rabbit polyclonal anti-β1 integrin antibody or a rabbit IgG isotype antibody. The cells were then probed with NL637-conjugated anti-rabbit IgG antibody and examined by fluorescence microscopy as above. An increase in fluorescence was detected on the cells probed with the anti-β1 integrin antibody compared to the IgG isotype control (Figure 5.19).

In order to assess the suitability of PLA for the analysis of the interaction between TF and β1 integrin on the surface of cells, PLA was performed using the mouse anti-TF antibody (HTF-1) and a rabbit polyclonal anti-β1 integrin antibody tested above. The MDA-MB-231 cells exhibited 41 ± 4.2 interactions between TF and β1 integrin on the surface membrane (Figure 5.20). This was comparable to the number of interactions observed between αv integrin and β1 integrin (49 ± 3.7 incidences/cell) which form an integrin complex that is reported to be prevalent on MDA-MB-231

Figure 5.17: Assessment of the transfection of FLAG-HA plasmid into MDA-MB-231 cells

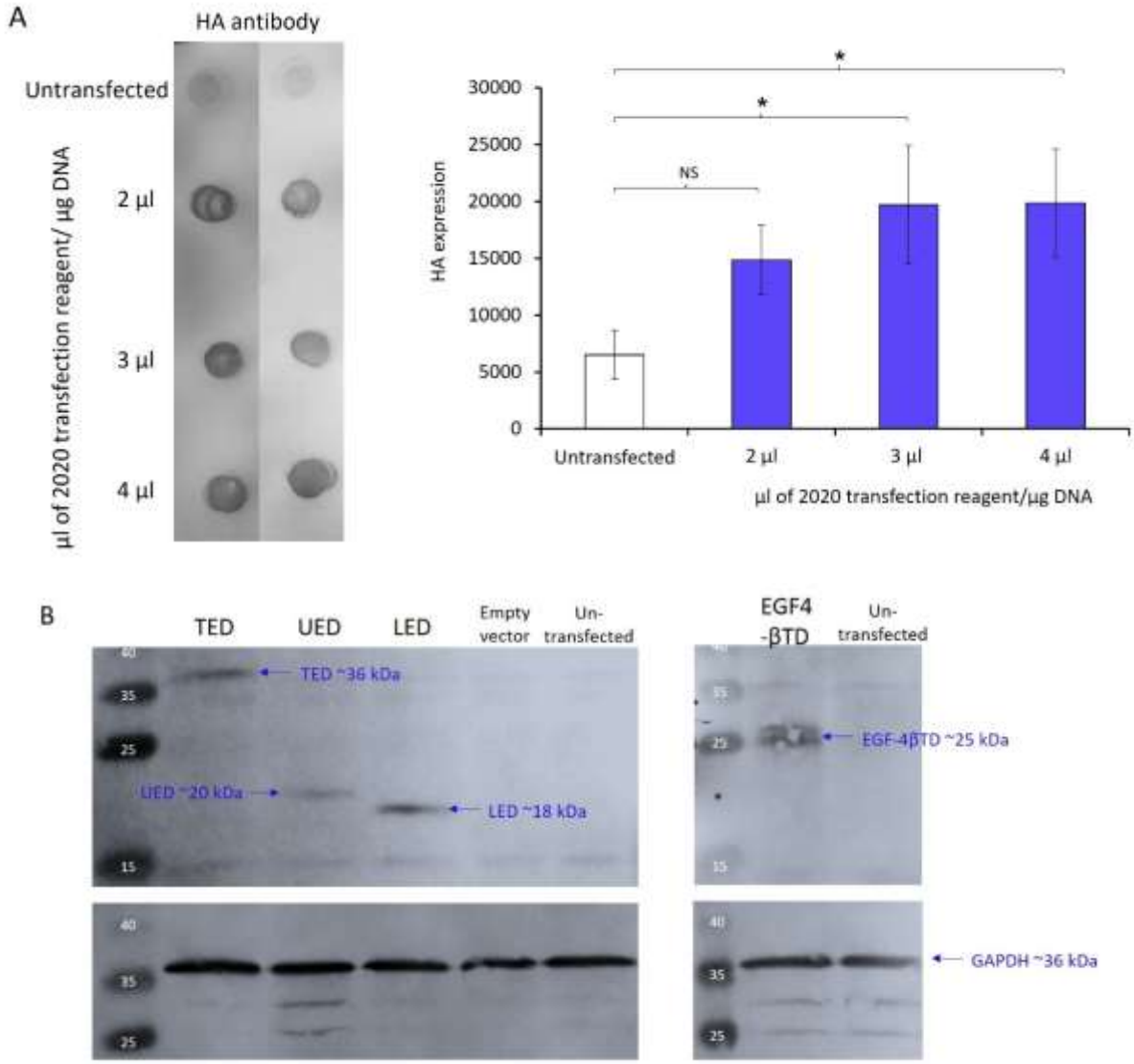

A) MDA-MB-231 cells (1.5 x 10^5) were transfected to express TED in tandem with FLAG and HA tags using a range of amounts of TransIT 2020 transfection reagent (2-4 µl) along with an untreated sample. The expression levels of the peptide were examined by dot blot using an anti-HA antibody and quantified using ImageJ (n=4, Images represent two experiments carried out in duplicate; data = mean values ± SEM; independent t-test, * = $p < 0.05$, NS = not significant). B) MDA-MB-231 cells (1.5 x 10^5) were transfected to express EGF4-βTD, TED, LED or UED in tandem with FLAG and HA tags or the FLAG-HA tag control peptide (EV). The expressed peptides were visualised by western blot using an anti-HA antibody (diluted 1:3000 v/v in TBST). The membranes were incubated with AP-conjugated anti-rabbit IgG or AP-conjugated anti-goat IgG antibodies (diluted 1:3000 v/v in TBST), respectively. The membranes were then developed using Western Blue stabilised substrate for AP (Images are representative of 2 experiments).

Figure 5.18: Detection of cell-surface TF by fluorescence microscopy

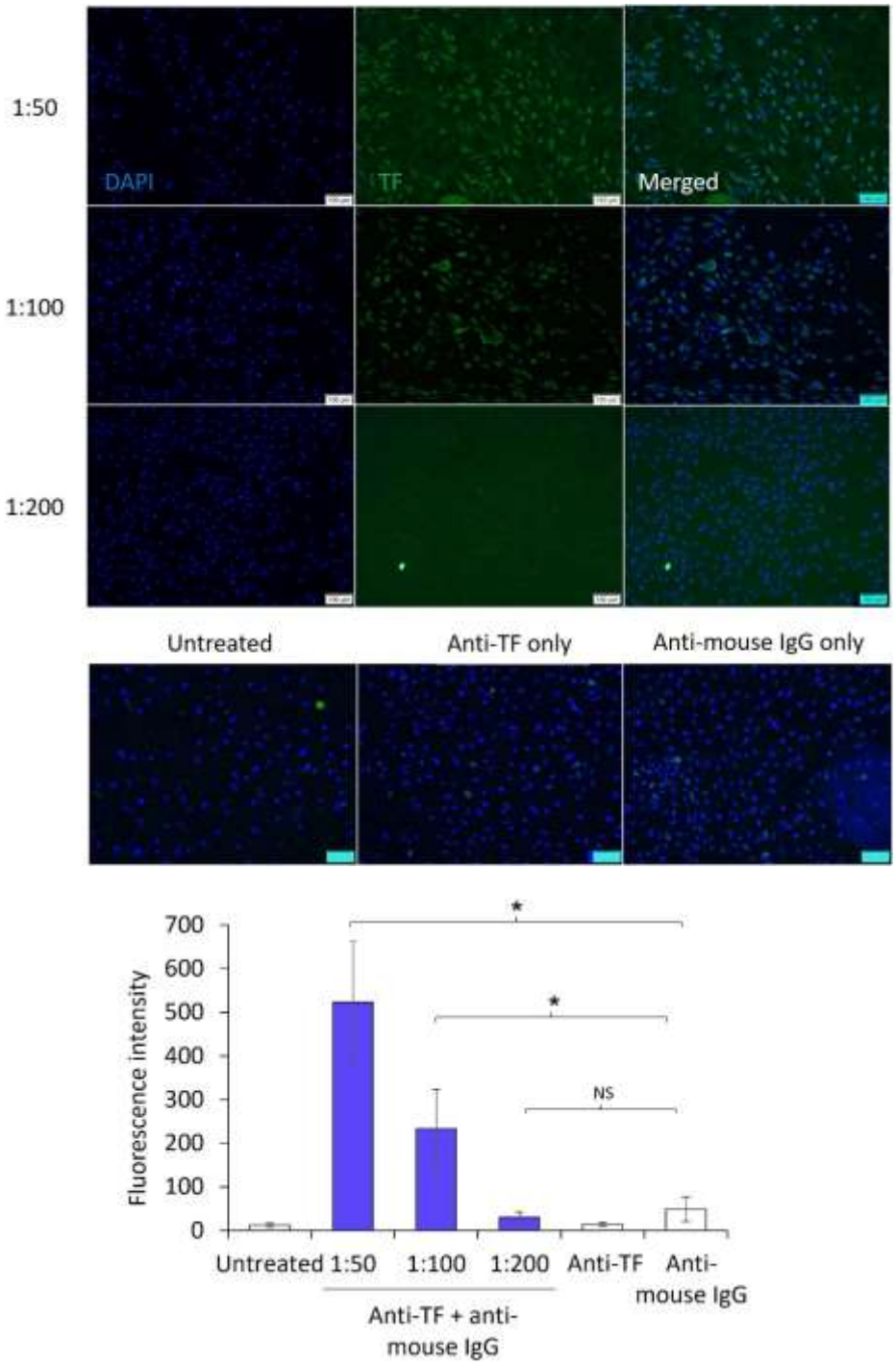

MDA-MB-231 cells (5 x 10^4) were plated in 10-well chamber glass slides. TF antigen was detected using an anti-TF antibody (HTF-1) diluted 1:50, 1:100 or 1:200 (v/v) in the provided antibody diluent and developed with NL493-conjugated anti-mouse IgG antibody (diluted 1:100 v/v in antibody diluent). The cells were assessed by fluorescence microscopy at x10 magnification and the fluorescence intensities were quantified using ImageJ (Images represent 4 fields of view from 2 independent experiments; data = mean values ± SEM; independent t-test, * = $p < 0.05$, NS = not significant).

Figure 5.19: Detection of cell-surface β1 integrin by fluorescence microscopy

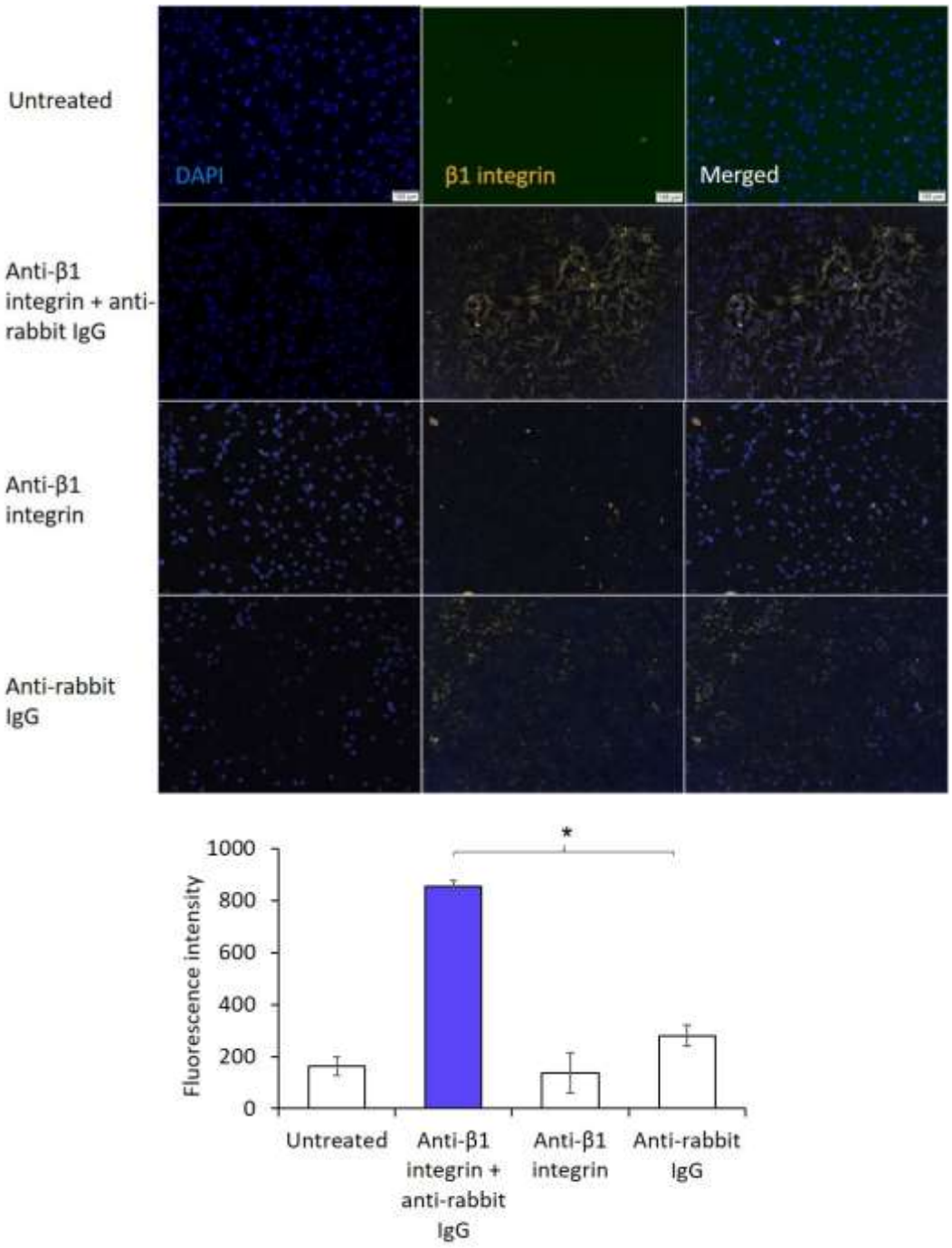

MDA-MB-231 cells (5 x 10^4) were plated in 10-well chamber glass slides. β1 integrin antigen was detected using an anti-β1 integrin antibody diluted 1:50 (v/v) in the provided antibody diluent, followed by NL637-conjugated anti-rabbit IgG antibody (diluted 1:100 v/v in antibody diluent). The cells were assessed by fluorescence microscopy at x10 magnification and the fluorescence intensities were quantified using ImageJ (Images represent 4 fields of view from 2 independent experiments; data = mean values ± SEM; independent t-test * = $p < 0.05$).

Figure 5.20: Visualisation of the interaction between TF and β1 integrin on the surface of MDA-MB-231 cells

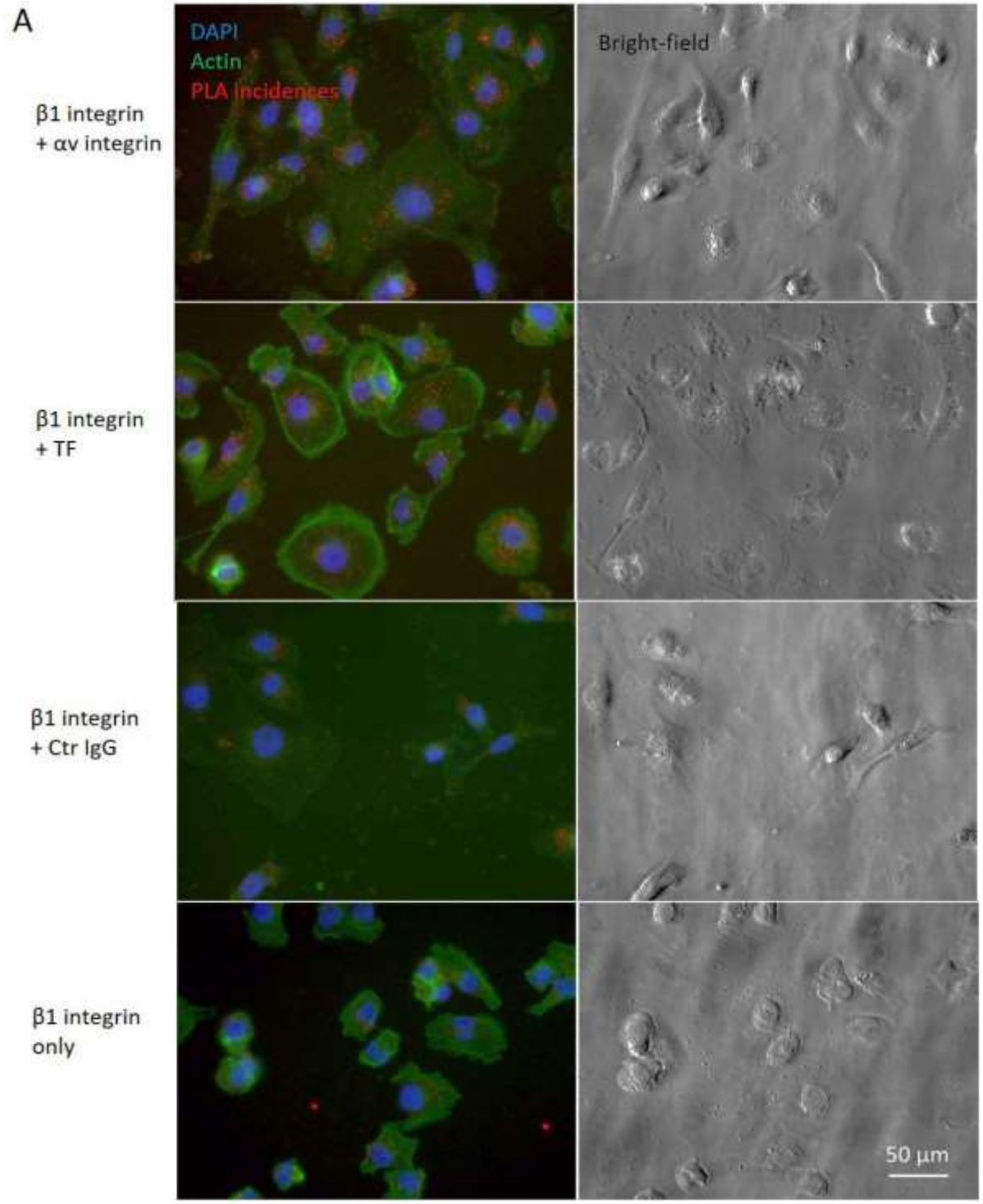

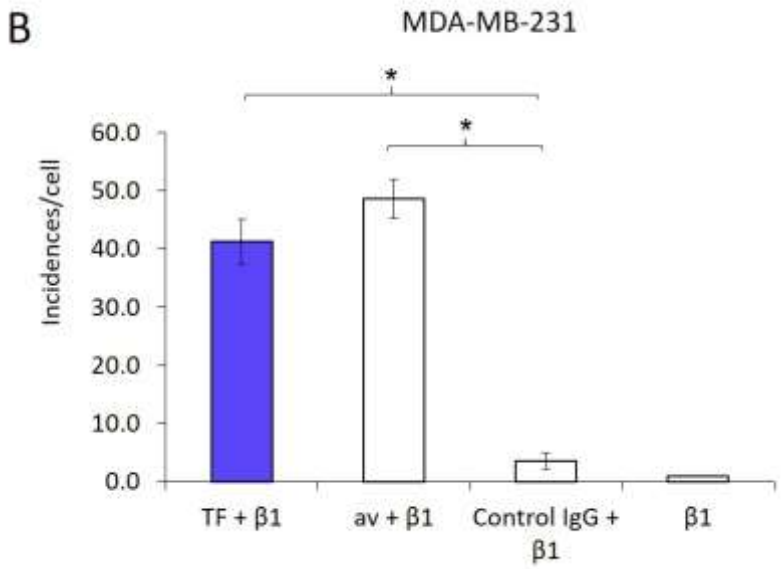

MDA-MB-231 cells (10^4) were seeded into glass bottomed cell culture plates. Interactions between the cell-surface proteins were examined by PLA, using a rabbit anti-β1 integrin, a mouse anti-αv integrin and a mouse anti-TF antibody (diluted 1:50 v/v in antibody diluent). A) The cells were examined by fluorescence microscopy at x40 magnification and B) the number of interactions in each field of view was quantified using ImageJ (Images represent 10 fields of view from 2 independent experiments; data = mean values ± SEM; independent t-test * = $p < 0.05$).

cells (Taherian et al., 2011; Zovein et al., 2010). The number of interactions observed on control cells following probing with an IgG isotype and β1 integrin antibody pairing was 3.5 ± 1.1 incidences/cell and therefore precludes any non-specific antibody or probe interactions. Similarly, the specificity of PLA for detecting the interaction between TF and β1 integrin was confirmed using HDBEC which do not express TF under normal conditions (Contrino et al., 1996; Drake et al., 1989). The number of interactions between TF and β1 integrin (1.7 ± 0.1 incidences/cell) on HDBEC was not significantly different from those examined using a mouse IgG isotype and rabbit β1 integrin antibody (0.9 ± 0.2 incidences/cell) (Figure 5.21). This again precludes any non-specific binding of the TF antibody or the probes to other cell-surface molecules. In contrast, the transfection of the HDBEC to express TF resulted in an increase in the number of interactions to 5.8 ± 0.4 incidences/cell (Figure 5.21). Collectively, these data confirm the suitability of the PLA assay to specifically examine and to quantify the interactions between TF and β1 integrin molecules on the surface of cells.

5.3.8 Investigation of the requirement for fVIIa in the interaction of TF and β1 integrin

Initially, the optimal quantity of siRNA for the suppression of fVII expression was optimised and the efficiency of two different transfection reagents determined. Western blot analysis of the expression of fVII demonstrated that maximal suppression (to 33% of original expression level) was achievable with 300 pmol fVII siRNA delivered using Viromer RED transfection reagent (Figure 5.22). Therefore, these experimental conditions were used for the knockdown of fVII expression in all further experiments.

PLA analysis of fVII knockdown cells indicated a reduction in the number of interactions between TF and β1 integrin from 33.8 ± 4.6 incidences/cell to 22.1 ± 1.4 incidences/cell following the suppression of fVII expression. Moreover, supplementation of the fVII knockdown cells with exogenous purified fVIIa restored the level of interactions to 39.8 ± 7.8 incidences/cell, which was comparable to the level observed in the untreated control cells (Figure 5.23) indicating a dependence on the presence of fVII/fVIIa.

5.3.9 Analysis of the association of the cloned peptides on the cell surface

In order to assess the interaction between the cloned peptides and either the cell-surface TF, or β1 integrin, it is essential that the expressed proteins are translocated to the surface of the cells. To confirm the presence of the peptides on the cell surface, cells expressing the FLAG-HA-tagged TED peptide were probed with either anti-FLAG-tag (FG4R) or anti-HA-tag (C29F4) antibodies and then developed with NL493-conjugated anti-mouse IgG antibody. Higher intensities were observed on cells expressing TED than on non-transfected cells, when probed with the anti-HA antibody

Figure 5.21: Visualisation of the interaction between TF and β1 integrin on the surface of HDEBC cells

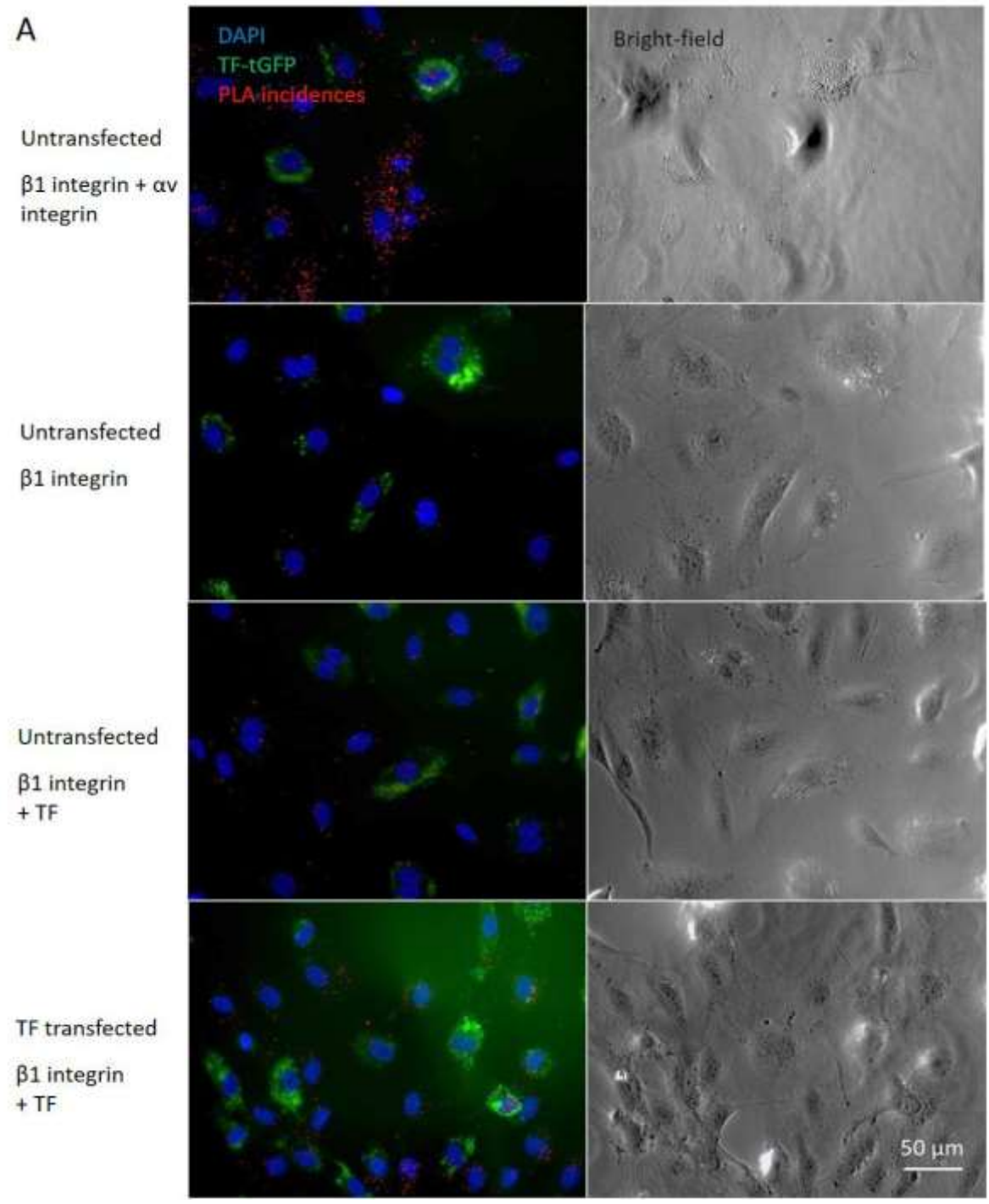

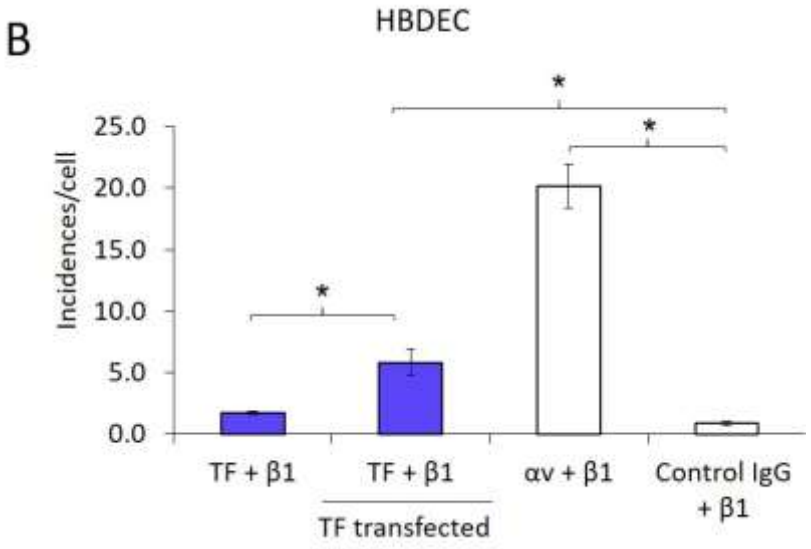

HDBEC (5 x 10^4) were seeded into glass bottomed cell culture plates. One set of cells was transfected with pCMV6-AC-F3-tGFP plasmid. Interactions between the cell-surface proteins were examined by PLA, using a rabbit anti-β1 integrin, a mouse anti-αv integrin and a mouse anti-TF antibody (diluted 1:50 v/v in antibody diluent). A) The cells were examined by fluorescence microscopy at x40 magnification and B) the number of interactions in each field of view was quantified using ImageJ (Images represent 10 fields of view from 2 independent experiments; data = mean values ± SEM; independent t-test * = $p < 0.05$).

Figure 5.22: Confirmation of suppression of the expression of fVII using siRNA

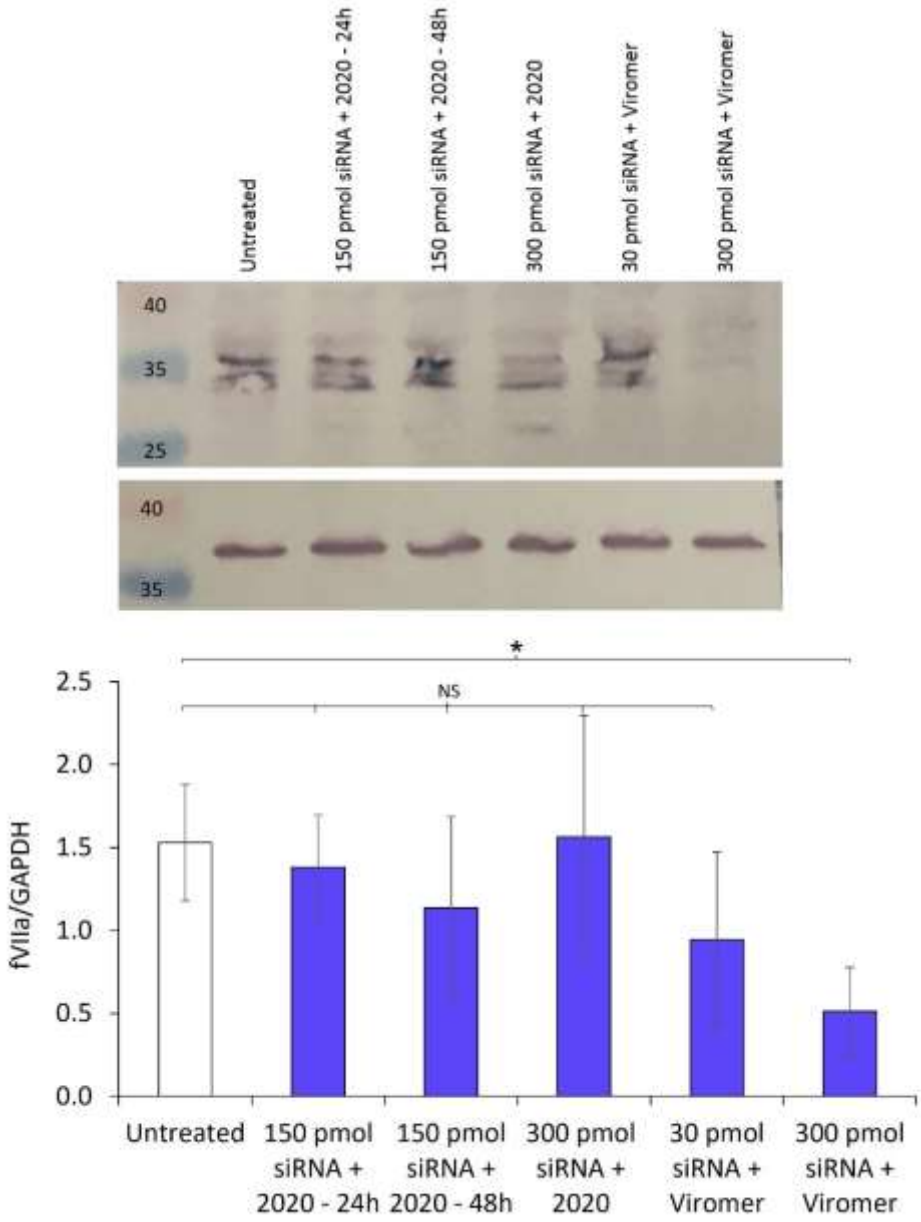

MDA-MB-231 cells (1.5 x 10^5) were transfected with a fVII siRNA (30-300 pmol) using either TransIT 2020 or Viromer RED transfection reagent and incubated for 2 days. The cells were then lysed in Laemmli buffer, proteins were separated by SDS-PAGE and the fVII expression assessed by western blot assay using an anti-fVII antibodies (diluted 1:3000 v/v in TBST). The membranes were incubated with AP-conjugated anti-rabbit IgG or AP-conjugated anti-goat IgG antibodies (diluted 1:3000 v/v in TBST), respectively. The membranes were then developed using Western Blue stabilised substrate for AP (n=4, Images represent two experiment carried out in duplicate; data = mean values ± SEM; one-way ANOVA, * = $p < 0.05$, NS = not significant).

Figure 5.23: Assessment of the influence of fVII on the interaction between TF and β1 integrin

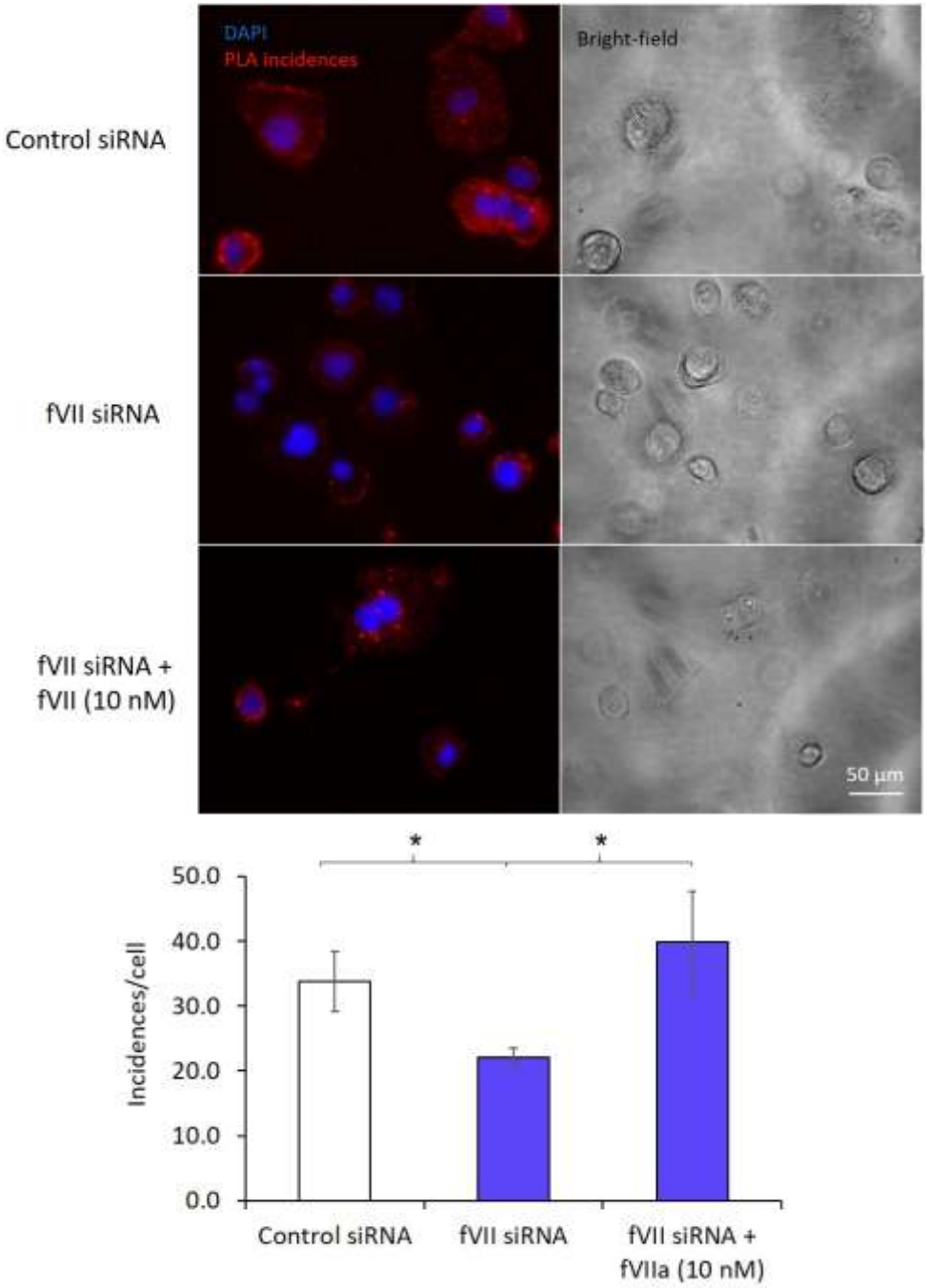

MDA-MB-231 cells (10^4) were transfected with either a fVII siRNA (300 pmol) or the silencer® select negative control #1 siRNA (300 pmol) and incubated for 2 days. One set of cells were treated with 10 nM recombinant fVII for 1 h. The interactions between TF and β1 integrin were examined by PLA performed using a mouse anti-TF antibody (HTF-1) and a polyclonal rabbit anti-β1 integrin antibody (diluted 1:50 v/v in antibody diluent). The cells were examined by fluorescence microscopy at x40 magnification and the number of interactions in each field of view was quantified using ImageJ (Images represent 10 fields of view from 2 independent experiments; data = mean values ± SEM; independent t-test * = $p < 0.05$).

(Figure 5.24). Furthermore, the use of intact cells, without using any permeabilization agent, confirmed the presence of TED on the cell surface. However, probing of cells with the anti-FLAG-tag antibody produced comparable fluorescence levels on TED-expressing and non-transfected cells (Figure 5.25) indicating the lack of specificity of the primary antibody. Consequently, the anti-FLAG-tag antibody was not used in further studies.

To preclude the possibility of non-specific interactions between the expressed peptides and cell-surface proteins, the proximity of TED peptide to cellular β1 integrin was compared to that of a FLAG-HA-tag control peptide prior to, and after PBST washes. The number of interactions between the FLAG-HA-tag control peptide and β1 integrin prior to the PBST washes was 6.3 ± 0.3 incidences/cell but was reduced to 2.8 ± 0.2 incidences/cell following the PBST washes (Figure 5.26). This indicated that any non-specific association of the control peptide was abolished by PBST washing. In contrast, the number of interactions between TED peptide and β1 integrin remained at 5.6 ± 0.5 incidences/cell after the washes (Figure 5.26) indicating a specific interaction between TED peptide and β1 integrin.

5.3.10 Investigation of the association of extracellular domain peptides of TF with β1 integrin

PLA analysis of the association between the TED, LED and UED peptides and β1 integrin on the surface of MDA-MB-231 cells showed that all three peptides were capable of interacting with β1 integrin (TED = 3.6 ± 0.2, LED = 3.9 ± 0.4, UED = 4.1 ± 0.4 incidences/cell) (Figure 5.27). Similarly, the three peptides were also capable of associating with β1 integrin on the surface of HDBEC (TED = 50.8 ± 8.6, LED = 50.0 ± 7.5, UED = 48.1 ± 4.7 incidences/cell) (Figure 5.28). Furthermore, the association between the TED, LED and UED peptides and β1 integrin on HDBEC was blocked by pre-incubation of the cells with an inhibitory anti-β1 integrin antibody (AIIB2) (Figure 5.29).

The interaction between the TED, LED and UED peptides and β1 integrin was confirmed by co-IP, next. In each case, the HA-tagged peptide was captured using an anti-HA-tag antibody and the presence of β1 integrin assessed. Western blot assessment of the co-purified precipitates showed the co-IP of β1 integrin with the expressed LED peptide. The levels of β1 integrin co-purified with UED and TED were comparable to background levels, indicating β1 integrin was not co-immunoprecipitated with these peptides (Figure 5.30A & Figure 5.30B). However, western blot analysis, following immunocapture of β1 integrin with an anti-β1 integrin antibody did not indicate the co-purification of any of the TED, LED or UED peptides (Figure 5.30C).

Figure 5.24: Detection of expressed FLAG-HA-tagged peptides on the surface of cells using an anti-HA antibody

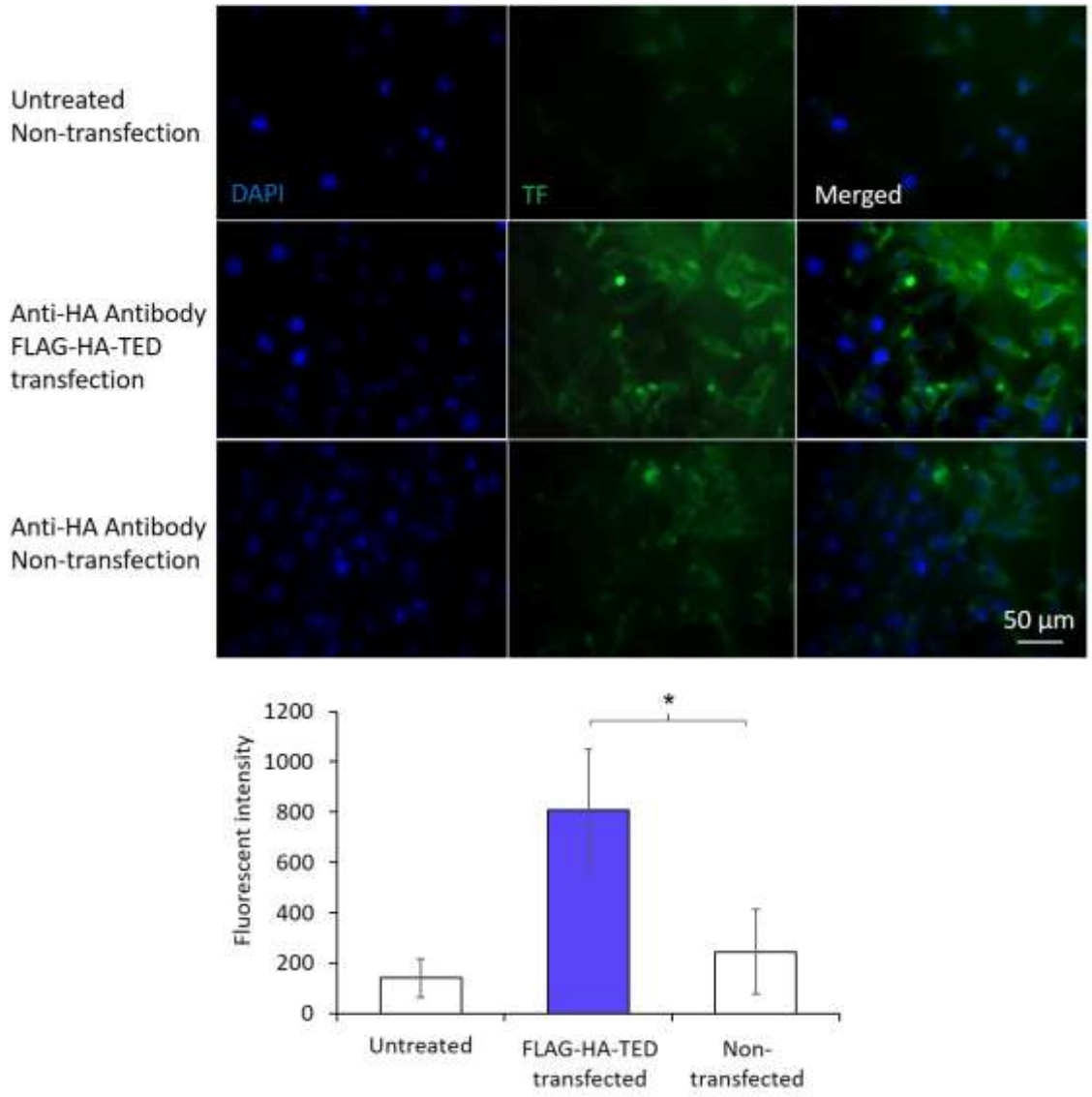

MDA-MB-231 cells (5 x 10^4) were transfected to express TED in tandem with the FLAG and HA tags. The presence of the TED peptide on the cell surface was detected using an anti-HA-tag antibody (C29F4) (diluted 1:50 v/v in antibody diluent) and developed with NL493-conjugated anti-rabbit IgG antibody (diluted 1:100 v/v in antibody diluent). The cells were assessed by fluorescence microscopy at x40 magnification and the fluorescence intensities were quantified using ImageJ (Images represent 4 fields of view from 2 independent experiments; data = mean values ± SEM; independent t-test * = $p < 0.05$).

Figure 5.25: Detection of expressed FLAG-HA-tagged peptides on the surface of cells using an anti-FLAG antibody

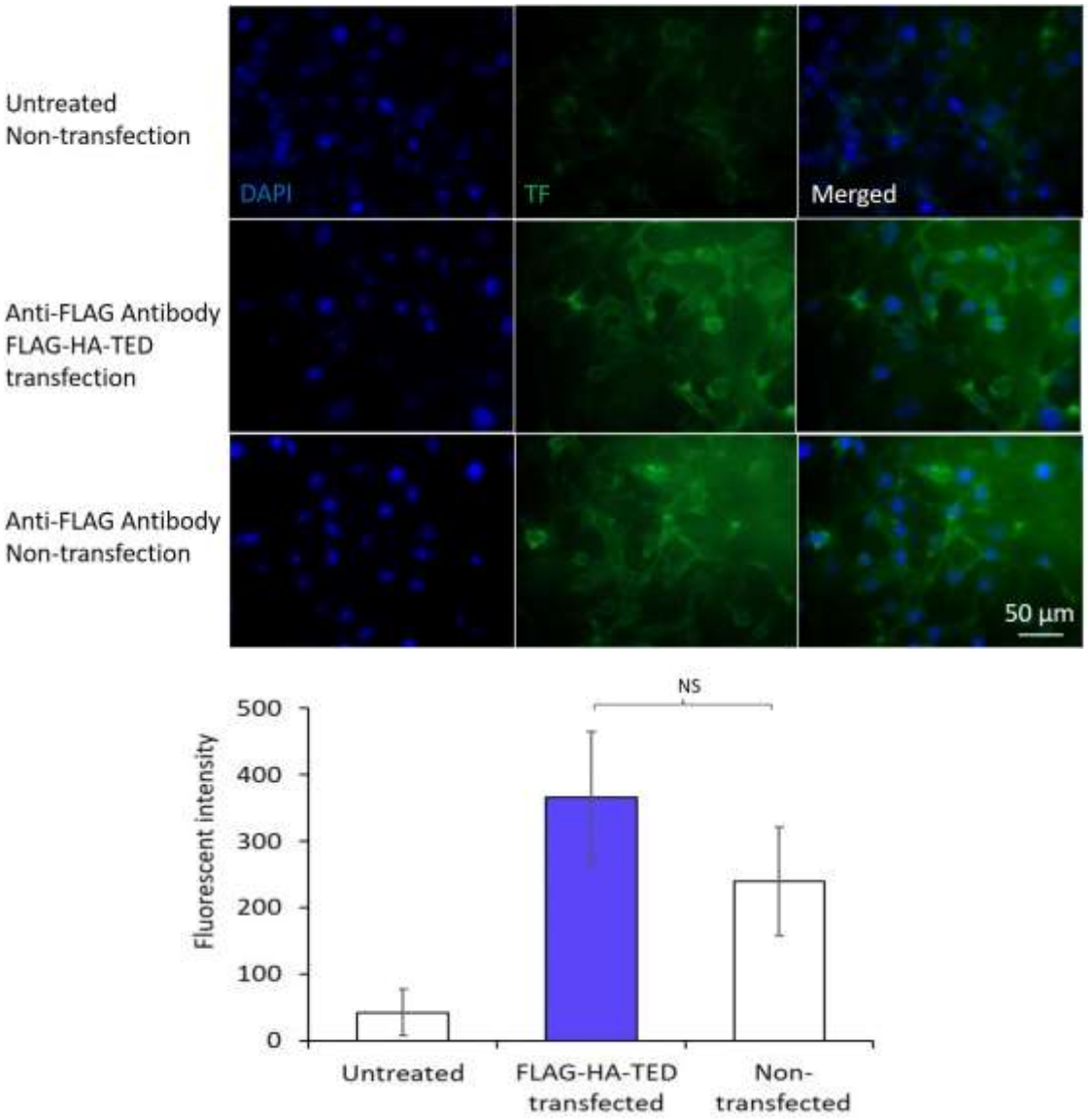

MDA-MB-231 cells (5 x 10^4) were transfected to express TED in tandem with the FLAG and HA tags. The presence of the TED peptide on the cell surface was detected using an anti-FLAG-tag antibody (FG4R) diluted 1:50 (v/v) in antibody diluent and developed with NL493-conjugated anti-rabbit IgG antibody (diluted 1:100 v/v in antibody diluent). The cells were assessed by fluorescence microscopy at x40 magnification and the fluorescence intensities were quantified using ImageJ (Images represent 4 fields of view from 2 independent experiments; data = mean values ± SEM; independent t-test NS = not significant).

Figure 5.26: The influence of washing of the cells on the association of the expressed TF-peptides with cell-surface proteins

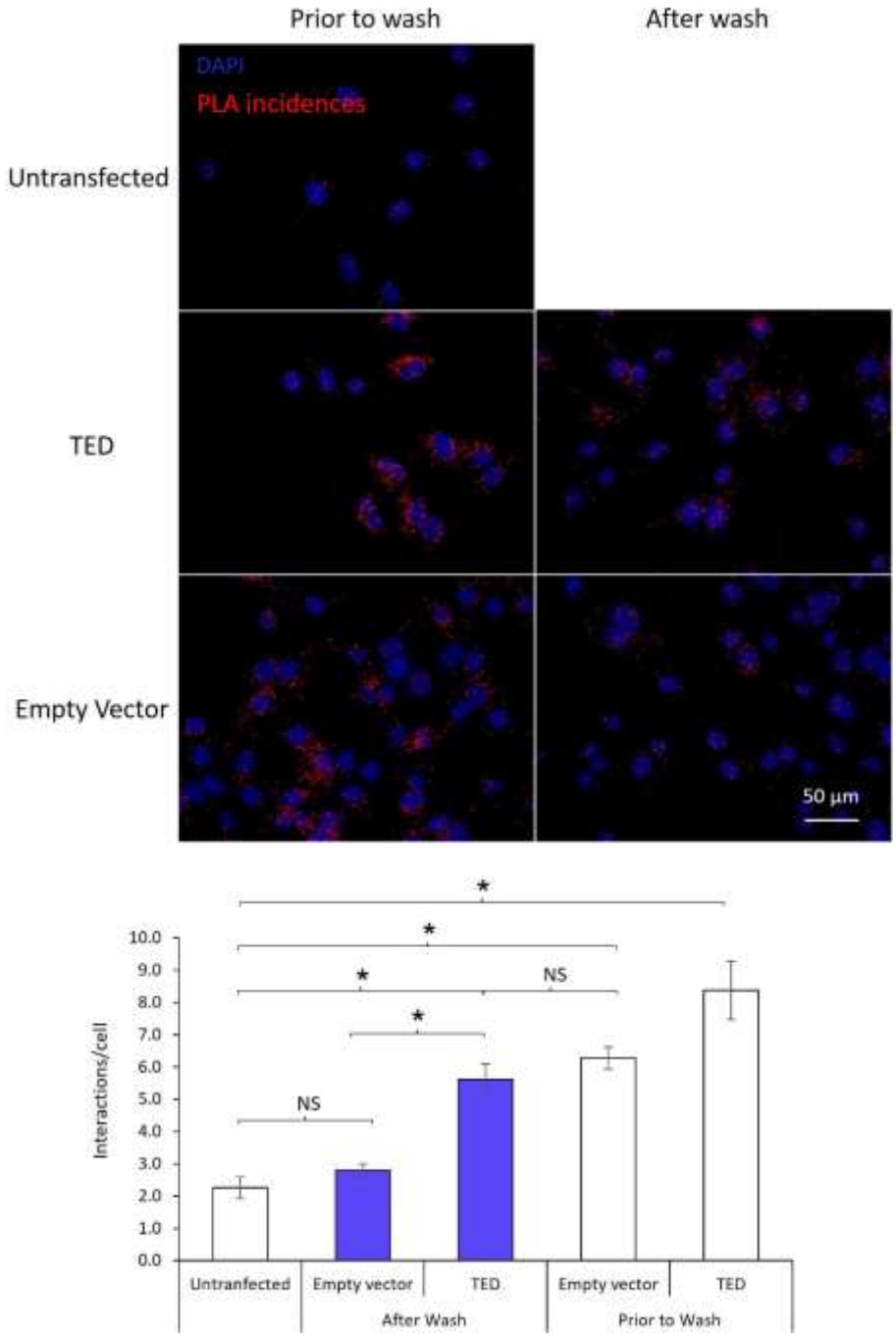

MDA-MB-231 cells (10^4) were transfected to express TED in tandem with the FLAG and HA tags or the FLAG-HA tag control peptide. The interactions between the TED peptide and β1 integrin was assessed by PLA using mouse anti-HA-tag (C29F4) and rabbit anti-β1 integrin antibodies (diluted 1:50 v/v in antibody diluent). The cells were examined by fluorescence microscopy at x40 magnification and the number of interactions in each field of view was quantified using ImageJ (Images represent 10 fields of view from 2 independent experiments; data = mean values ± SEM; one-way ANOVA, * = $p < 0.05$, NS = not significant).

Figure 5.27: Analysis of the association of the TF peptides with β1 integrin on the surface of MDA-MB-231 cells

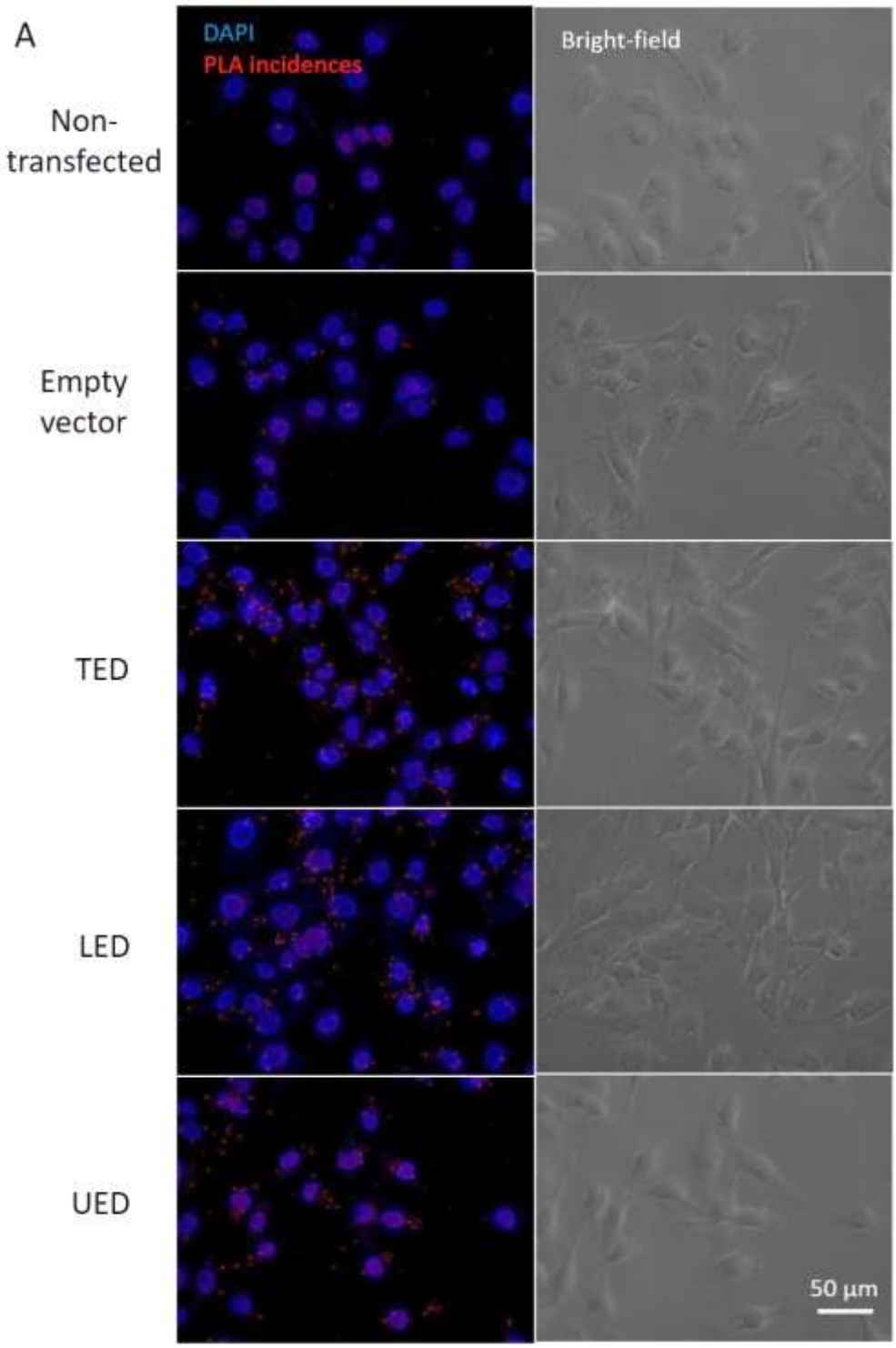

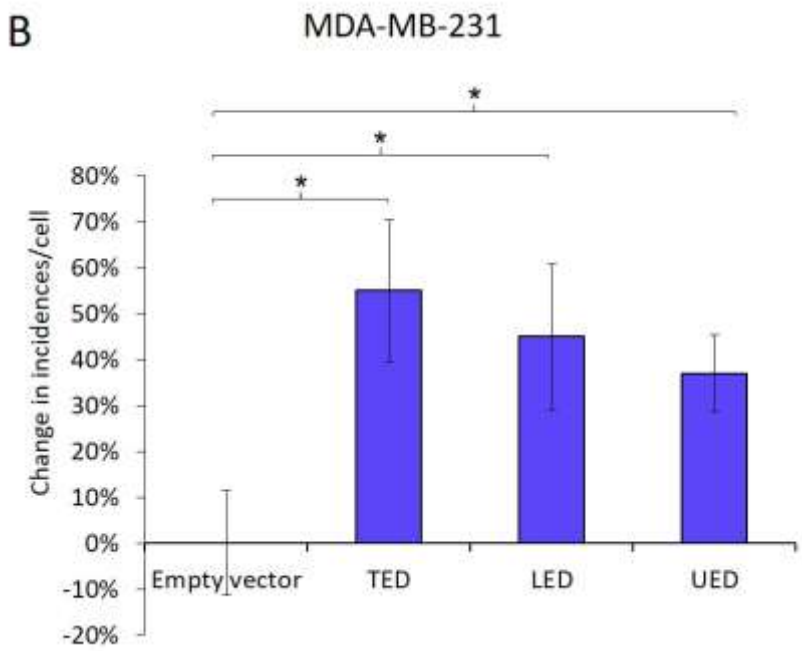

MDA-MB-231 cells (10^4) were transfected to express TED, LED or UED in tandem with the FLAG and HA tags or the FLAG-HA tag control peptide. The interactions between the expressed peptides and β1 integrin were assessed by PLA using mouse anti-HA-tag (C29F4) and rabbit anti-β1 integrin antibodies (diluted 1:50 v/v in antibody diluent). A) The cells were examined by fluorescence microscopy at x40 magnification and B) the number of interactions in each field of view was quantified using ImageJ. Percentage change was calculated as 100 x (treated - control) / control (Images represent 10 fields of view from 2 independent experiments; data = mean values ± SEM; independent t-test * = $p < 0.05$).

Figure 5.28: Analysis of the association of the TF peptides with β1 integrin on the surface of HDBEC

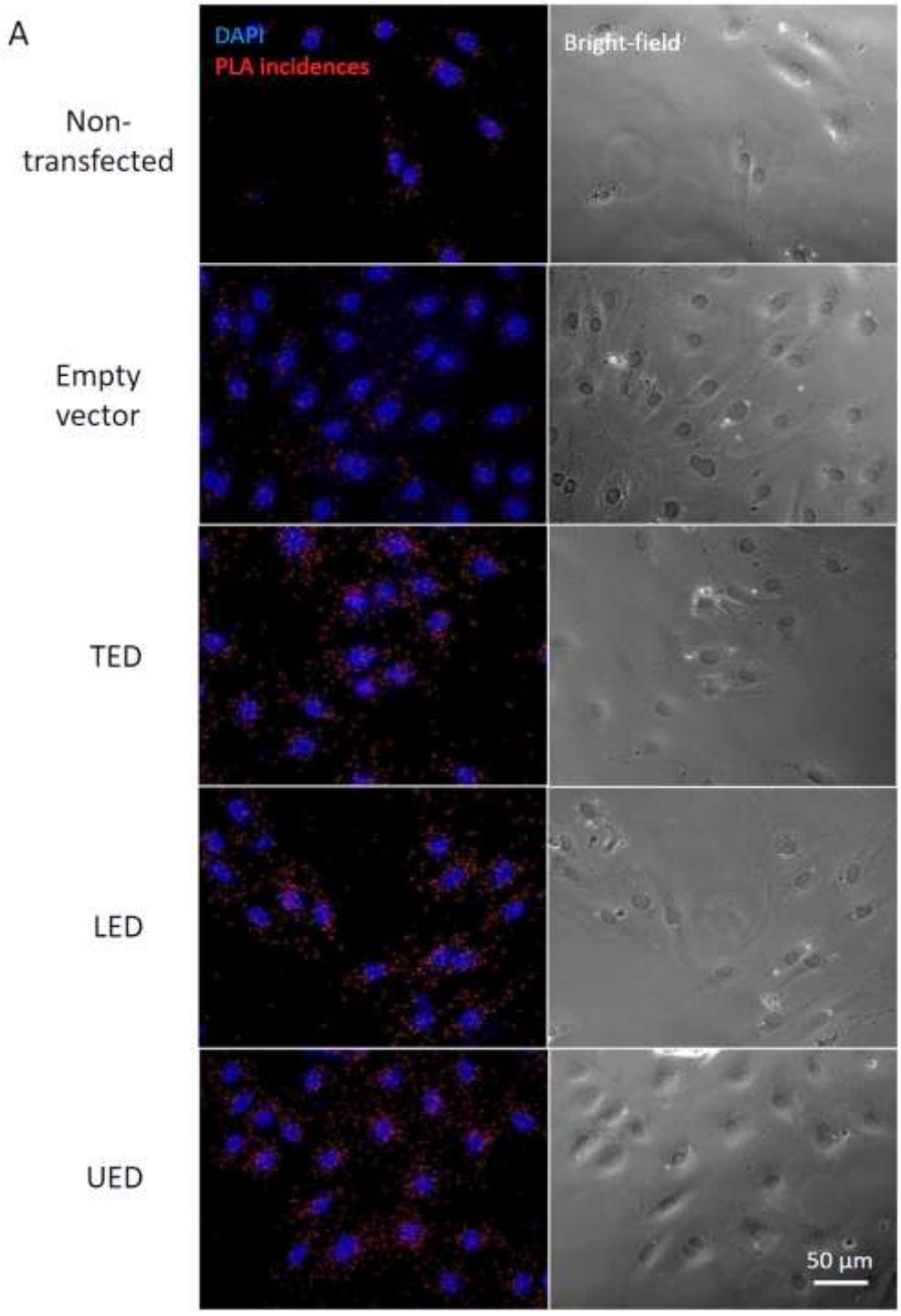

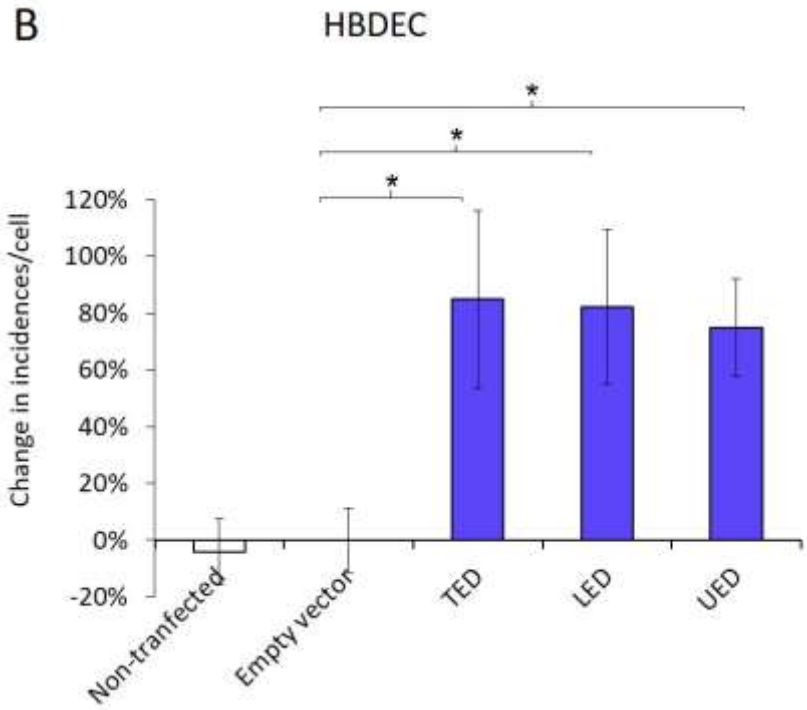

HDBEC (5 x 10^4) were transfected to express TED, LED or UED in tandem with the FLAG and HA tags or the FLAG-HA tag control peptide. The interactions between the expressed peptides and β1 integrin were assessed by PLA using mouse anti-HA-tag (C29F4) and rabbit anti-β1 integrin antibodies (diluted 1:50 v/v in antibody diluent). A) The cells were examined by fluorescence microscopy at x40 magnification and B) the number of interactions in each field of view was quantified using ImageJ. Percentage change was calculated as 100 x (treated - control) / control (Images represent 10 fields of view from 2 independent experiments; data = mean values ± SEM; independent t-test * = $p < 0.05$).

Figure 5.29: Examination of the influence of an inhibitory anti-β1 integrin antibody on the association of TF domain peptides with β1 integrin

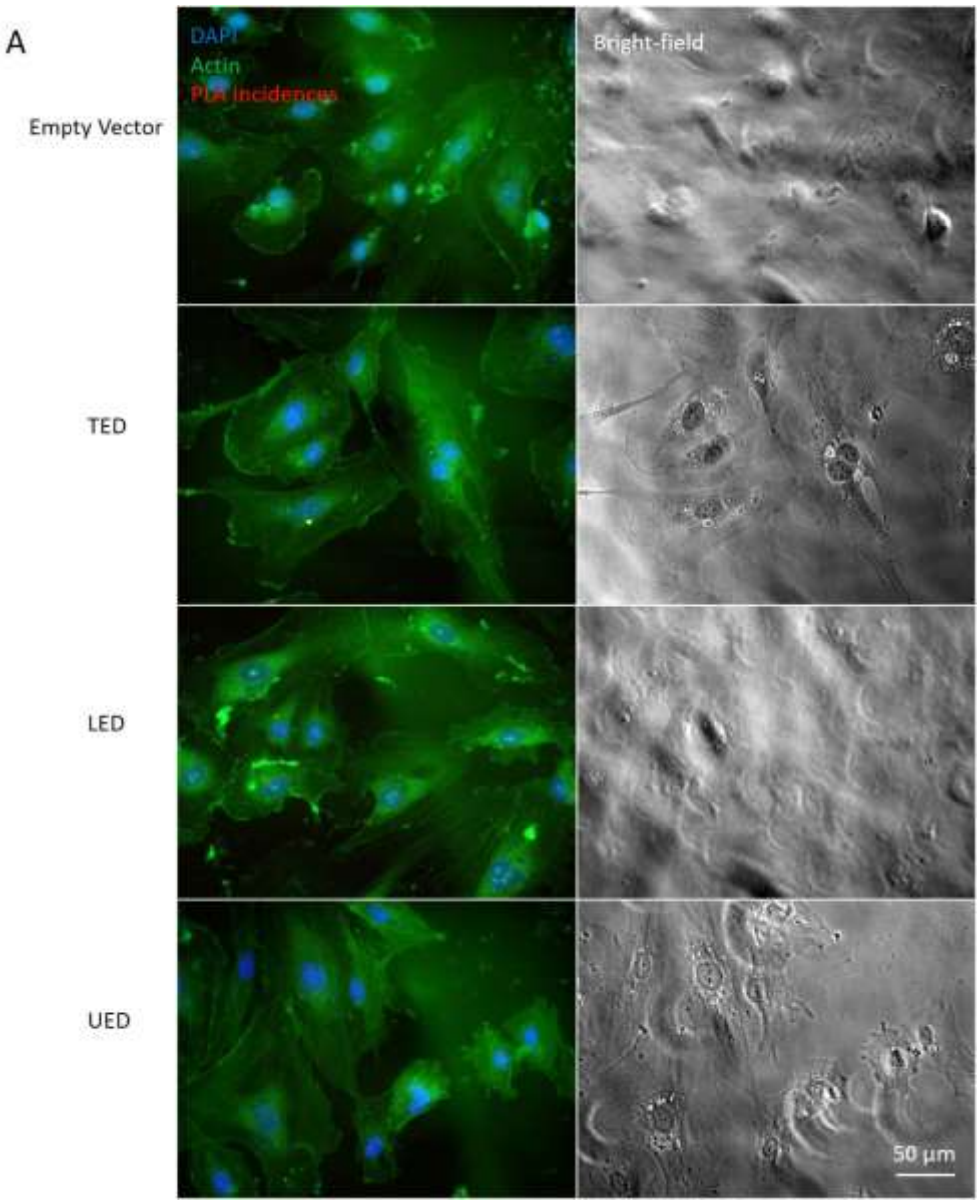

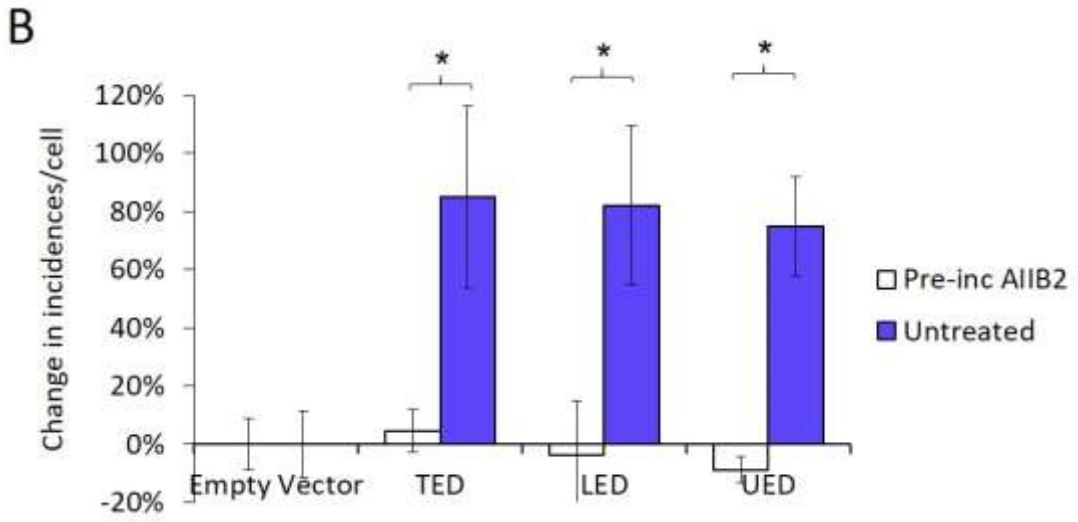

HDBEC (5 x 10^4) were transfected to express TED, LED or UED in tandem with the FLAG and HA tags or the FLAG-HA tag control peptide. The cells were pre-incubated with an blocking anti-β1 integrin antibody (AIIB2; 10 µg/ml) for 1 h prior to analysis. The interactions between the expressed peptides and β1 integrin were assessed by PLA using mouse anti-HA-tag (C29F4) and rabbit anti-β1 integrin antibodies (diluted 1:50 v/v in antibody diluent). A) The cells were examined by fluorescence microscopy at x40 magnification and B) the number of interactions in each field of view was quantified using ImageJ. Percentage change was calculated as 100 x (treated - control) / control (Images represent 10 fields of view from 2 independent experiments; data = mean values ± SEM; independent t-test * = $p < 0.05$).

Figure 5.30: Examination of the interaction of the TF domain peptides with β1 integrin by co-IP

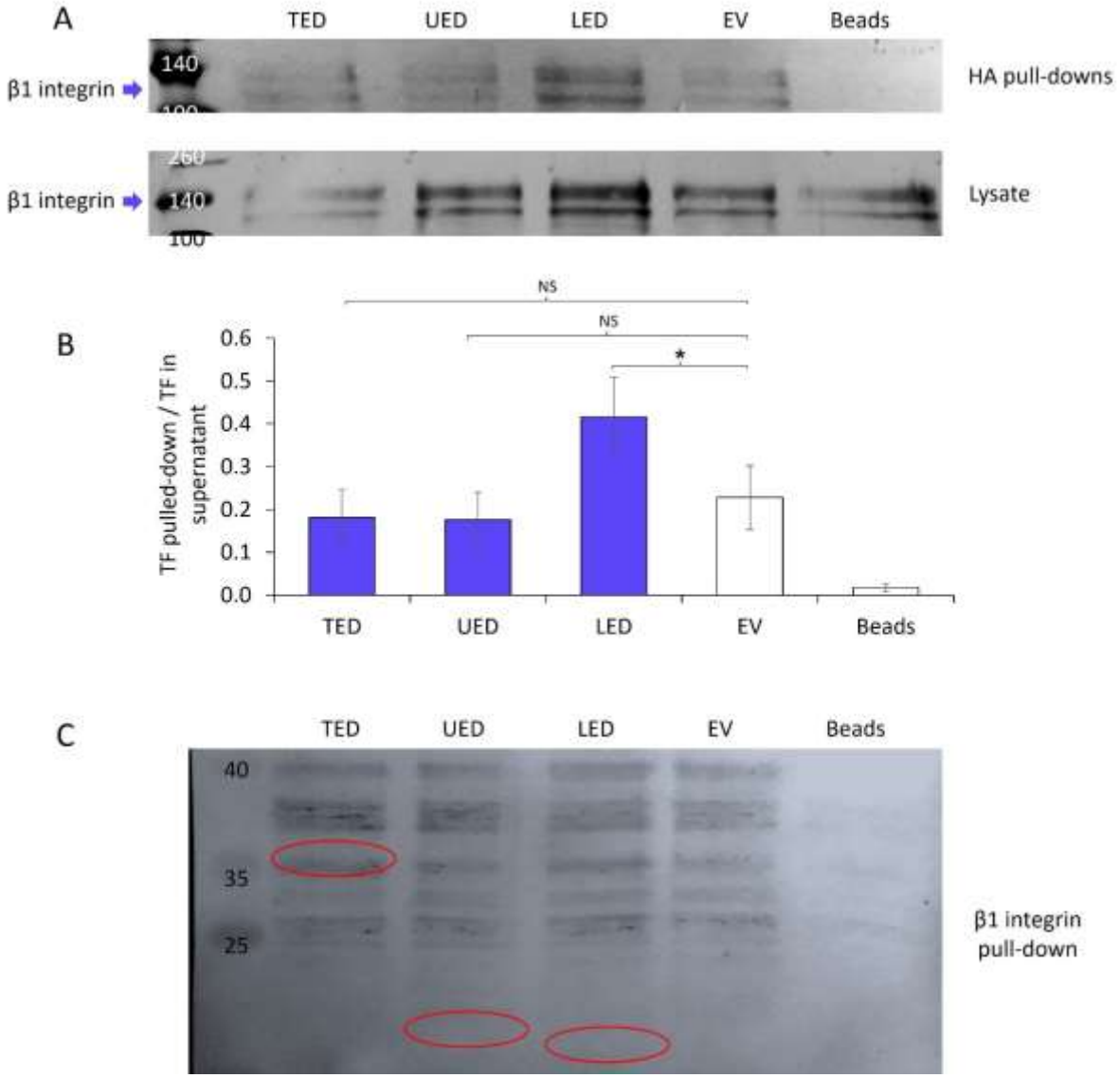

MDA-MB-231 cells (1.5 x 10^5) were transfected to express TED, LED or UED in tandem with the FLAG and HA tags or the FLAG-HA tag control peptide. A) The peptides were precipitated using an anti-HA-tag antibody and the presence of co-purified β1 integrin was examined by western blot using an anti-β1 integrin antibody. B) The intensities of the western blot bands were quantified using ImageJ (n=4, Images represent 2 experiments carried out in duplicate; data = mean values ± SEM; independent t-test, * = $p < 0.05$, NS = not significant). C) β1 integrin was precipitated using an anti-β1 integrin antibody and the presence of co-purified HA-tagged peptides was examined by western blot using an anti-HA antibody. The red circles indicate the positions where the co-purified proteins were expected to be detected.

5.3.11 Investigation of the association of the EGF4-βTD domain peptides with TF

PLA analysis indicated that EGF4-βTD peptide was capable of associating with TF on the surface of MDA-MB-231 cells (4.4 ± 0.5 incidences/cell) (Figure 5.31). However, only 3.2 ± 0.3 incidences/cell were detected between the EGF4 peptide and TF, which was comparable with that of the control peptide (3.3 ± 0.3 incidences/cell) (Figure 5.31). This indicates that the combined EGF4-βTD peptide may be capable of associating with TF, however, the EGF4 domain alone was not sufficient to sustain the interaction.

The interaction between EGF4-βTD peptide and TF was confirmed by co-IP, next. The HA-tagged peptide was captured using an anti-HA-tag antibody and the presence of TF assessed. Western blot analysis of the co-purified precipitates following immunocapture showed the co-IP of cellular TF with the expressed EGF4-βTD peptide (Figure 5.32A & Figure 5.32B). However, analysis of co-purified proteins, following immunocapture of TF with an anti-TF integrin antibody did not indicate the presence of the EGF4-βTD peptide in the immunoprecipitate (Figure 5.32C).

5.3.12 Examination of the ability of TF extracellular domain peptides to alter the steric availability of the EGF4-βTD within β1 integrin

To further investigate the involvement of the EGF4-βTD domains as a binding target for TF, the ability of the TED, LED and UED peptides to compete with the binding of a specific antibody against the EGF4-βTD region of β1 integrin was evaluated. The expression of LED peptide was capable of reducing the binding of the EGF4-βTD antibody, in HDBEC (Figure 5.33). This indicated that the LED peptide may bind on or near to the EGF4-βTD domains and therefore disrupt the binding of the antibody due to steric hinderance. The binding of the EGF4-βTD specific antibody was not significantly altered on expression of UED, TED or the control peptide. In contrast, the expression of either of the three peptides in MDA-MB-231 cells resulted in a reduction in the binding of the EGF4-βTD specific antibody although, due to the large variation in the data, none of these alterations were statistically significant.

5.3.13 Examination of the influence of the TF and β1 integrin peptides on ERK1/2 phosphorylation

In order to determine if any of the regions of TF extracellular domain are capable of influencing ERK signalling, the influence of the expression of the TED, LED and UED peptides on ERK1/2 phosphorylation was assessed. Expression of UED peptide in MDA-MB-231 cells resulted in the reduction in the pERK:tERK ratio (1.25 ± 0.07) compared to the cells expressing the control peptide (1.6 ± 0.2 pERK:tERK ratio) (Figure 5.34A). Furthermore, pre-incubation of cells with an inhibitory

Figure 5.31: Analysis of the association of the EGF4-βTD peptide with TF on the surface of MDA-MB-231 cells

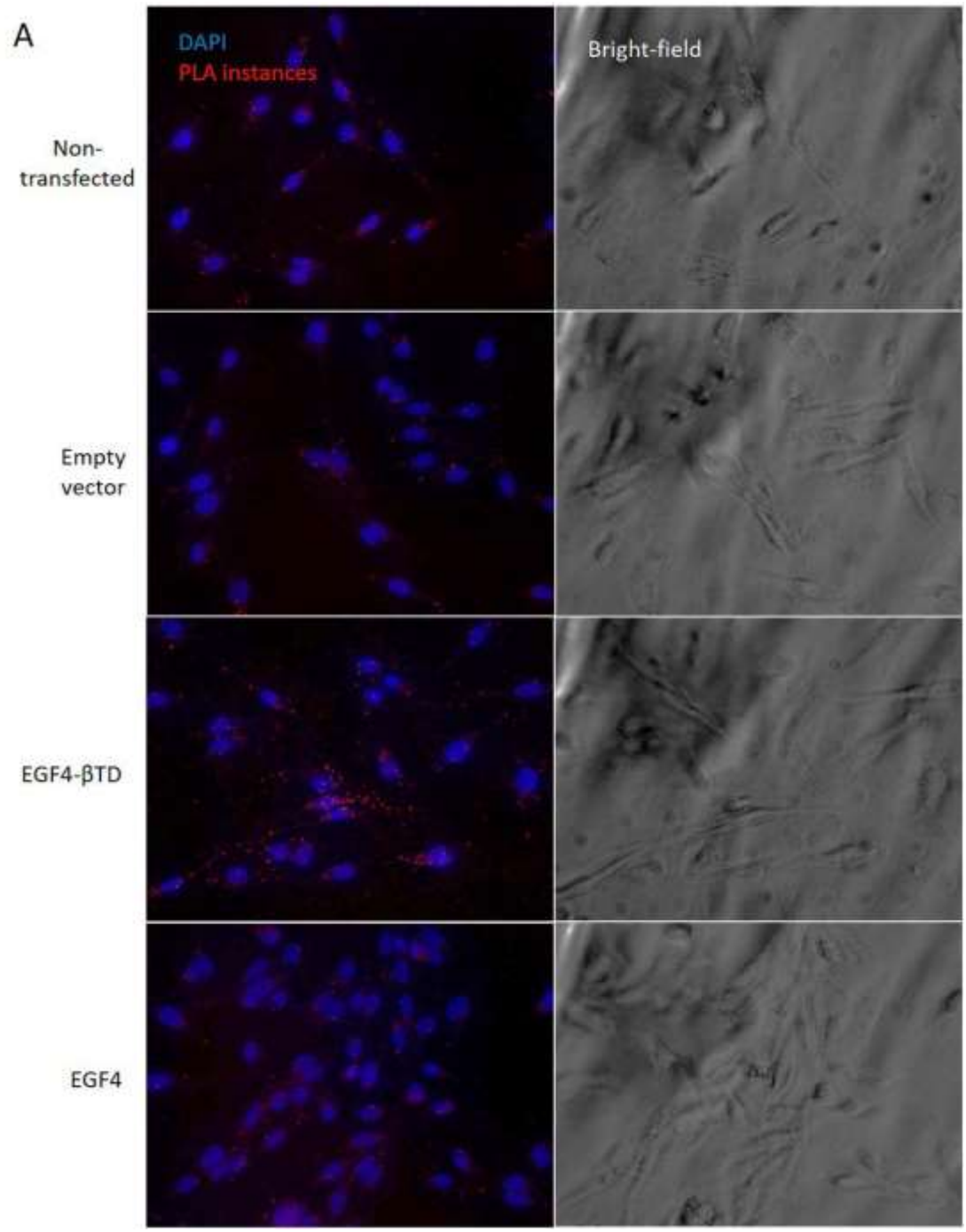

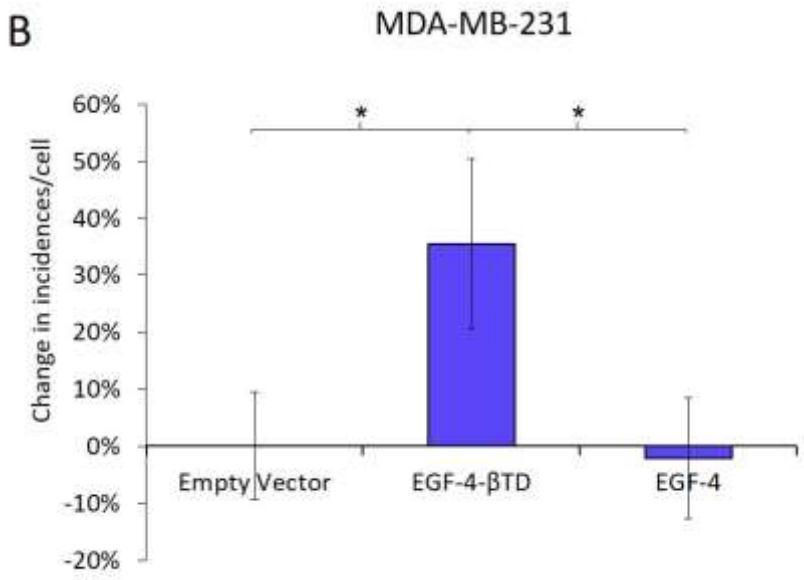

MDA-MB-231 cells (10^4) were transfected to express EGF4-βTD or EGF4 in tandem with the FLAG and HA tags or the FLAG-HA tag control peptide. The interactions between the expressed peptides and β1 integrin were assessed by PLA using mouse anti-HA-tag (C29F4) and rabbit anti-TF antibodies (diluted 1:50 v/v in antibody diluent). A) The cells were examined by fluorescence microscopy at x40 magnification and B) the number of interactions in each field of view was quantified using ImageJ. Percentage change was calculated as 100 x (treated - control) / control (Images represent 10 fields of view from 2 independent experiments; data = mean values ± SEM; independent t-test * = $p < 0.05$).

Figure 5.32: Examination of the interaction of the EGF4-βTD peptide with TF by co-IP

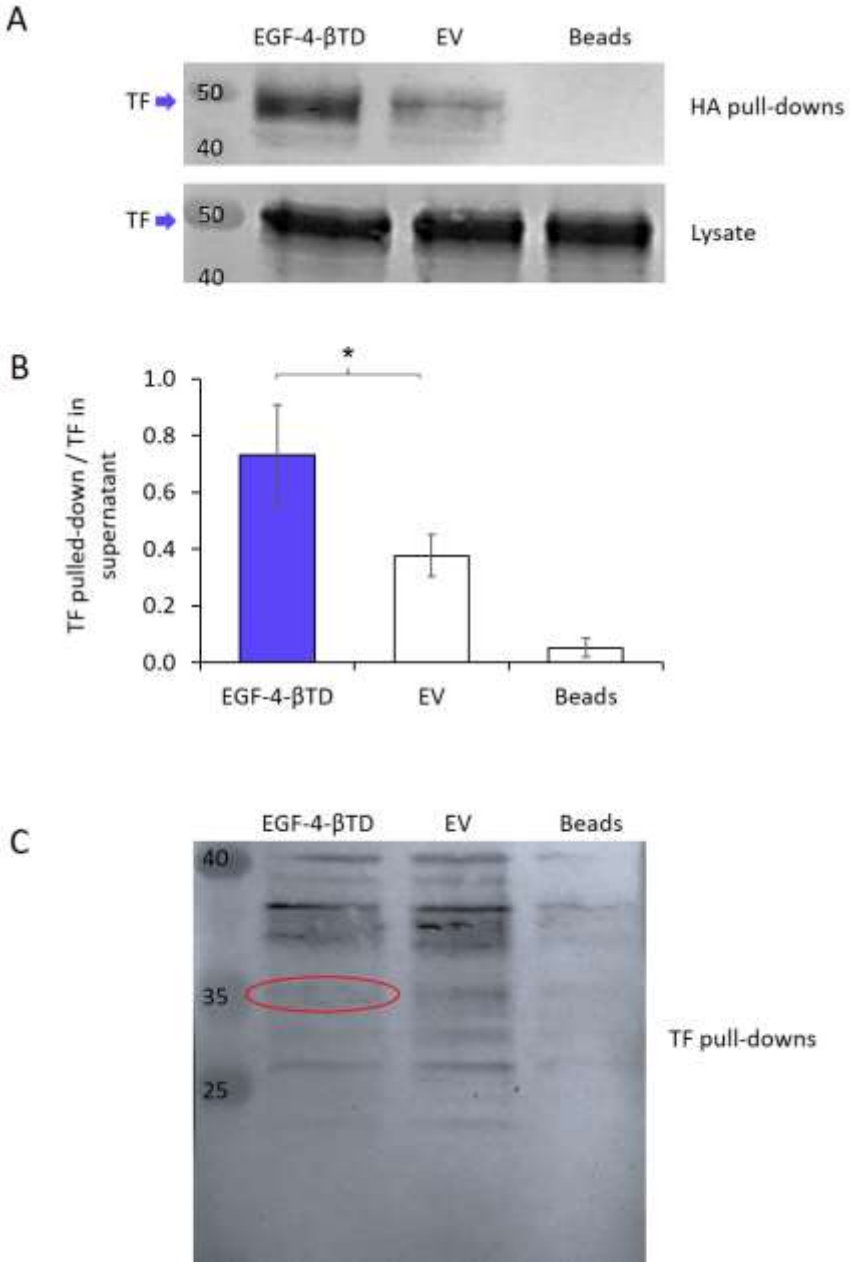

MDA-MB-231 cells (1.5 x 10^5) were transfected to express EGF4-βTD in tandem with the FLAG and HA tags or the FLAG-HA tag control peptide. A) The EGF4-βTD peptide was precipitated using an anti-HA-tag antibody and the presence of co-purified TF protein was examined by western blot using an anti-TF antibody. B) The intensities of the western blot bands were quantified using ImageJ (n=4, Images represent 2 experiments carried out in duplicate; data = mean values ± SEM; independent t-test * = $p < 0.05$). C) TF was precipitated using an anti-TF antibody and the presence of co-purified EGF4-βTD peptide was examined by western blot using an anti-HA antibody. The red circles indicate the position where the co-purified protein was expected to be detected.

Figure 5.33: Examination of the influence of expression of TF peptides on the binding of an EGF4-βTD domain-specific anti-β1 integrin antibody

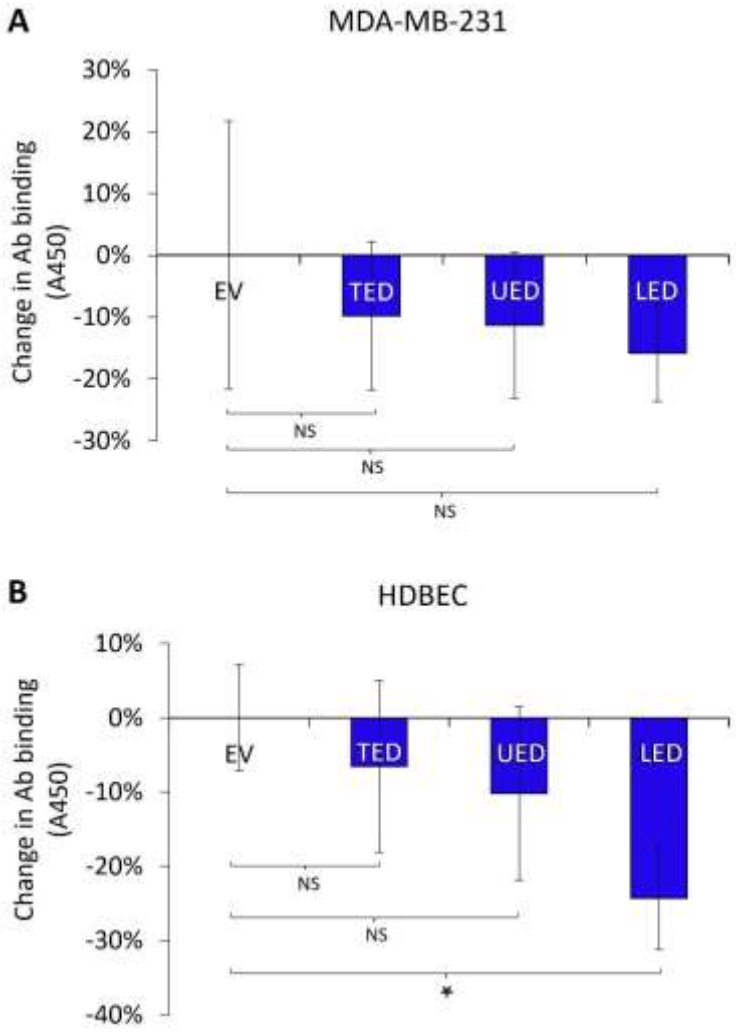

A) MDA-MB-231 cells (10^4) and B) HDBEC (5 x 10^4) were transfected to express TED, LED, UED or the control peptide. The cells were probed with an anti-β1 integrin antibody specific to the EGF4-βTD domain of β1 integrin and then with HRP-conjugated anti-rabbit IgG antibody. The samples were developed using TMB-one solution HRP substrate and the amount of bound antibody was quantified by measuring the absorptions at 450 nm using a plate reader. Percentage change values were calculated as 100 x (treated - control) / control (n=8, two experiment carried out in quadruplicate; data = mean values ± SEM; independent t-test, * = $p < 0.05$, NS = not significant).

Figure 5.34: Examination of the influence of the expression of TF and β1 integrin peptides on the phosphorylation of cellular ERK1/2

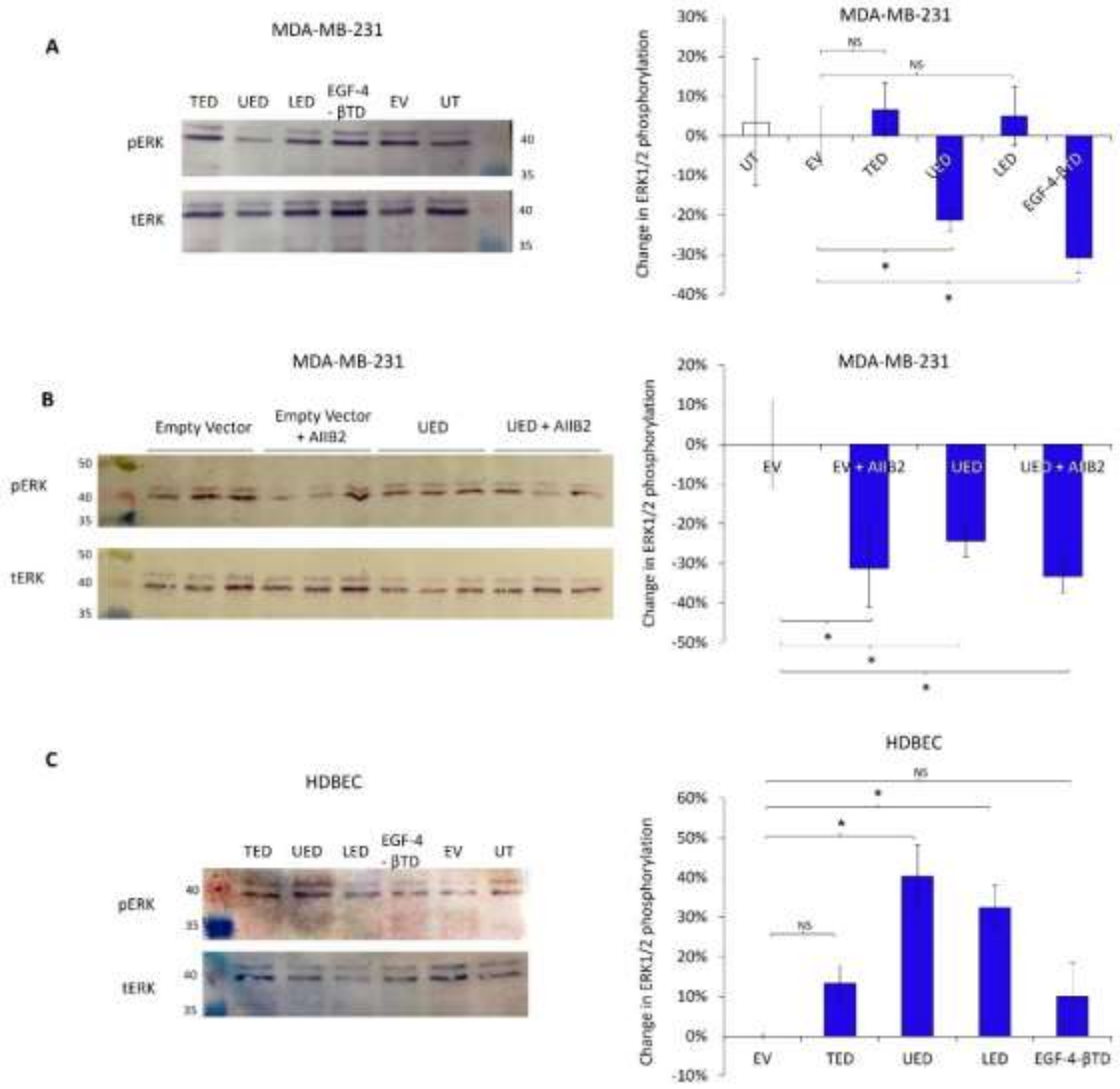

A) MDA-MB-231 cells (1.5 x 10^5) and B) HDBEC (5 x 10^5) were transfected to express TED, LED, UED, EGF4-βTD or the control peptide. C) Additional sets of MDA-MB-231 cells (1.5 x 10^5) expressing UED or the control peptide were pre-incubated with an inhibitory anti-β1 integrin antibody (AIIB2; 10 µg/ml) for 16 h prior to collection. All cells were then lysed with Laemmli buffer and western blot analysis was carried out using antibodies against ERK1/2 and phosphorylated ERK1/2 (diluted 1:2000 v/v in TBST) and against GAPDH (diluted 1:5000 v/v in TBST). The membranes were incubated with AP-conjugated anti-rabbit IgG or AP-conjugated anti-goat IgG antibodies (diluted 1:3000 v/v in TBST), respectively. The membranes were then developed using Western Blue stabilised substrate for AP. Band intensities were quantified using ImageJ and the ratio of pERK/tERK was calculated. Percentage change values were calculated as 100 x (treated - control) / control (n=6, two independent experiments carried out in triplicate; data = mean values ± SEM; independent t-test * = $p < 0.05$, NS = not significant).

anti-β1 integrin antibody (AIIB2) resulted in a comparable reduction of the pERK:tERK ratio to 1.1 ± 0.5 (Figure 5.34C). However, pre-incubation of the cells expressing UED peptide, with the inhibitory anti-β1 integrin antibody did not further reduce ERK phosphorylation beyond this level (1.1 ± 0.2 pERK:tERK ratio) (Figure 5.34C). In contrast, the expression of LED and TED peptide did not influence the phosphorylation of ERK in MDA-MB-231 cells.

The expression of either the UED or LED peptide in HDBEC resulted in pERK:tERK ratios of 1.0 ± 0.1 or 1.1 ± 0.3 respectively, which were higher than that observed in cells expressing the control peptide (0.5 ± 0.01) (Figure 5.34B). Moreover, the expression of TED peptide did not influence the phosphorylation of ERK in these cells.

In addition to the TF-derived peptides, the influence of the expression of EGF4-βTD peptide on ERK phosphorylation was also measured. Expression of EGF4-βTD peptide in MDA-MB-231 cells reduced the pERK:tERK ratio to 1.1 ± 0.1, compared to 1.6 ± 0.2 observed in cells expressing the control peptide (Figure 5.34A). However, expression of EGF4-βTD peptide in HDBEC did not influence the phosphorylation of ERK (Figure 5.34B).

5.3.14 Examination of the influence of the TF and β1 integrin peptides on cyclin D1 expression

To further investigate any influence of the TED, LED and UED peptides on cellular signalling, the outcome of the expression of these peptides on cyclin D1 mRNA expression was assessed by semi-quantitative RT-PCR. Expression of UED peptide resulted in the downregulation of cyclin D1 expression to 0.42 ± 0.07, compared with cells expressing LED (1.2 ± 0.5), TED (1.0 ± 0.07) or the control peptide (1.0 ± 0.2) (Figure 5.35A). In addition, pre-incubation of cells with an inhibitory anti-β1 integrin antibody (AIIB2) resulted in the downregulation of cyclin D1 expression to 0.7 ± 0.2 (Figure 5.35C). However, pre-incubation of cells expressing UED peptide with the inhibitory anti-β1 integrin antibody did not further reduce the level of cyclin D1 mRNA expression (0.5 ± 0.03) (Figure 5.35C). Finally, expression of either of the TED, LED or UED peptides in HDBEC did not alter the levels of cyclin D1 mRNA expression in these cells (Figure 5.35B). The expression of EGF4-βTD peptide was also shown to downregulate cyclin D1 expression to 0.35 ± 0.03 in MDA-MB-231 cells (Figure 5.35A), but had no influence in HDBEC (Figure 5.35B).

5.3.15 Examination of the influence of the TF and β1 integrin peptides on cell proliferation

To examine the influence of the expression of TED, LED and UED peptides on cell proliferation, cell numbers were determined after 4 days, following the transfection of cells. Cell numbers were shown to be reduced on the expression of UED peptide (92,200 cells ± 2,200) compared to those

Figure 5.35: Examination of the influence of expression of TF and β1 integrin peptides on cyclin D1 mRNA levels

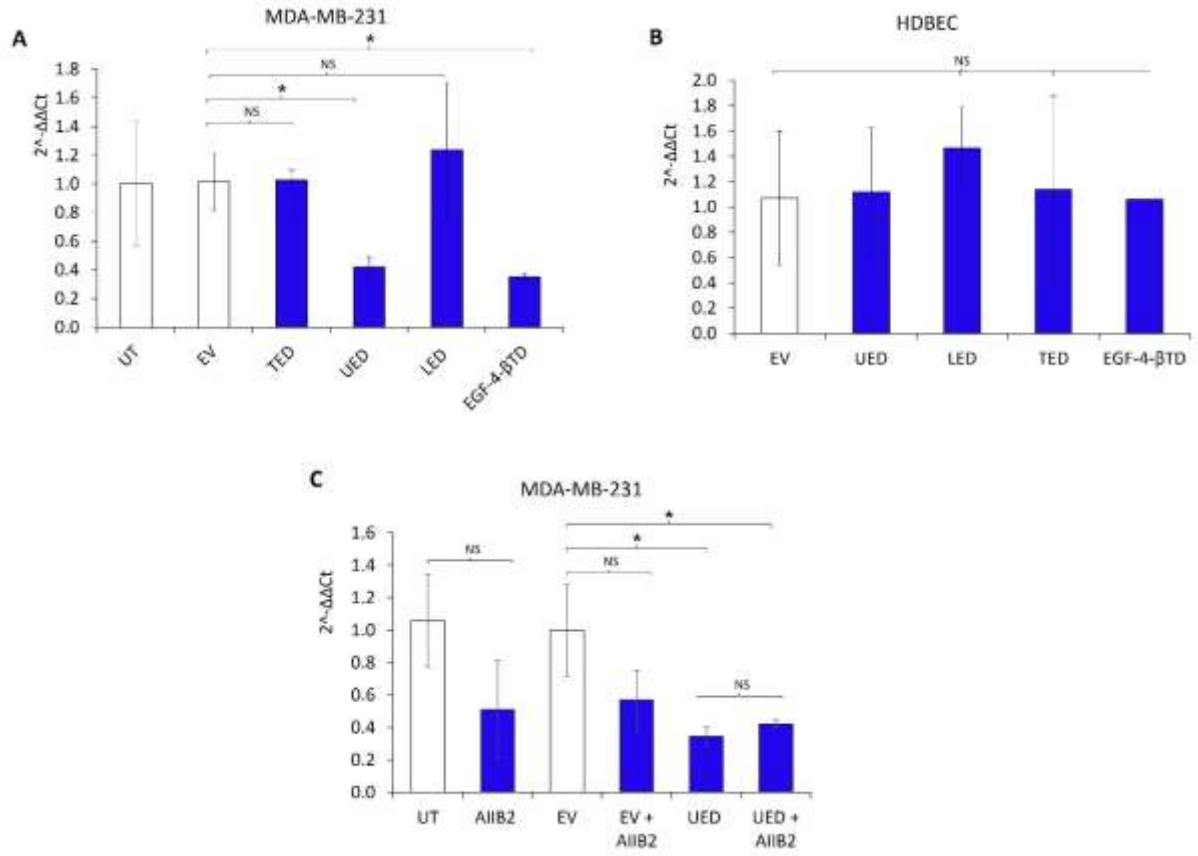

A) MDA-MB-231 cells (1.5 x 10^5) and B) HDBEC (5 x 10^5) were transfected to express TED, LED, UED, EGF4-βTD or the control peptide. C) Additional sets of MDA-MB-231 cells (1.5 x 10^5) expressing UED or the control peptide were pre-incubated with an inhibitory anti-β1 integrin antibody (AIIB2; 10 µg/ml) for 16 h prior to collection. The cells were then lysed, the mRNA extracted and converted to cDNA using cell-2-cDNA kit. The expression of cyclin D1 and β-actin mRNA were measured using RT-PCR and the relative cyclin D1 expression levels calculated using the $2^{-\Delta\Delta Ct}$ method (n=6, two independent experiments carried out in triplicate; data = mean values ± SEM; independent t-test * = $p < 0.05$, NS = not significant).

expressing the control peptide (98,600 cells ± 1,800). In contrast, expression of either LED (96,600 cells ± 1,900) or TED (98,500 cells ± 3,200) peptide had no significant influence on cell numbers compared to that of the control peptide (Figure 5.36A). Similarly, expression of any of the TED, LED or UED peptides in HDBEC did not influence cell numbers compared to those of the control peptide (Figure 5.36B). Finally, expression of EGF4-βTD peptide did not alter the rate of cell proliferation (97,600 cells ± 900) in MDA-MB-231 cells, which was comparable to that of the control sample (98,600 cells ± 1,800) (Figure 5.36A).

5.3.16 Examination of the influence of the TF extracellular domain peptides on the conformation of β1 integrin

To detect any change in the configuration of β1 integrin on cells, monoclonal antibodies 9EG7 and AIIB2 were used which distinguish between configurations by specifically binding to the active/open and inactive/closed configurations of β1 integrin, respectively. To confirm the specificity of these antibodies, cell-surface β1 integrin was activated by pre-incubation with Mn^{2+} ions and was then probed with these antibodies. The activation of β1 integrin resulted in an increase in the binding of 9EG7 antibody as indicated by a rise in the absorption from 0.77 ± 0.001 in non-treated cells, to 0.93 ± 0.002 (Figure 5.37A). In contrast, activation of β1 integrin resulted in a reduction in the binding of the AIIB2 antibody which was indicated by a decrease in absorption from 3.52 ± 0.07 in non-treated cells, to 3.04 ± 0.02 (Figure 5.37B). These data demonstrated the suitability of these antibodies for the selective identification of the active/open and inactive/closed configurations of β1 integrin.

Expression of UED peptide in MDA-MB-231 cells reduced the binding of the 9EG7 antibody (0.56 ± 0.07) compared to cells expressing the control peptide (0.81 ± 0.09) (Figure 5.38A). In contrast, the expression of neither the TED nor LED peptide significantly influenced the binding of the 9EG7 antibody in these cells. In addition, the expression of either LED or UED peptide in HDBEC reduced the binding of the 9EG7 antibody to 1.45 ± 0.11 and 1.41 ± 0.10, respectively, compared to cells expressing the control peptide (1.736 ± 0.07) (Figure 5.38B).

Furthermore, expression of LED peptide in MDA-MB-231 cells resulted in increased binding of the AIIB2 antibody (1.14 ± 0.14) compared to that of the control peptide (0.93 ± 0.31). In contrast, the expression of UED peptide decreased the binding of the AIIB2 antibody (0.72 ± 0.09) (Figure 5.38C). However due to large inter-experimental variations, the changes indicated by the data were not statistically significant. The expression of TED peptide did not influence the binding of the AIIB2 antibody in MDA-MB-231 cells. Additionally, the expression of the TED peptide increased the binding of AIIB2 antibody (2.35 ± 0.18) on HDBEC compared to that of the control peptide (1.98 ± 0.17) whilst the expression of either UED or LED peptide had no detectable influence (Figure 5.38D).

Figure 5.36: Examination of the influence of expression of TF and β1 integrin peptides on cell proliferation

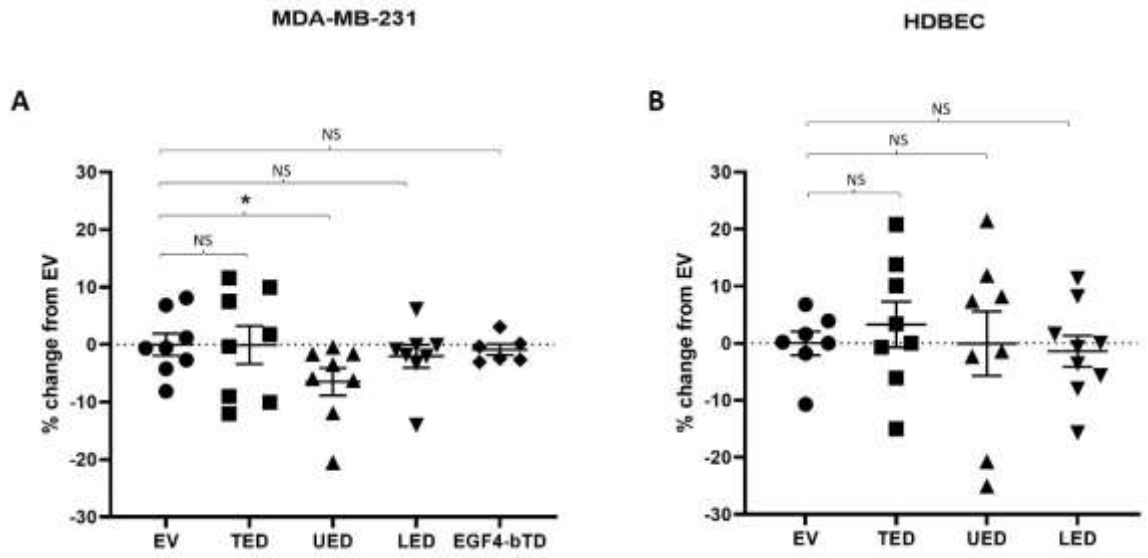

A) MDA-MB-231 cells and B) HDBEC (5 x 10^4) were transfected to express TED, LED, UED, EGF4-βTD or control peptide. The cells were incubated for 3 days and the number of cells were determined using the crystal violet assay. Percentage change was calculated as 100 x (treated - control) / control (n=8, two independent experiments carried out in quadruplicate; data = mean values ± SEM; independent t-test * = $p < 0.05$, NS = not significant).

Figure 5.37: Confirmation of the specificity of the monoclonal antibodies for the determination of β1 integrin conformation

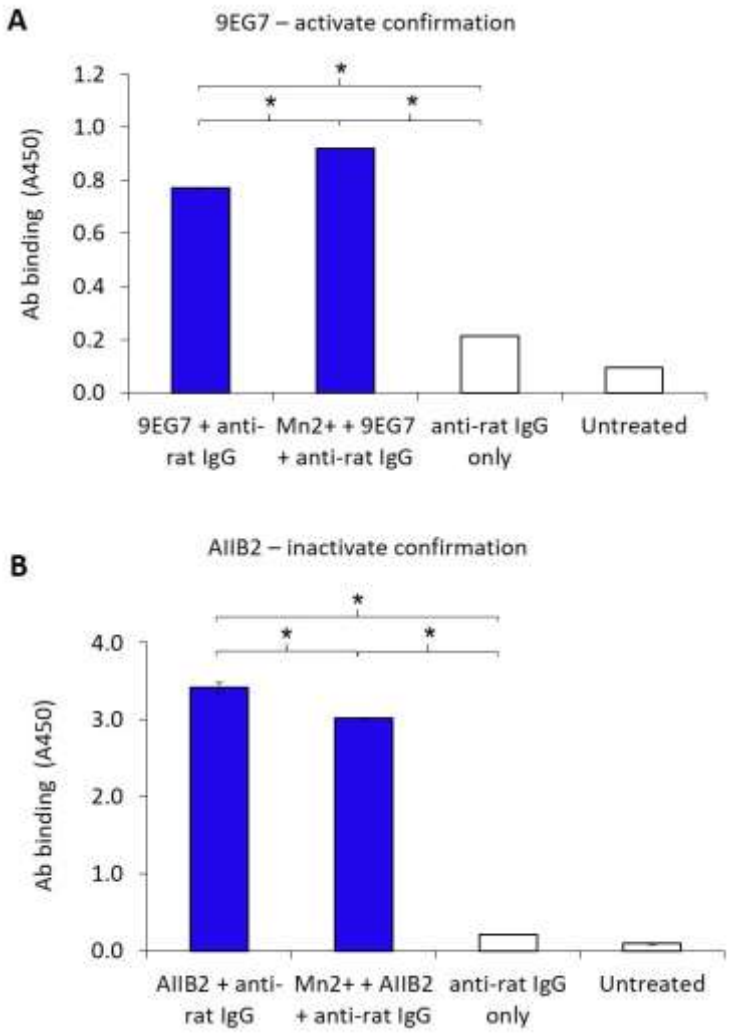

MDA-MB-231 cells (5 x 10^4) were plated in 96-well plates. Selected wells were treated with 1 mM Mn^{2+} ions for 30 min. The cells were then probed with antibodies against the A) active/open (9EG7) or B) inactive/closed (AIIB2) conformations of β1 integrin. The cells were probed with HRP-conjugated anti-rat IgG antibody and then developed using TMB-one solution HRP substrate. The amount of bound antibody was quantified by measuring the absorptions at 450 nm using a plate reader (n=4, two experiments carried out in duplicate; data = mean values ± SEM; one-way ANOVA * = $p < 0.05$).

Figure 5.38: Examination of the influence of the expression of TF peptides on the binding of monoclonal antibodies to β1 integrin

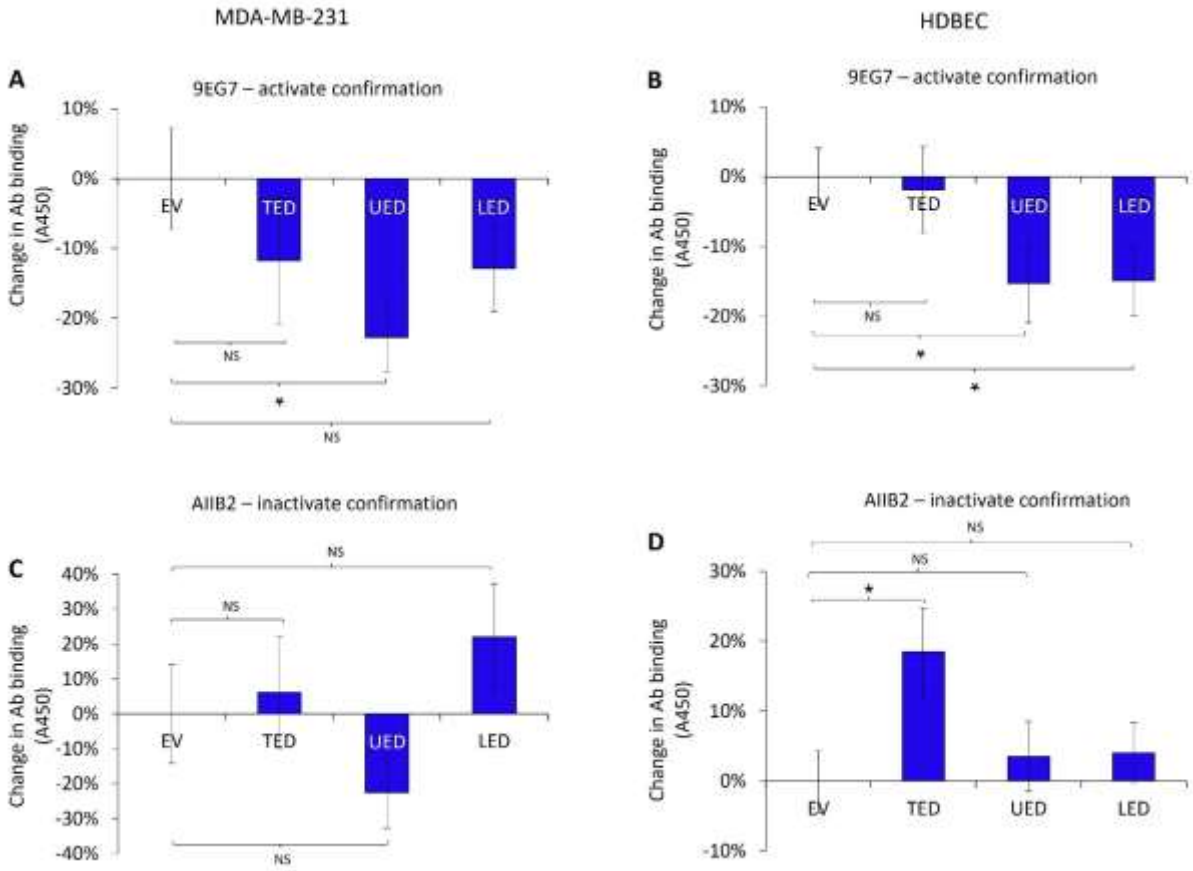

A) & C) MDA-MB-231 cells (10^4) and B) & D) HDBEC (5 x 10^4) were transfected to express TED, LED, UED or control peptide. The cells were probed with antibodies against the A) & B) active/open (9EG7) or C) & D) inactive/closed (AIIB2) conformation of β1 integrin. The cells were probed with HRP-conjugated anti-rat IgG antibody and developed using TMB-one solution HRP substrate. The amount of bound antibody was quantified by measuring the absorptions at 450 nm using a plate reader. Percentage change values were calculated as 100 x (treated - control) / control (n=8, two experiment carried out in quadruplicate; data = mean values ± SEM; independent t-test * = $p < 0.05$, NS = not significant).

5.4 Discussion

5.4.1 Elucidation of the role of factor fVII(a) in the interaction of TF and β1 integrin

The interaction between TF and β1 integrin is known to influence cell migration, angiogenesis and proliferation (Kocaturk & Versteeg, 2013). However, the specific requirements for complex formation between these proteins have not been investigated. In the current study, it was demonstrated that suppression of fVIIa expression in MDA-MB-231 cells reduced the association between TF and β1 integrin (Figure 5.23). This agrees with previous findings that incubation of PC3, HaCaT and A7 cells with recombinant human fVIIa increased the number of interactions between TF and β1 integrin as measured by PLA or by co-IP (Aberg et al., 2020; Versteeg et al., 2008b). Therefore, these findings confirm that the presence of fVIIa, either endogenously expressed or from sources external to the cell, is critical for the interaction between TF and β1 integrin.

5.4.2 Investigation of the function of the upper extracellular domain (UED) of TF in the interaction with β1 integrin

The extracellular region of TF has previously been shown to associate with β1 integrin and influence integrin-mediated cellular signalling (Dorfleutner et al., 2004; Kocaturk et al., 2013). The extracellular region of TF contains 2 fibronectin-like domains which have been suggested to have distinct functions in the interaction with β1 integrin. Therefore, the ability of an expressed UED peptide to bind to β1 integrin, as well as the outcome on cell signalling was assessed. The UED peptide was shown to associate with the cell-surface β1 integrin on both MDA-MB-231 cells and HDBEC as examined by PLA (Figure 5.27 & Figure 5.28). However, UED peptide did not co-purify with β1 integrin in co-IP experiments (Figure 5.30). This may suggest that the association between TF and β1 integrin occurs at multiple points and the UED participates as one of these required interactions. Consequently, the binding between the UED and β1 integrin may be interrupted during the IP procedure. The target site for the interaction for UED peptide within β1 integrin was determined to be located in the EGF3 and EGF4 regions (residues 495-602) of the latter protein. This was demonstrated by the ability of expressed UED peptide to reduce the binding of the 9EG7 antibody, which is specific for the EGF3 and EGF4 regions of β1 integrin (Figure 5.38). However, the 9EG7 antibody is also known to be selective for the active/open configuration of β1 integrin (Figure 5.37) (Bazzoni et al., 1995). Therefore, the reduction in the binding of the 9EG7 antibody may also reflect the ability of UED peptide to impede the activation of β1 integrin.

The interaction between TF and β1 integrin is also known to promote cellular proliferation (Collier & Ettelaie, 2010; Rothmeier et al., 2018). Therefore, the ability of UED peptide to influence cell proliferation was examined next. Expression of UED peptide in MDA-MB-231 cells resulted in the

reduction in the rate of cell proliferation (Figure 5.36A). This suppression in cell growth was concurrent with reduced ERK1/2 phosphorylation (Figure 5.34A) and cyclin D1 mRNA expression (Figure 5.35A). In addition, no further reduction was observed on antibody-mediated inhibition of β1 integrin in these cells (Figure 5.34C & Figure 5.35C) indicating that the ability of UED peptide to reduce cell proliferation in MDA-MB-231 cells was dependent on β1 integrin. Therefore, it was proposed that the expressed UED peptide may reduce the rate of proliferation by acting as a competitor to cellular TF, hence disrupting its interaction with cellular β1 integrin (Figure 5.39A). However, this also indicates that the UED alone does not contain the necessary motif(s) essential for initiating the integrin-mediated pro-proliferative signals. In contrast, expression of UED peptide in HDBEC resulted in increased ERK1/2 phosphorylation (Figure 5.34B) although the increase in ERK signalling was not translated into significant changes in cyclin D1 expression (Figure 5.35B) or in the promotion of cell proliferation (Figure 5.36B). The discrepancy between the outcomes observed in MDA-MB-231 cells and HDBEC may be due to the transient nature of the interaction between UED and β1 integrin. Transient binding of UED peptide to β1 integrin may be sufficient to disrupt the cellular-TF and β1 integrin complex in MDA-MB-231 cells, but can only induce short-term activation of ERK when bound (Figure 5.40A). Since sustained activation of ERK is essential for the induction of cyclin D1 expression (Walker & Assoian, 2005), the short-term activation of ERK is not sufficient to promote gene expression. An alternative explanation for the discrepancies between the outcome of UED peptide expression in these two cells may arise from differences in growth factor receptor expression. Signals originating from both integrins and growth factor receptors converge in order to regulate cell proliferation (Le Gall et al., 1998; Moreno-Layseca & Streuli, 2014). Since cancer cells commonly overexpress growth factor receptors, any complimentary stimuli to UED peptide/β1 integrin signalling may be amplified in MDA-MB-231 cells but not in HDBEC.

5.4.3 Investigation of the function of the lower extracellular domain (LED) of TF in interaction with β1 integrin

In addition to the upper domain, the LED peptide was shown to associate with cell-surface β1 integrin in both MDA-MB-231 cells and HDBEC using PLA (Figure 5.27 & Figure 5.28). However, unlike the UED peptide, LED peptide was co-immunoprecipitated along with β1 integrin (Figure 5.30), suggesting that the lower region of TF may be responsible for high affinity binding to β1 integrin. This finding is supported by the presence of certain amino acids within LED that are responsible for the binding of TF to the EGF domain of fXa during TF/fVIIa/fXa complex formation (Krudysz-Amblo et al., 2011). The EGF domain of fXa and EGF4 domain of β1 integrin contain similar amino acids that are also in comparable positions within the 3D structures of these protein (Collier, 2008). Therefore,

Figure 5.39: Model of the influence of TF extracellular domain peptides on integrin signalling in the presence of endogenous TF

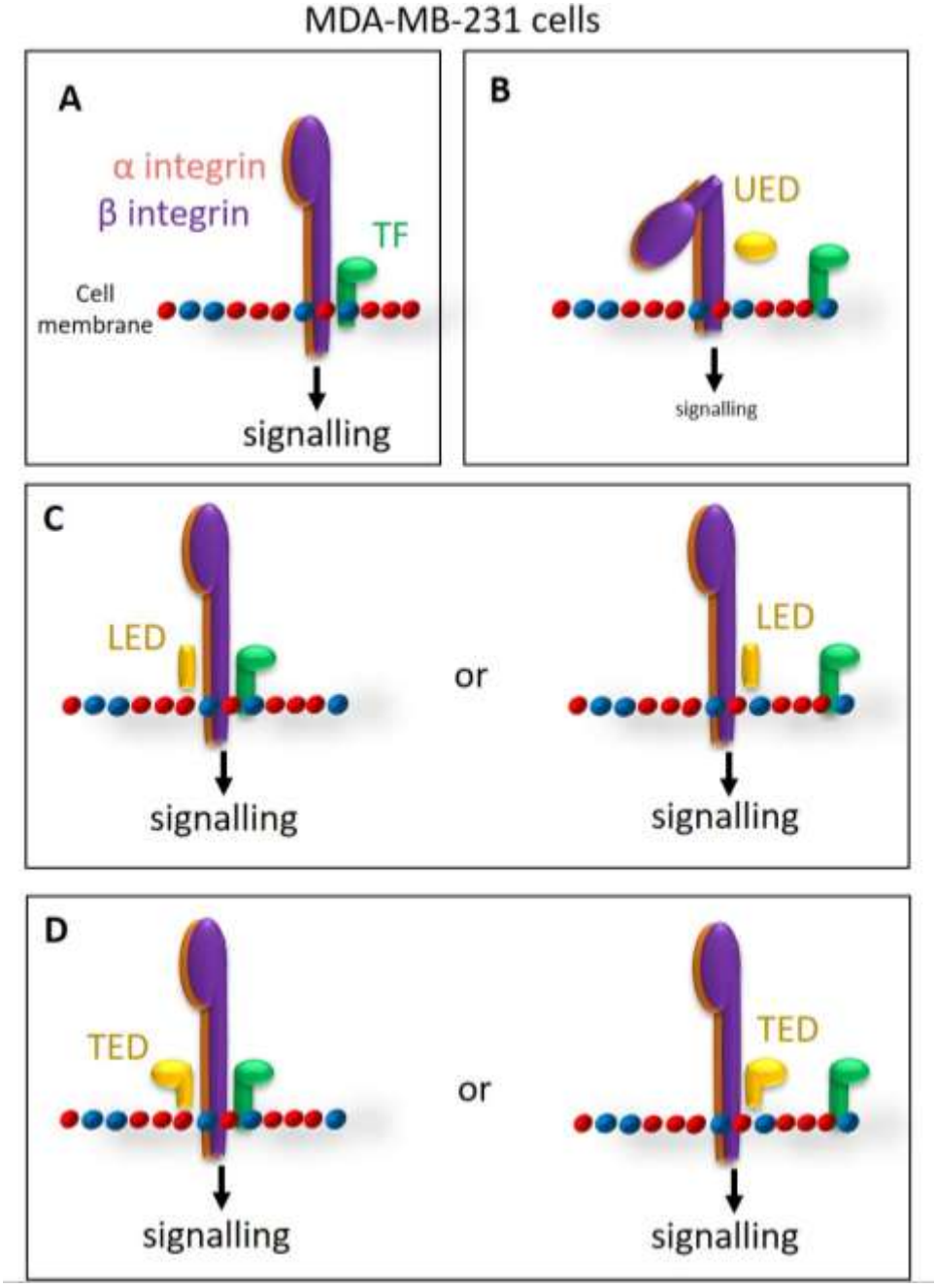

A) A model of the interactions between TF (green) and an α integrin (orange)/β integrin (purple) complex on the surface of MDA-MB-231 cells and the subsequent induction of cell signalling. B) UED peptide (yellow) acts as a competitor to cellular TF, disrupting the interaction between TF and the integrin receptor and reducing the subsequent signalling. C) LED peptide and D) TED peptide bind to the integrin receptor but have no influence on the TF/integrin complex and signalling (left of panels). Alternatively, LED and TED peptides may displace cellular-TF from the complex with the integrin receptor, but are capable of maintaining cell signalling (right of panels).

Figure 5.40: Model of the influence of TF extracellular domain peptides on integrin signalling in the absence of endogenous TF

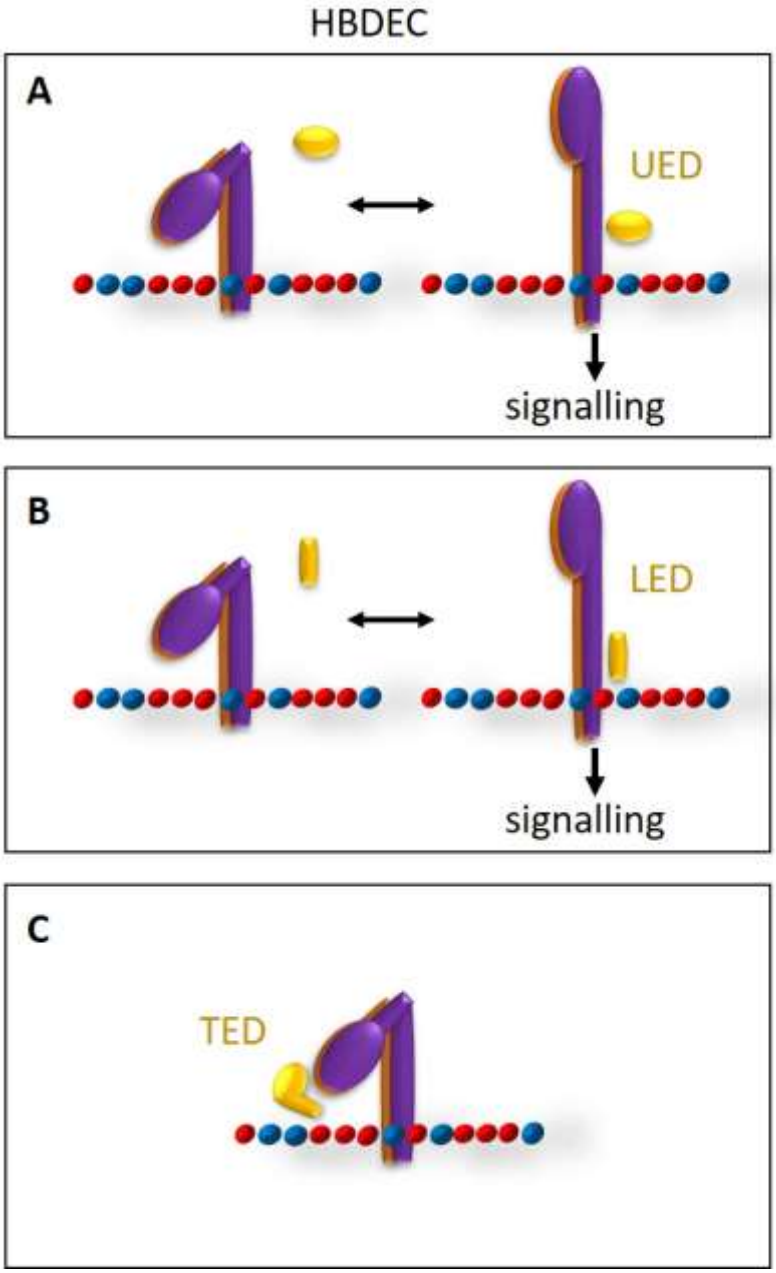

A model of the interactions between TF extracellular domain peptides (yellow) and an α integrin (orange)/β integrin (purple) complex on the surface of HDBEC and the subsequent induction of cell signalling. Transient binding of expressed A) UED and B) LED peptide to β1 integrin results in short-lived ERK signalling. C) Expressed TED peptide binds to β1 integrin and restrains the integrin receptor in the closed/inactive conformation preventing signalling.

it is proposed that the LED would be capable of binding to the EGF4 of β1 integrin in a similar manner to the interaction with the EGF domain in fXa. Furthermore, the binding of a monoclonal antibody specific to the EGF4-βTD domain of β1 integrin (residues 579-799) was significantly obstructed on expression of LED peptide in HDBEC (Figure 5.33B). Additionally, expression of LED peptide prevented the binding of the 9EG7 antibody specific to the EGF3 and EGF4 domains of β1 integrin (residues 495-602) in HDBEC (Figure 5.38B). Collectively these data indicate that the docking site of the lower region of TF is located around residues 579-602 of β1 integrin. In contrast, in cells expressing endogenous TF, the expressed LED peptide did not influence the binding of either the antibody specific to the EGF4-βTD (Figure 5.33A) or 9EG7 antibody (Figure 5.38A). This suggests a large proportion of the sites targeted by the two antibodies may be occupied with the endogenous TF. Therefore, the expression and binding of LED peptide in MDA-MB-231 cells does not result in a statistically significant change in the availability of the sites targeted by the EGF4-βTD specific and 9EG7 antibodies. In additional experiments, a peptide corresponding to the combined EGF4-βTD domains of β1 integrin (residues 572-728) was shown to associate with cell-surface TF (Figure 5.31) and also, co-purified with immunoprecipitated TF (Figure 5.32). In contrast, a peptide corresponding to the EGF4 domain alone was not sufficient to associate with cell-surface TF (Figure 5.31) indicating that the βTD domain may be the target docking site for TF. However, since construction of the plasmid to express the βTD domain alone was not successful (Figure 5.15), this hypothesis could not be examined.

The ability of LED peptide to influence cell proliferation was also examined. Expression of LED peptide did not influence ERK1/2 phosphorylation (Figure 5.34A), cyclin D1 mRNA expression (Figure 5.35A) or the rate of cell growth (Figure 5.36A) in MDA-MB-231 cells. This may indicate that LED peptide does not impact the signalling following the interaction of TF and β1 integrin in these cells. Alternatively, LED peptide may act as a competitor to cellular-TF in the same manner as UED peptide, although unlike UED, LED contains the motif(s) to sustain a proliferative signal (Figure 5.39B). Previous studies showed that a peptide corresponding to a section of LED (residues 202-219) was capable of inducing signals which enhanced the rate of migration in endothelial cells (Randolph et al., 1998). However in that study, the influence of this peptide on cell proliferation was not examined. In the present study, the expression of LED peptide in HDBEC resulted in increased ERK1/2 phosphorylation (Figure 5.34B) which indicates that LED peptide may be capable of inducing cell signalling. However, as with the UED peptide, the increase in ERK signalling in HDBEC was not translated into significant changes in cyclin D1 expression (Figure 5.35B) or in promotion of cell growth (Figure 5.36B). The lack of effectiveness of this signal may also arise from the transient

nature of the interaction between LED and β1 integrin (Figure 5.40B). Therefore, such short-term activation of ERK would not be sufficient to promote gene expression.

Since the docking site for the LED peptide was shown to be localised to the EGF4 and/or βTD domain, the ability of the EGF4-βTD domain (residues 572-728) of β1 integrin to alter cellular signalling and the rate of cellular proliferation was also examined. Expression of the EGF4-βTD peptide in MDA-MB-231 cells resulted in the reduction in ERK phosphorylation as well as the downregulation of cyclin D1 mRNA expression (Figure 5.34 & Figure 5.35). However, these alterations in proliferative signalling did not result in a reduction in the rate of cell proliferation (Figure 5.36). These data are in agreement with previous reports showing that a peptide corresponding to the EGF4-βTD of β1 integrin (residues 579-799) did not influence cellular proliferation in MDA-MB-231 cells (Kocaturk et al., 2013). However, this EGF4-βTD peptide was capable of inhibiting the rate of proliferation in MDA-MB-231mfp cells and MCF-7 cells (Kocaturk et al., 2013). In addition, treatment of HCAEC with EGF4-βTD peptide (residues 579-799) reversed both the increase in of ERK1/2 phosphorylation and the acceleration of cell proliferation which followed stimulation with recombinant TF (Collier & Ettelaie, 2010). This data further supports the hypothesis that transient interactions of peptides are capable of disrupting existing interactions between TF and β1 integrin on the cell surface, but may not initiate sustained signalling by themselves. Consequently, EGF4-βTD peptides acts as an inhibitor of proliferative signalling, in cells in which full-length TF is present.

5.4.4 Investigation of the function of the total extracellular domain (TED) of TF in interaction with β1 integrin

In the final study, the peptide corresponding to the complete extracellular domain of TF (TED) was expressed and the interaction and signalling properties compared to those of UED and LED peptides. Using PLA, TED peptide was shown to associate with cell-surface β1 integrin (Figure 5.27 & Figure 5.28). However, attempts at co-IP did not result in the co-purification of this peptide with β1 integrin (Figure 5.30). Therefore, the TED peptide appears to have a similar binding affinity for β1 integrin to that of UED peptide. Expression of TED peptide did not influence ERK1/2 phosphorylation (Figure 5.34A), cyclin D1 mRNA expression (Figure 5.35A) or the rate of cell growth (Figure 5.36A) in MDA-MB-231 cells. The lack of any inhibitory influence may indicate that TED peptide is capable of disrupting the interaction between cellular TF and β1 integrin, but concurrently contains the protein motif(s) sufficient to sustain some proliferative signalling (Figure 5.39C). Additionally, expression of TED peptide did not influence proliferation in HDBEC, which lack TF (Figure 5.35B & Figure 5.36B). Again, the transient nature of the interaction between TED peptide and β1 integrin may explain the lack of signalling in HDBEC. However, increases in ERK phosphorylation observed on transient

interactions between LED or UED peptides with β1 integrin were absent in cells expressing the TED peptide (Figure 5.34B). Furthermore, unlike the LED or UED peptides, the expression of TED peptide enhanced the binding of AIIB2 antibody which is specific to the closed configuration of β1 integrin (Figure 5.38D). This may suggest that TED peptide is capable of binding to β1 integrin in a manner which holds the latter protein in the inactive/closed conformation.

Comparison of TED to the naturally observed TF variant, asTF, which arises from a frameshift in the TF gene, shows that a major proportion of the protein is homologous to TED. The major difference between the two proteins is that the last 13 residues at the c-terminus of the TED are substituted with a stretch of 40 unique amino acids in asTF. In agreement with the observations following the expression of TED, asTF is also incapable of inducing proliferation in endothelial cells (van den Berg et al., 2009). Similarly, expression of asTF in MDA-MB-231 cells did not influence cell proliferation (Kocaturk et al., 2013). Although the expression of asTF in MCF-7 cells, which express low levels of full-length TF (Lima et al., 2013; Zhang et al., 2011), increases proliferation through interaction with β1 integrin (Kocaturk et al., 2013).

5.4.5 A proposed model for the binding of TF to β1 integrin

The data generated in this study suggest a model in which the binding of TF to β1 integrin occurs through both the upper and lower fibronectin-like domains within the extracellular region of TF. This two-pronged interaction appears to occur through the binding of the upper region of TF with the EGF4 domain of β1 integrin, and the lower region with the βTD domain (Figure 5.41A). The mechanism by which this two-pronged interaction influences cell signalling is thought to be dependent on a structural loop within the βTD which comes into contact with residues within the head group of the β-integrin subunit (Figure 5.42). This interaction is presumed to retain the integrin in the closed/inactive conformation (Arnaout et al., 2005). Therefore, it is likely that the binding of the LED to the βTD region of the integrin disrupts this interaction which would in turn release the integrin head-group, allowing β1 integrin to adopt the open/active conformation. Consequently, a larger proportion of cell surface β1 integrin will be in the inactive/closed conformation in cells that do not express TF, compared to those that constituently express this protein. This mechanism accounts for the discrepancies in the influences of the TED, LED and UED peptides observed in the presence or absence of endogenous TF. In cells devoid of endogenous TF, despite a proportion of β1 integrin being in the inactive/closed conformation, the expressed LED and UED peptides were capable of accessing their respective binding sites on β1 integrin, due to the small size of these peptides. In contrast, the larger combined peptide (TED) was not able to approach the relevant binding sites within the closed conformation of β1 integrin (Figure 5.41B). As a result, the expression

Figure 5.41: The proposed model of the association between TF and β1 integrin

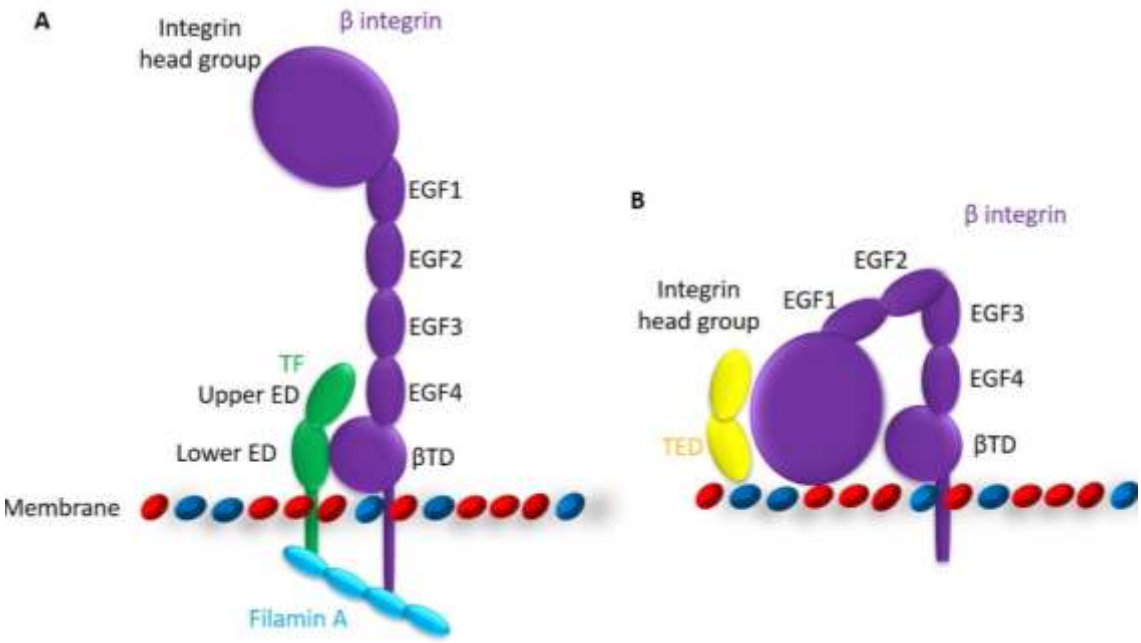

A) The proposed positioning for the interacting domains during complex formation between TF (green) and β1 integrin (purple). Complex formation is facilitated through the interaction of the cytoplasmic domains of TF and β1 integrin with filamin A. As a result, the upper extracellular domain of TF binds to the EGF4 domain of β1 integrin, and the lower extracellular domain binds to the βTD. B) In the absence of complex formation with filamin A, the TF extracellular domain peptide (TED; yellow) cannot gain access to the EGF4 and βTD within the closed β1 integrin conformation.

Figure 5.42: The interaction of the βTD domain with the integrin head group within β-type integrin subunits

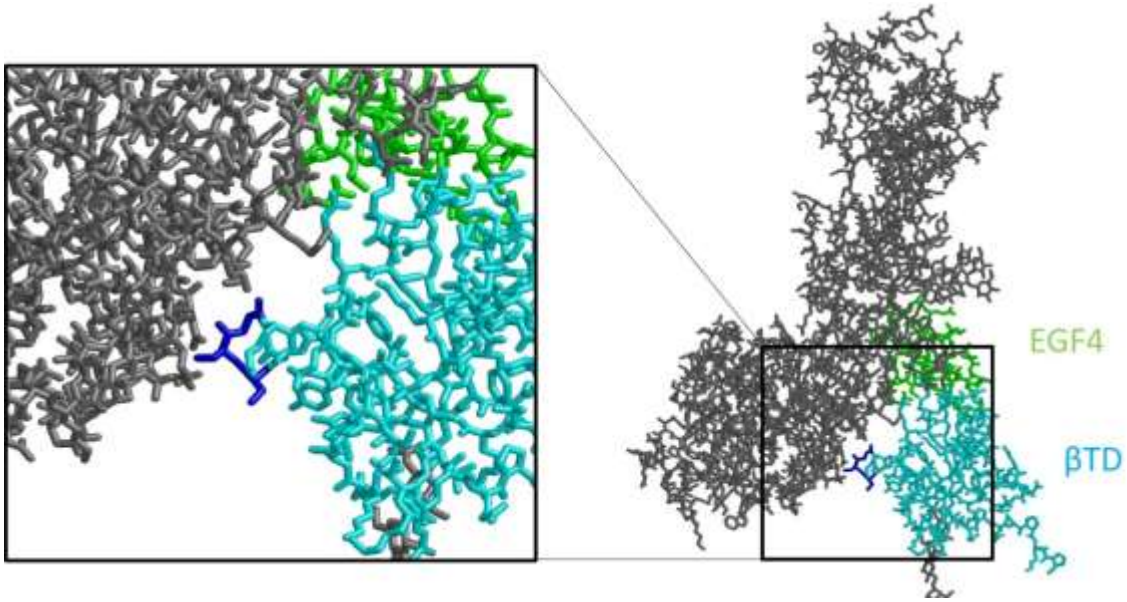

A structural loop (blue) within the βTD (cyan) of a β3 integrin that interacts with residues in the head group of the integrin molecule holding the integrin in a closed configuration.

of TED peptide did not induce proliferative signalling in HDBEC, which lack TF. However, the conformation of β1 integrin may be altered by inside-out signalling which involves the binding of focal adhesion proteins to the cytoplasmic domain of β1 integrin (De Franceschi & Ivaska, 2015; Kim et al., 2011). One such adaptor protein is the large structural protein filamin A which consists of an N-terminal actin-binding domain and 24 immunoglobulin (Ig)-like repeats (Gorlin et al., 1990). β1 integrin has been shown to bind within Ig-like repeats 21 (Kiema et al., 2006; Loo et al., 1998). Interestingly, the cytoplasmic domain of TF has also been shown to bind to filamin A following phosphorylation of Ser253 (Collier et al., 2017; Ott et al., 1998). The binding site for TF on filamin A has been reported to be located between Ig-like repeats 22–24 (Collier et al., 2017). This molecular arrangement not only permits the proximation of TF and β1 integrin but also may alter the structure of β1 integrin sufficiently to allow the required access for TF. This explains the difference in the action of full-length TF compared to TED, which lacks the intracellular domain and therefore cannot bind to filamin A.

The activation of β1 integrin resulting from the binding of TF suggests a potential mechanism by which β1 integrin can induce cellular signalling independently of ligation to the extracellular matrix. The resultant signals would provide a mechanism for cancer cells to bypass the pro-apoptotic influence which arises from the loss of cell adhesion, known as anoiksis. In support of this hypothesis, the up-regulation of TF expression in cancer cells has been reported to increase adhesion-free cell survival (Versteeg et al., 2004). This mechanism would facilitate cancer progression by allowing increased cell mobility and metastases (Desgrosellier & Cheresh, 2010; Versteeg et al., 2004).

Chapter 6

Assessment of the role of TF depalmitoylation on cellular function

6.1 Introduction

In the previous chapters it was shown that TF enhances the rate of cell proliferation by interacting with PAR2 and β1 integrin. However, it is also known that the post-translational modification of TF regulates the signals initiated by this protein (Belting et al., 2004). The post-translational modifications which influence TF signalling have been demonstrated to include phosphorylation of Ser253 and Ser258 and palmitoylation of Cys245. Furthermore, it has also been shown that depalmitoylation of TF enhances and precedes TF phosphorylation (Collier & Ettelaie, 2011; Dorfleutner & Ruf, 2003). It has been proposed that the mechanisms by which these modifications regulate TF signalling may be by influencing the association of TF with lipid-rafts as well as the packaging and release of TF in MV (Collier et al., 2017).

6.1.1 The role of MV release in the maintenance of cell TF levels

The phosphorylation of TF cytoplasmic domain at Ser253 enhances the packaging of TF into MV and subsequent release from the cell (Collier et al., 2014; Ott et al., 1998). The expression of a mutant form of TF which could not be phosphorylated (Ser253Ala) in HCAEC prevented the release of TF within MV. The prevention of the release of TF in turn leads to the accumulation of TF within cells and was shown to cause cell apoptosis (ElKeeb et al., 2015; Ethaeb et al., 2020). Furthermore, high concentrations of TF (500 nM) have been shown to initiate cellular apoptosis whereas at lower concentrations (5-50 nM) increased rates of cell proliferation were detected (Alkistis Frentzou et al., 2010; Pradier & Ettelaie, 2008). Therefore, the release of TF in MV has been proposed to be a mechanism by which cells can regulate the levels of TF and therefore prevent any pro-apoptotic signalling arising from TF. Additionally, since the depalmitoylation of TF at Cys245 is required for phosphorylation to take place (Collier & Ettelaie, 2011; Collier et al., 2014; Dorfleutner & Ruf, 2003), the palmitoylation of TF may indirectly regulate and discriminate between the rates of cell proliferation and apoptosis.

6.1.2 The association of TF with lipid rafts and the significance in MV release

Lipid rafts are regions within the cell membrane which contain higher than normal proportions of saturated lipids, cholesterol and sphingolipids (Levental et al., 2020). Furthermore, areas of cell surface membrane from which MV are released have been reported to be rich in lipid rafts (Davizon et al., 2010). Therefore, by targeting TF to the lipid rafts, TF may be more readily packaged into MV. The palmitoylation of proteins has been shown to promote the translocation of proteins to lipid rafts. This partly occurs due to the high affinity of palmitic acid chains for the association with cholesterol and sphingolipid molecules (Edidin, 2003; Levental et al., 2010). In support of this hypothesis, studies

using buoyant density gradient centrifugation and immunofluorescence confocal microscopy have shown TF to localise within lipid rafts (Awasthi et al., 2007).

The membrane in lipid raft domains tends to be thicker than other areas of the membrane. This is due to the interaction of cholesterol with the hydrocarbon chains of neighbouring phospholipids, resulting in the phospholipids adopting a more extended conformation (Cassera et al., 2002; Maulik & Shipley, 1996). These differences in the thickness of the membrane determine the membrane proteins that can be accommodated and therefore influences the distribution of transmembrane proteins in accordance with the length of their transmembrane domain (Figure 6.1) (Bretscher & Munro, 1993; Munro, 1995). The transmembrane domain of TF consists of 22 amino acid residues (Figure 6.2A). This is slightly shorter than the average length for an integral plasma membrane protein which is 24 residues (Butenas, 2012). However, the domain also contains a hydrophobic leucine residue (Leu242) at the cytoplasmic end. The Leu242 residue is separated from the rest of the hydrophobic residues of the transmembrane domain by a hydrophilic serine residue (Ser241) (Morrissey et al., 1987; Spicer et al., 1987). Therefore, it is possible that the Ser241 and Leu242 residues may also be capable of contributing to the length of the transmembrane domain under some circumstances (Figure 6.2B). Furthermore, palmitoylation of TF may further regulate the length of the transmembrane domain by altering the local hydrophobicity. Consequently, this configuration may maintain the TF in a conformation which favours the association with the thicker domains of the membrane.

Previous work has shown that preventing the phosphorylation of TF initiates cellular signalling that results in cell apoptosis. The phosphorylation of TF is also known to be a pre-requisite requirement for the depalmitoylation of the protein. Therefore, it was hypothesised that the depalmitoylation of TF was a required step within this cellular signalling pathway that results in cell apoptosis. In addition, the mechanism by which depalmitoylation participates in the signalling pathway was hypothesised to be by altering the translocation of TF to different membrane domains such as lipid rafts.

Figure 6.1:Proposed mechanisms for the sorting of proteins into different membrane domains according to the length of the transmembrane domain

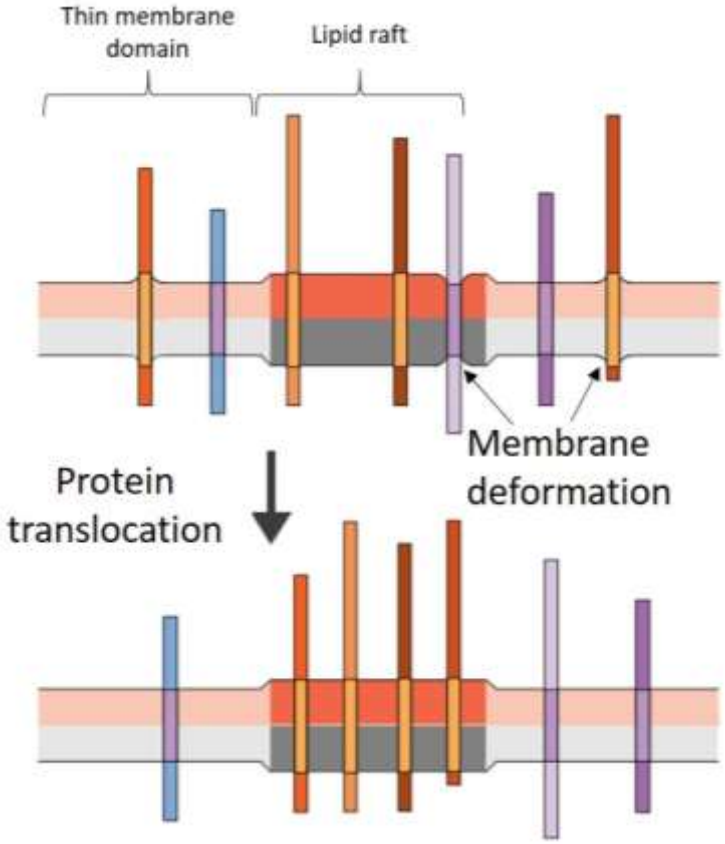

The localising of integral proteins, which have long transmembrane domains (orange), within thinner membrane domains results in deformation of the membrane which is energetically unfavourable. As a result of this deformation, the proteins will be translocated into thicker lipid raft domains within the membrane (Mouritsen & Bloom, 1993) (Diagram adapted from Sharpe et al. (2010)).

Figure 6.2: TF transmembrane domain

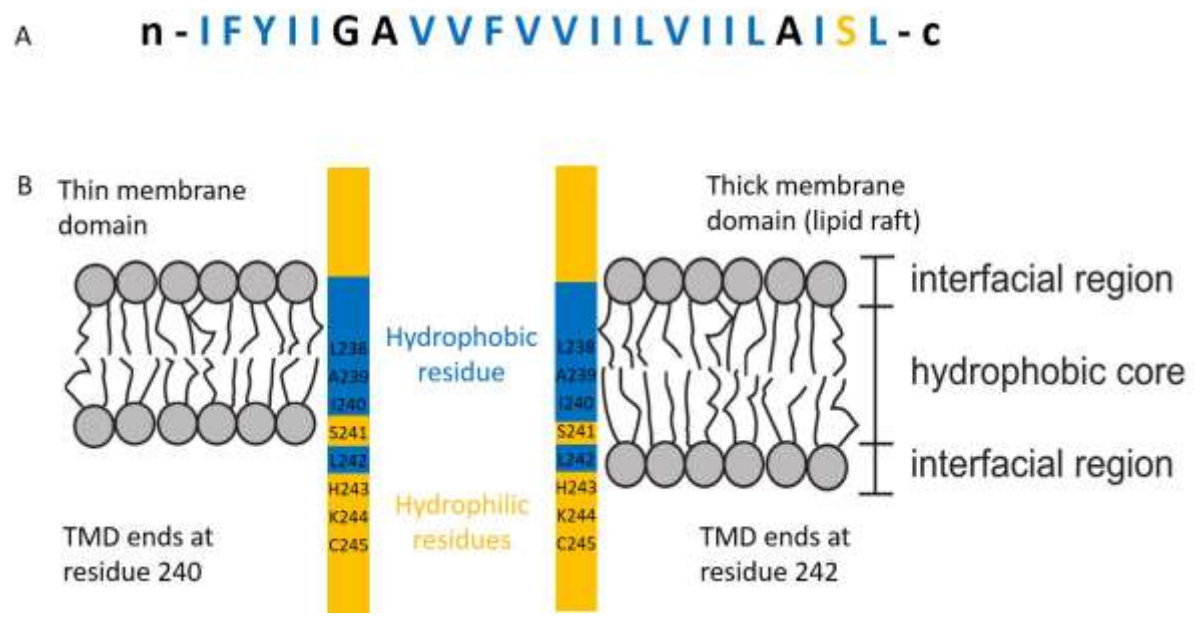

A) The amino acid sequence of TF transmembrane domain (residues 220-242). Hydrophobic residues are depicted in blue, hydrophilic residues in orange and neutral residues in black. B) Suggested positioning of residues at the c-terminus of TF transmembrane domain when situated in membrane domains of different thicknesses.

6.1.3 Aims

The aim of this study was to investigate the influence of phosphorylation and palmitoylation of the cytoplasmic domain of TF on the regulation of cell proliferation and apoptosis. Mutant forms of TF were utilised which either mimicked phosphorylated and palmitoylated forms of TF, or were prepared to prevent these post-translational modifications. In addition, mutant forms of TF in which the length of the transmembrane domain had been altered were used to assess the influence of the association of TF with different membrane domains, and its outcome on cellular proliferation and apoptosis. Cell lines and primary cells were transfected to express these mutant forms of TF and the rates of proliferation and apoptosis were assessed.

6.2 Methods

6.2.1 Transfection of cells to express wild-type or mutated forms of TF

MCF-7 cells and HCAEC were plated as specified in sections 6.2.2.2 and 6.2.3. All plates were then incubated at 37°C overnight to allow cells to adhere. Sets of cells were transfected with the pCMV6-AC-tGFP plasmid containing wild-type or mutated forms of TF (detailed in Table 6.1), as well as empty vector, using TransIT 2020 transfection reagent (section 2.3.2.6). The cells were incubated for 2 days to allow the expression of the TF proteins. The media was removed from the cells and replaced with either fresh media containing PAR2-AP (20 µM) or untreated fresh media. The plates were then incubated for a further 24 h prior to use in either the crystal violet assay or TiterTACS™ apoptosis assay.

6.2.2 Assessment of the influence of the phosphorylation or palmitoylation of TF on cell apoptosis

6.2.2.1 Principle of the TiterTACS apoptosis assay

The TiterTACS™ Colourimetric Apoptosis Detection Kit detects DNA fragmentation which occurs in the late stages of apoptosis. A terminal deoxynucleotidyl transferase (TdT) enzyme catalyses the addition of biotinylated nucleotide to the 3' hydroxyl terminus of single- or double-stranded DNA breaks. A streptavidin-HRP complex is then used to label the biotinylated nucleotides. The amount of streptavidin-HRP complex bound is then measured by using a chromogenic HRP substrate (Figure 6.3). This assay was previously optimised for use with MCF-7 cells and HCAEC within the laboratory (Ethaeb, 2018).

6.2.2.2 TiterTACS assay protocol

In order to assess the influence of the phosphorylation or palmitoylation of TF on the rate of cell apoptosis, MCF-7 cells and HCAEC (3×10^4) were plated out in 96-well plates. The cells were transfected with wild-type or mutated forms of TF and were then activated with PAR2-AP as detailed in section 6.2.1. The cells were fixed, first by incubation with formaldehyde (4% v/v) for 5 min and then with methanol (100%) for 20 min. The cells were washed twice with PBS (200 µl) and were then permeabilised using 50 µl Cytonin (provided in the kit) for 15 min. The cells were washed twice with distilled water (200 µl), incubated with hydrogen peroxide (3% v/v in methanol) for 5 min and washed once more with distilled water (200 µl). The cells were then incubated with 100 µl of TdT labelling buffer (TACS Safe-TdT™ Buffer (0.1 M), BSA (0.05 mg/ml) and 2-mercaptoethanesulfonic acid (0.06 mM) for 5 min at room temperature. The buffer was removed and replace with 30 µl of TdT labelling solution (TdT labelling buffer, biotinylated nucleotide (1.75 µM), TdT enzyme (7 µl/ml)

Table 6.1: Residue changes in mutant forms of TF and predicted results of the mutations

Residue position	WT residue	Mutant residue	Effect of mutation
253	Ser	Ala	Can not be phosphorylated
253	Ser	Arg	Phosphorylation mimic
245	Cys	Ser	Can not be palmitoylated
245	Cys	Phe	Palmitoylated mimic
241/242	Ser/Leu	Deletion	Shorten the transmembrane domain
243/244	Ser/Leu	Addition	Lengthening the transmembrane domain

Figure 6.3: Schematic of the TiterTACS™ colourimetric apoptosis detection kit

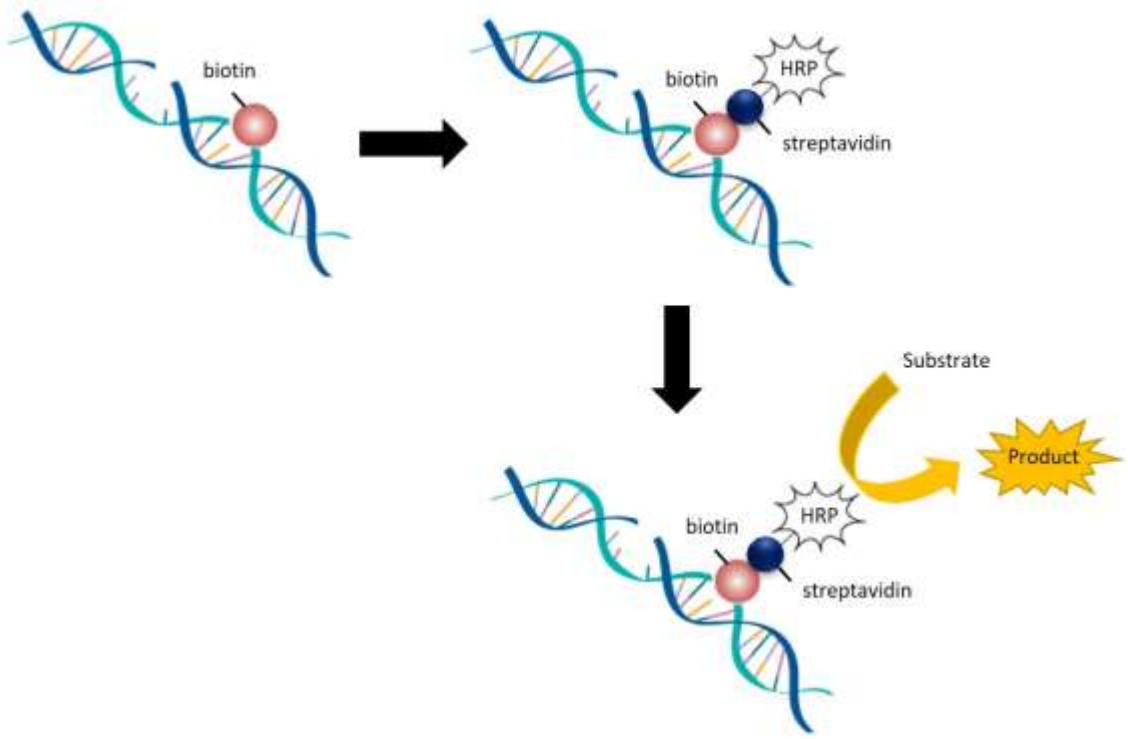

TiterTACS detects DNA breaks generated during apoptosis by using terminal deoxynucleotidyl transferase to attach biotinylated nucleotide to the 3’ hydroxyl terminus of single- or double-stranded DNA breaks. The biotin is bound by streptavidin conjugated to a HRP enzymes, which acts on a chromogenic substrate and produces a coloured product that can be detected and quantified using a plate reader.

and Mn^{2+} (20 µl/ml)) and the cells were incubated for 1 h at 37°C. The labelling reaction was stopped using 100 µl of stop solution (0.01 M EDTA, pH 8.0) and the cells were incubated for 5 min at room temperature. The cells were then washed twice with PBS and the provided streptavidin-HRP solution (50 µl) was added to each well. The cells were incubated for 10 min at room temperature and were then washed 4 times with PBST. The provided TACS-Sapphire solution (100 µl) was added to each well and the colour developed for 30 min, at room temperature in the dark. The reaction was stopped using 100 µl of hydrochloric acid (0.2 M) and the absorption of the samples was measured at 450 nm using a plate reader. The plates were retained in order to determine the number of cells using the crystal violet assay (section 2.3.2.10).

6.2.3 Assessment of the influence of the phosphorylation or palmitoylation of TF on cell proliferation

Prior to experiments, a standard curve was generated by plating a range of quantities of MCF-7 cells (0.01-0.2 million cells) in 12-well plates. The cells were incubated for 5 h at 37°C to allow the cells to adhere. The cells were then fixed with 3% (v/v) glutaraldehyde and the crystal violet assay performed as detailed in section 2.3.2.10. The absorption values were determined at 584 nm using a plate reader and a standard curve constructed (Figure 6.4). A standard curve for primary endothelial cells had previously been generated (Figure 4.7).

In order to assess the influence of the phosphorylation or palmitoylation of TF on the rate of cell proliferation, MCF-7 cells and HCAEC (1.5×10^5) were plated in 12-well plates. The cells were transfected with wild-type or mutated forms of TF and were then activated with PAR2-AP as detailed in section 6.2.1. The absorption values were determined at 584 nm using a plate reader and were used to determine the cell number from the respective standard curve.

Figure 6.4: Standard curve for determining cell numbers using the crystal violet assay

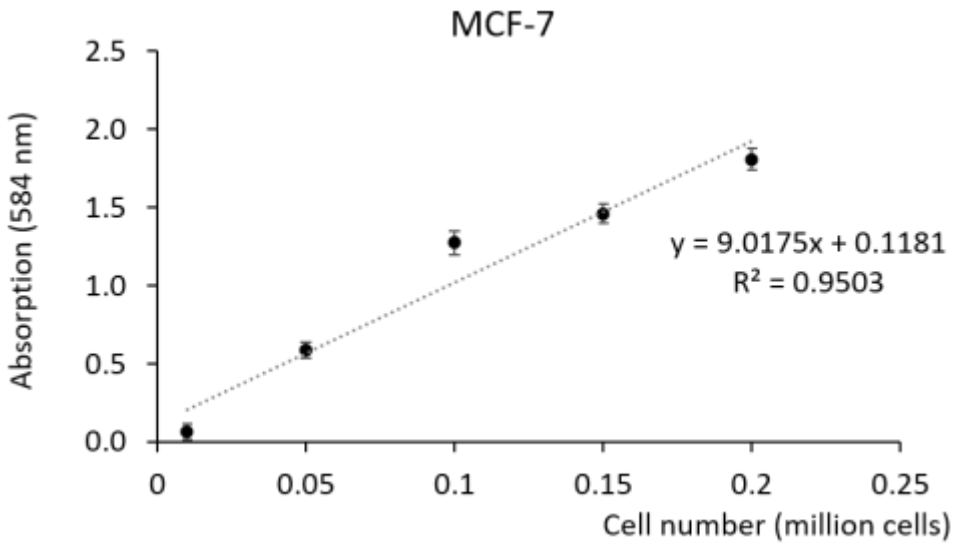

MCF-7 cells (0.01-0.2 x 10^6 cells) were plated in 12-well plates and allowed to adhere overnight. The number of cells were determined using the crystal violet assay and the absorption measured at 584 nm using a plate reader (n=4).

6.3 Results

6.3.1 Assessment of the influence of the phosphorylation of TF on cell apoptosis and proliferation

Mutation of Ser253Ala within TF has previously been used to prevent the phosphorylation of TF and the subsequent incorporation and release of the protein within MV (Collier et al., 2014; Ott et al., 1998). Furthermore, following activation of PAR2 on primary endothelial cells, the inability of cells to disperse excess TF within MV leads to the induction of apoptosis in the cells (ElKeeb et al., 2015; Ethaeb et al., 2020). Initially, the ability of the Ser253Ala substituted TF to promote cell apoptosis was confirmed in HCAEC and MCF-7 cells. The activation of PAR2 in cells expressing this form of TF resulted in increased levels of apoptosis (Figure 6.5A & Figure 6.5B). These increases were also concurrent with reductions in cell numbers (MCF-7 = 24,500 cells ± 4,000, HCAEC = 24,800 cells ± 1,100) compared to cells expressing the wild-type TF (MCF-7 = 71,700 cells ± 9,000, HCAEC = 59,200 cells ± 2,000) (Figure 6.5C & Figure 6.5D). In contrast, expression of the Ser253Asp substituted TF, which mimicked the phosphorylated protein, did not influence the level of apoptosis in MCF-7 cells (Figure 6.5A). This is in agreement with a previous study performed using HCAEC (ElKeeb et al., 2015). However, expression of the Ser253Asp substituted TF in MCF-7 cells resulted in a decrease in cell numbers to 20,500 ± 3,100 compared with cells expressing wild-type protein (71,700 cells ± 9,000) (Figure 6.5C). This is in contrast to the study performed using HCAEC, which reported that expression of the Ser253Asp substituted TF resulted in a small increase in cell proliferation (ElKeeb et al., 2015).

6.3.2 Assessment of the influence of the palmitoylation of TF on cell apoptosis and proliferation

Since depalmitoylation precedes and is required for the phosphorylation of TF (Collier & Ettelaie, 2011; Collier et al., 2014; Dorfleutner & Ruf, 2003), the influence of the palmitoylation of TF on cell apoptosis was assessed next. Expression of TF in which palmitoylation was mimicked by Cys245Phe substitution resulted in increased levels of apoptosis in HCAEC (Figure 6.6B) but not MCF-7 cells (Figure 6.6A). In addition, expression of the Cys245Phe substituted TF in HCAEC resulted in a concurrent decrease in cell numbers to 11,600 ± 800 compared with cells expressing wild-type TF (59,200 cells ± 4,000) (Figure 6.6D). In contrast, expression of Cys245Ser substituted TF which could not be palmitoylated resulted in a reduction in the level of apoptosis (Figure 6.6B). This reduction in apoptosis was reflected in the increase in cell numbers to 69,900 ± 600 compared to cells expressing the wild-type TF (59,200 cells ± 4,000) (Figure 6.6D). However, the expression of the Cys245Ser

Figure 6.5: Assessment of the influence of the phosphorylation of TF on cell proliferation and apoptosis

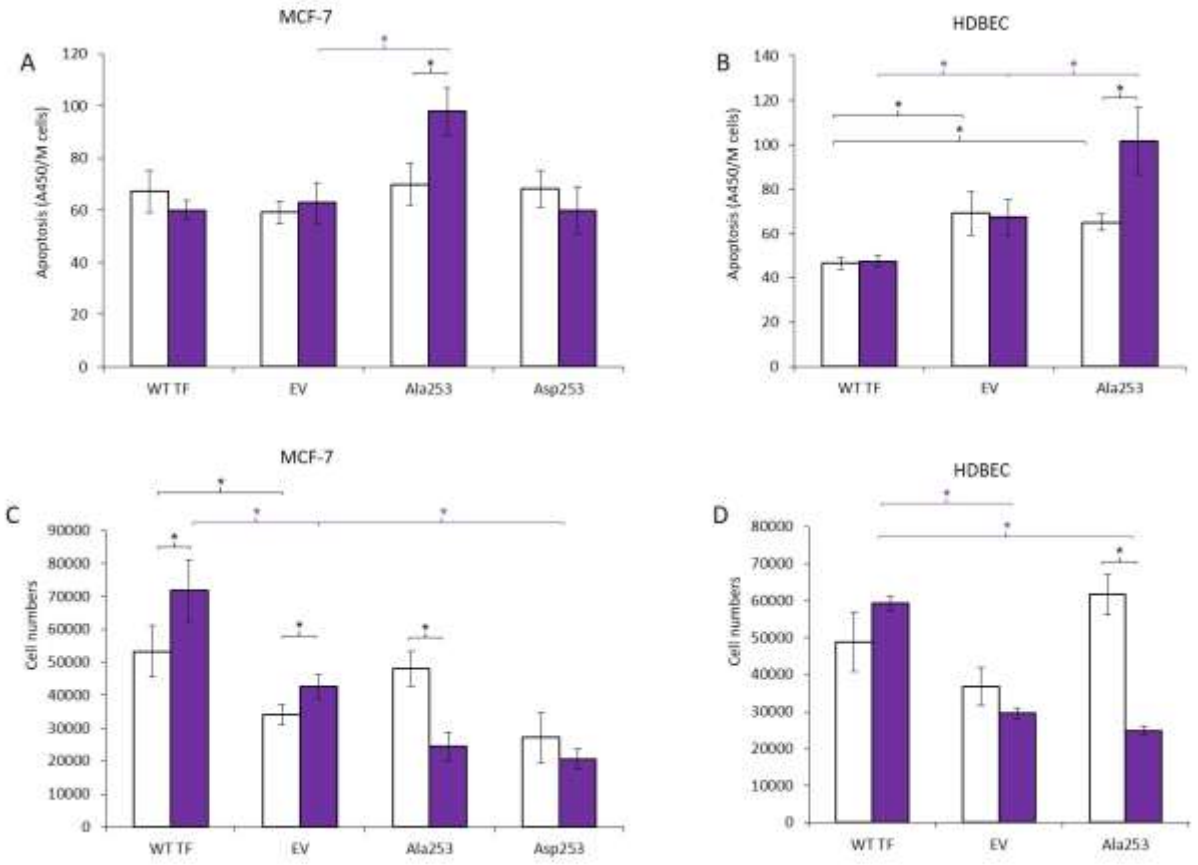

A) MCF-7 cells and B) HCAEC (3×10^4) were transfected to express either wild-type (WT) TF, the Ala253 and Asp253 mutant forms of TF or empty vector (EV). Sets of the cells were activated using PAR2-AP (20 µM) for 24 h prior to assessment. The rate of apoptosis was determined using the TiterTACS chromogenic TUNEL assay (n=6; two experiments carried out in triplicate; * = $p < 0.05$). C) MCF-7 cells and D) HCAEC (5×10^4) were transfected to express either wild-type (WT) TF, the Ala253 and Asp253 mutant forms of TF or empty vector (EV). Sets of the cells were activated using PAR2-AP (20 µM) for 24 h prior to assessment. The cells were examined by crystal violet assay to quantify cell numbers (n=9; three experiments carried out in triplicate; data = mean values ± SEM; one-way ANOVA, * = $p < 0.05$, unmarked = not significant).

Figure 6.6: Assessment of the influence of the palmitoylation of TF on cell proliferation and apoptosis

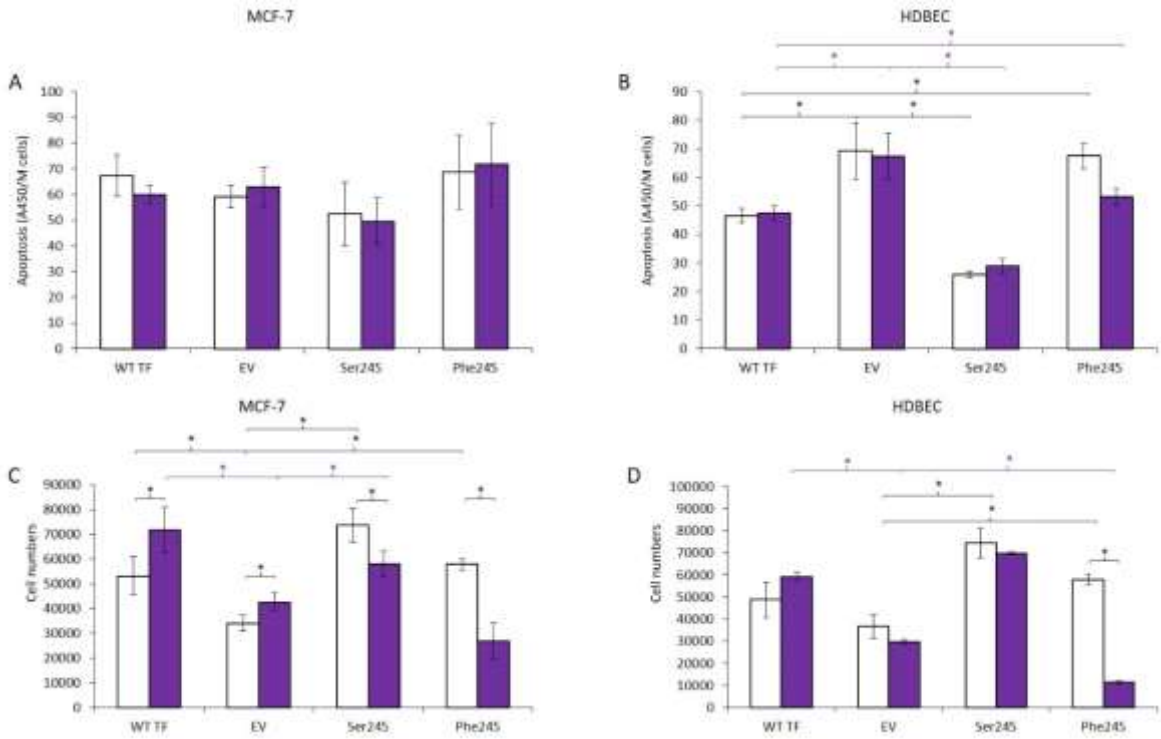

A) MCF-7 cells and B) HCAEC (3×10^4) were transfected to express either wild-type (WT) TF, the Ser245 and Phe245 mutant forms of TF or empty vector (EV). Sets of the cells were activated using PAR2-AP (20 µM) for 24 h prior to assessment. The rate of apoptosis was determined using the TiterTACS chromogenic TUNEL assay (n=6; two experiments carried out in triplicate; * = $p < 0.05$). C) MCF-7 cells and D) HCAEC (5×10^4) were transfected to express either wild-type (WT) TF, the Ser245 and Phe245 mutant forms of TF or empty vector (EV). Sets of the cells were activated using PAR2-AP (20 µM) for 24 h prior to assessment. The cells were examined by crystal violet assay to quantify cell numbers (n=9; three experiments carried out in triplicate; data = mean values ± SEM; one-way ANOVA, * = $p < 0.05$, unmarked = not significant).

substituted TF in MCF-7 cells had no influence on either cell apoptosis or numbers (Figure 6.6A & Figure 6.6C).

6.3.3 Assessment of the influence of the palmitoylation of TF on cell apoptosis and proliferation

The translocation of integral proteins between membrane domains with different thicknesses is known to be dependent on the length of the transmembrane domain within the protein (Mouritsen & Bloom, 1993). Therefore, alterations in the length of transmembrane domain of TF may interfere with the trafficking of the protein. Expression of TF in which residues Ser241 and Leu242 were deleted (ShortTM) in HCAEC resulted in significant increases in the levels of apoptosis (Figure 6.7B) and concurrent reduction in cell numbers to 14,800 ± 800 compared with cells expressing the wild-type TF (59,200 cells ± 2,000) (Figure 6.7D). Expression of the ShortTM mutant also resulted in a reduction in the number of MCF-7 cells to 22,900 ± 4,200 compared with cells expressing wild-type TF (71,700 cells ± 9,000) (Figure 6.7C) however interestingly, did not influence the rate of apoptosis of MCF-7 cells (Figure 6.7A). Finally, expression of TF in which additional Ser and Leu residues were inserted at positions 243 and 244 (LongTM) resulted in a reduction in the rate of apoptosis (Figure 6.7B) and a concurrent increase in cell numbers (MCF-7 = 57,700 cells ± 7,800, HCAEC = 104,000 cells ± 3,600) (Figure 6.7C & Figure 6.7D).

Figure 6.7: Assessment of the influence of the length of the transmembrane domain of TF on cell proliferation and apoptosis

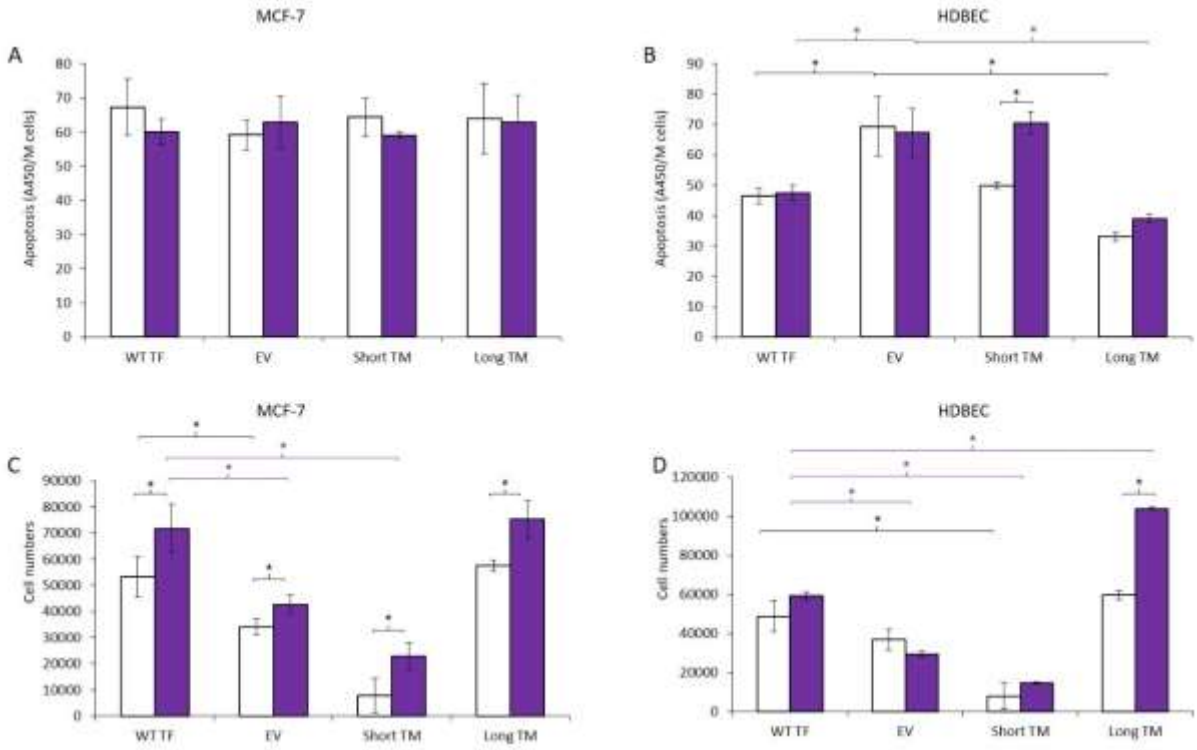

A) MCF-7 cells and B) HCAEC (3×10^4) were transfected to express either wild-type (WT) TF, the ShortTM and LongTM mutant forms of TF or empty vector (EV). Sets of the cells were activated using PAR2-AP (20 μM) for 24 h prior to assessment. The rate of apoptosis was determined using the TiterTACS chromogenic TUNEL assay (n=6; two experiments carried out in triplicate; * = $p < 0.05$). C) MCF-7 cells and D) HCAEC (5×10^4) were transfected to express either wild-type (WT) TF, the ShortTM and LongTM mutant forms of TF or empty vector (EV). Sets of the cells were activated using PAR2-AP (20 μM) for 24 h prior to assessment. The cells were examined by crystal violet assay to quantify cell numbers (n=9; three experiments carried out in triplicate; data = mean values ± SEM; one-way ANOVA, * = $p < 0.05$, unmarked = not significant).

6.4 Discussion

Following injury to the vasculature, endothelial cells are exposed to high levels of TF through the sequestering of TF-bearing MV from the bloodstream (Lima et al., 2013). Additionally, the exposure of the cells to pro-inflammatory factors can also induce TF expression in these cells (Herbert et al., 1992; Martin et al., 1993). However, cells located closer to the site of the injury acquire much higher levels of TF then those in the surrounding area. The acquisition of TF by the cells initiates a signalling pathway which, depending on the amount of TF that the cells are exposed to, determines the fate of the cells (Ethaeb et al., 2020). Therefore, TF signalling must be stringently regulated to prevent inappropriate termination or propagation of cells. One way by which TF signalling may be regulated is by trafficking of the protein to different membrane domains (Morrissey et al., 2012). The localisation of integral proteins within different membrane domains is determined by the length of the transmembrane domain of proteins (Mouritsen & Bloom, 1993). Furthermore, altering the length of the transmembrane domain is known to influence the function of various receptor proteins. One means by which the length of the transmembrane domain of TF may be modified is through the palmitoylation/depalmitoylation of the protein (Charollais & Van Der Goot, 2009). Therefore, in this study the influence of mutating the Cys245 palmitoylation site or altering the transmembrane domain length of TF on cellular apoptosis was assessed. The expression of mutant forms of TF in which the transmembrane domain had been artificially extended prevented cell apoptosis, whereas shortening the length of the domain promoted apoptosis (Figure 6.7). Additionally, this was also achievable by mutating the site of palmitoylation within TF. The expression of mutant forms of TF which mimicked the palmitoylation resulted in the increase in the rates of apoptosis in cells, while preventing palmitoylation suppressed cellular apoptosis (Figure 6.6). Therefore, this study suggested that depalmitoylation of TF occurs in response to PAR2 activation and result in the extension of the transmembrane domain of the protein. Furthermore, these findings may suggest that depalmitoylation of TF is the first stage in a signalling pathway which determines cell fate following injury to vasculature. The consequence of the extension of the transmembrane domain of TF is that it allows the protein to translocate into thicker lipid raft membrane domains (Cassera et al., 2002; Mouritsen & Bloom, 1993). Lipid rafts are known to facilitate cell signalling by being the site of assembly of receptor-coreceptor complexes and secondary signalling proteins (Simons & Toomre, 2000). One of the signalling proteins associated with lipid rafts is PKCα (Davizon et al., 2010) which is known to be responsible for the phosphorylation of TF at Ser253 (Wu et al., 2013; Zioncheck et al., 1992). The phosphorylation of TF allows the binding of filamin-A which leads to the incorporation of TF into MV (Collier & Ettelaie, 2011; Ott et al., 1998). In addition, TF-bearing MV are known to form from membrane regions which are rich in lipid rafts (Davizon et al., 2010), therefore, the presence of

TF within lipid rafts may also enhance the incorporation of TF into MV. The incorporation and release of TF within MV in turn results in the reduction in the amount of remaining TF on the cell surface. Subsequently, if the TF levels on the cell persist at an elevated level, for example when in close proximity of the injury, cellular apoptosis may be initiated to prevent aberrant growth. In contrast, if the majority of the cellular TF is dissipated, for example in less injured cells, then the processing of TF will induce a transient increase in cell proliferation. In addition, since the majority of the cellular TF is removed, no further activation of PAR2 may occur and the cell would return to a resting state. This mechanism ensures the self-regulation of the signalling pathway allowing for the determination of the level of injury. It is therefore clear that TF signalling requires strict regulation to prevent the growth of unhealthy cells. Moreover, inappropriate activation of the pathway could lead to uncontrolled cell growth as observed in some cancer cells.

In conclusion, this study examined the regulatory function of palmitoylation for the strict control of TF signalling. It was indicated that depalmitoylation of TF leads to the elongation of the transmembrane domain which in turn, results in the trafficking and release of TF within MV. This pathway results in the self-regulation of the amount of TF on a cell as well as determining the fate of cells as a response to injury.

Chapter 7

General Discussion

Cancer patients are known to develop a hypercoagulable state which often manifests as increased prevalence of VTE (Langer & Bokemeyer, 2012; Nadir, 2019). In turn, this hypercoagulable state has been shown to promote tumour growth, metastasis and angiogenesis (Langer & Bokemeyer, 2012; Unruh & Horbinski, 2020). Therefore, the control of coagulation using anticoagulants may have benefits other than preventing VTE such as having specific anti-cancer actions. The evidence for the beneficial properties of the LMWH family of anticoagulants has not just been limited to clinical observations and administration of LMWH in animal models has been shown to reduce the growth of xenograft tumours and associated vasculature (Lee et al., 2009; Takahashi et al., 2005). Among the possible mechanisms proposed for the effectiveness of LMWH in inhibiting cancer growth, one explanation involves the suppression of the effects of coagulation proteases within the tumour environment. In this study, the actions of two therapeutic LMWH preparations were compared to those of the direct fXa inhibitors, apixaban and rivaroxaban. While tinzaparin was capable of reducing cancer cell adhesion, invasion and angiogenesis, these outcomes were not observed with apixaban and rivaroxaban. Therefore, the inhibition of coagulation was ruled out as a possible mechanism for the anticancer properties of LMWH. However, the observation in this study that LMWH possess anticancer properties beyond their anticoagulant activities may provide an explanation for the reports that cancer patients treated with anticoagulants other than LMWH did not receive the significant improvements in long-term survival compared to patients treated with LMWH (Altinbas et al., 2004; Di Nisio et al., 2016; Kakkar et al., 2004; Klerk et al., 2005). Other proposed mechanisms by which LMWH suppress cancer growth and angiogenesis include interfering with the binding of growth factors to their respective receptors (Norrby, 2006). Therefore in this study, the anti-angiogenic influence of tinzaparin was compared to that of the VEGF blocker, bevacizumab. Tinzaparin was found to reduce both the density and the diameter of CAM blood vessels, indicated by inhibition of the formation of both capillaries and larger arterioles and venules (Figure 3.16). This is in agreement with findings that the LMWH nadroparin reduced the average dimeter of vessels within a rodent dorsal skinfold chamber model (Debergh et al., 2010). In contrast, bevacizumab reduced the density of the CAM vessels, but not the average dimeter, by inhibiting the formation of capillaries alone (Figure 3.17). This suggested that the mechanisms by which tinzaparin inhibits angiogenesis is through the blockage of the binding of multiple growth factors which induce both capillary formation and vessel maturation. Whereas VEGF and bFGF are known to induce the endothelial cell proliferation and migration which occurs at the early stages of angiogenesis (Steffens et al., 2004), PDGF and HB-EGF stimulate the migration of pericytes and vascular smooth muscles cells which encapsulate and stabilise blood vessels during vessel maturation (Abramsson et al., 2003; Stratman et al., 2010). LMWH have previously been shown to interfere with the binding of all 4 of

these growth factors (Ettelaie et al., 2011b; Lustig et al., 1996), therefore, supporting the finding that LMWH may influence both endothelial cells and pericytes during vessel formation. Interestingly, there is evidence that pericyte recruitment reduces the susceptibility of tumour vessels to anti-angiogenic treatment (Haibe et al., 2020). For example, treatment of cancer xenografts with bevacizumab resulted in increased pericyte coverage around the remaining vessels which in turn lead to decreased vessel permeability to therapeutic compounds (Arjaans et al., 2013). Therefore, the combined inhibition of endothelial cells and pericytes may have advantages over treatment targeting just endothelial cells. In support of this, tyrosine kinase inhibitors that block both VEGFR and PDGFR have been shown to be more effective in combination then when used separately (Bergers et al., 2003; Erber et al., 2004). Therefore, the ability of LMWH to inhibit both capillary formation and vessel maturation may give it advantages over anti-VEGF therapies.

Although the treatment of CAM-implanted xenografts with apixaban did not inhibit blood vessel formation, it did result in the reduction in the growth of the xenograft tumours (Figure 3.19). Interestingly, this property was unique to apixaban and not observed on treatment with rivaroxaban. In addition, apixaban, but not rivaroxaban was also observed to reduce MV release from cancer cells in the absence of exogenous proteases (Figure 4.27). This demonstration of the ability of apixaban to inhibit tumour growth is a novel finding and suggests that apixaban may have additional activities aside from the inhibition of fXa. Subsequently, an attempt was made to characterise the mode of action of apixaban in the inhibition of cancer growth and MV release. It is known that the activation of PAR2 on cells results in increased proliferation (Nishibori et al., 2005; Shimamoto et al., 2004) and the induction of MV release (Collier & Ettelaie, 2011; Koizume et al., 2016). Therefore, it was proposed that apixaban may suppress cancer growth and MV release by inhibiting the activation of PAR2. In fact the data generated in this study indicated that apixaban was capable of inhibiting activation of PAR2 by fVIIa (Figure 4.36) to a similar magnitude as an inhibitory anti-fVIIa antibody (Figure 4.35). Recently it has been reported that multiple cancer cell types express fVII(a) (Koizume et al., 2006; Madkhali et al., 2019; Magnus et al., 2010; Yokota et al., 2009). This suggested that apixaban may suppress cell proliferation by inhibiting the actions of endogenously expressed fVIIa and is also the first report showing that endogenous expression of fVIIa may promote cancer cell proliferation. However, the expression of fVIIa has previously been reported to be capable of increasing cancer cell migration and invasion, as well as the release of MV in ovarian cancer cells (Koizume et al., 2006; Yokota et al., 2009). Therefore, it is possible that apixaban may also suppress cancer migration and invasion. Importantly, whilst apixaban suppressed the growth of cancer cells, the growth of primary endothelial cells remained unaltered since these cells do not normally express

TF. Therefore, the inhibition of TF/fVIIa by apixaban may selectively inhibit the growth of cancer cells whilst leaving healthy cells unaffected. The lack of any direct cytotoxic effects of apixaban, as evident by the lack of activity against endothelial cells, stipulates that apixaban may potentially be utilised in combination with chemotherapy treatments.

On the whole, the examination of the anticancer properties of different anticoagulants indicated that tinzaparin inhibits cancer cell invasion and may interfere with the binding of growth factors which promote angiogenesis and vessel maturation within tumours. In contrast, apixaban suppressed cancer cell proliferation by inhibiting the activation of PAR2 by the TF/fVIIa complex. This knowledge of the specific mechanisms of the anticancer properties of anticoagulants may aid the selection of appropriate treatments, specific for different patients.

In addition to activating PAR2, TF may also influence cell proliferation through direct interaction with β1 integrin (Collier & Ettelaie, 2010; Kocaturk et al., 2013). The mechanism by which the interaction between TF and integrins can promote cell proliferation is not currently well understood. However, a competitor-peptide corresponding to the EGF4 and βTD domains of β1 integrin has been shown to inhibit TF-induced proliferation (Collier & Ettelaie, 2010). Therefore, the binding site for the interaction of TF and β1 integrin appeared to be located within the EGF4-βTD domains of the latter protein. In agreement with the previous report, this study identified the lower fibronectin-like domain of TF as capable of interacting with the βTD domain while the upper fibronectin-like domain interacted with the EGF4 domain of β1 integrin (Figure 5.41). The βTD domain contains a structural loop which is in contact with residues within the head group of the protein (Figure 5.42) and maintains the integrin in the closed/inactive conformation (Arnaout et al., 2005). Therefore, the interaction of TF with the βTD domain is likely to disrupt the structural loop releasing the head-group. This in turn allows β1 integrin to adopt the open/active conformation and initiate signalling which promotes cell proliferation (Vitale et al., 1997). Furthermore, this mechanism of activation of β1 integrin by TF may permits integrin signalling even in the absence of engagement with extracellular matrix which allows anchorage-independent survival, often associated with metastasising cancer cells (Desgrosellier & Cheresh, 2010; Versteeg et al., 2004). This is in agreement with previous studies which report TF is capable of enhancing anchorage-independent survival (Shaker et al., 2017; Versteeg et al., 2004).

In addition to identifying the interacting sites between TF and β1 integrin, in this study it was also shown that knockdown of fVIIa in cells reduces the interaction between TF and β1 integrin (Figure 5.23). This agrees with previous reports that the association between TF and β1 integrin in cancer cells is dependent on fVIIa (Rothmeier et al., 2017; Versteeg et al., 2008b). However, there is also evidence that fVIIa is not essential for TF/β1 integrin complex formation in primary endothelial cells (Collier & Ettelaie, 2010). Therefore, the role of fVIIa in the interaction between TF and β1 integrin formation requires further clarification. In addition, it has been proposed that β1 integrin regulates the proliferative signal arising from the activation of PAR2 by the TF/fVIIa complex (Versteeg et al., 2008b). In support of this, blockage of the activation of β1 integrin with an inhibitory antibody (AIIB2) was shown to inhibit IL-8 mRNA expression following activation of PAR2 (Versteeg et al., 2008b). Similarly, blocking of β1 integrin using the same antibody suppressed the phosphorylation of Src1 in response to PAR2 activation (Ethaeb et al., 2020). The mechanism by which β1 integrin regulates PAR2 signalling has been proposed to involve the direct interaction of β1 integrin to the TF/fVIIa complex. This interaction may alter the conformation of the TF/fVIIa complex into a configuration that is capable of digesting PAR2 at an accelerated rate (Versteeg et al., 2008b). However, in addition to the above evidence indicating a regulatory role of β1 integrin in TF/PAR2 signalling, there is also evidence that the TF/β1 integrin complex may induce signals independently of PAR2. For example, supplementation of HCAEC with TF induced proliferation which was not suppressed by incubation with a fVIIa-blocking antibody (Collier & Ettelaie, 2010). Similarly, the interaction between the TF/fVIIa complex with β1 integrin has been reported to result in increased ERK phosphorylation and up-regulation of IL-8 expression. These increases were not dependant on fVIIa activity and were not altered by substitution by active site-blocked fVIIa (Rothmeier et al., 2018). Furthermore, a recent study reported that binding of β1 integrin to the TF/fVIIa complex in HUVEC actively impedes the activation of PAR2 by trafficking the TF/fVIIa complex to endosomal compartments (Rothmeier et al., 2019). To date the capability of β1 integrin to form a complex with PAR2 has not been assessed. To further elucidate the mechanisms by which TF signalling occurs, the associations of TF, fVIIa, PAR2 and β1 integrin on the cell membrane needs to be examined and compared to that in cells lacking either fVIIa, or TF. Furthermore, examination of the association between TF/fVIIa/β1 integrin in the presence or absence of PAR2 activation should produce further indications of the mechanisms involved.

The stated interactions of TF with fVIIa, β1 integrin and PAR2 at the cell surface and signalling arising from these interactions has been shown to influence cell proliferation and apoptosis. High concentrations of TF have been shown to initiate cellular apoptosis whereas lower concentrations of

TF promote cell proliferation (Alkistis Frentzou et al., 2010; Pradier & Ettelaie, 2008). In addition, some cell lines have been shown to utilise the release of TF within MV as a means of self-regulating the level of TF within the cell. The phosphorylation of TF cytoplasmic domain at Ser253 enhances the packaging of TF into MV (Collier et al., 2014; Ott et al., 1998). Therefore, mutant forms of TF which cannot be phosphorylated cannot be packaged into MV and released from cells (Collier et al., 2014). The subsequent build-up of TF within the cell was shown to be capable of inducing apoptosis (ElKeeb et al., 2015). In addition, the cellular localisation of the protein has also been suggested to influence the packaging of the protein into MV. In this study, elongation of the transmembrane domain of TF resulted in a decrease in apoptosis (Figure 6.7). This was proposed to arise from the longer transmembrane domain allowing the translocation of TF to lipid rafts. The membrane composition of lipid rafts has been reported to favour the blebbing of the plasma membrane that produces MV (Davizon et al., 2010; Del Conde et al., 2005). In support of this, cholesterol enrichment of monocytes/macrophages has been shown to stimulate the production of larger quantities of MV in these cells (Liu et al., 2007) whereas pharmacological depletion of cholesterol in activated neutrophils impaired MV release (Del Conde et al., 2005). Furthermore, lipid analysis of MV indicate the presence of relatively high concentrations of cholesterol (Biro et al., 2005) as well as the presence of lipid raft-associated proteins, such as P-selectin glycoprotein ligand-1 (Del Conde et al., 2005). Collectively these data indicate lipid rafts are the domains within the cell membrane from which MV are released. Therefore, the translocation of TF to lipid rafts may be essential for the incorporation of TF into MV. Additionally, the translocation of TF to the lipid raft domains may enhance intracellular signalling since lipid raft domains have been proposed to be sites of assembly of receptors, co-receptors and secondary signalling proteins (Simons & Toomre, 2000). Therefore, the association of TF with lipid rafts may facilitate the interaction of TF with other membrane and signalling proteins. In support of this, the expression of a mutant form of TF with an extended transmembrane domain, which was proposed to localise to lipid rafts, increased the rate of cell proliferation (Figure 6.7). Interestingly, it is possible that the association of TF with lipid rafts may facilitate TF-signalling via both PAR2 and β1 integrin. PAR2 has been observed to be located within lipid rafts and depletion of cholesterol from cell membranes reduces the activation of PAR2 by the TF/fVIIa complex (Awasthi et al., 2007). Similarly, β1 integrin has been shown to reside within lipid rafts in melanoma and epidermoid carcinoma cells (Claas et al., 2001; Thorne et al., 2000). Moreover, activation of the α6β1 integrin receptor with Mg^{2+} ions resulted in increased localisation of this receptor within lipid rafts (Decker & ffrench-Constant, 2004). Previously, it has been suggested that the association between TF and β1 integrin may be important in the incorporation of TF into MV. In support of this hypothesis, TF and β1 integrin have been observed to be co-expressed in MV derived

from numerous cell types, including HCAEC (Ettelaie et al., 2013a), HUVEC (Rothmeier et al., 2019), macrophages (Furlan-Freguia et al., 2011; Rothmeier et al., 2017) and smooth muscle cells (Furlan-Freguia et al., 2011; Schecter et al., 2000). Furthermore, disruption of TF/β1 integrin complexes with a polyclonal anti-TF antibody resulted in a decrease in the levels of β1 integrin on endothelial cell-derived MV (Ettelaie et al., 2013a). The physiological function for the inclusion of β1 integrin in TF-bearing MV may be to permit the binding of MV to exposed extracellular matrix proteins such as collagen, and fibronectin during injury (Ettelaie et al., 2013a; Muralidharan-Chari et al., 2009b). Therefore, the localisation of TF-bearing MV activity to the exposed extracellular matrix could augment the local procoagulant activity at the site of injuries. Finally, as a whole, the various interactions of TF involving fVIIa, PAR2 and β1 integrin as studied in the last two chapters of this work corroborate the precise control of TF signalling. These findings permit opportunities for the use of novel anticoagulants in controlling TF mediated signalling in the future.

7.1 Further research

This study was the first to demonstrate that apixaban suppressed proliferation in cancer cells without having a detrimental effect on primary endothelial cells. Therefore, future research including animal and clinical trials would determine if this *in vitro* finding was translatable by testing if apixaban suppresses cancer growth *in vivo*. In addition, in this study the comparison of the anticancer properties of different anticoagulants indicated distinct mechanisms of action of tinzaparin and apixaban. Furthermore, the efficacy of both anticoagulants varied when utilised on cancer cell lines of differing origins. Therefore, clinical trials on both LMWH and apixaban may identify specific sub-sets of patients who would most benefit from the different anticancer properties of each of the anticoagulants.

In addition, the studies examining TF-mediated signalling indicated that the interaction between TF and β1 integrin required the presence of fVIIa. Therefore, it would be informative to conduct further work to investigate whether the activation of PAR2 by TF/fVIIa is a precursory step which enables the interaction between TF and β1 integrin. Alternatively, the interaction between TF and β1 integrin may enhance the ability of TF/fVIIa to cleave PAR2, a hypothesis that may also be investigated. Finally, there is also evidence that the interaction between TF and β1 integrin influences the packaging and release of both proteins within MV. Therefore, further investigations into the role of the interaction between TF and β1 integrin in the protein composition of MV, and subsequence functions of the vesicles, may prove insightful.

7.2 Concluding Statement

The bidirectional association between coagulation and cancer and the ability of tumours to promote thrombosis has been established for two centuries (Trousseau, 1867). This study examined and demonstrated the anticancer properties of various anticoagulants as potential therapeutic agents, but with dissimilar mechanisms of action. In particular, the novel anticoagulant apixaban, that was previously unknown to possess any anticancer properties. Finally, the study attempted to decipher the molecular interactions of TF with the cell-surface proteins which influence cell proliferation, apoptosis and MV release. In conclusion this study has further elucidated some of the interlinking mechanism between coagulation and cancer.

List of References

Abe, K., Shoji, M., Chen, J., Bierhaus, A., Danave, I., Micko, C., Casper, K., Dillehay, D. L., Nawroth, P. P. & Rickles, F. R. (1999) Regulation of vascular endothelial growth factor production and angiogenesis by the cytoplasmic tail of tissue factor. *Proc Natl Acad Sci U S A*, 96(15), 8663-8.

Aberg, M., Eden, D. & Siegbahn, A. (2020) Activation of beta1 integrins and caveolin-1 by TF/FVIIa promotes IGF-1R signaling and cell survival. *Apoptosis*.

Aberg, M. & Siegbahn, A. (2013) Tissue factor non-coagulant signaling - molecular mechanisms and biological consequences with a focus on cell migration and apoptosis. *J Thromb Haemost*, 11(5), 817-25.

Abramsson, A., Lindblom, P. & Betsholtz, C. (2003) Endothelial and nonendothelial sources of PDGF-B regulate pericyte recruitment and influence vascular pattern formation in tumors. *J Clin Invest*, 112(8), 1142-51.

Adams, M. N., Ramachandran, R., Yau, M. K., Suen, J. Y., Fairlie, D. P., Hollenberg, M. D. & Hooper, J. D. (2011) Structure, function and pathophysiology of protease activated receptors. *Pharmacol Ther*, 130(3), 248-82.

Addgene (2020) *Plasmid Cloning by PCR*, 2020. Available online: https://www.addgene.org/protocols/pcr-cloning/ [Accessed.

Ahamed, J. & Ruf, W. (2004) Protease-activated receptor 2-dependent phosphorylation of the tissue factor cytoplasmic domain. *J Biol Chem*, 279(22), 23038-44.

Ahamed, J., Versteeg, H. H., Kerver, M., Chen, V. M., Mueller, B. M., Hogg, P. J. & Ruf, W. (2006) Disulfide isomerization switches tissue factor from coagulation to cell signaling. *Proceedings of the National Academy of Sciences of the United States of America*, 103(38), 13932-13937.

Akl, E. A., Kamath, G., Kim, S. Y., Yosuico, V., Barba, M., Terrenato, I., Sperati, F. & Schunemann, H. J. (2007) Oral anticoagulation may prolong survival of a subgroup of patients with cancer: a cochrane systematic review. *J Exp Clin Cancer Res*, 26(2), 175-84.

Al-Ani, B., Saifeddine, M., Kawabata, A. & Hollenberg, M. D. (1999) Proteinase activated receptor 2: role of extracellular loop 2 for ligand-mediated activation. *British Journal of Pharmacology*, 128(5), 1105-1113.

Al-Nedawi, K., Meehan, B., Kerbel, R. S., Allison, A. C. & Rak, J. (2009a) Endothelial expression of autocrine VEGF upon the uptake of tumor-derived microvesicles containing oncogenic EGFR. *Proc Natl Acad Sci U S A*, 106(10), 3794-9.

Al-Nedawi, K., Meehan, B., Micallef, J., Lhotak, V., May, L., Guha, A. & Rak, J. (2008) Intercellular transfer of the oncogenic receptor EGFRvIII by microvesicles derived from tumour cells. *Nat Cell Biol*, 10(5), 619-24.

Al-Nedawi, K., Meehan, B. & Rak, J. (2009b) Microvesicles: messengers and mediators of tumor progression. *Cell Cycle*, 8(13), 2014-8.

Alberts, B. (2015) *Molecular biology of the cell*, Sixth edition. edition. New York, NY: Garland Science, Taylor and Francis Group.

Albrektsen, T., Sorensen, B. B., Hjorto, G. M., Fleckner, J., Rao, L. V. & Petersen, L. C. (2007) Transcriptional program induced by factor VIIa-tissue factor, PAR1 and PAR2 in MDA-MB-231 cells. *J Thromb Haemost*, 5(8), 1588-97.

Alkistis Frentzou, G., Collier, M. E., Seymour, A. M. & Ettelaie, C. (2010) Differential induction of cellular proliferation, hypertrophy and apoptosis in H9c2 cardiomyocytes by exogenous tissue factor. *Mol Cell Biochem*, 345(1-2), 119-30.

Altinbas, M., Coskun, H. S., Er, O., Ozkan, M., Eser, B., Unal, A., Cetin, M. & Soyuer, S. (2004) A randomized clinical trial of combination chemotherapy with and without low-molecular-weight heparin in small cell lung cancer. *Journal of Thrombosis and Haemostasis*, 2(8), 1266-1271.

Aoudjit, F. & Vuori, K. (2001) Integrin signaling inhibits paclitaxel-induced apoptosis in breast cancer cells. *Oncogene*, 20(36), 4995-5004.

Arakaki, A. K. S., Pan, W. A. & Trejo, J. (2018) GPCRs in cancer: protease-activated receptors, endocytic adaptors and signaling. *International Journal of Molecular Sciences*, 19(7).
Arderiu, G., Pena, E., Aledo, R. & Badimon, L. (2012) Tissue factor-Akt signaling triggers microvessel formation. *J Thromb Haemost*, 10(9), 1895-905.
Arderiu, G., Pena, E., Aledo, R., Juan-Babot, O. & Badimon, L. (2011) Tissue factor regulates microvessel formation and stabilization by induction of chemokine (C-C motif) ligand 2 expression. *Arterioscler Thromb Vasc Biol*, 31(11), 2607-15.
Arjaans, M., Oude Munnink, T. H., Oosting, S. F., Terwisscha van Scheltinga, A. G., Gietema, J. A., Garbacik, E. T., Timmer-Bosscha, H., Lub-de Hooge, M. N., Schroder, C. P. & de Vries, E. G. (2013) Bevacizumab-induced normalization of blood vessels in tumors hampers antibody uptake. *Cancer Res*, 73(11), 3347-55.
Arnaout, M. A., Mahalingam, B. & Xiong, J. P. (2005) Integrin structure, allostery, and bidirectional signaling. *Annu Rev Cell Dev Biol*, 21, 381-410.
Assoian, R. K. & Schwartz, M. A. (2001) Coordinate signaling by integrins and receptor tyrosine kinases in the regulation of G1 phase cell-cycle progression. *Curr Opin Genet Dev*, 11(1), 48-53.
Awasthi, V., Mandal, S. K., Papanna, V., Rao, L. V. & Pendurthi, U. R. (2007) Modulation of tissue factor-factor VIIa signaling by lipid rafts and caveolae. *Arterioscler Thromb Vasc Biol*, 27(6), 1447-55.
Ay, C., Pabinger, I. & Cohen, A. T. (2017) Cancer-associated venous thromboembolism: Burden, mechanisms, and management. *Thromb Haemost*, 117(2), 219-230.
Ay, C. & Unal, U. K. (2016) Epidemiology and risk factors for venous thromboembolism in lung cancer. *Curr Opin Oncol*, 28(2), 145-9.
Ayers, L., Harrison, P., Kohler, M. & Ferry, B. (2014) Procoagulant and platelet-derived microvesicle absolute counts determined by flow cytometry correlates with a measurement of their functional capacity. *J Extracell Vesicles*, 3.
Ayers, L., Nieuwland, R., Kohler, M., Kraenkel, N., Ferry, B. & Leeson, P. (2015) Dynamic microvesicle release and clearance within the cardiovascular system: triggers and mechanisms. *Clinical Science*, 129(11), 915-931.
Ayoub, M. A. & Pin, J. P. (2013) Interaction of protease-activated receptor 2 with G proteins and beta-arrestin 1 studied by bioluminescence resonance energy transfer. *Front Endocrinol (Lausanne)*, 4, 196.
Bach, R., Konigsberg, W. H. & Nemerson, Y. (1988) Human tissue factor contains thioester-linked palmitate and stearate on the cytoplasmic half-cystine. *Biochemistry*, 27(12), 4227-31.
Bach, R. R. (2006) Tissue factor encryption. *Arterioscler Thromb Vasc Biol*, 26(3), 456-61.
Baker, B. M. & Chen, C. S. (2012) Deconstructing the third dimension: how 3D culture microenvironments alter cellular cues. *J Cell Sci*, 125(Pt 13), 3015-24.
Bao, B., Ali, S., Kong, D., Sarkar, S. H., Wang, Z., Banerjee, S., Aboukameel, A., Padhye, S., Philip, P. A. & Sarkar, F. H. (2011) Anti-tumor activity of a novel compound-CDF is mediated by regulating miR-21, miR-200, and PTEN in pancreatic cancer. *PLoS One*, 6(3), e17850.
Bar-Ner, M., Eldor, A., Wasserman, L., Matzner, Y., Cohen, I. R., Fuks, Z. & Vlodavsky, I. (1987) Inhibition of heparanase-mediated degradation of extracellular matrix heparan sulfate by non-anticoagulant heparin species. *Blood*, 70(2), 551-7.
Bazzoni, G., Shih, D. T., Buck, C. A. & Hemler, M. E. (1995) Monoclonal-antibody 9EG7 defines a novel beta(1) integrin epitope induced by soluble ligand and manganese, but inhibited by calcium. *Journal of Biological Chemistry*, 270(43), 25570-25577.
Beauvais, D. M. & Rapraeger, A. C. (2004) Syndecans in tumor cell adhesion and signaling. *Reprod Biol Endocrinol*, 2, 3.
Belting, M., Ahamed, J. & Ruf, W. (2005) Signaling of the tissue factor coagulation pathway in angiogenesis and cancer. *Arterioscler Thromb Vasc Biol*, 25(8), 1545-50.
Belting, M., Dorrell, M. I., Sandgren, S., Aguilar, E., Ahamed, J., Dorfleutner, A., Carmeliet, P., Mueller, B. M., Friedlander, M. & Ruf, W. (2004) Regulation of angiogenesis by tissue factor cytoplasmic domain signaling. *Nat Med*, 10(5), 502-9.

Bereczky, B., Gilly, R., Raso, E., Vago, A., Timar, J. & Tovari, J. (2005) Selective antimetastatic effect of heparins in preclinical human melanoma models is based on inhibition of migration and microvascular arrest. *Clin Exp Metastasis*, 22(1), 69-76.
Bergers, G., Song, S., Meyer-Morse, N., Bergsland, E. & Hanahan, D. (2003) Benefits of targeting both pericytes and endothelial cells in the tumor vasculature with kinase inhibitors. *J Clin Invest*, 111(9), 1287-95.
Bertolesi, G. E., Lauria de Cidre, L. & Eijan, A. M. (1994) Growth inhibition in vitro of murine mammary adenocarcinoma cells by heparin and chemically modified heparins. *Tumour Biol*, 15(5), 275-83.
Bian, X., Xiao, Y. T., Wu, T., Yao, M., Du, L., Ren, S. & Wang, J. (2019) Microvesicles and chemokines in tumor microenvironment: mediators of intercellular communications in tumor progression. *Mol Cancer*, 18(1), 50.
Bianco, F., Perrotta, C., Novellino, L., Francolini, M., Riganti, L., Menna, E., Saglietti, L., Schuchman, E. H., Furlan, R., Clementi, E., Matteoli, M. & Verderio, C. (2009) Acid sphingomyelinase activity triggers microparticle release from glial cells. *EMBO J*, 28(8), 1043-54.
Bijwaard, K. E., Aguilera, N. S., Monczak, Y., Trudel, M., Taubenberger, J. K. & Lichy, J. H. (2001) Quantitative real-time reverse transcription-PCR assay for cyclin D1 expression: utility in the diagnosis of mantle cell lymphoma. *Clin Chem*, 47(2), 195-201.
Biosciences, B. (2007) BD FACSCalibur Instructions For Use. Available online: [Accessed Feb 2020].
Biro, E., Akkerman, J. W., Hoek, F. J., Gorter, G., Pronk, L. M., Sturk, A. & Nieuwland, R. (2005) The phospholipid composition and cholesterol content of platelet-derived microparticles: a comparison with platelet membrane fractions. *J Thromb Haemost*, 3(12), 2754-63.
Biro, E., Sturk-Maquelin, K. N., Vogel, G. M., Meuleman, D. G., Smit, M. J., Hack, C. E., Sturk, A. & Nieuwland, R. (2003) Human cell-derived microparticles promote thrombus formation in vivo in a tissue factor-dependent manner. *J Thromb Haemost*, 1(12), 2561-8.
Blandin, A. F., Renner, G., Lehmann, M., Lelong-Rebel, I., Martin, S. & Dontenwill, M. (2015) Beta 1 integrins as therapeutic targets to disrupt hallmarks of cancer. *Frontiers in Pharmacology*, 6.
Bobek, V. & Kovarik, J. (2004) Antitumor and antimetastatic effect of warfarin and heparins. *Biomed Pharmacother*, 58(4), 213-9.
Bohm, E., Seyfried, B. K., Dockal, M., Graninger, M., Hasslacher, M., Neurath, M., Konetschny, C., Matthiessen, P., Mitterer, A. & Scheiflinger, F. (2015) Differences in N-glycosylation of recombinant human coagulation factor VII derived from BHK, CHO, and HEK293 cells. *BMC Biotechnol*, 15, 87.
Bohm, S. K., Khitin, L. M., Grady, E. F., Aponte, G., Payan, D. G. & Bunnett, N. W. (1996) Mechanisms of desensitization and resensitization of proteinase-activated receptor-2. *Journal of Biological Chemistry*, 271(36), 22003-22016.
Bonnekoh, B., Wevers, A., Jugert, F., Merk, H. & Mahrle, G. (1989) Colorimetric growth assay for epidermal cell cultures by their crystal violet binding capacity. *Arch Dermatol Res*, 281(7), 487-90.
Booden, M. A., Eckert, L. B., Der, C. J. & Trejo, J. (2004) Persistent signaling by dysregulated thrombin receptor trafficking promotes breast carcinoma cell invasion. *Mol Cell Biol*, 24(5), 1990-9.
Borges, F. T., Reis, L. A. & Schor, N. (2013) Extracellular vesicles: structure, function, and potential clinical uses in renal diseases. *Braz J Med Biol Res*, 46(10), 824-30.
Bouchard, B. A., Krudysz-Amblo, J. & Butenas, S. (2012) Platelet tissue factor is not expressed transiently after platelet activation. *Blood*, 119(18), 4338-9; author reply 4339-41.
Brakebusch, C. & Fassler, R. (2003) The integrin-actin connection, an eternal love affair. *EMBO J*, 22(10), 2324-33.
Bretscher, M. S. & Munro, S. (1993) Cholesterol and the Golgi apparatus. *Science*, 261(5126), 1280-1.
Browder, T., Folkman, J. & Pirie-Shepherd, S. (2000) The hemostatic system as a regulator of angiogenesis. *J Biol Chem*, 275(3), 1521-4.
Broze, G. J., Jr. (1995) Tissue factor pathway inhibitor. *Thromb Haemost*, 74(1), 90-3.
Broze, G. J., Jr. & Majerus, P. W. (1980) Purification and properties of human coagulation factor VII. *J Biol Chem*, 255(4), 1242-7.

Brummel-Ziedins, K., Vossen, C. Y., Rosendaal, F. R., Umezaki, K. & Mann, K. G. (2005) The plasma hemostatic proteome: thrombin generation in healthy individuals. *J Thromb Haemost*, 3(7), 1472-81.
Buijs, J. T., Laghmani, E., van den Akker, R. F. P., Tieken, C., Vletter, E. M., van der Molen, K. M., Crooijmans, J. J., Kroone, C., Le Devedec, S. E., van der Pluijm, G. & Versteeg, H. H. (2019) The direct oral anticoagulants rivaroxaban and dabigatran do not inhibit orthotopic growth and metastasis of human breast cancer in mice. *Journal of Thrombosis and Haemostasis*, 17(6), 951-963.
Burger, D., Turner, M., Xiao, F. X., Munkonda, M. N., Akbari, S. & Burns, K. D. (2017) High glucose increases the formation and pro-oxidative activity of endothelial microparticles. *Diabetologia*, 60(9), 1791-1800.
Butenas, S. (2012) Tissue factor structure and function. *Scientifica (Cairo)*, 2012, 964862.
Butenas, S., Amblo-Krudysz, J. & Mann, K. G. (2012) Posttranslational modifications of tissue factor. *Front Biosci (Elite Ed)*, 4, 381-91.
Buzas, E. I., Gyorgy, B., Nagy, G., Falus, A. & Gay, S. (2014) Emerging role of extracellular vesicles in inflammatory diseases. *Nat Rev Rheumatol*, 10(6), 356-64.
Callander, N. S., Varki, N. & Rao, L. V. (1992) Immunohistochemical identification of tissue factor in solid tumors. *Cancer*, 70(5), 1194-201.
Camerer, E., Gjernes, E., Wiiger, M., Pringle, S. & Prydz, H. (2000a) Binding of factor VIIa to tissue factor on keratinocytes induces gene expression. *J Biol Chem*, 275(9), 6580-5.
Camerer, E., Huang, W. & Coughlin, S. R. (2000b) Tissue factor- and factor X-dependent activation of protease-activated receptor 2 by factor VIIa. *Proc Natl Acad Sci U S A*, 97(10), 5255-60.
Camerer, E., Kataoka, H., Kahn, M., Lease, K. & Coughlin, S. R. (2002) Genetic evidence that protease-activated receptors mediate factor Xa signaling in endothelial cells. *J Biol Chem*, 277(18), 16081-7.
Camerer, E., Rottingen, J. A., Gjernes, E., Larsen, K., Skartlien, A. H., Iversen, J. G. & Prydz, H. (1999) Coagulation factors VIIa and Xa induce cell signaling leading to up-regulation of the egr-1 gene. *J Biol Chem*, 274(45), 32225-33.
Campbell, I. D. & Humphries, M. J. (2011) Integrin structure, activation, and interactions. *Cold Spring Harb Perspect Biol*, 3(3).
Campello, E., Spiezia, L., Radu, C. M., Bulato, C., Castelli, M., Gavasso, S. & Simioni, P. (2011) Endothelial, platelet, and tissue factor-bearing microparticles in cancer patients with and without venous thromboembolism. *Thromb Res*, 127(5), 473-7.
Carmazzi, Y., Iorio, M., Armani, C., Cianchetti, S., Raggi, F., Neri, T., Cordazzo, C., Petrini, S., Vanacore, R., Bogazzi, F., Paggiaro, P. & Celi, A. (2012) The mechanisms of nadroparin-mediated inhibition of proliferation of two human lung cancer cell lines. *Cell Prolif*, 45(6), 545-56.
Carmeliet, P. (2005) Angiogenesis in life, disease and medicine. *Nature*, 438(7070), 932-6.
Carmeliet, P. & Jain, R. K. (2000) Angiogenesis in cancer and other diseases. *Nature*, 407(6801), 249-57.
Carmeliet, P., Mackman, N., Moons, L., Luther, T., Gressens, P., Van Vlaenderen, I., Demunck, H., Kasper, M., Breier, G., Evrard, P., Muller, M., Risau, W., Edgington, T. & Collen, D. (1996) Role of tissue factor in embryonic blood vessel development. *Nature*, 383(6595), 73-5.
Carmeliet, P., Moons, L., Dewerchin, M., Mackman, N., Luther, T., Breier, G., Ploplis, V., Muller, M., Nagy, A., Plow, E., Gerard, R., Edgington, T., Risau, W. & Collen, D. (1997) Insights in vessel development and vascular disorders using targeted inactivation and transfer of vascular endothelial growth factor, the tissue factor receptor, and the plasminogen system. *Ann N Y Acad Sci*, 811, 191-206.
Carneiro-Lobo, T. C., Konig, S., Machado, D. E., Nasciutti, L. E., Forni, M. F., Francischetti, I. M., Sogayar, M. C. & Monteiro, R. Q. (2009) Ixolaris, a tissue factor inhibitor, blocks primary tumor growth and angiogenesis in a glioblastoma model. *J Thromb Haemost*, 7(11), 1855-64.
Carneiro-Lobo, T. C., Schaffner, F., Disse, J., Ostergaard, H., Francischetti, I. M., Monteiro, R. Q. & Ruf, W. (2012) The tick-derived inhibitor Ixolaris prevents tissue factor signaling on tumor cells. *J Thromb Haemost*, 10(9), 1849-58.

Carvalho, E., Hugo de Almeida, V., Rondon, A. M. R., Possik, P. A., Viola, J. P. B. & Monteiro, R. Q. (2018) Protease-activated receptor 2 (PAR2) upregulates granulocyte colony stimulating factor (G-CSF) expression in breast cancer cells. *Biochem Biophys Res Commun*, 504(1), 270-276.
Cassera, M. B., Silber, A. M. & Gennaro, A. M. (2002) Differential effects of cholesterol on acyl chain order in erythrocyte membranes as a function of depth from the surface. An electron paramagnetic resonance (EPR) spin label study. *Biophys Chem*, 99(2), 117-27.
Casu, B. (1985) Structure and biological activity of heparin. *Adv Carbohydr Chem Biochem*, 43, 51-134.
Casu, B., Guerrini, M., Naggi, A., Perez, M., Torri, G., Ribatti, D., Carminati, P., Giannini, G., Penco, S., Pisano, C., Belleri, M., Rusnati, M. & Presta, M. (2002) Short heparin sequences spaced by glycol-split uronate residues are antagonists of fibroblast growth factor 2 and angiogenesis inhibitors. *Biochemistry*, 41(33), 10519-28.
Caunt, M., Hu, L., Tang, T., Brooks, P. C., Ibrahim, S. & Karpatkin, S. (2006) Growth-regulated oncogene is pivotal in thrombin-induced angiogenesis. *Cancer Res*, 66(8), 4125-32.
Caunt, M., Huang, Y. Q., Brooks, P. C. & Karpatkin, S. (2003) Thrombin induces neoangiogenesis in the chick chorioallantoic membrane. *Journal of Thrombosis and Haemostasis*, 1(10), 2097-2102.
Chang, L. H., Pan, S. L., Lai, C. Y., Tsai, A. C. & Teng, C. M. (2013) Activated PAR-2 regulates pancreatic cancer progression through ILK/HIF-alpha-induced TGF-alpha expression and MEK/VEGF-A-mediated angiogenesis. *Am J Pathol*, 183(2), 566-75.
Charollais, J. & Van Der Goot, F. G. (2009) Palmitoylation of membrane proteins (Review). *Mol Membr Biol*, 26(1), 55-66.
Che, S. P. Y., Park, J. Y. & Stokol, T. (2017) Tissue factor-expressing tumor-derived extracellular vesicles activate quiescent endothelial cells via protease-activated receptor-1. *Frontiers in Oncology*, 7.
Chen, V. M. & Hogg, P. J. (2013) Encryption and decryption of tissue factor. *J Thromb Haemost*, 11 Suppl 1, 277-84.
Cimpean, A. M., Ribatti, D. & Raica, M. (2008) The chick embryo chorioallantoic membrane as a model to study tumor metastasis. *Angiogenesis*, 11(4), 311-9.
Cirillo, P., Cali, G., Golino, P., Calabro, P., Forte, L., De Rosa, S., Pacileo, M., Ragni, M., Scopacasa, F., Nitsch, L. & Chiariello, M. (2004) Tissue factor binding of activated factor VII triggers smooth muscle cell proliferation via extracellular signal-regulated kinase activation. *Circulation*, 109(23), 2911-6.
Claas, C., Stipp, C. S. & Hemler, M. E. (2001) Evaluation of prototype transmembrane 4 superfamily protein complexes and their relation to lipid rafts. *J Biol Chem*, 276(11), 7974-84.
Clancy, J. W., Sedgwick, A., Rosse, C., Muralidharan-Chari, V., Raposo, G., Method, M., Chavrier, P. & D'Souza-Schorey, C. (2015) Regulated delivery of molecular cargo to invasive tumour-derived microvesicles. *Nat Commun*, 6, 6919.
Cocucci, E., Racchetti, G. & Meldolesi, J. (2009) Shedding microvesicles: artefacts no more. *Trends Cell Biol*, 19(2), 43-51.
Collier, M. E. (2008) *A study of the regulation of oestrogen receptor alpha by tissue factor in breast cancer cells*. Doctor of Philosophy PhD thesis. The University of Hull.
Collier, M. E. & Ettelaie, C. (2010) Induction of endothelial cell proliferation by recombinant and microparticle-tissue factor involves beta1-integrin and extracellular signal regulated kinase activation. *Arterioscler Thromb Vasc Biol*, 30(9), 1810-7.
Collier, M. E. & Ettelaie, C. (2011) Regulation of the incorporation of tissue factor into microparticles by serine phosphorylation of the cytoplasmic domain of tissue factor. *J Biol Chem*, 286(14), 11977-84.
Collier, M. E., Li, C. & Ettelaie, C. (2008) Influence of exogenous tissue factor on estrogen receptor alpha expression in breast cancer cells: involvement of beta1-integrin, PAR2, and mitogen-activated protein kinase activation. *Mol Cancer Res*, 6(12), 1807-18.
Collier, M. E., Maraveyas, A. & Ettelaie, C. (2014) Filamin-A is required for the incorporation of tissue factor into cell-derived microvesicles. *Thromb Haemost*, 111(4), 647-55.

Collier, M. E. W., Ettelaie, C., Goult, B. T., Maraveyas, A. & Goodall, A. H. (2017) Investigation of the filamin A-dependent mechanisms of tissue factor incorporation into microvesicles. *Thromb Haemost*, 117(11), 2034-2044.
Collier, M. E. W., Mah, P. M., Xiao, Y. P., Maraveyas, A. & Ettelaie, C. (2013) Microparticle-associated tissue factor is recycled by endothelial cells resulting in enhanced surface tissue factor activity. *Thrombosis and Haemostasis*, 110(5), 966-976.
Conti, S., Guercini, F. & Iorio, A. (2003) Low-molecular-weight heparin and cancer survival: review of the literature and pooled analysis of 1,726 patients treated for at least three months. *Pathophysiol Haemost Thromb*, 33(4), 197-201.
Contrino, J., Hair, G., Kreutzer, D. L. & Rickles, F. R. (1996) In situ detection of tissue factor in vascular endothelial cells: correlation with the malignant phenotype of human breast disease. *Nat Med*, 2(2), 209-15.
Cooper, J. & Giancotti, F. G. (2019) Integrin signaling in cancer: mechanotransduction, stemness, epithelial plasticity, and therapeutic resistance. *Cancer Cell*, 35(3), 347-367.
Cui, H., Tan, Y. X., Osterholm, C., Zhang, X., Hedin, U., Vlodavsky, I. & Li, J. P. (2016) Heparanase expression upregulates platelet adhesion activity and thrombogenicity. *Oncotarget*, 7(26), 39486-39496.
Curtis, A. M., Wilkinson, P. F., Gui, M., Gales, T. L., Hu, E. & Edelberg, J. M. (2009) p38 mitogen-activated protein kinase targets the production of proinflammatory endothelial microparticles. *J Thromb Haemost*, 7(4), 701-9.
D'Souza-Schorey, C. & Chavrier, P. (2006) ARF proteins: roles in membrane traffic and beyond. *Nat Rev Mol Cell Biol*, 7(5), 347-58.
Damiano, B. P., Cheung, W. M., Santulli, R. J., Fung-Leung, W. P., Ngo, K., Ye, R. D., Darrow, A. L., Derian, C. K., de Garavilla, L. & Andrade-Gordon, P. (1999) Cardiovascular responses mediated by protease-activated receptor-2 (PAR-2) and thrombin receptor (PAR-1) are distinguished in mice deficient in PAR-2 or PAR-1. *J Pharmacol Exp Ther*, 288(2), 671-8.
Darmoul, D., Gratio, V., Devaud, H. & Laburthe, M. (2004) Protease-activated receptor 2 in colon cancer - Trypsin-induced MAPK phosphorylation and cell proliferation are mediated by epidermal growth factor receptor transactivation. *Journal of Biological Chemistry*, 279(20), 20927-20934.
Das, K., Prasad, R., Roy, S., Mukherjee, A. & Sen, P. (2018a) The protease activated receptor 2 promotes Rab5a mediated generation of pro-metastatic microvesicles. *Sci Rep*, 8(1), 7357.
Das, K., Prasad, R., Singh, A., Bhattacharya, A., Roy, A., Mallik, S., Mukherjee, A. & Sen, P. (2018b) Protease-activated receptor 2 promotes actomyosin dependent transforming microvesicles generation from human breast cancer. *Molecular Carcinogenesis*, 57(12), 1707-1722.
Davie, E. W. & Ratnoff, O. D. (1964) Waterfall sequence for intrinsic blood clotting. *Science*, 145(3638), 1310-2.
Davizon, P., Munday, A. D. & Lopez, J. A. (2010) Tissue factor, lipid rafts, and microparticles. *Semin Thromb Hemost*, 36(8), 857-64.
de Bono, J. S., Concin, N., Hong, D. S., Thistlethwaite, F. C., Machiels, J. P., Arkenau, H. T., Plummer, R., Jones, R. H., Nielsen, D., Windfeld, K., Ghatta, S., Slomovitz, B. M., Spicer, J. F., Yachnin, J., Ang, J. E., Mau-Sorensen, P. M., Forster, M. D., Collins, D., Dean, E., Rangwala, R. A. & Lassen, U. (2019) Tisotumab vedotin in patients with advanced or metastatic solid tumours (InnovaTV 201): a first-in-human, multicentre, phase 1-2 trial. *Lancet Oncol*, 20(3), 383-393.
De Franceschi, N. & Ivaska, J. (2015) Integrin bondage: filamin takes control. *Nat Struct Mol Biol*, 22(5), 355-7.
de Oliveira, A. D. S., Lima, L. G., Mariano-Oliveira, A., Machado, D. E., Nasciutti, L. E., Andersen, J. F., Petersen, L. C., Francischetti, I. M. & Monteiro, R. Q. (2012) Inhibition of tissue factor by ixolaris reduces primary tumor growth and experimental metastasis in a murine model of melanoma. *Thromb Res*, 130(3), e163-70.

Debergh, I., Van Damme, N., Pattyn, P., Peeters, M. & Ceelen, W. P. (2010) The low-molecular-weight heparin, nadroparin, inhibits tumour angiogenesis in a rodent dorsal skinfold chamber model. *Br J Cancer*, 102(5), 837-43.
Decker, L. & ffrench-Constant, C. (2004) Lipid rafts and integrin activation regulate oligodendrocyte survival. *J Neurosci*, 24(15), 3816-25.
DeFea, K. A., Zalevsky, J., Thoma, M. S., Dery, O., Mullins, R. D. & Bunnett, N. W. (2000) beta-Arrestin-dependent endocytosis of proteinase-activated receptor 2 is required for intracellular targeting of activated ERK1/2. *Journal of Cell Biology*, 148(6), 1267-1281.
Defeo, K., Hayes, C., Chernick, M., Van Ryn, J. & Gilmour, S. K. (2010) Use of dabigatran etexilate to reduce breast cancer progression. *Cancer Biology & Therapy*, 10(10), 1001-1008.
Deitcher, S. R., Kessler, C. M., Merli, G., Rigas, J. R., Lyons, R. M., Fareed, J. & Investigators, O. (2006) Secondary prevention of venous thromboembolic events in patients with active cancer: enoxaparin alone versus initial enoxaparin followed by warfarin for a 180-day period. *Clin Appl Thromb Hemost*, 12(4), 389-96.
Del Conde, I., Shrimpton, C. N., Thiagarajan, P. & Lopez, J. A. (2005) Tissue-factor-bearing microvesicles arise from lipid rafts and fuse with activated platelets to initiate coagulation. *Blood*, 106(5), 1604-11.
del Pozo, M. A., Price, L. S., Alderson, N. B., Ren, X. D. & Schwartz, M. A. (2000) Adhesion to the extracellular matrix regulates the coupling of the small GTPase Rac to its effector PAK. *EMBO J*, 19(9), 2008-14.
Dery, O., Corvera, C. U., Steinhoff, M. & Bunnett, N. W. (1998) Proteinase-activated receptors: novel mechanisms of signaling by serine proteases. *Am J Physiol*, 274(6), C1429-52.
Deryugina, E. I. & Quigley, J. P. (2008) Chick embryo chorioallantoic membrane model systems to study and visualize human tumor cell metastasis. *Histochem Cell Biol*, 130(6), 1119-30.
Desgrosellier, J. S. & Cheresh, D. A. (2010) Integrins in cancer: biological implications and therapeutic opportunities. *Nat Rev Cancer*, 10(1), 9-22.
Di Nisio, M., Porreca, E., Candeloro, M., De Tursi, M., Russi, I. & Rutjes, A. W. (2016) Primary prophylaxis for venous thromboembolism in ambulatory cancer patients receiving chemotherapy. *Cochrane Database Syst Rev*, 12, CD008500.
Dogan, O. T., Polat, Z. A., Karahan, O., Epozturk, K., Altun, A., Akkurt, I. & Cetin, A. (2011) Antiangiogenic activities of bemiparin sodium, enoxaparin sodium, nadroparin calcium and tinzaparin sodium. *Thromb Res*, 128(4), e29-32.
Dohle, D. S., Pasa, S. D., Gustmann, S., Laub, M., Wissler, J. H., Jennissen, H. P. & Dunker, N. (2009) Chick ex ovo culture and ex ovo CAM assay: how it really works. *J Vis Exp*(33).
Dorfleutner, A., Hintermann, E., Tarui, T., Takada, Y. & Ruf, W. (2004) Cross-talk of integrin alpha3beta1 and tissue factor in cell migration. *Mol Biol Cell*, 15(10), 4416-25.
Dorfleutner, A. & Ruf, W. (2003) Regulation of tissue factor cytoplasmic domain phosphorylation by palmitoylation. *Blood*, 102(12), 3998-4005.
Drake, T. A., Morrissey, J. H. & Edgington, T. S. (1989) Selective cellular expression of tissue factor in human tissues. Implications for disorders of hemostasis and thrombosis. *Am J Pathol*, 134(5), 1087-97.
Dvorak, H. F., Brown, L. F., Detmar, M. & Dvorak, A. M. (1995) Vascular permeability factor/vascular endothelial growth factor, microvascular hyperpermeability, and angiogenesis. *Am J Pathol*, 146(5), 1029-39.
Edidin, M. (2003) The state of lipid rafts: from model membranes to cells. *Annu Rev Biophys Biomol Struct*, 32, 257-83.
Edovitsky, E., Elkin, M., Zcharia, E., Peretz, T. & Vlodavsky, I. (2004) Heparanase gene silencing, tumor invasiveness, angiogenesis, and metastasis. *J Natl Cancer Inst*, 96(16), 1219-30.
Eigenbrot, C. (2002) Structure, function, and activation of coagulation factor VII. *Current Protein & Peptide Science*, 3(3), 287-299.

ElKeeb, A. M., Collier, M. E., Maraveyas, A. & Ettelaie, C. (2015) Accumulation of tissue factor in endothelial cells induces cell apoptosis, mediated through p38 and p53 activation. *Thromb Haemost*, 114(2), 364-78.
Ellinghaus, P., Perzborn, E., Hauenschild, P., Gerdes, C., Heitmeier, S., Visser, M., Summer, H. & Laux, V. (2016) Expression of pro-inflammatory genes in human endothelial cells: Comparison of rivaroxaban and dabigatran. *Thrombosis Research*, 142, 44-51.
Ender, F., Freund, A., Quecke, T., Steidel, C., Zamzow, P., von Bubnoff, N. & Gieseler, F. (2020) Tissue factor activity on microvesicles from cancer patients. *J Cancer Res Clin Oncol*, 146(2), 467-475.
Enjeti, A. K., Ariyarajah, A., D'Crus, A., Seldon, M. & Lincz, L. F. (2016) Correlative analysis of nanoparticle tracking, flow cytometric and functional measurements for circulating microvesicles in normal subjects. *Thromb Res*, 145, 18-23.
Erber, R., Thurnher, A., Katsen, A. D., Groth, G., Kerger, H., Hammes, H. P., Menger, M. D., Ullrich, A. & Vajkoczy, P. (2004) Combined inhibition of VEGF and PDGF signaling enforces tumor vessel regression by interfering with pericyte-mediated endothelial cell survival mechanisms. *FASEB J*, 18(2), 338-40.
Escolar, G., Fernandez-Gallego, V., Arellano-Rodrigo, E., Roquer, J., Reverter, J. C., Sanz, V. V., Molina, P., Lopez-Vilchez, I., Diaz-Ricart, M. & Galan, A. M. (2013) Reversal of apixaban induced alterations in hemostasis by different coagulation factor concentrates: significance of studies in vitro with circulating human blood. *PLoS One*, 8(11), e78696.
Ethaeb, A. M. (2018) *Elucidation of the signalling mechanisms involved in TF-mediated apoptosis in endothelial cells*. Doctor of Philosophy University of Hull.
Ethaeb, A. M., Mohammad, M. A., Madkhali, Y., Featherby, S., Maraveyas, A., Greenman, J. & Ettelaie, C. (2020) Accumulation of tissue factor in endothelial cells promotes cellular apoptosis through over-activation of Src1 and involves beta1-integrin signalling. *Apoptosis*, 25(1-2), 29-41.
Ettelaie, C., Collier, M. E., Featherby, S., Greenman, J. & Maraveyas, A. (2015) The potential of cancer cell lines to release tissue factor-containing microvesicles correlates with tissue factor and PAR2 mRNA levels but not tissue factor protein or surface activity. *Journal of Thrombosis and Haemostasis*, 13, 463-464.
Ettelaie, C., Collier, M. E., Maraveyas, A. & Ettelaie, R. (2014) Characterization of physical properties of tissue factor-containing microvesicles and a comparison of ultracentrifuge-based recovery procedures. *J Extracell Vesicles*, 3.
Ettelaie, C., Collier, M. E., Mei, M. P., Xiao, Y. P. & Maraveyas, A. (2013a) Enhanced binding of tissue factor-microparticles to collagen-IV and fibronectin leads to increased tissue factor activity in vitro. *Thromb Haemost*, 109(1), 61-71.
Ettelaie, C., Collier, M. E. W., Featherby, S., Benelhaj, N. E., Greenman, J. & Maraveyas, A. (2016) Analysis of the potential of cancer cell lines to release tissue factor-containing microvesicles: correlation with tissue factor and PAR2 expression. *Thrombosis Journal*, 14.
Ettelaie, C., Elkeeb, A. M., Maraveyas, A. & Collier, M. E. (2013b) p38alpha phosphorylates serine 258 within the cytoplasmic domain of tissue factor and prevents its incorporation into cell-derived microparticles. *Biochim Biophys Acta*, 1833(3), 613-21.
Ettelaie, C., Fountain, D., Collier, M. E., Beeby, E., Xiao, Y. P. & Maraveyas, A. (2011a) Low molecular weight heparin suppresses tissue factor-mediated cancer cell invasion and migration in vitro. *Exp Ther Med*, 2(2), 363-367.
Ettelaie, C., Fountain, D., Collier, M. E., Elkeeb, A. M., Xiao, Y. P. & Maraveyas, A. (2011b) Low molecular weight heparin downregulates tissue factor expression and activity by modulating growth factor receptor-mediated induction of nuclear factor-kappaB. *Biochim Biophys Acta*, 1812(12), 1591-600.
Fair, D. S. & Bahnak, B. R. (1984) Human hepatoma cells secrete single chain factor X, prothrombin, and antithrombin III. *Blood*, 64(1), 194-204.
Falanga, A. (2005) Mechanisms of thrombosis in cancer. *Thromb Res*, 115 Suppl 1, 21-4.

Falanga, A., Marchetti, M. & Russo, L. (2015) The mechanisms of cancer-associated thrombosis. *Thromb Res*, 135 Suppl 1, S8-S11.
Falanga, A., Marchetti, M. & Vignoli, A. (2013) Coagulation and cancer: biological and clinical aspects. *J Thromb Haemost*, 11(2), 223-33.
Falanga, A., Russo, L., Milesi, V. & Vignoli, A. (2017) Mechanisms and risk factors of thrombosis in cancer. *Crit Rev Oncol Hematol*, 118, 79-83.
Fan, L., Yotov, W. V., Zhu, T., Esmailzadeh, L., Joyal, J. S., Sennlaub, F., Heveker, N., Chemtob, S. & Rivard, G. E. (2005) Tissue factor enhances protease-activated receptor-2-mediated factor VIIa cell proliferative properties. *J Thromb Haemost*, 3(5), 1056-63.
Fareed, J., Jeske, W., Hoppensteadt, D., Clarizio, R. & Walenga, J. M. (1996) Are the available low-molecular-weight heparin preparations the same? *Semin Thromb Hemost*, 22 Suppl 1, 77-91.
Featherby, S., Madkhali, Y., Maraveyas, A. & Ettelaie, C. (2019) Apixaban Suppresses the Release of TF-Positive Microvesicles and Restrains Cancer Cell Proliferation through Directly Inhibiting TF-fVIIa Activity. *Thromb Haemost*.
Feng, Q., Zhang, C., Lum, D., Druso, J. E., Blank, B., Wilson, K. F., Welm, A., Antonyak, M. A. & Cerione, R. A. (2017) A class of extracellular vesicles from breast cancer cells activates VEGF receptors and tumour angiogenesis. *Nat Commun*, 8, 14450.
Fox, J. E., Austin, C. D., Reynolds, C. C. & Steffen, P. K. (1991) Evidence that agonist-induced activation of calpain causes the shedding of procoagulant-containing microvesicles from the membrane of aggregating platelets. *J Biol Chem*, 266(20), 13289-95.
Franco, M., Roswall, P., Cortez, E., Hanahan, D. & Pietras, K. (2011) Pericytes promote endothelial cell survival through induction of autocrine VEGF-A signaling and Bcl-w expression. *Blood*, 118(10), 2906-17.
Frost, C., Wang, J., Nepal, S., Schuster, A., Barrett, Y. C., Mosqueda-Garcia, R., Reeves, R. A. & LaCreta, F. (2013) Apixaban, an oral, direct factor Xa inhibitor: single dose safety, pharmacokinetics, pharmacodynamics and food effect in healthy subjects. *Br J Clin Pharmacol*, 75(2), 476-87.
Furlan-Freguia, C., Marchese, P., Gruber, A., Ruggeri, Z. M. & Ruf, W. (2011) P2X7 receptor signaling contributes to tissue factor-dependent thrombosis in mice. *J Clin Invest*, 121(7), 2932-44.
Gale, A. J. & Gordon, S. G. (2001) Update on tumor cell procoagulant factors. *Acta Haematologica*, 106(1-2), 25-32.
Ge, L., Ly, Y., Hollenberg, M. & DeFea, K. (2003) A beta-arrestin-dependent scaffold is associated with prolonged MAPK activation in pseudopodia during protease-activated receptor-2-induced chemotaxis. *J Biol Chem*, 278(36), 34418-26.
Geddings, J. E. & Mackman, N. (2013) Tumor-derived tissue factor-positive microparticles and venous thrombosis in cancer patients. *Blood*, 122(11), 1873-1880.
Gong, J., Jaiswal, R., Dalla, P., Luk, F. & Bebawy, M. (2015) Microparticles in cancer: A review of recent developments and the potential for clinical application. *Semin Cell Dev Biol*, 40, 35-40.
Gorlin, J. B., Yamin, R., Egan, S., Stewart, M., Stossel, T. P., Kwiatkowski, D. J. & Hartwig, J. H. (1990) Human endothelial actin-binding protein (ABP-280, nonmuscle filamin): a molecular leaf spring. *J Cell Biol*, 111(3), 1089-105.
Graf, C. & Ruf, W. (2018) Tissue factor as a mediator of coagulation and signaling in cancer and chronic inflammation. *Thromb Res*, 164 Suppl 1, S143-S147.
Graf, C., Wilgenbus, P., Pagel, S., Pott, J., Marini, F., Reyda, S., Kitano, M., Macher-Goppinger, S., Weiler, H. & Ruf, W. (2019) Myeloid cell-synthesized coagulation factor X dampens antitumor immunity. *Sci Immunol*, 4(39).
Graf, C. W., P.; Kitano, M.; Macher-Göppinger, S.; Ruf, W. (2018) Macrophage factor Xa signaling promotes cancer immune evasion. *Blood*, 132 Suppl 1(135).
Griffin, C. T., Srinivasan, Y., Zheng, Y. W., Huang, W. & Coughlin, S. R. (2001) A role for thrombin receptor signaling in endothelial cells during embryonic development. *Science*, 293(5535), 1666-70.
Grover, S. P. & Mackman, N. (2018) Tissue factor: an essential mediator of hemostasis and trigger of thrombosis. *Arterioscler Thromb Vasc Biol*, 38(4), 709-725.

Guasti, L., Squizzato, A., Moretto, P., Vigetti, D., Ageno, W., Dentali, F., Maresca, A. M., Campiotti, L., Grandi, A. M. & Passi, A. (2017) In vitro effects of Apixaban on 5 different cancer cell lines. *PLoS One*, 12(10), e0185035.
Guo, D., Zhou, H., Wu, Y., Zhou, F., Xu, G., Wen, H. & Zhang, X. (2011) Involvement of ERK1/2/NF-kappaB signal transduction pathway in TF/FVIIa/PAR2-induced proliferation and migration of colon cancer cell SW620. *Tumour Biol*, 32(5), 921-30.
Hadjipanayi, E., Kuhn, P. H., Moog, P., Bauer, A. T., Kuekrek, H., Mirzoyan, L., Hummel, A., Kirchhoff, K., Salgin, B., Isenburg, S., Dornseifer, U., Ninkovic, M., Machens, H. G. & Schilling, A. F. (2015) The fibrin matrix regulates angiogenic responses within the hemostatic microenvironment through biochemical control. *PLoS One*, 10(8), e0135618.
Haibe, Y., Kreidieh, M., El Hajj, H., Khalifeh, I., Mukherji, D., Temraz, S. & Shamseddine, A. (2020) Resistance Mechanisms to Anti-angiogenic Therapies in Cancer. *Front Oncol*, 10, 221.
Halper, J. & Carter, B. J. (1989) Modulation of growth of human carcinoma SW-13 cells by heparin and growth factors. *J Cell Physiol*, 141(1), 16-23.
Han, X., Guo, B., Li, Y. & Zhu, B. (2014) Tissue factor in tumor microenvironment: a systematic review. *J Hematol Oncol*, 7, 54.
Hankins, H. M., Baldridge, R. D., Xu, P. & Graham, T. R. (2015) Role of flippases, scramblases and transfer proteins in phosphatidylserine subcellular distribution. *Traffic*, 16(1), 35-47.
Haralabopoulos, G. C., Grant, D. S., Kleinman, H. K. & Maragoudakis, M. E. (1997) Thrombin promotes endothelial cell alignment in Matrigel in vitro and angiogenesis in vivo. *Am J Physiol*, 273(1 Pt 1), C239-45.
Harburger, D. S. & Calderwood, D. A. (2009) Integrin signalling at a glance. *J Cell Sci*, 122(Pt 2), 159-63.
Harlos, K., Martin, D. M., O'Brien, D. P., Jones, E. Y., Stuart, D. I., Polikarpov, I., Miller, A., Tuddenham, E. G. & Boys, C. W. (1994) Crystal structure of the extracellular region of human tissue factor. *Nature*, 370(6491), 662-6.
Harris, S. L. & Levine, A. J. (2005) The p53 pathway: positive and negative feedback loops. *Oncogene*, 24(17), 2899-908.
Hartjes, T. A., Mytnyk, S., Jenster, G. W., van Steijn, V. & van Royen, M. E. (2019) Extracellular vesicle quantification and characterization: common methods and emerging approaches. *Bioengineering (Basel)*, 6(1).
Harvey, J. R., Mellor, P., Eldaly, H., Lennard, T. W., Kirby, J. A. & Ali, S. (2007) Inhibition of CXCR4-mediated breast cancer metastasis: a potential role for heparinoids? *Clin Cancer Res*, 13(5), 1562-70.
Hatton, C. S. R. (2013) *Haematology*, 9th ed. / Chris S.R. Hatton ... [et al.]. edition. Oxford: Wiley-Blackwell.
Hedstrom, L. (2002) Serine protease mechanism and specificity. *Chem Rev*, 102(12), 4501-24.
Hembrough, T. A., Swartz, G. M., Papathanassiu, A., Vlasuk, G. P., Rote, W. E., Green, S. J. & Pribluda, V. S. (2003) Tissue factor/factor VIIa inhibitors block angiogenesis and tumor growth through a nonhemostatic mechanism. *Cancer Research*, 63(11), 2997-3000.
Hempel, D., Sierko, E. & Wojtukiewicz, M. Z. (2016) Protease-activated receptors - biology and role in cancer. *Postepy Higieny I Medycyny Doswiadczalnej*, 70, 775-786.
Henrikson, K. P., Salazar, S. L., Fenton, J. W., 2nd & Pentecost, B. T. (1999) Role of thrombin receptor in breast cancer invasiveness. *Br J Cancer*, 79(3-4), 401-6.
Herbert, J. M., Savi, P., Laplace, M. C. & Lale, A. (1992) IL-4 inhibits LPS-, IL-1 beta- and TNF alpha-induced expression of tissue factor in endothelial cells and monocytes. *FEBS Lett*, 310(1), 31-3.
Hernandez, C., Orbe, J., Roncal, C., Alvarez-Hernandez, M., Martinez de Lizarrondo, S., Alves, M. T., Garcia Mata, J. & Paramo, J. A. (2013) Tissue factor expressed by microparticles is associated with mortality but not with thrombosis in cancer patients. *Thromb Haemost*, 110(3), 598-608.
Heuberger, D. M. & Schuepbach, R. A. (2019) Protease-activated receptors (PARs): mechanisms of action and potential therapeutic modulators in PAR-driven inflammatory diseases. *Thromb J*, 17, 4.

Hillyer, C. D. (2009) *Transfusion medicine and hemostasis : clinical and laboratory aspects*. Burlington, MA. ; London: Elsevier.
Hirota, Y., Osuga, Y., Hirata, T., Harada, M., Morimoto, C., Yoshino, O., Koga, K., Yano, T., Tsutsumi, O. & Taketani, Y. (2005) Activation of protease-activated receptor 2 stimulates proliferation and interleukin (IL)-6 and IL-8 secretion of endometriotic stromal cells. *Hum Reprod*, 20(12), 3547-53.
Hisada, Y. & Mackman, N. (2019) Tissue factor and cancer: regulation, tumor growth, and metastasis. *Semin Thromb Hemost*, 45(4), 385-395.
Hjortoe, G. M., Petersen, L. C., Albrektsen, T., Sorensen, B. B., Norby, P. L., Mandal, S. K., Pendurthi, U. R. & Rao, L. V. M. (2004) Tissue factor-factor VIIa-specific up-regulation of IL-8 expression in MDA-MB-231 cells is mediated by PAR-2 and results in increased cell migration. *Blood*, 103(8), 3029-3037.
Hobbs, J. E., Zakarija, A., Cundiff, D. L., Doll, J. A., Hymen, E., Cornwell, M., Crawford, S. E., Liu, N., Signaevsky, M. & Soff, G. A. (2007) Alternatively spliced human tissue factor promotes tumor growth and angiogenesis in a pancreatic cancer tumor model. *Thromb Res*, 120 Suppl 2, S13-21.
Hollenberg, M. D. & Compton, S. J. (2002) International Union of Pharmacology. XXVIII. Proteinase-activated receptors. *Pharmacol Rev*, 54(2), 203-17.
Holliday, L. S., Faria, L. P. & Rody, W. J., Jr. (2019) Actin and actin-associated proteins in extracellular vesicles shed by osteoclasts. *Int J Mol Sci*, 21(1).
Hong, D. S., Concin, N., Vergote, I., de Bono, J. S., Slomovitz, B. M., Drew, Y., Arkenau, H. T., Machiels, J. P., Spicer, J. F., Jones, R., Forster, M. D., Cornez, N., Gennigens, C., Johnson, M. L., Thistlethwaite, F. C., Rangwala, R. A., Ghatta, S., Windfeld, K., Harris, J. R., Lassen, U. N. & Coleman, R. L. (2020) Tisotumab vedotin in previously treated recurrent or metastatic cervical cancer. *Clin Cancer Res*, 26(6), 1220-1228.
Horton, J. (2005) Venous thrombotic events in cancer: the bottom line. *Cancer Control*, 12 Suppl 1, 31-7.
Hostettler, N., Naggi, A., Torri, G., Ishai-Michaeli, R., Casu, B., Vlodavsky, I. & Borsig, L. (2007) P-selectin- and heparanase-dependent antimetastatic activity of non-anticoagulant heparins. *FASEB J*, 21(13), 3562-72.
Hou, S., Isaji, T., Hang, Q., Im, S., Fukuda, T. & Gu, J. (2016) Distinct effects of beta1 integrin on cell proliferation and cellular signaling in MDA-MB-231 breast cancer cells. *Sci Rep*, 6, 18430.
Howlett, A. R., Bailey, N., Damsky, C., Petersen, O. W. & Bissell, M. J. (1995) Cellular growth and survival are mediated by beta 1 integrins in normal human breast epithelium but not in breast carcinoma. *J Cell Sci*, 108 (Pt 5), 1945-57.
Hu, L., Xia, L., Zhou, H., Wu, B., Mu, Y., Wu, Y. & Yan, J. (2013) TF/FVIIa/PAR2 promotes cell proliferation and migration via PKCalpha and ERK-dependent c-Jun/AP-1 pathway in colon cancer cell line SW620. *Tumour Biol*, 34(5), 2573-81.
Hugel, B., Carmen, M., Martinez, M. C., Kunzelmann, C. & Freyssinet, J. M. (2005) Membrane microparticles: Two sides of the coin. *Physiology*, 20, 22-27.
Hughes, C. S., Postovit, L. M. & Lajoie, G. A. (2010) Matrigel: a complex protein mixture required for optimal growth of cell culture. *Proteomics*, 10(9), 1886-90.
Humphries, J. D., Byron, A. & Humphries, M. J. (2006) Integrin ligands at a glance. *J Cell Sci*, 119(Pt 19), 3901-3.
Humphries, M. J. (1996) Integrin activation: the link between ligand binding and signal transduction. *Curr Opin Cell Biol*, 8(5), 632-40.
Hynes, R. O. (2002) Integrins: bidirectional, allosteric signaling machines. *Cell*, 110(6), 673-87.
Ilan, N., Elkin, M. & Vlodavsky, I. (2006) Regulation, function and clinical significance of heparanase in cancer metastasis and angiogenesis. *Int J Biochem Cell Biol*, 38(12), 2018-39.
Jakob, W., Jentzsch, K. D., Mauersberger, B. & Heder, G. (1978) The chick embryo choriallantoic membrane as a bioassay for angiogenesis factors: reactions induced by carrier materials. *Exp Pathol (Jena)*, 15(5), 241-9.
Jayson, G. C. & Gallagher, J. T. (1997) Heparin oligosaccharides: inhibitors of the biological activity of bFGF on Caco-2 cells. *Br J Cancer*, 75(1), 9-16.

Jeanes, A. I., Wang, P., Moreno-Layseca, P., Paul, N., Cheung, J., Tsang, R., Akhtar, N., Foster, F. M., Brennan, K. & Streuli, C. H. (2012) Specific beta-containing integrins exert differential control on proliferation and two-dimensional collective cell migration in mammary epithelial cells. *J Biol Chem*, 287(29), 24103-12.
Jia, D. Y., Tan, Y., Liu, H. J., Ooi, S., Li, L., Wright, K., Bennett, S., Addison, C. L. & Wang, L. S. (2016) Cardamonin reduces chemotherapy-enriched breast cancer stem-like cells in vitro and in vivo. *Oncotarget*, 7(1), 771-785.
Jiang, D. L., Li, Y., Ma, H., Li, L. H., Zhan, S. H. & Gao, Y. Q. (2017) PAR2 activates autocrine IL-8 signaling pathway to promote proliferation and migration of colorectal cancer cells. *International Journal of Clinical and Experimental Pathology*, 10(5), 5600-5605.
Jiang, X., Bailly, M. A., Panetti, T. S., Cappello, M., Konigsberg, W. H. & Bromberg, M. E. (2004) Formation of tissue factor-factor VIIa-factor Xa complex promotes cellular signaling and migration of human breast cancer cells. *Journal of Thrombosis and Haemostasis*, 2(1), 93-101.
Jiang, Y., Yau, M. K., Lim, J., Wu, K. C., Xu, W., Suen, J. Y. & Fairlie, D. P. (2018) A potent antagonist of protease-activated receptor 2 that inhibits multiple signaling functions in human cancer cells. *J Pharmacol Exp Ther*, 364(2), 246-257.
Johnson, M. J., Sproule, M. W. & Paul, J. (1999) The prevalence and associated variables of deep venous thrombosis in patients with advanced cancer. *Clin Oncol (R Coll Radiol)*, 11(2), 105-10.
Jones, D. S., Wallace, A. C. & Fraser, E. E. (1971) Sequence of events in experimental metastases of Walker 256 tumor: light, immunofluorescent, and electron microscopic observations. *J Natl Cancer Inst*, 46(3), 493-504.
Jung, O., Trapp-Stamborski, V., Purushothaman, A., Jin, H., Wang, H., Sanderson, R. D. & Rapraeger, A. C. (2016) Heparanase-induced shedding of syndecan-1/CD138 in myeloma and endothelial cells activates VEGFR2 and an invasive phenotype: prevention by novel synstatins. *Oncogenesis*, 5, e202.
Jung, Y. K., Woo, M. A., Soh, H. T. & Park, H. G. (2014) Aptamer-based cell imaging reagents capable of fluorescence switching. *Chem Commun (Camb)*, 50(82), 12329-32.
Jurasz, P., Alonso-Escolano, D. & Radomski, M. W. (2004) Platelet--cancer interactions: mechanisms and pharmacology of tumour cell-induced platelet aggregation. *Br J Pharmacol*, 143(7), 819-26.
Kakkar, A. K., Lemoine, N. R., Scully, M. F., Tebbutt, S. & Williamson, R. C. (1995) Tissue factor expression correlates with histological grade in human pancreatic cancer. *Br J Surg*, 82(8), 1101-4.
Kakkar, A. K., Levine, M. N., Kadziola, Z., Lemoine, N. R., Low, V., Patel, H. K., Rustin, G., Thomas, M., Quigley, M. & Williamson, R. C. (2004) Low molecular weight heparin, therapy with dalteparin, and survival in advanced cancer: the fragmin advanced malignancy outcome study (FAMOUS). *J Clin Oncol*, 22(10), 1944-8.
Katagiri, H., Itoh, S., Uchida, T., Kawai, Y. & Watanabe, K. (1999) [Monitoring of plasma concentration of low molecular weight heparin--comparative evaluation with chromogenic and clotting assays]. *Rinsho Byori*, 47(11), 1046-51.
Katrancioglu, N., Karahan, O., Kilic, A. T., Altun, A., Katrancioglu, O. & Polat, Z. A. (2012) Comparison of the antiangiogenic effects of heparin sodium, enoxaparin sodium, and tinzaparin sodium by using chorioallantoic membrane assay. *Blood Coagul Fibrinolysis*, 23(3), 218-21.
Kaufman, R. J. (1998) Post-translational modifications required for coagulation factor secretion and function. *Thromb Haemost*, 79(6), 1068-79.
Kawaguchi, M., Yamamoto, K., Kataoka, H., Izumi, A., Yamashita, F., Kiwaki, T., Nishida, T., Camerer, E. & Fukushima, T. (2020) Protease-activated receptor-2 accelerates intestinal tumor formation through activation of nuclear factor-kappaB signaling and tumor angiogenesis in Apc(Min/+) mice. *Cancer Sci*, 111(4), 1193-1202.
Kawamoto, T., Ohga, N., Akiyama, K., Hirata, N., Kitahara, S., Maishi, N., Osawa, T., Yamamoto, K., Kondoh, M., Shindoh, M., Hida, Y. & Hida, K. (2012) Tumor-derived microvesicles induce proangiogenic phenotype in endothelial cells via endocytosis. *PLoS One*, 7(3), e34045.
Kempton, C. L., Hoffman, M., Roberts, H. R. & Monroe, D. M. (2005) Platelet heterogeneity: variation in coagulation complexes on platelet subpopulations. *Arterioscler Thromb Vasc Biol*, 25(4), 861-6.

Khajah, M. A., Al Saleh, S., Mathew, P. M. & Luqmani, Y. A. (2012) Differential effect of growth factors on invasion and proliferation of endocrine resistant breast cancer cells. *PLoS One*, 7(7), e41847.
Khalil, J., Bensaid, B., Elkacemi, H., Afif, M., Bensaid, Y., Kebdani, T. & Benjaafar, N. (2015) Venous thromboembolism in cancer patients: an underestimated major health problem. *World J Surg Oncol*, 13, 204.
Khorana, A. A., Francis, C. W., Culakova, E., Kuderer, N. M. & Lyman, G. H. (2007a) Frequency, risk factors, and trends for venous thromboembolism among hospitalized cancer patients. *Cancer*, 110(10), 2339-46.
Khorana, A. A., Francis, C. W., Culakova, E., Kuderer, N. M. & Lyman, G. H. (2007b) Thromboembolism is a leading cause of death in cancer patients receiving outpatient chemotherapy. *J Thromb Haemost*, 5(3), 632-4.
Khorana, A. A., Noble, S., Lee, A. Y. Y., Soff, G., Meyer, G., O'Connell, C. & Carrier, M. (2018) Role of direct oral anticoagulants in the treatment of cancer-associated venous thromboembolism: guidance from the SSC of the ISTH. *J Thromb Haemost*, 16(9), 1891-1894.
Khorana, A. A., Sahni, A., Altland, O. D. & Francis, C. W. (2003) Heparin inhibition of endothelial cell proliferation and organization is dependent on molecular weight. *Arteriosclerosis Thrombosis and Vascular Biology*, 23(11), 2110-2115.
Khwaja, A., Rodriguez-Viciana, P., Wennstrom, S., Warne, P. H. & Downward, J. (1997) Matrix adhesion and Ras transformation both activate a phosphoinositide 3-OH kinase and protein kinase B/Akt cellular survival pathway. *EMBO J*, 16(10), 2783-93.
Kiema, T., Lad, Y., Jiang, P., Oxley, C. L., Baldassarre, M., Wegener, K. L., Campbell, I. D., Ylanne, J. & Calderwood, D. A. (2006) The molecular basis of filamin binding to integrins and competition with talin. *Mol Cell*, 21(3), 337-47.
Kim, C., Ye, F. & Ginsberg, M. H. (2011) Regulation of integrin activation. *Annu Rev Cell Dev Biol*, 27, 321-45.
Kim, M., Carman, C. V., Yang, W., Salas, A. & Springer, T. A. (2004) The primacy of affinity over clustering in regulation of adhesiveness of the integrin {alpha}L{beta}2. *J Cell Biol*, 167(6), 1241-53.
Kim, M. S., Kuppireddy, S. V., Sakamuri, S., Singal, M., Getnet, D., Harsha, H. C., Goel, R., Balakrishnan, L., Jacob, H. K. C., Kashyap, M. K., Tankala, S. G., Maitra, A., Iacobuzio-Donahue, C. A., Jaffee, E., Goggins, M. G., Velculescu, V. E., Hruban, R. H. & Pandey, A. (2012) Rapid Characterization of Candidate Biomarkers for Pancreatic Cancer Using Cell Microarrays (CMAs). *Journal of Proteome Research*, 11(11), 5556-5563.
Klerk, C. P., Smorenburg, S. M., Otten, H. M., Lensing, A. W., Prins, M. H., Piovella, F., Prandoni, P., Bos, M. M., Richel, D. J., van Tienhoven, G. & Buller, H. R. (2005) The effect of low molecular weight heparin on survival in patients with advanced malignancy. *J Clin Oncol*, 23(10), 2130-5.
Kocaturk, B., Tieken, C., Vreeken, D., Unlu, B., Engels, C. C., de Kruijf, E. M., Kuppen, P. J., Reitsma, P. H., Bogdanov, V. Y. & Versteeg, H. H. (2015) Alternatively spliced tissue factor synergizes with the estrogen receptor pathway in promoting breast cancer progression. *J Thromb Haemost*, 13(9), 1683-93.
Kocaturk, B., Van den Berg, Y. W., Tiekena, C., Mieog, J. S. D., de Kruijf, E. M., Engels, C. C., van der Ent, M. A., Kuppen, P. J., Van De Velde, C. J., Ruf, W., Reitsma, P. H., Osanto, S., Liefers, G. J., Bogdanov, V. Y. & Versteeg, H. H. (2013) Alternatively spliced tissue factor promotes breast cancer growth in a beta 1 integrin-dependent manner. *Proceedings of the National Academy of Sciences of the United States of America*, 110(28), 11517-11522.
Kocaturk, B. & Versteeg, H. H. (2013) Tissue factor-integrin interactions in cancer and thrombosis: every Jack has his Jill. *J Thromb Haemost*, 11 Suppl 1, 285-93.
Koizume, S., Ito, S., Miyagi, E., Hirahara, F., Nakamura, Y., Sakuma, Y., Osaka, H., Takano, Y., Ruf, W. & Miyagi, Y. (2012) HIF2alpha-Sp1 interaction mediates a deacetylation-dependent FVII-gene activation under hypoxic conditions in ovarian cancer cells. *Nucleic Acids Res*, 40(12), 5389-401.

Koizume, S., Ito, S., Yoshioka, Y., Kanayama, T., Nakamura, Y., Yoshihara, M., Yamada, R., Ochiya, T., Ruf, W., Miyagi, E., Hirahara, F. & Miyagi, Y. (2016) High-level secretion of tissue factor-rich extracellular vesicles from ovarian cancer cells mediated by filamin-A and protease-activated receptors. *Thromb Haemost*, 115(2), 299-310.
Koizume, S., Jin, M. S., Miyagi, E., Hirahara, F., Nakamura, Y., Piao, J. H., Asai, A., Yoshida, A., Tsuchiya, E., Ruf, W. & Miyagi, Y. (2006) Activation of cancer cell migration and invasion by ectopic synthesis of coagulation factor VII. *Cancer Res*, 66(19), 9453-60.
Koizume, S., Yokota, N., Miyagi, E., Hirahara, F., Nakamura, Y., Sakuma, Y., Yoshida, A., Kameda, Y., Tsuchiya, E., Ruf, W. & Miyagi, Y. (2009) Hepatocyte nuclear factor-4-independent synthesis of coagulation factor VII in breast cancer cells and its inhibition by targeting selective histone acetyltransferases. *Mol Cancer Res*, 7(12), 1928-36.
Komiyama, Y., Pedersen, A. H. & Kisiel, W. (1990) Proteolytic activation of human factors IX and X by recombinant human factor VIIa: effects of calcium, phospholipids, and tissue factor. *Biochemistry*, 29(40), 9418-25.
Krishnamurthy, M. & Freedman, M. L. (2005) Complications of anticoagulation with heparin. *Virtual Mentor*, 7(4).
Krudysz-Amblo, J., Jennings, M. E., Matthews, D. E., Mann, K. G. & Butenas, S. (2011) Differences in the fractional abundances of carbohydrates of natural and recombinant human tissue factor. *Biochimica Et Biophysica Acta-General Subjects*, 1810(4), 398-405.
Langer, F. & Bokemeyer, C. (2012) Crosstalk between cancer and haemostasis. Implications for cancer biology and cancer-associated thrombosis with focus on tissue factor. *Hamostaseologie*, 32(2), 95-104.
Lazo-Langner, A., Goss, G. D., Spaans, J. N. & Rodger, M. A. (2007) The effect of low-molecular-weight heparin on cancer survival. A systematic review and meta-analysis of randomized trials. *J Thromb Haemost*, 5(4), 729-37.
Le Gall, M., Grall, D., Chambard, J. C., Pouyssegur, J. & Van Obberghen-Schilling, E. (1998) An anchorage-dependent signal distinct from p42/44 MAP kinase activation is required for cell cycle progression. *Oncogene*, 17(10), 1271-7.
Lee, E., Kim, Y. S., Bae, S. M., Kim, S. K., Jin, S., Chung, S. W., Lee, M., Moon, H. T., Jeon, O. C., Park, R. W., Kim, I. S., Byun, Y. & Kim, S. Y. (2009) Polyproline-type helical-structured low-molecular weight heparin (LMWH)-taurocholate conjugate as a new angiogenesis inhibitor. *Int J Cancer*, 124(12), 2755-65.
Lerner, D. J., Chen, M., Tram, T. & Coughlin, S. R. (1996) Agonist recognition by proteinase-activated receptor 2 and thrombin receptor. Importance of extracellular loop interactions for receptor function. *J Biol Chem*, 271(24), 13943-7.
Leung, D. W., Cachianes, G., Kuang, W. J., Goeddel, D. V. & Ferrara, N. (1989) Vascular endothelial growth factor is a secreted angiogenic mitogen. *Science*, 246(4935), 1306-9.
Levental, I., Levental, K. R. & Heberle, F. A. (2020) Lipid Rafts: Controversies Resolved, Mysteries Remain. *Trends Cell Biol*, 30(5), 341-353.
Levental, I., Lingwood, D., Grzybek, M., Coskun, U. & Simons, K. (2010) Palmitoylation regulates raft affinity for the majority of integral raft proteins. *Proc Natl Acad Sci U S A*, 107(51), 22050-4.
Lever, R., Hoult, J. R. & Page, C. P. (2000) The effects of heparin and related molecules upon the adhesion of human polymorphonuclear leucocytes to vascular endothelium in vitro. *Br J Pharmacol*, 129(3), 533-40.
Levine, M. N., Gu, C., Liebman, H. A., Escalante, C. P., Solymoss, S., Deitchman, D., Ramirez, L. & Julian, J. (2012) A randomized phase II trial of apixaban for the prevention of thromboembolism in patients with metastatic cancer. *Journal of Thrombosis and Haemostasis*, 10(5), 807-814.
Li, B., Antonyak, M. A., Zhang, J. & Cerione, R. A. (2012) RhoA triggers a specific signaling pathway that generates transforming microvesicles in cancer cells. *Oncogene*, 31(45), 4740-4749.

Lim, S. T., Chen, X. L., Lim, Y., Hanson, D. A., Vo, T. T., Howerton, K., Larocque, N., Fisher, S. J., Schlaepfer, D. D. & Ilic, D. (2008) Nuclear FAK promotes cell proliferation and survival through FERM-enhanced p53 degradation. *Mol Cell*, 29(1), 9-22.
Lima, L. G., Leal, A. C., Vargas, G., Porto-Carreiro, I. & Monteiro, R. Q. (2013) Intercellular transfer of tissue factor via the uptake of tumor-derived microvesicles. *Thromb Res*, 132(4), 450-6.
Lin, R. Z. & Chang, H. Y. (2008) Recent advances in three-dimensional multicellular spheroid culture for biomedical research. *Biotechnol J*, 3(9-10), 1172-84.
Lin, R. Z., Chou, L. F., Chien, C. C. & Chang, H. Y. (2006) Dynamic analysis of hepatoma spheroid formation: roles of E-cadherin and beta1-integrin. *Cell Tissue Res*, 324(3), 411-22.
Lin, Z. M., Zhao, J. X., Duan, X. N., Zhang, L. B., Ye, J. M., Xu, L. & Liu, Y. H. (2014) Effects of tissue factor, PAR-2 and MMP-9 expression on human breast cancer cell line MCF-7 invasion. *Asian Pac J Cancer Prev*, 15(2), 643-6.
Lindblom, P., Gerhardt, H., Liebner, S., Abramsson, A., Enge, M., Hellstrom, M., Backstrom, G., Fredriksson, S., Landegren, U., Nystrom, H. C., Bergstrom, G., Dejana, E., Ostman, A., Lindahl, P. & Betsholtz, C. (2003) Endothelial PDGF-B retention is required for proper investment of pericytes in the microvessel wall. *Genes Dev*, 17(15), 1835-40.
Linhardt, R. J. (2003) 2003 Claude S. Hudson Award address in carbohydrate chemistry. Heparin: structure and activity. *J Med Chem*, 46(13), 2551-64.
Linhardt, R. J. & Gunay, N. S. (1999) Production and chemical processing of low molecular weight heparins. *Semin Thromb Hemost*, 25 Suppl 3, 5-16.
Liu, M. L., Reilly, M. P., Casasanto, P., McKenzie, S. E. & Williams, K. J. (2007) Cholesterol enrichment of human monocyte/macrophages induces surface exposure of phosphatidylserine and the release of biologically-active tissue factor-positive microvesicles. *Arterioscler Thromb Vasc Biol*, 27(2), 430-5.
Liu, Y., Jiang, P., Capkova, K., Xue, D., Ye, L., Sinha, S. C., Mackman, N., Janda, K. D. & Liu, C. (2011) Tissue factor-activated coagulation cascade in the tumor microenvironment is critical for tumor progression and an effective target for therapy. *Cancer Res*, 71(20), 6492-502.
Liu, Y. & Mueller, B. M. (2006) Protease-activated receptor-2 regulates vascular endothelial growth factor expression in MDA-MB-231 cells via MAPK pathways. *Biochem Biophys Res Commun*, 344(4), 1263-70.
Livak, K. J. & Schmittgen, T. D. (2001) Analysis of relative gene expression data using real-time quantitative PCR and the 2(T)(-Delta Delta C) method. *Methods*, 25(4), 402-408.
Lodish, H. F. (2008) *Molecular cell biology*, 1 vols., 6th edition. New York: W.H. Freeman.
Loo, D. T., Kanner, S. B. & Aruffo, A. (1998) Filamin binds to the cytoplasmic domain of the beta1-integrin. Identification of amino acids responsible for this interaction. *J Biol Chem*, 273(36), 23304-12.
Losche, W., Scholz, T., Temmler, U., Oberle, V. & Claus, R. A. (2004) Platelet-derived microvesicles transfer tissue factor to monocytes but not to neutrophils. *Platelets*, 15(2), 109-15.
Loury, D. J., Thiemann, P., Prescoutt, J. E. & Buggy, J. (2007) PCI-27483, a small molecule inhibitor of factor VIIa, inhibits tumor growth in vivo. *Molecular Cancer Therapeutics*, 6(12), 3523s-3523s.
Lugano, R., Ramachandran, M. & Dimberg, A. (2020) Tumor angiogenesis: causes, consequences, challenges and opportunities. *Cell Mol Life Sci*, 77(9), 1745-1770.
Luo, B. H., Carman, C. V. & Springer, T. A. (2007) Structural basis of integrin regulation and signaling. *Annu Rev Immunol*, 25, 619-47.
Luo, R., Wang, X. W., Dong, Y. X., Wang, L. & Tian, C. L. (2014) Activation of protease-activated receptor 2 reduces glioblastoma cell apoptosis. *Journal of Biomedical Science*, 21.
Luo, W., Shitaye, H., Friedman, M., Bennett, C. N., Miller, J., Macdougald, O. A. & Hankenson, K. D. (2008) Disruption of cell-matrix interactions by heparin enhances mesenchymal progenitor adipocyte differentiation. *Exp Cell Res*, 314(18), 3382-91.
Lustig, F., Hoebeke, J., Ostergren-Lunden, G., Velge-Roussel, F., Bondjers, G., Olsson, U., Ruetschi, U. & Fager, G. (1996) Alternative splicing determines the binding of platelet-derived growth factor (PDGF-AA) to glycosaminoglycans. *Biochemistry*, 35(37), 12077-85.

Lyman, G. H., Khorana, A. A., Falanga, A., Clarke-Pearson, D., Flowers, C., Jahanzeb, M., Kakkar, A., Kuderer, N. M., Levine, M. N., Liebman, H., Mendelson, D., Raskob, G., Somerfield, M. R., Thodiyil, P., Trent, D., Francis, C. W. & American Society of Clinical, O. (2007) American Society of Clinical Oncology guideline: recommendations for venous thromboembolism prophylaxis and treatment in patients with cancer. *J Clin Oncol*, 25(34), 5490-505.
Ma, L., Perini, R., McKnight, W., Dicay, M., Klein, A., Hollenberg, M. D. & Wallace, J. L. (2005) Proteinase-activated receptors 1 and 4 counter-regulate endostatin and VEGF release from human platelets. *Proc Natl Acad Sci U S A*, 102(1), 216-20.
Ma, Y., Bao-Han, W., Lv, X., Su, Y., Zhao, X., Yin, Y., Zhang, X., Zhou, Z., MacNaughton, W. K. & Wang, H. (2013) MicroRNA-34a mediates the autocrine signaling of PAR2-activating proteinase and its role in colonic cancer cell proliferation. *PLoS One*, 8(8), e72383.
Macfarlane, R. G. (1964) An enzyme cascade in the blood clotting mechanism, and Its function as a biochemical amplifier. *Nature*, 202, 498-9.
Mackman, N. (2004) Role of tissue factor in hemostasis, thrombosis, and vascular development. *Arterioscler Thromb Vasc Biol*, 24(6), 1015-22.
Mackman, N. (2009) The role of tissue factor and factor VIIa in hemostasis. *Anesth Analg*, 108(5), 1447-52.
Mackman, N., Sawdey, M. S., Keeton, M. R. & Loskutoff, D. J. (1993) Murine tissue factor gene expression in vivo. Tissue and cell specificity and regulation by lipopolysaccharide. *Am J Pathol*, 143(1), 76-84.
Madkhali, Y., Featherby, S., Collier, M. E., Maraveyas, A., Greenman, J. & Ettelaie, C. (2019) The ratio of factor VIIa:Tissue factor content within microvesicles determines the differential influence on endothelial cells. *TH Open*, 3(2), e132-e145.
Madkhali, Y. A. (2020) *An investigation into the regulation of cellular homeostasis through modulation of cell-surface tissue factor*PhD. University of Hull
Magnus, N., Garnier, D. & Rak, J. (2010) Oncogenic epidermal growth factor receptor up-regulates multiple elements of the tissue factor signaling pathway in human glioma cells. *Blood*, 116(5), 815-8.
Majewski, M. W., Gandhi, D. M., Holyst, T., Wang, Z., Hernandez, I., Rosas, R., Jr., Zhu, J., Weiler, H. & Dockendorff, C. (2020) Synthesis and initial pharmacology of dual-targeting ligands for putative complexes of integrin alphaVbeta3 and PAR2. *RSC Med Chem*, 11(8), 940-949.
Mandala, M., Falanga, A., Piccioli, A., Prandoni, P., Pogliani, E. M., Labianca, R., Barni, S. & working group, A. (2006) Venous thromboembolism and cancer: guidelines of the Italian Association of Medical Oncology (AIOM). *Crit Rev Oncol Hematol*, 59(3), 194-204.
Manduteanu, I., Voinea, M., Capraru, M., Dragomir, E. & Simionescu, M. (2002) A novel attribute of enoxaparin: inhibition of monocyte adhesion to endothelial cells by a mechanism involving cell adhesion molecules. *Pharmacology*, 65(1), 32-7.
Mangieri, D., Nico, B., Benagiano, V., De Giorgis, M., Vacca, A. & Ribatti, D. (2008) Angiogenic activity of multiple myeloma endothelial cells in vivo in the chick embryo chorioallantoic membrane assay is associated to a down-regulation in the expression of endogenous endostatin. *J Cell Mol Med*, 12(3), 1023-8.
Mann, K. G. (1999) Biochemistry and physiology of blood coagulation. *Thromb Haemost*, 82(2), 165-74.
Maqsood, A., Hisada, Y., Garratt, K. B., Homeister, J. & Mackman, N. (2019) Rivaroxaban does not affect growth of human pancreatic tumors in mice. *J Thromb Haemost*.
Maraveyas, A., Ettelaie, C., Echrish, H., Li, C., Gardiner, E., Greenman, J. & Madden, L. A. (2010) Weight-adjusted dalteparin for prevention of vascular thromboembolism in advanced pancreatic cancer patients decreases serum tissue factor and serum-mediated induction of cancer cell invasion. *Blood Coagul Fibrinolysis*, 21(5), 452-8.
Maraveyas, A., Waters, J., Roy, R., Fyfe, D., Propper, D., Lofts, F., Sgouros, J., Gardiner, E., Wedgwood, K., Ettelaie, C. & Bozas, G. (2012) Gemcitabine versus gemcitabine plus dalteparin thromboprophylaxis in pancreatic cancer. *Eur J Cancer*, 48(9), 1283-92.

Marchetti, M., Vignoli, A., Russo, L., Balducci, D., Pagnoncelli, M., Barbui, T. & Falanga, A. (2008) Endothelial capillary tube formation and cell proliferation induced by tumor cells are affected by low molecular weight heparins and unfractionated heparin. *Thromb Res*, 121(5), 637-45.
Martin, N. B., Jamieson, A. & Tuffin, D. P. (1993) The effect of interleukin-4 on tumour necrosis factor-alpha induced expression of tissue factor and plasminogen activator inhibitor-1 in human umbilical vein endothelial cells. *Thromb Haemost*, 70(6), 1037-42.
Martins, V. R., Dias, M. S. & Hainaut, P. (2013) Tumor-cell-derived microvesicles as carriers of molecular information in cancer. *Curr Opin Oncol*, 25(1), 66-75.
Maryanoff, B. E., Santulli, R. J., McComsey, D. F., Hoekstra, W. J., Hoey, K., Smith, C. E., Addo, M., Darrow, A. L. & Andrade-Gordon, P. (2001) Protease-activated receptor-2 (PAR-2): structure-function study of receptor activation by diverse peptides related to tethered-ligand epitopes. *Arch Biochem Biophys*, 386(2), 195-204.
Masola, V., Zaza, G., Gambaro, G., Franchi, M. & Onisto, M. (2020) Role of heparanase in tumor progression: Molecular aspects and therapeutic options. *Semin Cancer Biol*, 62, 86-98.
Maulik, P. R. & Shipley, G. G. (1996) Interactions of N-stearoyl sphingomyelin with cholesterol and dipalmitoylphosphatidylcholine in bilayer membranes. *Biophys J*, 70(5), 2256-65.
MBinfo (2018) *What is integrin?*, 2018. Available online: https://www.mechanobio.info/what-is-mechanosignaling/what-is-the-extracellular-matrix-and-the-basal-lamina/what-is-integrin/ [Accessed.
McBane, R. D., 2nd, Wysokinski, W. E., Le-Rademacher, J. G., Zemla, T., Ashrani, A., Tafur, A., Perepu, U., Anderson, D., Gundabolu, K., Kuzma, C., Perez Botero, J., Leon Ferre, R. A., Henkin, S., Lenz, C. J., Houghton, D. E., Vishnu, P. & Loprinzi, C. L. (2020) Apixaban and dalteparin in active malignancy-associated venous thromboembolism: The ADAM VTE trial. *J Thromb Haemost*, 18(2), 411-421.
McCoy, K. L., Traynelis, S. F. & Hepler, J. R. (2010) PAR1 and PAR2 couple to overlapping and distinct sets of G proteins and linked signaling pathways to differentially regulate cell physiology. *Molecular Pharmacology*, 77(6), 1005-1015.
Mebratu, Y. & Tesfaigzi, Y. (2009) How ERK1/2 activation controls cell proliferation and cell death: Is subcellular localization the answer? *Cell Cycle*, 8(8), 1168-75.
Menck, K., Sonmezer, C., Worst, T. S., Schulz, M., Dihazi, G. H., Streit, F., Erdmann, G., Kling, S., Boutros, M., Binder, C. & Gross, J. C. (2017) Neutral sphingomyelinases control extracellular vesicles budding from the plasma membrane. *Journal of Extracellular Vesicles*, 6(1).
MERCK (2019) *How Proximity Ligation Assays (PLA) Work*, 2019. Available online: https://www.sigmaaldrich.com/GB/en/technical-documents/technical-article/protein-biology/protein-and-nucleic-acid-interactions/how-pla-works [Accessed.
Mertens, K. & Bertina, R. M. (1980) Pathways in the activation of human coagulation factor X. *Biochem J*, 185(3), 647-58.
Milia, A. F., Salis, M. B., Stacca, T., Pinna, A., Madeddu, P., Trevisani, M., Geppetti, P. & Emanueli, C. (2002) Protease-activated receptor-2 stimulates angiogenesis and accelerates hemodynamic recovery in a mouse model of hindlimb ischemia. *Circ Res*, 91(4), 346-52.
Mirza, H., Yatsula, V. & Bahou, W. F. (1996) The proteinase activated receptor-2 (PAR-2) mediates mitogenic responses in human vascular endothelial cells - Molecular characterization and evidence for functional coupling to the thrombin receptor. *Journal of Clinical Investigation*, 97(7), 1705-1714.
Mitra, S. K. & Schlaepfer, D. D. (2006) Integrin-regulated FAK-Src signaling in normal and cancer cells. *Curr Opin Cell Biol*, 18(5), 516-23.
Miyata, S., Miyagi, Y., Koshikawa, N., Nagashima, Y., Kato, Y., Yasumitsu, H., Hirahara, F., Misugi, K. & Miyazaki, K. (1998) Stimulation of cellular growth and adhesion to fibronectin and vitronectin in culture and tumorigenicity in nude mice by overexpression of trypsinogen in human gastric cancer cells. *Clinical & Experimental Metastasis*, 16(7), 613-622.
Moreno-Layseca, P. & Streuli, C. H. (2014) Signalling pathways linking integrins with cell cycle progression. *Matrix Biol*, 34, 144-53.

Moro, L., Dolce, L., Cabodi, S., Bergatto, E., Boeri Erba, E., Smeriglio, M., Turco, E., Retta, S. F., Giuffrida, M. G., Venturino, M., Godovac-Zimmermann, J., Conti, A., Schaefer, E., Beguinot, L., Tacchetti, C., Gaggini, P., Silengo, L., Tarone, G. & Defilippi, P. (2002) Integrin-induced epidermal growth factor (EGF) receptor activation requires c-Src and p130Cas and leads to phosphorylation of specific EGF receptor tyrosines. *J Biol Chem*, 277(11), 9405-14.
Morris, D. R., Ding, Y., Ricks, T. K., Gullapalli, A., Wolfe, B. L. & Trejo, J. (2006) Protease-activated receptor-2 is essential for factor VIIa and Xa-induced signaling, migration, and invasion of breast cancer cells. *Cancer Research*, 66(1), 307-314.
Morrissey, J. H., Davis-Harrison, R. L., Tavoosi, N., Ke, K., Pureza, V., Boettcher, J. M., Clay, M. C., Rienstra, C. M., Ohkubo, Y. Z., Pogorelov, T. V. & Tajkhorshid, E. (2010) Protein-phospholipid interactions in blood clotting. *Thromb Res*, 125 Suppl 1, S23-5.
Morrissey, J. H., Fakhrai, H. & Edgington, T. S. (1987) Molecular cloning of the cDNA for tissue factor, the cellular receptor for the initiation of the coagulation protease cascade. *Cell*, 50(1), 129-35.
Morrissey, J. H., Macik, B. G., Neuenschwander, P. F. & Comp, P. C. (1993) Quantitation of activated factor VII levels in plasma using a tissue factor mutant selectively deficient in promoting factor VII activation. *Blood*, 81(3), 734-44.
Morrissey, J. H., Tajkhorshid, E., Sligar, S. G. & Rienstra, C. M. (2012) Tissue factor/factor VIIa complex: role of the membrane surface. *Thromb Res*, 129 Suppl 2, S8-10.
Mouritsen, O. G. & Bloom, M. (1993) Models of lipid-protein interactions in membranes. *Annu Rev Biophys Biomol Struct*, 22, 145-71.
Mousa, S. A. (2013) Comparative pharmacodynamic assessment of the antiangiogenesis activity of heparin and low-molecular-weight heparin fractions: structure-function relationship. *Clin Appl Thromb Hemost*, 19(1), 48-54.
Mousa, S. A., Bozarth, J. M., Larnkjaer, A. & Johansen, K. (2000) Vascular effects of heparin molecular weight fractions and low molecular weight heparins (LMWH) on the release of tissue factor pathway inhibitor (TFPI) from human endothelial cells. *Blood*, 96(11), 59b-59b.
Mousa, S. A., Linhardt, R., Francis, J. L. & Amirkhosravi, A. (2006) Anti-metastatic effect of a non-anticoagulant low-molecular-weight heparin versus the standard low-molecular-weight heparin, enoxaparin. *Thromb Haemost*, 96(6), 816-21.
Mousa, S. A. & Mohamed, S. (2004a) Anti-angiogenic mechanisms and efficacy of the low molecular weight heparin, tinzaparin: anti-cancer efficacy. *Oncol Rep*, 12(4), 683-8.
Mousa, S. A. & Mohamed, S. (2004b) Inhibition of endothelial cell tube formation by the low molecular weight heparin, tinzaparin, is mediated by tissue factor pathway inhibitor. *Thromb Haemost*, 92(3), 627-33.
Mousa, S. A. & Petersen, L. J. (2009) Anti-cancer properties of low-molecular-weight heparin: preclinical evidence. *Thromb Haemost*, 102(2), 258-67.
Mueck, W., Stampfuss, J., Kubitza, D. & Becka, M. (2014) Clinical pharmacokinetic and pharmacodynamic profile of rivaroxaban. *Clin Pharmacokinet*, 53(1), 1-16.
Mueller, B. M., Reisfeld, R. A., Edgington, T. S. & Ruf, W. (1992) Expression of tissue factor by melanoma cells promotes efficient hematogenous metastasis. *Proc Natl Acad Sci U S A*, 89(24), 11832-6.
Muller, M., Albrecht, S., Golfert, F., Hofer, A., Funk, R. H., Magdolen, V., Flossel, C. & Luther, T. (1999) Localization of tissue factor in actin-filament-rich membrane areas of epithelial cells. *Exp Cell Res*, 248(1), 136-47.
Munro, S. (1995) An investigation of the role of transmembrane domains in Golgi protein retention. *EMBO J*, 14(19), 4695-704.
Munster, M., Fremder, E., Miller, V., Ben-Tsedek, N., Davidi, S., Scherer, S. J. & Shaked, Y. (2014) Anti-VEGF-A affects the angiogenic properties of tumor-derived microparticles. *PLoS One*, 9(4), e95983.

Muralidharan-Chari, V., Clancy, J., Plou, C., Romao, M., Chavrier, P., Raposo, G. & D'Souza-Schorey, C. (2009a) ARF6-regulated shedding of tumor cell-derived plasma membrane microvesicles. *Curr Biol*, 19(22), 1875-85.
Muralidharan-Chari, V., Clancy, J., Plou, C., Romao, M., Chavrier, P., Raposo, G. & D'Souza-Schorey, C. (2009b) ARF6-Regulated Shedding of Tumor Cell-Derived Plasma Membrane Microvesicles. *Current Biology*, 19(22), 1875-1885.
Muralidharan-Chari, V., Clancy, J. W., Sedgwick, A. & D'Souza-Schorey, C. (2010) Microvesicles: mediators of extracellular communication during cancer progression. *J Cell Sci*, 123(Pt 10), 1603-11.
Nadir, Y. (2019) Decreasing tumor growth and angiogenesis by inhibition of coagulation. *Semin Thromb Hemost*, 45(6), 622-628.
Nadir, Y., Brenner, B., Zetser, A., Ilan, N., Shafat, I., Zcharia, E., Goldshmidt, O. & Vlodavsky, I. (2006) Heparanase induces tissue factor expression in vascular endothelial and cancer cells. *J Thromb Haemost*, 4(11), 2443-51.
Nawaz, M., Shah, N., Zanetti, B. R., Maugeri, M., Silvestre, R. N., Fatima, F., Neder, L. & Valadi, H. (2018) Extracellular vesicles and matrix remodeling enzymes: the emerging roles in extracellular matrix remodeling, progression of diseases and tissue repair. *Cells*, 7(10).
NEBiolabs *Guidelines for PCR Optimization with Thermophilic DNA Polymerases*Available online: https://www.neb.com/tools-and-resources/usage-guidelines/guidelines-for-pcr-optimization-with-thermophilic-dna-polymerases [Accessed 2018].
NEBiolabs (2020) *Q5® Site-Directed Mutagenesis Kit - manual*, 2020. Available online: https://www.neb.com/-/media/catalog/datacards-or-manuals/manuale0554.pdf [Accessed 2018].
Nieswandt, B., Hafner, M., Echtenacher, B. & Mannel, D. N. (1999) Lysis of tumor cells by natural killer cells in mice is impeded by platelets. *Cancer Res*, 59(6), 1295-300.
Nishibori, M., Mori, S. & Takahashi, H. K. (2005) Physiology and pathophysiology of proteinase-activated receptors (PARs): PAR-2-mediated proliferation of colon cancer cell. *J Pharmacol Sci*, 97(1), 25-30.
Norrby, K. (2000) 2.5 kDa and 5.0 kDa heparin fragments specifically inhibit microvessel sprouting and network formation in VEGF165-mediated mammalian angiogenesis. *Int J Exp Pathol*, 81(3), 191-8.
Norrby, K. (2006) Low-molecular-weight heparins and angiogenesis. *APMIS*, 114(2), 79-102.
Nystedt, S., Emilsson, I. E., Wahlestedt, C. & Sundelin, J. (1994) Molecular-cloning of a potential proteinase activated receptor. *Proceedings of the National Academy of Sciences of the United States of America*, 91(20), 9208-9212.
Nystedt, S., Emilsson, K., Larsson, A. K., Strombeck, B. & Sundelin, J. (1995) Molecular cloning and functional expression of the gene encoding the human proteinase-activated receptor 2. *Eur J Biochem*, 232(1), 84-9.
O'Brien, P. J., Molino, M., Kahn, M. & Brass, L. F. (2001) Protease activated receptors: theme and variations. *Oncogene*, 20(13), 1570-81.
Ollivier, V., Chabbat, J., Herbert, J. M., Hakim, J. & de Prost, D. (2000) Vascular endothelial growth factor production by fibroblasts in response to factor VIIa binding to tissue factor involves thrombin and factor Xa. *Arterioscler Thromb Vasc Biol*, 20(5), 1374-81.
Olson, M. F., Ashworth, A. & Hall, A. (1995) An essential role for Rho, Rac, and Cdc42 GTPases in cell cycle progression through G1. *Science*, 269(5228), 1270-2.
Olson, S. T., Bjork, I., Sheffer, R., Craig, P. A., Shore, J. D. & Choay, J. (1992) Role of the antithrombin-binding pentasaccharide in heparin acceleration of antithrombin-proteinase reactions. Resolution of the antithrombin conformational change contribution to heparin rate enhancement. *J Biol Chem*, 267(18), 12528-38.
Osterud, B. (2010) Tissue factor expression in blood cells. *Thromb Res*, 125 Suppl 1, S31-4.
Osterud, B. & Olsen, J. O. (2013) Human platelets do not express tissue factor. *Thromb Res*, 132(1), 112-5.

Ott, I., Fischer, E. G., Miyagi, Y., Mueller, B. M. & Ruf, W. (1998) A role for tissue factor in cell adhesion and migration mediated by interaction with actin-binding protein 280. *Journal of Cell Biology*, 140(5), 1241-1253.
Ott, I., Weigand, B., Michl, R., Seitz, I., Sabbari-Erfani, N., Neumann, F. J. & Schomig, A. (2005) Tissue factor cytoplasmic domain stimulates migration by activation of the GTPase Rac1 and the mitogen-activated protein kinase p38. *Circulation*, 111(3), 349-55.
Paborsky, L. R., Caras, I. W., Fisher, K. L. & Gorman, C. M. (1991) Lipid association, but not the transmembrane domain, is required for tissue factor activity. Substitution of the transmembrane domain with a phosphatidylinositol anchor. *J Biol Chem*, 266(32), 21911-6.
Paborsky, L. R. & Harris, R. J. (1990) Post-translational modifications of recombinant human tissue factor. *Thromb Res*, 60(5), 367-76.
Palta, S., Saroa, R. & Palta, A. (2014) Overview of the coagulation system. *Indian J Anaesth*, 58(5), 515-23.
Parisis, N., Metodieva, G. & Metodiev, M. V. (2013) Pseudopodial and beta-arrestin-interacting proteomes from migrating breast cancer cells upon PAR2 activation. *J Proteomics*, 80, 91-106.
Park, C. C., Zhang, H., Pallavicini, M., Gray, J. W., Baehner, F., Park, C. J. & Bissell, M. J. (2006) Beta1 integrin inhibitory antibody induces apoptosis of breast cancer cells, inhibits growth, and distinguishes malignant from normal phenotype in three dimensional cultures and in vivo. *Cancer Res*, 66(3), 1526-35.
Pawar, N. R., Buzza, M. S. & Antalis, T. M. (2019) Membrane-anchored serine proteases and protease-activated receptor-2-mediated signaling: co-conspirators in cancer progression. *Cancer Research*, 79(2), 301-310.
Piccin, A., Murphy, W. G. & Smith, O. P. (2007) Circulating microparticles: pathophysiology and clinical implications. *Blood Rev*, 21(3), 157-71.
Pike, A. C. W., Brzozowski, A. M., Roberts, S. M., Olsen, O. H. & Persson, E. (1999) Structure of human factor VIIa and its implications for the triggering of blood coagulation. *Proceedings of the National Academy of Sciences of the United States of America*, 96(16), 8925-8930.
Pinto, D. J., Orwat, M. J., Koch, S., Rossi, K. A., Alexander, R. S., Smallwood, A., Wong, P. C., Rendina, A. R., Luettgen, J. M., Knabb, R. M., He, K., Xin, B., Wexler, R. R. & Lam, P. Y. (2007) Discovery of 1-(4-methoxyphenyl)-7-oxo-6-(4-(2-oxopiperidin-1-yl)phenyl)-4,5,6,7-tetrahydro-1H -pyrazolo[3,4-c]pyridine-3-carboxamide (apixaban, BMS-562247), a highly potent, selective, efficacious, and orally bioavailable inhibitor of blood coagulation factor Xa. *J Med Chem*, 50(22), 5339-56.
Pisano, C., Aulicino, C., Vesci, L., Casu, B., Naggi, A., Torri, G., Ribatti, D., Belleri, M., Rusnati, M. & Presta, M. (2005) Undersulfated, low-molecular-weight glycol-split heparin as an antiangiogenic VEGF antagonist. *Glycobiology*, 15(2), 1C-6C.
Poon, R. T., Lau, C. P., Ho, J. W., Yu, W. C., Fan, S. T. & Wong, J. (2003) Tissue factor expression correlates with tumor angiogenesis and invasiveness in human hepatocellular carcinoma. *Clin Cancer Res*, 9(14), 5339-45.
Poulsen, L. K., Jacobsen, N., Sorensen, B. B., Bergenhem, N. C., Kelly, J. D., Foster, D. C., Thastrup, O., Ezban, M. & Petersen, L. C. (1998) Signal transduction via the mitogen-activated protein kinase pathway induced by binding of coagulation factor VIIa to tissue factor. *J Biol Chem*, 273(11), 6228-32.
Pradier, A. & Ettelaie, C. (2008) The influence of exogenous tissue factor on the regulators of proliferation and apoptosis in endothelial cells. *J Vasc Res*, 45(1), 19-32.
Prescott, J. T., P. Loury, D. (2008) PCI-27483, a small molecule inhibitor of factor VIIa, inhibits growth of BxPC3 pancreatic adenocarcinoma xenograft tumors, *American Association for Cancer Research Annual Meeting.* San Diego, CA.
Prieto-Martínez FD, A. M., Medina-Franco JL. (2018) Molecular docking: current advances and challenges. *TIP Rev Esp Cienc Quim Biol.*, 21(Suppl: 1), 65-87.
Rackov, G., Garcia-Romero, N., Esteban-Rubio, S., Carrion-Navarro, J., Belda-Iniesta, C. & Ayuso-Sacido, A. (2018) Vesicle-mediated control of cell function: the role of extracellular matrix and microenvironment. *Front Physiol*, 9, 651.

Ramanathan, R. K., Thomas, G. W., Khorana, A. A., Shah, S., Zhou, C., Wong, S., Cole, G., James, D. & Gabrail, N. Y. (2019) A Phase 2 Study of PCI-27483, a Factor VIIa Inhibitor in Combination with Gemcitabine for Advanced Pancreatic Cancer. *Oncology*, 96(4), 217-222.
Rand, M. L., Wang, H., Bang, K. W., Packham, M. A. & Freedman, J. (2006) Rapid clearance of procoagulant platelet-derived microparticles from the circulation of rabbits. *J Thromb Haemost*, 4(7), 1621-3.
Randolph, G. J., Luther, T., Albrecht, S., Magdolen, V. & Muller, W. A. (1998) Role of tissue factor in adhesion of mononuclear phagocytes to and trafficking through endothelium in vitro. *Blood*, 92(11), 4167-4177.
Rao, B., Gao, Y., Huang, J., Gao, X., Fu, X., Huang, M., Yao, J., Wang, J., Li, W., Zhang, J., Liu, H., Wang, L. & Wang, J. (2011) Mutations of p53 and K-ras correlate TF expression in human colorectal carcinomas: TF downregulation as a marker of poor prognosis. *Int J Colorectal Dis*, 26(5), 593-601.
Rao, C. N., Lakka, S. S., Kin, Y., Konduri, S. D., Fuller, G. N., Mohanam, S. & Rao, J. S. (2001) Expression of tissue factor pathway inhibitor 2 inversely correlates during the progression of human gliomas. *Clin Cancer Res*, 7(3), 570-6.
Rao, L. V., Kothari, H. & Pendurthi, U. R. (2012) Tissue factor encryption and decryption: facts and controversies. *Thromb Res*, 129 Suppl 2, S13-7.
Raposo, G. & Stoorvogel, W. (2013) Extracellular vesicles: exosomes, microvesicles, and friends. *J Cell Biol*, 200(4), 373-83.
Raskob, G. E., van Es, N., Verhamme, P., Carrier, M., Di Nisio, M., Garcia, D., Grosso, M. A., Kakkar, A. K., Kovacs, M. J., Mercuri, M. F., Meyer, G., Segers, A., Shi, M., Wang, T. F., Yeo, E., Zhang, G., Zwicker, J. I., Weitz, J. I., Buller, H. R. & Hokusai, V. T. E. C. I. (2018) Edoxaban for the treatment of cancer-associated venous thromboembolism. *N Engl J Med*, 378(7), 615-624.
Rauch, U., Bonderman, D., Bohrmann, B., Badimon, J. J., Himber, J., Riederer, M. A. & Nemerson, Y. (2000) Transfer of tissue factor from leukocytes to platelets is mediated by CD15 and tissue factor. *Blood*, 96(1), 170-5.
Ribatti, D. (2014) The chick embryo chorioallantoic membrane as a model for tumor biology. *Experimental Cell Research*, 328(2), 314-324.
Richard, D. E., Vouret-Craviari, V. & Pouyssegur, J. (2001) Angiogenesis and G-protein-coupled receptors: signals that bridge the gap. *Oncogene*, 20(13), 1556-62.
Rickles, F. R., Hancock, W. W., Edwards, R. L. & Zacharski, L. R. (1988) Antimetastatic agents. I. Role of cellular procoagulants in the pathogenesis of fibrin deposition in cancer and the use of anticoagulants and/or antiplatelet drugs in cancer treatment. *Semin Thromb Hemost*, 14(1), 88-94.
Rickles, F. R., Shoji, M. & Abe, K. (2001) The role of the hemostatic system in tumor growth, metastasis, and angiogenesis: tissue factor is a bifunctional molecule capable of inducing both fibrin deposition and angiogenesis in cancer. *Int J Hematol*, 73(2), 145-50.
Riewald, M. & Ruf, W. (2001) Mechanistic coupling of protease signaling and initiation of coagulation by tissue factor. *Proc Natl Acad Sci U S A*, 98(14), 7742-7.
Roehrig, S., Straub, A., Pohlmann, J., Lampe, T., Pernerstorfer, J., Schlemmer, K. H., Reinemer, P. & Perzborn, E. (2005) Discovery of the novel antithrombotic agent 5-chloro-N-({(5S)-2-oxo-3- [4-(3-oxomorpholin-4-yl)phenyl]-1,3-oxazolidin-5-yl}methyl)thiophene- 2-carboxamide (BAY 59-7939): an oral, direct factor Xa inhibitor. *J Med Chem*, 48(19), 5900-8.
Rong, Y., Belozerov, V. E., Tucker-Burden, C., Chen, G., Durden, D. L., Olson, J. J., Van Meir, E. G., Mackman, N. & Brat, D. J. (2009) Epidermal growth factor receptor and PTEN modulate tissue factor expression in glioblastoma through JunD/activator protein-1 transcriptional activity. *Cancer Res*, 69(6), 2540-9.
Rong, Y., Hu, F., Huang, R., Mackman, N., Horowitz, J. M., Jensen, R. L., Durden, D. L., Van Meir, E. G. & Brat, D. J. (2006) Early growth response gene-1 regulates hypoxia-induced expression of tissue factor in glioblastoma multiforme through hypoxia-inducible factor-1-independent mechanisms. *Cancer Res*, 66(14), 7067-74.

Rothmeier, A. S., Liu, E., Chakrabarty, S., Disse, J., Mueller, B. M., Ostergaard, H. & Ruf, W. (2018) Identification of the integrin-binding site on coagulation factor VIIa required for proangiogenic PAR2 signaling. *Blood*, 131(6), 674-685.
Rothmeier, A. S., Marchese, P., Langer, F., Kamikubo, Y., Schaffner, F., Cantor, J., Ginsberg, M. H., Ruggeri, Z. M. & Ruf, W. (2017) Tissue factor prothrombotic activity is regulated by integrin-arf6 trafficking. *Arterioscler Thromb Vasc Biol*, 37(7), 1323-1331.
Rothmeier, A. S., Versteeg, H. H. & Ruf, W. (2019) Factor VIIa-induced interaction with integrin controls the release of tissue factor on extracellular vesicles from endothelial cells. *J Thromb Haemost*, 17(4), 627-634.
Rousseau, A., Van Dreden, P., Khaterchi, A., Larsen, A. K., Elalamy, I. & Gerotziafas, G. T. (2017) Procoagulant microparticles derived from cancer cells have determinant role in the hypercoagulable state associated with cancer. *International Journal of Oncology*, 51(6), 1793-1800.
Ruf, W., Disse, J., Carneiro-Lobo, T. C., Yokota, N. & Schaffner, F. (2011) Tissue factor and cell signalling in cancer progression and thrombosis. *J Thromb Haemost*, 9 Suppl 1, 306-15.
Ruf, W. & Mueller, B. M. (1999) Tissue factor signaling. *Thromb Haemost*, 82(2), 175-82.
Ruf, W., Yokota, N. & Schaffner, F. (2010) Tissue factor in cancer progression and angiogenesis. *Thromb Res*, 125 Suppl 2, S36-8.
Ryden, L., Grabau, D., Schaffner, F., Jonsson, P. E., Ruf, W. & Belting, M. (2010) Evidence for tissue factor phosphorylation and its correlation with protease-activated receptor expression and the prognosis of primary breast cancer. *Int J Cancer*, 126(10), 2330-40.
Sabri, A., Muske, G., Zhang, H., Pak, E., Darrow, A., Andrade-Gordon, P. & Steinberg, S. F. (2000) Signaling properties and functions of two distinct cardiomyocyte protease-activated receptors. *Circ Res*, 86(10), 1054-61.
Saffarzadeh, M., Grunz, K., Nguyen, T. S., Lee, Y. K., Kitano, M., Danckwardt, S., Rodrigues, C. D. S., Weiler, H., Reyda, S. & Ruf, W. (2020) Macrophage protease-activated receptor 2 regulates fetal liver erythropoiesis in mice. *Blood Adv*, 4(22), 5810-5824.
Santa Cruz Biotechnology, I. (2020) *PAR-2 Antibody (SAM11): sc-13504*, 2020. Available online: https://datasheets.scbt.com/sc-13504.pdf [Accessed.
Sato, T., Yamaguchi, A., Goi, T., Hirono, Y., Takeuchi, K., Katayama, K. & Matsukawa, S. (2004) Heparanase expression in human colorectal cancer and its relationship to tumor angiogenesis, hematogenous metastasis, and prognosis. *J Surg Oncol*, 87(4), 174-81.
Sato, Y., Asada, Y., Marutsuka, K., Hatakeyama, K. & Sumiyoshi, A. (1996) Tissue factor induces migration of cultured aortic smooth muscle cells. *Thromb Haemost*, 75(3), 389-92.
Schaffner, F. & Ruf, W. (2008) Tissue factor and protease-activated receptor signaling in cancer. *Semin Thromb Hemost*, 34(2), 147-53.
Schaffner, F. & Ruf, W. (2009) Tissue factor and PAR2 signaling in the tumor microenvironment. *Arterioscler Thromb Vasc Biol*, 29(12), 1999-2004.
Schaffner, F., Versteeg, H. H., Schillert, A., Yokota, N., Petersen, L. C., Mueller, B. M. & Ruf, W. (2010) Cooperation of tissue factor cytoplasmic domain and PAR2 signaling in breast cancer development. *Blood*, 116(26), 6106-6113.
Schecter, A. D., Spirn, B., Rossikhina, M., Giesen, P. L., Bogdanov, V., Fallon, J. T., Fisher, E. A., Schnapp, L. M., Nemerson, Y. & Taubman, M. B. (2000) Release of active tissue factor by human arterial smooth muscle cells. *Circ Res*, 87(2), 126-32.
Schlesinger, M. (2018) Role of platelets and platelet receptors in cancer metastasis. *J Hematol Oncol*, 11(1), 125.
Schwartz, M. A. & Assoian, R. K. (2001) Integrins and cell proliferation: regulation of cyclin-dependent kinases via cytoplasmic signaling pathways. *J Cell Sci*, 114(Pt 14), 2553-60.
Scientific, T. (2020) *Co-immunoprecipitation (Co-IP)*, 2020. Available online: https://www.thermofisher.com/uk/en/home/life-science/protein-biology/protein-biology-learning-center/protein-biology-resource-library/pierce-protein-methods/co-immunoprecipitation-co-ip.html [Accessed.

Scott, G., Leopardi, S., Parker, L., Babiarz, L., Seiberg, M. & Han, R. J. (2003) The proteinase-activated receptor-2 mediates phagocytosis in a Rho-dependent manner in human keratinocytes. *Journal of Investigative Dermatology*, 121(3), 529-541.
Sedgwick, A. E., Clancy, J. W., Olivia Balmert, M. & D'Souza-Schorey, C. (2015) Extracellular microvesicles and invadopodia mediate non-overlapping modes of tumor cell invasion. *Sci Rep*, 5, 14748.
Seeliger, D. & de Groot, B. L. (2010) Ligand docking and binding site analysis with PyMOL and Autodock/Vina. *Journal of Computer-Aided Molecular Design*, 24(5), 417-422.
Seto, S., Onodera, H., Kaido, T., Yoshikawa, A., Ishigami, S., Arii, S. & Imamura, M. (2000) Tissue factor expression in human colorectal carcinoma: correlation with hepatic metastasis and impact on prognosis. *Cancer*, 88(2), 295-301.
Sevenet, P. O., Kaczor, D. A. & Depasse, F. (2017) Factor VII deficiency: from basics to clinical laboratory diagnosis and patient management. *Clin Appl Thromb Hemost*, 23(7), 703-710.
Shaker, H., Bundred, N. J., Landberg, G., Pritchard, S. A., Albadry, H., Nicholson, S. L., Harries, L. J., Heah, J. Y. E., Castle, J. & Kirwan, C. C. (2020) Breast cancer stromal clotting activation (Tissue Factor and thrombin): A pre-invasive phenomena that is prognostic in invasion. *Cancer Med*, 9(5), 1768-1778.
Shaker, H., Harrison, H., Clarke, R., Landberg, G., Bundred, N. J., Versteeg, H. H. & Kirwan, C. C. (2017) Tissue Factor promotes breast cancer stem cell activity in vitro. *Oncotarget*, 8(16), 25915-25927.
Shanshan, H., Lan, X., Xia, L., Huang, W., Meifang, Z. & Ling, Y. (2019) Inhibition of protease-activated receptor-2 induces apoptosis in cervical cancer by inhibiting signal transducer and activator of transcription-3 signaling. *J Int Med Res*, 47(3), 1330-1338.
Sharpe, H. J., Stevens, T. J. & Munro, S. (2010) A comprehensive comparison of transmembrane domains reveals organelle-specific properties. *Cell*, 142(1), 158-69.
Shen, B., Zheng, M. Q., Lu, J. W., Jiang, Q., Wang, T. H. & Huang, X. E. (2013) CXCL12-CXCR4 promotes proliferation and invasion of pancreatic cancer cells. *Asian Pac J Cancer Prev*, 14(9), 5403-8.
Shigemori, C., Wada, H., Matsumoto, K., Shiku, H., Nakamura, S. & Suzuki, H. (1998) Tissue factor expression and metastatic potential of colorectal cancer. *Thromb Haemost*, 80(6), 894-8.
Shimamoto, R., Sawada, T., Uchima, Y., Inoue, M., Kimura, K., Yamashita, Y., Yamada, N., Nishihara, T., Ohira, M. & Hirakawa, K. (2004) A role for protease-activated receptor-2 in pancreatic cancer cell proliferation. *Int J Oncol*, 24(6), 1401-6.
Shoji, M., Hancock, W. W., Abe, K., Micko, C., Casper, K. A., Baine, R. M., Wilcox, J. N., Danave, I., Dillehay, D. L., Matthews, E., Contrino, J., Morrissey, J. H., Gordon, S., Edgington, T. S., Kudryk, B., Kreutzer, D. L. & Rickles, F. R. (1998) Activation of coagulation and angiogenesis in cancer: immunohistochemical localization in situ of clotting proteins and vascular endothelial growth factor in human cancer. *Am J Pathol*, 152(2), 399-411.
Short, S. M., Talbott, G. A. & Juliano, R. L. (1998) Integrin-mediated signaling events in human endothelial cells. *Mol Biol Cell*, 9(8), 1969-80.
Sideras, K., Schaefer, P. L., Okuno, S. H., Sloan, J. A., Kutteh, L., Fitch, T. R., Dakhil, S. R., Levitt, R., Alberts, S. R., Morton, R. F., Rowland, K. M., Novotny, P. J. & Loprinzi, C. L. (2006) Low-molecular-weight heparin in patients with advanced cancer: a phase 3 clinical trial. *Mayo Clin Proc*, 81(6), 758-67.
Sierko, E., Wojtukiewicz, M. Z., Zimnoch, L., Tokajuk, P., Ostrowska-Cichocka, K. & Kisiel, W. (2012) Co-localization of Protein Z, Protein Z-Dependent protease inhibitor and coagulation factor X in human colon cancer tissue: implications for coagulation regulation on tumor cells. *Thromb Res*, 129(4), e112-8.
Simons, K. & Toomre, D. (2000) Lipid rafts and signal transduction. *Nat Rev Mol Cell Biol*, 1(1), 31-9.
Skog, J., Wurdinger, T., van Rijn, S., Meijer, D. H., Gainche, L., Sena-Esteves, M., Curry, W. T., Jr., Carter, B. S., Krichevsky, A. M. & Breakefield, X. O. (2008) Glioblastoma microvesicles transport RNA

and proteins that promote tumour growth and provide diagnostic biomarkers. *Nat Cell Biol*, 10(12), 1470-6.
Smorenburg, S. M. & Van Noorden, C. J. (2001) The complex effects of heparins on cancer progression and metastasis in experimental studies. *Pharmacol Rev*, 53(1), 93-105.
Smyrek, I., Mathew, B., Fischer, S. C., Lissek, S. M., Becker, S. & Stelzer, E. H. K. (2019) E-cadherin, actin, microtubules and FAK dominate different spheroid formation phases and important elements of tissue integrity. *Biol Open*, 8(1).
Soker, S., Goldstaub, D., Svahn, C. M., Vlodavsky, I., Levi, B. Z. & Neufeld, G. (1994) Variations in the size and sulfation of heparin modulate the effect of heparin on the binding of VEGF165 to its receptors. *Biochem Biophys Res Commun*, 203(2), 1339-47.
Sorensen, B. B., Freskgard, P. O., Nielsen, L. S., Rao, L. V., Ezban, M. & Petersen, L. C. (1999) Factor VIIa-induced p44/42 mitogen-activated protein kinase activation requires the proteolytic activity of factor VIIa and is independent of the tissue factor cytoplasmic domain. *J Biol Chem*, 274(30), 21349-54.
Spicer, E. K., Horton, R., Bloem, L., Bach, R., Williams, K. R., Guha, A., Kraus, J., Lin, T. C., Nemerson, Y. & Konigsberg, W. H. (1987) Isolation of cDNA clones coding for human tissue factor: primary structure of the protein and cDNA. *Proc Natl Acad Sci U S A*, 84(15), 5148-52.
Spiess, M., Hernandez-Varas, P., Oddone, A., Olofsson, H., Blom, H., Waithe, D., Lock, J. G., Lakadamyali, M. & Stromblad, S. (2018) Active and inactive beta1 integrins segregate into distinct nanoclusters in focal adhesions. *J Cell Biol*, 217(6), 1929-1940.
Sriwai, W., Mahavadi, S., Al-Shboul, O., Grider, J. R. & Murthy, K. S. (2013) Distinctive G protein-dependent signaling by protease-activated peceptor 2 (PAR2) in smooth muscle: feedback inhibition of RhoA by cAMP-independent PKA. *PLoS One*, 8(6), e66743.
Stachowiak, J. C., Schmid, E. M., Ryan, C. J., Ann, H. S., Sasaki, D. Y., Sherman, M. B., Geissler, P. L., Fletcher, D. A. & Hayden, C. C. (2012) Membrane bending by protein-protein crowding. *Nat Cell Biol*, 14(9), 944-9.
Stalheim, L., Ding, Y., Gullapalli, A., Paing, M. M., Wolfe, B. L., Morris, D. R. & Trejo, J. (2005) Multiple independent functions of arrestins in the regulation of protease-activated receptor-2 signaling and trafficking. *Molecular Pharmacology*, 67(1), 78-87.
Steffens, G. C., Yao, C., Prevel, P., Markowicz, M., Schenck, P., Noah, E. M. & Pallua, N. (2004) Modulation of angiogenic potential of collagen matrices by covalent incorporation of heparin and loading with vascular endothelial growth factor. *Tissue Eng*, 10(9-10), 1502-9.
Stevenson, J. L., Choi, S. H. & Varki, A. (2005) Differential metastasis inhibition by clinically relevant levels of heparins--correlation with selectin inhibition, not antithrombotic activity. *Clin Cancer Res*, 11(19 Pt 1), 7003-11.
Stevenson, J. L., Varki, A. & Borsig, L. (2007) Heparin attenuates metastasis mainly due to inhibition of P- and L-selectin, but non-anticoagulant heparins can have additional effects. *Thromb Res*, 120 Suppl 2, S107-11.
Stoker, M., O'Neill, C., Berryman, S. & Waxman, V. (1968) Anchorage and growth regulation in normal and virus-transformed cells. *Int J Cancer*, 3(5), 683-93.
Stratman, A. N., Schwindt, A. E., Malotte, K. M. & Davis, G. E. (2010) Endothelial-derived PDGF-BB and HB-EGF coordinately regulate pericyte recruitment during vasculogenic tube assembly and stabilization. *Blood*, 116(22), 4720-30.
Su, Y., Xia, W., Li, J., Walz, T., Humphries, M. J., Vestweber, D., Cabanas, C., Lu, C. & Springer, T. A. (2016) Relating conformation to function in integrin alpha5beta1. *Proc Natl Acad Sci U S A*, 113(27), E3872-81.
Sudha, T., Yalcin, M., Lin, H. Y., Elmetwally, A. M., Nazeer, T., Arumugam, T., Phillips, P. & Mousa, S. A. (2014) Suppression of pancreatic cancer by sulfated non-anticoagulant low molecular weight heparin. *Cancer Lett*, 350(1-2), 25-33.
Suen, J. Y., Gardiner, B., Grimmond, S. & Fairlie, D. P. (2010) Profiling gene expression induced by protease-activated receptor 2 (PAR2) activation in human kidney cells. *PLoS One*, 5(11), e13809.

Sun, L., Li, P. B., Yao, Y. F., Xiu, A. Y., Peng, Z., Bai, Y. H. & Gao, Y. J. (2018a) Proteinase-activated receptor 2 promotes tumor cell proliferation and metastasis by inducing epithelial-mesenchymal transition and predicts poor prognosis in hepatocellular carcinoma. *World J Gastroenterol*, 24(10), 1120-1133.
Sun, Q., Zhou, C., Ma, R., Guo, Q., Huang, H., Hao, J., Liu, H., Shi, R. & Liu, B. (2018b) Prognostic value of increased integrin-beta 1 expression in solid cancers: a meta-analysis. *Onco Targets Ther*, 11, 1787-1799.
Suttie, J. W. (1980) Mechanism of action of vitamin K: synthesis of gamma-carboxyglutamic acid. *CRC Crit Rev Biochem*, 8(2), 191-223.
Szatanek, R., Baran, J., Siedlar, M. & Baj-Krzyworzeka, M. (2015) Isolation of extracellular vesicles: Determining the correct approach (Review). *International Journal of Molecular Medicine*, 36(1), 11-17.
Taherian, A., Li, X. L., Liu, Y. Q. & Haas, T. A. (2011) Differences in integrin expression and signaling within human breast cancer cells. *Bmc Cancer*, 11.
Takada, Y. & Puzon, W. (1993) Identification of a regulatory region of integrin beta 1 subunit using activating and inhibiting antibodies. *J Biol Chem*, 268(23), 17597-601.
Takahashi, H., Ebihara, S., Okazaki, T., Asada, M., Sasaki, H. & Yamaya, M. (2005) A comparison of the effects of unfractionated heparin, dalteparin and danaparoid on vascular endothelial growth factor-induced tumour angiogenesis and heparanase activity. *Br J Pharmacol*, 146(3), 333-43.
Tang, J. Q., Fan, Q., Wu, W. H., Jia, Z. C., Li, H., Yang, Y. M., Liu, Y. C. & Wan, Y. L. (2010) Extrahepatic synthesis of coagulation factor VII by colorectal cancer cells promotes tumor invasion and metastasis. *Chin Med J (Engl)*, 123(24), 3559-65.
Tang, W., Nakamura, Y., Tsujimoto, M., Sato, M., Wang, X., Kurozumi, K., Nakahara, M., Nakao, K., Nakamura, M., Mori, I. & Kakudo, K. (2002) Heparanase: a key enzyme in invasion and metastasis of gastric carcinoma. *Mod Pathol*, 15(6), 593-8.
Teplyakov, A., Obmolova, G., Malia, T. J., Wu, B., Zhao, Y., Taudte, S., Anderson, G. M. & Gilliland, G. L. (2017) Crystal structure of tissue factor in complex with antibody 10H10 reveals the signaling epitope. *Cell Signal*, 36, 139-144.
Thaler, J., Ay, C., Mackman, N., Bertina, R. M., Kaider, A., Marosi, C., Key, N. S., Barcel, D. A., Scheithauer, W., Kornek, G., Zielinski, C. & Pabinger, I. (2012) Microparticle-associated tissue factor activity, venous thromboembolism and mortality in pancreatic, gastric, colorectal and brain cancer patients. *J Thromb Haemost*, 10(7), 1363-70.
Thaler, J., Koder, S., Kornek, G., Pabinger, I. & Ay, C. (2014) Microparticle-associated tissue factor activity in patients with metastatic pancreatic cancer and its effect on fibrin clot formation. *Transl Res*, 163(2), 145-50.
Thery, C., Amigorena, S., Raposo, G. & Clayton, A. (2006) Isolation and characterization of exosomes from cell culture supernatants and biological fluids. *Curr Protoc Cell Biol*, Chapter 3, Unit 3 22.
Thery, C., Witwer, K. W., Aikawa, E., Alcaraz, M. J., Anderson, J. D., Andriantsitohaina, R., Antoniou, A., Arab, T., Archer, F., Atkin-Smith, G. K., Ayre, D. C., Bach, J. M., Bachurski, D., Baharvand, H., Balaj, L., Baldacchino, S., Bauer, N. N., Baxter, A. A., Bebawy, M., Beckham, C., Zavec, A. B., Benmoussa, A., Berardi, A. C., Bergese, P., Bielska, E., Blenkiron, C., Bobis-Wozowicz, S., Boilard, E., Boireau, W., Bongiovanni, A., Borras, F. E., Bosch, S., Boulanger, C. M., Breakefield, X., Breglio, A. M., Brennan, M. A., Brigstock, D. R., Brisson, A., Broekman, M. L. D., Bromberg, J. F., Bryl-Gorecka, P., Buch, S., Buck, A. H., Burger, D., Busatto, S., Buschmann, D., Bussolati, B., Buzas, E. I., Byrd, J. B., Camussi, G., Carter, D. R. F., Caruso, S., Chamley, L. W., Chang, Y. T., Chen, C. C., Chen, S., Cheng, L., Chin, A. R., Clayton, A., Clerici, S. P., Cocks, A., Cocucci, E., Coffey, R. J., Cordeiro-da-Silva, A., Couch, Y., Coumans, F. A. W., Coyle, B., Crescitelli, R., Criado, M. F., D'Souza-Schorey, C., Das, S., Chaudhuri, A. D., de Candia, P., De Santana, E. F., De Wever, O., del Portillo, H. A., Demaret, T., Deville, S., Devitt, A., Dhondt, B., Di Vizio, D., Dieterich, L. C., Dolo, V., Rubio, A. P. D., Dominici, M., Dourado, M. R., Driedonks, T. A. P., Duarte, F. V., Duncan, H. M., Eichenberger, R. M., Ekstrom, K., Andaloussi, S. E. L., Elie-Caille, C., Erdbrugger, U., Falcon-Perez, J. M., Fatima, F., Fish, J. E., Flores-Bellver, M., Forsonits, A., Frelet-

Barrand, A., et al (2018) Minimal information for studies of extracellular vesicles 2018 (MISEV2018): a position statement of the International Society for Extracellular Vesicles and update of the MISEV2014 guidelines. *Journal of Extracellular Vesicles*, 7(1).
Thorne, R. F., Marshall, J. F., Shafren, D. R., Gibson, P. G., Hart, I. R. & Burns, G. F. (2000) The integrins alpha3beta1 and alpha6beta1 physically and functionally associate with CD36 in human melanoma cells. Requirement for the extracellular domain OF CD36. *J Biol Chem*, 275(45), 35264-75.
Timp, J. F., Braekkan, S. K., Versteeg, H. H. & Cannegieter, S. C. (2013) Epidemiology of cancer-associated venous thrombosis. *Blood*, 122(10), 1712-23.
Toomey, J. R., Kratzer, K. E., Lasky, N. M., Stanton, J. J. & Broze, G. J., Jr. (1996) Targeted disruption of the murine tissue factor gene results in embryonic lethality. *Blood*, 88(5), 1583-7.
Trevigen (2016) *Cultrex® Spheroid Invasion Matrix*, 2016. Available online: https://trevigen.com/products-services/physiologic-cell-culture/spheroid-assays/matrices/cultrex-spheroid-invasion-matrix/ [Accessed.
Tricarico, C., Clancy, J. & D'Souza-Schorey, C. (2017) Biology and biogenesis of shed microvesicles. *Small GTPases*, 8(4), 220-232.
Triplett, D. A. (2000) Coagulation and bleeding disorders: review and update. *Clin Chem*, 46(8 Pt 2), 1260-9.
Trousseau, A. (1867) Lectures on clinical medicine, *New Sydenham Society*. Hotel-Dieu, Paris.
Tryggvason, K., Hoyhtya, M. & Salo, T. (1987) Proteolytic degradation of extracellular matrix in tumor invasion. *Biochim Biophys Acta*, 907(3), 191-217.
Tsopanoglou, N. E. & Maragoudakis, M. E. (1999) On the mechanism of thrombin-induced angiogenesis. Potentiation of vascular endothelial growth factor activity on endothelial cells by up-regulation of its receptors. *J Biol Chem*, 274(34), 23969-76.
Tzanakakis, E. S., Hansen, L. K. & Hu, W. S. (2001) The role of actin filaments and microtubules in hepatocyte spheroid self-assembly. *Cell Motil Cytoskeleton*, 48(3), 175-89.
Ueno, T., Toi, M., Koike, M., Nakamura, S. & Tominaga, T. (2000) Tissue factor expression in breast cancer tissues: its correlation with prognosis and plasma concentration. *Br J Cancer*, 83(2), 164-70.
Unruh, D. & Horbinski, C. (2020) Beyond thrombosis: the impact of tissue factor signaling in cancer. *J Hematol Oncol*, 13(1), 93.
Unruh, D., Turner, K., Srinivasan, R., Kocaturk, B., Qi, X., Chu, Z., Aronow, B. J., Plas, D. R., Gallo, C. A., Kalthoff, H., Kirchhofer, D., Ruf, W., Ahmad, S. A., Lucas, F. V., Versteeg, H. H. & Bogdanov, V. Y. (2014) Alternatively spliced tissue factor contributes to tumor spread and activation of coagulation in pancreatic ductal adenocarcinoma. *Int J Cancer*, 134(1), 9-20.
Uusitalo-Jarvinen, H., Kurokawa, T., Mueller, B. M., Andrade-Gordon, P., Friedlander, M. & Ruf, W. (2007) Role of protease activated receptor 1 and 2 signaling in hypoxia-induced angiogenesis. *Arterioscler Thromb Vasc Biol*, 27(6), 1456-62.
Valdramidou, D., Humphries, M. J. & Mould, A. P. (2008) Distinct roles of beta1 metal ion-dependent adhesion site (MIDAS), adjacent to MIDAS (ADMIDAS), and ligand-associated metal-binding site (LIMBS) cation-binding sites in ligand recognition by integrin alpha2beta1. *J Biol Chem*, 283(47), 32704-14.
van den Berg, Y. W., van den Hengel, L. G., Myers, H. R., Ayachi, O., Jordanova, E., Ruf, W., Spek, C. A., Reitsma, P. H., Bogdanov, V. Y. & Versteeg, H. H. (2009) Alternatively spliced tissue factor induces angiogenesis through integrin ligation. *Proc Natl Acad Sci U S A*, 106(46), 19497-502.
van der Pol, E., Coumans, F. A. W., Grootemaat, A. E., Gardiner, C., Sargent, I. L., Harrison, P., Sturk, A., van Leeuwen, T. G. & Nieuwland, R. (2014) Particle size distribution of exosomes and microvesicles determined by transmission electron microscopy, flow cytometry, nanoparticle tracking analysis, and resistive pulse sensing. *Journal of Thrombosis and Haemostasis*, 12(7), 1182-1192.
van Gastel, J., Hendrickx, J. O., Leysen, H., Santos-Otte, P., Luttrell, L. M., Martin, B. & Maudsley, S. (2018) beta-Arrestin Based Receptor Signaling Paradigms: Potential Therapeutic Targets for Complex Age-Related Disorders. *Front Pharmacol*, 9, 1369.

van Niel, G., D'Angelo, G. & Raposo, G. (2018) Shedding light on the cell biology of extracellular vesicles. *Nat Rev Mol Cell Biol*.
Varki, A. (2007) Trousseau's syndrome: multiple definitions and multiple mechanisms. *Blood*, 110(6), 1723-9.
Venkateswarlu, D., Perera, L., Darden, T. & Pedersen, L. G. (2002) Structure and dynamics of zymogen human blood coagulation factor X. *Biophysical Journal*, 82(3), 1190-1206.
Vermeulen, K., Van Bockstaele, D. R. & Berneman, Z. N. (2003) The cell cycle: a review of regulation, deregulation and therapeutic targets in cancer. *Cell Prolif*, 36(3), 131-49.
Versteeg, H. H., Schaffner, F., Kerver, M., Ellies, L. G., Andrade-Gordon, P., Mueller, B. M. & Ruf, W. (2008a) Protease-activated receptor (PAR) 2, but not PAR1, signaling promotes the development of mammary adenocarcinoma in polyoma middle T mice. *Cancer Research*, 68(17), 7219-7227.
Versteeg, H. H., Schaffner, F., Kerver, M., Petersen, H. H., Ahamed, J., Felding-Habermann, B., Takada, Y., Mueller, B. M. & Ruf, W. (2008b) Inhibition of tissue factor signaling suppresses tumor growth. *Blood*, 111(1), 190-9.
Versteeg, H. H., Spek, C. A., Richel, D. J. & Peppelenbosch, M. P. (2004) Coagulation factors VIIa and Xa inhibit apoptosis and anoikis. *Oncogene*, 23(2), 410-7.
Vitale, M., Illario, M., Di Matola, T., Casamassima, A., Fenzi, G. & Rossi, G. (1997) Integrin binding to immobilized collagen and fibronectin stimulates the proliferation of human thyroid cells in culture. *Endocrinology*, 138(4), 1642-8.
Vlodavsky, I., Ilan, N., Nadir, Y., Brenner, B., Katz, B. Z., Naggi, A., Torri, G., Casud, B. & Sasisekharan, R. (2007) Heparanase, heparin and the coagulation system in cancer progression. *Thrombosis Research*, 120, S112-S120.
Vrana, J. A., Stang, M. T., Grande, J. P. & Getz, M. J. (1996) Expression of tissue factor in tumor stroma correlates with progression to invasive human breast cancer: paracrine regulation by carcinoma cell-derived members of the transforming growth factor beta family. *Cancer Res*, 56(21), 5063-70.
Walker, A. J., Card, T. R., West, J., Crooks, C. & Grainge, M. J. (2013) Incidence of venous thromboembolism in patients with cancer - a cohort study using linked United Kingdom databases. *Eur J Cancer*, 49(6), 1404-13.
Walker, J. L. & Assoian, R. K. (2005) Integrin-dependent signal transduction regulating cyclin D1 expression and G1 phase cell cycle progression. *Cancer Metastasis Rev*, 24(3), 383-93.
Wang, H. Y., Zheng, Y. S. & He, S. H. (2006) Induction of release and up-regulated gene expression of interleukin (IL)-8 in A549 cells by serine proteinases. *Bmc Cell Biology*, 7.
Wang, J., Pendurthi, U. R. & Rao, L. V. M. (2017) Sphingomyelin encrypts tissue factor: ATP-induced activation of A-SMase leads to tissue factor decryption and microvesicle shedding. *Blood Advances*, 1(13), 849-862.
Wang, T., Gilkes, D. M., Takano, N., Xiang, L., Luo, W., Bishop, C. J., Chaturvedi, P., Green, J. J. & Semenza, G. L. (2014) Hypoxia-inducible factors and RAB22A mediate formation of microvesicles that stimulate breast cancer invasion and metastasis. *Proc Natl Acad Sci U S A*, 111(31), E3234-42.
Wells, A. (2000) Tumor invasion: role of growth factor-induced cell motility. *Adv Cancer Res*, 78, 31-101.
Wildgoose, P., Nemerson, Y., Hansen, L. L., Nielsen, F. E., Glazer, S. & Hedner, U. (1992) Measurement of basal levels of factor VIIa in hemophilia A and B patients. *Blood*, 80(1), 25-8.
Witwer, K. W., Buzas, E. I., Bemis, L. T., Bora, A., Lasser, C., Lotvall, J., Nolte-'t Hoen, E. N., Piper, M. G., Sivaraman, S., Skog, J., Thery, C., Wauben, M. H. & Hochberg, F. (2013) Standardization of sample collection, isolation and analysis methods in extracellular vesicle research. *J Extracell Vesicles*, 2.
Wojtukiewicz, M. Z., Hempel, D., Sierko, E., Tucker, S. C. & Honn, K. V. (2015) Protease-activated receptors (PARs)--biology and role in cancer invasion and metastasis. *Cancer Metastasis Rev*, 34(4), 775-96.
Wojtukiewicz, M. Z., Sierko, E., Hempel, D., Tucker, S. C. & Honn, K. V. (2017) Platelets and cancer angiogenesis nexus. *Cancer Metastasis Rev*, 36(2), 249-262.

Wolfenson, H., Lavelin, I. & Geiger, B. (2013) Dynamic regulation of the structure and functions of integrin adhesions. *Dev Cell*, 24(5), 447-58.
Wu, B., Zhou, H., Hu, L., Mu, Y. & Wu, Y. (2013) Involvement of PKCalpha activation in TF/VIIa/PAR2-induced proliferation, migration, and survival of colon cancer cell SW620. *Tumour Biol*, 34(2), 837-46.
Wygant, G. D., Guo, J., Rosenblatt, L., Weycker, D., Li, S., Lee, T., Luo, X. M., Mardekian, J., Hanau, A., Atwood, M., Pan, X. Y. & Cohen, A. (2019) Comparative effectiveness of apixaban versus warfarin for treatment of venous thromboembolism in patients with and without active cancer. *Journal of the American College of Cardiology*, 73(9), 1926-1926.
Wysokinski, W. E., Houghton, D. E., Casanegra, A. I., Vlazny, D. T., Bott-Kitslaar, D. M., Froehling, D. A., Hodge, D. O., Peterson, L. G. & Mcbane, R. D. (2019) Comparison of apixaban to rivaroxaban and enoxaparin in acute cancer-associated venous thromboembolism. *American Journal of Hematology*, 94(11), 1185-1192.
Xie, C., Zhu, J., Chen, X., Mi, L., Nishida, N. & Springer, T. A. (2010) Structure of an integrin with an alphaI domain, complement receptor type 4. *EMBO J*, 29(3), 666-79.
Xie, L. Q., Duan, Z. X., Liu, C. J., Zheng, Y. M. & Zhou, J. (2015) Protease-activated receptor 2 agonist increases cell proliferation and invasion of human pancreatic cancer cells. *Experimental and Therapeutic Medicine*, 9(1), 239-244.
Xie, L. Q., Zheng, Y. M., Li, X., Zhao, J. Y., Chen, X. Y., Chen, L., Zhou, J., Hai, O. & Li, F. (2012) Enhanced proliferation of human hepatoma cells by PAR-2 agonists via the ERK/AP-1 pathway. *Oncology Reports*, 28(5), 1665-1672.
Xiong, J. P., Stehle, T., Diefenbach, B., Zhang, R., Dunker, R., Scott, D. L., Joachimiak, A., Goodman, S. L. & Arnaout, M. A. (2001) Crystal structure of the extracellular segment of integrin alpha Vbeta3. *Science*, 294(5541), 339-45.
Xue, M., Chan, A., Seol, J., Sambrook, P., March, L. & Jackson, C. (2011) Protease activated receptor (PAR)2, but not PAR1, promotes synovial fibroblast proliferation and invasion. *Internal Medicine Journal*, 41, 33-33.
Yau, M. K., Liu, L. & Fairlie, D. P. (2013) Toward drugs for protease-activated receptor 2 (PAR2). *J Med Chem*, 56(19), 7477-97.
Yavuz, C., Caliskan, A., Karahan, O., Yazici, S., Guclu, O., Demirtas, S. & Mavitas, B. (2014) Investigation of the antiangiogenic behaviors of rivaroxaban and low molecular weight heparins. *Blood Coagul Fibrinolysis*, 25(4), 303-8.
Yokota, N., Koizume, S., Miyagi, E., Hirahara, F., Nakamura, Y., Kikuchi, K., Ruf, W., Sakuma, Y., Tsuchiya, E. & Miyagi, Y. (2009) Self-production of tissue factor-coagulation factor VII complex by ovarian cancer cells. *British Journal of Cancer*, 101(12), 2023-2029.
Young, A. M., Marshall, A., Thirlwall, J., Chapman, O., Lokare, A., Hill, C., Hale, D., Dunn, J. A., Lyman, G. H., Hutchinson, C., MacCallum, P., Kakkar, A., Hobbs, F. D. R., Petrou, S., Dale, J., Poole, C. J., Maraveyas, A. & Levine, M. (2018) Comparison of an oral factor Xa inhibitor with low molecular weight heparin in patients with cancer with venous thromboembolism: results of a randomized trial (SELECT-D). *J Clin Oncol*, 36(20), 2017-2023.
Yu, J., May, L., Milsom, C., Anderson, G. M., Weitz, J. I., Luyendyk, J. P., Broze, G., Mackman, N. & Rak, J. (2008) Contribution of host-derived tissue factor to tumor neovascularization. *Arterioscler Thromb Vasc Biol*, 28(11), 1975-81.
Yu, J. L., May, L., Lhotak, V., Shahrzad, S., Shirasawa, S., Weitz, J. I., Coomber, B. L., Mackman, N. & Rak, J. W. (2005) Oncogenic events regulate tissue factor expression in colorectal cancer cells: implications for tumor progression and angiogenesis. *Blood*, 105(4), 1734-1741.
Zcharia, E., Metzger, S., Chajek-Shaul, T., Aingorn, H., Elkin, M., Friedmann, Y., Weinstein, T., Li, J. P., Lindahl, U. & Vlodavsky, I. (2004) Transgenic expression of mammalian heparanase uncovers physiological functions of heparan sulfate in tissue morphogenesis, vascularization, and feeding behavior. *FASEB J*, 18(2), 252-63.

Zetser, A., Bashenko, Y., Edovitsky, E., Levy-Adam, F., Vlodavsky, I. & Ilan, N. (2006) Heparanase induces vascular endothelial growth factor expression: correlation with p38 phosphorylation levels and Src activation. *Cancer Res*, 66(3), 1455-63.
Zhang, K. & Chen, J. (2012) The regulation of integrin function by divalent cations. *Cell Adh Migr*, 6(1), 20-9.
Zhang, W. & Liu, H. T. (2002) MAPK signal pathways in the regulation of cell proliferation in mammalian cells. *Cell Res*, 12(1), 9-18.
Zhang, X., Yu, H., Lou, J. R., Zheng, J., Zhu, H., Popescu, N. I., Lupu, F., Lind, S. E. & Ding, W. Q. (2011) MicroRNA-19 (miR-19) regulates tissue factor expression in breast cancer cells. *J Biol Chem*, 286(2), 1429-35.
Zhang, Y., Deng, Y., Luther, T., Muller, M., Ziegler, R., Waldherr, R., Stern, D. M. & Nawroth, P. P. (1994) Tissue factor controls the balance of angiogenic and antiangiogenic properties of tumor cells in mice. *J Clin Invest*, 94(3), 1320-7.
Zhang, Y., Feng, J., Fu, H., Liu, C., Yu, Z., Sun, Y., She, X., Li, P., Zhao, C., Liu, Y., Liu, T., Liu, Q., Liu, Q., Li, G. & Wu, M. (2018) Coagulation factor X regulated by CASC2c recruited macrophages and induced M2 polarization in glioblastoma multiforme. *Front Immunol*, 9, 1557.
Zhao, J., Aguilar, G., Palencia, S., Newton, E. & Abo, A. (2009) rNAPc2 inhibits colorectal cancer in mice through tissue factor. *Clin Cancer Res*, 15(1), 208-16.
Zhao, J. H., Reiske, H. & Guan, J. L. (1998) Regulation of the cell cycle by focal adhesion kinase. *J Cell Biol*, 143(7), 1997-2008.
Zhu, J., Luo, B. H., Xiao, T., Zhang, C., Nishida, N. & Springer, T. A. (2008) Structure of a complete integrin ectodomain in a physiologic resting state and activation and deactivation by applied forces. *Mol Cell*, 32(6), 849-61.
Zhu, X., Ohtsubo, M., Bohmer, R. M., Roberts, J. M. & Assoian, R. K. (1996) Adhesion-dependent cell cycle progression linked to the expression of cyclin D1, activation of cyclin E-cdk2, and phosphorylation of the retinoblastoma protein. *J Cell Biol*, 133(2), 391-403.
Zioncheck, T. F., Roy, S. & Vehar, G. A. (1992) The cytoplasmic domain of tissue factor is phosphorylated by a protein kinase C-dependent mechanism. *J Biol Chem*, 267(6), 3561-4.
Zovein, A. C., Luque, A., Turlo, K. A., Hofmann, J. J., Yee, K. M., Becker, M. S., Fassler, R., Mellman, I., Lane, T. F. & Iruela-Arispe, M. L. (2010) Beta 1 integrin establishes endothelial cell polarity and arteriolar lumen formation via a PAR3-dependent mechanism. *Developmental Cell*, 18(1), 39-51.

Appendix 1

Figure A-1: Nanoparticle tracking analysis of cancer cell-derived MV

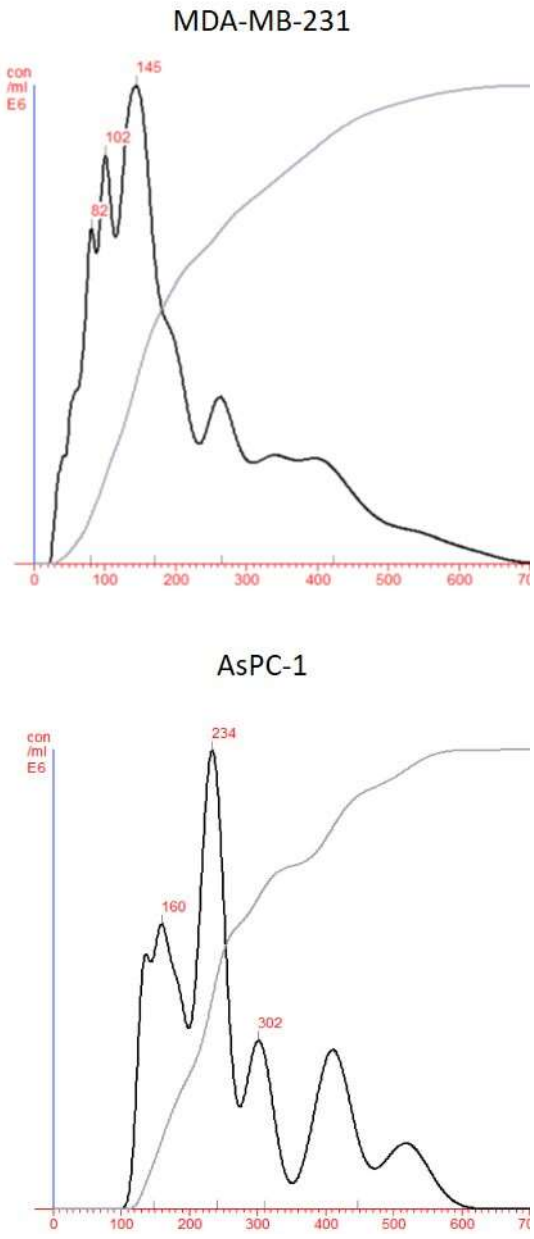

Microparticles were isolated from the conditioned media of MDA-MB-231 and AsCP-1 cells by ultracentrifugation at 100,000 *g* for 1 h at 20˚C, and resuspended in 0.1 µm-filtered PBS. The size distributions of the microvesicles were determined using a Nanosight NTA 2.3 instrument.